

Jia-Nan Zhang *Editor*

Carbon-Based Nanomaterials for Energy Conversion and Storage

Applications in Electrochemical Catalysis

Springer Series in Materials Science

Volume 325

Series Editors

Robert Hull, Center for Materials, Devices, and Integrated Systems, Rensselaer Polytechnic Institute, Troy, NY, USA

Chennupati Jagadish, Research School of Physics and Engineering, Australian National University, Canberra, ACT, Australia

Yoshiyuki Kawazoe, Center for Computational Materials, Tohoku University, Sendai, Japan

Jamie Kruzic, School of Mechanical & Manufacturing Engineering, UNSW Sydney, Sydney, NSW, Australia

Richard Osgood jr., Columbia University, Wenham, MA, USA

Jürgen Parisi, Universität Oldenburg, Oldenburg, Germany

Udo W. Pohl, Institute of Solid State Physics, Technical University of Berlin, Berlin, Germany

Tae-Yeon Seong, Department of Materials Science & Engineering, Korea University, Seoul, Korea (Republic of)

Shin-ichi Uchida, Electronics and Manufacturing, National Institute of Advanced Industrial Science and Technology, Tsukuba, Ibaraki, Japan

Zhiming M. Wang, Institute of Fundamental and Frontier Sciences - Electronic, University of Electronic Science and Technology of China, Chengdu, China

The Springer Series in Materials Science covers the complete spectrum of materials research and technology, including fundamental principles, physical properties, materials theory and design. Recognizing the increasing importance of materials science in future device technologies, the book titles in this series reflect the state-of-the-art in understanding and controlling the structure and properties of all important classes of materials.


Jia-Nan Zhang
Editor

Carbon-Based Nanomaterials for Energy Conversion and Storage

Applications in Electrochemical Catalysis

 Springer

Editor

Jia-Nan Zhang 

College of Materials Science
and Engineering
Zhengzhou University
Zhengzhou, Henan, China

ISSN 0933-033X

ISSN 2196-2812 (electronic)

Springer Series in Materials Science

ISBN 978-981-19-4624-0

ISBN 978-981-19-4625-7 (eBook)

<https://doi.org/10.1007/978-981-19-4625-7>

© The Editor(s) (if applicable) and The Author(s), under exclusive license to Springer Nature Singapore Pte Ltd. 2022

This work is subject to copyright. All rights are solely and exclusively licensed by the Publisher, whether the whole or part of the material is concerned, specifically the rights of translation, reprinting, reuse of illustrations, recitation, broadcasting, reproduction on microfilms or in any other physical way, and transmission or information storage and retrieval, electronic adaptation, computer software, or by similar or dissimilar methodology now known or hereafter developed.

The use of general descriptive names, registered names, trademarks, service marks, etc. in this publication does not imply, even in the absence of a specific statement, that such names are exempt from the relevant protective laws and regulations and therefore free for general use.

The publisher, the authors, and the editors are safe to assume that the advice and information in this book are believed to be true and accurate at the date of publication. Neither the publisher nor the authors or the editors give a warranty, expressed or implied, with respect to the material contained herein or for any errors or omissions that may have been made. The publisher remains neutral with regard to jurisdictional claims in published maps and institutional affiliations.

This Springer imprint is published by the registered company Springer Nature Singapore Pte Ltd.

The registered company address is: 152 Beach Road, #21-01/04 Gateway East, Singapore 189721, Singapore

Preface

The increasing demand of energy and scarcity of fossil fuel are major concerns today and have attracted much attention on utilizing renewable energy sources for better storage and conversion of energy. To meet the increasing demand of energy, most researches have focused on developing high-performance energy conversion and storage. The extensive studies have been carried out on catalysts used in different types of electrochemical reaction. The optimal design of catalysts is considered as one of the main routes to achieve high performance of the electrochemical energy conversion and storage. In this regard, carbon-based nanomaterials have been drawn considerable attention due to their special properties of high surface areas which providing large number of active sites for electrochemical reaction and ion/electron diffusion. Among various materials, carbon-based materials can be used as effective catalytic materials for different electrochemical reactions, from metal-free carbon-based nanomaterials to metal-heteroatom-carbon-based nanomaterials, as well as metal nanoparticles supported or encapsulated to carbon-based materials with their unique properties, tailored sizes and morphologies and. With the flourishing development of diverse carbon-based nanomaterials, further insights into the design and mechanisms of ideal electrocatalysts have been gained.

This book aims to cover all these aspects and discuss recent achievements and various electrochemical reactions processes including energy conversion and storage, as well as the corresponding advanced electrocatalysts mechanism understanding. The book comprises four sections. The first section discusses the fundamental synthesis, characterization techniques, and catalytic effects related to the energy conversion and storage mechanism from different types of electrochemical reactions. The next section elaborately reviews different types of electrocatalytic reactions based on different carbon-based materials and their performance reported till date. The third section is focused on batteries based on different carbon-based materials with different storage mechanism and their performances as reported. Finally, the enlightenment in terms of theoretical development and experimental research will be provided to the general reader.

It is anticipated that the content will further supply unambiguous understanding for all these components and the importance of the field and discuss current trends of different carbon-based materials for current ongoing works.

Zhengzhou, China

Prof. Jia-Nan Zhang

Acknowledgments

This book was supported by the National Natural Science Foundation of China (No. 21875221, U1604123, 21571157, 21101141, 22102156, and 22109140), the Youth Talent Support Program of High-Level Talents Special Support Plan in Henan Province (No. ZYQR201810148), the Creative talents in the Education Department of Henan Province (No. 19HASTIT039), the Outstanding Young Talent Research Fund of Zhengzhou University (No. 1521320001), and Distinguished Young Scholars Innovation Team of Zhengzhou University (No. 32320275).

Zhengzhou, China

Prof. Jia-Nan Zhang

Contents

1	Introduction	1
	Siran Xu, Yajin Wang, Dongping Xue, Huicong Xia, and Jia-Nan Zhang	
	References	9
2	Synthesis of Carbon-Based Nanomaterials	15
	Yu Du, Su Jiang, Yuan Li, and Jia-Nan Zhang	
2.1	Introduction	16
2.2	Synthesis of Metal-Free Carbon-Based Nanomaterials	18
	2.2.1 Intrinsic Defect Carbon	19
	2.2.2 Heteroatom-Doped Carbon	23
2.3	Synthesis of Atomically Dispersed Metal Carbon-Based Nanomaterials	27
	2.3.1 Single Metal-Heteroatom Doped Carbon-Based Nanomaterials	29
	2.3.2 Double/Multi-Metal-Heteroatom Doped Carbon-Based Nanomaterials	30
	2.3.3 Atomically Dispersed Metal Multi-Heteroatom Co-doped Carbon-Based Nanomaterials	32
2.4	Synthesis of Metal Nanoparticles Encapsulated Carbon-Based Nanomaterials	34
	2.4.1 Metal Hybrids Encapsulated Carbon-Based Nanomaterials	35
	2.4.2 Alloys Encapsulated Carbon-Based Nanomaterials	36
2.5	Synthesis of Metal Nanoparticles Supported Carbon-Based Nanomaterials	38
	2.5.1 Metal Hybrids Supported Carbon-Based Nanomaterials	39
	2.5.2 Alloys Supported Carbon-Based Nanomaterials	40
2.6	Conclusion and Perspectives	43
	References	44

3	Characterization	53
	Miaoying Chen, Dongping Xue, and Bang-An Lu	
3.1	Introduction	53
3.2	Direct Visualization	56
3.2.1	Scanning Electron Microscope and Transmission Electron Microscope	56
3.2.2	Scanning Transmission Electron Microscopy	58
3.2.3	Scanning Tunnel Microscope	61
3.2.4	Energy Dispersive Spectrometer and Electron Energy Loss Spectrometer	62
3.3	Indirect Verification	62
3.3.1	X-ray Diffraction	63
3.3.2	Raman Spectrum	65
3.3.3	N ₂ Adsorption–Desorption Curve	66
3.3.4	X-ray Photoelectron Spectroscopy	66
3.3.5	X-ray Absorption Spectroscopy	69
3.3.6	Electron Paramagnetic Resonance	71
3.3.7	Other Advanced Techniques	72
3.4	Simulation and Calculation	75
3.5	Conclusion and Perspectives	77
	References	77
4	Catalytic Effect of Carbon-Based Nanomaterials in Electrochemical Catalysis	83
	Yajin Wang, Xiaoyu Zhang, Huicong Xia, and Jia-Nan Zhang	
4.1	Introduction	84
4.2	Confinement Effect	87
4.2.1	Chemical Coordination Confinement Effect	87
4.2.2	Spatial Confinement Effect	89
4.3	Interface Engineering Effect	90
4.4	Electric Field Effect	91
4.5	Conclusion and Perspectives	95
	References	97
5	Carbon-Based Nanomaterials for Oxygen Reduction Reaction	103
	Xiaoyu Zhang, Dongping Xue, Siran Xu, Bang-An Lu, and Jia-Nan Zhang	
5.1	Introduction	104
5.2	Metal-Free Carbon-Based Electrocatalysts for ORR	105
5.3	Atomically Dispersed Metal Carbon-Based Electrocatalysts for ORR	108
5.4	Metal Nanoparticles Encapsulated Carbon-Based Electrocatalysts for ORR	112
5.5	Metal Nanoparticles Supported Carbon-Based Electrocatalysts for ORR	114

5.6	Conclusion and Perspectives	117
	References	119
6	Carbon-Based Nanomaterials for Hydrogen Evolution Reaction	123
	Reaction	123
	Bin Zhao and Siran Xu	
6.1	Introduction	123
6.2	Metal-Free Carbon-Based Electrocatalysts for HER	126
6.3	Atomically Dispersed Metal Carbon-Based Electrocatalysts for HER	129
6.4	Metal Nanoparticles Supported Carbon-Based Electrocatalysts for HER	133
6.5	Metal Nanoparticles Encapsulated Carbon-Based Electrocatalysts for HER	137
6.6	Conclusion and Prospects	139
	References	140
7	Carbon-Based Nanomaterials for Oxygen Evolution Reaction	147
	Mengli Liu, Siran Xu, and Bang-An Lu	
7.1	Introduction	147
7.2	Metal-Free Carbon-Based Electrocatalysts for OER	150
7.3	Atomically Dispersed Metal Carbon-Based Electrocatalysts for OER	153
7.4	Metal Nanoparticles Encapsulated Carbon-Based Electrocatalysts for OER	156
7.5	Metal Nanoparticles Supported Carbon-Based Electrocatalysts for OER	160
7.6	Conclusion and Perspective	161
	References	163
8	Carbon-Based Nanomaterials for Carbon Dioxide Reduction Reaction	169
	Reaction	169
	Dongping Xue and Yifan Wei	
8.1	Introduction	169
8.2	Metal-Free Carbon-Based Electrocatalysts for CO ₂ RR	172
8.3	Atomically Dispersed Metal Carbon-Based Electrocatalysts for CO ₂ RR	176
8.4	Metal Nanoparticles Encapsulated/Supported Carbon-Based Electrocatalysts for CO ₂ RR	179
8.5	Conclusion and Perspectives	181
	References	182
9	Carbon-Based Nanomaterials for Nitrogen Reduction Reaction	187
	Reaction	187
	Yajin Wang, Dongping Xue, Siran Xu, and Bang-An Lu	
9.1	Introduction	188
9.2	Metal-Free Carbon-Based Electrocatalysts for NRR	192

9.3	Atomically Dispersed Metal Carbon-Based Electrocatalysts for NRR	194
9.4	Metal Nanoparticles Encapsulated Carbon-Based Electrocatalysts for NRR	195
9.5	Metal Nanoparticles Supported Carbon-Based Electrocatalysts for NRR	199
9.6	Conclusion and Perspectives	202
	References	203
10	Carbon-Based Nanomaterials for Metal-Ion Batteries	209
	Yifan Wei, Huicong Xia, and Gan Qu	
10.1	Introduction	210
10.2	Metal-Free Carbon-Based Materials for MIBs	212
10.3	Atomically Dispersed Metal on Carbon Materials for MIBs	215
10.4	Metal Nanoparticles Encapsulated Carbon-Based Materials for MIBs	217
10.5	Metal Nanoparticles Supported Carbon-Based Materials for MIBs	219
10.6	Conclusion and Perspectives	223
	References	224
11	Carbon-Based Nanomaterials for Metal-Sulfur/Selenium Batteries	227
	Weijie Chen, Kai Guo, Huicong Xia, and Gan Qu	
11.1	Introduction	228
11.2	Metal-Free Carbon-Based Materials for MSBs	232
11.3	Atomically Dispersed Metal on Carbon-Based Materials for MSBs	235
11.4	Metal Nanoparticles Encapsulated by Carbon-Based Materials for MSBs	238
11.5	Metal Nanoparticles Supported Carbon-Based Materials for MSBs	238
11.6	Conclusion and Perspectives	242
	References	243
12	Carbon-Based Nanomaterials for Metal-Air Batteries	249
	Yue Yu and Huicong Xia	
12.1	Introduction	249
12.2	Metal-Free Carbon-Based Materials for MABs	253
12.3	Atomically Dispersed Metal Carbon-Based Materials for MABs	257
12.4	Metal Nanoparticles Encapsulated Carbon-Based Materials for MABs	259
12.5	Metal Nanoparticles Supported Carbon-Based Materials	263
12.6	Conclusion and Perspectives	266
	References	267

13 Summary and Perspectives 271
Huicong Xia, Dongping Xue, and Jia-Nan Zhang

Index 273

Contributors

Chen Miaoying College of Materials Science and Engineering, Zhengzhou University, Zhengzhou, P. R. China

Chen Weijie College of Materials Science and Engineering, Zhengzhou University, Zhengzhou, P. R. China

Du Yu College of Materials Science and Engineering, Zhengzhou University, Zhengzhou, P. R. China

Guo Kai College of Materials Science and Engineering, Zhengzhou University, Zhengzhou, P. R. China

Jiang Su College of Materials Science and Engineering, Zhengzhou University, Zhengzhou, P. R. China

Li Yuan College of Materials Science and Engineering, Zhengzhou University, Zhengzhou, P. R. China

Liu Mengli College of Materials Science and Engineering, Zhengzhou University, Zhengzhou, P. R. China

Lu Bang-An College of Materials Science and Engineering, Zhengzhou University, Zhengzhou, P. R. China

Qu Gan College of Materials Science and Engineering, Zhengzhou University, Zhengzhou, P. R. China

Wang Yajin College of Materials Science and Engineering, Zhengzhou University, Zhengzhou, P. R. China

Wei Yifan College of Materials Science and Engineering, Zhengzhou University, Zhengzhou, P. R. China

Xia Huicong College of Materials Science and Engineering, Zhengzhou University, Zhengzhou, P. R. China

Xu Siran College of Materials Science and Engineering, Zhengzhou University, Zhengzhou, P. R. China

Xue Dongping College of Materials Science and Engineering, Zhengzhou University, Zhengzhou, P. R. China

Yu Yue College of Materials Science and Engineering, Zhengzhou University, Zhengzhou, P. R. China

Zhang Jia-Nan College of Materials Science and Engineering, Zhengzhou University, Zhengzhou, P. R. China

Zhang Xiaoyu College of Materials Science and Engineering, Zhengzhou University, Zhengzhou, P. R. China

Zhao Bin College of Materials Science and Engineering, Zhengzhou University, Zhengzhou, P. R. China

Chapter 1

Introduction



Siran Xu, Yajin Wang, Dongping Xue, Huicong Xia, and Jia-Nan Zhang

Nanotechnology refers to the study of the properties and interactions of substances (including the manipulation of atoms and molecules) on the nanometer scale (between 1 and 100 nm), as well as the multidisciplinary science and technology that utilizes these properties, covering multiple fields such as physics, chemistry, materials, science, engineering, biology and medicine [1]. Its ultimate goal is to directly synthesis products with specific functions based on the novel physical, chemical, and biological properties of atoms, molecules, and nanoscale substances. Nanotechnology is another major technology that profoundly affects social development after information technology and biotechnology [2].

Nanomaterials are the core component of nanotechnology. When the substance reaches nanometer scale (about 1–100 nm), quantum effect, locality of substance, huge surface, and interface effects make many properties of the substance qualitatively change, showing lots of differences from macroscopic objects and the strange phenomenon of single atoms [2, 3]. However, if only the scale reaches nanometers without special properties, it cannot be called nanomaterials. After 1990, nanomaterials have developed rapidly. The most worth mentioning before this is the discovery of carbon nano-atom cluster—buckminsterfullerene (C_{60}) in 1985 [3]. The successful

S. Xu · Y. Wang · D. Xue · H. Xia · J.-N. Zhang (✉)
College of Materials Science and Engineering, Zhengzhou University, Zhengzhou 450001,
P. R. China
e-mail: zjn@zzu.edu.cn

S. Xu
e-mail: siranxuhbnu@163.com

Y. Wang
e-mail: 13283861570@163.com

D. Xue
e-mail: xdongping1231@126.com

H. Xia
e-mail: summer9209@126.com

development of this material has made people see that it has special properties that ordinary carbon material does not have. Pure C_{60} solid is an insulator, but it becomes a material with good conductivity after being doped with alkali metals, which can be compared with metals and even become superconductors [4]. With the development of nanotechnology, the classification of nanomaterials has become more detailed, including nano-particles, nano-blocks, nano-films, and nano-assembly systems [5]. At the beginning of the twenty-first century, people are more and more interested in the emerging fields of modern nanotechnology. With the help of various special properties of nanomaterials, which have a wide range of applications in the fields of catalytic, environmental protection, construction materials, [6] biomedical materials, [7] electromagnetic materials, [8] optical materials, [9] degradable materials [10] and so on. After decades of research and exploration on nanotechnology, it has been developed by leaps and bounds, and now scientists have been able to manipulate individual atoms in the laboratory, making nanomaterials the basis for preparing various required functional devices.

Some people say that electricity has brought about human civilization; others say that it is a human civilization that has created electricity. Regardless of the judgment, we can be sure that the emergence of electricity has changed the history of mankind, and the energy that brings electricity is an important driving force for the progress of mankind, society, and civilization. Because of this, our huge social system still relies on fossil energy which has naturally penetrated all aspects of our lives until now. 85% of the energy used by human beings is fossil energy sources, such as coal, oil, and natural gas, and overuse of these fossil energy sources has caused them to be in a crisis of energy exhaustion [11]. Moreover, the excessive use of traditional fossil energy has brought about global warming, ecological system destruction, endangerment of rare species, frequent extreme weather events, sea-level rise crisis, air pollution, and other problems, which seriously threaten survival and development of human society. If there is clean, safe, efficient, inexhaustible energy for our use, the “energy crisis” will cease to exist. Therefore, it is urgent to find clean energy, get rid of fossil energy dependence, promote economic growth, eliminate energy inequality and poverty, and protect the environment, to realize the sustainable development of all mankind [12]. Electrochemical energy storage and conversion systems, such as fuel cells, [13] metal-air batteries, [14] electrolytic water devices, [15] and carbon dioxide reduction technology [16] have become important means to deal with environmental and energy crises. In energy conversion equipment, catalyst design is an important link. Traditional electrocatalysts and energy storage materials still face technical problems such as complex preparation processes, low porosity, poor catalytic activity and stability, which severely restrict their commercial applications. Therefore, there is an urgent need to develop catalytic materials with high conversion efficiency and excellent stability. In recent years, researchers have focused their attention on nanocatalysts. Because of their unique crystal structure and surface characteristics, they have the advantages of large specific surface area, excellent stability, and high surface activity. Moreover, the bonding and electronic state on the surface of the nanocatalysts are different from the inside of the particle, and the incomplete coordination of surface atoms will also lead to an increase in surface active sites,

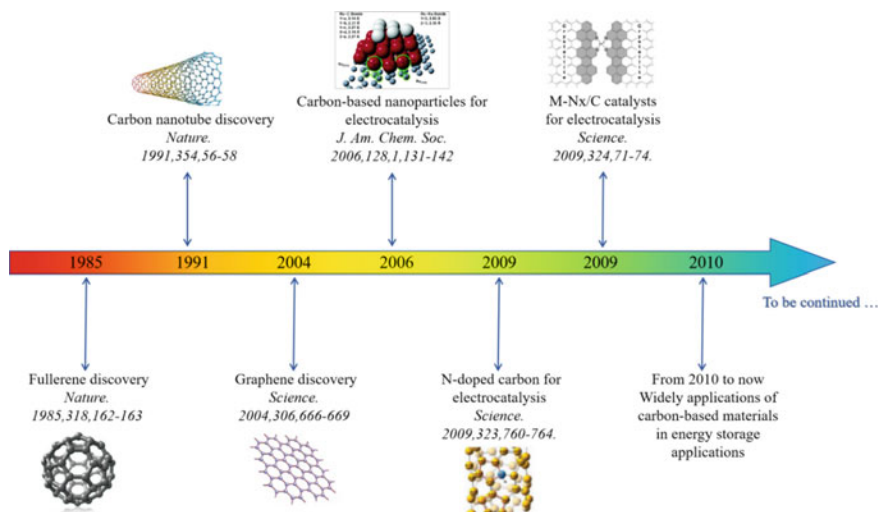


Fig. 1.1 Timeline of the important breakthrough of the development of carbon nanomaterials

and improve the catalytic performance [17]. Therefore, nanocatalysts show great application prospects in energy conversion and storage [18].

Carbon nanomaterials (CNMs) stand out to be one of the highly efficient nanomaterials due to its vast availability and lower cost compared to other nanomaterials [19, 20]. The development history of carbon-based nanomaterials is shown in Fig. 1.1. Meanwhile, CNMs, benefiting from their unique properties in exceptional electrical, thermal, chemical, and mechanical fields, have occupied a unique position in nanoscience [20–22]. Indeed, CNMs, thanks to the various allotropes (graphite, diamond, fullerenes), as well as the abundant dimensions from zero-dimensional (0D) to three-dimensional (3D) and variable forms of existence (powders, fibers, films, foams, fabrics, and hybrids) have captured immense attention as attractive materials with great potential and promising applications in massive fields [23]. In recent years, fullerenes, expanded graphite (EG), carbon nanotubes (CNTs), carbon nanofibers (CNFs), graphene, reduced graphene oxide (rGO), and other CNMs have been extensively applied in energy storage, electronics, catalysis, biomaterials, and medical fields [24–26]. CNMs are widely popular because of their low cost, abundant resources, various morphologies, excellent electrical and thermal conductivity, large surface areas, highly tunable electronic structures, and mechanical/chemical strength [24, 27]. These properties are all advantageous for advanced development in catalysis. The diversification of carbon nanostructures also provides more possibilities and directions for further exploration of electrochemical properties, mainly involving 0D fullerenes, carbon dots, one-dimensional (1D) CNTs, nanofibres, two-dimensional (2D) graphene, and 3D nanocrystal or self-assembled carbon [28]. Fullerenes, as typical 0D CNMs, usually exhibit hollow spheres or ellipsoidal shapes [29]. Among

them, C_{60} as an allotrope of carbon with an ideal spherical structure has been considered as the most representative 0D carbon material [30]. Subsequently, fullerenes have been studied extensively since 1990, when Kratschmer et al. [4] successfully achieved scalable production of C_{60} by evaporating graphite electrodes in a helium atmosphere. Numerous studies have reported that fullerene C_{60} , with its precise structure and abundant unsaturated bonds, can be easily functionalized to produce various derivatives, which can effectively reduce the structural/combinatorial heterogeneity problems that plague many CNMs [29, 31, 32]. Fullerenes also exhibit excellent redox properties, endowing them unique research properties in batteries and catalysis [31, 33]. 1D CNMs have shown extensive potential for energy conversion and storage as well as for commercial industrial production due to their low-cost, large specific surface areas, and controlled synthesis [23, 25, 34]. CNTs, as the most studied 1D carbon material, exhibit a tubular structure rolled by graphene sheets with a high length-to-diameter ratio [35, 36]. CNTs are usually divided into single-walled carbon nanotube (SWCNTs) and multi-walled carbon nanotube (MWCNTs) [21]. SWCNTs consists of a single layer graphene sheet, while MWCNTs are composed of multiple layers of graphene nanosheet, both of which have hollow lamellar structure, ultra-high electrical conductivity, significant charge transport mobility, good thermal stability, and large specific surface areas [37, 38]. Since the discovery of 2D graphene as a new member of the carbon family by Novoselov et al. in 2004, a new chapter in the development of graphene in materials science has been opened [39]. 2D graphene, a single layer of carbon atoms with a hexagonal lattice, consists of sp^2 carbon atoms bonded to adjacent carbon atoms in 3σ bonds [8, 40, 41]. The unique structural advantages of graphene endow the large theoretical specific surface areas with numerous mass transfer channels to fast deliver electrolyte to the active centers, high electrical conductivity to fast catalytic reaction kinetics, and strong corrosion resistance and chemical stability [40, 42, 43]. In addition, 2D graphene is an ideal carrier for dispersed active materials; graphene can not only modulate the morphology and microstructure of active materials and expose more electrochemical active sites, but also induce strong synergistic coupling effects [44, 45]. 3D nanocarbon material represents the growth in all dimensions, unlike 1D and 2D CNMs that expand only along one and two directions [25, 41]. Apart from the traditional activated carbon, mesoporous carbon and nanocrystals, more reports have focused on the self-assembly of low-dimensional CNMs, and flexible and highly selective assembly materials make it possible to design 3D CNMs in a controlled manner [25]. Thus, they not only inherit the characteristics of individual components, but also obtain some new features endowed by the assembly of all the components.

In 2009, Dai and his colleagues successfully fabricated nitrogen (N)-doped vertically aligned carbon nanotubes as metal-free catalysts to replace Pt for oxygen reduction reaction (ORR) in alkaline fuel cells, which exhibit extremely high catalytic activity, ultra-high long-term stability [46]. Since then, metal-free carbon-based materials have been widely explored as a new class of potential catalysts and have shown excellent catalytic performance in energy conversion and storage, green catalysis, and industrial production [47]. Various CNMs, including heteroatom doping (B, O, P, S, N, F), edge doping, defect doping, and charge transfer doping, have attracted

immense attention as high-efficient metal-free catalysts for various key reactions in energy conversion and storage processes [16, 48, 49]. Although metal-based materials often suffer from some shortcomings, such as high cost, low utilization, easy deactivation, and poor stability, the outstanding electrochemical activity decided that metal-based materials occupy the dominant status during nanomaterials [47, 50]. Therefore, the use of CNMs as a carrier to support or encapsulate metal-based carbon catalysts can effectively solve the above challenges. In addition, there are multiple advantages for diverse CNMs as a carrier to construct carbon-based materials: (1) Numerous researches imply that loading the active phases into the carbon skeleton not only improves the overall electrical conductivity and accelerates the electron transfer rate, but also modulates the electronic density of states of carbon and generates new active sites [51]. (2) The introduction of defects or heteroatoms can cause a positive impact on the charge state of the carbon skeleton, resulting in an increase in the variety and density of potential active sites [48, 52, 53]. (3) Metal-support interaction, confinement effect, and other catalytic effects can induce rapid charge transfer between metal site and carbon matrix, modulate the electronic structure of the loaded metal, and thus significantly enhance the electrochemical performance of carbon-based electrocatalysts [54, 55]. It is worth mentioning that the highly agglomerative nature of metal nanoparticles greatly limits the atomic utilization of metal sites and reduces the number of accessible active sites. In 2011, Zhang et al. [56] reported the preparation and performance of single-atom catalysts consisting of isolated single Pt atoms supported on the surface of iron oxide (Pt_1/FeO_x) for the first time, which exhibited outstanding activity and strong stability for CO oxidation and proposed the concept of “single-atom catalysis” on this basis. It is not difficult to speculate that the uniform dispersion of single metal atoms on CNMs can maximize the utilization of metal atoms and expose a large number of active sites [57, 58]. Single-atom catalysis is now a foreword and a hot object in the field of nanomaterials.

Previously, 0D metal nanoparticles have been the focus of materials research due to their high surface-to-volume ratio, better exposure of metal sites compared with their bulk counterparts, and their excellent electrical, magnetic, optical, and catalytic properties [59, 60]. However, due to the high surface energy of metal nanoparticles, migration and agglomeration of nanoparticles are very likely to occur during the catalytic process, and these structural and morphological changes often have a great negative impact on catalytic activity, selectivity, and stability, resulting in a dramatic decrease in catalytic performance, which greatly limits the further exploration of metal nanoparticles in energy conversion and storage [61–63]. Since 1994, when Planeix et al. [64] first reported the synthesis and application of nanohybrids consisting of Ru nanoparticles supported on carbon nanotube, the development of carbon-based nanomaterials has entered a new phase, with the exponential growth of a large amount of literature about metal nanoparticles supported on CNMs. Although the stability of conventional carbon-based supported metal nanoparticles can be improved by strong metal-support interactions, they may still undergo migration and agglomeration under harsh conditions. Fortunately, with the continuous innovation and development of carbon-based nanomaterials, a class of encapsulated metal

nanoparticles has emerged. Since CNMs are ideal carriers for metal nanoparticles due to their large surface areas, good thermal stability, tunable electronic structure, rich structural variety, good electrical conductivity, and acid and base resistance, encapsulating metal nanoparticles into CNMs have become a mainstream trend [65]. Numerous researches imply that encapsulated metal nanoparticles into CNMs can endow dramatically enhanced stability (due to the combination of spatial constraints and metal-support interactions) and recyclability, improved catalytic selectivity, strong electronic transfer, and interfacial catalysis between metal nanoparticles and carbon matrix [61, 66, 67]. In recent years, a great deal of research has focused on the development of low-cost, high-abundance, highly active and stable nanomaterials for energy conversion and storage applications. The emergence of carbon-based nanomaterials has brought a new light to the advanced development in this field.

To address the global energy crisis and the growing environmental pollution problem, various advanced electrochemical energy conversion devices (e.g., fuel cells, metal-air batteries, electrochemical water splitting, etc.) has been intensively studied to develop a green, economical, sustainable, and reliable alternative to traditional fossil fuel [68, 69]. However, their in-depth development is limited by the lack of ideal electrocatalysts to drive key electrode reactions, such as the cathode ORR reaction in proton exchange membrane fuel cells (PMFC), the oxygen evolution reaction (OER) and ORR processes in rechargeable Zn-air batteries, and the two half-reactions of hydrogen evolution reaction (HER) and OER in water splitting [15, 70, 71]. In addition, converting the greenhouse gas CO₂ into valuable chemical fuels using renewable electricity (CO₂ reduction reaction (CO₂RR)) offers new opportunities to reduce resource extraction and achieve a carbon-neutral [16, 19]. In addition, the conversion of airborne N₂ to NH₃ by electrochemical reduction (Nitrogen reduction reaction (NRR)) is considered to be a sustainable alternative process [72]. Although the specific mechanisms involved in each of the catalytic reactions mentioned above are different, they all undergo sluggish electron transfer kinetics and all require low-cost, highly active, and strong stable electrochemical catalysts to speed up the reaction process. Currently, carbon-based nanomaterials have emerged as the most promising candidates to replace precious metal catalysts due to the complex catalytic effects between active phase and carbon matrix, and CNMs' unique properties: (1) Natural reserves are abundant and cost-effective; (2) Excellent acid and alkali resistance and chemical stability; (3) High theoretical specific surface area; (4) Strong electric conductivity; (5) Various structures available. Meanwhile, with the advanced development of carbon-based nanomaterials, numerous studies were reported about various key reactions of energy conversion, such as ORR, HER, OER, CO₂RR, and NRR, as shown in Fig. 1.2 [19, 26, 71, 73–76].

Electrochemical energy storage (EES) devices, especially lithium-ion batteries (LIBs), have become the most commonly used power source due to their high energy density, safety, long cycle life, and environmental friendliness, as well as being the most widely used rechargeable battery today [77, 78]. In addition to these, the other electrochemical energy storage devices such as metal-sulfur (selenium) batteries (especially Li-S(Se) batteries) and metal-air batteries are also receiving

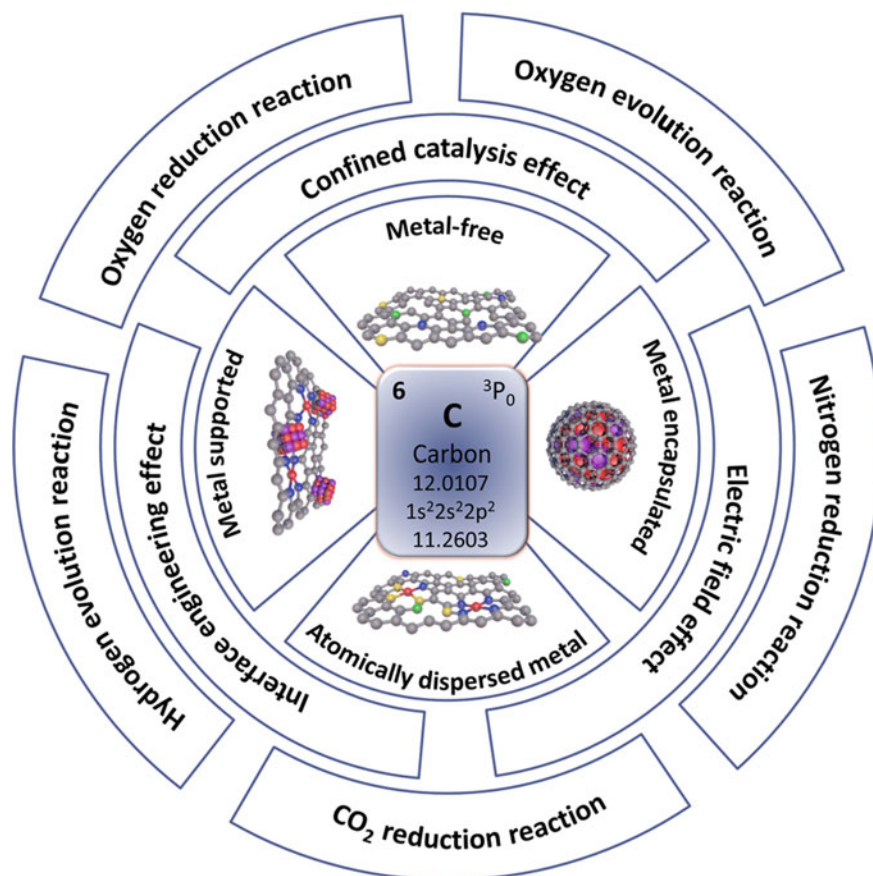


Fig. 1.2 Illustration of carbon-based nanomaterials for electrochemical catalysis

increasing attention due to their unique characteristics [77, 79, 80]. However, all these EES devices are facing the defects of low energy density and need to be recharged frequently, so it is crucial to develop a lightweight, large volume EES device that can be recharged quickly and has a long life, which has become an inevitable trend for future development [77]. Therefore, the development of suitable battery electrode materials to limit their energy density and specific density is essential for the development of EES devices. CNMs exhibit high electrical conductivity, high specific surface area, and good stability with low volume expansion during charging and discharging. The high conductivity facilitates charge transfer, and the high specific surface area provides a channel for the diffusion of electrolytes and oxygen. The adjustable pore structure with a high specific surface area enables rapid diffusion and charge transfer of electrolyte, which is conducive to rapid charging and discharging (Fig. 1.3) [81, 82]. These properties of carbon materials make them show great potential in the EES field.

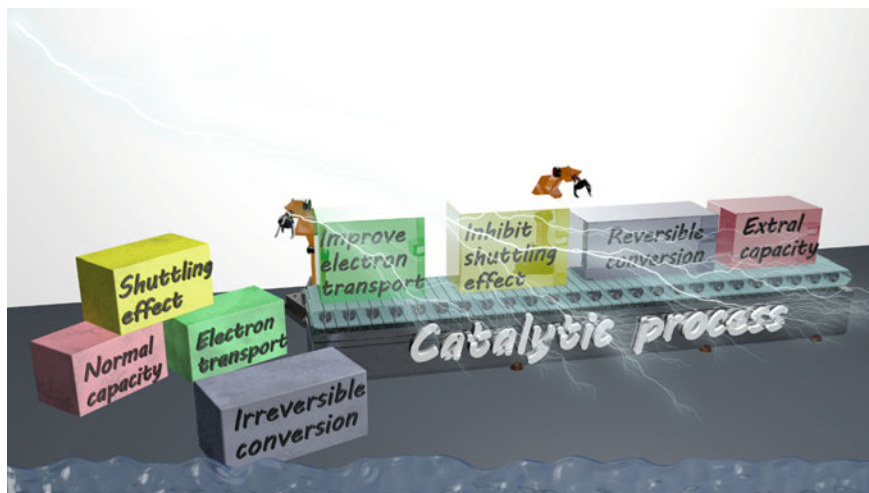


Fig. 1.3 Challenges and perspectives of catalytic processes for energy storage devices

In this chapter, first of all, according to the current environment and energy development status, we propose that an electrochemical-based energy conversion and storage system is one of the cleanest and renewable ways to alleviate energy and environmental problems. Secondly, based on the application of electrochemical energy conversion and storage, we propose that the key to these applications is the catalyst and electrode materials. Among the catalytic materials, carbon-based nanomaterials have been widely studied in energy conversion and storage applications due to their rich sources, low price, large specific surface area, adjustable morphology, and electronic structure. Finally, we propose that this book will comprehensively and deeply reveal the regulation rules and catalytic mechanism of carbon-based catalyst surface and interface defect structures by combining the current synthesis design principles of carbon-based nanomaterials and advanced characterization techniques, hoping to help scientific researchers, especially new researchers, quickly get in touch with cutting-edge science.

This book aims to systematically summarize the advanced development of carbon-based nanomaterials for electrochemical catalysis. It is our sincere hope that this book will provide researchers with further knowledge about carbon-based nanomaterials and that researchers interested in carbon-based nanomaterials will explore new ideas or answers in this book, which is the real meaning of this book. We also hope that new researchers will develop a stronger scientific interest through the interpretation of this book. We apologize to the authors of many outstanding research papers that we have missed due to the large amount of literature produced in this field over time.

References

1. R.P. Andres, R.S. Averback, W.L. Brown, L.E. Brus, W.A. Goddard, A. Kaldor, S.G. Louie, M. Moscovits, P.S. Peercy, S.J. Riley, R.W. Siegel, F. Spaepen, Y. Wang, Research opportunities on clusters and cluster-assembled materials—A department of energy, council on materials science panel report. *J. Mater. Res.* **4**, 704–736 (2011). <https://doi.org/10.1557/jmr.1989.0704>
2. P. Moriarty, Nanostructured materials. *Rep. Prog. Phys.* **64**, 297–381 (2001). <https://doi.org/10.1088/0034-4885/64/3/201>
3. R.F. Curl, R.E. Smalley, Probing C₆₀. *Science* **242**, 1017–1022 (1988). <https://doi.org/10.1126/science.242.4881.1017>
4. W. Krätschmer, L.D. Lamb, K. Fostiropoulos, D.R. Huffman, Solid C₆₀: A new form of carbon. *Nature* **347**, 354–358 (1990). <https://doi.org/10.1038/347354a0>
5. H. Gleiter, Nanostructured materials: Basic concepts and microstructure. *Acta Mater.* **48**, 1–29 (2000). [https://doi.org/10.1016/s1359-6454\(99\)00285-2](https://doi.org/10.1016/s1359-6454(99)00285-2)
6. A.S. Dahlan, Smart and functional materials based nanomaterials in construction styles in nano-architecture. *SILICON* **11**, 1949–1953 (2019). <https://doi.org/10.1007/s12633-018-0015-x>
7. Gkika DA, Vordos N, Nolan JW, Mitropoulos AC, Vansant EF, Cool P, Braet J (2017) Price tag in nanomaterials?. *J. Nanopart. Res.* **19**. <https://doi.org/10.1007/s11051-017-3875-x>
8. P. Kumar, Ultrathin 2D nanomaterials for electromagnetic interference shielding. *Adv. Mater. Interfaces* **6**, 1901454 (2019). <https://doi.org/10.1002/admi.201901454>
9. S. Muhammad, M. Nakano, A.G. Al-Sehemi, Y. Kitagawa, A. Irfan, A.R. Chaudhry, R. Kishi, S. Ito, K. Yoneda, K. Fukuda, Role of a singlet diradical character in carbon nanomaterials: A novel hot spot for efficient nonlinear optical materials. *Nanoscale* **8**, 17998–18020 (2016). <https://doi.org/10.1039/c6nr06097h>
10. P. Qu, M. Zhang, K. Fan, Z. Guo, Microporous modified atmosphere packaging to extend shelf life of fresh foods: A review. *Crit. Rev. Food Sci. Nutr.* **62**, 51–65 (2022). <https://doi.org/10.1080/10408398.2020.1811635>
11. S. Erker, R. Stangl, G. Stoeglehner, Resilience in the light of energy crises—Part I: A framework to conceptualise regional energy resilience. *J. Clean. Prod.* **164**, 420–433 (2017). <https://doi.org/10.1016/j.jclepro.2017.06.163>
12. H.J. Smith, The PACE of clean energy development. *Science* **355**, 921–922 (2017). <https://doi.org/10.1126/science.355.6328.921-c>
13. A. Bailey, L. Andrews, A. Khot, L. Rubin, J. Young, T.D. Allston, G.A. Takacs, Hydrogen storage experiments for an undergraduate laboratory course—clean energy: Hydrogen/fuel cells. *J. Chem. Educ.* **92**, 688–692 (2014). <https://doi.org/10.1021/ed5006294>
14. H.-F. Wang, Q. Xu, Materials design for rechargeable metal-air batteries. *Matter* **1**, 565–595 (2019). <https://doi.org/10.1016/j.matt.2019.05.008>
15. J. Zhang, Q. Zhang, X. Feng, Support and interface effects in water-splitting electrocatalysts. *Adv. Mater.* **31**, 1808167 (2019). <https://doi.org/10.1002/adma.201808167>
16. M. de Jesus Gálvez-Vázquez, P. Moreno-García, H. Xu, Y. Hou, H. Hu, I.Z. Montiel, A.V. Rudnev, S. Alinejad, V. Grozovski, B.J. Wiley, M. Arenz, P. Broekmann, Environment matters: CO₂RR electrocatalyst performance testing in a gas-fed zero-gap electrolyzer. *ACS Catal.* **10**, 13096–13108 (2020). <https://doi.org/10.1021/acscatal.0c03609>
17. H. Tong, S. Ouyang, Y. Bi, N. Umezawa, M. Oshikiri, J. Ye, Nano-photocatalytic materials: Possibilities and challenges. *Adv. Mater.* **24**, 229–251 (2012). <https://doi.org/10.1002/adma.201102752>
18. Q. Zhang, E. Uchaker, S.L. Candelaria, G. Cao, Nanomaterials for energy conversion and storage. *Chem. Soc. Rev.* **42**, 3127–3171 (2013). <https://doi.org/10.1039/c3cs00009e>
19. D. Xue, H. Xia, W. Yan, J. Zhang, S. Mu, Defect engineering on carbon-based catalysts for electrocatalytic CO₂ reduction. *Nano-Micro Lett.* **13**, 5 (2020). <https://doi.org/10.1007/s40820-020-00538-7>
20. N. Choudhary, S. Hwang, W. Choi, Carbon nanomaterials: A review, in *Handbook of nano-materials properties*. ed. by B. Bhushan, D. Luo, S.R. Schriker, W. Sigmund, S. Zauscher (Springer, Berlin Heidelberg, Berlin, 2014), pp. 709–769

21. F. Ghaemi, M. Ali, R. Yunus, R.N. Othman, Synthesis of carbon nanomaterials using catalytic chemical vapor deposition technique, in *Synthesis, technology and applications of carbon nanomaterials*, eds. by S.A. Rashid, R.N.I. Raja Othman, M.Z. Hussein (Elsevier, 2019), pp. 1–27
22. A.D. Goswami, D.H. Trivedi, N.L. Jadhav, D.V. Pinjari, Sustainable and green synthesis of carbon nanomaterials: A review. *J. Environ. Chem. Eng.* **9**, 106118 (2021). <https://doi.org/10.1016/j.jece.2021.106118>
23. S. Kumar, G. Saeed, L. Zhu, K.N. Hui, N.H. Kim, J.H. Lee, 0D to 3D carbon-based networks combined with pseudocapacitive electrode material for high energy density supercapacitor: A review. *Chem. Eng. J.* **403**, 126352 (2021). <https://doi.org/10.1016/j.cej.2020.126352>
24. K.P. Gopinath, D.-V.N. Vo, D. Gnana Prakash, A. Adithya Joseph, S. Viswanathan, J. Arun, Environmental applications of carbon-based materials: A review. *Environ. Chem. Lett.* **19**, 557–582 (2020). <https://doi.org/10.1007/s10311-020-01084-9>
25. J. Ni, Y. Li, Carbon nanomaterials in different dimensions for electrochemical energy storage. *Adv. Energy Mater.* **6**, 1600278 (2016). <https://doi.org/10.1002/aenm.201600278>
26. S. Peng, L. Li, J. Kong Yoong Lee, L. Tian, M. Srinivasan, S. Adams, S. Ramakrishna, Electrospun carbon nanofibers and their hybrid composites as advanced materials for energy conversion and storage. *Nano Energy* **22**, 361–395 (2016). <https://doi.org/10.1016/j.nanoen.2016.02.001>
27. D. Jariwala, V.K. Sangwan, L.J. Lauhon, T.J. Marks, M.C. Hersam, Carbon nanomaterials for electronics, optoelectronics, photovoltaics, and sensing. *Chem. Soc. Rev.* **42**, 2824–2860 (2013). <https://doi.org/10.1039/c2cs35335k>
28. H. Yi, D. Huang, L. Qin, G. Zeng, C. Lai, M. Cheng, S. Ye, B. Song, X. Ren, X. Guo, Selective prepared carbon nanomaterials for advanced photocatalytic application in environmental pollutant treatment and hydrogen production. *Appl. Catal. B* **239**, 408–424 (2018). <https://doi.org/10.1016/j.apcatb.2018.07.068>
29. T. Xu, W. Shen, W. Huang, X. Lu, Fullerene micro/nanostructures: Controlled synthesis and energy applications. *Mat. Today Nano* **11**, 100081 (2020). <https://doi.org/10.1016/j.mtnano.2020.100081>
30. H.W. Kroto, J.R. Heath, S.C. O'Brien, R.F. Curl, R.E. Smalley, C₆₀: Buckminsterfullerene. *Nature* **318**, 162–163 (1985). <https://doi.org/10.1038/318162a0>
31. Z. Jiang, Y. Zhao, X. Lu, J. Xie, Fullerenes for rechargeable battery applications: Recent developments and future perspectives. *J. Energy Chem.* **55**, 70–79 (2021). <https://doi.org/10.1016/j.jechem.2020.06.065>
32. M. Chen, R. Guan, S. Yang, Hybrids of fullerenes and 2D nanomaterials. *Adv. Sci.* **6**, 1800941 (2019). <https://doi.org/10.1002/advs.201800941>
33. C. Shan, H.-J. Yen, K. Wu, Q. Lin, M. Zhou, X. Guo, D. Wu, H. Zhang, G. Wu, H.-L. Wang, Functionalized fullerenes for highly efficient lithium ion storage: Structure-property-performance correlation with energy implications. *Nano Energy* **40**, 327–335 (2017). <https://doi.org/10.1016/j.nanoen.2017.08.033>
34. J. Restivo, O.S. Gonçalves Pinto Soares, M.F. Ribeiro Pereira, Processing methods used in the fabrication of macrostructures containing 1D carbon nanomaterials for catalysis. *Processes* **8**, (2020). <https://doi.org/10.3390/pr8111329>
35. S.S. Mahmood, A.J. Atiya, F.H. Abdulrazzak, A.F. Alkaim, F.H. Hussein, A review on applications of carbon nanotubes (CNTs) in solar cells. *J. Med. Chem. Sci.* **4**, 225–229 (2021). <https://doi.org/10.26655/jmchemsci.2021.3.2>
36. S. Iijima, Helical microtubules of graphitic carbon. *Nature* **354**, 56–58 (1991). <https://doi.org/10.1038/354056a0>
37. R.K. Thines, N.M. Mubarak, S. Nizamuddin, J.N. Sahu, E.C. Abdullah, P. Ganesan, Application potential of carbon nanomaterials in water and wastewater treatment: A review. *J. Taiwan Inst. Chem. Eng.* **72**, 116–133 (2017). <https://doi.org/10.1016/j.jtice.2017.01.018>
38. Q. Wu, L. Yang, X. Wang, Z. Hu, From carbon-based nanotubes to nanocages for advanced energy conversion and storage. *Acc. Chem. Res.* **50**, 435–444 (2017). <https://doi.org/10.1021/acs.accounts.6b00541>

39. K.S. Novoselov, A.K. Geim, S.V. Morozov, D. Jiang, Y. Zhang, S.V. Dubonos, I.V. Grigorieva, A.A. Firsov, Electric field effect in atomically thin carbon films. *Science* **306**, 666–669 (2004). <https://doi.org/10.1126/science.1102896>
40. N.G. Sahoo, Y. Pan, L. Li, S.H. Chan, Graphene-based materials for energy conversion. *Adv. Mater.* **24**, 4203–4210 (2012). <https://doi.org/10.1002/adma.201104971>
41. Y. Wang, P. Yang, L. Zheng, X. Shi, H. Zheng, Carbon nanomaterials with sp² or/and sp hybridization in energy conversion and storage applications: A review. *Energy Storage Mater.* **26**, 349–370 (2020). <https://doi.org/10.1016/j.ensm.2019.11.006>
42. S. Stankovich, D.A. Dikin, G.H. Dommett, K.M. Kohlhaas, E.J. Zimney, E.A. Stach, R.D. Piner, S.T. Nguyen, R.S. Ruoff, Graphene-based composite materials. *Nature* **442**, 282–286 (2006). <https://doi.org/10.1038/nature04969>
43. F. Schedin, A.K. Geim, S.V. Morozov, E.W. Hill, P. Blake, M.I. Katsnelson, K.S. Novoselov, Detection of individual gas molecules adsorbed on graphene. *Nat. Mater.* **6**, 652–655 (2007). <https://doi.org/10.1038/nmat1967>
44. A. Ali, P.K. Shen, Nonprecious metal’s graphene-supported electrocatalysts for hydrogen evolution reaction: Fundamentals to applications. *Carbon Energy* **2**, 99–121 (2019). <https://doi.org/10.1002/cey2.26>
45. X. Li, X. Yang, J. Zhang, Y. Huang, B. Liu, In situ/operando techniques for characterization of single-atom catalysts. *ACS Catal.* **9**, 2521–2531 (2019). <https://doi.org/10.1021/acscatal.8b04937>
46. K. Gong, F. Du, Z. Xia, M. Durstock, L. Dai, Nitrogen-doped carbon nanotube arrays with high electrocatalytic activity for oxygen reduction. *Science* **323**, 760–764 (2009). <https://doi.org/10.1126/science.1168049>
47. S. Zhao, D.W. Wang, R. Amal, L. Dai, Carbon-based metal-free catalysts for key reactions involved in energy conversion and storage. *Adv. Mater.* **31**, 1801526 (2019). <https://doi.org/10.1002/adma.201801526>
48. W. Chen, M. Wan, Q. Liu, X. Xiong, F. Yu, Y. Huang, Heteroatom-doped carbon materials: Synthesis, mechanism, and application for sodium-ion batteries. *Small Methods* **3**, 1800323 (2018). <https://doi.org/10.1002/smt.201800323>
49. T. Asefa, X. Huang, Heteroatom-doped carbon materials for electrocatalysis. *Chemistry* **23**, 10703–10713 (2017). <https://doi.org/10.1002/chem.201700439>
50. X. Wang, A. Vasileff, Y. Jiao, Y. Zheng, S.Z. Qiao, Electronic and structural engineering of carbon-based metal-free electrocatalysts for water splitting. *Adv. Mater.* **31**, 1803625 (2019). <https://doi.org/10.1002/adma.201803625>
51. W. Zhou, J. Jia, J. Lu, L. Yang, D. Hou, G. Li, S. Chen, Recent developments of carbon-based electrocatalysts for hydrogen evolution reaction. *Nano Energy* **28**, 29–43 (2016). <https://doi.org/10.1016/j.nanoen.2016.08.027>
52. L. Tao, Y. Wang, Y. Zou, N. Zhang, Y. Zhang, Y. Wu, Y. Wang, R. Chen, S. Wang, Charge transfer modulated activity of carbon-based electrocatalysts. *Adv. Energy Mater.* **10**, 1901227 (2019). <https://doi.org/10.1002/aenm.201901227>
53. A. Ferre-Vilaplana, E. Herrero, Charge transfer, bonding conditioning and solvation effect in the activation of the oxygen reduction reaction on unclustered graphitic-nitrogen-doped graphene. *Phys. Chem. Chem. Phys.* **17**, 16238–16242 (2015). <https://doi.org/10.1039/c5cp00918a>
54. J. Yang, W. Li, D. Wang, Y. Li, Electronic metal-support interaction of single-atom catalysts and applications in electrocatalysis. *Adv. Mater.* **32**, 2003300 (2020). <https://doi.org/10.1002/adma.202003300>
55. A. Beck, X. Huang, L. Artiglia, M. Zabilskiy, X. Wang, P. Rzepka, D. Palagin, M.G. Willinger, J.A. van Bokhoven, The dynamics of overlayer formation on catalyst nanoparticles and strong metal-support interaction. *Nat. Commun.* **11**, 3220 (2020). <https://doi.org/10.1038/s41467-020-17070-2>
56. B. Qiao, A. Wang, X. Yang, L.F. Allard, Z. Jiang, Y. Cui, J. Liu, J. Li, T. Zhang, Single-atom catalysis of CO oxidation using Pt₁/FeO_x. *Nat. Chem.* **3**, 634–641 (2011). <https://doi.org/10.1038/nchem.1095>

57. M.B. Gawande, P. Fornasiero, R. Zbořil, Carbon-based single-atom catalysts for advanced applications. *ACS Catal.* **10**, 2231–2259 (2020). <https://doi.org/10.1021/acscatal.9b04217>
58. Y. Peng, B. Lu, S. Chen, Carbon-supported single atom catalysts for electrochemical energy conversion and storage. *Adv. Mater.* **30**, e1801995 (2018). <https://doi.org/10.1002/adma.201801995>
59. B. Wu, Y. Kuang, X. Zhang, J. Chen, Noble metal nanoparticles/carbon nanotubes nanohybrids: Synthesis and applications. *Nano Today* **6**, 75–90 (2011). <https://doi.org/10.1016/j.nantod.2010.12.008>
60. R. Narayanan, M.A. El-Sayed, Catalysis with transition metal nanoparticles in colloidal solution: Nanoparticle shape dependence and stability. *J. Phys. Chem. B* **109**, 12663–12676 (2005). <https://doi.org/10.1021/jp051066p>
61. C. Gao, F. Lyu, Y. Yin, Encapsulated metal nanoparticles for catalysis. *Chem. Rev.* **121**, 834–881 (2021). <https://doi.org/10.1021/acs.chemrev.0c00237>
62. N. Wang, Q. Sun, J. Yu, Ultrasmall metal nanoparticles confined within crystalline nanoporous materials: A fascinating class of nanocatalysts. *Adv. Mater.* **31**, 1803966 (2019). <https://doi.org/10.1002/adma.201803966>
63. Q.-L. Zhu, Q. Xu, Immobilization of ultrafine metal nanoparticles to high-surface-area materials and their catalytic applications. *Chem* **1**, 220–245 (2016). <https://doi.org/10.1016/j.chemmpr.2016.07.005>
64. J.M. Planeix, N. Coustel, B. Coq, V. Brotons, P.S. Kumbhar, R. Dutartre, P. Geneste, P. Bernier, P.M. Ajayan, Application of carbon nanotubes as supports in heterogeneous catalysis. *J. Am. Chem. Soc.* **116**, 7935–7936 (2002). <https://doi.org/10.1021/ja00096a076>
65. X. Yan, Y. Jia, X. Yao, Defects on carbons for electrocatalytic oxygen reduction. *Chem. Soc. Rev.* **47**, 7628–7658 (2018). <https://doi.org/10.1039/c7cs00690j>
66. J. Lu, S. Yin, P.K. Shen, Carbon-encapsulated electrocatalysts for the hydrogen evolution reaction. *Electrochem Energy Rev* **2**, 105–127 (2018). <https://doi.org/10.1007/s41918-018-0025-9>
67. N. Rao, R. Singh, L. Bashambu, Carbon-based nanomaterials: Synthesis and prospective applications. *Mater. Today Proc.* **44**, 608–614 (2021). <https://doi.org/10.1016/j.matpr.2020.10.593>
68. Y. Zhang, M. Luo, Y. Yang, Y. Li, S. Guo, Advanced multifunctional electrocatalysts for energy conversion. *ACS Energy Lett.* **4**, 1672–1680 (2019). <https://doi.org/10.1021/acsenergylett.9b01045>
69. Z.P. Cano, D. Banham, S. Ye, A. Hintennach, J. Lu, M. Fowler, Z. Chen, Batteries and fuel cells for emerging electric vehicle markets. *Nat. Energy* **3**, 279–289 (2018). <https://doi.org/10.1038/s41560-018-0108-1>
70. H. Yin, H. Xia, S. Zhao, K. Li, J. Zhang, S. Mu, Atomic level dispersed metal–nitrogen–carbon catalyst toward oxygen reduction reaction: Synthesis strategies and chemical environmental regulation. *Energy Environ. Mater.* **4**, 5–18 (2020). <https://doi.org/10.1002/eem2.12085>
71. Y. Qiao, P. Yuan, Y. Hu, J. Zhang, S. Mu, J. Zhou, H. Li, H. Xia, J. He, Q. Xu, Sulfuration of an Fe–N–C catalyst containing Fe_xC/Fe species to enhance the catalysis of oxygen reduction in acidic media and for use in flexible Zn–air batteries. *Adv. Mater.* **30**, 1804504 (2018). <https://doi.org/10.1002/adma.201804504>
72. W. Tong, B. Huang, P. Wang, L. Li, Q. Shao, X. Huang, Crystal-phase-engineered PdCu electrocatalyst for enhanced ammonia synthesis. *Angew. Chem. Int. Ed.* **59**, 2649–2653 (2020). <https://doi.org/10.1002/anie.201913122>
73. Y. Guo, P. Yuan, J. Zhang, H. Xia, F. Cheng, M. Zhou, J. Li, Y. Qiao, S. Mu, Q. Xu, Co₂P–CoN double active centers confined in N-doped carbon nanotube: Heterostructural engineering for trifunctional catalysis toward HER, ORR, OER, and Zn–air batteries driven water splitting. *Adv. Func. Mater.* **28**, 1805641 (2018). <https://doi.org/10.1002/adfm.201805641>
74. Y. Guo, P. Yuan, J. Zhang, Y. Hu, I.S. Aminu, X. Wang, J. Zhou, H. Xia, Z. Song, Q. Xu, S. Mu, Carbon nanosheets containing discrete Co–N_x–B_y–C active sites for efficient oxygen electrocatalysis and rechargeable Zn–air batteries. *ACS Nano* **12**, 1894–1901 (2018). <https://doi.org/10.1021/acsnano.7b08721>

75. X. Xue, J. Zhang, I.A. Saana, J. Sun, Q. Xu, S. Mu, Rational inert-basal-plane activating design of ultrathin 1T' phase MoS₂ with a MoO₃ heterostructure for enhancing hydrogen evolution performances. *Nanoscale* **10**, 16531–16538 (2018). <https://doi.org/10.1039/c8nr05270k>
76. K. Shen, X. Chen, J. Chen, Y. Li, Development of MOF-derived carbon-based nanomaterials for efficient catalysis. *ACS Catal.* **6**, 5887–5903 (2016). <https://doi.org/10.1021/acscatal.6b01222>
77. C. Zhang, W. Lv, Y. Tao, Q.-H. Yang, Towards superior volumetric performance: Design and preparation of novel carbon materials for energy storage. *Energy Environ. Sci.* **8**, 1390–1403 (2015). <https://doi.org/10.1039/c5ee00389j>
78. M.S. Dresselhaus, I.L. Thomas, Alternative energy technologies. *Nature* **414**, 332–337 (2001). <https://doi.org/10.1038/35104599>
79. H. Xia, G. Qu, H. Yin, J. Zhang, Atomically dispersed metal active centers as a chemically tunable platform for energy storage devices. *J. Mater. Chem. A* **8**, 15358–15372 (2020). <https://doi.org/10.1039/d0ta04019c>
80. K. Guo, G. Qu, J. Li, H. Xia, W. Yan, J. Fu, P. Yuan, J. Zhang, Polysulfides shuttling remedies by interface-catalytic effect of Mn₃O₄-MnP_x heterostructure. *Energy Storage Mater.* **36**, 496–503 (2021). <https://doi.org/10.1016/j.ensm.2021.01.021>
81. Y. Pan, K. Xu, C. Wu, Recent progress in supercapacitors based on the advanced carbon electrodes. *Nanotechnol. Rev.* **8**, 299–314 (2019). <https://doi.org/10.1515/ntrev-2019-0029>
82. X. Wang, L. Liu, Z. Niu, Carbon-based materials for lithium-ion capacitors. *Mater. Chem. Frontiers* **3**, 1265–1279 (2019). <https://doi.org/10.1039/c9qm00062c>

Chapter 2

Synthesis of Carbon-Based Nanomaterials



Yu Du, Su Jiang, Yuan Li, and Jia-Nan Zhang

Abstract Carbon-based catalytic materials have the advantage of structural stability, adjustable morphology, and high tolerance to acid/alkaline media, for which they have always been a research hotspot in the field of catalysis. However, the original carbon material is inert to electrochemical reactions, so the activation and enhancement of its catalytic performance is very important. In addition to improving the carbon materials themselves, more and more researchers are devoted to promoting the development of metal carbon-based catalysts. Recently, based on the relationship between structure and performance, synthetic strategies such as defect engineering, surface engineering, and confinement effects have been proposed to modify and rationally design the morphology and structure of carbon-based nanomaterials. At the same time, with the continuous in-depth understanding of the catalytic mechanism, the carbon-based materials are doped with metal atoms, doped with heteroatoms, metal particles and hybrids are loaded, in order to obtain more excellent catalytic performance is feasible. In this chapter, the synthesis of carbon-based catalytic nanomaterials with different catalytic sites is firstly summarized. Based on the synthesis strategies and methods proposed in recent years as well as the understanding of the catalytic mechanism of the catalytic active center, the composition and the modified rational design of carbon-based catalysts have also reviewed. Hope it would provide reference and guidance for the application of carbon-based nanomaterials in the field of energy conversion.

Y. Du · S. Jiang · Y. Li · J.-N. Zhang (✉)
College of Materials Science and Engineering, Zhengzhou University, Zhengzhou 450001,
P. R. China
e-mail: zjn@zzu.edu.cn

Y. Du
e-mail: aiyegreen@163.com

S. Jiang
e-mail: jiangszzu@163.com

2.1 Introduction

According to the demand for an ideal catalyst with high performance, various structures, and compositions of the catalyst can have been numerous researched. Carbon-based nanomaterials have received extensive attention due to their multiple advantages, such as earth abundance, low cost, and high conductivity [1].

Many types of carbon nanomaterials, such as activated carbon, fullerene, carbon nanotube (CNT), graphene, diamond, and carbon nitride (C_3N_4), have been studied as chemical substances of potential catalysts due to their rich structure, electronic properties, and low cost [2]. Although they show great potential in the catalytic field, pure carbon is generally inert in chemistry. Therefore, adjusting the structure and electronic properties of pure carbon materials through physical or chemical modification to improve the catalytic activity of carbon nanomaterials is necessary [3].

Generally speaking, defect engineering and heteroatom doping are considered as effective strategies to modify the properties of metal-free carbon materials. Graphene, as typical carbon nanomaterials, often perform as active at defects and edges. Defect engineering is proposed to modify the structure and morphology of carbon materials by constructing inherent pores, edge sites, vacancies, etc. In 2009, Hiroto et al. [4] used density functional theory and direct molecular orbital-molecular dynamics (MO-MD) methods for the first time to clarify the effect of defects on the electronic state of graphene through evaluating normal graphene and defective graphene (one carbon atom was removed from the normal graphene), defective graphene anions (defective graphene plus an excess electron), and defective graphene cations (defective graphene plus one hole). In addition, Jia et al. [5] developed defective two-dimensional graphene by removing nitrogen from intentionally doped precursors, and introduced various types of graphene edges such as pentagons, heptagons, and octagons structural defects. Theoretical calculation results showed that edge defects can significantly improve the catalytic activity of oxygen reduction reaction (ORR), oxygen evolution reaction (OER), and hydrogen evolution reaction (HER). A series of characterizations have confirmed that the defect level of graphite was greatly increased after ball milling. Therefore, designing abundant defect sites in carbon-based materials has broad prospects in future research. In addition to defects, the formation of vacancies can also effectively tune the electronic structure of carbon-based catalysts and promote their electrochemical performance. For vacancies, especially the presence of oxygen vacancies, the band gap of the semiconductor can be effectively adjusted, and the distribution of electrons on the surface of the material can be changed. The carbon materials synthesized under the guidance of these strategies will make the carbon atoms at the defect as active sites exhibit better activity. However, the in-plane atoms of graphene show poor chemical activity when used as catalytic sites. Therefore, in order to trigger the activity of carbon atoms, it is feasible to introduce different heteroatoms such as O, N, B, S, P and their corresponding functional groups to enhance the activity of in-plane structures. In this way, the structure of carbon atoms around the electrons can be changed, which can promote the adsorption

of catalytic reaction intermediates, thereby improving the catalytic activity of carbon atoms. Studies have shown that the introduction of N atoms induces the redistribution of the charges between N atoms and adjacent C atoms, thereby obtaining excellent catalytic performance [6]. Since then, heteroatom-doped carbon materials have been intensively studied, and the types and doping methods of doped heteroatoms have also been continuously developed and studied [7].

In addition to the carbon material itself as catalyst material, due to its incredibly high surface area, excellent electrical conductivity, and chemical stability, carbon-based substrates as catalyst support attached to other active substances have also been extensively studied. The substrate material can firmly fix metal nanoparticles to prevent them from further agglomeration and improve catalytic activity [8]. This metal-support interaction has been the focus of researches on carbon-based material catalysts in recent years [9]. Based on this effect, a series of carbon-based metal catalyst are designed and synthesized, including metal nanoparticles supported carbon-based nanomaterials and atomically dispersed metal carbon-based nanomaterials. Previous reports indicated that the size and morphology of the metal particles and the surface structure of the substrate greatly affect the metal supporting structure, which has a great influence on promoting the catalytic reaction that occurs at the interface. Therefore, the rational design of the metal-support interface structure is very important. In addition, the intrinsic property of metal nanoparticles or their hybrids and the interaction between metals are also critical to catalytic performance. The factors mentioned above all need to be considered clearly when designing and synthesizing such catalysts.

Substrates such as carbon materials not only provide anchor points for single metal atoms, but also change the charge density and electronic structure of metal atoms due to the strong interfacial interaction between metal atoms and adjacent carbon atoms. When the size of the nanoparticle is reduced to the single-atom level, the metal-support interaction will be maximized, resulting in the generation of new catalytically active sites, new reaction pathways, and ultimately improved catalytic performance [10]. In this case, metal atoms are often regarded as catalytically active centers. Therefore, for the synthesis of atomically dispersed metal carbon-based nanomaterials, researchers not only pay attention to the selection of metal atoms, but also lay emphasis on the regulation of the microenvironment of metal atoms [11]. Choosing an appropriate central metal atom is the most direct and effective strategy for synthesizing high-activity atom-dispersed metal carbon-based catalysts [12]. For the case where multiple metal atoms are loaded, the mutual influence and synergy between different metal atoms are also one of the research hotspots [13, 14]. When the active metal center is definite, the doping of heteroatoms is a common effective method to improve the activity of the catalytic active sites. Heteroatom doping of metal-loaded carbon-based materials can not only affect the electronic structure of the carbon material, but also anchor the metal center or adjust the charge density distribution and change its bond formation [15]. The doped heteroatoms usually form coordination with the metal center and/or carbon atoms [16]. Therefore, adjusting the type and structure of coordination atoms will effectively adjust the electronic structure of the metal-carbon site (especially the d electron of the central metal atom)

to obtain better electrocatalytic activity. In addition, the types of coordination atoms and the chemical environment can be adjusted. Therefore, the study of heteroatom doping here not only involves the doping of monometallic, bimetallic, and even multi-metal materials, but also includes the effect of co-doping of different heteroatoms [17].

As mentioned above, particle size, defects and heteroatom doping are important factors that affect the electrocatalytic activity of the catalyst. There are still huge challenges in the precise control of the active structure of carbon materials and the design and synthesis of a definite catalytic center structure. The existing synthesis methods, such as pyrolysis, wet chemical methods, physical and chemical deposition methods, ball milling, and graphene vacancies oriented synthesis have been extensively studied in the field of synthesizing heterogeneous catalyst [18]. With the in-depth understanding of the catalytic mechanism and the relationship between the structure and performance of the catalytic center, the research on synthesis methods has been continuously explored and developed. In this chapter, the design and synthesis strategies of several carbon-based catalysts from the perspective of structure–activity relationship according to different catalytic active sites have been summarized (Fig. 2.1). The synthesis strategies and development trends of carbon-based materials are also reviewed, hoping to provide methodological references for future research.

2.2 Synthesis of Metal-Free Carbon-Based Nanomaterials

Carbon nanomaterials have high reserves in nature, which are easily obtainable. Original carbon materials have structural stability, adjustable morphology, and show high tolerance to acid/alkaline media. Therefore, they have been regarded as potential candidates of catalytic materials used in energy conversion reactions. However, since the original carbon materials are inert to electrochemical reactions, the activation and enhancement of their catalytic performance is of great importance. In recent years, researchers have mainly started from two aspects to improve the performance of metal-free carbon-based materials. On the one hand, for the synthesis of intrinsic defect carbon, the introduction of defects will interfere with the electron symmetry of the active sites, so as to provide non-uniform components and catalytic active centers by adjusting the charge density and spin density of the carbon atoms. In fact, there are inherent defects in carbon materials, but their density is too low to obtain high electrocatalytic performance on a macroscopic scale. Therefore, the production of high-density uniform defects in carbon materials is the key to improving the catalytic performance of carbon-based materials through defect engineering strategies. On the other hand, the charge transfer that can also be induced by doping heteroatoms in the carbon material can effectively adjust the electronic characteristics of the carbon near the doping site, which can provide the carbon matrix with an optimized charge carrier concentration and create new active sites, which can further optimize

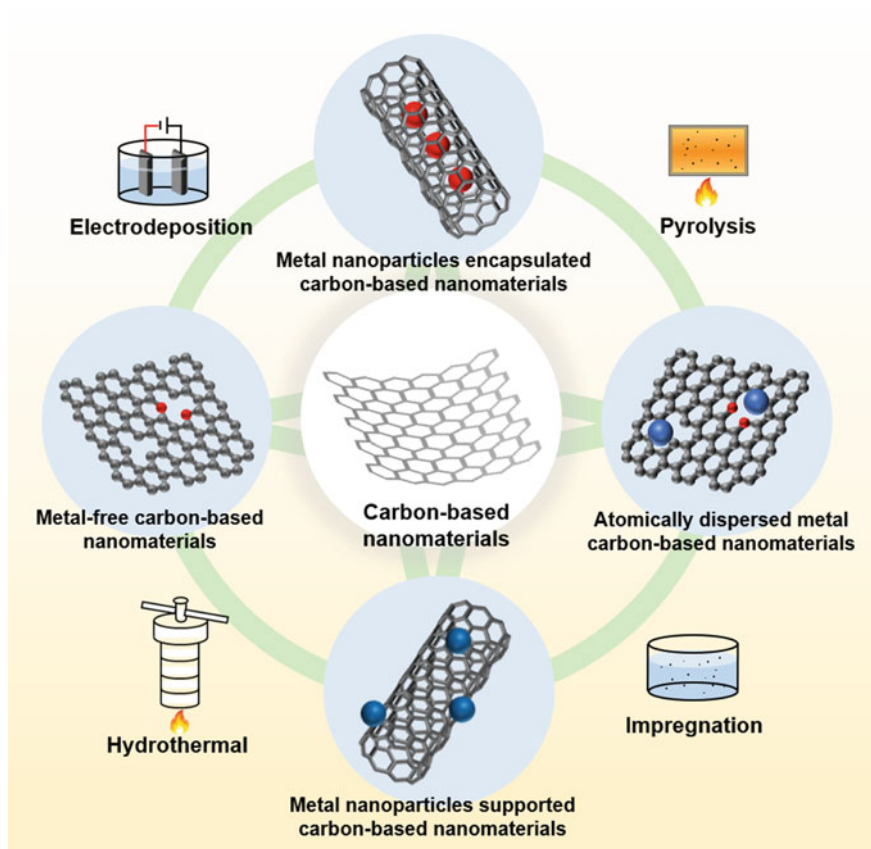


Fig. 2.1 Types of carbon-based nanomaterials and their synthesis methods

the performance of carbon nanomaterials in energy conversion by improving the electronic arrangement.

2.2.1 *Intrinsic Defect Carbon*

Defect engineering is an effective strategy to control the surface physical and chemical properties of catalytic materials. In recent years, plenty of efforts have been made to increase the defect density of carbon materials to increase the catalytically active sites of carbon materials. At the same time, researchers are constantly exploring the influence of different defect structures on catalytic performance. At present, the most studied carbon defect structures mainly include edge defects, surface defects, vacancy defects, and topological defects.

Edge sites versus basal plane defect. Constructing controllable defects with different structures and positions is a hot spot in defect engineering research. The exploration and comparison of defect types mainly focus on edge defects and internal defects. A large number of studies have shown that edge defects have a stronger ability to redistribute electrons, so they can provide more catalytic sites than defects inside the plane. The synthesis methods of edge defects mainly include edge engineering, [19, 20] electrochemical reduction-reoxidation, [21] ultrasonic-assisted liquid phase exfoliation, [22] molten salt-assisted acid exfoliation, [23] spontaneous gas foaming, [24] biomass synthesis, [25] etc. Wang et al. [19] developed a general edge engineering method to transform the corresponding specific nitrogen doping sites to produce carbon defect configurations. Three corresponding configurations were mainly synthesized, graphite-N with vacancies in place (C585), pyridine-N to separated pentagons (S-C5), and pyrrole-N to adjacent pentagons (A-C5). It shows good intrinsic activity in both oxygen reduction reaction (ORR) and hydrogen evolution reaction (HER). Among them, A-C5 has the highest ORR activity, and C585 has the highest HER activity. This work provides insights for the design of high-performance carbon-based catalysts based on the principle of defect formation (Fig. 2.2a). Yao et al. [5] reported the assembly of a two-dimensional graphene (DG) material with carbon defects, prepared from an N-doped precursor through a simple denitrification procedure. Experimental results show that the material has triple functions of ORR, OER, and HER, and its half-wave potential has good performance in the three reactions, and its activity is better than that of N-doped graphene. Zinc-air battery shows that DG has very stable charge and discharge voltage, high current and power density, comparable to Pt/C catalyst. This is the first reported three-function metal-free catalyst based on defect mechanism, which provides a new idea for the application of defect mechanism in electrocatalysts (Fig. 2.2b-e).

Vacancy/hole. As a kind of lattice defects, the introduction of vacancy defects can promote the electron conduction of carbon-based catalytic materials and improve the conductivity of carbon materials. According to research, vacancy defects can be obtained by fast flame method, [26] heteroatom doping, [27] thermally induced defects, [28] co-precipitation, [29] irradiation, [30] KOH activation [31] and other methods. Among them, oxygen holes supported by oxides are the focus of the study of vacancy defects. Zheng et al. [32] proposed a simple solution reduction method for the synthesis of mesoporous Co_3O_4 nanowires with high specific surface area. The oxygen vacancies on the surface of the reduced Co_3O_4 nanowires are greatly increased, and the current density and electrochemical supercapacitor capacitance are also increased. Density functional theory calculations show that the generation of oxygen vacancies leads to the formation of new energy gap states, in which the electrons originally associated with the Co-O bond tend to delocalize, resulting in higher conductivity and electrocatalytic activity (Fig. 2.3a-c). Hu et al. [33] reported a series of $\text{Co}_3\text{O}_4/\text{rGO}$ (reduced graphene oxide) nanocomposites with adjustable oxygen vacancy defect concentration, synthesized by simple alkali etching. The synergistic effect of the thermal assist effect of the reduced graphene oxide and the oxygen vacancy defect provides the composite material with excellent catalytic activity.

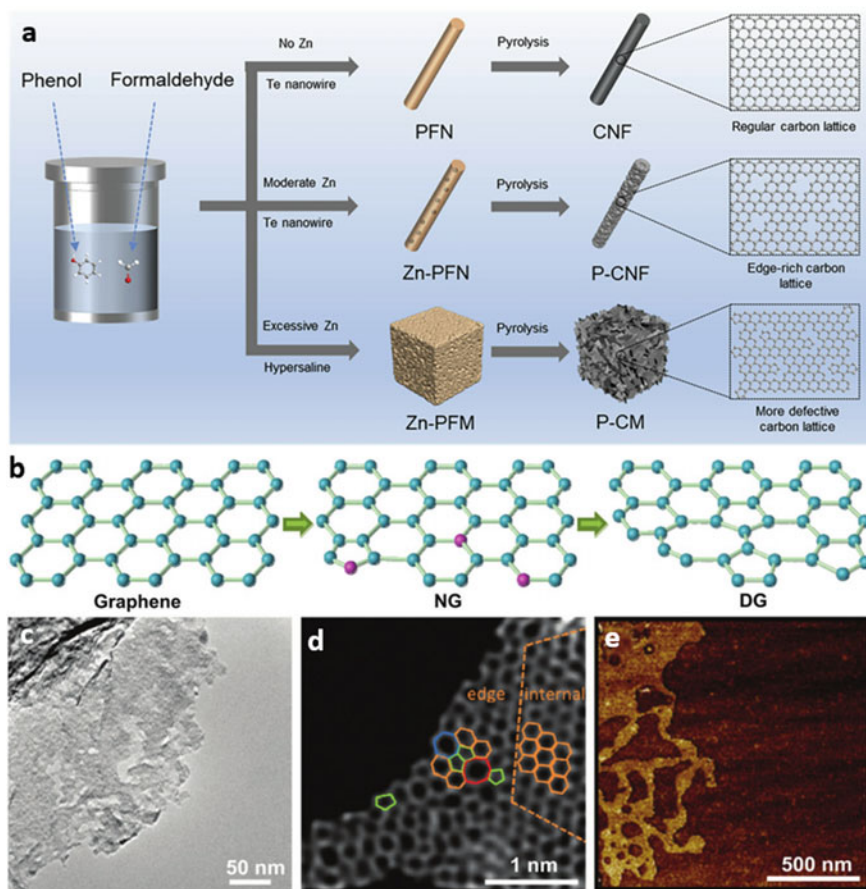


Fig. 2.2 Synthesis of carbon nanotubes with edge site and basal plane defects. **a** Schematic illustration of fabricating three types of carbon materials, edge-deficient carbon nanofibers (CNFs), edge-rich porous CNFs (P-CNFs), highly porous carbon monolith (P-CM). Reproduced with permission [19]. Copyright 2020, Elsevier. **b** The schematic of the formation of DG. **c** The TEM, **d** HAADF and **e** AFM image of DG. Hexagons, pentagons, heptagons, and octagons were labeled in orange, green, blue, and red, respectively. Reproduced with permission [5]. Copyright 2016, WILEY-VCH

Deng et al. [34] reported a molybdenum disulfide as a catalyst for the hydrogenation of carbon dioxide to methanol. Experiments have shown that the sulfur vacancies generated on the surface drive the selective hydrogenation of CO_2 to methanol. The catalyst has superior conversion efficiency and long-term stability, and is a strong candidate for industrial applications.

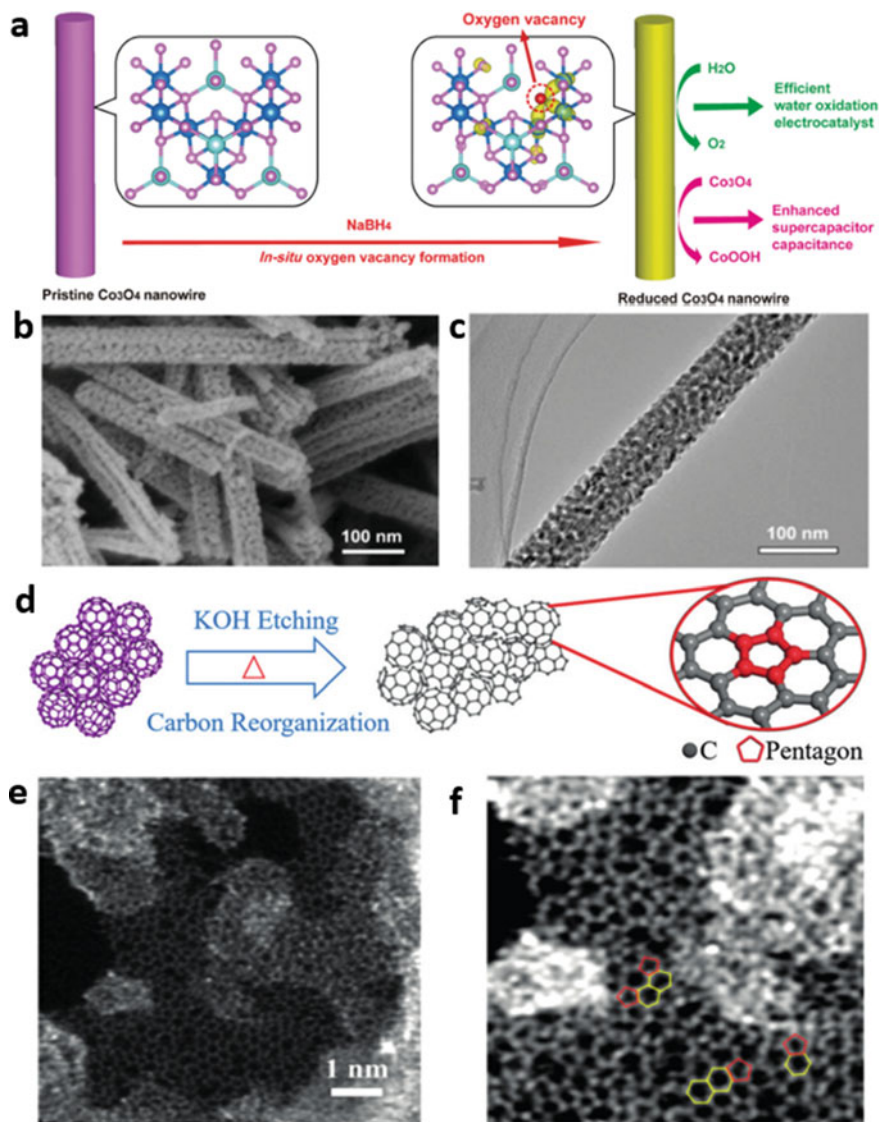


Fig. 2.3 Synthesis of topologically defective carbon nanomaterials. **a** Schematic of the NaBH_4 reduction for in situ creation of oxygen vacancies in Co_3O_4 NWs. **b** SEM and **c** TEM images of the reduced Co_3O_4 NWs. Reproduced with permission [32]. Copyright 2014, WILEY-VCH. **d** Illustration of the synthetic method of PD-C; **e** ac-STEM image of PD-C; **f** cropped image of (b). Reproduced with permission [40]. Copyright 2019, WILEY-VCH

Topological defect. Mismatches and/or missing atoms of lattice units often lead to in-plane topological defects in the framework of graphene-based carbon materials. They can significantly redistribute electrons on the surface of carbon materials and improve the electron transport capacity on the surface of carbon materials. Based on the above understanding, various methods have been demonstrated to successfully synthesize defective carbon materials with topological structures, such as direct carbonization, [35] doping evaporation, [36] surface coupling reaction, [37] synthesis of intramolecular defect formers [38] and low temperature thermal solution method [39]. However, due to the high formation energy, deliberately creating high-density uniform topological defects in the carbon network is still challenging. Mu et al. [40] constructed a carbon nanomaterial rich in pentagonal defects by in-situ etching of fullerene molecules (C₆₀). The experiment verified that the intrinsic pentagonal shape of the basal plane contributes to the local redistribution of electrons in the carbon matrix. And energy band gap contraction can improve electrochemical activity, which corresponds to the calculation result of density functional theory. It shows that the intrinsic pentagonal defects have far-reaching significance for the development of carbon-based nanomaterials in the field of energy storage and conversion (Fig. 2.3d–f).

2.2.2 *Heteroatom-Doped Carbon*

In addition to the effect of intrinsic defects on the catalyst, the doping of heteroatoms with different electronegativity (such as B, N, P, and F) into the carbon network can introduce asymmetric charges and redistribute the spin density. The electrical neutrality of the matrix optimizes the electrical properties of the carbon material and induces the generation of charged active sites. The three main methods for preparing heteroatom-doped carbon-based catalysts are pyrolysis, chemical vapor deposition (CVD) and solvothermal process. Pyrolysis is a synthetic material obtained by heating heteroatom precursors and matrix materials in a crucible within a certain temperature range. In the process of synthesizing heteroatom-doped carbon nanomaterials by CVD, the doping sites are formed mainly by the deposition of heteroatoms on the surface of carbon-based materials. The solvothermal method is a simple thermal reaction that achieves the successful introduction of heteroatoms through the synergistic interaction of polymers and ionic liquids as structure directing agents and carbon sources [41].

Nitrogen doping. The combination of electron-accepting nitrogen atoms and carbon materials can supply adjacent carbon atoms with a relatively high positive charge density. It is the earliest and most widely studied type of heteroatom doping in carbon materials. N-doped carbon materials are mostly synthesized by pyrolysis. Frequently selected nitrogen sources are urea, amine compounds, such as hexamethylenetetramine, 1,6-hexanediamine, etc. The main product of the pyrolysis of amines is the imine group, which is doped in the carbon source through a coupling

reaction [43]. After pyrolysis, urea mostly exists in the material in the form of pyridine nitrogen [44]. The introduction of nitrogen can form different structural sites on the surface of carbon materials, which can be studied as potential catalytic sites. And nitrogen doping in carbon-based nanomaterials also induces changes in electronic structure, thus providing more binding options for the introduction of other metals [43]. Yao et al. [42] synthesized a three-dimensional (3D) carbon aerogel with a novel N-S-C coordination active site constructed using N-modified S defects, where the active sites originated from the integrity of edge thiophene S, graphite N, and pentagonal defects. This catalyst exhibited excellent ORR activity, stability and high current density under acidic conditions. It provided new insights for the application of nano-carbon structural defects in carbon-based ORR catalysts (Fig. 2.4).

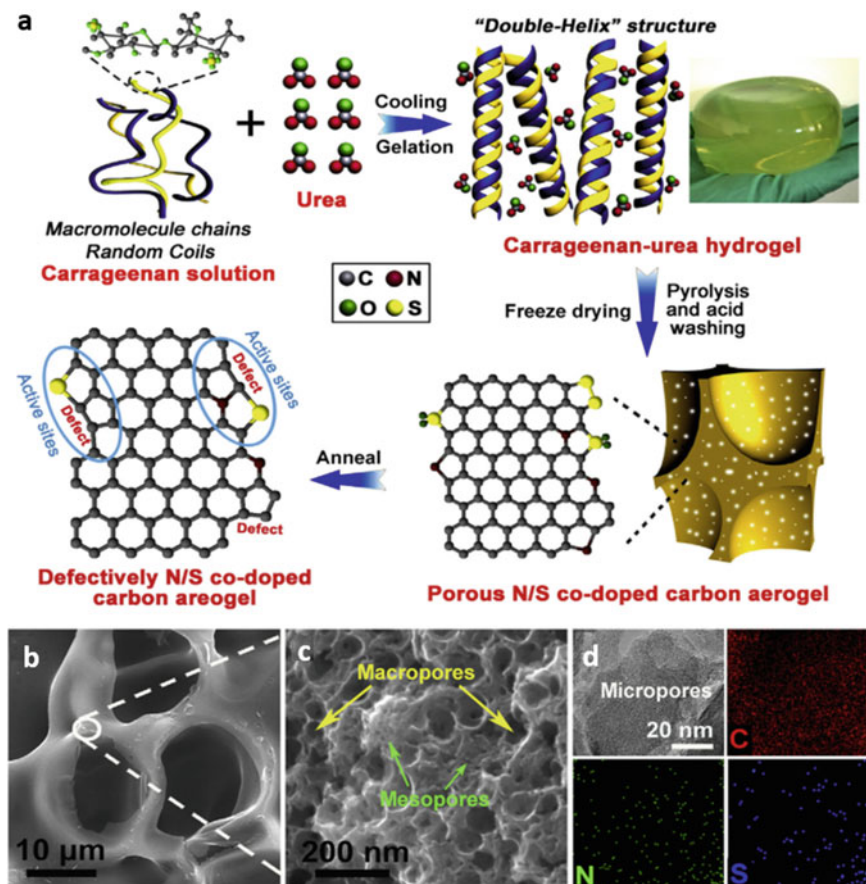


Fig. 2.4 Synthesis of N-doped carbon materials. **a** The Synthesis Process and Morphology of N-Modified S-Defect Carbon Aerogel. **b, c** Low-resolution and high-resolution FESEM images of NSCA-700-1000. **d** TEM image and the corresponding EDS mapping for C, N, and S elements of NSCA-700-1000. Reproduced with permission [42]. Copyright 2018, Elsevier

Boron doping. The B-C bond produced by introducing boron atoms into the carbon substrate can have a beneficial effect on the adsorption or fixation of gases or intermediates in the energy conversion reaction. The typical methods for boron doping include liquid-phase electrodeposition, [45] high-temperature annealing, [46] and one-pot solvent evaporation-induced self-assembly [47]. Mu et al. [14] developed a metal-free and controllable strategy to prepare B and Cl dual-doped CNTs (BCICNTs) by chemically tailoring two-dimensional (2D) boron carbide (B_4C) with Cl_2 . Among them, Cl_2 partially extracts B atoms in B_4C , and the remaining B and C atoms combine with Cl atoms to form a nanotube microstructure. Experimental results showed that as a metal-free ORR catalyst, it had a higher half-wave potential and stability than commercial Pt/C catalysts. And the doping configuration of B and Cl can be controlled by choosing different chlorine-carbide molar ratios (Fig. 2.5).

Phosphorus doping. Phosphorus atom doping can usually be combined with template method to prepare heteroatom-doped porous carbon-based catalytic materials, so as to obtain unique pore structure and large specific surface area while regulating the electronic structure of catalytic sites. The materials obtained by the template method are generally easier to obtain more regular nanoporous structures and suitable sizes. Yuan et al. [48] used F127 as the soft template, organic phosphoric acid as the P source, and phenolic resin as the C source to synthesize a P-doped mesoporous carbon material with good pore structure and high specific surface area. In the synthesis process, a small amount of iron was introduced as a catalyst to optimize the texture properties and graphitization degree of carbon materials. The experimental result showed that the synthesized material had excellent catalytic activity and durability for ORR, highlighting the possibility of its application in electrode materials and electronic nanodevices for metal-air batteries and fuel cells.

Sulfur doping. Similar to the effect of other heteroatom doping, sulfur atom doping can improve the surface reactivity of inert carbon materials, leading to the enrichment of surface charges and promoting the transfer of electrons during the reaction. Annealing and template methods can easily introduce sulfur atoms. Different pyrolysis temperatures will have different effects on the specific surface area, pore size and sulfur doping content of the material. Yang et al. [49] prepared S-doped graphene with high specific surface area. The synthesis method was to heat ultrathin graphene oxide-porous silica sheet through graphene oxide and guest gas H_2S under high temperature conditions. The study proved for the first time that sulfur can be doped into graphene flakes through the main form of thiophene-like S, which exhibited excellent electrocatalytic activity, long durability and high selectivity as an ORR catalyst.

Oxygen doping. Researchers usually dope carbon materials with oxygen atoms in the form of oxygen-containing functional groups. The introduction of oxygen-containing functional groups can improve the gas adsorption strength and the binding strength of intermediates during the catalytic reaction. At the same time, its electron-withdrawing ability can also rearrange the electrons of the surrounding carbon atoms.

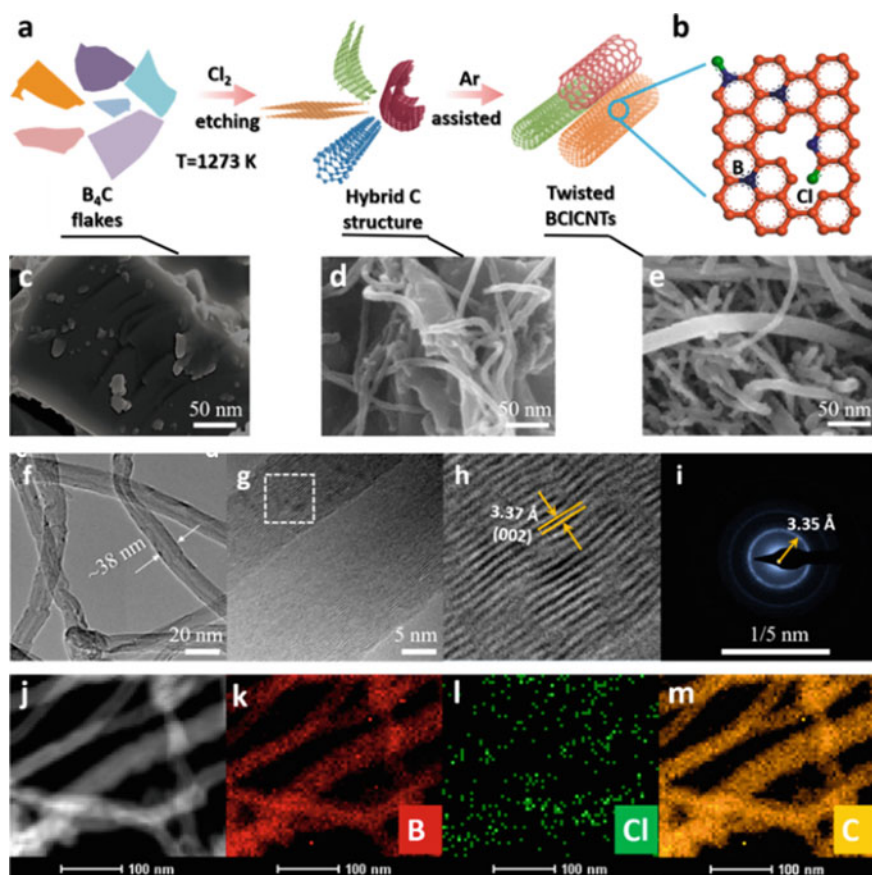


Fig. 2.5 Synthesis of B-doped carbon nanotubes. **a** Schematic illumination of one-step evolution from B₄C to BCICNTs. **b** Possible locations for B and Cl co-incorporation into CNTs. **c–e** SEM images of the pristine B₄C nanoflakes (**c**), transitional hybrid carbon structure (**d**), and the resultant BCICNTs **e**. Low-magnified and **f** high-magnified TEM **g** and its intercepted part **h** and SAED images **i** of the as-synthesized BCICNTs. **j** STEM-HAADF images of the typical BCICNTs. (**k–m**) HAADF intensity mapping: boron mapping **k**, chlorine mapping **l**, and carbon mapping (**m**). Reproduced with permission [14]. Copyright 2019, ACS Energy Letters

Simple pyrolytic synthesis methods and microwave-assisted synthesis are also applicable to oxygen-doped carbon-based materials [50]. Sun et al. [51] synthesized O-doped graphene derived from sodium gluconate using sodium gluconate argon annealing method as an excellent 2D NRR catalyst, which exhibited excellent electrochemical activity and structural stability in an acidic environment, due to the O-doped graphene can more effectively adsorb N₂. Density functional theory calculations showed that C = O and O–C = O groups had a greater contribution to NRR, which was higher than that of C–O groups.

Co-doping. A large number of studies have confirmed the effectiveness of single heteroatom doping as a strategy to improve the catalytic performance of carbon materials. Further studies have shown that the co-doping of two or more heteroatoms (such as N–S, N–P, N–B, etc.) brings about a more complex and attractive electronic interaction that produces a synergistic effect in enhancing the catalysis of carbon materials. Its performance also has a high potential for improvement. Compared with single heteroatom doping, the synthesis of co-doping is more restricted and complicated to control. In the existing reports, the methods of template method, carbonization and freeze-drying activation, [52] flame synthesis, [53] post-treatment synthesis [54] and hydrothermal synthesis [55] are all feasible. Yuan et al. [56] reported an in-situ self-sacrifice and self-template strategy, which used in-situ nanostructures and catalytically active site engineering to synthesize N and S co-doped hierarchical porous carbon electrocatalyst during the carbonization of a single polymer precursor. The research results showed that the N, S-doped porous network provided abundant active sites and transport channels for efficient charge transport, and the catalyst exhibited excellent ORR activity in both alkaline and acidic electrolytes (Fig. 2.6). The combination of N doping and other heteroatoms doping is mainly considered when designing to introduction multiple heteroatoms. Xie et al. [57] developed a simple strategy to directly synthesize natural N/O-doped ultra-thin few-layer carbon nanosheets by pyrolyzing three-dimensional guanine without using any template. Its catalytic performance was excellent, the half-wave potential can reach 0.84 V, which was better than most graphene-based electrocatalysts. The combination of heteroatom doping, high specific surface area and abundant structural defects enhances the ORR activity of the catalyst.

Both the defect structure and the doping of heteroatoms are based on the adjustment of the electronic structure of the active sites of non-metallic carbon materials to improve the shortcomings of the inertness of the catalytic performance of the carbon materials. Research based on these two synthesis strategies has provided a favorable basis for its effectiveness. However, the precise control of defect positions and types, and the effective doping of heteroatoms require further exploration by researchers.

2.3 Synthesis of Atomically Dispersed Metal Carbon-Based Nanomaterials

The effective synthesis and application of single-atom catalysts (SACs) or atomically dispersed metal carbon-based catalysts is a very important research direction in the field of catalytic materials research in recent years. Due to the high dispersion of active components, the almost 100% metal utilization efficiency and the interaction between the active center and the adjacent coordination atoms, compared with metal nanoparticles, clusters, blocks, etc., atomically dispersed metal catalysts show superior activity, stability, and selectivity in many energy conversion reactions. Bimetallic and even multiple metals may have a synergistic effect of metal sites, resulting in

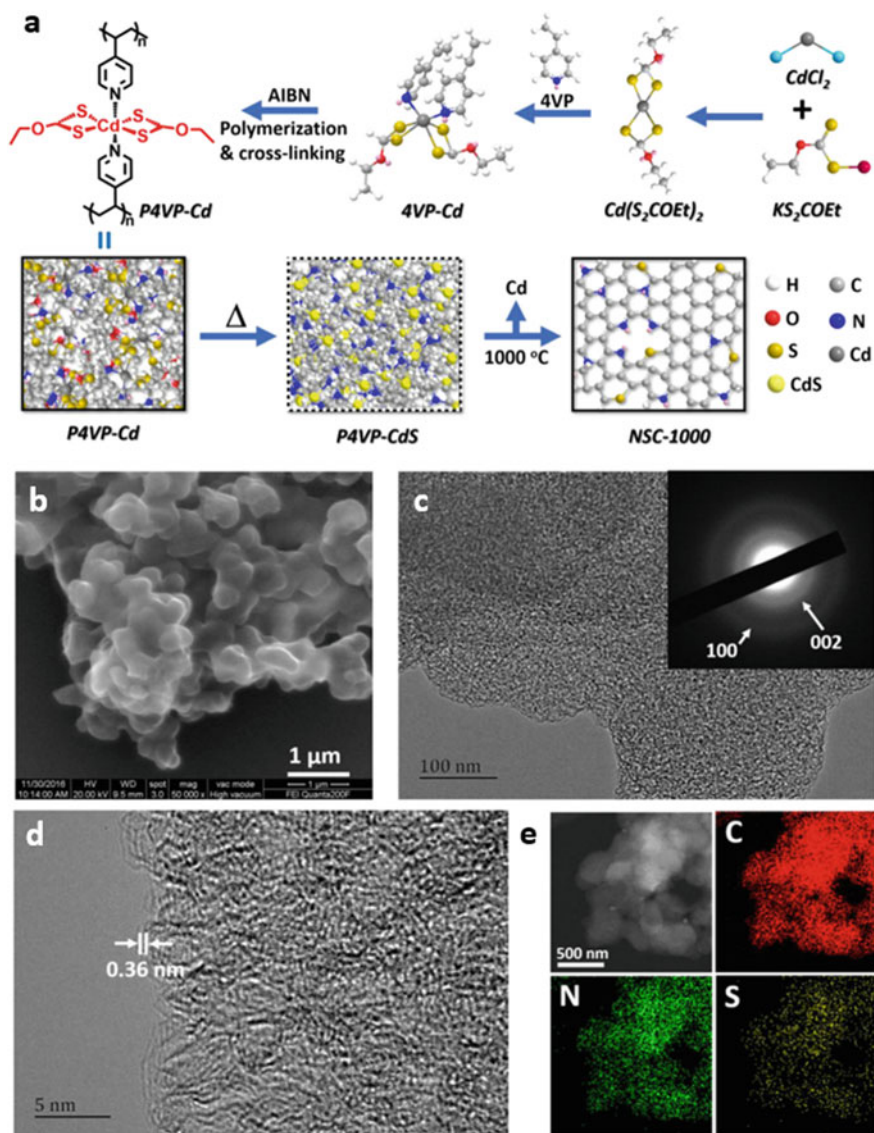


Fig. 2.6 Synthesis of co-doped carbon nanomaterials. **a** Schematic of the fabrication process of N, S co-doped porous carbon materials. Morphology and microstructure characterizations. **b** SEM, **c** TEM (inset is the SAED pattern), and **d** HR-TEM images of NSC-1000. **e** HAADF-STEM image of NSC-1000 and the corresponding element mapping images for C, N, and S. Reproduced with permission [56]. Copyright 2019, Elsevier

better performance than single-metal catalysts. It is very important for the synthesis of well-dispersed carbon-based catalysts to make the metal uniformly dispersed on the carbon substrate in the form of atoms.

Among them, a common type of research is the anchoring of metal atoms by introducing heteroatoms into the carbon support. The introduction of heteroatoms can form bonds with single metal atoms and/or carbon substrates, generate electron transfer, prevent metal atoms from agglomerating through unique electronic structures and coordination environments, and form atomically dispersed metal-carbon-based nanomaterials as catalysts [58]. The synthesis methods of single-atom catalysts mainly include pyrolysis, [59] hydrothermal, [60] electrodeposition, [61] impregnation, [62] etc., and metal atoms are introduced into the nanocarbon matrix. In the following, various synthetic methods will be introduced from the dispersion methods of different metal atoms.

2.3.1 Single Metal-Heteroatom Doped Carbon-Based Nanomaterials

Due to the small specific surface area and high surface energy, isolated metal single atoms are prone to aggregate and form metal nanoparticles during the synthesis process, especially under harsh pretreatment or catalytic conditions [63]. Studies have found that heteroatoms can act as coordination sites to fix metal atoms by forming M-H bonds (H represents heteroatoms including N, O, S, etc., and M represents metals including Zn, Fe, Co, Ni, Mn, etc.) [64, 65]. Because the electronegativity of N atoms is relatively high and the size of atoms is similar to that of C, the N-doped M-H-C structured metal single-atom catalyst is the most widely studied. The resulting M-N_x-C structure not only fixes the metal atom through M-N coordination, but also changes the electronic structure of the metal atom through the binding effect of C and N. On the other hand, the defect effects and porous channels brought about by the introduction of nitrogen bring more favorable bonding for the anchoring of metal atoms [66]. Different types of N (such as pyrrole, pyridine, graphite nitrogen, etc.) also have different effects on the catalytic performance of the catalyst [67].

The design and research of the synthesis process have been extensively explored to accurately control the N in the catalyst according to the application prospects. Li et al. [68] reported a synthesis strategy for stabilizing single cobalt atoms on nitrogen-doped porous carbon under metal loadings as high as 4 wt%. By pyrolyzing the pre-designed Zn/Co metal-organic framework, Zn has been selectively evaporated above 800 °C, and Co has been carbonized and reduced by the organic linker. Co-N unit point had excellent ORR activity with the half-wave potential of 0.881 V, and exhibited the strong chemical stability and thermal stability.

The introduction of various heteroatoms has formed different coordination structures and coordination numbers, which may differently influence the electron cloud density of the carbon substrate and self-spin of the metal center. Compared with

electrocatalysts without heteroatoms, the synergistic effect of heteroatoms such as O, S, P, and B will make the prepared materials have unique structural characteristics and higher electrocatalytic activity [69]. The general synthesis method is similar to that of the M–N_x–C material, which requires precise control of multiple steps to obtain the product with the desired structure, such as high temperature annealing, [70] bottom-up stepwise synthesis methods, [71] in situ template synthesis, [72] etc.

Zhang et al. [10] introduced two methods to achieve atomic dispersion of metal species on the stent. The mass-selective soft landing technology can use mass-selected molecular or atomic beams to precisely control the size of the metal species and precisely adjust the surface structure of the carrier. The use of wet chemical methods can chemically fix the metal species on the bracket (Fig. 2.7a–c). Zhang et al. [73] reported a simple and scalable way to produce thermally stable single-atom catalysts, using commercial RuO₂ as a raw material, by physically mixing submicron RuO₂ aggregates with MgAl_{1.2}Fe_{0.8}O₄ spinel. Studies have shown that the diffusion process is caused by strong covalent carrier interaction. This simple and easy-to-obtain synthesis strategy provides a direction for large-scale manufacturing of single-atom catalysts for industrial applications.

2.3.2 Double/Multi-Metal-Heteroatom Doped Carbon-Based Nanomaterials

The introduction of multiple metals not only reduces the demand for precious metals, but also optimizes the geometry and electronic structure of the metal sites, which is conducive to improving activity and selectivity. The synergistic effect brought by multiple metal centers is often the key to its superior performance to single metal catalysts. The synergy between the bimetallic atoms either changes the availability of active surface sites or modulates the binding energy to achieve a suitable metal state between the catalytic site and the reactants, intermediates and products [75]. The synergistic effect of carbon-supported multi-metal SACs is similar to that of metal alloy catalysts. Bimetallic atom pairs with dual catalytic sites are beneficial to adjust the activity and selectivity of the electrocatalysts.

Common synthetic methods of bimetallic atom-dispersed carbon-based nanomaterials include template method, [76] solution processing, [77] one-pot method, [78] high temperature treatment, [79] and electrospinning method [80]. As a porous material with high porosity, low density, large specific surface area, regular pore channels, and adjustable pore size, metal–organic frameworks (MOFs) are also commonly used to restrict the introduction of metal atoms into carbon sources. Kern et al. [81] proposed a metal–organic network, which promoted the production of oxygen from water by heterogeneous bimetallic catalysts by appropriately inserting Co and Fe metal centers in an organic environment. Compared with homogeneous metal catalysts, the catalytic activity had a nonlinear increase. Due to the weak electron coupling between the two metal centers of the π -electron system of the porphyrin

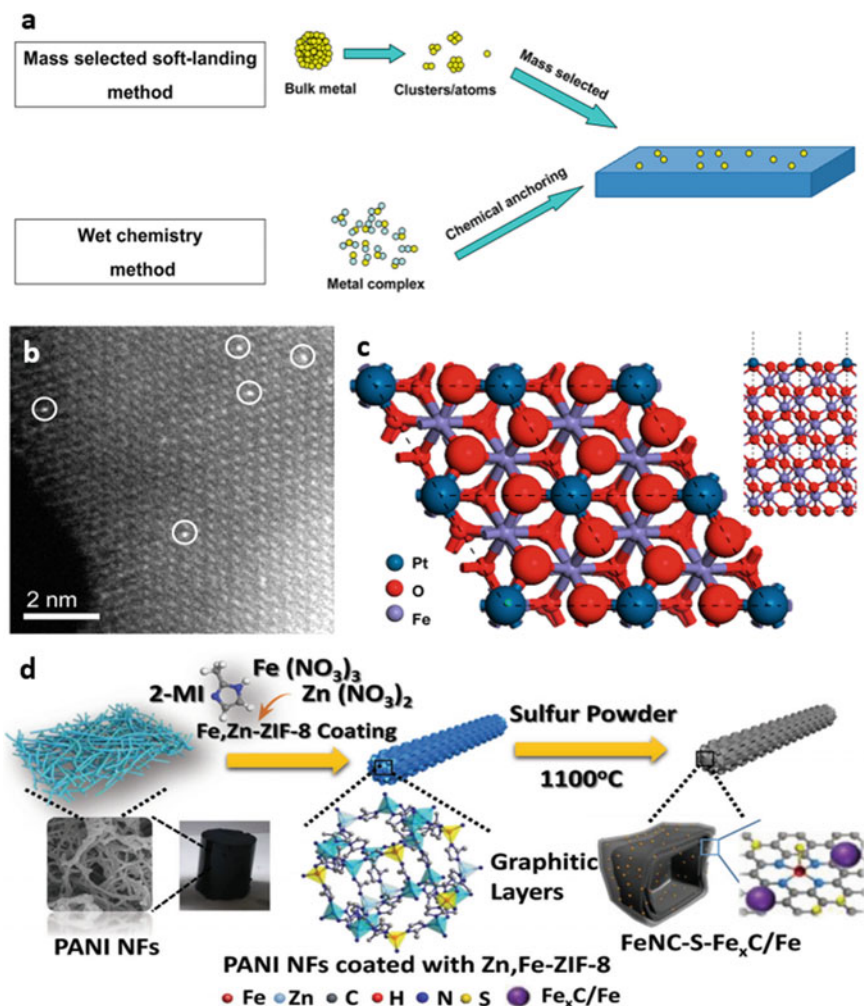


Fig. 2.7 Synthesis of single-metal heteroatom-doped carbon-based nanomaterials. **a** Methods for preparing SACs: mass-selected soft-landing and wet chemistry. **b** HAADF-STEM image and **c** Density functional modeling of Pt_1/FeO_x . Reproduced with permission [10]. Copyright 2013, American Chemical Society. **d** Synthesis scheme of the $\text{FeNC-S-Fe}_x\text{C}/\text{Fe}$ catalyst. Reproduced with permission [74]. Copyright 2018, WILEY-VCH

macrocycle, which promoted the improvement of OER activity. The proposal of this metal–organic network embodied the reliable prospect of bimetallic electrocatalysts as OER electrocatalysts.

Besides the above synthetic methods, there are many other effective methods to synthesize bimetallic atomic catalysts. Liu et al. [82] developed a Fenton-like catalyst with a single cobalt atom anchored on porous nitrogen-doped graphene. The content of pyrrole N in N-doped graphene was adjusted by Fe doping and changing

the calcination temperature. This catalyst had dual active sites, high activity and stability, and can efficiently catalyze and oxidize refractory organics by activating peroxymonosulfate (PMS). Density functional theory calculations showed that the Co–N₄ position was the best binding site for PMS activation (Fig. 2.8a). Zhang et al. [83] designed and synthesized Fe, Mn/N–C catalysts dispersed with bimetallic atoms, revealing the true reaction mechanism in the electrocatalytic process. This catalyst had a Fe–N₄/C system with an intermediate spin state, and oxygen reduction will occur preferentially on ferric iron. Theoretical calculations showed that the divalent iron sites were activated by the spin state transition of the Mn–N part dispersed by adjacent atoms, thereby improving the ORR performance and durability of this electrocatalyst (Fig. 2.8b–e).

2.3.3 *Atomically Dispersed Metal Multi-Heteroatom Co-doped Carbon-Based Nanomaterials*

Since different heteroatoms have different regulatory effects on the metal catalytic center, people try to further optimize the electronic structure of carbon-based materials by designing doping a variety of heteroatoms. Different heteroatom doping may bring more complex forms of M–H bonds. The bonding mode of atoms, the interaction between metal and heteroatoms and the interaction between heteroatoms may have a significant impact on the charge transfer and the adsorption of intermediates, thereby promoting mass transfer and electron transfer in the catalytic process, which allow the catalyst with excellent catalytic activity and stability [84].

Because the introduced heteroatoms are more complex, the requirements for the corresponding synthesis steps are also higher. Appropriate methods are required to tune the corresponding doping sites and the adsorption of metal atoms. A commonly used synthesis strategy is thermal decomposition, in which the introduction of heteroatoms is regulated by controlling the temperature and atmosphere.

Xu et al. [74] proposed an improved system to increase the activity of Fe_xC/Fe through sulfidation, and synthesized FeNC–S–Fe_xC/Fe catalyst. Experimental results showed that this catalyst exhibited excellent activity with higher ORR activity and better durability in acidic media. Its half-wave potential is 0.821 V, which was better than commercial Pt/C catalysts, and had a certain OER activity, which can be used as a high-performance dual-function catalyst for zinc-air batteries. It can be found through theoretical calculations that the introduction of sulfur has a certain effect on the enhancement of the active center (Fig. 2.7d). Lu et al. [17] developed a mesoporous carbon composite material with co-coordination of nitrogen and phosphorus with manganese atoms, which was prepared by polymerization of *o*-phenylenediamine and high-temperature calcination. This electrocatalyst exhibited high ORR activity in alkaline media, with a half-wave potential of 0.84 V, which was comparable to the Pt/C catalyst. The research results showed that the introduction of phosphorus promoted the formation of mesopores during the pyrolysis process and the mass

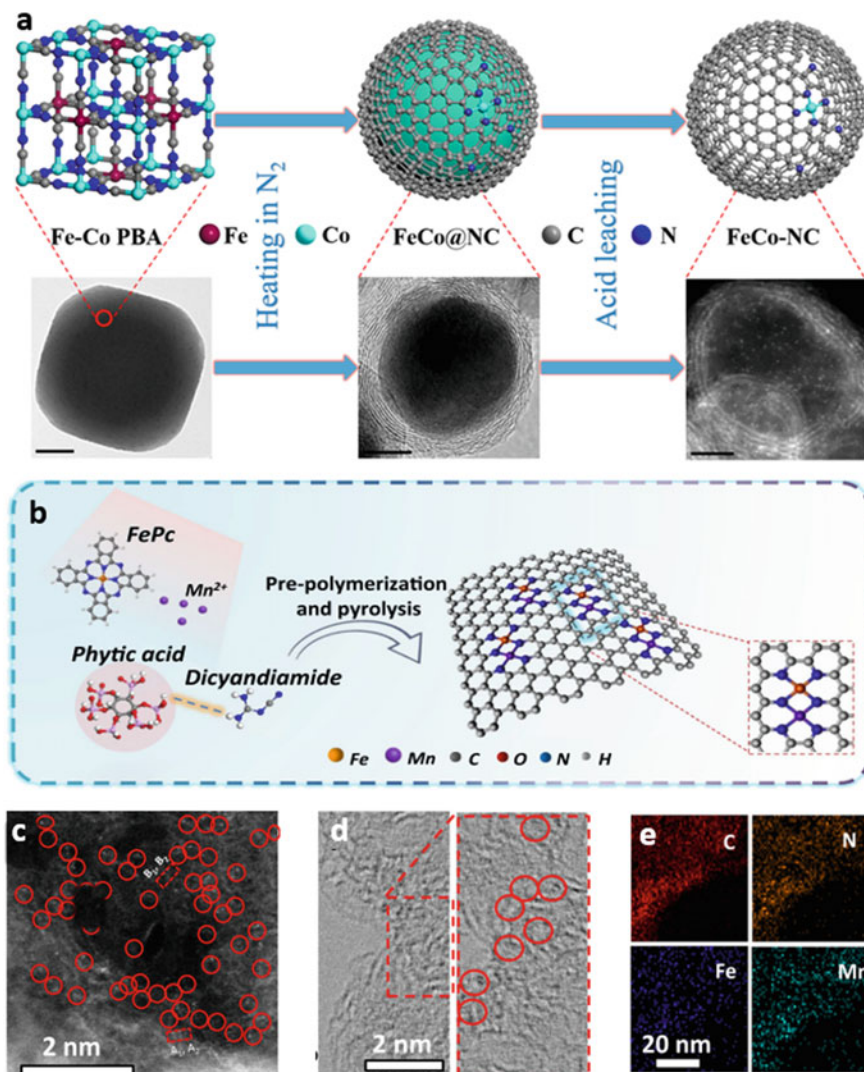


Fig. 2.8 Synthesis of polymetallic heteroatom-doped carbon-based nanomaterials. **a** Preparation route and model of single-Co-atom catalyst. Scale bars: (left) 50 nm, (middle) 4 nm, and (right) 2 nm. Reproduced with permission [82]. Copyright 2018, American Chemical Society. **b** Schematic illustration of synthesis procedure for Fe, Mn/N-C catalysts. **c** Aberration-corrected HAADF-STEM image and some of bimetallic Fe/Mn sites are highlighted by larger red circles. **d** HR-TEM of Fe, Mn/N-C, in which some lattice distortions are highlighted by red circles. **e** HAADF-STEM image of Mn, Fe/N-C with mappings of individual elements. Reproduced with permission [83]. Copyright 2021, Springer Nature

transfer process. On the other hand, the atomic-scale co-coordination between N, P, and Mn changed the configuration of Mn, thereby improving ORR activity. Wu et al. [85] synthesized a sulfur-doped Mn–N–C catalyst (Mn–N–C–S) through effective adsorption and pyrolysis. In acidic medium, Mn–N–C–S exhibited excellent ORR activity, high current density, and good stability. Theoretical calculations showed that there was a repulsion between the ORR intermediate and the adjacent sulfur dopants, which caused a steric effect and leads to an increase in ORR activity.

Although the research on atom-dispersed metal–carbon-based nanomaterials has achieved vigorous development so far, this type of catalyst still has some limitations that need to be resolved. First of all, the content of atomically dispersed metals is often very low. Despite the maximum atom utilization, the number of effective catalytic sites is small, making it impossible to optimize the catalytic performance [86]. Secondly, the low amount of heteroatoms and the difficult-to-control doping type make it impossible to obtain an ideal catalyst structure according to the experimental design [87]. Catalysts with complex structures, such as multi-heteroatom-doped catalysts with multiple metal catalytic sites, often inevitably occur agglomeration of metal atoms, which has a negative impact on catalytic performance. Therefore, precisely control the type and content of heteroatom doping and increase the loading of single metal atoms will become the main issue of research in this field for a long time in the future.

2.4 Synthesis of Metal Nanoparticles Encapsulated Carbon-Based Nanomaterials

At present, the most advanced catalysts are still based on precious metals, but the high cost, limited resources and general durability limit their large-scale application in industry. Therefore, the development of non-precious metal electrocatalysts with economic benefits has become a major research topic in the current field. More and more studies have shown that, compared with metal nanoparticles deposited on the surface of carbon-based nanomaterials, encapsulating the same metal or metal oxide in carbon-based nanomaterials can exhibit different catalytic activities. It mainly includes various oxides, [88] sulfides, [89] phosphides, [90] nitrides, [91] carbides, [92] selenide metal nanoparticles, [93] etc., wrapped in carbon shells, as well as alloy nanoparticles wrapped in carbon shells: CoNi, FeNi, etc. Meanwhile, different coating structures will show different morphology, structure, and chemical composition. More importantly, the unique shape, structure, and chemical composition will lead to superior performance. For example, the core–shell structure is generally made of a graphite layer as the outer shell, and metal hybrids or alloys are wrapped in it to form a nano-scale ordered assembly structure [94].

The main synthesis methods for synthesizing metal nanoparticles encapsulated carbon-based nanomaterials include continuous reduction method, co-reduction method, microemulsion synthesis method, solvated metal atom dispersion method,

and other liquid phase synthesis methods. The advantage of the liquid phase synthesis method is that the reactants and precursors can be uniformly dispersed in the liquid phase, making the reaction more complete. The carbon nanotube packaging structure is mainly synthesized by filling carbon nanotubes with metal hybrids or alloy nanoparticles through pyrolysis [95] and wet chemical methods [96]. These assembled structures can effectively limit the volume change and polymerization of metal particles during charging and discharging, and provide better support conditions for the stability of catalytic performance. The related synthetic methods will be described in detail below.

2.4.1 *Metal Hybrids Encapsulated Carbon-Based Nanomaterials*

During the electrochemical reaction process, metal agglomeration often occurs and thus resulting in low ion transmission efficiency of the system, and causes poor performance. In this case, the structure of carbon-based nanomaterials coated with metal hybrids provides an effective solution to improve electron transfer efficiency. The outer carbon shell provides a conductive path for efficient transmission and can protect the internal metal structure stability.

Pyrolysis is a common synthetic method in encapsulating metal compounds. Under space-constrained conditions, metal compounds can be facily encapsulated in carbon-based nanoshell structures by a high temperature of 1000 °C. Xu et al. [97] reported that a simple self-assembly and pyrolysis strategy can be used to expand the preparation of cobalt phosphide (Co₂P)-cobalt nitride (CoN) core-shell nanoparticles with dual active sites. This non-noble metal electrocatalyst was coated in nitrogen-doped carbon nanotubes. Density functional theory calculations showed that Co-N-C was the site with the highest OER and ORR activity, and the active nitrogen site coupled with Co₂P was the main source of HER activity. The experimental results confirmed the above conclusions and reflected the excellent electrochemical performance of the electrocatalyst (Fig. 2.9). Lin et al. [98] successfully prepared a new pea-like Co@C and Co₃O₄@C composite nanostructure for the first time. Co and Co₃O₄ nanoparticles were encapsulated in a carbon coating with good graphitization. In lithium-ion battery tests, the unique nanostructure of this material exhibits excellent stability, cyclability, and high charge-discharge rate, making it a promising candidate for lithium-ion battery anodes. In addition, this study showed that the excellent electrochemical performance was significantly related to the unique structure of the sample, which proved that it was possible to change the corresponding electrochemical performance by rationally designing the layered structure of the material. Guo et al. [99] developed a one-step *in-situ* nano-space confinement pyrolysis strategy to solve the problem of large volume changes and dissolution of Fe₃O₄ nanomaterials during insertion/extraction of lithium ions. This material had an egg-yolk shell nano-spindle structure with sufficient internal void space, which can well limit the

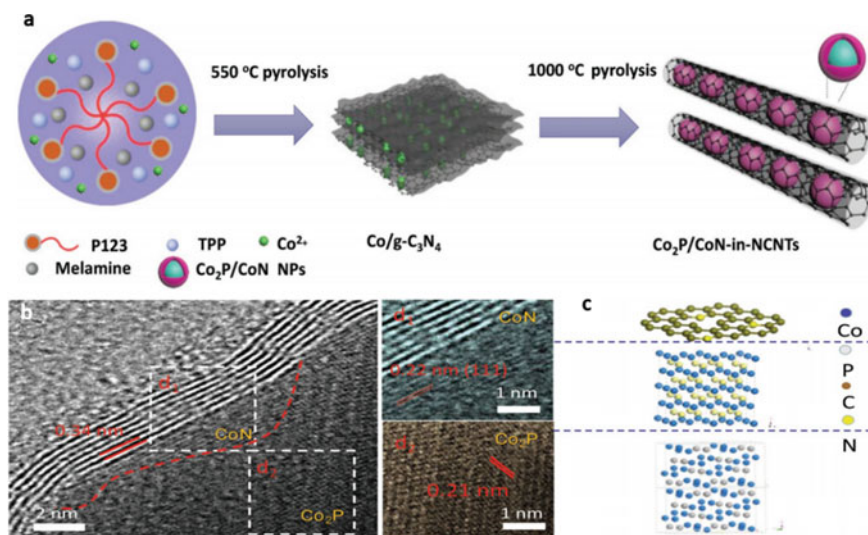


Fig. 2.9 Synthesis of alloy-encapsulated carbon-based nanomaterials. **a** The synthetic route for $\text{Co}_2\text{P}/\text{CoN}$ -in-NCNTs. **b** Crystal structures and **c** molecular Structures of $\text{Co}_2\text{P}/\text{CoN}$ -in-NCNTs core/shell models. Reproduced with permission [97]. Copyright 2018, WILEY-VCH

change of Fe_3O_4 nanomaterials and adapt to it. Therefore, the $\text{Fe}_3\text{O}_4@/\text{Fe}_3\text{C}$ core-shell structure material had high reversible capacity, high rate, and excellent cycle life, and was currently reported as an excellent Fe_3O_4 -based anode material.

2.4.2 Alloys Encapsulated Carbon-Based Nanomaterials

Compared with metal hybrids, alloy nanoparticles contain more metal species, which can provide more abundant active sites. The relative quantity of each component phase in the alloy, the volume size of the different phase metal particles and the different structure will all have an impact on the properties of the material. More optimized reactivity and stability by adjusting the different components in these alloys can be obtained. Bao et al. [100] introduced a synthetic strategy to uniformly disperse metal nanoparticles in carbon nanotubes. The focus was on homogeneous dispersion of metal particles in multi-walled carbon nanotubes (MWCNTs) with an inner diameter of less than 10 nm and double-walled carbon nanotubes with an inner diameter of 1.0–1.5 nm. The research results showed that the size of metal particles can be adjusted by changing the channel diameter, thereby affecting the adsorption activity and catalytic performance of the catalyst. The confinement effect can also be further adjusted by controlling the electronic structure of the curved graphene wall. Therefore, the possibility of carbon nanotube electrocatalysts in commercial applications was enhanced (Fig. 2.10a, b).

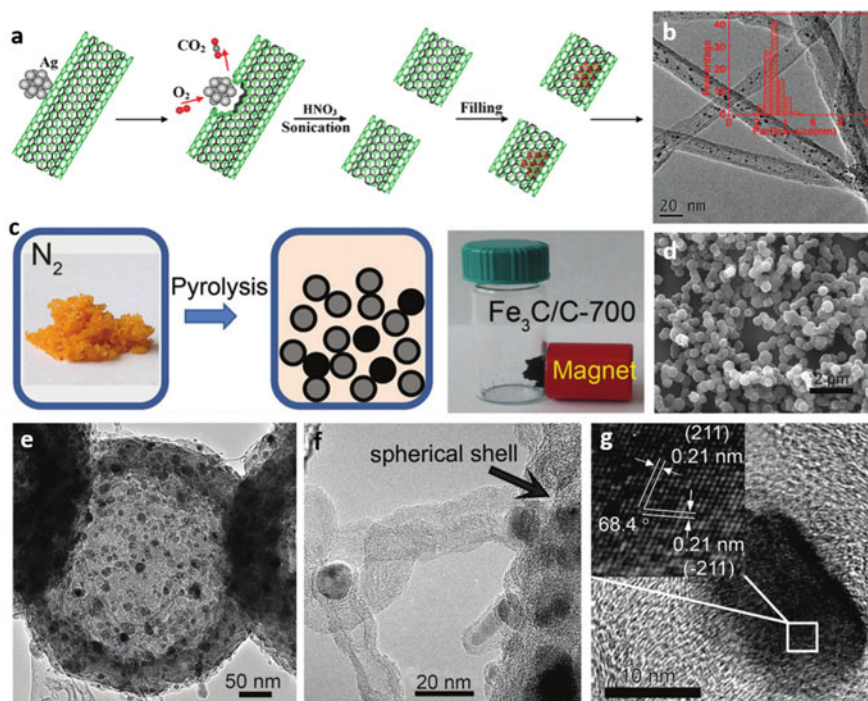


Fig. 2.10 Synthesis of alloy-encapsulated carbon-based nanomaterials. **a** Scheme for introducing nanoparticles inside MWCNTs (i.d. 4–8 nm) by a wet chemistry method. **b** The TEM image displays Ru nanoparticles confined in MWCNTs with the inset showing their particle size distribution. Reproduced with permission [97]. Copyright 2011, American Chemical Society. **c** Synthesis of $\text{Fe}_3\text{C}/\text{C}$ hollow spheres. **d** SEM image of $\text{Fe}_3\text{C}/\text{C}$ -700. **e** TEM image of one typical hollow catalyst sphere of $\text{Fe}_3\text{C}/\text{C}$ -700. **f** TEM image of bamboo-like carbon nanotubes grown on the surface of the hollow spheres. **g** HRTEM image of a Fe_3C nanoparticle in $\text{Fe}_3\text{C}/\text{C}$ -700 and the index crystal plane shown in the inset. Reproduced with permission [104] Copyright 2014, WILEY-VCH

The current main research direction is the synthesis method of Fe, Co, Ni, Cu and other transition metal elements mixed and encapsulated in carbon-based nanomaterials. More in-depth mechanism research is also needed to obtain more excellent catalytic performance. Common synthesis methods of existing alloy-encapsulated carbon-based nanomaterials include CVD method, [101] pyrolysis method, [102] and hydrothermal method [103]. Li et al. [104] reported a hollow spherical high-pressure pyrolysis catalyst composed of uniformly coated iron carbide (Fe_3C) nanoparticles with a graphite layer. The surface had only a few nitrogen and metal functions. In acidic media, the outer graphite shell can play a stabilizing role and reduce the loss of ORR performance of metal particles. Therefore, this electrocatalyst had good activity and stability, which provides new insights for the development of ORR catalysts (Fig. 2.10c–g). Xi et al. [105] used the atmospheric pressure chemical vapor deposition method to successfully encapsulate nickel copper (NiCu) alloy nanoparticles into a graphite shell. Through research, it was found that the synthesized

material has obvious core–shell structure and adjustable shell thickness, which can be used as HER electrocatalyst. Electrochemical measurement results showed that the catalytic activity of carbon-coated Ni-Cu nanoalloy particles (NiCu@C) was related to the thickness of the shell, and the nickel-copper nanoparticles coated with a single-layer graphite shell showed good HER activity and durability. Density functional theory (DFT) calculations showed that NiCu@C had ideal hydrogen adsorption performance, which corresponds to the higher HER activity.

Although in the past research, encapsulated carbon-based nanomaterials have made some progress in the study of electrocatalytic activity, it still has a long way to go before commercial applications. First, the active sites between metals and carbon-based materials cannot be eliminated and the interactions between metals and metals cannot be eliminated. They influence each other and restrict each other, and the effect on the performance of the material is still unclear. Second, the durability of metal nanoparticles coated carbon-based nanomaterials still needs to be improved. Compared with precious metal-based catalysts, many performance aspects still need to be improved. In short, in the future, it is necessary to combine experimental results and theoretical calculations to explore the synthesis of more high-performance electrocatalysts.

2.5 Synthesis of Metal Nanoparticles Supported Carbon-Based Nanomaterials

Among heterogeneous catalysts, supported catalysts occupy a large proportion. So far, there have been many research examples of carbon-based nanomaterials loaded with metal nanoparticles. The surface ligands of nanomaterials will largely affect their molecular properties [106]. This means that regulating the interaction between carbon-based nanomaterials and the metal particles supported by them will play a crucial role in the construction of suitable catalysts. Different substrate materials and different load materials will have a huge impact on the performance and internal interaction of the composite material. This chapter mainly introduces metal hybrid-supported carbon-based nanomaterials and alloy-supported carbon-based nanomaterials, such as self-supporting materials, materials using carbon substrates for secondary growth, and some of their synthesis methods and properties.

In the traditional synthesis process, the raw materials needed as the catalyst electrode are often in powder form, and some inactive binders need to be used to bond them together. These substances can easily lead to the uncontrollable microstructure of the material and the reduction of the active surface area, which greatly affects the performance of the catalyst. The self-supporting material is a material that directly grows in situ on the substrate without adding an adhesive [107]. This material has a variety of forms, due to the strong interaction between the substrate and the supported material, the active sites will be evenly dispersed. In addition, self-supporting catalysts usually have the characteristics of high specific surface area, high conductivity,

and long-term durability. This material is considered a favorable choice for the further development of electrochemical catalysis.

The typical synthesis method is mainly high-temperature annealing, and metal precursors are supported on carbon-based nanomaterials by calcination. The desired metals are mostly obtained by impregnation, co-precipitation or direct chemical reduction of metal precursors on carbon sources [108]. Several synthetic methods of supported metal nanoparticles will be introduced in detail below.

2.5.1 Metal Hybrids Supported Carbon-Based Nanomaterials

The synthesis methods of metal hybrid supported carbon-based nanomaterials are relatively abundant, and their applications are also relatively wide. A simple one-pot heat treatment method can be applied to this material synthesis. The metal hybrids can be fully supported on the carbon substrate through the process of heating, heat preservation and cooling of the uniform mixture, and their uniform dispersion can be controlled. In electrochemical reactions, the efficiency of water splitting is closely related to the production of O_2 and H_2 . Wang et al. [109] used a one-pot method to synthesize N-doped carbon hybrids loaded with Co, CoO, Co_3O_4 , etc., in order to improve the overall efficiency and use it as a dual-function electrocatalyst. The synergistic effect between metallic cobalt and its hybrids provided superior activity for HER, and the introduction of electron-rich nitrogen also played a role. The high conductivity of carbon and the structural characteristics of nanocomposite materials also made the material exhibit excellent reactivity when used as an OER electrocatalyst.

Solvothermal reactions are also commonly used here. This method has a relatively simple process, the process is easy to control, and the experiment can be carried out slowly. The closed reaction space will make the substrate react more fully and uniformly, avoiding contamination. For example, Ding et al. [110] successfully prepared a Ni_3N /graphene nanocomposite material for use as a supercapacitor. The material was synthesized by anchoring Ni_3N nanoparticles on redox graphene nanosheets. The smaller size of the hybrid metal significantly increased the Faraday redox reaction of the pseudocapacitor material.

In order to suppress the shuttle effect in lithium-sulfur batteries, Sun et al. [111] designed and synthesized a Co_2B -loaded carbon nanotube composite material coated on a commercial polypropylene separator as an effective barrier layer for inhibiting polysulfide in lithium sulfur batteries (LSBs). The calculation results of density functional theory showed that the empty orbital in the boride can not only absorb polysulfides, but also had a cobalt-sulfur absorption effect, which was stronger than other barrier materials. Zhang et al. [112] reported a HER electrocatalyst synthesized by diruthenium triboride (Ru_2B_3) dispersed in B, N-doped carbon nanofibers (BNC). The material was obtained by self-assembly and connection of ruthenium complexes on BNC and melamine through an in-situ pyrolysis method. Experimental results showed that it had excellent performance in terms of HER, which was better than

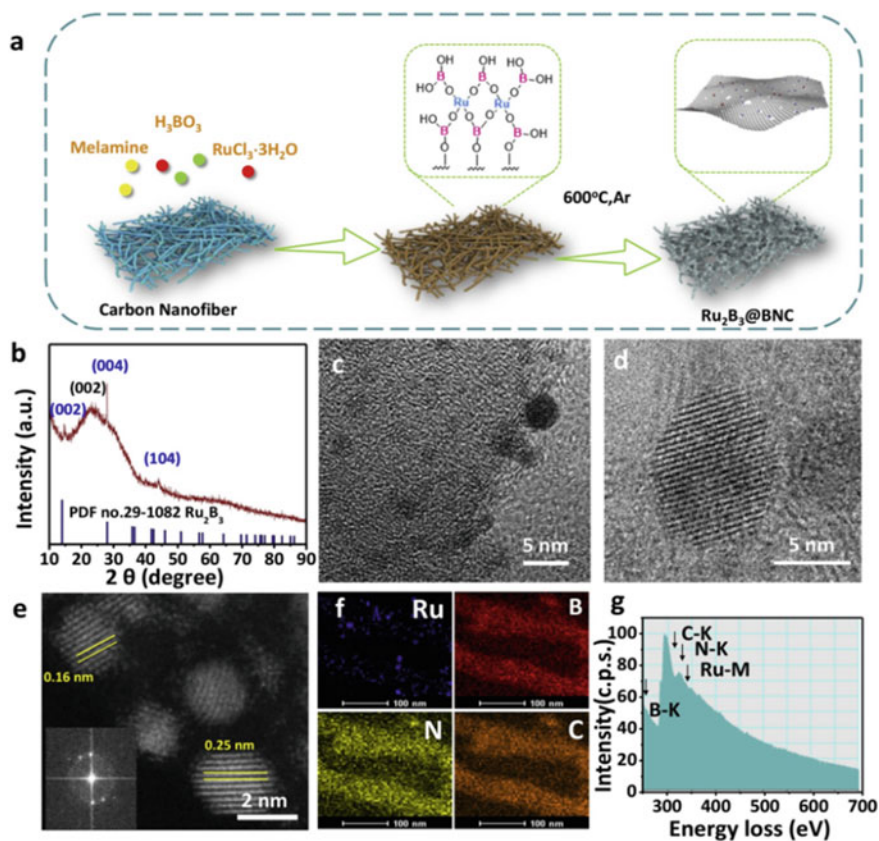


Fig. 2.11 Metal hybrids support the synthesis of carbon-based nanomaterials. **a** Synthetic illustration of the $\text{Ru}_2\text{B}_3@\text{BNC}$ electrocatalyst. **b** XRD pattern of $\text{Ru}_2\text{B}_3@\text{BNC}$. **c** low- and **d** high-magnification TEM, **e** HAADF-STEM, **f** EDS elemental mapping of Ru, B, N, and C for $\text{Ru}_2\text{B}_3@\text{BNC}$. **g** EELS spectrum of $\text{Ru}_2\text{B}_3@\text{BNC}$. Reproduced with permission [112]. Copyright 2020, Elsevier

other HER electrocatalysts on the market at that time, and its durability was also excellent (Fig. 2.11).

2.5.2 Alloys Supported Carbon-Based Nanomaterials

Alloy-supported carbon-based nanomaterials have unique physicochemical properties. It not only has the good stability and durability of self-supporting materials, but also has various metal properties of alloy materials. The two or more metals mix with each other, the electronic structure changes, and the internally generated electron transfer interacts with the carbon-based material. At the same time, when

exposed on the surface of the substrate, it is easier to contact the reactant for activation, so the catalytic activity can be greatly improved. Existing reports have introduced various synthesis methods, such as thermal treatment, microwave dielectric loss heating, pore volume impregnation, in situ growth, solvothermal methods, etc. These synthetic strategies are described in detail below.

Baker et al. [113] proposed for the first time that carbon nanofibers were used to support alloy particles as a catalyst. They loaded Fe and Cu nanoparticles on carbon nanoparticles by thermal treatment and found that their catalytic activity and stability for hydrogenation reactions were significantly superior to that of similar metals adsorbed on carbon-based materials. The research results showed that the epitaxial growth of metal particles on carbon nanofibers occurs, and the special crystalline form led to the excellent catalytic performance of this catalyst.

Lukehart et al. [68] synthesized an electrocatalyst material with Pt/Ru nano-alloy particles supported on a powdered carbon carrier by microwave dielectric loss heating method. And they also reported the catalytic performance of this nanocomposite in the direct methanol fuel cell (DMFC) anode catalyst, which was more stable and catalytically active than previously known unsupported catalysts for commercial applications. This pointed out the direction for the future research prospects of supported electrocatalysts, and opened a variety of potential research roads.

Wei et al. [114] prepared electrocatalysts with transition metal elements such as Mo and Co supported on carbon nanotubes, and prepared a corresponding control group to measure its effective catalytic efficiency. Transmission Electron Microscope (TEM) images showed that the synthesized carbon nanotubes have a higher specific surface area, which facilitates the adsorption of reactants in the catalytic reaction. It can be seen from the diffraction of X-rays (XRD) image that the supported active phase was more uniformly dispersed on the surface of the carbon nanotubes, which laid the foundation for the improvement of catalytic activity.

Wang et al. [115] developed a self-made graphite carbon nanocage supported Pr-Ir nanoalloy composite catalyst to improve the catalytic activity and durability of polymer electrolyte membrane electrolysis cell (PEMEC). This catalyst was synthesized by pore volume impregnation in aqueous solution. It was verified through experiments that the excellent performance of this graphite carbon nanocage when loaded with Pr-Ir alloy was even better than when loaded with pure platinum, so that the amount of platinum can be reduced by 50% in the application of platinum catalyst. This provided an effective method for the wider use of platinum-based catalysts.

Ji et al. [116] reported a simple MOF *in-situ* growth strategy to synthesize an electrocatalyst with dual functions of HER/OER. They used carbonization and heat treatment to graft Co-N-C nanosheets loaded with MoS₂ on carbon nanofibers. The material did not use a binder, and showed a unique hierarchical structure. The carbon nanofibers were connected to each other and have excellent electrical conductivity. They can be directly used as electrodes and were a typical self-supporting catalyst material (Fig. 2.12a-e).

Hu et al. [117] reported a solvothermal synthesized heterogeneous bimetallic cobalt diselenide nanoparticle (CoSe₂/FeSe₂@C) composite supported by carbon nanorods as a high-efficiency OER electrocatalyst. It had abundant holes and strong

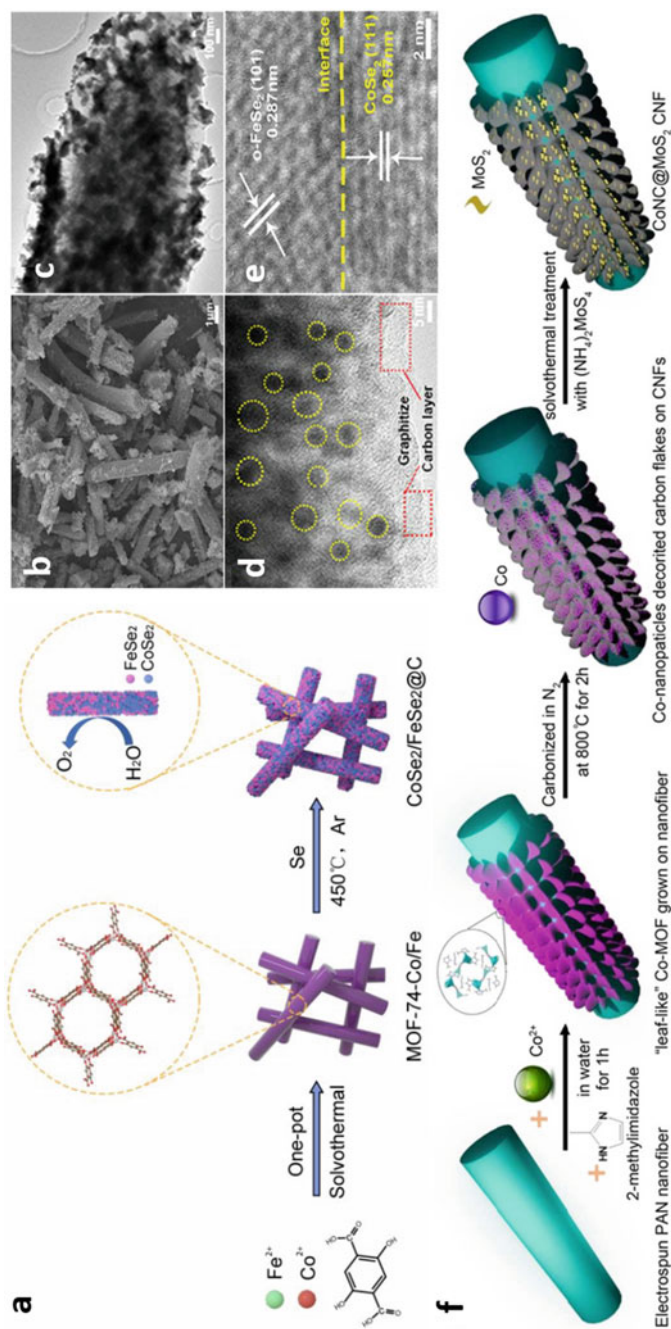


Fig. 2.12 Synthesis of alloy-supported carbon-based nanomaterials. **a** Schematic illustration of the synthesis process of CoSe₂/FeSe₂@C. **b** SEM image of CoSe₂/FeSe₂@C. **c** TEM image of CoSe₂/FeSe₂@C. **d** TEM image of CoSe₂/FeSe₂@C showing the carbon layer. **e** TEM image of CoSe₂/FeSe₂@C showing the interface. **f** Schematic illustration of the fabrication process of free-standing CoNC@MoS₂/CNF films. Reproduced with permission [117]. Copyright 2020, American Chemical Society

electron couplings to increase the active sites of the catalyst and adjust the electronic structure, which greatly improved the electrocatalytic activity. At the same time, its unique heterostructure also provided the material with vacancy defects and strong electronic interaction, which made the material exhibit excellent OER performance (Fig. 2.12f).

In summary, these different synthesis methods have brought more excellent electrochemical performance for the metal nanoparticles loaded with carbon-based nanomaterials by adjusting the physical and chemical interaction between the metal particles and the carbon-based materials.

2.6 Conclusion and Perspectives

In this chapter, the synthesis of various carbon-based nanomaterials, including metal defect-free carbon and carbon-doped nanomaterials, atom-dispersed metal carbon-based nanomaterials, metal nanoparticles coated carbon-based nanomaterials, and metal nanoparticles support carbon-based nanomaterials have been systematically introduced. The application of carbon-based nanomaterials in the field of electrocatalysis continues to develop, and there are more and more synthesis schemes. In metal-free carbon, several synthesis methods of carbon defects are mainly introduced, including the introduction of edge defects, vacancies and topological structure. There are many kinds of heteroatoms that can be incorporated in heteroatom-doped carbon. The currently known synthesis methods are mainly N, B, P, S, and O introduced in this chapter, and the incorporation of other heteroatoms needs to be explored in the future. It is necessary to optimize the synthesis method to obtain higher catalytic activity. Research on atomically dispersed metal carbon-based nanomaterials, metal nanoparticle-coated metal carbon-based nanomaterials, and metal nanoparticle-supported metal carbon-based nanomaterials still needs to be developed. Metals and carbon-based materials can be combined in a variety of ways through different synthesis methods, resulting in different electrochemical properties.

In general, there are still many synthesis methods to be developed for carbon-based nanomaterials used in catalysis. The various properties of the catalyst can be optimized by adjusting their coordination structure and electronic effects. Compared with the noble metal-based catalysts in commercial applications, although carbon-based materials have good electrical conductivity, they still have great shortcomings in catalytic performance. If they are put into application, they still need a high amount to reach the same level as Pt-based catalysts. The activity indicates that its intrinsic activity is still low. Therefore, the catalytic activity, stability and durability of carbon-based nanomaterials electrocatalysts need to be improved by more suitable synthesis methods. It is necessary to further study the various synthesis methods and mechanisms of carbon-based nanomaterials.

References

1. S. Zhao, D.W. Wang, R. Amal, L. Dai, Carbon-based metal-free catalysts for key reactions involved in energy conversion and storage. *Adv. Mater.* **31**, 1801526 (2018). <https://doi.org/10.1002/adma.201801526>
2. R. Paul, Q. Dai, C. Hu, L. Dai, Ten years of carbon-based metal-free electrocatalysts. *Carbon Energy* **1**, 19–31 (2019). <https://doi.org/10.1002/cey2.5>
3. J. Kotakoski, A.V. Krasheninnikov, U. Kaiser, J.C. Meyer, From point defects in graphene to two-dimensional amorphous carbon. *Phys. Rev. Lett.* **106**, 105505 (2011). <https://doi.org/10.1103/PhysRevLett.106.105505>
4. H. Tachikawa, H. Kawabata, Electronic states of defect sites of graphene model compounds: A DFT and direct molecular orbital-molecular dynamics study. *J. Phys. Chem. C* **113**, 7603–7609 (2009). <https://doi.org/10.1021/jp900365h>
5. Y. Jia, L. Zhang, A. Du, G. Gao, J. Chen, X. Yan, C.L. Brown, X. Yao, Defect graphene as a trifunctional catalyst for electrochemical reactions. *Adv. Mater.* **28**, 9532–9538 (2016). <https://doi.org/10.1002/adma.201602912>
6. K. Gong, F. Du, Z. Xia, M. Durstock, L. Dai, Nitrogen-doped carbon nanotube arrays with high electrocatalytic activity for oxygen reduction. *Science* **323**, 760–764 (2009). <https://doi.org/10.1126/science.1168049>
7. C. Zhang, N. Mahmood, H. Yin, F. Liu, Y. Hou, Synthesis of phosphorus-doped graphene and its multifunctional applications for oxygen reduction reaction and lithium ion batteries. *Adv. Mater.* **25**, 4932–4937 (2013). <https://doi.org/10.1002/adma.201301870>
8. Y.N. Chen, X. Zhang, Z. Zhou, Carbon-based substrates for highly dispersed nanoparticle and even single-atom electrocatalysts. *Small Methods* **3**, 1900050 (2019). <https://doi.org/10.1002/smt.201900050>
9. C.T. Campbell, Electronic perturbations. *Nat. Chem.* **4**, 597–598 (2012). <https://doi.org/10.1038/nchem.1412>
10. X.-F. Yang, A. Wang, B. Qiao, J. Li, J. Liu, T. Zhang, Single-atom catalysts: A new frontier in heterogeneous catalysis. *Acc. Chem. Res.* **46**, 1740–1748 (2013). <https://doi.org/10.1021/ar300361m>
11. J. Zhang, H. Yang, B. Liu, Coordination engineering of single-atom catalysts for the oxygen reduction reaction: A review. *Adv. Energy Mater.* **11**, 2002473 (2020). <https://doi.org/10.1002/aenm.202002473>
12. X. Xie, C. He, B. Li, Y. He, D.A. Cullen, E.C. Wegener, A.J. Kropf, U. Martinez, Y. Cheng, M.H. Engelhard, M.E. Bowden, M. Song, T. Lemmon, X.S. Li, Z. Nie, J. Liu, D.J. Myers, P. Zelenay, G. Wang, G. Wu, V. Ramani, Y. Shao, Performance enhancement and degradation mechanism identification of a single-atom Co–N–C catalyst for proton exchange membrane fuel cells. *Nat. Catal.* **3**, 1044–1054 (2020). <https://doi.org/10.1038/s41929-020-00546-1>
13. M. Xiao, Y. Chen, J. Zhu, H. Zhang, X. Zhao, L. Gao, X. Wang, J. Zhao, J. Ge, Z. Jiang, S. Chen, C. Liu, W. Xing, Climbing the apex of the ORR volcano plot via binuclear site construction: Electronic and geometric engineering. *J. Am. Chem. Soc.* **141**, 17763–17770 (2019). <https://doi.org/10.1021/jacs.9b08362>
14. Z. Kou, B. Guo, D. He, J. Zhang, S. Mu, Transforming two-dimensional boron carbide into boron and chlorine dual-doped carbon nanotubes by chlorination for efficient oxygen reduction. *ACS Energy Lett.* **3**, 184–190 (2017). <https://doi.org/10.1021/acsenergylett.7b01133>
15. P. Yin, T. Yao, Y. Wu, L. Zheng, Y. Lin, W. Liu, H. Ju, J. Zhu, X. Hong, Z. Deng, G. Zhou, S. Wei, Y. Li, Single cobalt atoms with precise N-coordination as superior oxygen reduction reaction catalysts. *Angew. Chem. Int. Ed.* **55**, 10800–10805 (2016). <https://doi.org/10.1002/anie.201604802>
16. J. Wang, H. Li, S. Liu, Y. Hu, J. Zhang, M. Xia, Y. Hou, J. Tse, J. Zhang, Y. Zhao, Turning on Zn 4s electrons in a N₂–Zn–B₂ configuration to stimulate remarkable ORR performance. *Angew. Chem. Int. Ed.* **60**, 181–185 (2021). <https://doi.org/10.1002/anie.202009991>

17. X. Zhu, R. Amal, X. Lu, N. P Co-coordinated manganese atoms in mesoporous carbon for electrochemical oxygen reduction. *Small* **15**, e1804524 (2019). <https://doi.org/10.1002/sml.201804524>
18. T.N. Nguyen, M. Salehi, Q.V. Le, A. Seifitokaldani, C.T. Dinh, Fundamentals of electrochemical CO₂ reduction on single-metal-atom catalysts. *ACS Catal.* **10**, 10068–10095 (2020). <https://doi.org/10.1021/acscatal.0c02643>
19. X. Wang, Y. Jia, X. Mao, L. Zhang, D. Liu, L. Song, X. Yan, J. Chen, D. Yang, J. Zhou, K. Wang, A. Du, X. Yao, A directional synthesis for topological defect in carbon. *Chemistry* **6**, 2009–2023 (2020). <https://doi.org/10.1016/j.chempr.2020.05.010>
20. S. Yang, Q. Cheng, J. Mao, Q. Xu, Y. Zhang, Y. Guo, T. Tan, W. Luo, H. Yang, Z. Jiang, Rational design of edges of covalent organic networks for catalyzing hydrogen peroxide production. *Appl. Catal. B* **298**, 120605 (2021). <https://doi.org/10.1016/j.apcatb.2021.120605>
21. A. Yu, G. Ma, L. Zhu, R. Zhang, Y. Li, S. Yang, H.-Y. Hsu, P. Peng, F.-F. Li, Conversion of CO₂ to defective porous carbons in one electro-redox cycle for boosting electrocatalytic H₂O₂ production. *Appl. Catal. B* **307**, 121161 (2022). <https://doi.org/10.1016/j.apcatb.2022.121161>
22. L. Lu, Y. Zhu, C. Shi, Y.T. Pei, Large-scale synthesis of defect-selective graphene quantum dots by ultrasonic-assisted liquid-phase exfoliation. *Carbon* **109**, 373–383 (2016). <https://doi.org/10.1016/j.carbon.2016.08.023>
23. S. Huo, P. Zhang, M. He, W. Zhang, B. Liang, M. Zhang, H. Wang, K. Li, Sustainable development of ultrathin porous carbon nanosheets with highly accessible defects from biomass waste for high-performance capacitive desalination. *Green Chem.* **23**, 8554–8565 (2021). <https://doi.org/10.1039/d1gc02576g>
24. H. Jiang, J. Gu, X. Zheng, M. Liu, X. Qiu, L. Wang, W. Li, Z. Chen, X. Ji, J. Li, (2019) Defect-rich and ultrathin n doped carbon nanosheets as advanced trifunctional metal-free electrocatalysts for the ORR, OER and HER. *Energy Environ. Sci.* **12**, 322–333. <https://doi.org/10.1039/c8ee03276a>
25. C. Xu, Y. Hei, J. Liu, M. Sun, T. Sha, N. Wang, M. Hassan, X. Bo, M. Zhou, Synthesis of a three-dimensional interconnected carbon nanorod aerogel from wax gourd for amperometric sensing. *Microchim. Acta* **185**, 482 (2018). <https://doi.org/10.1007/s00604-018-3008-y>
26. C. Ma, X. Zou, A. Li, Z. Gao, L. Luo, S. Shen, J. Zhang, Z. Huang, L. Zhu, Rapid flame synthesis of carbon doped defective ZnO for electrocatalytic CO₂ reduction to syngas. *Electrochim. Acta* **411**, 140098 (2022). <https://doi.org/10.1016/j.electacta.2022.140098>
27. J. Li, Y. Du, M. Zhang, J. Zhang, J. Mu, L. Gao, C. Zhang, X. Dai, Y. Ma, Tuning the electronic and optical properties of two-dimensional hydrogenated c-BN nanosheets by Be and C dopants and vacancy defects. *Chem. Phys.* **555**, 111441 (2022). <https://doi.org/10.1016/j.chemphys.2021.111441>
28. M. Honda, F. Tokuda, Y. Ichikawa, Effects of carbon defects on ZnO nanorods directly grown on graphene. *Jpn. J. Appl. Phys.* **56**, 110306 (2017). <https://doi.org/10.7567/jjap.56.110306>
29. J. Liu, Y. Guan, S. Liu, S. Li, C. Gao, J. Du, C. Qiu, D. Li, D. Zhang, X. Wang, Y. Wang, Y. Hu, Y. Rong, A. Mei, H. Han, Modulating oxygen vacancies in BaSnO₃ for printable carbon-based mesoscopic perovskite solar cells. *ACS Appl. Energy Mater.* **4**, 11032–11040 (2021). <https://doi.org/10.1021/acsaem.1c01966>
30. A. Csóré, N. Mukesh, G. Károlyházy, D. Beke, A. Gali, Photoluminescence spectrum of divacancy in porous and nanocrystalline cubic silicon carbide. *J. Appl. Phys.* **131**, 071102 (2022). <https://doi.org/10.1063/5.0080514>
31. L. Zong, K. Fan, W. Wu, L. Cui, L. Zhang, B. Johannessen, D. Qi, H. Yin, Y. Wang, P. Liu, L. Wang, H. Zhao, Anchoring single copper atoms to microporous carbon spheres as high-performance electrocatalyst for oxygen reduction reaction. *Adv. Func. Mater.* **31**, 2104864 (2021). <https://doi.org/10.1002/adfm.202104864>
32. Y. Wang, T. Zhou, K. Jiang, P. Da, Z. Peng, J. Tang, B. Kong, W.-B. Cai, Z. Yang, G. Zheng, Reduced mesoporous Co₃O₄ nanowires as efficient water oxidation electrocatalysts and supercapacitor electrodes. *Adv. Energy Mater.* **4**, 1400696 (2014). <https://doi.org/10.1002/aenm.201400696>

33. Y. Zeng, J. Zhong, H. Wang, M. Fu, D. Ye, Y. Hu, Synergistic effect of tunable oxygen-vacancy defects and graphene on accelerating the photothermal degradation of methanol over $\text{Co}_3\text{O}_4/\text{rGO}$ nanocomposites. *Chem. Eng. J.* **425**, 131658 (2021). <https://doi.org/10.1016/j.cej.2021.131658>
34. F. Studt, Catalysis by unusual vacancies. *Nat. Catal.* **4**, 184–185 (2021). <https://doi.org/10.1038/s41929-021-00593-2>
35. C. Tang, H.-F. Wang, X. Chen, B.-Q. Li, T.-Z. Hou, B. Zhang, Q. Zhang, M.-M. Titirici, F. Wei, Topological defects in metal-free nanocarbon for oxygen electrocatalysis. *Adv. Mater.* **28**, 6845–6851 (2016). <https://doi.org/10.1002/adma.201601406>
36. S. Yang, S. Xu, J. Tong, D. Ding, G. Wang, R. Chen, P. Jin, X.C. Wang, Overlooked role of nitrogen dopant in carbon catalysts for peroxymonosulfate activation: Intrinsic defects or extrinsic defects? *Appl. Catal. B* **295**, 120291 (2021). <https://doi.org/10.1016/j.apcatb.2021.120291>
37. Q. Fan, D. Martin-Jimenez, D. Ebeling, C.K. Krug, L. Brechmann, C. Kohlmeier, G. Hilt, W. Hieringer, A. Schirmeisen, J.M. Gottfried, Nanoribbons with nonalternant topology from fusion of polyazulene: Carbon allotropes beyond graphene. *J. Am. Chem. Soc.* **141**, 17713–17720 (2019). <https://doi.org/10.1021/jacs.9b08060>
38. F. Liu, B. He, Supermicroporous carbons with nitrogen and defect co-doped as high-efficient oxygen reduction catalysts in both alkaline and acidic medium. *Electrochim. Acta* **362**, 137225 (2020). <https://doi.org/10.1016/j.electacta.2020.137225>
39. Z. Xie, Y. Wang, Facile synthesis of MOF-derived $\text{Co}@\text{CoN}_x$ /bamboo-like carbon tubes for efficient electrocatalytic water oxidation. *Electrochim. Acta* **296**, 372–378 (2019). <https://doi.org/10.1016/j.electacta.2018.11.071>
40. J. Zhu, Y. Huang, W. Mei, C. Zhao, C. Zhang, J. Zhang, I.S. Amiinu, S. Mu, Effects of intrinsic pentagon defects on electrochemical reactivity of carbon nanomaterials. *Angew. Chem. Int. Ed.* **58**, 3859–3864 (2019). <https://doi.org/10.1002/anie.201813805>
41. H. Liu, H. Hu, J. Wang, P. Niehoff, X. He, E. Paillard, D. Eder, M. Winter, J. Li, Hierarchical ternary $\text{MoO}_2/\text{MoS}_2$ /heteroatom-doped carbon hybrid materials for high-performance lithium-ion storage. *ChemElectroChem* **3**, 922–932 (2016). <https://doi.org/10.1002/celec.201600062>
42. D. Li, Y. Jia, G. Chang, J. Chen, H. Liu, J. Wang, Y. Hu, Y. Xia, D. Yang, X. Yao, A defect-driven metal-free electrocatalyst for oxygen reduction in acidic electrolyte. *Chem* **4**, 2345–2356 (2018). <https://doi.org/10.1016/j.chempr.2018.07.005>
43. P. Yang, J. Zhang, D. Liu, M. Liu, H. Zhang, P. Zhao, C. Zhang, Facile synthesis of porous nitrogen-doped carbon for aerobic oxidation of amines to imines. *Microporous Mesoporous Mater.* **266**, 198–203 (2018). <https://doi.org/10.1016/j.micromeso.2018.03.002>
44. Y. Liu, Z. Gao, Synthesis of hierarchically porous nitrogen-doped carbon for sodium-ion batteries. *ChemElectroChem* **4**, 1059–1065 (2017). <https://doi.org/10.1002/celec.201600834>
45. N. Suo, H. Huang, X. Wang, X. Hou, Z. Shao, G. Zhang, Facile synthesis and electrocatalytic performance for oxygen reduction of boron-doped carbon catalysts on graphene sheets. *Fuel Cells* **21**, 328–336 (2021). <https://doi.org/10.1002/fuce.202000175>
46. N. Suo, H. Huang, A.M. Wu, G.Z. Cao, G.F. Zhang, A novel method of synthesizing boron-doped carbon catalysts. *Fuel Cells* **18**, 681–687 (2018). <https://doi.org/10.1002/fuce.201700233>
47. J. Su, X. Cao, J. Wu, C. Jin, J.-H. Tian, R. Yang, One-pot synthesis of boron-doped ordered mesoporous carbons as efficient electrocatalysts for the oxygen reduction reaction. *RSC Adv.* **6**, 24728–24737 (2016). <https://doi.org/10.1039/c6ra01296e>
48. H. Zhao, Z.-P. Hu, Y.-P. Zhu, L. Ge, Z.-Y. Yuan, P-doped mesoporous carbons for high-efficiency electrocatalytic oxygen reduction. *Chin. J. Catal.* **40**, 1366–1374 (2019). [https://doi.org/10.1016/s1872-2067\(19\)63363-2](https://doi.org/10.1016/s1872-2067(19)63363-2)
49. S. Yang, L. Zhi, K. Tang, X. Feng, J. Maier, K. Müllen, Efficient synthesis of heteroatom (N or S)-doped graphene based on ultrathin graphene oxide-porous silica sheets for oxygen reduction reactions. *Adv. Func. Mater.* **22**, 3634–3640 (2012). <https://doi.org/10.1002/adfm.201200186>

50. X. Zheng, Q. Zhang, T. Chen, Y. Wu, J. Hao, C. Tan, P. Chen, F. Wang, H. Liu, W. Lv, G. Liu, A novel synthetic carbon and oxygen doped stalactite-like g-C₃N₄ for broad-spectrum-driven indometacin degradation. *J. Hazard. Mater.* **386**, 121961 (2020). <https://doi.org/10.1016/j.jhazmat.2019.121961>
51. T. Wang, L. Xia, J.J. Yang, H. Wang, W.H. Fang, H. Chen, D. Tang, A.M. Asiri, Y. Luo, G. Cui, X. Sun, Electrocatalytic N₂-to-NH₃ conversion using oxygen-doped graphene: Experimental and theoretical studies. *Chem. Commun.* **55**, 7502–7505 (2019). <https://doi.org/10.1039/c9cc01999e>
52. S. Huo, M. Liu, L. Wu, M. Liu, M. Xu, W. Ni, Y.-M. Yan, Methanesulfonic acid-assisted synthesis of N/S co-doped hierarchically porous carbon for high performance supercapacitors. *J. Power Sources* **387**, 81–90 (2018). <https://doi.org/10.1016/j.jpowsour.2018.03.061>
53. W. Wang, P. Wang, Y. Kang, J. Zhao, P. Tao, Z. Lei, Flame synthesis of nitrogen, boron co-doped carbon as efficient electrocatalyst for oxygen reduction reaction. *Int. J. Hydrogen Energy* **44**, 4771–4779 (2019). <https://doi.org/10.1016/j.ijhydene.2019.01.022>
54. M. Liu, Y. Liu, Z. Gao, C. Wang, W. Ye, R. Lu, S. Zhang, Nitrogen and sulfur co-doped carbon nanospheres for highly efficient oxidation of ethylbenzene. *New J. Chem.* **42**, 15962–15967 (2018). <https://doi.org/10.1039/c8nj02948b>
55. L. Lin, Y. Wang, Y. Xiao, W. Liu, Hydrothermal synthesis of carbon dots codoped with nitrogen and phosphorus as a turn-on fluorescent probe for cadmium(ii). *Microchim. Acta* **186**, 147 (2019). <https://doi.org/10.1007/s00604-019-3264-5>
56. K. Yuan, C. Lu, S. Sfaelou, X. Liao, X. Zhuang, Y. Chen, U. Scherf, X. Feng, In situ nanoarchitecturing and active-site engineering toward highly efficient carbonaceous electrocatalysts. *Nano Energy* **59**, 207–215 (2019). <https://doi.org/10.1016/j.nanoen.2019.02.043>
57. B. Huang, Y. Liu, X. Huang, Z. Xie, Multiple heteroatom-doped few-layer carbons for the electrochemical oxygen reduction reaction. *J. Mater. Chem. A* **6**, 22277–22286 (2018). <https://doi.org/10.1039/c8ta06743k>
58. H. Yin, H. Xia, S. Zhao, K. Li, J. Zhang, S. Mu, Atomic level dispersed metal-nitrogen-carbon catalyst toward oxygen reduction reaction: Synthesis strategies and chemical environmental regulation. *Energy Environ. Mater.* **4**, 5–18 (2020). <https://doi.org/10.1002/eem2.12085>
59. S. Ding, H.-A. Chen, O. Mekasuwandumrong, M.J. Hülsey, X. Fu, Q. He, J. Panpranot, C.-M. Yang, N. Yan, High-temperature flame spray pyrolysis induced stabilization of Pt single-atom catalysts. *Appl. Catal. B* **281**, 119471 (2021). <https://doi.org/10.1016/j.apcatb.2020.119471>
60. S. Zhao, J. Lin, P. Wu, C. Ye, Y. Li, A. Li, X. Jin, Y. Zhao, G. Chen, Y. Qiu, D. Ye, A hydrothermally stable single-atom catalyst of Pt supported on high-entropy oxide/Al₂O₃: Structural optimization and enhanced catalytic activity. *ACS Appl. Mater. Interfaces.* **13**, 48764–48773 (2021). <https://doi.org/10.1021/acsami.1c14456>
61. Y. Shi, W.-M. Huang, J. Li, Y. Zhou, Z.-Q. Li, Y.-C. Yin, X.-H. Xia, Site-specific electrodeposition enables self-terminating growth of atomically dispersed metal catalysts. *Nat. Commun.* **11**, 4558 (2020). <https://doi.org/10.1038/s41467-020-18430-8>
62. V. Muravev, G. Spezzati, Y.-Q. Su, A. Parastaev, F.-K. Chiang, A. Longo, C. Escudero, N. Kosinov, E.J.M. Hensen, Interface dynamics of Pd-CeO₂ single-atom catalysts during CO oxidation. *Nat. Catal.* **4**, 469–478 (2021). <https://doi.org/10.1038/s41929-021-00621-1>
63. Y. Zhou, E. Song, W. Chen, C.U. Segre, J. Zhou, Y.C. Lin, C. Zhu, R. Ma, P. Liu, S. Chu, T. Thomas, M. Yang, Q. Liu, K. Suenaga, Z. Liu, J. Liu, J. Wang, Dual-metal interbonding as the chemical facilitator for single-atom dispersions. *Adv. Mater.* **32**, 2003484 (2020). <https://doi.org/10.1002/adma.202003484>
64. X. Li, Q. Zhou, S. Wang, Y. Li, Y. Liu, Q. Gao, Q. Wu, Tuning the coordination environment to effect the electrocatalytic behavior of a single-atom catalyst toward the nitrogen reduction reaction. *J. Phys. Chem. C* **125**, 11963–11974 (2021). <https://doi.org/10.1021/acs.jpcc.1c02161>
65. Y. Shao, Z. Zha, H. Wang, Heteroatom-doped porous carbon-supported single-atom catalysts for electrocatalytic energy conversion. *J. Energy Chem.* **63**, 54–73 (2021). <https://doi.org/10.1016/j.ijechem.2021.04.041>

66. J. Guo, J. Huo, Y. Liu, W. Wu, Y. Wang, M. Wu, H. Liu, G. Wang, Nitrogen-doped porous carbon supported nonprecious metal single-atom electrocatalysts: From synthesis to application. *Small Methods* **3**, 1900159 (2019). <https://doi.org/10.1002/smtd.201900159>
67. X. Zhang, X. Xu, S. Yao, C. Hao, C. Pan, X. Xiang, Z.Q. Tian, P.K. Shen, Z. Shao, S.P. Jiang, Boosting electrocatalytic activity of single atom catalysts supported on nitrogen-doped carbon through N coordination environment engineering. *Small* **18**, 2105329 (2022). <https://doi.org/10.1002/smll.202105329>
68. D.L. Boxall, G.A. Deluga, E.A. Kenik, W.D. King, C.M. Lukehart, Rapid synthesis of a Pt₁Ru₁/carbon nanocomposite using microwave irradiation: A DMFC anode catalyst of high relative performance. *Chem. Mater.* **13**, 891–900 (2001). <https://doi.org/10.1021/cm000652m>
69. J. Zhang, H. Zhao, J. Li, H. Jin, X. Yu, Y. Lei, S. Wang, In situ encapsulation of iron complex nanoparticles into biomass-derived heteroatom-enriched carbon nanotubes for high-performance supercapacitors. *Adv. Energy Mater.* **9**, 1803221 (2019). <https://doi.org/10.1002/aenm.201803221>
70. C.-L. Yang, L.-N. Wang, P. Yin, J. Liu, M.-X. Chen, Q.-Q. Yan, Z.-S. Wang, S.-L. Xu, S.-Q. Chu, C. Cui, H. Ju, J. Zhu, Y. Lin, J. Shui, H.-W. Liang, Sulfur-anchoring synthesis of platinum intermetallic nanoparticle catalysts for fuel cells. *Science* **374**, 459–464 (2021). <https://doi.org/10.1126/science.abj9980>
71. J. Tzadikov, R. Geva, A. Azoulay, M. Shalom, Facile synthesis of carbon-sulfur scaffold with transition-metal sulfides and oxides as efficient electrocatalysts for oxygen evolution reaction. *ChemCatChem* **13**, 3749–3753 (2021). <https://doi.org/10.1002/cctc.202100572>
72. J. Zhu, Q. Lai, Y. Zhao, J. Zhong, Y. Liang, An effective FeCl₃ template assisted synthesis of nitrogen, sulfur and iron-tridoped carbon nanosheets from a protic salt for oxygen reduction electrocatalysis. *Chin. J. Catal.* **39**, 1453–1462 (2018). [https://doi.org/10.1016/s1872-2067\(18\)63124-9](https://doi.org/10.1016/s1872-2067(18)63124-9)
73. K. Liu, X. Zhao, G. Ren, T. Yang, Y. Ren, A.F. Lee, Y. Su, X. Pan, J. Zhang, Z. Chen, J. Yang, X. Liu, T. Zhou, W. Xi, J. Luo, C. Zeng, H. Matsumoto, W. Liu, Q. Jiang, K. Wilson, A. Wang, B. Qiao, W. Li, T. Zhang, Strong metal-support interaction promoted scalable production of thermally stable single-atom catalysts. *Nat. Commun.* **11**, 1263 (2020). <https://doi.org/10.1038/s41467-020-14984-9>
74. Y. Qiao, P. Yuan, Y. Hu, J. Zhang, S. Mu, J. Zhou, H. Li, H. Xia, J. He, Q. Xu, Sulfuration of an Fe–N–C catalyst containing Fe_xC/Fe species to enhance the catalysis of oxygen reduction in acidic media and for use in flexible Zn-air batteries. *Adv. Mater.* **30**, e1804504 (2018). <https://doi.org/10.1002/adma.201804504>
75. M. Liu, N. Li, S. Cao, X. Wang, X. Lu, L. Kong, Y. Xu, X.H. Bu, A “pre-constrained metal twins” strategy to prepare efficient dual-metal-atom catalysts for cooperative oxygen electrocatalysis. *Adv. Mater.* **34**, 2107421 (2022). <https://doi.org/10.1002/adma.202107421>
76. M. Tan, T. He, J. Liu, H. Wu, Q. Li, J. Zheng, Y. Wang, Z. Sun, S. Wang, Y. Zhang, Supramolecular bimetallogels: A nanofiber network for bimetal/nitrogen co-doped carbon electrocatalysts. *J. Mater. Chem. A* **6**, 8227–8232 (2018). <https://doi.org/10.1039/c8ta01898g>
77. W. Zhang, S. Wang, F. Yang, Z. Yang, H. Wei, Y. Yang, J. Wei, Synthesis of catalytically active bimetallic nanoparticles within solution-processable metal-organic-framework scaffolds. *CrystrEngComm* **21**, 3954–3960 (2019). <https://doi.org/10.1039/c9ce00238c>
78. A.A. Vasilev, M.I. Ivantsov, E.L. Dzidziguri, M.N. Efimov, D.G. Muratov, M.V. Kulikova, N.A. Zhilyaeva, G.P. Karpacheva, Size effect of the carbon-supported bimetallic Fe–Co nanoparticles on the catalytic activity in the fischer-tropsch synthesis. *Fuel* **310**, 122455 (2022). <https://doi.org/10.1016/j.fuel.2021.122455>
79. L.-J. Zuo, S.-L. Xu, A. Wang, P. Yin, S. Zhao, H.-W. Liang, High-temperature synthesis of carbon-supported bimetallic nanocluster catalysts by enlarging the interparticle distance. *Inorg. Chem.* **61**, 2719–2723 (2022). <https://doi.org/10.1021/acs.inorgchem.1c03965>
80. M.A. Alvi, M.S. Akhtar, An effective and low cost Pd Ce bimetallic decorated carbon nanofibers as electro-catalyst for direct methanol fuel cells applications. *J. Alloy. Compd.* **684**, 524–529 (2016). <https://doi.org/10.1016/j.jallcom.2016.05.101>

81. B. Wurster, D. Grumelli, D. Hotger, R. Gutzler, K. Kern, Driving the oxygen evolution reaction by nonlinear cooperativity in bimetallic coordination catalysts. *J. Am. Chem. Soc.* **138**, 3623–3626 (2016). <https://doi.org/10.1021/jacs.5b10484>
82. X. Li, X. Huang, S. Xi, S. Miao, J. Ding, W. Cai, S. Liu, X. Yang, H. Yang, J. Gao, J. Wang, Y. Huang, T. Zhang, B. Liu, Single cobalt atoms anchored on porous N-doped graphene with dual reaction sites for efficient fenton-like catalysis. *J. Am. Chem. Soc.* **140**, 12469–12475 (2018). <https://doi.org/10.1021/jacs.8b05992>
83. G. Yang, J. Zhu, P. Yuan, Y. Hu, G. Qu, B.A. Lu, X. Xue, H. Yin, W. Cheng, J. Cheng, W. Xu, J. Li, J. Hu, S. Mu, J.N. Zhang, Regulating Fe-spin state by atomically dispersed Mn–N in Fe–N–C catalysts with high oxygen reduction activity. *Nat. Commun.* **12**, 1734 (2021). <https://doi.org/10.1038/s41467-021-21919-5>
84. M.B.Z. Hegazy, M.R. Berber, Y. Yamauchi, A. Pakdel, R. Cao, U.-P. Apfel, Synergistic electrocatalytic hydrogen evolution in Ni/NiS nanoparticles wrapped in multi-heteroatom-doped reduced graphene oxide nanosheets. *ACS Appl. Mater. Interfaces.* **13**, 34043–34052 (2021). <https://doi.org/10.1021/acsami.1c05888>
85. L. Guo, S. Hwang, B. Li, F. Yang, M. Wang, M. Chen, X. Yang, S.G. Karakalos, D.A. Cullen, Z. Feng, G. Wang, G. Wu, H. Xu, Promoting atomically dispersed Mn₄ sites via sulfur doping for oxygen reduction: Unveiling intrinsic activity and degradation in fuel cells. *ACS Nano* **15**, 6886–6899 (2021). <https://doi.org/10.1021/acs.nano.0c10637>
86. L. Zhao, Y. Zhang, L.-B. Huang, X.-Z. Liu, Q.-H. Zhang, C. He, Z.-Y. Wu, L.-J. Zhang, J. Wu, W. Yang, L. Gu, J.-S. Hu, L.-J. Wan, Cascade anchoring strategy for general mass production of high-loading single-atomic metal-nitrogen catalysts. *Nat. Commun.* **10**, 1278 (2019). <https://doi.org/10.1038/s41467-019-09290-y>
87. C.H. Choi, M. Kim, H.C. Kwon, S.J. Cho, S. Yun, H.-T. Kim, K.J.J. Mayrhofer, H. Kim, M. Choi, Tuning selectivity of electrochemical reactions by atomically dispersed platinum catalyst. *Nat. Commun.* **7**, 10922 (2016). <https://doi.org/10.1038/ncomms10922>
88. D. Sun, L. Ye, F. Sun, H. García, Z. Li, From mixed-metal mofs to carbon-coated core–shell metal alloy@metal oxide solid solutions: Transformation of Co/Ni-MOF-74 to Co_xNi_{1-x}@Co_yNi_{1-y}O@C for the oxygen evolution reaction. *Inorg. Chem.* **56**, 5203–5209 (2017). <https://doi.org/10.1021/acs.inorgchem.7b00333>
89. K. Yang, H. Fu, Y. Duan, M. Wang, M.X. Tran, J.K. Lee, W. Yang, G. Liu, Uniform metal sulfide@N-doped carbon nanospheres for sodium storage: Universal synthesis strategy and superior performance. *Energy Environ. Mater.* (2022). <https://doi.org/10.1002/eam2.12380>
90. W. Li, R. Zhao, K. Zhou, C. Shen, X. Zhang, H. Wu, L. Ni, H. Yan, G. Diao, M. Chen, Cage-structured M_xP_y@CNCs (M = Co and Zn) from MOF confined growth in carbon nanocages for superior lithium storage and hydrogen evolution performance. *J. Mater. Chem. A* **7**, 8443–8450 (2019). <https://doi.org/10.1039/c9ta00054b>
91. B.K. Kang, Y.J. Choi, H.W. Choi, S.B. Kwon, S. Kim, Y.J. Kim, J.S. Park, W.S. Yang, D.H. Yoon, W.-H. Ryu, Rational design and in-situ formation of nickel–cobalt nitride multi-core/hollow N-doped carbon shell anode for Li-ion batteries. *Chem. Eng. J.* **420**, 129630 (2021). <https://doi.org/10.1016/j.cej.2021.129630>
92. J. Nishijo, C. Okabe, O. Oishi, N. Nishi, Synthesis, structures and magnetic properties of carbon-encapsulated nanoparticles via thermal decomposition of metal acetylide. *Carbon* **44**, 2943–2949 (2006). <https://doi.org/10.1016/j.carbon.2006.05.037>
93. X. Li, X. Liu, Y. Xiang, Q. Zheng, X. Wei, D. Lin, Metal-organic frameworks derived carbon-coated ZnSe/Co_{0.85}Se@N-doped carbon microcuboid as an advanced anode material for sodium-ion batteries. *Chin. Chem. Lett.* (2021). <https://doi.org/10.1016/j.ccllet.2021.10.014>
94. H.-S. Park, S.-B. Han, D.-H. Kwak, J.-H. Han, K.-W. Park, Fe nanoparticles encapsulated in doped graphitic shells as high-performance and stable catalysts for oxygen reduction reaction in an acid medium. *J. Catal.* **370**, 130–137 (2019). <https://doi.org/10.1016/j.jcat.2018.12.015>
95. Z. Peng, Y. Yu, D. Jiang, Y. Wu, B.Y. Xia, Z. Dong, N-doped carbon shell coated CoP nanocrystals encapsulated in porous N-doped carbon substrate as efficient electrocatalyst of water splitting. *Carbon* **144**, 464–471 (2019). <https://doi.org/10.1016/j.carbon.2018.12.085>

96. R. Li, H. Yuan, Z. Ma, B. Tang, J. Li, X. Wang, Facile coupling of content design and efficient modulation on the activity of CNT-supported PdAgCu nanoparticle electrocatalysts: Leaching lift-up and annealing fall-off. *Electrochim. Acta* **293**, 149–159 (2019). <https://doi.org/10.1016/j.electacta.2018.10.024>
97. Y. Guo, P. Yuan, J. Zhang, H. Xia, F. Cheng, M. Zhou, J. Li, Y. Qiao, S. Mu, Q. Xu, Co₂P-CoN double active centers confined in N-doped carbon nanotube: Heterostructural engineering for trifunctional catalysis toward HER, ORR, OER, and Zn-air batteries driven water splitting. *Adv. Func. Mater.* **28**, 1805641 (2018). <https://doi.org/10.1002/adfm.201805641>
98. Y. Wang, H.J. Zhang, L. Lu, L.P. Stubbs, C.C. Wong, J. Lin, Designed functional systems from peapod-like Co@carbon to Co₃O₄@carbon nanocomposites. *ACS Nano* **4**, 4753–4761 (2010). <https://doi.org/10.1021/nn1004183>
99. J. Zhang, K. Wang, Q. Xu, Y. Zhou, F. Cheng, S. Guo, Beyond yolk-shell nanoparticles: Fe₃O₄@Fe₃C core@shell nanoparticles as yolks and carbon nanospindles as shells for efficient lithium ion storage. *ACS Nano* **9**, 3369–3376 (2015). <https://doi.org/10.1021/acsnano.5b00760>
100. X. Pan, X. Bao, The effects of confinement inside carbon nanotubes on catalysis. *Acc. Chem. Res.* **44**, 553–562 (2011). <https://doi.org/10.1021/ar100160t>
101. D. Kuang, L. Hou, S. Wang, H. Luo, L. Deng, J.L. Mead, H. Huang, M. Song, Large-scale synthesis and outstanding microwave absorption properties of carbon nanotubes coated by extremely small FeCo–C core-shell nanoparticles. *Carbon* **153**, 52–61 (2019). <https://doi.org/10.1016/j.carbon.2019.06.105>
102. Y.P. Chen, L. Zhang, J.J. Feng, X.S. Li, A.J. Wang, Water-regulated and bioinspired one-step pyrolysis of iron-cobalt nanoparticles-capped carbon nanotubes/porous honeycombed nitrogen-doped carbon composite for highly efficient oxygen reduction. *J. Colloid Interface Sci.* **618**, 352–361 (2022). <https://doi.org/10.1016/j.jcis.2022.03.083>
103. L. Liu, F. Gao, P. Concepción, A. Corma, A new strategy to transform mono and bimetallic non-noble metal nanoparticles into highly active and chemoselective hydrogenation catalysts. *J. Catal.* **350**, 218–225 (2017). <https://doi.org/10.1016/j.jcat.2017.03.014>
104. Y. Hu, J.O. Jensen, W. Zhang, L.N. Cleemann, W. Xing, N.J. Bjerrum, Q. Li, Hollow spheres of iron carbide nanoparticles encased in graphitic layers as oxygen reduction catalysts. *Angew. Chem. Int. Ed.* **53**, 3675–3679 (2014). <https://doi.org/10.1002/anie.201400358>
105. Y. Shen, Y. Zhou, D. Wang, X. Wu, J. Li, J. Xi, Nickel-copper alloy encapsulated in graphitic carbon shells as electrocatalysts for hydrogen evolution reaction. *Adv. Energy Mater.* **8**, 1701759 (2018). <https://doi.org/10.1002/aenm.201701759>
106. P. Liu, R. Qin, G. Fu, N. Zheng, Surface coordination chemistry of metal nanomaterials. *J. Am. Chem. Soc.* **139**, 2122–2131 (2017). <https://doi.org/10.1021/jacs.6b10978>
107. J. Wang, N. Zang, C. Xuan, B. Jia, W. Jin, T. Ma, Self-supporting electrodes for gas-involved key energy reactions. *Adv. Func. Mater.* **31**, 2104620 (2021). <https://doi.org/10.1002/adfm.202104620>
108. T.Y. Yoo, J.M. Yoo, A.K. Sinha, M.S. Bootharaju, E. Jung, H.S. Lee, B.-H. Lee, J. Kim, W.H. Antink, Y.M. Kim, J. Lee, E. Lee, D.W. Lee, S.-P. Cho, S.J. Yoo, Y.-E. Sung, T. Hyeon, Direct synthesis of intermetallic platinum-alloy nanoparticles highly loaded on carbon supports for efficient electrocatalysis. *J. Am. Chem. Soc.* **142**, 14190–14200 (2020). <https://doi.org/10.1021/jacs.0c05140>
109. H. Jin, J. Wang, D. Su, Z. Wei, Z. Pang, Y. Wang, In situ cobalt-cobalt oxide/N-doped carbon hybrids as superior bifunctional electrocatalysts for hydrogen and oxygen evolution. *J. Am. Chem. Soc.* **137**, 2688–2694 (2015). <https://doi.org/10.1021/ja5127165>
110. Y. Yu, W. Gao, Z. Shen, Q. Zheng, H. Wu, X. Wang, W. Song, K. Ding, A novel Ni₃N/graphene nanocomposite as supercapacitor electrode material with high capacitance and energy density. *J. Mater. Chem. A* **3**, 16633–16641 (2015). <https://doi.org/10.1039/c5ta03830h>
111. B. Guan, Y. Zhang, L. Fan, X. Wu, M. Wang, Y. Qiu, N. Zhang, K. Sun, Blocking polysulfide with Co₂B@CNT via “synergetic adsorptive effect” toward ultrahigh-rate capability and robust lithium-sulfur battery. *ACS Nano* **13**, 6742–6750 (2019). <https://doi.org/10.1021/acsnano.9b01329>

112. Y. Qiao, P. Yuan, C.-W. Pao, Y. Cheng, Z. Pu, Q. Xu, S. Mu, J. Zhang, Boron-rich environment boosting ruthenium boride on B, N doped carbon outperforms platinum for hydrogen evolution reaction in a universal pH range. *Nano Energy* **75**, 104881 (2020). <https://doi.org/10.1016/j.nanoen.2020.104881>
113. N.M. Rodriguez, M.-S. Kim, R.T.K. Baker, Carbon nanofibers: A unique catalyst support medium. *J. Phys. Chem.* **98**, 13108–13111 (2002). <https://doi.org/10.1021/j100101a003>
114. H. Shang, C. Liu, Y. Xu, J. Qiu, F. Wei, States of carbon nanotube supported Mo-based HDS catalysts. *Fuel Process. Technol.* **88**, 117–123 (2007). <https://doi.org/10.1016/j.fuproc.2004.08.010>
115. M. Zeng, X.X. Wang, Z.H. Tan, X.X. Huang, J.N. Wang, Remarkable durability of pPt-Ir alloy catalysts supported on graphitic carbon nanocages. *J. Power Sources* **264**, 272–281 (2014). <https://doi.org/10.1016/j.jpowsour.2014.04.097>
116. D. Ji, S. Peng, L. Fan, L. Li, X. Qin, S. Ramakrishna, Thin MoS₂ nanosheets grafted mofs-derived porous Co–N–C flakes grown on electrospun carbon nanofibers as self-supported bifunctional catalysts for overall water splitting. *J. Mater. Chem. A* **5**, 23898–23908 (2017). <https://doi.org/10.1039/c7ta08166a>
117. W. Li, Y. Niu, X. Wu, F. Wu, T. Li, W. Hu, Heterostructured CoSe₂/FeSe₂ nanoparticles with abundant vacancies and strong electronic coupling supported on carbon nanorods for oxygen evolution electrocatalysis. *ACS Sustain. Chem. Eng.* **8**, 4658–4666 (2020). <https://doi.org/10.1021/acssuschemeng.0c00839>

Chapter 3

Characterization



Miaoying Chen, Dongping Xue, and Bang-An Lu

Abstract The characterization approach is one of the most challenging aspects of researching carbon-based nanomaterials, particularly carbon-based catalysts with defects and atomically dispersion. It's difficult to precisely identify the active sites of catalysts using early characterization approaches, which makes disclosing the catalytic mechanism and constructing high-efficiency catalysts challenging. High-efficiency carbon-based catalysts have improved in recent years, thanks to extensive use of current characterization techniques (e.g., *ex-situ*, *in-situ*, and operando) and simulation calculation approaches (e.g., first-principles and molecular dynamics simulation calculations). This chapter emphasizes the characterization methodologies that reveal the true active sites, catalytic processes, and structure–activity relationships of carbon-based nanomaterials from three perspectives: direct visualization, indirect validation, and simulation calculations.

3.1 Introduction

Carbon-based nanomaterials utilized for energy storage and transformation must be described and studied in terms of shape, size, surface structure, stability, and the interaction between materials and their environment [1–3]. Defects and heteroatoms can be used to effectively control the electronic structure of catalyst active sites and stimulate the production and transition of reaction intermediates, which is helpful to specific electrochemical reactions [4–6]. However, the current characterization techniques for the electronic structure of defects and heteroatoms are not comprehensive

M. Chen · D. Xue · B.-A. Lu (✉)
College of Materials Science and Engineering, Zhengzhou University, Zhengzhou 450001,
P. R. China
e-mail: balu@zzu.edu.cn

M. Chen
e-mail: chenmiaoying11@163.com

D. Xue
e-mail: xdongping1231@126.com

enough, and more research is still needed to explore the relationship between defects, heteroatoms and electrocatalytic activity. Carbon electrons can hybridize with one of three different electronic orbitals: sp , sp^2 , and sp^3 , and carbon-based entities display nanomaterial properties such as surface and interface effects and quantum size effects. Because of these numerous complex effects, studies on the characterization methods of carbon-based nanomaterials, specifically defects and atomic dispersion carbon-based catalysts, are complicated. It is difficult to use early characterization methods to accurately identify catalytic active sites in different electrocatalytic reactions to fully understand the experimental role of different active site types in different electrocatalytic reactions, posing significant challenges in uncovering the catalytic mechanism and designing efficient catalysts [7–9].

With the widespread use of modern nanomaterial characterization techniques (such as *ex-situ*, *in-situ*, and operando) and simulation calculation methods in recent years (such as first-principles and molecular dynamics simulation calculation), [10–12] especially the establishment and development of various *in-situ* spectroscopy methods, high-efficiency carbon-based catalysts have developed rapidly. Understanding materials at the atomic and molecular levels have two critical implications for nanomaterials development [13, 14]. As a result, research on carbon-based catalysts shifts from the traditional mode of material synthesis and performance testing to the mode of rational design and performance management based on the structure–activity connection. For example, Wu et al. [15] used scanning electron microscopy (SEM) and transmission electron microscopy (TEM) to determine the interaction force (covalent bond, van der Waals force, and hydrogen bond) between host and guest in carbon materials, and determined the structure–activity relationship by combining electrochemical properties, thus improving electrocatalytic performance. Liu et al. [16] compared diamond graphite core–shell structure supported Pd catalysts (1% Pd/ND@G), onion-like carbon (OLC) supported Pd catalysts (1% Pd/OLC), traditional carbon nanotubes (CNTs) supported Pd catalysts (1% Pd/CNTs), and commercial carbon-supported Pd catalysts (commercial Pd/C) and discovered that the strong metal-support interaction (SMSI) between Pd nanoclusters and defective graphene shells.

The characterization of material is important to identify the active sites, understand the reaction mechanism, and further improve the electrocatalytic performance of carbon-based nanomaterials by using *in-situ* and operando characterization techniques that can monitor catalyst surface evolution and atomic structure changes in real time [17, 18]. For example, using *in-situ* infrared detection (also known as surface-enhanced infrared absorption spectroscopy, SEIRAS), the Seh's group discovered that the intermediates of the CO₂ reduction reaction differed depending on the presence of other catalysts, thereby determining the reaction pathway [19]. Using operando X-ray absorption spectroscopy, Wang et al. discovered that during CO₂ reduction, the structure and oxidation state of the catalyst surface changed from Cu(ii) phthalocyanine to Cu nanoclusters [9].

For carbon-based nanomaterials, this chapter describes the characterization approaches for revealing the true active sites, catalytic mechanism, and structure–activity relationship. SEM, TEM, aberration correction-scanning transmission electron microscopy (AC-STEM), and similar techniques can provide a clear picture of a material’s structure and element distribution. All these techniques can be used to gain information about the structure of individual elements in a material; this information can then be used to infer the overall structure. Using simulation and computation, one may confirm current carbon-based material forms and changes in their catalytic process. Carbon-based nanomaterials can now be used in practical applications thanks to a mathematical model and results that are in agreement with those obtained in the lab [20–22] (Fig. 3.1).

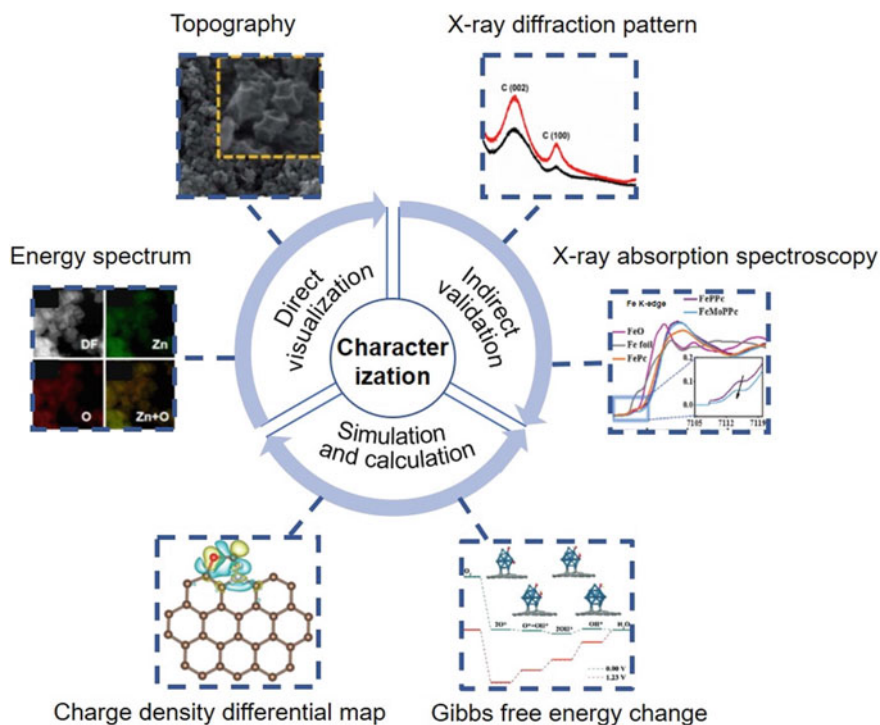


Fig. 3.1 Classification of characterization techniques for carbon-based nanomaterials. Reproduced with permission [20]. Copyright 2018, WILEY–VCH. Reproduced with permission [21]. Copyright 2021, WILEY–VCH. Reproduced with permission [22]. Copyright 2019, WILEY–VCH

3.2 Direct Visualization

It refers to the use of computer image processing to directly visualize collected signal data without additional processing. With the use of SEM, TEM, scanning tunneling microscope (STM), energy dispersive spectrometer (EDS), electron energy loss spectrum (EELS) and other methods of characterization, it is possible to see details about carbon-based nanomaterials, such as their surface morphology, structure, element distribution, and atomic coordination state. This chapter summarizes and analyzes the most commonly used methods for detecting carbon-based materials in order to provide readers with more in-depth study on related topics.

3.2.1 *Scanning Electron Microscope and Transmission Electron Microscope*

SEM can visually observe the surface morphology of samples [23, 24]. However, due to the low resolution of SEM, it is difficult to capture signals at the atomic or molecular scale [25, 26], which hinders understanding the catalytic mechanism of carbon-based catalysts at the atomic level. TEM has a higher resolution compared with SEM, so it plays a vital role in the direct imaging of the catalytic center (the size and morphology of the catalytic metal species) of the atomic-level heterogeneous carbon-based catalyst [25], especially the resolution of the AC-TEM has been significantly improved [23]. It can achieve high-quality imaging with single-atom resolution, which can deepen the understanding of the catalytic mechanism of carbon-based catalysts at the atomic level. As an additional feature, selected area electron diffraction (SAED) can be used to determine the crystal structure of carbon-based nanomaterials.

The support and surface morphology of electrocatalysts will affect various physical properties (such as particle size, dispersion, and specific surface area) and their electrochemical properties (such as activity and stability) [30]. It also affects the electron conduction and mass transfer of catalysts. Carbon-based nanomaterials are often used as ideal catalyst supports because of their high specific surface area, high thermal stability, and good electrical conductivity [30, 31]. SEM can directly observe the surface morphology of carbon support, which plays a vital role in studying the relationship between the structure (such as mass transfer channel, pore size, and distribution, etc.) and electrochemical performance of carbon-based nanomaterials. For example, Lee et al. [27] formed LbL-MWNT/MnO₂ (Layer-by-layer-multi-walled carbon nanotubes/MnO₂) electrodes by using an electrochemical deposition method, utilizing the high electrical conductivity of MWNTs and the porous structure of LbL-MWNT films to effectively promote MnO₂ energy storage. In Fig. 3.2a, b, the assembled LbL-MWNT films have a porous network structure, and the MWNT surface is covered with a uniform thickness of porous MnO₂ film with the progress of electrochemical deposition. The interface between the ITO glass substrate and the

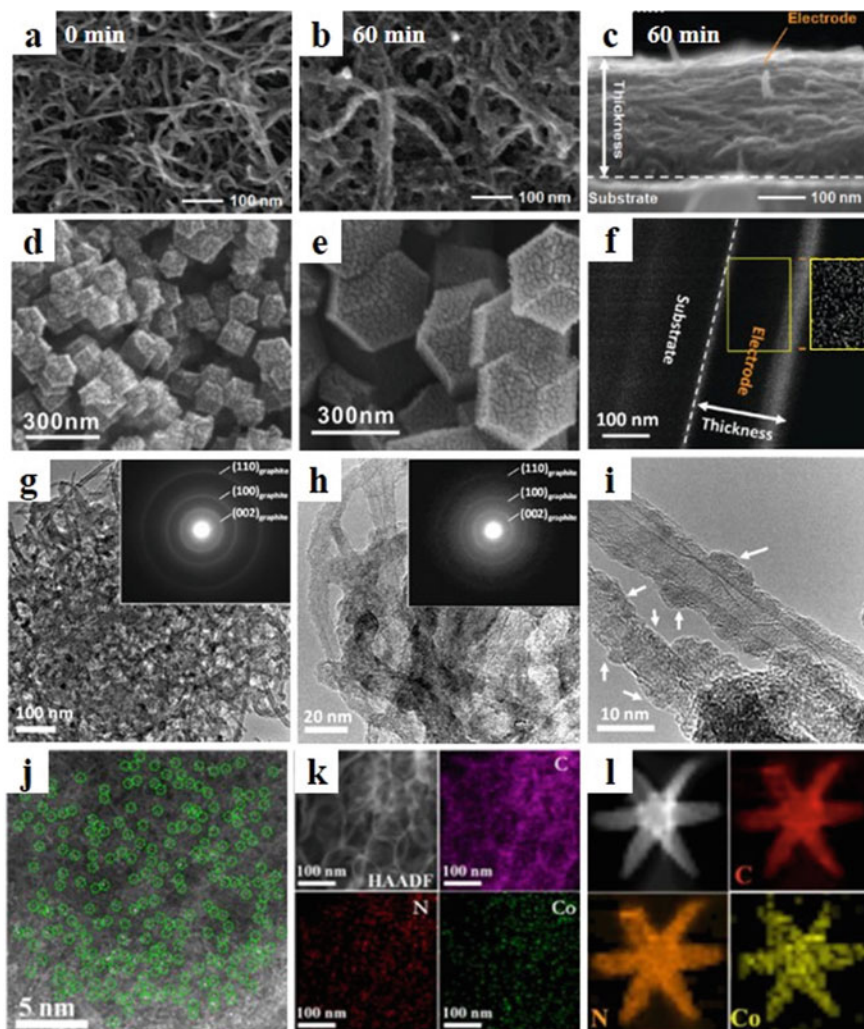


Fig. 3.2 SEM, TEM, and EDS images. **a** SEM images of pristine LbL-MWNT electrode. **b** SEM images and **c** cross-section view of LbL-MWNT/MnO₂ electrodes prepared by dipping LbL-MWNT electrodes into 0.1 M KMnO₄/0.1 M K₂SO₄ solution at a deposition of 60 min. Reproduced with permission [27]. Copyright 2010, American Chemical Society. **d** SEM images of N-C. **e** SEM images of Fe-N-C. Reproduced with permission [20]. Copyright 2018, WILEY-VCH. **f** Cross-section SEM image and elemental mapping of Mn for an LbL-MWNT/MnO₂ electrode (60 min dipping). Reproduced with permission [27]. Copyright 2010, American Chemical Society. **g** TEM image with selected-area diffraction pattern (SAED) of an LbL-MWNT. **h** TEM of an LbL-MWNT/MnO₂ electrode (10 bilayers, 60 min dipping). **i** High-magnification image of an LbL-MWNT/MnO₂ electrode (60 min dipping). Reproduced with permission [27]. Copyright 2010, American Chemical Society. **j** AC HAADF-STEM image of ISAS-Co/HNCS. **k** HAADF-STEM image and corresponding EDS of ISAS-Co/HNCS. Reproduced with permission [28]. Copyright 2017, American Chemical Society. **l** EDS of the CoSA-N-C. Reproduced with permission [29]. Copyright 2020, Elsevier

electrode is shown in the cross-sectional view (Fig. 3.2c), indicating the formation of a nanocomposite electrode of uniform thickness, and the cross-sectional view and the elemental mapping of Mn (Fig. 3.2f) show a uniform distribution of Mn on the electrodes, further confirming that MnO_2 is uniformly distributed on the LbL-MWNT films. Wang et al. [20] used ZIF-8 as the catalytic carbon precursor, due to the unique cavity structure (pore size 3.4 Å, cavity diameter 11 Å) of ZIF-8, to prepare Fe–N–C monatomic catalyst, in which the network of ZIF-8 can not only prevent the agglomeration of Fe atoms, but also protect and fix the position of Fe atoms. Figure 3.2d, e show that N–C and Fe–N–C after pyrolysis both retain the rhombic dodecahedron porous structure of ZIF-8 with a high specific surface area. TEM with atomic resolution can obtain the internal structure information of carbon-based nanomaterials, visualize the specific position details of the physical state of carbon-based catalysts, and identify the existing forms of metals (the existing forms of atoms or clusters) and the positions of metals on carbon supports [26]. Choi et al. [32] reported a sulfur-doped zeolite template carbon. The TEM image shows that with the increase of doped sulfur content, Pt clusters change from 4 nm to 1–2 nm and finally are highly dispersed. Lee et al. [27] used TEM and SAED to analyze the crystallinity of MnO_2 and the microstructure of the electrodes prepared by experiments. As shown in Fig. 3.2g, the multi-walled carbon nanotubes in LbL-MWNT films are randomly oriented and form a porous network structure. The SAED illustrations correspond to the (002), (100), and (110) crystal planes of graphite. Figure 3.2h is the TEM picture of LbL-MWNT/ MnO_2 electrode formed after 10 bilayers of LbL-MWNT film were immersed in KMnO_4 solution for 60 min, which shows that MnO_2 with uniform thickness was formed on the film surface, and the unchanged SAED picture shows that the carbon support is stable before and after immersion, and MnO_2 deposited on LbL-MWNT film is amorphous. The white arrows in Fig. 3.2i indicate that MnO_2 nanoparticles are uniformly distributed on MWNT.

However, TEM is insensitive to distinguishing the different oxidation states of the same elements. Fortunately, this can be overcome by combining scanning transmission electron microscopy of the high-angle annular dark-field with spectrometers sensitive to elements and electronic states.

3.2.2 Scanning Transmission Electron Microscopy

STEM imaging is a raster scanning on the sample surface by a small probe formed by highly converging electron beams. Electrons pass through the sample surface and interact with atoms in the sample, causing elastic and inelastic scattering. An electronic detector collects the scattered electrons to form an image. Electrons with large scattering angle are collected by a high-angle annular dark-field (HAADF) detector. Similar to SEM, the number of scattered electrons increases with the increase of atomic number, which is used to show atomic number contrast [33]. Electrons with small scattering angles (mainly coherently scattered electrons) collected by the annular bright-field (ABF) detector show low atomic number contrast. Therefore,

HAADF images are more conducive to observing the distribution of active sites in carbon-based metal electrocatalysts and identifying defect types on carbon-based surfaces [33, 34].

Generally speaking, STEM has a higher resolution than SEM and TEM and it can directly judge metal atoms' position and coordination structure in carbon-based materials [26, 35]. It can also be connected with EDS, EELS and other auxiliary devices to further achieve sub-Ångstrom resolution [23]. For SACs, the atomic numbers of heavy metal sites (such as transition metals) and lighter element support materials (such as carbon supports) are quite different, and heavy metal elements are clearly visible [36]. Therefore, HAADF-STEM diagram can be used as direct evidence of monatomic catalysts. For example, Chen et al. [37] prepared fully exposed Pt₃ clusters on the defective graphene-coated nano-diamond (ND@G) core-shell structure by means of atomic dispersed Sn with dilution effect. HAADF-STEM is used to explore the metal atom distribution of the prepared Pt-Sn co-doped catalyst (Fig. 3.3a-f). Pt and Sn are easily distinguished due to the difference in atomic number contrast. In the picture, the green circle represents the atomically distributed Sn species, whereas the red circle represents the Pt cluster. Figure 3.3a-e shows that Pt atoms are highly dispersed and exist in the form of irregular fine Pt clusters. Atomic dispersed Sn surrounds Pt clusters. The particle size distribution diagram in Fig. 3.3a shows that the average size of nanoparticles is about 0.83 nm, and Fig. 3.3f corresponds to the intensity diagram of red line extraction contour in Fig. 3.3e, in which the intensity of Pt atoms does not reach the intensity of Pt monatomic layer, indicating that all Pt atoms are exposed on the carbon support and there is no mutual covering phenomenon. Zhang et al. [34] proposed to fill Ni species in graphene defects (Ni@DG) to form a whole with excellent oxygen evolution reaction (OER) and hydrogen evolution reaction (HER) activity. No obvious nanoparticles were found in TEM images, but Ni was found in its corresponding EDS, indicating that some minor Ni was invisible in TEM. Therefore, HAADF-STEM was used to observe the surface defects of Ni@DG and the distribution of Ni. Figure 3.3g shows that there are obvious depressions and peaks in the defect-rich graphene grid, which are respectively attributed to Di vacancy (Fig. 3.3h) and Di vacancy with defect Ni (Fig. 3.3i).

In addition, *in-situ* STEM can directly visualize the dynamic surface and subsurface structure of the catalyst as well as monitor the formation of the catalyst during the synthesis process and the reconstruction and degradation of active sites under the reaction conditions in real-time, thus providing great inspiration for further research into the formation mechanism and reaction mechanism of the catalyst. For example, Gai et al. [38] showed the sequence of small particles undergoing structural rearrangement through STEM which controlled the monatomic dynamics in the environment (Fig. 3.3j-l). The yellow arrow in Fig. 3.3j shows that a single atom migrates from the cluster or particle P to the white spot on the amorphous carbon support in Fig. 3.3k, and finally forms a new small cluster (Fig. 3.3l).

Therefore, STEM is essential for visualizing carbon-based nanomaterials, especially carbon-based monatomic electrocatalysts [33]. HAADF-STEM can distinguish different elements in carbon-based materials and judge the aggregation state of heavy atoms. AC-STEM can reach sub-Ångstrom spatial resolution, which can

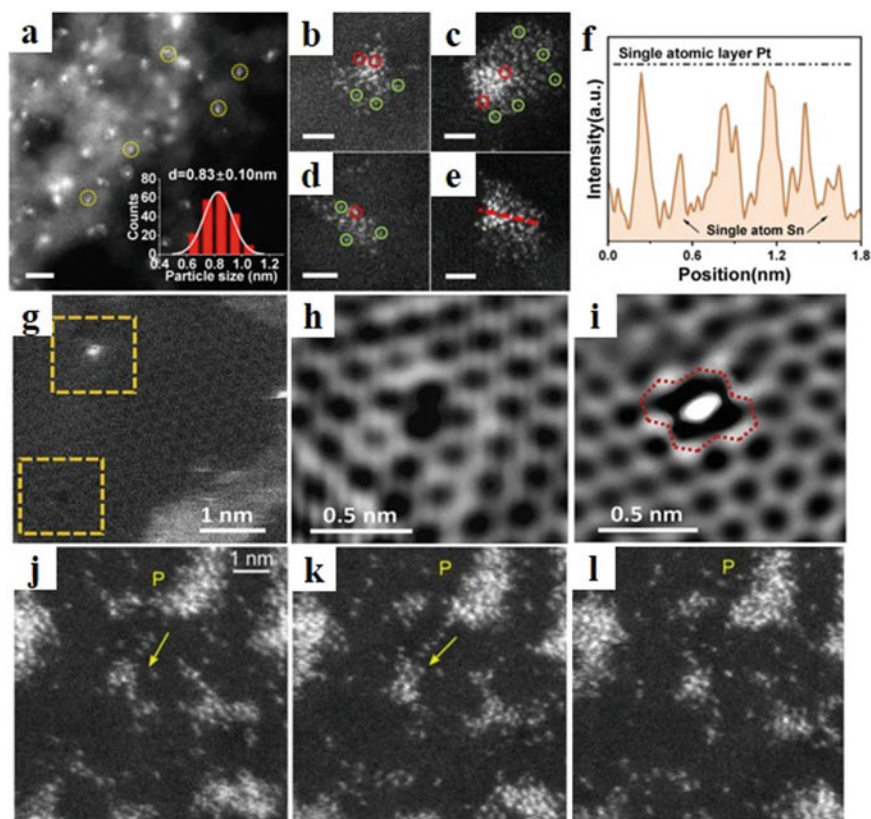


Fig. 3.3 STEM, STM, and EELS images. **a–e** HAADF-STEM images of $\text{Pt}_{6.8}\text{Sn}/\text{ND}@G$. **f** are the extracted line profiles along with red directions in **e**. Reproduced with permission [37]. Copyright 2017, Royal Society of Chemistry. **g** HADDF-STEM image of Ni-SAC. The Zoomed-in image of vacancy **h** without single Ni atom trapped and **i** with single Ni atom trapped. Reproduced with permission [30]. Copyright 2017, Elsevier. **j–l** *In-situ* ESTEM images of Pt/C. Migration of single atoms **j–k** leading to increased faceting of the particle and the formation of clusters **l**. Reproduced with permission [38]. Copyright 2014, IOP Publishing. **m** STM image NG-2 with defects arranged measured at a *Bias* = 0.9 V versus RHE and *I* = 104 pA. Reproduced with permission [40]. Copyright 2011, American Chemical Society. **n–o** STM images of the Fe-N-C catalyst at different bias conditions. **n** *Us* = -1.0 V versus RHE, *I* = 0.3 nA. **o** *Us* = 1.0 V versus RHE, *I* = 0.2 nA. Reproduced with permission [41]. Copyright 2017, Elsevier. **p** EELS spectra from pristine graphene and atoms C1, C2, and C3. Reproduced with permission [42]. Copyright 2013, American Chemical Society. **q** EELS spectra of the N K-edge (Nk) and Fe L-edge (FeL) acquired from single atoms 1 and 2 and few-layer graphene 3. Reproduced with permission [36]. Copyright 2017, American Association for the Advancement of Science. **r** EELS spectrum of $\text{Ru}_2\text{B}_3@BNC$. Reproduced with permission [43]. Copyright 2020, Elsevier

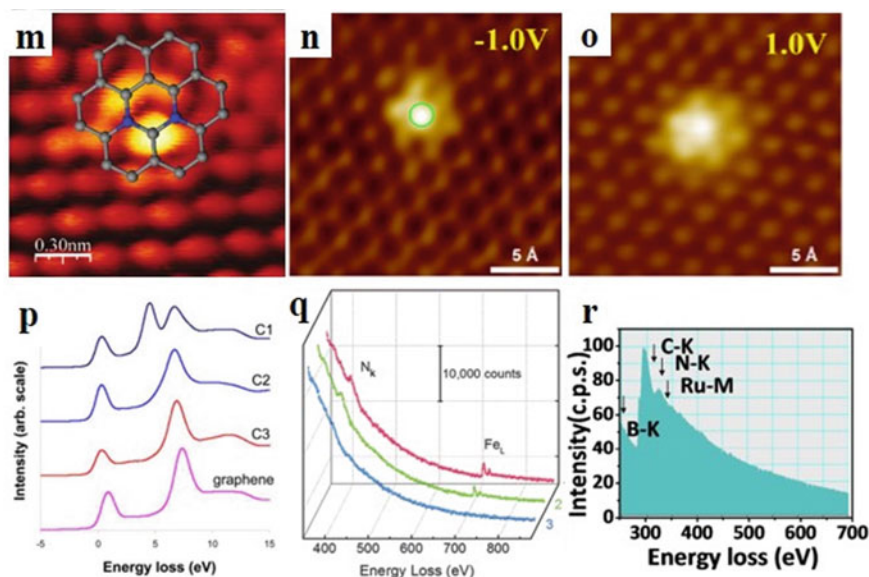


Fig. 3.3 (continued)

confirm the existence of single-atom in carbon-based monatomic catalysts and even make more complex characterization [23, 39].

3.2.3 Scanning Tunnel Microscope

In carbon-based nanomaterials, STM can directly study the nano-scale surface morphology, reveal the electronic characteristics of carbon-based monatomic catalyst surface atoms, and indirectly distinguish elements with similar atomic numbers. For example, Deng et al. [40] synthesized N-doped graphene by a new synthesis method, and studied the structure and electronic characteristics of surface atoms of N-doped graphene by STM. Figure 3.3m shows a graphene layer with a definite honeycomb structure. It can be seen that there are bright spots on the graphene network (the diameter of the bright area is less than 0.5 nm), which indicates that the existence of defects interferes with the electronic structure of graphene. After the density functional theory (DFT) calculation, it is determined that the doping of N atoms leads to the increase of electron density of adjacent C atoms. Liu et al. [41] characterized the local electronic properties of iron atom sites in Fe–N–C catalyst, and found that the bright spot remained stable and had no obvious difference under different bias voltages (Fig. 3.3n, o), which indicated that the electronic structure of the bright spot was strongly hybridized with the electronic structure of its adjacent

atoms. After DFT calculation, it is confirmed that Fe in FePc exists in the form of Fe–N₄.

In addition, STM can identify reaction intermediates on the surface of carbon-based catalysts under ultra-high vacuum or ultra-low temperature conditions. Electrochemical scanning tunneling microscopy (ECSTM) can observe the reaction process of carbon electrode in situ at constant potential, which broadens the scope of STM for exploring the solid surface of carbon-based catalysts.

3.2.4 Energy Dispersive Spectrometer and Electron Energy Loss Spectrometer

EDS and EELS are auxiliary devices equipped with electron microscopes, and EELS can be used as a complementary technique to EDS. EDS uses the characteristic X-rays generated by the interaction of electrons and matter to identify the element types, and EELS can obtain more details related to the electronic structure. Combined with HAADF-STEM, the spatial distribution, relative content, and coordination of each element on carbon-based electrocatalysts are explained. In turn, it reflects the influence of heteroatoms or defects in the carbon matrix on the electronic structure of the carbon matrix. For example, Han et al. [28] obtained nitrogen-doped hollow carbon spheres containing isolated Co single atoms by means of assisted pyrolysis. They characterized the carbon-based catalyst with AC-HAADF-STEM and clarified that Co exists in the form of atoms (Fig. 3.2j), and the elemental map shows that Co, C and N are uniformly distributed on the hollow substrate (Fig. 3.2k). Similarly, in Fig. 3.2l, Co, C and N are uniformly distributed in the star-shaped carbon-based nanostructures [29]. Nicholls et al. [42] simulated three different C atom sites in N-doped graphene in order to determine the coordination of N-doped graphene (C1, C2 and C3 represent the adjacent carbon, the next adjacent carbon and the farthest carbon from the nitrogen atom after N-doping in a six-membered ring) and the original graphene structure. EELS spectrum (Fig. 3.3p) showed that the electronic distribution and energy band structure of C1, C2 and C3 changed after N-doping, and C1 was 4.6 at.%. Chung et al. [36] used EELS to explain the coordination on carbon matrix, and compared with mark 3 (multilayer graphene), it showed that there were *n* atoms around Fe (Fig. 3.3q). Similarly, Qiao et al. [43] used EELS to illustrate the existence of C, N, B, and Ru (Fig. 3.3r).

3.3 Indirect Verification

SEM for observing surface morphology, X-ray diffractometer (XRD) for analyzing phase, and X-ray photoelectron spectroscopy (XPS) for determining coordination structure are all indispensable means for characterizing carbon-based nanomaterials.

However, each characterization technique has its own advantages and disadvantages, so it is impossible to use a single characterization means to characterize a certain material completely, and the structure information inferred by any characterization means should be verified more effectively by other characterization means. In this chapter, XRD, Raman spectrometer (Raman), XPS, and X-ray absorption spectrometer (XAS) are taken as examples to illustrate the importance of indirectly verifying the structure, atomic chemical characteristics and coordination state of carbon-based materials for the characterization of carbon-based nanomaterials.

3.3.1 X-ray Diffraction

XRD is the result of diffraction of X-ray with specific wavelength interacting with specific crystal. Among them, the position of X-ray diffraction line determines the cell parameters, the relative intensity of diffraction line determines the type, number and arrangement of atoms in the crystal lattice, and the shape of the characteristic peak can judge the crystallization state of the crystal. For carbon-based nanomaterials, it can be used for conventional qualitative and quantitative phase analysis, but this is only applicable to materials with definite crystal structure, not to amorphous nanocatalysts, monatomic catalysts and molecular catalysts [44, 45].

Huang et al. [46] reported an electrocatalyst supported on carbon nanotubes and characterized the structural evolution of the catalyst in the preparation process in detail. It can be seen from Fig. 3.4a that ethylene diamine tetra acetic acid/carbon nanotubes (EDTA/CNT) can be regarded as a physical mixture of Na_2EDTA and CNT, and the XRD images of EDTA/CNT are similar to $\text{Na}_2\text{EDTA/CNT}$, indicating that this synthesis step has not changed the original crystal structure. Similarly, Han et al. [44] XRD to explore carbon-based catalysts' structural changes during each synthesis process. The (211) and (220) faces of N-doped ordered mesoporous carbon (N-OMC) skeleton are clearly shown in Fig. 3.4b, indicating that Fe-N-C/N-OMC produced a mesoporous structure very similar to porous silicon (KIT-6) after removing the ordered mesoporous silica template.

In addition, *in-situ* and operando XRD can monitor the structural changes and phase transition process of carbon-based nanomaterials under different electrochemical conditions, and track the evolution of the crystal structure and composition of carbon-based electrode materials during the cell cycle in specific environments, which is helpful to explore the reaction mechanism and degradation mechanism of carbon-based catalysts. For example, Liu et al. [47] determined by *in-situ* XRD that during CO_2 reduction reaction (CO_2RR), the potential ranged from 0.4 V to -0.8 V versus RHE, which was beneficial to the generation of active PdH species for CO desorption (Fig. 3.4c). At 0.4 to -0.2 V versus RHE, only Pd exists on Pd/C samples. With the further decrease of potential, the XRD peak of Pd/C gradually shifts negatively, which is due to lattice expansion caused by PdH formation. At -0.4 V versus RHE, Pd and PdH coexist in Pd/C catalyst. At -0.6 V and -0.8 V versus RHE, only

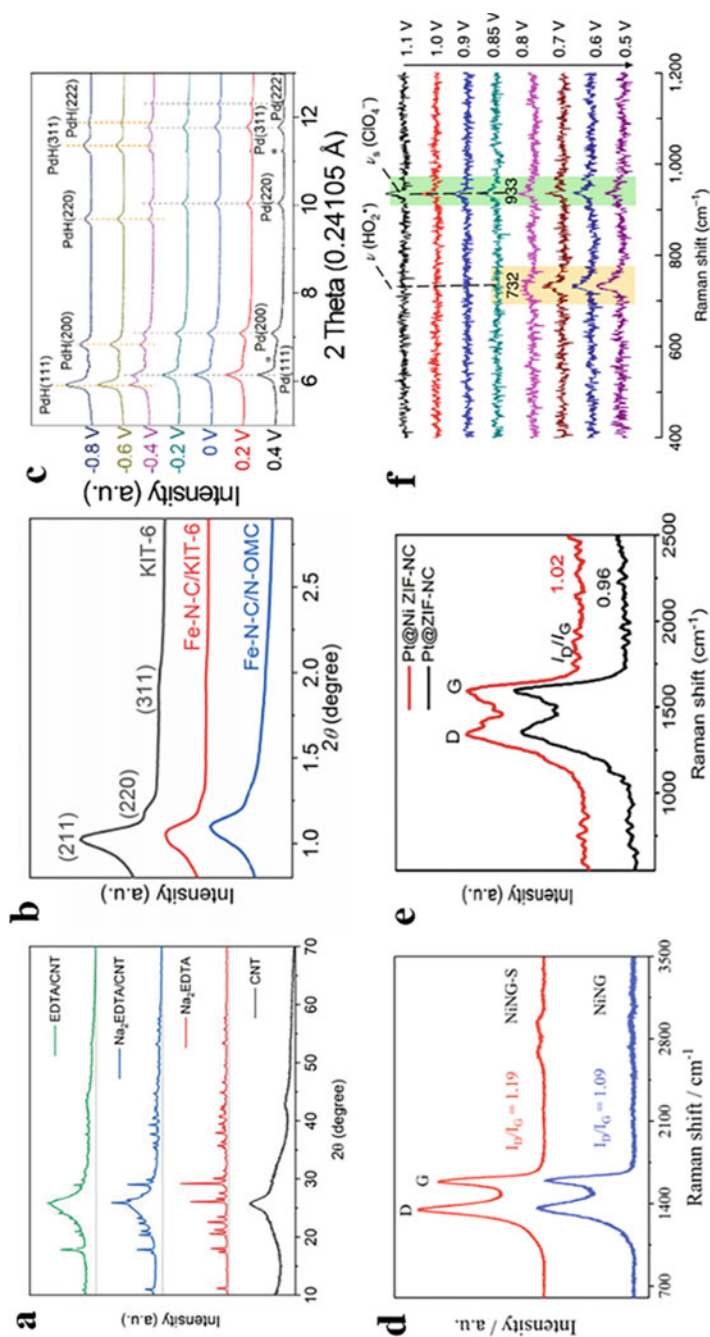


Fig. 3.4 XRD and Raman spectra. **a** XRD patterns of CNT, Na₂EDTA, Na₂EDTA/CNT and EDTA/CNT. Reproduced with permission [46]. Copyright 2021, WILEY-VCH. **b** Small-angle X-ray diffraction patterns of KIT-6, Fe-N-C/KIT-6 and Fe-N-C/N-OMC. Reproduced with permission [44]. Copyright 2020, Elsevier. **c** In-situ XRD analyses for Pd/C. Asterisk (*) marks point out the peaks from the carbon substrate. Reproduced with permission [47]. Copyright 2020, WILEY-VCH. **d** Raman spectra of NING and NING-S. Reproduced with permission [48]. Copyright 2021, WILEY-VCH. **e** Raman spectra of Pt@Ni-ZIF-NC and Pt@ZIF-NC. Reproduced with permission [49]. Copyright 2021, Elsevier. **f** In-situ Raman spectra of the ORR system at a Pt(111) electrode surface in a 0.1 M HClO₄ solution saturated with O₂. Reproduced with permission [12]. Copyright 2018, Springer Nature

PcH species existed. This provides support for exploring the reaction mechanism in CO₂RR process.

However, due to its surface insensitivity. Therefore, operando XRD is not suitable for studying the electrochemical reaction process of carbon-based catalysts. Still, it can be used as a supplement to other characterization methods.

3.3.2 Raman Spectrum

Because nonpolar groups (such as C–C, C = C, etc.) have vigorous Raman activity, Raman spectra can be used to analyze the carbon matrix of carbon-based catalysts, and usually show the characteristic peaks of D band and G band (D peak represents the defects of C atom lattice and G peak represents the in-plane stretching vibration of sp² hybridization of C atom). The two peaks' intensity ratio (I_D/I_G) can evaluate the degree of defects and graphitization [50–52] in the carbon matrix. For example, Jia et al. [48] improved the catalytic activity of atom-dispersed Ni–N–C by doping S atoms, and determined that the catalyst doped with S had higher I_D/I_G by Raman technique (Fig. 3.4d), which indicated that S doping led to an increase in defect density in graphene, which was beneficial to adsorption of more active sites and improvement of catalytic performance. Liang et al. [49] inhibited the aggregation of Pt atoms in the reaction process by introducing Ni atoms. In Raman spectrum (Fig. 3.4e), the I_D/I_G of Pt@Ni ZIF–NC was 1.02, which was higher than that of Pt@ZIF–NC, indicating that the defects of carbon matrix increased during the formation of Ni sites on ZIF–NC, which was beneficial to the dispersion of Pt atoms.

In addition, Raman spectroscopy is very sensitive to adsorption and bonding on the catalyst surface [12]. Therefore, it is often used to detect the adsorption species on the catalyst surface and the coordination structure of the catalytic metal center, so as to determine the changes on the catalyst surface during the catalytic process and infer the catalytic mechanism [53]. Moreover, due to the extremely low Raman scattering of water, Raman spectroscopy has become an essential tool to study the catalytic mechanism of electrocatalysts in an aqueous solution [54]. For example, Jin et al. [12] used electrochemical surface-enhanced Raman spectroscopy (SERS) to characterize the ORR process on Pt surface to deeply understand the mechanism of ORR on Pt surface, and found that with the decrease of potential, an increasing HO₂^{*} peak appeared at the wave number of 732 cm⁻¹, indicating the formation of intermediate HO₂^{*} (Fig. 3.4f).

In short, Raman technology can judge the defect degree of the carbon matrix, and operando Raman is helpful to identify the active species in the electrochemical reaction, judge the adsorbed species on the catalyst surface, and even verify the oxidation state of metal atoms at the active sites.

3.3.3 N_2 Adsorption–Desorption Curve

The specific surface area of carbon-based catalyst calculated by the Brunner–Emmet–Teller (BET) measurements is generally proportional to the density of active sites adsorbed on the carbon-based surface, and its size can be related to the activity of carbon-based catalyst. The shape and pore size distribution of mesopores in carbon materials (such as molecular sieves and microporous activated carbon) can be preliminarily determined by the shape of hysteresis loops, which is instructive for uniformly dispersed catalytic sites. In the analysis of pore size or pore volume, the total pore volume of carbon material is calculated by the single point method, and the micropore volume of carbon material is calculated by t-plot method. The mesopore and macropore volume can be obtained by subtracting the micropore volume from the total pore volume. In carbon materials, micropores are beneficial to increase the density of active sites, and mesopores are beneficial to mass transfer. The existence of these two kinds of pores is beneficial to the improvement of catalytic activity, while the existence of macropores makes the carbon matrix collapse during electrochemical cycle, which is extremely unfavorable to the stability of the catalyst.

Xie et al. [55] explored a new synthetic method in order to improve the utilization rate of metal Co atoms and inhibit the agglomeration of Co atoms or the formation of nanoparticles. According to the particle size distribution diagram (Fig. 3.5b), it is judged that $\text{Co}(\text{acac})_3$ and $\text{Co}(\text{mlm})_4$ occupy micropores filled with ZIF-8, and ZIF-8 structure hinders the movement of Co atoms, forming a relatively stable Co monatomic catalyst. The N_2 isothermal adsorption–desorption curves of catalysts with different Co contents (Fig. 3.5a) show that all the $\text{Co}(\text{mlm})\text{-NC}$ synthesized in this paper have similar pore structures. Similarly, in order to enhance the stability of perovskite quantum dots, Qiao et al. [56] encapsulated them in an organic framework (MOF). By comparing the BET specific surface area and particle size distribution of perovskite before and after encapsulation, it was confirmed that perovskite was encapsulated in the air of MOF (Fig. 3.5c, d).

In a word, N_2 isothermal adsorption–desorption test is a powerful characterization method for measuring specific surface area, pore size distribution, pore volume or pore volume of carbon materials and analyzing pore structure.

3.3.4 X-ray Photoelectron Spectroscopy

The most outstanding advantage of XPS in electrocatalysis research is its high sensitivity to the material surface [24]. XPS is widely used in carbon-based nanomaterials to study the surface element species and electronic structure of specific elements (such as C, N, etc.) [33] and to measure the binding energy of electrons in the inner layer of specific elements. Zhang et al. [6] simulated the distribution of various nitrogen species in nitrogen-doped graphite carbon (Fig. 3.6f), and used XPS to show the binding energy of various nitrogen species on graphite carbon support, indicating

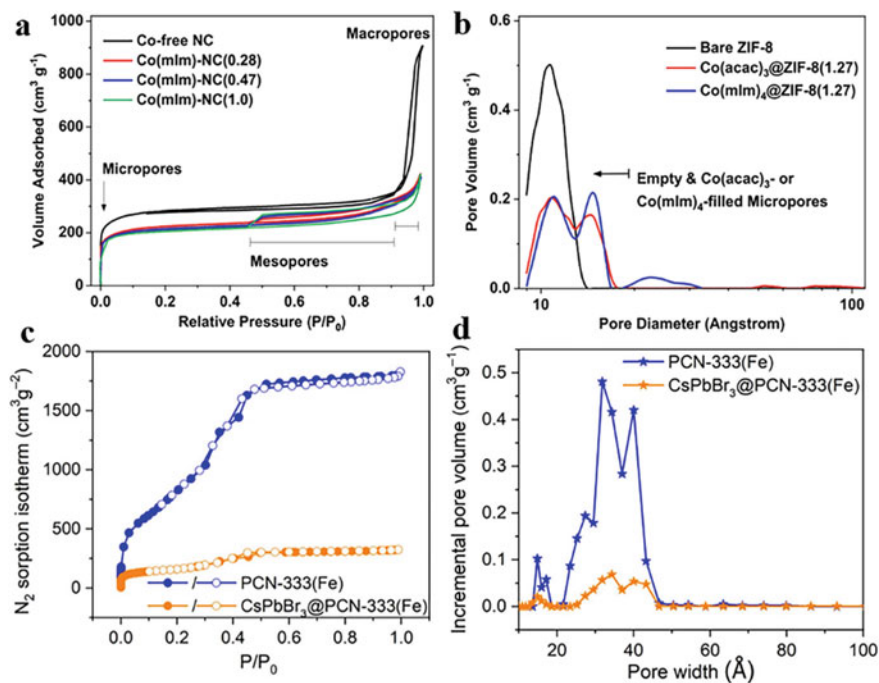


Fig. 3.5 N₂ adsorption–desorption curve and pore size distribution. **a** N₂ isothermal adsorption/desorption of Co(mIm)-NC with different Co content. **b** Pore size distribution for the bare ZIF-8, Co(acac)₃@ZIF-8(1.27) and Co(mIm)₄@ZIF-8(1.27) precursors determined from non-local density functional theory (NLDFT) model of the N₂ adsorption data. Reproduced with permission [55]. Copyright 2020, Springer Nature. **c** N₂ adsorption/desorption of PCN-333(Fe) and CsPbBr₃@PCN-333(Fe) at 77 K and 1 atm. **d** DFT pore size distributions before and after encapsulating the perovskite. Reproduced with permission [56]. Copyright 2021, American Chemical Society

that different N configurations can change the electronic structure of adjacent carbon atoms, thus affecting the electrocatalytic activity. Guo et al. [14] doped Mn–N–C with S to improve the intrinsic activity of Mn–N–C catalyst. XPS was used to characterize the composition and chemical state of Mn–N–C–S catalyst surface layer (Fig. 3.6a–c). Figure 3.6a shows the broad spectrum of NC, NCS, Mn–N–C and Mn–N–C–S catalysts, which shows that Mn, N, C and S exist in Mn–N–C–S at the same time, and the atomic percentage of S is about 2.7 times that of Mn. Figure 3.6b shows that the chemical state of Mn atoms in the two catalysts is the same, both of which are +2 valence, indicating that S element has no substantial influence on Mn atoms in Mn–N–C–S catalysts. In Fig. 3.5c, compared with other samples, the peak at 399.2 eV is the peak of Mn–N coordination, which confirms the existence of Mn–N coordination in the catalyst. Similarly, in order to improve the intrinsic activity of Mn–N–C catalyst, Chen et al. [57] developed an acid-assisted step-by-step pyrolysis synthesis strategy. The valence of the Mn atom in Mn–N–C–HCl–00/1100 was

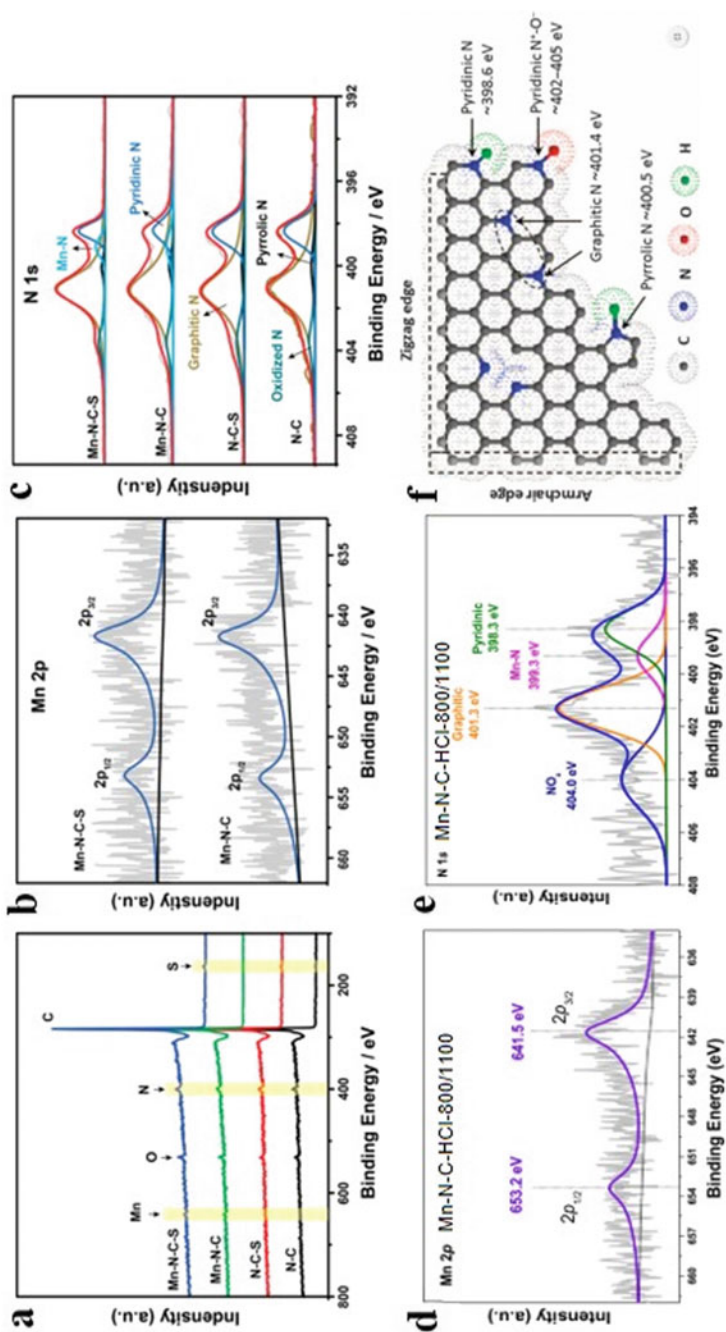


Fig. 3.6 XPS analysis. **a** XPS patterns of N-C, N-C-S, Mn-N-C, and Mn-N-C-S catalysts. **b** high-resolution Mn 2p XPS spectra of Mn-N-C and Mn-N-C-S catalysts. **c** high-resolution N 1s XPS spectra of N-C, N-C-S, Mn-N-C, and Mn-N-C-S catalysts. Reproduced with permission [6]. Copyright 2021, American Chemical Society. **d** high resolution of Mn 2p XPS spectra of the Mn-N-C-HCl-800/1100. **e** high resolution of N 1s XPS spectra of the Mn-N-C-HCl-800/1100. Reproduced with permission [14]. Copyright 2020, American Chemical Society. **f** Scheme illustration of nitrogen species in nitrogen-containing graphitic carbons. Reproduced with permission [57]. Copyright 2015, American Association for the Advancement of Science

+2 (Fig. 3.6d), and the existence of Mn–N coordination was confirmed by XPS characterization (Fig. 3.6e).

However, XPS needs to probe the surface of carbon-based catalyst in an ultra-high vacuum environment. At present, the quasi-operando research is to carefully move the electrocatalytic catalyst into the vacuum chamber of XPS, and then probe, which limits the application and development of in-situ/operando XPS at the electrode–electrolyte interface.

3.3.5 X-ray Absorption Spectroscopy

XAS can obtain the regional structure information and electronic state of target atoms in carbon-based nanomaterials on the atomic scale. According to the spectral region division, it can be divided into two types of spectra. One is X-ray absorption near-edge structure spectrum (XANES), and the threshold is in the low-energy region of 30–50 eV. Because the shell electrons of target atoms absorb photons, it can be used to detect the valence state and coordination charge of atoms in carbon-based materials [33, 58]. The other is extended X-ray absorption fine structure spectroscopy (EXAFS), with a spectral range of 50–1000 eV, which can be used to detect atomic coordination geometry, such as atomic proximity structure, coordination number and bond length [58]. It is worth noting that when XAS is used to characterize carbon-based catalysts with dispersed atoms, its relatively uniform structure is helpful to extract the local coordination structure of heavy atoms in carbon-based catalysts from the average structure information obtained by XAS.

As shown in Fig. 3.7a–f, Wang et al. [21] adjusted the spin state of Fe in adjacent Fe–N₄ through Mo–N₄, thus producing FeMoPPc catalyst with high catalytic activity for nitrogen reduction reaction (NRR). XAS analysis was used to judge the coordination environment and electronic state of Fe atoms and Mo atoms in FeMoPPc. XANES spectra of the Fe K-edge show that the chemical valence state of Fe in FeMoPPc and FePPc is almost the same, but the peak intensity of the front edge of FeMoPPc is lower than that of FePPc, which indicates that the introduction of Mo atoms has changed the coordination environment of Fe (Fig. 3.7a). In FT-EXAFS spectrum of Fe K-edge, the existence of Fe–N coordination in FeMoPPc is confirmed by comparing with other standard spectra, and there is no peak corresponding to Fe–Fe coordination, which further confirms the previous characterization results of Fe existing forms (Fig. 3.7b). The wavelet transform (WT) of Fe K-edge EXAFS is used to further study the state of iron atoms (Fig. 3.7c). By EXAFS fitting, it is determined that the coordination number (CN) of Fe–N_x in FeMoPPc is 4, the bond length of Fe–N is 1.96 Å, and finally the structure of Fe–N₄ is determined. In the same way, Fig. 3.7d–f shows that Mo in FeMoPPc has very close chemical valence, and Mo in FeMoPPc exists in Mo–N₄ structure.

However, for dimer with long bond length, EXAFS is a great challenge for dimer detection because of weak signal with long bond length or being blocked by scattering path with destructive interference. However, the existence of dimer can be determined

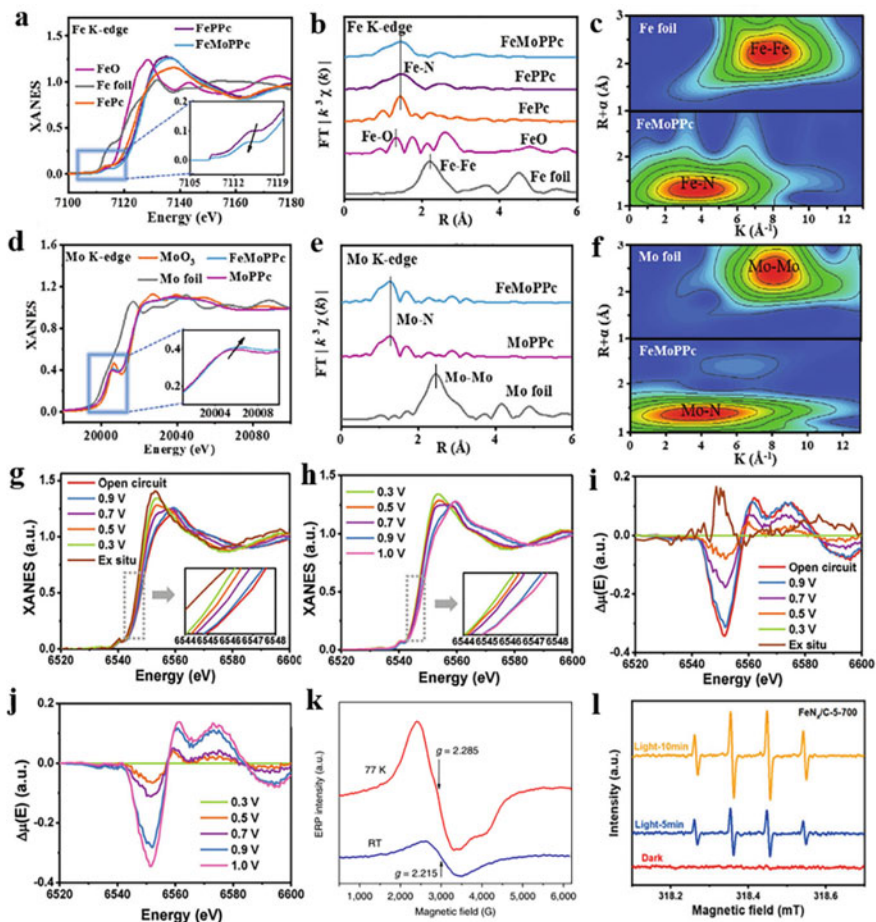


Fig. 3.7 XAS and EPR. **a** Fe K-edge XANES and **b** EXAFS for the catalyst FeMoPPc and other standard samples. **c** Wavelet transform of Fourier-transformed EXAFS data of Fe foil, FeMoPPc. **d** Mo K-edge XANES and **e** EXAFS for the catalyst FeMoPPc and other standard samples. R is the distance in Ångströms ($1 \text{ \AA} = 10^{-10} \text{ m}$); k is the wave number. **f** Wavelet transform of Fourier-transformed EXAFS data of Mo foil, FeMoPPc. Reproduced with permission [21]. Copyright 2021, WILEY-VCH. **g, h** Operando XANES and **i, j** $\Delta\mu$ -XANES ($\mu_E - \mu_{0.3V}$) of Mn-SAS/CN catalyst collected ex situ and **g, i** at the open circuit from 0.9 to 0.3 V versus RHE and **h, j** from 0.3 to 0.9 V versus RHE in O₂-saturated KOH. Reproduced with permission [59]. Copyright 2020, WILEY-VCH. **k** EPR spectra of A-Ni-NG measured at room temperature (RT) and 77 K. Reproduced with permission [60]. Copyright 2018, Springer Nature. **l** EPR spectra of DMPO-trapped FeNx/C-5-T and an H₂O₂-aqueous system under light irradiation. Reproduced with permission [61]. Copyright 2021, WILEY-VCH

by high-resolution HAADF-STEM imaging. There may be different coordination structures in carbon-based materials with complex structures, because the coordination structure information obtained by EXAFS is often the result of the average coordination of elements. For example, when there are equal four-coordination and six-coordination structures in the materials at the same time, the spectrum shows that the average coordination number is 5, which will lead to misleading structural information. Therefore, the accurate discrimination of atomic coordination geometry should be combined with other characterization methods.

In addition, *in-situ* and operando XAS can monitor the changes of electronic environment and geometric structure of catalytic sites in carbon-based nanomaterials on an atomic scale in real-time. [62, 63] For example, Han et al. [59] judged the influence of hydroxyl radical (OH^*) on the electronic environment of Mn in Mn–N–C catalyst using operando XAS characterization, thus inferring the relationship between the desorption of reaction intermediates and the reaction mechanism. Figure 3.7 g and h show that when the applied potential decreases from 0.9 V to 0.3 V versus RHE, the spectral lines of XANES gradually move towards low energy. When the applied potential is reversed, the spectral lines also change in the opposite direction. This indicates that with the increase of overpotential, the chemical valence of Mn atom decreases, which leads to the decrease of its adsorption capacity for OH, thus accelerating the desorption of OH^- , that is, the applied potential can adjust the valence state of Mn, thus regulating the adsorption/desorption capacity for reaction intermediate (OH^*). Figure 3.7i, j show the results of μ -XANES sensitive to the surface, which can be used to evaluate the coverage of OH_{ads} at Mn site quantitatively. It can be seen from the figures that the coverage rate of OH_{ads} decreases with the decrease of potential, which indicates that Mn– N_4 site is gradually released during ORR under the action of Mn–N–C, indicating that this is a process mediated by surface oxidation. Although the analysis of *in-situ*/operando spectral changes is very complicated, it is quite beneficial to further study the reaction mechanism and electrochemical reaction process.

3.3.6 Electron Paramagnetic Resonance

The unpaired electrons in the molecules of paramagnetic substances produce energy level splits under the action of a DC magnetic field. The electrons in the lower energy levels will absorb the electromagnetic wave energy and jump to the higher energy levels. This is the electron paramagnetic resonance (EPR) effect. The EPR spectrometer records the absorption signal generated by electromagnetic wave stimulation to obtain the first-order differential spectrum of the absorption signal, which can be used to directly judge the existence of stable paramagnetic substances. For example, Yang et al. [60] obtained by EPR spectroscopy that the number of unpaired electrons of Ni(i) $3d_x^2-y^2$ orbitals were 2.215 and 2.285 at room temperature and 77 K, respectively, and determined that the monovalent Ni(i) with higher reactivity is the catalyst. The active sites are prone to change under the influence of heat (Fig. 3.7k).

In the electrochemical reaction process, for high-activity and short-lived intermediates, EPR-spin trap technology is generally used, which uses a spin trap (ST, such as coumarin) to react with active free radicals in the reaction. To generate a relatively stable spin adduct, which can qualitatively and quantitatively determine the short-lived intermediate product in the electrochemical reaction process. Xing et al. [61] used EPR to confirm further the formation of hydroxyl radicals ($\cdot\text{OH}$) in the catalytic process, corresponding to the intensity ratio in the spectrum of 1:2:2:1 (Fig. 3.71).

In sum, EPR can determine the presence of paramagnetic substances and activity reflecting intermediates in carbon-based nanomaterials, especially carbon-based materials containing unpaired electronic substances. In addition, in catalysis, the capture of free radicals can also clarify the electron transfer reaction so that the surface properties of the catalyst can be inferred.

3.3.7 Other Advanced Techniques

Infrared absorption spectrum (IR). Since the characteristic absorption peak of the group corresponds to the change of the dipole moment caused by the vibration of each group, the infrared absorption (IR) spectrum of the substance can be used to determine the chemical group. During the electrochemical reaction of carbon materials, it can be used to determine the chemical groups and bonds adsorbed on the surface of carbon-based catalysts [64]. Fig. 3.8a is a Fourier transform infrared spectrum (FT-IR) of an electrocatalyst based on carbon nanotubes (CNTs) [46]. The figure shows the ethylenediaminetetraacetic acid/carbon nanotubes before and after the electrochemical cycle test. (EDTA/CNT) The surface contains CN, COO^- , COOH and OH, which confirms the stability of the carbon matrix. In order to prevent the oxidation and agglomeration of metal halide perovskite quantum dots, Qiao et al. [56] encapsulated CsPbBr_3 into an iron-based metal-organic framework (MOF), and used TEM, EDS, IR and other means to verify the successful synthesis of the composite material. The one-to-one correspondence of the characteristic peaks in Fig. 3.8b illustrates this point. In order to improve the selectivity of CO_2 hydrogenation to methanol, Chen et al. [65] prepared a single-atom platinum catalyst coordinated with oxygen (denoted as Pt_1 @MIL, and the platinum nanocrystal catalyst corresponding to oxygen-free coordination is Pt_n @MIL). They used *in-situ* diffuse reflectance infrared Fourier transform spectroscopy (DRIFTS) technology to dynamically monitor the changes in the catalyst surface bond during the reaction process, thereby judging the different reaction paths under the action of Pt_1 @MIL and Pt_n @MIL, and confirming that the two are calculated based on DFT. The difference in the judged response path. Figure 3.8c shows that after Pt_1 @MIL is treated with H_2 at 150°C for 0.5 h, the 3197 cm^{-1} corresponds to the OH bond, and there is no Pt-H peak, while the Pt_n @MIL 1949 cm^{-1} corresponds to the Pt-H bond, no OH peak. This result is consistent with the DFT result. Similarly, when the catalyst is used for CO_2 reaction and hydrogenation, the reaction intermediates corresponding to Pt_1 @MIL and Pt_n @MIL are HCOO^* and COOH^* , respectively. Therefore, the

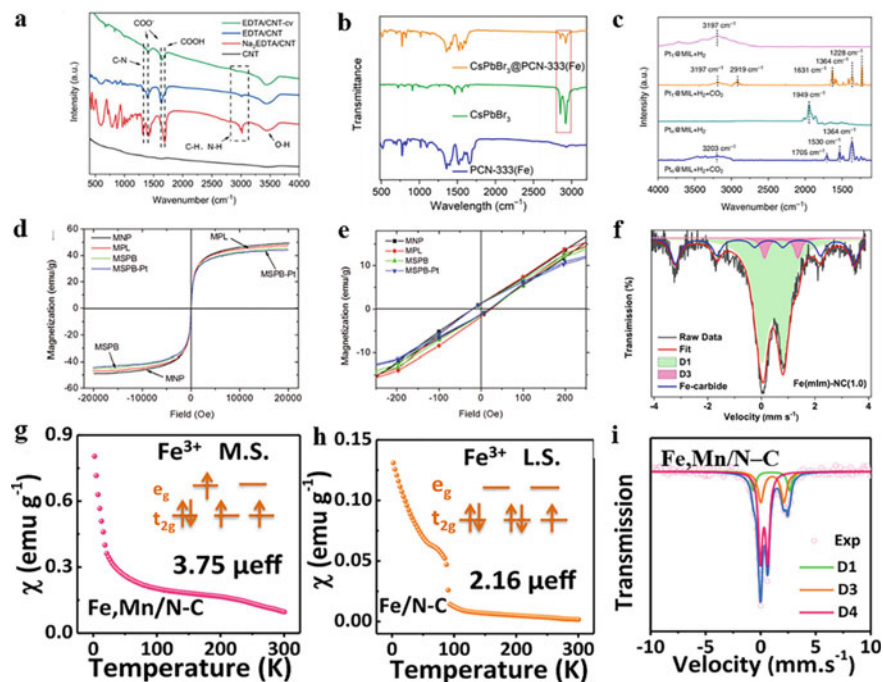


Fig. 3.8 IR, Mössbauer spectroscopy, and magnetization curve. **a** FT-IR spectra of CNT, Na₂EDTA/CNT, EDTA/CNT and EDTA/CNT-cv. Reproduced with permission [46]. Copyright 2021, WILEY-VCH. **b** IR spectra of CsPbBr₃@PCN-333(Fe), CsPbBr₃ and PCN-333(Fe). Reproduced with permission [56]. Copyright 2021, American Chemical Society. **c** In-situ DRIFTS spectra of Pt₁@MIL and Pt_n@MIL after the treatment with H₂, as well as H₂ and CO₂ in sequence at 150 °C. Reproduced with permission [65]. Copyright 2019, Springer Nature. **d** Magnetization curves and **e** magnetization curves at low magnetic field of bare MNPs, MPL, MSPB, and MSPB-Pt observed by VSM at room temperature. Reproduced with permission [66]. Copyright 2012, American Chemical Society. **f** Mössbauer spectrum of Fe(mIm)-NC(1.0) catalyst. Reproduced with permission [55]. Copyright 2020, Springer Nature. **g, h** VSM spectra of **(g)** Fe, Mn/N-C and **(h)** Fe/N-C. **i** Room-temperature ⁵⁷Fe Mossbauer spectrum of Fe, Mn/N-C. Reproduced with permission [67]. Copyright 2021, Springer Nature

single Pt atom in Pt₁@MIL can activate its coordinated oxygen atom and change the reaction path of catalytic hydrogenation.

In addition, IR technology can also detect the interaction between the probe molecules and the catalyst center to reflect their dispersion state and oxidation state; the change in the vibration frequency of the probe molecule can distinguish the carbon base during the electrochemical reaction. Changes in the coordination environment of the catalytic center of the catalyst.

Vibrating sample magnetometer (VSM). VSM is one of the important means to measure the magnetic properties of materials, which can be used to detect the intrinsic magnetic properties of various materials, such as magnetization, coercivity,

magnetic moment, etc. In carbon-based nanomaterials, VSM can measure hysteresis loops or magnetization curves of ferromagnetic, paramagnetic or diamagnetic parts on carbon-based catalysts. For example, Wu et al. [66] synthesized platinum nano catalyst immobilized on magnetic supports, and used the magnetic properties of the catalysts to recover the substances after catalytic reaction, so as to reduce the cost. Through VSM test, it is determined that the synthesized composite catalyst is super paramagnetic material, and the residual magnetization and coercivity under low magnetic field are in the super paramagnetism range (Fig. 3.8d, e). Therefore, after the catalyst participates in the reaction and its catalytic performance is degraded, the catalyst is separated by using external permanent magnets.

In addition, the information about valence electrons of specific atoms can be obtained through the effective magnetic moment, which is beneficial to judge the relationship between the spin states of atoms in active sites and catalytic performance. For example, Yang et al. [67] synthesized a bimetallic atom-dispersed Fe, Mn/N–C catalyst, and found that atom-dispersed Mn(III) can interact with neighboring Fe(III), resulting in redistribution of valence layer electrons of neighboring Fe, which changed from low spin state to medium spin state (Fig. 3.8 g, h). The activity and stability of this bimetallic catalyst were improved.

Mössbauer Spectroscopy. Mössbauer spectroscopy is a science that studies the behavior of extranuclear electrons by observing the resonance and absorption of gamma rays by nuclei. In the field of heterogeneous catalysis of carbon-based materials, Mössbauer spectroscopy is one of the most effective methods to characterize the structure, valence, spin state and electronic environment of metal species in carbon-based catalysts, especially ^{57}Fe and ^{119}Sn . At present, Mössbauer spectroscopy has been widely used to distinguish the structure, coordination state and valence of Fe species in Fe–N–C catalysts, and the relative content of each species. For Fe catalysts, it is helpful to discuss the structure–activity relationship between active sites and catalytic properties, and the possible activation or deactivation process of surface materials in the electrochemical reaction process. For example, Xie et al. [55] determined that the synthesized Fe(mlm)-NC catalyst mainly exists in the form of $\text{FeN}_4\text{C}_{12}$ similar to porphyrin structure (corresponding to the D1 part of Fig. 3.8f), and there is very little $\text{FeN}_{2+2}\text{C}_{4+4}$ with pyridine structure (corresponding to the D3 part of Fig. 3.8f) in order to determine the structural form of Fe. Yang et al. [67] in order to distinguish different Fe species and their relative contents, determined Fe with large isomer shift (IS) and quadrupole split (QS) by Mossbauer spectrum, and Mn/N–C has high content of D4 in medium spin state and low content of D3 in high spin state. according to the is value used to describe the valence state of Mossbauer absorption atom, it is determined that Fe mainly exists in the form of + 3 valence. Therefore, Mössbauer spectroscopy is indispensable for the analysis of carbon-based catalysts with Fe and/or Sn atoms as active sites.

3.4 Simulation and Calculation

In the aspect of energy storage and transformation of carbon-based nanomaterials, molecular dynamics simulation and calculation are seldom used, and first-principles simulation and calculation are often used [68–70]. Before the experiment begins, simulation and calculation can judge the feasibility of the experimental method. After the experiment, it can verify the experimental results and further illustrate the correctness of the conclusion. In carbon-based catalysts, the DFT calculation can infer the possible crystal structure of substances, and DFT-optimized structure can determine the coordination structure and electronic characteristics (Bader charge, density of states (DOS), energy band, etc.) of metal atoms in carbon-based catalysts. Moreover, DFT calculation can calculate Gibbs free energy of reaction in electrochemical reaction, infer the possibility of reaction and determine the reaction path [71, 72]. When evaluating the catalytic performance, the geometric configuration and electronic structure of active sites in the catalyst are beneficial to evaluate the activity of carbon-based catalysts, and the adsorption energy of reactants and reaction intermediates, decomposition potential of substances or reaction potential of reactions calculated by DFT are beneficial to evaluate the activity or stability of carbon-based catalysts.

For example, Chen et al. [22] developed Ir monatomic catalyst and Ir₁₉ cluster catalyst, and the simulation of charge density difference diagram shows that the metal states of Ir atoms in these two catalysts are significantly different (Fig. 3.9a), showing different catalytic activities in catalytic performance. Gibbs free energy diagram of Ir₁₉ cluster determines the path of oxygen reduction reaction (ORR), which shows that the rate determination step (RDS) of Ir₁₉ cluster catalyst is the resolution of hydroxyl radical when $U = 0$ V vs. RHE (Fig. 3.9b), and the adsorption of ORR intermediate *OH by the catalyst can help to understand the catalytic mechanism [22]. Li et al. [73] simulated DOS of Fe 3d orbitals in two FeN₄ structures (planar structure and non-planar structure) (Fig. 3.9c), and judged that with the shortening of Fe–N bond length, Fe 3d electron orbitals moved forward, which was beneficial for FeN₄ site to absorb oxygen, thus explaining the relationship between Fe–N bond length and catalytic activity. Figure 3.9d [74] shows the difference of charge density and Bader charge of ZnB₂N₂. It is determined that the Bader charge of Zn is 0.75 and that of B is 3.00, and the electrons of B are more easily obtained by adjacent N atoms, thus retaining the 3d¹⁰ configuration of Zn. Figure 3.9f is the volcano map of ORR corresponding to various carbon-based catalysts (the starting electrode potential of RDS calculated by DFT on the left side and the current measured by rotating disk ring electrode on the right side) [1]. The reliability of the data is illustrated according to the consistency between DFT calculation and experimental results. Choi et al. [75] simulated and calculated the surface oxidized Fe–N–C by DFT in order to deeply understand the fatal weakness of Fe–N–C in acidic medium. Figure 3.9e shows the calculated binding energy and electron work function of O₂ at different positions, and Fig. 3.9h shows that after the carbon surface is oxidized (there are electron-withdrawing groups on the surface), the d orbital of Fe decreases, which reduces

the ability of absorbing oxygen at the Fe site and exhausts the p electrons of C, thus improving the electron work function (corresponding to the green column in Fig. 3.9e). Figure 3.9g depicts the ORR path of FeN₄.

In addition, DFT simulation can be combined with other characterization methods to characterize samples together. For example, people often use EXAFS fitting curve combined with DFT to judge the local coordination configuration of synthesized samples. Combining STM with DFT to judge the existing forms of light atoms on the surface of carbon-based monatomic catalysts.

In a word, in carbon-based nanomaterials, simulation and calculation are powerful tools to explore the coordination structure and electronic structure of active sites in

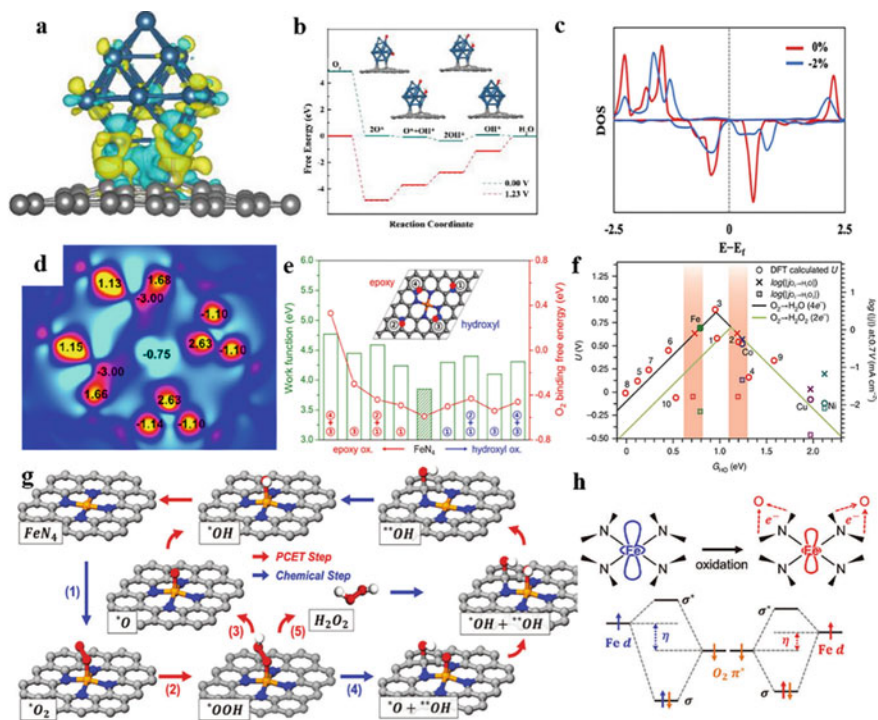


Fig. 3.9 Simulation and calculation. **a** Charge density difference for Ir₁₉ cluster on graphene. **b** Gibbs free energy diagram for ORR on Ir₁₉ cluster. Reproduced with permission [22]. Copyright 2019, WILEY-VCH. **c** DOS of the 3d orbitals of the central Fe ion in the two modeled FeN₄ sites. Reproduced with permission [73]. Copyright 2019, WILEY-VCH. **d** Charge density difference and Bader charge. Reproduced with permission [74]. Copyright 2020, WILEY-VCH. **e** O₂-binding energy of FeN₄ and electron work function. Reproduced with permission [75]. Copyright 2018, Royal Society of Chemistry. **f** The ORR volcano activity plot. Reproduced with permission [1]. Copyright 2020, Springer Nature. **g** ORR pathways at FeN₄. Single and double asterisks denote reaction intermediates adsorbed on the Fe-center and nearest C-center, respectively. **h** Scheme of electron depletion at the FeN₄ center induced by surface oxidation. Reproduced with permission [75]. Copyright 2018, Royal Society of Chemistry

carbon-based catalysts, and are very important to verify the relationship between atomic coordination configuration and catalyst activity and selectivity. If the calculation model and results are consistent with the experimental results, it can provide powerful theoretical guidance for the practical application of carbon-based nanomaterials.

3.5 Conclusion and Perspectives

This chapter describes in detail the methodologies for characterization of carbon-based nanomaterials for energy storage and conversion from three perspectives: direct visualization, indirect verification, simulation, and computation. The characterization of carbon-based nanomaterials is critical for carbon-based material research and development. Using early characterization methodologies, it is challenging to precisely identify the active sites of the catalysts and monitor the changes in the electronic structure and coordination state of the catalytic sites during the reaction process in carbon-based nano-catalysts. From an experimental standpoint, this makes it difficult to completely comprehend the true functions of the active site types in various electrocatalytic reactions, unveil the catalytic mechanism and build efficient catalysts. The development and widespread application of advanced characterization techniques, particularly the establishment of various *in-situ* spectroscopy methods, have deepened the understanding of the catalytic mechanism of carbon-based nano-catalysts, and facilitated the rational design the catalysts. However, each characterization technique has its advantages and disadvantages, so the information derived by any characterization tool should be better validated by other techniques. Meanwhile, to precisely reveal the catalytic mechanism of carbon-based catalysts, as many reliable characterizations as possible of the reaction behavior of substrates or intermediates on the active site are required. Undoubtedly, further refinement and development of reliable characterization techniques are needed to precisely reveal the catalytic reaction mechanism and efficiently guide high-performance carbon-based catalysts.

References

1. F. Luo, A. Roy, L. Silvioli, D.A. Cullen, A. Zitolo, M.T. Sougrati, I.C. Oguz, T. Mineva, D. Teschner, S. Wagner, J. Wen, F. Dionigi, U.I. Kramm, J. Rossmeisl, F. Jaouen, P. Strasser, P-block single-metal-site tin/nitrogen-doped carbon fuel cell cathode catalyst for oxygen reduction reaction. *Nat. Mater.* **19**, 1215–1223 (2020). <https://doi.org/10.1038/s41563-020-0717-5>
2. X. Chen, M. Peng, X. Cai, Y. Chen, Z. Jia, Y. Deng, B. Mei, Z. Jiang, D. Xiao, X. Wen, N. Wang, H. Liu, D. Ma, Regulating coordination number in atomically dispersed Pt species on defect-rich graphene for n-butane dehydrogenation reaction. *Nat. Commun.* **12**, 2664 (2021). <https://doi.org/10.1038/s41467-021-22948-w>

3. T. Wang, X. Cao, H. Qin, L. Shang, S. Zheng, F. Fang, L. Jiao, P-block atomically dispersed antimony catalyst for highly efficient oxygen reduction reaction. *Angew. Chem. Int. Ed.* **60**, 21237–21241 (2021). <https://doi.org/10.1002/anie.202108599>
4. Z. Xiao, C. Xie, Y. Wang, R. Chen, S. Wang, Recent advances in defect electrocatalysts: Preparation and characterization. *J. Energy Chem.* **53**, 208–225 (2021). <https://doi.org/10.1016/j.jechem.2020.04.063>
5. W.J. Jiang, L. Gu, L. Li, Y. Zhang, X. Zhang, L.J. Zhang, J.Q. Wang, J.S. Hu, Z. Wei, L.J. Wan, Understanding the high activity of Fe–N–C electrocatalysts in oxygen reduction: Fe/Fe₃C nanoparticles boost the activity of Fe–N_(x). *J. Am. Chem. Soc.* **138**, 3570–3578 (2016). <https://doi.org/10.1021/jacs.6b00757>
6. L. Guo, S. Hwang, B. Li, F. Yang, M. Wang, M. Chen, X. Yang, S.G. Karakalos, D.A. Cullen, Z. Feng, G. Wang, G. Wu, H. Xu, Promoting atomically dispersed MnN₄ sites via sulfur doping for oxygen reduction: Unveiling intrinsic activity and degradation in fuel cells. *ACS Nano* **15**, 6886–6899 (2021). <https://doi.org/10.1021/acsnano.0c10637>
7. R.R. Shahi, O.N. Srivastava, WITHDRAWN: Carbon nanomaterials as catalysts for hydrogen uptake and release by nanocrystalline MgH₂. *J. Phys. Chem. Solids* (2013). <https://doi.org/10.1016/j.jpcs.2013.06.015>
8. P. Jiang, J. Chen, C. Wang, K. Yang, S. Gong, S. Liu, Z. Lin, M. Li, G. Xia, Y. Yang, J. Su, Q. Chen, Tuning the activity of carbon for electrocatalytic hydrogen evolution via an iridium-cobalt alloy core encapsulated in nitrogen-doped carbon cages. *Adv. Mater.* **30**, 1705324 (2018). <https://doi.org/10.1002/adma.201705324>
9. Z. Weng, Y. Wu, M. Wang, J. Jiang, K. Yang, S. Huo, X.F. Wang, Q. Ma, G.W. Brudvig, V.S. Batista, Y. Liang, Z. Feng, H. Wang, Active sites of copper-complex catalytic materials for electrochemical carbon dioxide reduction. *Nat. Commun.* **9**, 415 (2018). <https://doi.org/10.1038/s41467-018-02819-7>
10. D.A. Welch, B.L. Mehdi, H.J. Hatchell, R. Faller, J.E. Evans, N.D. Browning, Using molecular dynamics to quantify the electrical double layer and examine the potential for its direct observation in the *in-situ* TEM. *Adv. Struct. Chem. Imaging* **1**, 1 (2015). <https://doi.org/10.1186/s40679-014-0002-2>
11. D. Liu, K. Ni, J. Ye, J. Xie, Y. Zhu, L. Song, Tailoring the structure of carbon nanomaterials toward high-end energy applications. *Adv. Mater.* **30**, e1802104 (2018). <https://doi.org/10.1002/adma.201802104>
12. J.C. Dong, X.G. Zhang, V. Briega Martos, X. Jin, J. Yang, S. Chen, Z.L. Yang, D.Y. Wu, J.M. Feliu, C.T. Williams, Z.Q. Tian, J.F. Li, In situ Raman spectroscopic evidence for oxygen reduction reaction intermediates at platinum single-crystal surfaces. *Nat. Energy* **4**, 60–67 (2018). <https://doi.org/10.1038/s41560-018-0292-z>
13. J. Zhang, Z. Gao, S. Wang, G. Wang, X. Gao, B. Zhang, S. Xing, S. Zhao, Y. Qin, Origin of synergistic effects in bicomponent cobalt oxide-platinum catalysts for selective hydrogenation reaction. *Nat. Commun.* **10**, 4166 (2019). <https://doi.org/10.1038/s41467-019-11970-8>
14. M. Chen, X. Li, F. Yang, B. Li, T. Stracensky, S. Karakalos, S. Mukerjee, Q. Jia, D. Su, G. Wang, G. Wu, H. Xu, Atomically dispersed MnN₄ catalysts via environmentally benign aqueous synthesis for oxygen reduction: Mechanistic understanding of activity and stability improvements. *ACS Catal.* **10**, 10523–10534 (2020). <https://doi.org/10.1021/acscatal.0c02490>
15. H. Geng, Y. Peng, L. Qu, H. Zhang, M. Wu, Structure design and composition engineering of carbon-based nanomaterials for lithium energy storage. *Adv. Energy Mater.* **10**, 1903030 (2020). <https://doi.org/10.1002/aenm.201903030>
16. F. Huang, Z. Jia, J. Diao, H. Yuan, D. Su, H. Liu, Palladium nanoclusters immobilized on defective nanodiamond-graphene core-shell supports for semihydrogenation of phenylacetylene. *J. Energy Chem.* **33**, 31–36 (2019). <https://doi.org/10.1016/j.jechem.2018.08.006>
17. J. King, C. Liu, S.S.C. Chuang, In situ infrared approach to unravel reaction intermediates and pathways on catalyst surfaces. *Res. Chem. Intermed.* **45**, 5831–5847 (2019). <https://doi.org/10.1007/s11164-019-04004-x>
18. X. Li, H.Y. Wang, H. Yang, W. Cai, S. Liu, B. Liu, In situ/Operando characterization techniques to probe the electrochemical reactions for energy conversion. *Small Methods* **2**, 1700395 (2018). <https://doi.org/10.1002/smt.201700395>

19. A.D. Handoko, F. Wei, B.S. Jenndy, Z.W.S. Yeo, Understanding heterogeneous electrocatalytic carbon dioxide reduction through operando techniques. *Nat. Catal.* **1**, 922–934 (2018). <https://doi.org/10.1038/s41929-018-0182-6>
20. J. Wang, G. Han, L. Wang, L. Du, G. Chen, Y. Gao, Y. Ma, C. Du, X. Cheng, P. Zuo, G. Yin, ZIF-8 with ferrocene encapsulated: A promising precursor to single-atom Fe embedded nitrogen-doped carbon as highly efficient catalyst for oxygen electroreduction. *Small* **14**, 1704282 (2018). <https://doi.org/10.1002/sml.201704282>
21. Y. Wang, W. Cheng, P. Yuan, G. Yang, S. Mu, J. Liang, H. Xia, K. Guo, M. Liu, S. Zhao, G. Qu, B.A. Lu, Y. Hu, J. Hu, J.N. Zhang, Boosting nitrogen reduction to ammonia on FeN₄ sites by atomic spin regulation. *Adv. Sci.* **8**, e2102915 (2021). <https://doi.org/10.1002/adv.202102915>
22. M. Xiao, J. Zhu, G. Li, N. Li, S. Li, Z.P. Cano, L. Ma, P. Cui, P. Xu, G. Jiang, H. Jin, S. Wang, T. Wu, J. Lu, A. Yu, D. Su, Z. Chen, A single-atom iridium heterogeneous catalyst in oxygen reduction reaction. *Angew. Chem. Int. Ed.* **58**, 9640–9645 (2019). <https://doi.org/10.1002/anie.201905241>
23. P. Tieu, X. Yan, M. Xu, P. Christopher, X. Pan, Directly probing the local coordination, charge state, and stability of single atom catalysts by advanced electron microscopy: A review. *Small* **17**, e2006482 (2021). <https://doi.org/10.1002/small.202006482>
24. R. Qin, K. Liu, Q. Wu, N. Zheng, Surface coordination chemistry of atomically dispersed metal catalysts. *Chem. Rev.* **120**, 11810–11899 (2020). <https://doi.org/10.1021/acs.chemrev.0c00094>
25. M.W. Glasscott, A.D. Pendergast, M.H. Choudhury, J.E. Dick, Advanced characterization techniques for evaluating porosity, nanopore tortuosity, and electrical connectivity at the single-nanoparticle level. *ACS Appl. Nano Mater.* **2**, 819–830 (2018). <https://doi.org/10.1021/acsnm.8b02051>
26. Y. Wang, H. Su, Y. He, L. Li, S. Zhu, H. Shen, P. Xie, X. Fu, G. Zhou, C. Feng, D. Zhao, F. Xiao, X. Zhu, Y. Zeng, M. Shao, S. Chen, G. Wu, J. Zeng, C. Wang, Advanced electrocatalysts with single-metal-atom active sites. *Chem. Rev.* **120**, 12217–12314 (2020). <https://doi.org/10.1021/acs.chemrev.0c00594>
27. S.W. Lee, J. Kim, S. Chen, P.T. Hammond, Y. Shao-Horn, Carbon nanotube/manganese oxide ultrathin film electrodes for electrochemical capacitors. *ACS Nano* **4**, 3889–3896 (2010). <https://doi.org/10.1021/nn100681d>
28. Y. Han, Y.G. Wang, W. Chen, R. Xu, L. Zheng, J. Zhang, J. Luo, R.A. Shen, Y. Zhu, W.C. Cheong, C. Chen, Q. Peng, D. Wang, Y. Li, Hollow N-doped carbon spheres with isolated cobalt single atomic sites: Superior electrocatalysts for oxygen reduction. *J. Am. Chem. Soc.* **139**, 17269–17272 (2017). <https://doi.org/10.1021/jacs.7b10194>
29. L. Zhou, P. Zhou, Y. Zhang, B. Liu, P. Gao, S. Guo, 3D star-like atypical hybrid MOF derived single-atom catalyst boosts oxygen reduction catalysis. *J. Energy Chem.* **55**, 355–360 (2021). <https://doi.org/10.1016/j.jechem.2020.06.059>
30. J. Chen, Z. Ou, H. Chen, S. Song, K. Wang, Y. Wang, Recent developments of nanocarbon based supports for PEMFCs electrocatalysts. *Chin. J. Catal.* **42**, 1297–1326 (2021). [https://doi.org/10.1016/s1872-2067\(20\)63736-6](https://doi.org/10.1016/s1872-2067(20)63736-6)
31. J. Pan, S. Yu, Z. Jing, Q. Zhou, Y. Dong, X. Lou, F. Xia, Electrocatalytic hydrogen evolution reaction related to nanochannel materials. *Small Struct.* **2**, 2100076 (2021). <https://doi.org/10.1002/sstr.202100076>
32. C.H. Choi, M. Kim, H.C. Kwon, S.J. Cho, S. Yun, H.T. Kim, K.J. Mayrhofer, H. Kim, M. Choi, Tuning selectivity of electrochemical reactions by atomically dispersed platinum catalyst. *Nat. Commun.* **7**, 10922 (2016). <https://doi.org/10.1038/ncomms10922>
33. Y. Shang, X. Duan, S. Wang, Q. Yue, B. Gao, X. Xu, Carbon-based single atom catalyst: Synthesis, characterization, DFT calculations. *Chin. Chem. Lett.* (2021). <https://doi.org/10.1016/j.ccl.2021.07.050>
34. L.Z. Zhang, Y. Jia, G.P. Gao, X.C. Yan, N. Chen, J. Chen, M.T. Soo, B. Wood, D.J. Yang, A.J. Du, X.D. Yao, Graphene defects trap atomic Ni species for hydrogen and oxygen evolution reactions. *Chem* **4**, 285–297 (2018). <https://doi.org/10.1016/j.chempr.2017.12.005>
35. L. Fan, P.F. Liu, X. Yan, L. Gu, Z.Z. Yang, H.G. Yang, S. Qiu, X. Yao, Atomically isolated nickel species anchored on graphitized carbon for efficient hydrogen evolution electrocatalysis. *Nat. Commun.* **7**, 10667 (2016). <https://doi.org/10.1038/ncomms10667>

36. H.T. Chung, D.A. Cullen, D. Higgins, B.T. Sneed, E.F. Holby, K.L. More, P. Zelenay, Direct atomic-level insight into the active sites of a high-performance PGM-free ORR catalyst. *Science* **357**, 479–484 (2017). <https://doi.org/10.1126/science.aan2255>
37. X. Dai, Z. Chen, T. Yao, L. Zheng, Y. Lin, W. Liu, H. Ju, J. Zhu, X. Hong, S. Wei, Y. Wu, Y. Li, Single Ni sites distributed on N-doped carbon for selective hydrogenation of acetylene. *Chem. Commun.* **53**, 11568–11571 (2017). <https://doi.org/10.1039/c7cc04820c>
38. P.L. Gai, E.D. Boyes, In-situ environmental (scanning) transmission electron microscopy of catalysts at the atomic level. *J. Phys: Conf. Ser.* **522**, 012002 (2014). <https://doi.org/10.1088/1742-6596/522/1/012002>
39. D. Xue, H. Xia, W. Yan, J. Zhang, S. Mu, Defect engineering on carbon-based catalysts for electrocatalytic CO₂ reduction. *Nano-Micro Lett.* **13**, 5 (2020). <https://doi.org/10.1007/s40820-020-00538-7>
40. D. Deng, X. Pan, L. Yu, Y. Cui, Y. Jiang, J. Qi, W.X. Li, Q. Fu, X. Ma, Q. Xue, G. Sun, X. Bao, Toward N-doped graphene via solvothermal synthesis. *Chem. Mater.* **23**, 1188–1193 (2011). <https://doi.org/10.1021/cm102666r>
41. Q. Liu, Y. Liu, H. Li, L. Li, D. Deng, F. Yang, X. Bao, Towards the atomic-scale characterization of isolated iron sites confined in a nitrogen-doped graphene matrix. *Appl. Surf. Sci.* **410**, 111–116 (2017). <https://doi.org/10.1016/j.apsusc.2017.03.090>
42. R.J. Nicholls, A.T. Murdock, J. Tsang, J. Britton, T.J. Pennycook, A. Koos, P.D. Nellist, N. Grobert, J.R. Yates, Probing the bonding in nitrogen-doped graphene using electron energy loss spectroscopy. *ACS Nano* **7**, 7145–7150 (2013). <https://doi.org/10.1021/nn402489v>
43. Y. Qiao, P. Yuan, C.W. Pao, Y. Cheng, Z. Pu, Q. Xu, S. Mu, J. Zhang, Boron-rich environment boosting ruthenium boride on B, N doped carbon outperforms platinum for hydrogen evolution reaction in a universal pH range. *Nano Energy* **75**, 104881 (2020). <https://doi.org/10.1016/j.nanoen.2020.104881>
44. J. Han, H. Bao, J.Q. Wang, L. Zheng, S. Sun, Z.L. Wang, C. Sun, 3D N-doped ordered mesoporous carbon supported single-atom Fe–N–C catalysts with superior performance for oxygen reduction reaction and zinc-air battery. *Appl. Catal. B* **280**, 119411 (2021). <https://doi.org/10.1016/j.apcatb.2020.119411>
45. F. Yang, M. Wang, D. Zhang, J. Yang, M. Zheng, Y. Li, Chirality pure carbon nanotubes: Growth, sorting, and characterization. *Chem. Rev.* **120**, 2693–2758 (2020). <https://doi.org/10.1021/acs.chemrev.9b00835>
46. M. Huang, S. Gong, C. Wang, Y. Yang, P. Jiang, P. Wang, L. Hu, Q. Chen, Lewis-basic EDTA as a highly active molecular electrocatalyst for CO₂ reduction to CH₄. *Angew. Chem. Int. Ed.* **60**, 23002 (2021). <https://doi.org/10.1002/anie.202110594>
47. Y. Liu, D. Tian, A.N. Biswas, Z. Xie, S. Hwang, J.H. Lee, H. Meng, J.G. Chen, Transition metal nitrides as promising catalyst supports for tuning CO/H₂ syngas production from electrochemical CO₂ reduction. *Angew. Chem. Int. Ed.* **59**, 11345–11348 (2020). <https://doi.org/10.1002/anie.202003625>
48. C. Jia, X. Tan, Y. Zhao, W. Ren, Y. Li, Z. Su, S.C. Smith, C. Zhao, Sulfur-dopant-promoted electroreduction of CO₂ over coordinatively unsaturated Ni–N₂ moieties. *Angew. Chem. Int. Ed.* **60**, 23342 (2021). <https://doi.org/10.1002/anie.202109373>
49. L. Liang, H. jin, H. Zhou, B. Liu, C. Hu, D. Chen, J. Zhu, Z. Wang, H.W. Li, S. Liu, D. He, S. Mu, Ultra-small platinum nanoparticles segregated by nickle sites for efficient ORR and HER processes. *J. Energy Chem.* **65**, 48–54 (2022). <https://doi.org/10.1016/j.jechem.2021.05.033>
50. Y. He, H. Guo, S. Hwang, X. Yang, Z. He, J. Braaten, S. Karakalos, W. Shan, M. Wang, H. Zhou, Z. Feng, K.L. More, G. Wang, D. Su, D.A. Cullen, L. Fei, S. Litster, G. Wu, Single cobalt sites dispersed in hierarchically porous nanofiber networks for durable and high-power PGM-free cathodes in fuel cells. *Adv. Mater.* **32**, e2003577 (2020). <https://doi.org/10.1002/adma.202003577>
51. J. Zhang, J. Zhang, F. He, Y. Chen, J. Zhu, D. Wang, S. Mu, H.Y. Yang, Defect and doping co-engineered non-metal nanocarbon ORR electrocatalyst. *Nano-Micro Lett.* **13**, 65 (2021). <https://doi.org/10.1007/s40820-020-00579-y>

52. Y. Jia, L. Zhang, A. Du, G. Gao, J. Chen, X. Yan, C.L. Brown, X. Yao, Defect graphene as a trifunctional catalyst for electrochemical reactions. *Adv. Mater.* **28**, 9532–9538 (2016). <https://doi.org/10.1002/adma.201602912>
53. X. Li, X. Yang, J. Zhang, Y. Huang, B. Liu, In Situ/Operando techniques for characterization of single-atom catalysts. *ACS Catal.* **9**, 2521–2531 (2019). <https://doi.org/10.1021/acscatal.8b04937>
54. A.J. Jebaraj, D.A. Scherson, Microparticle electrodes and single particle microbatteries: electrochemical and in situ micro Raman spectroscopic studies. *Acc. Chem. Res.* **46**, 1192–1205 (2013). <https://doi.org/10.1021/ar300210q>
55. X. Xie, C. He, B. Li, Y. He, D.A. Cullen, E.C. Wegener, A.J. Kropf, U. Martinez, Y. Cheng, M.H. Engelhard, M.E. Bowden, M. Song, T. Lemmon, X.S. Li, Z. Nie, J. Liu, D.J. Myers, P. Zelenay, G. Wang, G. Wu, V. Ramani, Y. Shao, Performance enhancement and degradation mechanism identification of a single-atom Co–N–C catalyst for proton exchange membrane fuel cells. *Nat. Catal.* **3**, 1044–1054 (2020). <https://doi.org/10.1038/s41929-020-00546-1>
56. G.Y. Qiao, D. Guan, S. Yuan, H. Rao, X. Chen, J.A. Wang, J.S. Qin, J.J. Xu, J. Yu, Perovskite quantum dots encapsulated in a mesoporous metal-organic framework as synergistic photocathode materials. *J. Am. Chem. Soc.* **143**, 14253–14260 (2021). <https://doi.org/10.1021/jacs.1c05907>
57. J. Zhang, Z. Xia, L. Dai, Carbon-based electrocatalysts for advanced energy conversion and storage. *Sci. Adv.* **1**, e1500564 (2015). <https://doi.org/10.1126/sciadv.1500564>
58. S. Wang, N. Yan, X-ray absorption spectroscopy: An indispensable tool to study single-atom catalysts. *Synchrotron Radiat News* **33**, 18–26 (2020). <https://doi.org/10.1080/08940886.2020.1812354>
59. X. Han, T. Zhang, W. Chen, B. Dong, G. Meng, L. Zheng, C. Yang, X. Sun, Z. Zhuang, D. Wang, A. Han, J. Liu, MnN₄ oxygen reduction electrocatalyst: Operando investigation of active sites and high performance in zinc-air battery. *Adv. Energy Mater.* **11**, 2002753 (2020). <https://doi.org/10.1002/aenm.202002753>
60. H.B. Yang, S.F. Hung, S. Liu, K. Yuan, S. Miao, L. Zhang, X. Huang, H.Y. Wang, W. Cai, R. Chen, J. Gao, X. Yang, W. Chen, Y. Huang, H.M. Chen, C.M. Li, T. Zhang, B. Liu, Atomically dispersed Ni(I) as the active site for electrochemical CO₂ reduction. *Nat. Energy* **3**, 140–147 (2018). <https://doi.org/10.1038/s41560-017-0078-8>
61. Y. Xing, Z. Yao, W. Li, W. Wu, X. Lu, J. Tian, Z. Li, H. Hu, M. Wu, Fe/Fe₃C boosts H₂O₂ utilization for methane conversion overwhelming O₂ generation. *Angew. Chem. Int. Ed.* **60**, 8889–8895 (2021). <https://doi.org/10.1002/anie.202016888>
62. S. Song, J. Zhou, X. Su, Y. Wang, J. Li, L. Zhang, G. Xiao, C. Guan, R. Liu, S. Chen, H.J. Lin, S. Zhang, J.Q. Wang, Operando X-ray spectroscopic tracking of self-reconstruction for anchored nanoparticles as high-performance electrocatalysts towards oxygen evolution. *Energy Environ. Sci.* **11**, 2945–2953 (2018). <https://doi.org/10.1039/c8ee00773j>
63. J. Wei, S.N. Qin, J. Yang, H.L. Ya, W.H. Huang, H. Zhang, B.J. Hwang, Z.Q. Tian, J.F. Li, Probing single-atom catalysts and catalytic reaction processes by shell-isolated nanoparticle-enhanced Raman spectroscopy. *Angew. Chem. Int. Ed.* **60**, 9306–9310 (2021). <https://doi.org/10.1002/anie.202100198>
64. S. Chen, A. Chen, Electrochemical reduction of carbon dioxide on Au nanoparticles: An in situ FTIR study. *J. Phys. Chem. C* **123**, 23898–23906 (2019). <https://doi.org/10.1021/acs.jpcc.9b04080>
65. Y. Chen, H. Li, W. Zhao, W. Zhang, J. Li, W. Li, X. Zheng, W. Yan, W. Zhang, J. Zhu, R. Si, J. Zeng, Optimizing reaction paths for methanol synthesis from CO₂ hydrogenation via metal-ligand cooperativity. *Nat. Commun.* **10**, 1885 (2019). <https://doi.org/10.1038/s41467-019-09918-z>
66. S. Wu, J. Kaiser, X. Guo, L. Li, Y. Lu, M. Ballauff, Recoverable platinum nanocatalysts immobilized on magnetic spherical polyelectrolyte brushes. *Ind. Eng. Chem. Res.* **51**, 5608–5614 (2012). <https://doi.org/10.1021/ie2025147>
67. G. Yang, J. Zhu, P. Yuan, Y. Hu, G. Qu, B.A. Lu, X. Xue, H. Yin, W. Cheng, J. Cheng, W. Xu, J. Li, J. Hu, S. Mu, J.N. Zhang, Regulating Fe-spin state by atomically dispersed Mn–N in

- Fe–N–C catalysts with high oxygen reduction activity. *Nat. Commun.* **12**, 1734 (2021). <https://doi.org/10.1038/s41467-021-21919-5>
68. R. Jalem, Y. Morishita, T. Okajima, H. Takeda, Y. Kondo, M. Nakayama, T. Kasuga, Experimental and first-principles DFT study on the electrochemical reactivity of garnet-type solid electrolytes with carbon. *J. Mater. Chem. A* **4**, 14371–14379 (2016). <https://doi.org/10.1039/c6ta04280e>
69. T.K. Schwietert, A. Vasileiadis, M. Wagemaker, First-principles prediction of the electrochemical stability and reaction mechanisms of solid-state electrolytes. *JACS Au* **1**, 1488–1496 (2021). <https://doi.org/10.1021/jacsau.1c00228>
70. M.R. Philpott, J.N. Glosli, Molecular dynamics simulation of interfacial electrochemical processes: Electric double layer screening. *Solid-Liquid Electrochem Interfaces*, 13–30
71. A. Kumar, V.K. Vashista, D.K. Das, S. Ibraheem, G. Yasin, R. Iqbal, T.A. Nguyen, R.K. Gupta, M. Rasidul Islam, M–N–C-based single-atom catalysts for H₂, O₂ and CO₂ electrocatalysis: Activity descriptors, active sites identification, challenges and prospects. *Fuel* **304**, 121420 (2021). <https://doi.org/10.1016/j.fuel.2021.121420>
72. C. Chu, D. Huang, S. Gupta, S. Weon, J. Niu, E. Stavitski, C. Muhich, J.H. Kim, Neighboring Pd single atoms surpass isolated single atoms for selective hydrodehalogenation catalysis. *Nat. Commun.* **12**, 5179 (2021). <https://doi.org/10.1038/s41467-021-25526-2>
73. J. Li, H. Zhang, W. Samarakoon, W. Shan, D.A. Cullen, S. Karakalos, M. Chen, D. Gu, K.L. More, G. Wang, Z. Feng, Z. Wang, G. Wu, Thermally driven structure and performance evolution of atomically dispersed FeN₄ sites for oxygen reduction. *Angew. Chem. Int. Ed.* **58**, 18971–18980 (2019). <https://doi.org/10.1002/anie.201909312>
74. J. Wang, H. Li, S. Liu, Y. Hu, J. Zhang, M. Xia, Y. Hou, J. Tse, J. Zhang, Y. Zhao, Turning on Zn 4s electrons in a N₂–Zn–B₂ configuration to stimulate remarkable ORR performance. *Angew. Chem. Int. Ed.* **60**, 181–185 (2021). <https://doi.org/10.1002/anie.202009991>
75. C.H. Choi, H.K. Lim, M.W. Chung, G. Chon, N. Ranjbar Sahraie, A. Altin, M.T. Sougrati, L. Stievano, H.S. Oh, E.S. Park, F. Luo, P. Strasser, G. Dražić, K.J.J. Mayrhofer, H. Kim, F. Jaouen, The achilles' heel of iron-based catalysts during oxygen reduction in an acidic medium. *Energy Environ. Sci.* **11**, 3176–3182 (2018). <https://doi.org/10.1039/c8ee01855c>

Chapter 4

Catalytic Effect of Carbon-Based Nanomaterials in Electrochemical Catalysis



Yajin Wang, Xiaoyu Zhang, Huicong Xia, and Jia-Nan Zhang

Abstract Carbon materials have been widely studied and applied as electrocatalysts in recent years due to their advantages of good stability, adjustable pores, high specific surface area, and excellent electrical conductivity. Graphene, carbon nanotubes, and mesoporous carbon are commonly used in the preparation of electrocatalysts, which are good composite matrix materials. Load different active species on the carbon nanomaterial to increase the electron asymmetry density of carbon nanomaterials or break the electrical neutrality of the carbon surface to form more adsorption active sites, which is also more conducive to the free movement of sp^2 hybridized π electrons on the carbon surface, so that the electronic distribution and spatial structure of the composite material are changed. In the process of synthesizing carbon-based nanomaterials, these changes will cause different catalytic effects between the substrates and the supported materials. The catalytic effect can not only change the size of supported-materials and the coordination of the chemical environment, but also use the interaction between supported-materials and the substrates as a bridge for the electrons theoretical study of heterogeneous catalytic, and can also use the structural characteristics to form a local electric field to promote transmission. Therefore, the electrocatalytic activity of carbon-based nanomaterials can be effectively improved. In this chapter, several catalytic effects of carbon-based nanomaterials have been reviewed, including confinement effect, interface engineering effect, and electric field effect, and mechanisms of different catalytic effects and electrocatalytic applications have also been systematically discussed.

Y. Wang · X. Zhang · H. Xia · J.-N. Zhang (✉)
College of Materials Science and Engineering, Zhengzhou University, Zhengzhou 450001,
P. R. China
e-mail: zjn@zzu.edu.cn

Y. Wang
e-mail: 13283861570@163.com

X. Zhang
e-mail: zhangxiaoyu0321@163.com

H. Xia
e-mail: summer9209@126.com

4.1 Introduction

Carbon nanomaterials have good electrocatalytic properties as electrocatalytic catalysts due to their controllable electronic structure, excellent electrical/thermal conductivity, and abundant surface active sites [1, 2]. Meanwhile, a large number of studies have shown that precise control of the structure and morphology of the electrocatalyst can improve its catalytic performance for important reactions such as oxygen reduction/hydrogen evolution reaction (ORR/OER), hydroxide/hydrogen evolution reaction (HOR/HER), and carbon dioxide/nitrogen reduction reaction ($\text{CO}_2\text{RR}/\text{NRR}$), etc. [3]. In the process of preparing carbon-based nanomaterials and adjusting their structure and morphology, different catalytic effects will occur between the carbon support and active species, including confinement effect, [4] interface engineering effect, [5] and electric field effect, [6] which can improve the electrochemical performance of carbon-based nanomaterials (Fig. 4.1).

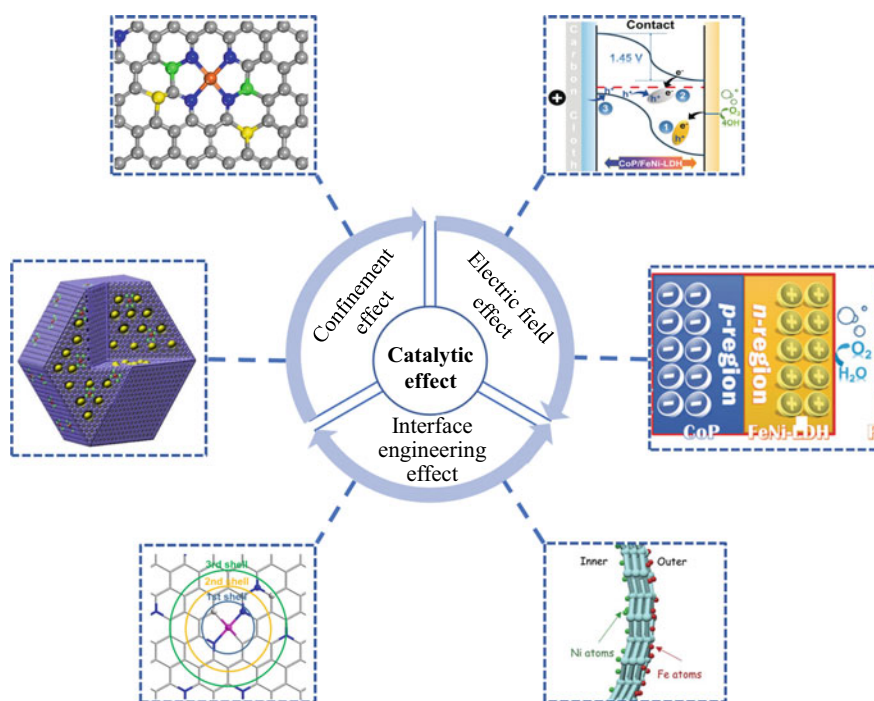


Fig. 4.1 Catalytic effect of carbon-based nanomaterials in electrochemical catalysis. Reproduced with permission [7]. Copyright 2019, WILEY-VCH. Reproduced with permission [8]. Copyright 2021, Springer Nature. Reproduced with permission [9]. Copyright 2020, WILEY-VCH. Reproduced with permission [10]. Copyright 2018, American Association for the Advancement of Science (AAAS). Reproduced with permission [11]. Copyright 2018, Springer Nature

Because of their large surface area, ordered pore size, and high porosity, porous carbon-based materials have a significant confinement effect when used as electrocatalysts: (1) The confinement engineering can disperse and stabilize single atoms, clusters, and nanoparticles (NPs) through space confinement to prevent agglomeration and improve the durability of the catalyst. The reactants are usually confined in nano-spaces such as micro/nanopores in 0D microporous carbon, one-dimensional (1D) channels in carbon nanotubes (CNTs), two-dimensional (2D) spaces in layered materials (e.g., 2D layered graphite, etc.), and three-dimensional (3D) spaces in metal-organic frameworks (MOF), etc. [4, 12]. Such materials hold uniform and limited nano-spaces to confine the growth of desired catalysts in certain dimensions. (2) The metal dimensions are controlled at the atomic level by means of coordination confinement. The chemical coordination confinement is an effective strategy for the synthesis of catalysts when the size further goes down to the atomic level. Anchoring the active atom on a substrate with the specific chemical coordination interaction from surface functional heteroatom, coordinative unsaturated atoms, defects, etc. enables to precisely prepare uniform atomic sites, giving various single-atom catalysts (SACs) or metal clusters [13].

Recently, improving the interface effect of transition-metal carbon-based catalysts to promote the interaction of metal carriers has been regarded as an effective strategy to improve the catalytic performance and stability [14]. The electronic metal-support interaction (EMSI) intensely affect electrocatalysts' performance in terms of intrinsic activity, active site density, and durability [15]. To date, constructing transition-metal carbon-based electrocatalysts with abundant engineered interfaces has been regarded as an effective strategy to facilitate the reaction rate [16]. Interface engineering to design composite can combine the merits of different materials, which is beneficial for exploring active catalysts [17]. The interplay at the interface can achieve simultaneous exposure of electron-rich and electron-deficient regions within a catalyst, which can facilitate both reduction and oxidation reactions. Benefiting from the significant interfacial interaction, which is unattainable for conventional catalysts, some transition-metal carbon-based catalysts even show high activity and stability that is comparable to noble-metal-based catalysts [14]. On the one hand, active species are encapsulated into the stable carbon layer to protect the inner metal core from the destructive reaction environment. Electron transfer from the active metal core to the carbon layer stimulates unique catalytic activity on the carbon surface which has been extensively utilized in a variety of catalytic reaction systems [18]. On the other hand, doping heteroatoms into carbon material (e.g., nitrogen-doped) is a practical strategy to regulate the electronic state of C atoms in doped area and thus adjust the performance [19]. Beyond that, the N-doped carbon material with the high affinity of nitrogen can also be combined with metal atoms [20]. The specific coordination structure participates in constructing the efficient active site [21]. Additionally, the formed interfacial chemical bonding can also alter the coordination state and valence state of metal atoms [22].

The design of carbon-based nanomaterials and the improvement of catalytic efficiency depend not only on the number of active sites in the catalyst, but also on the diffusion rate of the reactants. The typical pathway of the electrolysis reaction

mainly includes three steps: charge transfer and surface conversion (such as chemical adsorption of reactants and desorption of products from the electrode surface), charge transport and mass transfer [23]. After many efforts, it was found that the adsorption and desorption of intermediates can be balanced by increasing the density of catalyst active sites and adjusting the binding energy [24]. Adjusting the catalyst components [25] and introducing defects [26] are feasible methods to adjust the binding energy. For charge transport, specific materials can be used to reduce resistance [27]. However, slow mass transfer often becomes the bottleneck of the entire electrochemical reaction kinetics at high current densities [28]. According to reports, by increasing the wettability of the electrode surface, promoting the adsorption of polar reactants on the electrode surface, or forming a gas repellent surface through surface roughening and functionalization, the bubbles quickly dissipate to accelerate the mass transfer of the electrode reactants [29]. Numerous researches show that the corners and edges of the catalyst usually have good activity [30]. Researchers have also found that metal-containing materials with sharp tips [31] or high-curvature structures [32] will generate local electric fields, because this high-curvature structure will cause electrons to gather around the metal area. After a local electric field is formed, more metal cations will be attracted to the catalytic tip, thereby increasing the concentration of reactants around the catalytic site, thereby improving electrocatalytic performance [33]. The enhanced local field is also believed to lower the reaction barrier. For carbon-based nanomaterials, when metal sites are grown on a carbon-based substrate, a local electric field may be generated at the interface between the load and the substrate. For example, Yang et al. [23] synthesized the NiFe nanocone array, which had a sharp cone tip and optimized alloy composition, the generated local electric field enhanced the transfer of reactants and improved the catalytic activity of OER. And when a single metal atom embedded in the matrix to form a high-curvature surface may also generate a local electric field at the single-atom site of the metal. Song et al. [32] synthesized onion-like nanospheres of carbon (OLC) anchored atom-dispersed Pt structure (Pt₁/OLC) as the HER electrocatalyst. In an acidic medium, the Pt₁/OLC catalyst (0.27 wt% Pt) had a low overpotential (38 mV at 10 mA cm⁻²) and a high flipping frequency (40.78 H₂ s⁻¹ at 100 mV). It was better than the graphene-supported single-atom catalyst under the same Pt loading condition. The Nyquist diagram showed that Pt₁/OLC had an ultra-low charge transfer resistance (R_c), indicating that there was a rapid mass transfer process between the catalyst and the electrolyte interface. First-principles calculations showed that an *in-situ* strong local electric field was formed around the Pt site on the curved carrier and protruded from the curved OLC surface like a tip. There was significant proton enrichment around Pt, which promotes electrochemical reaction kinetics. In this chapter, several catalytic effects of carbon-based nanomaterials have been reviewed, including confinement effect, interface engineering effect, electric field effect, and systematically discussed the mechanism of different catalytic effects and electrocatalytic applications.

4.2 Confinement Effect

In general, confinement effect includes the following two aspects: Firstly, carbon nanomaterials disperse and stabilize single atoms or nanoparticles through space confinement to prevent agglomeration and improve the long-term stability of the catalyst [34–36]. Secondly, carbon nanomaterials alter the electronic structure of the active center and the chemical environment neighboring the active center through chemical coordination to improve the activity of the catalyst. Porous carbon nanomaterials with their unique characteristics: (1) excellent chemical and mechanical stability, (2) adjustable porosity and surface chemistry, (3) good electrical and thermal conductivity, (4) high specific surface area, (5) and excellent structural diversity [37–40]. Therefore, porous carbon-based materials have a good confinement effect when used as electrocatalysts. In this part, the confinement effect of porous carbon-based materials in electrochemical catalysis applications was discussed from two aspects of chemical coordination and spatial confinement.

4.2.1 Chemical Coordination Confinement Effect

The introduction of rich coordination atoms (such as N and O atoms) into porous carbon-based materials can provide rich anchoring sites to stabilize the target single metal atoms [38]. Porous carbon as a promising supporting material for single atoms due to its excellent physicochemical properties has been widely studied in recent years.

Yin et al. [41] developed a practical and controllable general strategy for the synthesis of porous carbon loaded with single atoms resulting from the pyrolysis of MOFs and the mixing of Zn as a “fence” (Fig. 4.2a). It has been shown that the atomic dispersion of Co atoms was stabilized by the generated N-doped porous carbon. The obtained Co SAs/N–C catalyst showed superior ORR performance. Wang et al. [42] developed a host–guest strategy for constructing N-doped porous carbon loaded with Fe–Co double sites. The synthesis was based on the bonding between the control Co node (host) and adsorbed Fe^{3+} ion (guest) within the confined space of MOFs. The catalyst exhibited excellent ORR performance under acidic conditions. Zhang et al. [43] utilized sulfur to boost the ORR and OER performance of a Fe–N–C catalytic system with embedded $\text{Fe}_x\text{C}/\text{Fe}$ species. Based on high-angle annular dark field scanning transmission electron microscope (HAADF-STEM), X-ray absorption near edge structure (XANES), and extended X-ray absorption fine structure (EXAFS) analysis, the Fe–S bonds formed at the interface between the $\text{Fe}_x\text{C}/\text{Fe}$ clusters can be observed and S-containing Fe–N–C matrix result in new types of active sites that can increase the activity of bifunctional catalysts for oxygen reactions. Density functional theory (DFT) calculations further confirmed that the atomically dispersed FeN_x sites of the Fe–N–C system, the Fe_xC clusters, and the S-containing sites were the active species and that their interactions played a significant role in catalytic

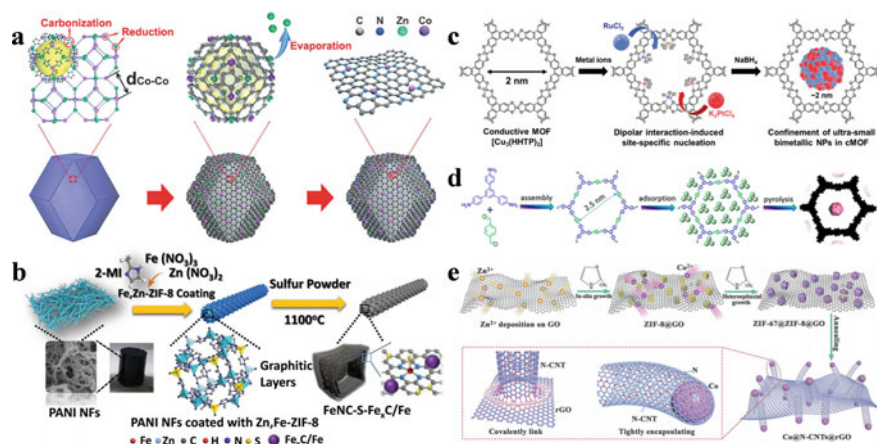


Fig. 4.2 Confinement effect of carbon-based nanomaterials in electrochemical catalysis. a The formation of Co SAs/N-C. Reproduced with permission [41]. Copyright 2016, WILEY-VCH. **b** Synthesis scheme of the FeNC-S-Fe_xC/Fe catalyst. Reproduced with permission [43]. Copyright 2018, WILEY-VCH. **c** Schematic illustration for the preparation of PtRu@cMOF. Reproduced with permission [46]. Copyright 2021, WILEY-VCH. **d** Illustration of the synthesis process of FeAC@FeSA-N-C. Reproduced with permission [47]. Copyright 2019, American Chemical Society. **e** Synthetic procedure for the preparation of Co@N-CNTs@rGO hybrid composites. Reproduced with permission [49]. Copyright 2018, WILEY-VCH

activity (Fig. 4.2b). Based on the pyrolysis of hollow MOF spheres, Yang et al. [44] rationally prepared a series of hollow porous carbons catalysts with uniform nitrogen doping and ultra-high load of single nitrogen atoms for epoxide catalysis of carbon dioxide cycloaddition. The ultra-high content of a single Zn atom was stabilized by surrounding N atoms, resulting in Zn-N₄ units, where Zn and N represented Lewis acid sites and Lewis base sites, respectively. This Zn-N₄ structure promoted the catalytic process under synergistic effect. Hu et al. [28] reported a dispersed single atomic Fe site catalyst with high carbon dioxide reduction activity. The active site was the discrete Fe³⁺ ion, which was compatible with the N-doped carbon carrier pyrrolidene (N) atom. Compared with the traditional Fe^{II} site, Fe^{III} site had a stronger carbon dioxide absorption capacity and a weaker CO absorption capacity, and thus leading to a better activity. Through the chemical coordination confinement, the abundant metal nodes and abundant ligands of MOFs made the metal single atom dispersed and stable, thus improving the activity and stability of the catalyst. Li et al. [8] reported an effective ORR catalyst consisting of graphite carbon with restricted Mn single atom. Using the unique characteristics of ZIF-8 precursors to obtain the doping and adsorption process, the density of the active sites can be effectively significantly increased. The catalyst exhibited excellent ORR activity, stability, and corrosion resistance under acidic conditions. In addition to single metal atom, MOF-derived metal nanoparticles carbon-based materials also exhibit excellent activity in confined catalysis. However, there are few examples of stabilization of nanoparticles by coordination confinement. Therefore, the design of new synthesis strategies to

confined more active sites is adjective for the future development of MOF-derived carbon-based catalysts.

4.2.2 *Spatial Confinement Effect*

Due to the existence of regular porous structures, carbon-based porous materials can spatially isolate and encapsulate suitable metal active sites through confinement effects. Chen et al. [45] produced an isolated single atomic Fe/N-porous carbon (ISA Fe/CN) catalyst with high ORR reactivity and stability by cage-encapsulated-precursor pyrolysis strategy. The spatially confined highly dispersed iron atoms were the main reasons for the enhanced catalytic activity and stability. DFT calculations showed that the potential barrier of atomically dispersed Fe at the rate-limiting step was much lower than that of Fe nanoparticles, indicating the key role of the confinement effect of MOF-derived carbon materials. Kim et al. [46] guided highly active and stable conductive MOF (cMOF), which were presented via the confinement of bimetallic nanoparticles (BNPs) in the pores of a 2D cMOF, where the confinement by dipolar-interaction-induced site-specific nucleation. Heterogeneous metal precursors were bound to the pores of 2D cMOFs by dipolar interactions, and the subsequent reduction produces ultrasmall (~1.54 nm) and well-dispersed PtRu NPs confined in the pores of the cMOF. PtRu NPs decorated cMOFs exhibited significantly enhanced chemiresistive NO₂ sensing performances, owing to the bimetallic synergies of PtRu NPs and the high surface area and porosity of cMOF. The approach paved the way for the synthesis of highly active and conductive porous materials via bimetallic and/or multimetallic NPs loading (Fig. 4.2c). Ao et al. [47] achieved coexistence of single Fe atoms and Fe nanoclusters through spatial isolation strategy using a COF template (Fig. 4.2d). Wang et al. [48] reported a two-dimensional bimetallic (Co/Zn) and leaf-like zeolitic imidazolate framework (ZIF-L) pyrolysis method for the low-cost preparation of nitrogen-doped carbon nanotubes encapsulating Co nanoparticles (Co-N-CNTs). Highly dispersed cobalt nanoparticles were completely encapsulated at the tips of N-CNTs, resulting in the complete formation of highly active cobalt for oxygen reduction and evolution reactions. The obtained Co-N-CNT had good electrocatalytic activity and stability. Chen et al. [49] used graphene oxide (GO) coated core-shell (Co, Zn) bimetallic ZIF as precursors, the synthetic carbon nanotubes were encapsulated and grafted onto GO by direct annealing (Fig. 4.2e). Uniquely core-shell ZIF-67@ZIF-8 assist in encapsulating ultrafine Co nanoparticles via N-CNT with a very thin carbon layer in situ formed, avoiding the accumulation of particles or carbon at high temperatures. In addition, ZIF-67@ZIF-8 covering GO can expose more catalytic sites and facilitate mass transfer. The prepared Co@N-CNTs@rGO composite showed excellent HER activity.

4.3 Interface Engineering Effect

As early as the 1930s, G. M. Schwab proposed the concept of “electronic factor” to describe the effect of electron interaction on the catalytic behavior of load type catalysts, and divide the electron interaction into structures and synergies [50]. When the catalytic reaction is involved, the electron transfer between the metal and the carrier is first considered. Thereafter, S. J. Tauster used the term of “strong metal-support interaction” to describe the chemical adsorption properties of VIII elements loaded by metal oxides (such as SiO_2 and MgO) in 1978 [51–53]. Later, this concept was extended to the interaction between any metal species and support based on the experimental phenomenon [53, 54]. Until then, based on the early characterization of surface science, researchers have realized that the active site may change from the metal state to the strong metal–support interaction state, indicating that the carrier covers or encapsulates the active site [55, 56]. After that, the metal-vector electron interaction is a bridge between the design of the electronic theory and the design of the multiphase catalyst, has received extensive attention [15]. The interaction between the metal and the carrier is one of the most basic strategies to improve electrocatalytic efficiency [57].

As the metal particles (nanoparticles, nanoclusters and single atoms) have decreased, the catalytic behavior of load-bearing metal species changes significantly for various chemical transformations [58, 59]. EMSI has a significant effect on the geometric structure and electron properties of the metal catalyst, and is generally considered to be a key role in adjusting the catalytic behavior of the load type metal species [60, 61]. At present, EMSI has been widely used as strategies for the stability, activity, selectivity, and screening catalytic mechanism of various load type catalyst systems [62]. However, due to the dimensional effect of the metal activity and the unique surface properties of different carriers, the EMSI is made difficult for EMSI global cognition [63, 64]. Therefore, the two factors in which the metal dimensional effect and the surface properties of the carrier are determined to determine the role of the EMSI, thereby imposing a better practical catalyst on this basis [65]. The carbon material is a carrier as an example, although it is very challenging of strong metal–carbon interactions by depositing metal species on perfect carbon-based surface [66] the suspenders of the edge carbon site can establish EMSI and effectively regulate the catalytic behavior of the metal species. For example, the carbon nanomaterial as support can minimize the agglomeration of metal NPs and stabilize the metal load by manufacturing defects, adding anchoring sites [34, 67]. The ligand can stabilize the metal surface by surface modification, thereby enhancing its activity and stability [68]. Moreover, the EMSI can change the electronic structure of the catalyst to increase its activity by changing the binding strength of the intermediate, thereby reducing the reaction energy barrier [69]. In short, EMSI plays a major role in regulating catalysis [63]. The EMSI in different types may exhibit a variety of properties during reaction [61, 70]. Although EMSI has attracted much attention, comprehensive research and operando tests are of a small amount, and may be a new opportunity for the full-scale understanding of the underlying factors in EMSI [15, 71].

Encapsulating transition metal nanoparticles inside carbon nanotubes (CNTs) or spheres has emerged as a novel strategy of designing high-durable non-precious metal catalysts. The stable carbon layer protects the inner metal core from the destructive reaction environment and thus is vividly described as chainmail for catalysts. Electron transfer from the active metal core to the carbon layer stimulates unique catalytic activity on the carbon surface which has been extensively utilized in a variety of catalytic reaction systems [18]. Bao et al. [72] reported a hierarchical architecture that consists of ultrathin graphene shells (only 1–3 layers) that encapsulate a uniform CoNi nanoalloy to enhance its HER performance in acidic media. DFT calculations indicated that the ultrathin graphene shells strongly promoted electron penetration from the CoNi nanoalloy to the graphene surface. With nitrogen dopants, they synergistically increased the electron density on the graphene surface, which resulted in superior HER activity on the graphene shells (Fig. 4.3a–c).

Product selectivity in multi-electron electrocatalytic reactions is crucial to energy conversion efficiency and chemical production. However, a present practical drawback is the limited understanding of actual catalytic active sites. Using as a prototype SACs in acidic ORR, Qiao et al. [73] reported the structure–property relationship of catalysts and firstly showed that molecular-level local structure, including first and second coordination spheres (CSs), rather than individual active atoms, synergistically determined the electrocatalytic response (Fig. 4.3d, e). ORR selectivity on Co-SACs can be tailored from a four-electron to a two-electron pathway by modifying first (N or/and O coordination) and second (C–O–C groups) CSs. Using combined theoretical predictions and experiments, including X-ray absorption fine structure analyses and in situ infrared spectroscopy, the unique selectivity change was confirmed, which originated from the structure dependent shift of active sites from the center Co atom to the O-adjacent C atom. That result showed that the optimized electronic structure and *OOH adsorption behavior on active sites enabled the present “best” activity and selectivity of >95% for acidic H₂O₂ electrosynthesis.

4.4 Electric Field Effect

The design of carbon-based nanomaterials and the improvement of catalytic efficiency depend not only on the number of active sites in the catalyst, but also on the diffusion rate of the reactants. The typical path of the electrolysis reaction mainly includes three steps of charge transfer and surface transformation (such as chemical adsorption of reactants and desorption of products from the electrode surface), charge/mass transfer [23]. However, under high current density, slow mass transfer often becomes the bottleneck of the entire electrochemical reaction kinetics[74].

Generally, changing the physical properties of the material interface can improve the local electronic structure and the catalytic performance of the material [75, 76]. And functionalization to form a gas repellent surface, so that the bubbles quickly dissipate, and can accelerate the mass transfer of the electrode reaction [23]. The resistance can also be reduced by using a binder-free catalyst, a metal (alloy) core

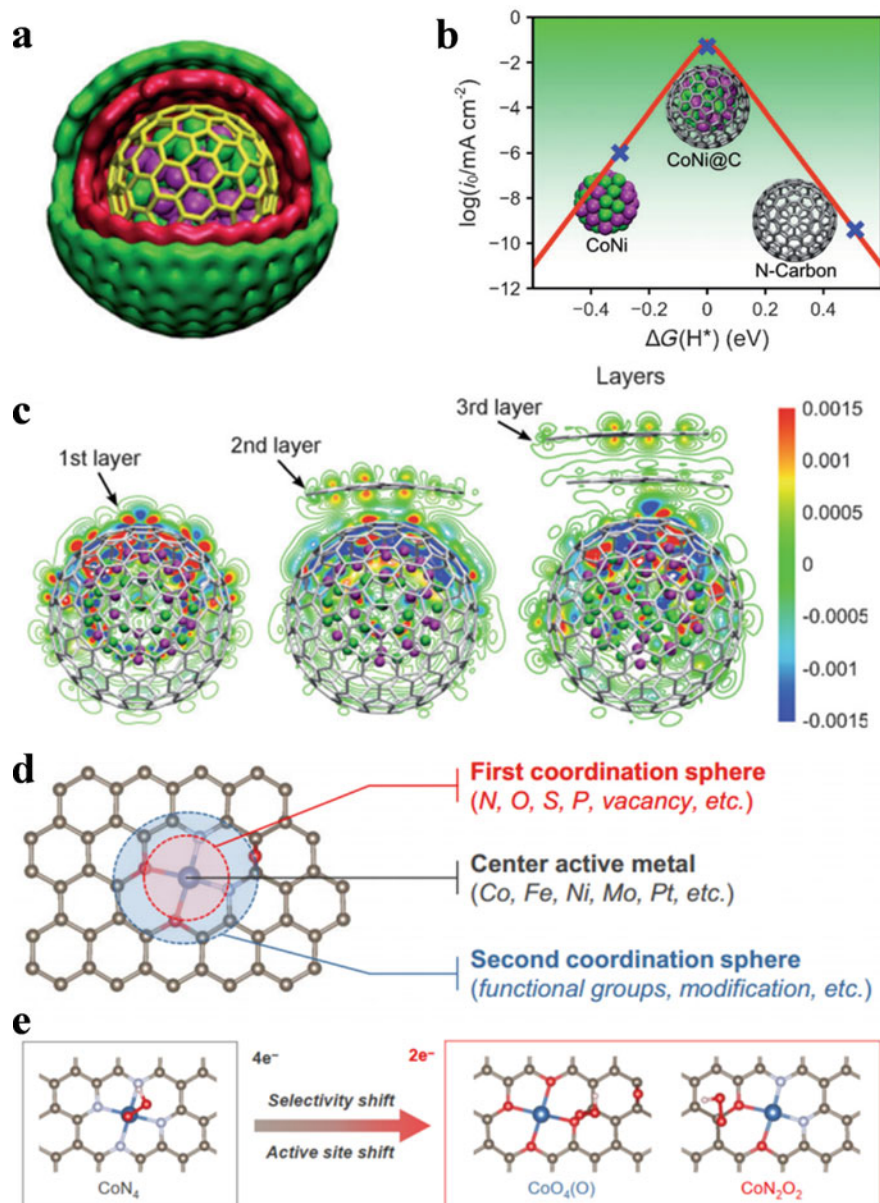


Fig. 4.3 Interface engineering effect of carbon-based nanomaterials in electrochemical catalysis. **a** Schematic illustration of a CoNi alloy encapsulated in three-layer graphene. **b** Volcano plot of the polarized current (i_0) versus $\Delta G(H^*)$ for a CoNi cluster, CoNi@C, and an N-doped graphene shell (N-carbon). **c** Redistribution of the electron densities after the CoNi clusters have been covered by one to three layers of graphene. Reproduced with permission [72]. Copyright 2015, WILEY-VCH. **d** Schematic of SACs, highlighting first and second coordination spheres and center active metal. **e** Optimized geometry structures of *OOH adsorption on CoN_4 , $CoO_4(O)$, and CoN_2O_2 moieties. Reproduced with permission [73]. Copyright 2021, American Chemical Society

catalyst, and a highly conductive carrier [29]. Karlberg et al. [77] evaluated the electric field effect of the oxygen reduction reaction based on DFT, and discussed how the local electric field affected the activity of the oxygen reduction reaction and how it changed the reaction mechanism predicted by the model. The author estimated the influence of the local electric field in the electric double layer on the ORR by changing the applied electric field in the DFT calculation. Potentially, including the local electric field can greatly change the adsorption energy and potential barrier, thereby affecting the prediction of the ORR reaction mechanism on different metals. The influence of the local electric field and the resulting electric double layer has been ignored before. In order to estimate the influence of local electric field on ORR, the DFT results under different external electric field strengths were combined with the previously developed electrochemical reaction model. The model fully considered the influence of electrode potential and found that the local electric field had little influence on the model output. Therefore, the general situation obtained without the electric field still exists. However, in order to accurately predict the oxygen reduction potential near the top of the volcano, local electric field effects may be important. Through this theoretical calculation and discussion on the influence of electric field effect on electrocatalysis, the researchers focused on the study of the electric field effect of electrocatalysts, especially the electric field effect produced by carbon-based nanomaterials in the process of electrocatalysis [77].

As shown in Fig. 4.4a, Liu et al. [6] reported a fibrous bifunctional three-dimensional electrocatalyst that can be used for HER and OER. The interface electrical effect of metallic nickel nitride nanoparticles/ NiCo_2O_4 nanosheets/graphite fibers promoted overall water splitting activity in a wide pH range. Its excellent electrochemical performance was mainly determined by the following factors: the metallic properties of the three components of Ni_3N , CoN , and NiCo_2O_4 ; electronic structure, nanosheet-nanosphere network with abundant electroactive sites and interfaces of different components the electric field effect at the place. These three compounds were all metallic in nature, the filled region represents an occupied state, and the energy of the highest occupied state was the Fermi level. The metal properties ensured efficient electron transfer. Their Fermi energy levels were 0.44, 0.16, and 2.4 eV, respectively (Fig. 4.4b).

Compared with the reversible hydrogen electrode, contact electric potential (CEP) serves as an additional potential provided an interfacial electric field and promoted electrochemical reactions (Fig. 4.4c) [27]. Song et al. [32] reported that onion-like carbon nanospheres (OLC) anchor stable atom-dispersed Pt as a HER catalyst (Pt_1/OLC). In the experiment, surface oxidized detonation nanodiamonds (DNDs) were selected as the starting materials for obtaining OLC, because their size distribution was very uniform. The material undergoes thermal deoxygenation treatments at different temperatures to precisely adjust the type and distribution density of oxygen species, and was automatically converted to OLC at high temperatures (>900 °C). Then, single-cycle atomic layer deposition (ALD) was used to generate isolated platinum atoms on all carriers (Fig. 4.4d). First-principles calculations showed that at the Pt site on the curved carrier, the local electric field enhanced by the tip promotes the kinetics of the hydrogen evolution reaction. Liu et al. [31] reported the generation

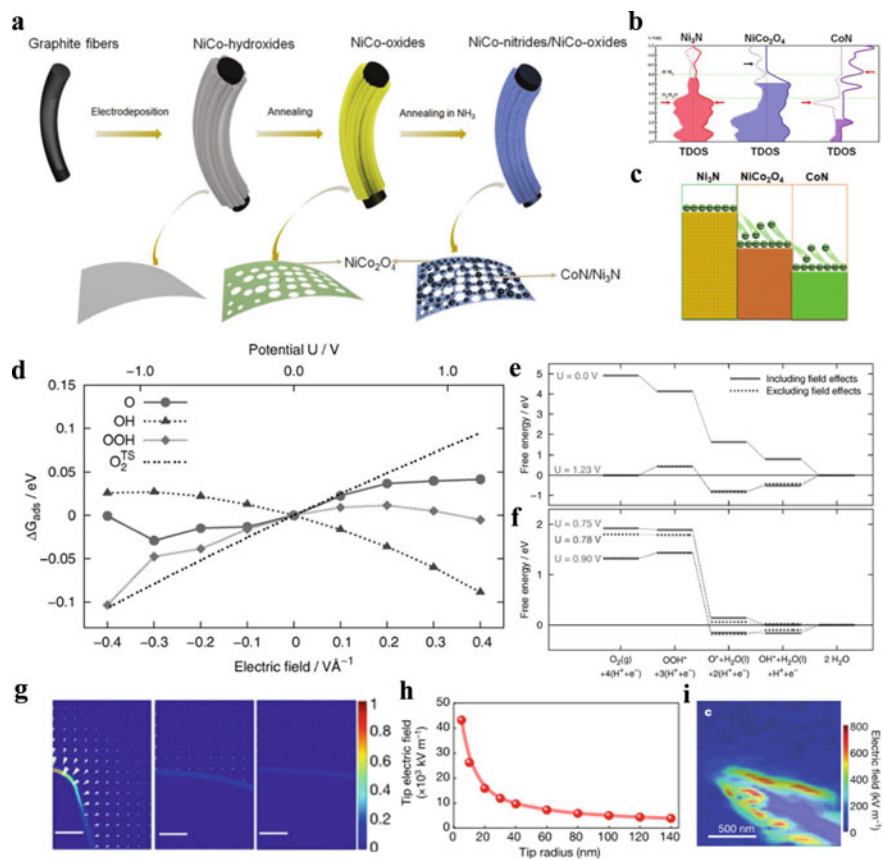


Fig. 4.4 Electric field effect of carbon-based nanomaterials in electrochemical catalysis. a Schematics of the fabrication processes of NiCo-nitride/NiCo₂O₄ supported graphite fibers. **b** Spin resolved total electron density of states (TDOS) for Ni₃N, NiCo₂O₄, and CoN. The filled area is the occupied state and the energy of the highest occupied state is the Fermi level. Reproduced with permission [6]. Copyright 2019, WILEY-VCH. **c** Schematics of interface electric field effect contributing to electrons transfer. Reproduced with permission [27]. Copyright 2020, American Chemical Society. **d** The change in adsorption energy for O, OH and OOH as a function of the electric field strength. Reproduced with permission [32]. Copyright 2019, Springer Nature. **e, f** Free energy diagrams for oxygen reduction on Pt(111). The top panel shows the free energy diagram for U = 0 V and U = 1.23 V. The lower panel shows a zoom in at interesting potentials **f**, such as the potential at which the reaction starts to become endothermic with (0.75 V) and without (0.78 V) an electric field. The potential of 0.9 V is interesting since the stability of adsorbed OH and adsorbed O are equal for this potential when the electric field effects are included. **g** Free electron density distribution on the surface of electrodes is shown as a color map. **h** Electrostatic field intensity at the electrode tip increases as the tip radius decreases. **i** Surface K⁺ density and current density distributions on the surface of Au needles. The tip radius is 5 nm. Reproduced with permission [31]. Copyright 2016, Springer Nature

of nano-structured electrodes, at low application of overpotential, local high electric field concentrates electrolyte cations, which in turn leads to high local concentration of CO₂ close to the active CO₂ reduction reaction surface. The simulation showed that the electric field of the metal nano-tip is 10 times higher than that of the quasi-planar electrode area. The gold nano-needle was used to measure the concentration of the field-inducing reagent and the CO is at -0.35 V (overpotential is 0.24 V). The lower geometric current density was 22 milliamperes per square centimeter (Fig. 4.4e, f). This performance exceeded the best performance of gold nanorods, nanoparticles and oxide-derived noble metal catalysts by an order of magnitude. The Kelvin probe atomic force microscope also confirmed that the metal nano-level tip can produce a strong electric field effect (Fig. 4.4g). The Faraday efficiency of the similarly designed palladium nanoneedle electrocatalyst to produce formate is over 90% , and the geometric current density of formate is 10 mA cm⁻² at -0.2 V, which showed the wider applicability of the field-induced reagent concentration concept.

With these insights, a possible solution is provided for the controllable application and development of the local electric field effect of carbon-based nanomaterials to accurately synthesize the next generation of well-defined electrocatalysts. From the macro- to the atomic level, exploring suitable electric field effects and integrating them with other technologies may provide opportunities to bridge the gap between basic research and industrial applications.

4.5 Conclusion and Perspectives

In this section, a periscope summary of electrocatalysts is provided from catalytic effect. Specifically, the confinement effect, interface engineering effect, and electric field effect are expected to have significant impact on the electronic structure of the active species, and hence improve the intrinsic activity accordingly. Despite the above-mentioned advancements in improving the performance of electrocatalysts through catalytic effect, challenges remain in the following contexts:

- (1) In-depth *in-situ* characterization of the structure of catalyst and understanding of relevant mechanisms. In most cases, the characterizations of the structure of catalyst focus on the state before the electrocatalysis. However, it is essential to comprehend how the structure of catalyst evolves during the reaction for better understanding the role of the structure of catalyst. Therefore, post-reaction analyses and advanced in situ characterization techniques are needed to reveal the evolution of geometry structure and electronic structure of electrocatalysts as well as the adsorption behaviors of reaction intermediates under working conditions. On this basis, more comprehensive understanding about the relevant reaction mechanisms and performance enhancement mechanisms is required.
- (2) Theoretical study of catalytic effect. Integrating theoretical analysis with experimental support is beneficial to elaborate the effect of interface and hence

give guidance to novel catalytic material design. However, there is still a gap between the theoretical model and practice electrocatalyst. To bridge this gap on the structure–performance relationship, a well-defined model system for theoretical calculation is needed.

- (3) Constructing a stable triple-phase interface. Contrary to the electrocatalytic measurement in a three-electrode system with the relatively ideal electrolyte, especially O_2 -saturated electrolyte for ORR, a stable three-phase interface (electrolyte-solid catalyst-gaseous oxygen) needs to be constructed in the practical application of Zn-air battery due to the extremely low O_2 solubility. This means additional challenges such as gas diffusion ability and wettability of air electrode need to be considered. In this regard, interface engineering to regulate the hydrophobicity and to construct mass transport channel also merits attention.
- (4) The catalytic effect of catalysts under extreme condition such as high pH, high temperature, high concentration of ion, and so on, is supposed to be very different from that under ambient condition. Like the superconductivity under temperatures around absolute zero, the catalytic effect under extreme condition may contribute to the appearance of some interesting phenomenon and ultrahigh catalytic efficiency.
- (5) The precise identification of genuine active sites is essential to guide the high-performance electrocatalyst design. The abovementioned advance in situ electrochemical operando techniques would allow for achieving this goal. Different from conventional modeling with ideal models in nonpractical conditions, the accurate theoretic modeling need consider the genuine chemical state and environments of active sites, the influences of electrolytes, applied potentials, and local fields in catalyst working conditions, as well as the dynamic evolution of catalytic sites. The machine-learning based computation and big-data processing will facilitate such modeling.
- (6) For targeting the practical application of the synthesized electrocatalysts, the device-level requirements should be paid more attention such as the collective catalyst layer design, mass transfer and diffusion issues at high output conditions, etc. A majority of current electrocatalysts for water splitting and CO_2RR have been assessed in traditional three-electrode system, which may not reflect their performance in the real devices. The evaluation of the catalysts in an operating pilot electrolyzer would be necessary and helpful for bridging the gap between the lab test and industry expectation. Moreover, the general, facile and controllable confined synthetic strategies allow for generating the uniform, efficient and stable catalytic sites at large scale, which may enable the mass production of electrocatalysts with reproducible performance at low cost. Combining the above-mentioned confinement strategies at various scales by delicately designing the precursors, which may open up possibilities for achieving such goal for bringing the research from lab scale to industrial scale.

This section sheds light on the rational design of electrocatalysts for board electrochemical applications from the fundamental understanding of confinement effect,

interface engineering effect, and electric field effect. Thus, hope that this chapter will bring significant attention in the field of electrochemistry by enabling more frontier researches in the fields of battery technology.

References

1. L. Yang, J. Shui, L. Du, Y. Shao, J. Liu, L. Dai, Z. Hu, Carbon-based metal-free ORR electrocatalysts for fuel cells: Past, present, and future. *Adv. Mater.* **31**, 1804799 (2019). <https://doi.org/10.1002/adma.201804799>
2. J. Zhu, S. Mu, Defect engineering in carbon-based electrocatalysts: Insight into intrinsic carbon defects. *Adv. Func. Mater.* **30**, 2001097 (2020). <https://doi.org/10.1002/adfm.202001097>
3. L.P. Yuan, T. Tang, J.S. Hu, L.J. Wan, Confinement strategies for precise synthesis of efficient electrocatalysts from the macroscopic to the atomic level. *Accounts of Materials Research* **2**, 907–919 (2021). <https://doi.org/10.1021/accountsmr.1c00135>
4. H. Tabassum, A. Mahmood, B. Zhu, Z. Liang, R. Zhong, S. Guo, R. Zou, Recent advances in confining metal-based nanoparticles into carbon nanotubes for electrochemical energy conversion and storage devices. *Energy Environ. Sci.* **12**, 2924–2956 (2019). <https://doi.org/10.1039/c9ee00315k>
5. Z. Geng, Y. Liu, X. Kong, P. Li, K. Li, Z. Liu, J. Du, M. Shu, R. Si, J. Zeng, Achieving a record-high yield rate of 120.9 $\mu\text{g NH}_3 \text{ mgcat}^{-1} \text{ h}^{-1}$ for N_2 electrochemical reduction over Ru single-atom catalysts. *Adv. Mater.* **30**, 1803498 (2018). <https://doi.org/10.1002/adma.201803498>
6. Z. Liu, H. Tan, D. Liu, X. Liu, J. Xin, J. Xie, M. Zhao, L. Song, L. Dai, H. Liu, Promotion of overall water splitting activity over a wide pH range by interfacial electrical effects of metallic NiCo-nitrides nanoparticle/NiCo₂O₄ nanoflake/graphite fibers. *Adv. Sci.* **6**, 1801829 (2019). <https://doi.org/10.1002/advs.201801829>
7. K. He, T. Tadesse Tsega, X. Liu, J. Zai, X.-H. Li, X. Liu, W. Li, N. Ali, X. Qian, Utilizing the space-charge region of the FeNi-LDH/CoP p-n junction to promote performance in oxygen evolution electrocatalysis. *Angew. Chem. Int. Ed.* **58**, 11903–11909 (2019). <https://doi.org/10.1002/anie.201905281>
8. J. Li, M. Chen, D.A. Cullen, S. Hwang, M. Wang, B. Li, K. Liu, S. Karakalos, M. Lucero, H. Zhang, C. Lei, H. Xu, G.E. Sterbinsky, Z. Feng, D. Su, K.L. More, G. Wang, Z. Wang, G. Wu, Atomically dispersed manganese catalysts for oxygen reduction in proton-exchange membrane fuel cells. *Nat. Catal.* **1**, 935–945 (2018). <https://doi.org/10.1038/s41929-018-0164-8>
9. J. Chen, H. Li, C. Fan, Q. Meng, Y. Tang, X. Qiu, G. Fu, T. Ma, Dual single-atomic Ni-N₄ and Fe-N₄ sites constructing janus hollow graphene for selective oxygen electrocatalysis. *Adv. Mater.* **32**, 2003134 (2020). <https://doi.org/10.1002/adma.202003134>
10. H. Zhang, P. An, W. Zhou, B. Y. Guan, P. Zhang, J. Dong, X. W. Lou, Dynamic traction of lattice-confined platinum atoms into mesoporous carbon matrix for hydrogen evolution reaction. *Sci. Adv.* **4**, eaao6657 (2018). <https://doi.org/10.1126/sciadv.aao6657>
11. Y. Chen, S. Ji, S. Zhao, W. Chen, J. Dong, W.-C. Cheong, R. Shen, X. Wen, L. Zheng, A.I. Rykov, S. Cai, H. Tang, Z. Zhuang, C. Chen, Q. Peng, D. Wang, Y. Li, Enhanced oxygen reduction with single-atomic-site iron catalysts for a zinc-air battery and hydrogen-air fuel cell. *Nat. Commun.* **9**, 5422 (2018). <https://doi.org/10.1038/s41467-018-07850-2>
12. Z. Li, X. Zhang, H. Cheng, J. Liu, M. Shao, M. Wei, D.G. Evans, H. Zhang, X. Duan, Confined synthesis of 2D nanostructured materials toward electrocatalysis. *Adv. Energy Mater.* **10**, 1900486 (2019). <https://doi.org/10.1002/aenm.201900486>
13. Y. Wang, H. Su, Y. He, L. Li, S. Zhu, H. Shen, P. Xie, X. Fu, G. Zhou, C. Feng, D. Zhao, F. Xiao, X. Zhu, Y. Zeng, M. Shao, S. Chen, G. Wu, J. Zeng, C. Wang, Advanced electrocatalysts with single-metal-atom active sites. *Chem. Rev.* **120**, 12217–12314 (2020). <https://doi.org/10.1021/acs.chemrev.0c00594>

14. M. Luo, W. Sun, B.B. Xu, H. Pan, Y. Jiang, Interface engineering of air electrocatalysts for rechargeable zinc-air batteries. *Adv. Energy Mater.* **11**, 2002762 (2020). <https://doi.org/10.1002/aenm.202002762>
15. J. Yang, W. Li, D. Wang, Y. Li, Electronic metal-support interaction of single-atom catalysts and applications in electrocatalysis. *Adv. Mater.* **32**, e2003300 (2020). <https://doi.org/10.1002/adma.202003300>
16. G. Zhao, K. Rui, S.X. Dou, W. Sun, Boosting electrochemical water oxidation: The merits of heterostructured electrocatalysts. *J. Mater. Chem. A* **8**, 6393–6405 (2020). <https://doi.org/10.1039/d0ta00708k>
17. C. Han, W. Li, H.K. Liu, S. Dou, J. Wang, Design strategies for developing non-precious metal based bi-functional catalysts for alkaline electrolyte based zinc-air batteries. *Mater. Horiz.* **6**, 1812–1827 (2019). <https://doi.org/10.1039/c9mh00502a>
18. L. Yu, D. Deng, X. Bao, Chain mail for catalysts. *Angew. Chem. Int. Ed.* **59**, 15294–15297 (2020). <https://doi.org/10.1002/anie.202007604>
19. T.C. Tseng, C. Urban, Y. Wang, R. Otero, S.L. Tait, M. Alcamí, D. Eciija, M. Trelka, J.M. Gallego, N. Lin, M. Konuma, U. Starke, A. Nefedov, A. Langner, C. Woll, M.A. Herranz, F. Martin, N. Martin, K. Kern, R. Miranda, Charge-transfer-induced structural rearrangements at both sides of organic/metal interfaces. *Nat. Chem.* **2**, 374–379 (2010). <https://doi.org/10.1038/nchem.591>
20. D. Wang, Q. Li, C. Han, Z. Xing, X. Yang, Single-atom ruthenium based catalyst for enhanced hydrogen evolution. *Appl. Catal. B* **249**, 91–97 (2019). <https://doi.org/10.1016/j.apcatb.2019.02.059>
21. H.J. Qiu, Y. Ito, W. Cong, Y. Tan, P. Liu, A. Hirata, T. Fujita, Z. Tang, M. Chen, Nanoporous graphene with single-atom nickel dopants: An efficient and stable catalyst for electrochemical hydrogen production. *Angew. Chem. Int. Ed.* **54**, 14031–14035 (2015). <https://doi.org/10.1002/anie.201507381>
22. W. Chen, J. Pei, C.T. He, J. Wan, H. Ren, Y. Wang, J. Dong, K. Wu, W.C. Cheong, J. Mao, X. Zheng, W. Yan, Z. Zhuang, C. Chen, Q. Peng, D. Wang, Y. Li, Single tungsten atoms supported on MOF-derived N-doped carbon for robust electrochemical hydrogen evolution. *Adv. Mater.* **30**, e1800396 (2018). <https://doi.org/10.1002/adma.201800396>
23. P. Liu, B. Chen, C. Liang, W. Yao, Y. Cui, S. Hu, P. Zou, H. Zhang, H.J. Fan, C. Yang, Tip-enhanced electric field: A new mechanism promoting mass transfer in oxygen evolution reactions. *Adv. Mater.* **33**, 2007377 (2021). <https://doi.org/10.1002/adma.202007377>
24. T. Ling, M. Jaroniec, S.Z. Qiao, Recent progress in engineering the atomic and electronic structure of electrocatalysts via cation exchange reactions. *Adv. Mater.* **32**, 2001866 (2020). <https://doi.org/10.1002/adma.202001866>
25. T. Wu, S. Sun, J. Song, S. Xi, Y. Du, B. Chen, W.A. Sasangka, H. Liao, C.L. Gan, G.G. Scherer, L. Zeng, H. Wang, H. Li, A. Grimaud, Z.J. Xu, Iron-facilitated dynamic active-site generation on spinel CoAl_2O_4 with self-termination of surface reconstruction for water oxidation. *Nat. Catal.* **2**, 763–772 (2019). <https://doi.org/10.1038/s41929-019-0325-4>
26. W. Xu, F. Lyu, Y. Bai, A. Gao, J. Feng, Z. Cai, Y. Yin, Porous cobalt oxide nanoplates enriched with oxygen vacancies for oxygen evolution reaction. *Nano Energy* **43**, 110–116 (2018). <https://doi.org/10.1016/j.nanoen.2017.11.022>
27. J. Xu, Z. Lian, B. Wei, Y. Li, O. Bondarchuk, N. Zhang, Z. Yu, A. Araujo, I. Amorim, Z. Wang, B. Li, L. Liu, Strong electronic coupling between ultrafine iridium-ruthenium nanoclusters and conductive, acid-stable tellurium nanoparticle support for efficient and durable oxygen evolution in acidic and neutral media. *ACS Catal.* **10**, 3571–3579 (2020). <https://doi.org/10.1021/acscatal.9b05611>
28. M.F. Lagadec, A. Grimaud, Water electrolyzers with closed and open electrochemical systems. *Nat. Mater.* **19**, 1140–1150 (2020). <https://doi.org/10.1038/s41563-020-0788-3>
29. C. Liang, P. Zou, A. Nairan, Y. Zhang, J. Liu, K. Liu, S. Hu, F. Kang, H.J. Fan, C. Yang, Exceptional performance of hierarchical Ni-Fe oxyhydroxide@NiFe alloy nanowire array electrocatalysts for large current density water splitting. *Energy Environ. Sci.* **13**, 86–95 (2020). <https://doi.org/10.1039/c9ee02388g>

30. D. Deng, K.S. Novoselov, Q. Fu, N. Zheng, Z. Tian, X. Bao, Catalysis with two-dimensional materials and their heterostructures. *Nat. Nanotechnol.* **11**, 218–230 (2016). <https://doi.org/10.1038/nnano.2015.340>
31. M. Liu, Y. Pang, B. Zhang, P. De Luna, O. Voznyy, J. Xu, X. Zheng, C.T. Dinh, F. Fan, C. Cao, F.P.G. de Arquer, T.S. Safaei, A. Mepham, A. Klinkova, E. Kumacheva, T. Filleter, D. Sinton, S.O. Kelley, E.H. Sargent, Enhanced electrocatalytic CO₂ reduction via field-induced reagent concentration. *Nature* **537**, 382–386 (2016). <https://doi.org/10.1038/nature19060>
32. D. Liu, X. Li, S. Chen, H. Yan, C. Wang, C. Wu, Y.A. Haleem, S. Duan, J. Lu, B. Ge, P.M. Ajayan, Y. Luo, J. Jiang, L. Song, Atomically dispersed platinum supported on curved carbon supports for efficient electrocatalytic hydrogen evolution. *Nat. Energy* **4**, 512–518 (2019). <https://doi.org/10.1038/s41560-019-0402-6>
33. H. Jiang, Z. Hou, Y. Luo, Unraveling the mechanism for the sharp-tip enhanced electrocatalytic carbon dioxide reduction: The kinetics decide. *Angew. Chem. Int. Ed.* **56**, 15617–15621 (2017). <https://doi.org/10.1002/anie.201708825>
34. S. Fang, X. Zhu, X. Liu, J. Gu, W. Liu, D. Wang, W. Zhang, Y. Lin, J. Lu, S. Wei, Y. Li, T. Yao, Uncovering near-free platinum single-atom dynamics during electrochemical hydrogen evolution reaction. *Nat. Commun.* **11**, 1029 (2020). <https://doi.org/10.1038/s41467-020-14848-2>
35. Y. Wang, Y. Pan, L. Zhu, H. Yu, B. Duan, R. Wang, Z. Zhang, S. Qiu, Solvent-free assembly of Co/Fe-containing MOFs derived N-doped mesoporous carbon nanosheets for ORR and HER. *Carbon* **146**, 671–679 (2019). <https://doi.org/10.1016/j.carbon.2019.02.002>
36. Y. Jia, L. Zhang, A. Du, G. Gao, J. Chen, X. Yan, C.L. Brown, X. Yao, Defect graphene as a trifunctional catalyst for electrochemical reactions. *Adv. Mater.* **28**, 9532–9538 (2016). <https://doi.org/10.1002/adma.201602912>
37. Y. Zhu, S. Murali, W. Cai, X. Li, J.W. Suk, J.R. Potts, R.S. Ruoff, Graphene and graphene oxide: Synthesis, properties, and applications. *Adv. Mater.* **22**, 3906–3924 (2010). <https://doi.org/10.1002/adma.201001068>
38. T. Tang, W.J. Jiang, X.Z. Liu, J. Deng, S. Niu, B. Wang, S.F. Jin, Q. Zhang, L. Gu, J.S. Hu, L.J. Wan, Metastable rock salt oxide-mediated synthesis of high-density dual-protected M@NC for long-life rechargeable zinc-air batteries with record power density. *J. Am. Chem. Soc.* **142**, 7116–7127 (2020). <https://doi.org/10.1021/jacs.0c01349>
39. C. He, Y. Zhang, Y. Zhang, L. Zhao, L.P. Yuan, J. Zhang, J. Ma, J.S. Hu, Molecular evidence for metallic cobalt boosting CO₂ electroreduction on pyridinic nitrogen. *Angew. Chem. Int. Ed.* **59**, 4914–4919 (2020). <https://doi.org/10.1002/anie.201916520>
40. J. Zhang, W.J. Jiang, S. Niu, H. Zhang, J. Liu, H. Li, G.F. Huang, L. Jiang, W.Q. Huang, J.S. Hu, W. Hu, Organic small molecule activates transitionmetal foam for efficient oxygen evolution reaction. *Adv. Mater.* **32**, e1906015 (2020). <https://doi.org/10.1002/adma.201906015>
41. P. Yin, T. Yao, Y. Wu, L. Zheng, Y. Lin, W. Liu, H. Ju, J. Zhu, X. Hong, Z. Deng, G. Zhou, S. Wei, Y. Li, Single cobalt atoms with precise N-coordination as superior oxygen reduction reaction catalysts. *Angew. Chem. Int. Ed.* **55**, 10800–10805 (2016). <https://doi.org/10.1002/anie.201604802>
42. J. Wang, Z. Huang, W. Liu, C. Chang, H. Tang, Z. Li, W. Chen, C. Jia, T. Yao, S. Wei, Y. Wu, Y. Li, Design of N-coordinated dual-metal sites: A stable and active Pt-free catalyst for acidic oxygen reduction reaction. *J. Am. Chem. Soc.* **139**, 17281–17284 (2017). <https://doi.org/10.1021/jacs.7b10385>
43. Y. Qiao, P. Yuan, Y. Hu, J. Zhang, S. Mu, J. Zhou, H. Li, H. Xia, J. He, Q. Xu, Sulfuration of an Fe–N–C catalyst containing FexC/Fe species to enhance the catalysis of oxygen reduction in acidic media and for use in flexible Zn-air batteries. *Adv. Mater.* **30**, e1804504 (2018). <https://doi.org/10.1002/adma.201804504>
44. Q. Yang, C.C. Yang, C.H. Lin, H.L. Jiang, Metal-organic-framework-derived hollow N-doped porous carbon with ultrahigh concentrations of single Zn atoms for efficient carbon dioxide conversion. *Angew. Chem. Int. Ed.* **58**, 3511–3515 (2019). <https://doi.org/10.1002/anie.201813494>

45. Y. Chen, S. Ji, Y. Wang, J. Dong, W. Chen, Z. Li, R. Shen, L. Zheng, Z. Zhuang, D. Wang, Y. Li, Isolated single iron atoms anchored on N-doped porous carbon as an efficient electrocatalyst for the oxygen reduction reaction. *Angew. Chem. Int. Ed.* **56**, 6937–6941 (2017). <https://doi.org/10.1002/anie.201702473>
46. C. Park, W.T. Koo, S. Chong, H. Shin, Y.H. Kim, H.J. Cho, J.S. Jang, D.H. Kim, J. Lee, S. Park, J. Ko, J. Kim, I.D. Kim, Confinement of ultrasmall bimetallic nanoparticles in conductive metal-organic frameworks via site-specific nucleation. *Adv. Mater.* **33**, e2101216 (2021). <https://doi.org/10.1002/adma.202101216>
47. X. Ao, W. Zhang, Z. Li, J.G. Li, L. Soule, X. Huang, W.H. Chiang, H.M. Chen, C. Wang, M. Liu, X.C. Zeng, Markedly enhanced oxygen reduction activity of single-atom Fe catalysts via integration with Fe nanoclusters. *ACS Nano* **13**, 11853–11862 (2019). <https://doi.org/10.1021/acsnano.9b05913>
48. T. Wang, Z. Kou, S. Mu, J. Liu, D. He, I.S. Amiinu, W. Meng, K. Zhou, Z. Luo, S. Chaemchuen, F. Verpoort, 2D dual-metal zeolitic-imidazolate-framework(ZIF)-derived bifunctional air electrodes with ultrahigh electrochemical properties for rechargeable zinc-air batteries. *Adv. Func. Mater.* **28**, 1705048 (2018). <https://doi.org/10.1002/adfm.201705048>
49. Z. Chen, R. Wu, Y. Liu, Y. Ha, Y. Guo, D. Sun, M. Liu, F. Fang, Ultrafine Co nanoparticles encapsulated in carbon-nanotubes-grafted graphene sheets as advanced electrocatalysts for the hydrogen evolution reaction. *Adv. Mater.* **30**, e1802011 (2018). <https://doi.org/10.1002/adma.201802011>
50. G.M. Schwab, Chemical effects at the solid/solid phase boundary. *J. Colloid Interface Sci.* **34**, 337–342 (1970). [https://doi.org/10.1016/0021-9797\(70\)90192-X](https://doi.org/10.1016/0021-9797(70)90192-X)
51. S.J. Tauster, S.C. Fung, R.L. Garten, Strong metal-support interactions. Group 8 noble metals supported on TiO₂. *J. Am. Chem. Soc.* **4**, 170–175 (1978). <https://doi.org/10.1021/ja00469a029>
52. S.J. Tauster, S.C. Fung, R.T.K. Baker, J.A. Horsley, Strong interactions in supported-metal catalysts. *Science* **211**, 1121–1125 (1981). <https://doi.org/10.1126/science.211.4487.1121>
53. S.J. Tauster, Strong metal-support interactions. *Acc. Chem. Res.* **20**, 389–394 (1987). <https://doi.org/10.1021/ar00143a001>
54. H. Tributsch, U.I. Koslowski, I. Dorbandt, Experimental and theoretical modeling of Fe-, Co-, Cu-, Mn-based electrocatalysts for oxygen reduction. *Electrochim. Acta* **53**, 2198–2209 (2008). <https://doi.org/10.1016/j.electacta.2007.09.027>
55. C.T. Campbell, Catalyst-support interactions: Electronic perturbations. *Nat. Chem.* **4**, 597–598 (2012). <https://doi.org/10.1038/nchem.1412>
56. J.L. Shi, J.H. Wu, X.J. Zhao, X.L. Xue, Y.F. Gao, Z.X. Guo, S.F. Li, Substrate co-doping modulates electronic metal-support interactions and significantly enhances single-atom catalysis. *Nanoscale* **8**, 19256–19262 (2016). <https://doi.org/10.1039/c6nr04292a>
57. P. Hu, Z. Huang, Z. Amghouz, M. Makkee, F. Xu, F. Kapteijn, A. Dikhtiarenko, Y. Chen, X. Gu, X. Tang, Electronic metal-support interactions in single-atom catalysts. *Angew. Chem. Int. Ed.* **53**, 3418–3421 (2014). <https://doi.org/10.1002/anie.201309248>
58. T.W. van Deelen, C. Hernández Mejía, K.P. de Jong, Control of metal-support interactions in heterogeneous catalysts to enhance activity and selectivity. *Nat. Catal.* **2**, 955–970 (2019). <https://doi.org/10.1038/s41929-019-0364-x>
59. I. Ro, J. Resasco, P. Christopher, Approaches for understanding and controlling interfacial effects in oxide-supported metal catalysts. *ACS Catal.* **8**, 7368–7387 (2018). <https://doi.org/10.1021/acscatal.8b02071>
60. M. Ahmadi, H. Mistry, B. Roldan Cuenya, Tailoring the catalytic properties of metal nanoparticles via support interactions. *J. Phys. Chem. Lett.* **7**, 3519–3533 (2016). <https://doi.org/10.1021/acs.jpcllett.6b01198>
61. Z. Li, R. Wu, L. Zhao, P. Li, X. Wei, J. Wang, J.S. Chen, T. Zhang, Metal-support interactions in designing noble metal-based catalysts for electrochemical CO₂ reduction: Recent advances and future perspectives. *Nano Res.* **14**, 3795–3809 (2021). <https://doi.org/10.1007/s12274-021-3363-6>
62. C.J. Pan, M.C. Tsai, W.N. Su, J. Rick, N.G. Akalework, A.K. Agegnehu, S.Y. Cheng, B.J. Hwang, Tuning/exploiting strong metal-support interaction (SMSI) in heterogeneous catalysis. *J. Taiwan Inst. Chem. Eng.* **74**, 154–186 (2017). <https://doi.org/10.1016/j.jtice.2017.02.012>

63. Y. Lou, J. Xu, Y. Zhang, C. Pan, Y. Dong, Y. Zhu, Metal-support interaction for heterogeneous catalysis: From nanoparticles to single atoms. *Materials Today Nano* **12**, 100093 (2020). <https://doi.org/10.1016/j.mtnano.2020.100093>
64. S. Tian, S. Chen, X. Ren, Y. Hu, H. Hu, J. Sun, F. Bai, An efficient visible-light photocatalyst for CO₂ reduction fabricated by cobalt porphyrin and graphitic carbon nitride via covalent bonding. *Nano Res.* **13**, 2665–2672 (2020). <https://doi.org/10.1007/s12274-020-2908-4>
65. D.H. Nam, P. De Luna, A. Rosas-Hernandez, A. Thevenon, F. Li, T. Agapie, J.C. Peters, O. Shekhah, M. Eddaoudi, E.H. Sargent, Molecular enhancement of heterogeneous CO₂ reduction. *Nat. Mater.* **19**, 266–276 (2020). <https://doi.org/10.1038/s41563-020-0610-2>
66. Y. Wang, Y. Liu, W. Liu, J. Wu, Q. Li, Q. Feng, Z. Chen, X. Xiong, D. Wang, Y. Lei, Regulating the coordination structure of metal single atoms for efficient electrocatalytic CO₂ reduction. *Energy Environ. Sci.* **13**, 4609–4624 (2020). <https://doi.org/10.1039/d0ee02833a>
67. Z. Jiang, T. Wang, J. Pei, H. Shang, D. Zhou, H. Li, J. Dong, Y. Wang, R. Cao, Z. Zhuang, W. Chen, D. Wang, J. Zhang, Y. Li, Discovery of main group single Sb-N₄ active sites for CO₂ electroreduction to formate with high efficiency. *Energy Environ. Sci.* **13**, 2856–2863 (2020). <https://doi.org/10.1039/d0ee01486a>
68. X. Ao, W. Zhang, B. Zhao, Y. Ding, G. Nam, L. Soule, A. Abdelhafiz, C. Wang, M. Liu, Atomically dispersed Fe-N-C decorated with Pt-alloy core-shell nanoparticles for improved activity and durability towards oxygen reduction. *Energy Environ. Sci.* **13**, 3032–3040 (2020). <https://doi.org/10.1039/d0ee00832j>
69. Q. He, J.H. Lee, D. Liu, Y. Liu, Z. Lin, Z. Xie, S. Hwang, S. Kattel, L. Song, J.G. Chen, Accelerating CO₂ electroreduction to CO over Pd single-atom catalyst. *Adv. Func. Mater.* **30**, 2000407 (2020). <https://doi.org/10.1002/adfm.202000407>
70. T. Zhang, X. Han, H. Yang, A. Han, E. Hu, Y. Li, X.Q. Yang, L. Wang, J. Liu, B. Liu, Atomically dispersed nickel(I) on an alloy-encapsulated nitrogen-doped carbon nanotube array for high-performance electrochemical CO₂ reduction reaction. *Angew. Chem. Int. Ed.* **59**, 12055–12061 (2020). <https://doi.org/10.1002/anie.202002984>
71. A. Vasileff, C. Xu, Y. Jiao, Y. Zheng, S.Z. Qiao, Surface and interface engineering in copper-based bimetallic materials for selective CO₂ electroreduction. *Chem* **4**, 1809–1831 (2018). <https://doi.org/10.1016/j.chempr.2018.05.001>
72. J. Deng, P. Ren, D. Deng, X. Bao, Enhanced electron penetration through an ultrathin graphene layer for highly efficient catalysis of the hydrogen evolution reaction. *Angew. Chem. Int. Ed.* **54**, 2100–2104 (2015). <https://doi.org/10.1002/anie.201409524>
73. C. Tang, L. Chen, H. Li, L. Li, Y. Jiao, Y. Zheng, H. Xu, K. Davey, S.Z. Qiao, Tailoring acidic oxygen reduction selectivity on single-atom catalysts via modification of first and second coordination spheres. *J. Am. Chem. Soc.* **143**, 7819–7827 (2021). <https://doi.org/10.1021/jacs.1c03135>
74. B. Zhang, L. Wang, Z. Cao, S.M. Kozlov, F.P. García de Arquer, C.T. Dinh, J. Li, Z. Wang, X. Zheng, L. Zhang, Y. Wen, O. Voznyy, R. Comin, P. De Luna, T. Regier, W. Bi, E.E. Alp, C.W. Pao, L. Zheng, Y. Hu, Y. Ji, Y. Li, Y. Zhang, L. Cavallo, H. Peng, E.H. Sargent, High-valence metals improve oxygen evolution reaction performance by modulating 3d metal oxidation cycle energetics. *Nat. Catal.* **3**, 985–992 (2020). <https://doi.org/10.1038/s41929-020-00525-6>
75. F. Li, X.V. Medvedev, J.J. Medvedev, E. Khairullina, H. Engelhardt, S. Chandrasekar, Y. Guo, J. Jin, A. Lee, H. Thérien-Aubin, A. Ahmed, Y. Pang, A. Klinkova, Interplay of electrochemical and electrical effects induces structural transformations in electrocatalysts. *Nat. Catal.* **4**, 479–487 (2021). <https://doi.org/10.1038/s41929-021-00624-y>
76. J. Lin, Y. Yan, T. Xu, J. Cao, X. Zheng, J. Feng, J. Qi, Rich P vacancies modulate Ni₂P/Cu₃P interfaced nanosheets for electrocatalytic alkaline water splitting. *J. Colloid Interface Sci.* **564**, 37–42 (2020). <https://doi.org/10.1016/j.jcis.2019.12.114>
77. G.S. Karlberg, J. Rossmeisl, J.K. Nørskov, Estimations of electric field effects on the oxygen reduction reaction based on the density functional theory. *Phys. Chem. Chem. Phys.* **9**, 5158–5161 (2007). <https://doi.org/10.1039/b705938h>

Chapter 5

Carbon-Based Nanomaterials for Oxygen Reduction Reaction



Xiaoyu Zhang, Dongping Xue, Siran Xu, Bang-An Lu, and Jia-Nan Zhang

Abstract The performance of proton exchange membrane fuel cell (PEMFC) and metal-air batteries are determined by the oxygen reduction reaction (ORR) on the cathode, whereas the kinetics of ORR is very sluggish. Therefore, it is urgent to design and develop efficient electrocatalysts to accelerate ORR. At present, as the highest activity catalyst, Pt-based catalysts have various issues such as high cost, easy poisoning, aggregation, and low durability. As a result, the investigation of high-activity, low-cost and stable ORR electrocatalysts is of significance to the practical implementation of fuel cell technology. The excellent electrical conductivity and high surface area of carbon-based materials make the catalysts good candidates for Pt-based catalysts. This chapter will cover the application of porous carbon-based materials in ORR from the aspects of the metal-free, single metallic atom, and metal nanoparticles (NPs), etc., reveal their deep catalytic mechanism, explain their unique structure–activity relationship, and clarify the future development direction and potential obstacles of carbon-based nanomaterials for ORR.

X. Zhang · D. Xue · S. Xu · B.-A. Lu · J.-N. Zhang (✉)
College of Materials Science and Engineering, Zhengzhou University, Zhengzhou 450001,
P. R. China
e-mail: zjn@zzu.edu.cn

X. Zhang
e-mail: zhangxiaoyu0321@163.com

D. Xue
e-mail: xdongping1231@126.com

S. Xu
e-mail: siranxuhbnu@163.com

B.-A. Lu
e-mail: balu@zzu.edu.cn

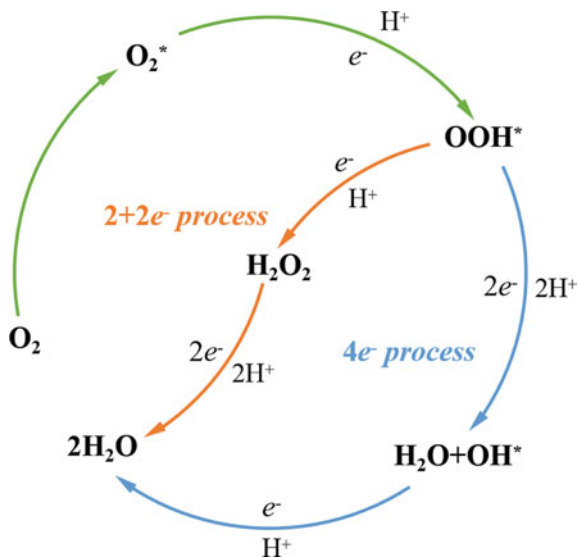
5.1 Introduction

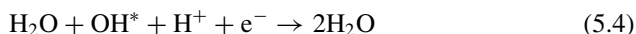
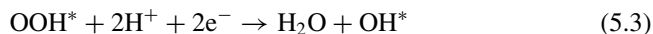
Proton exchange membrane fuel cell (PEMFC) is a vital medium for hydrogen energy utilization. The working steps of PEMFC involve the following processes: (1) The reaction fuel is fed to the electrode. In the normal operation of fuel cells, hydrogen or oxygen fuel needs to be supplied. The graphite plate in the PEMFC clamp contains fine serpentine grooves to ensure efficient fuel transport. (2) Electrochemical reaction. Oxygen is transported to the cathode, and hydrogen at the anode is then subjected to an electrochemical reaction with a catalyst. In PEMFC, chemical energy is converted to electrical energy through oxygen reduction reaction (ORR) at the cathode and hydrogen oxidation reaction (HOR) at the anode. Compared with the anode HOR, the cathode ORR dynamics is slower. Considerable amounts of precious metal Pt catalysts are needed to accelerate the sluggish kinetics of ORR, thus significantly increasing the cost of the cell. Therefore, it is imperative to design and develop efficient electrocatalysts to accelerate ORR.

ORR in PEMFC is a complex reaction process involving multi-electron reactions, which can be simply divided into two-electron ($2e^-$) paths and four-electron ($4e^-$) paths [1]. Generally, O_2 generates H_2O through $4e^-$ transfer, or H_2O_2 through $2e^-$ transfer, and H_2O_2 is unstable and may decompose into O_2 to participate in oxygen reduction again [2]. As shown in Fig. 5.1, the details can be described as below:



Fig. 5.1 Mechanism of ORR. The blue arrow and the orange arrow represent direct $4e^-$ transfer path and $2e^- + 2e^-$ transfer path, respectively





The reduction potential of 4e^- is higher than that of 2e^- , and the dissociation energy of the O–O bond in O_2 is larger than that of H_2O_2 . Therefore, when the catalytic activity is not strong, the reaction of 2e^- or the mixed reaction of 2e^- and 4e^- is likely to occur. Moreover, the H_2O_2 generated by the 2e^- process might cause damage to the proton exchange membrane, and the 4e^- process is the ideal oxygen reduction path for fuel cells [3]. However, for most catalysts, their catalysis process often occurs as a mixture of 2e^- and 4e^- reaction. Therefore, the 4e^- reaction selectivity of the catalyst has also become an important indicator for evaluating the quality of ORR catalysts. At present, Pt-based catalysts are ORR catalysts with the highest activity, the lowest overpotential and the highest 4e^- reaction selectivity. However, aside expensive cost, Pt-based catalysts also have various drawbacks such as rapid poisoning, aggregation, and low durability. As a result, the study of high-activity, low-cost and stable ORR electrocatalysts is of great significance to the practical application of fuel cell technology [4].

Porous carbon-based materials present the following metrics: (1) excellent chemical and mechanical stability, (2) higher porosity and adjustable pore size, (3) excellent electrical conductivity, (4) high specific surface area, (5) and the synthetic methods are simple and easy to obtain [5–7]. Therefore, porous carbon-based nanomaterials have been extensively studied as ORR electrocatalysts to solve the difficult problem of the industrial application of Pt-based catalysts. This part will review the application of porous carbon-based materials in ORR from the aspects of nonmetal, single metallic atom and metal nanoparticles (NPs), etc., and elaborate their unique structure–activity relationship and catalytic mechanism.

5.2 Metal-Free Carbon-Based Electrocatalysts for ORR

Among various carbon-based materials, the heteroatoms doped carbon nanomaterials have been regarded as one of the most promising ORR catalysts due to the several merits, including large specific surface area and favorable feasibility to structure/functionalization regulation [8]. To achieve a lower oxygen adsorption energy barrier and activate or significantly improve the electrocatalytic activity of ORR. Non-metallic heteroatom doping (N, P, S, B, and F) can be used to alter the intrinsic properties of functional carbon materials, such as internal micro-structure and composition, electronic structure, surface and partial electrochemical characteristics [9]. Therefore, heteroatom-doped carbon-based electrocatalysts show a huge research prospect for the development of ORR. N atom is the most commonly used heteroatoms to modify carbon materials among all heteroatoms. Because the electronic confinement effect derived from the conjugation between the graphene π

system and the N lone pair of electrons [10]. As such, intensive works have used MOFs as templates to build heteroatom-doped carbon-based materials and applied them to the electrocatalytic of ORR with excellent results.

Chueh et al. [11] successfully prepared a highly efficient nitrogen-doped carbon nanotubes (N-CNTs) electrocatalyst derived from nitrogen-doped carbon dots (N-C dots) and MOFs for ORR. The N-C dots with plenty of hydroxyl and amine groups can favor the formation of N-CNTs through the catalytic decomposition of MOFs in a lower temperature. On the other hand, the N-C dots function as inducers of the graphitic structure and supplied extra nitrogen, expanding a potential electrocatalytic activity of N-CNTs. Results revealed that the N-CNTs provided an exceptional ORR electrocatalytic performance, giving a positive onset potential of 0.88 V vs. RHE. and a high kinetic current density of up to 5.58 mA cm⁻² at 0.2 V. In addition, the N-CNTs catalyst displays excellent catalytic durability and tolerance to methanol in an alkaline media. Sung et al. [12] synthesized graphitic carbon nitride-carbon nanofiber (g-CN-CNF) as a bifunctional catalyst in an anion-exchange membrane water electrolyzer (AEMWE), and primary and rechargeable Zn-air cells. The g-CN-CNF catalyst showed high catalytic activity for oxygen reduction and evolution in half-cell, with low overpotentials and low Tafel slopes. The increased activity was attributed to the synergistic effect of abundant active sites and the electrical conductivity following the pyrolysis of g-CN and CNF. As a result, AEMWE with the g-CN-CNF anode exhibited outstanding performance. In addition, the performance and durability of Zn-air cells with g-CN-CNF cathode outperformed those fabricated with commercial platinum.

Furthermore, two or more heteroatoms co-doped carbon materials have also been developed, exhibiting better activity than the single heteroatom doped counterparts [13]. Zhang et al. [13] constructed P and N-coordinated fullerene-like carbon (N, P-FC) multi-functional catalyst via a facile soft template pyrolysis method, which achieved an impressive activity for electrochemical ORR with half-wave overpotential ($E_{1/2}$) of 0.910 V, 79 mV higher than that of commercial Pt/C and overperformed all the documented carbon-based electrocatalysts (Fig. 5.2a-e). Combined theoretical calculation studies suggested that the P-coordinated C site was more active for CO₂RR, while the N-coordinated neighboring C site was responsible for ORR in this catalyst. Similarly, Zhang et al. [14] successfully prepared nitrogen-and fluorine co-doped microporous carbon nanofibers (N, F-MCFs) via electrospinning polyacrylonitrile/polyvinylidene fluoride/polyvinyl pyrrolidone (PAN/PVDF/PVP) tricomponent polymers followed by a hydrothermal process and thermal treatment, which was achieved for the first time in the literature. The results indicated that N, F-MCFs exhibited a high catalytic activity (E_{onset} : 0.94 V vs. RHE., $E_{1/2}$: 0.81 V vs. RHE., and electron transfer number: 4.0) and considerably better stability and methanol tolerance for ORR in alkaline solutions as compared to commercial Pt/C (20 wt%) catalysts.

Recently, the defect mechanism of carbon-based electrocatalysts has a perfect role in promoting advanced electrocatalytic activity for the ORR [15–17]. The structural defects play a decisive role in the catalytic process because most electrochemical reactions occur at these sites [18]. Several methods are proposed to fabricate defects,

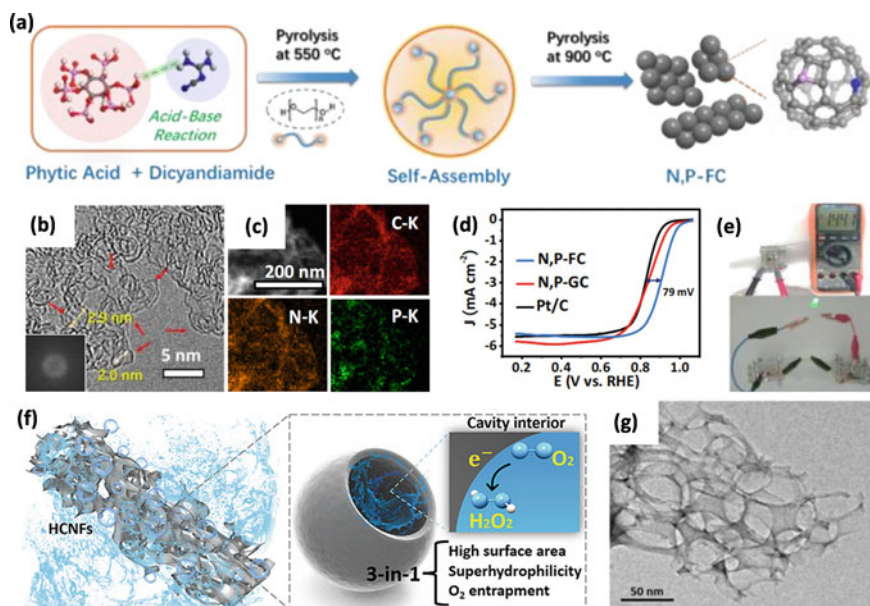


Fig. 5.2 Metal-free carbon-based electrocatalysts for ORR. **a** The illustration of the synthetic protocol of N, P-FC. **b** SEM image, **c** TEM image of the N, P-FC. **d** LSV curves of N, P-FC, N, P-GC, and Pt/C catalyst for ORR in 0.1 M KOH. **e** Photograph of all-solid-state Zn-air batteries with an open-circuit voltage of 1.441 V and luminous LED lamp lighting test. Reproduced with permission [13]. Copyright 2012, Royal Society of Chemistry. **f** 3-in-1 effect of HCNFs promotes O_2 -to- H_2O_2 conversion. **g** TEM images for HCNFs. Reproduced with permission [24]. Copyright 2021, WILEY-VCH

such as chemical modification, doping removal, and plasma etching [17, 19]. Since their respective advantages of defects and heteroatom doping as mentioned above, a well way to simultaneously introduce both target doping and appropriate defects will improve the ORR performance.

Liang et al. [20] reported a novel molecular design strategy to achieve 2D porous turbostratic carbon nanomesh with abundant N-doped carbon defects (NDC). Molecular-level integration of carbon source, N source, and sacrificial template into the polymer chains promised the formation of abundant and accessible carbon edge defects as well as efficient N doping sites synchronously. A special active site of carbon edge defect doped with graphitic valley N with the lowest theoretical ORR energy barrier of 0.56 eV was revealed to be responsible for the exceptional ORR electrocatalytic performance of prepared NDC materials in alkaline media. Notably, this method had a considerable advantage in modulating the composition and structures of the carbon precursor at the molecular level for carbon defect regulation via changing the building units and integration routes. This efficient molecular design strategy created a new avenue for rational development of high-performance N-doped

defective carbon ORR electrocatalysts and deeply understanding their ORR electrocatalytic mechanism. Similarly, Wen et al. [21] presented the scalable salt-templated synthesis of two-dimensional porous fluorine-doped carbon (FC) nanosheets. Due to the larger special surface area ($1031 \text{ m}^2 \text{ g}^{-1}$) and high active sites, FC-900 (pyrolyzed at $900 \text{ }^\circ\text{C}$) showed impressive ORR. The synergistic effect of fluoride doping and defects provided the richer density of active sites in these nanosheets. The results revealed F dopants and defects important roles in efficient ORR electrocatalysis owing to the synergistic effect, which was important for comprehending the origin of ORR [21].

Electrocatalytic two-electron oxygen reduction has emerged as a promising alternative to the energy- and waste intensive anthraquinone process for distributed H_2O_2 production [22]. This process, however, suffers from strong competition from the four-electron pathway leading to low H_2O_2 selectivity [23]. Sun et al. [24] reported using a superhydrophilic O_2 -entrapping electrocatalyst to enable superb two-electron oxygen reduction electrocatalysis (Fig. 5.2f, g). The honeycomb carbon nanofibers (HCNFs) were robust and capable of achieving a high H_2O_2 selectivity of 97.3%, much higher than that of its solid carbon nanofiber counterpart. Impressively, this catalyst achieved an ultrahigh mass activity of up to 220 A g^{-1} , surpassing all other catalysts for two-electron oxygen reduction reaction. The superhydrophilic porous carbon skeleton with rich oxygenated functional groups facilitated efficient electron transfer and better wetting of the catalyst by the electrolyte, and the interconnected cavities allowed for more effective entrapping of the gas bubbles.

5.3 Atomically Dispersed Metal Carbon-Based Electrocatalysts for ORR

The atomically dispersed metal carbon-based materials mainly consist of metallic atoms or coexistent of metallic atoms and clusters. Among them, transition single metallic atom catalysts have become one of the main research hotspots due to their high dispersibility and atomic availability. Significantly, the transition metal (Fe, Co, etc.)–N–C material is considered to be the most promising substitute for Pt-based catalyst [25]. The high intrinsic activity (such as turnover frequency) of the active center of M–N_x/C is generally believed to be mainly derived from the N coordinated single metallic atom confined in the carbon matrix. Thus, maximizing the number of metal sites is a top priority for improving ORR performance. Atomic dispersion catalysts can reasonably utilize metal resources and promote atomic economic efficiency by optimizing the use of atoms to a certain extent. The active center of atomic dispersion catalyst can form due to its unique electronic structure and unsaturated coordination environment [26]. In addition, the good atomic dispersion also allows the catalyst to have similar spatial effects and electronic interactions with the substrate, thus improving the catalytic performance. Many pioneers' work has suggested that the encapsulated metallic atom in heteroatom-doped (N, P, S, etc.)

carbon materials is an effective way to fine tuning the electron interactions between encapsulated metallic atoms and carbon, and hence generate rich active sites for electrocatalysis [10].

At present, Fe–N–C catalyst has become one of the most widely studied M–N–C materials because of its high ORR activity [27, 28]. Single Fe atoms are one of the most widely studied by researchers. Jia et al. [29] implemented chemical vapor deposition to synthesize Fe–N–C by flowing iron chloride vapor over a Zn–N–C substrate at 750 °C, leading to high-temperature trans-metalation of Zn–N₄ sites into Fe–N₄ sites. Characterization by multiple techniques showed that all Fe–N₄ sites formed via this approach are gas-phase and electrochemically accessible. As a result, the Fe–N–C catalyst had an active site density of 1.92×10^{20} sites per gram with 100% site utilization. This catalyst delivered an unprecedented oxygen reduction reaction activity of 33 mA cm⁻² at 0.90 V (iR-corrected; i, current; R, resistance) in a H₂–O₂ proton exchange membrane fuel cell at 1.0 bar and 80 °C. Lin et al. [20] used the ligand in the MOF precursor to confine a series of single metallic atoms. The metal was firstly coordinated with the ligand, and then pyrolysis and acid leaching were carried out to form a stable single-atom catalyst. It was worth noting that the obtained SAC/N–C catalyst was coordinated with pyridinic-N and had superior ORR activity, stability and good methanol tolerance. More importantly, by changing the metal precursor, this strategy can be successfully extended to the process of preparing other transition metal single-atom catalysis (SACs).

Meanwhile, S is less electronegative than N atoms and is a very effective non-metallic dopant. Mu et al. [30] prepared Fe, N, and S co-doped carbon matrix/CNTs nanocomposites (Fe–N–S CNN) by pyrolysis of ZIF-8 impregnated with iron salts. The carbon-based nanomaterial derived from ZIF-8 had a higher porosity, regular pores, and a larger specific surface area. CNTs grown in situ were conducive to electron transport, have good electrical conductivity, and can promote material transport and material exchange. In addition, the synergy between Fe, N, and S can jointly promote the increase in the number of active sites, improve ORR activity and long-term stability. In addition, Fe–N–S CNN also showed excellent performance and ability as the cathode of the primary Zn air battery.

P atoms, which are also electronegative, can grab electrons from metal atoms. Zhang et al. [31] designed a facial strategy to synthesize N, P-doped defective carbon nanosheets first (N, P–DC), then covered doped sites with well-defined metal–N₄ macrocyclic molecules (FePc@N, P–DC) through the non-pyrolysis process (Fig. 5.3e). The defective carbon boosted the high spin state of Fe center, thus bringing superior ORR performances (Fig. 5.3f).

Although Fe–N–C catalyst had excellent ORR activity, its poor stability was the main obstacle to important application [32]. Even worse, Fenton reactions occur between Fe²⁺ and H₂O₂. H₂O₂ will attack the active site of FeN₄ and the carbon carrier, thus accelerating the performance degradation [3, 33]. Therefore, some methods are needed to suppress the Fenton reaction of metallic Fe. First, the stability of the Fe-based catalyst can be enhanced by introducing other metals. By rational design and synthesis of dual-metal atomically dispersed Fe, Mn/N–C catalyst as a model object, Zhang et al. [34] unraveled that the O₂ reduction preferentially takes

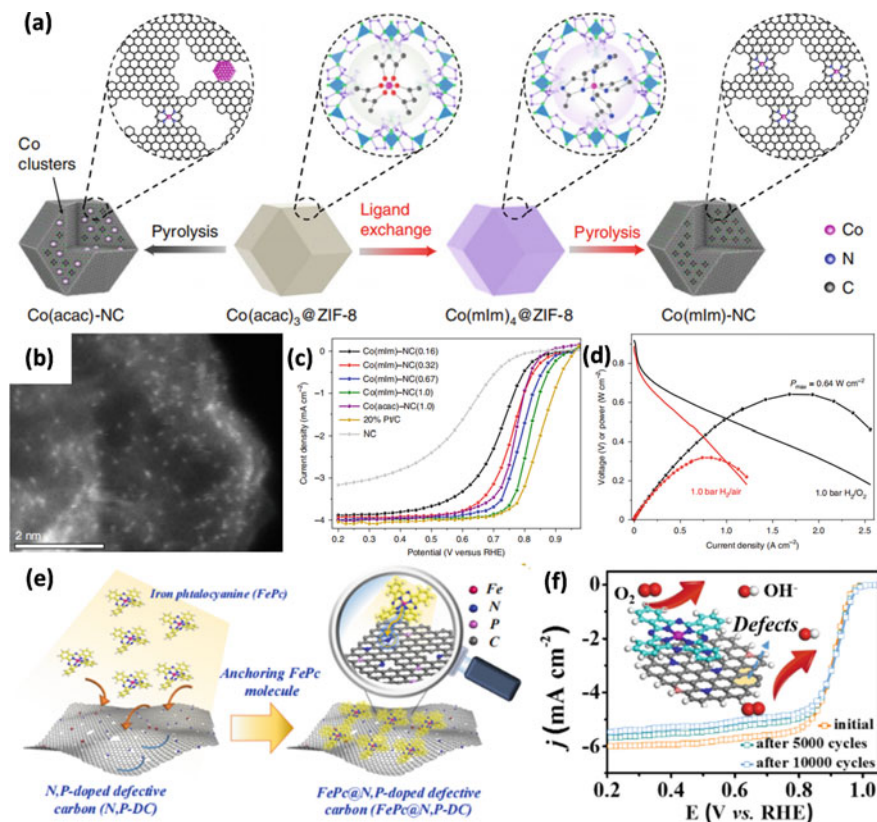


Fig. 5.3 Atomically dispersed metal carbon-based electrocatalysts for ORR. **a** A two-step encapsulation and ligand-exchange approach effectively introduces Co_4 complexes into the ZIF-8 micropores. **b** HAADF-STEM image of the Co(mIm)-NC(1.0) catalyst. **c** Steady-state ORR polarization plots for different Co(mIm)-NC catalysts as a function of Co content ($\text{Co(mIm)-NC}(x)$), Co(acac)-NC(1.0) and Co-free NC in 0.5 M H_2SO_4 , and for 20% Pt/C (60 μg Pt on the electrode disk) in 0.1 M HClO_4 under O_2 saturation. **d** Fuel cell performance (dashed-dot: power density, full line: polarization curves) of Co(mIm)-NC(1.0) . Reproduced with permission [32]. Copyright 2020, Springer Nature. **e** Synthetic procedure of FePc@N,P-DC catalyst. **f** ORR polarization LSV of FePc@N,P-DC measurement before and after 5000 and 10,000 cycles at the scan rate of 50 mV s^{-1} with the rotation speed of 1600 rpm. Reproduced with permission [31]. Copyright 2020, Elsevier

place on Fe^{III} in the Fe_4/C system with the intermediate spin state which possesses one e_g electron ($t_{2g}^4e_g^1$) readily penetrating the antibonding π -orbital of oxygen. Both magnetic measurements and theoretical calculation revealed that the adjacent atomically dispersed Mn-N moieties can effectively activate the Fe^{III} sites by both spin-state transition and electronic modulation, rendering the excellent ORR performances of Fe, Mn/N-C in both alkaline and acidic media (halfwave potentials are 0.928 V in 0.1 M KOH, and 0.804 V in 0.1 M HClO_4), and good durability, which outperforms and has almost the same activity of commercial Pt/C, respectively. Fe, Ni

bimetallic carbon-based catalysts is another interesting case. Zhao et al. [7] presented hetero-single-atom ORR electrocatalyst, which has atomically dispersed Fe and Ni co-anchored to a micro-sized nitrogen-doped graphitic carbon support with unique trimodal-porous structure configured by highly ordered macropores interconnected through mesopores. The obtained experimental results indicate that the achieved outstanding ORR performance results from the synergetic enhancement induced by the coexisting Fe-N₄ and Ni-N₄ sites and the superior mass-transfer capability promoted by the trimodal-porous-structured carbon support.

Alternatively, Fe atoms can be substituted by metals that do not catalyze the Fenton reaction, with Co being the most investigated. Wu et al. [32] synthesized an atomically dispersed Co-N-C catalyst by simple pyrolysis (Fig. 5.3a, b). Compared with Fe-N-C catalysts with similar synthesis methods, Co-N-C catalysts have similar ORR catalytic activity and much better durability (Fig. 5.3c, d).

Fenton reactions involving Mn ions are insignificant because of weak reactivity between Mn and H₂O₂. Therefore, with proper design, Mn can also be an excellent single atomic catalyst to replace Fe. Wu and co-workers reported an atomically dispersed Mn single-atom catalyst (Mn-NC) obtained by simple pyrolysis of ZIF-8 loaded with metal Mn, and the ORR half-wave of the obtained catalyst under acidic conditions the potential is 0.8 V versus RHE, which is close to Fe-NC catalyst [35]. In addition, since metal Mn does not promote the occurrence of Fenton reaction, it has excellent long-term stability under acidic conditions.

Clusters composed of several single atoms can also be synthesized by controlling the reaction conditions and the ratio of reactants. The formation of clusters can change the electronic structure of the active centers, and the synergistic interaction between metallic atoms and between clusters and heteroatoms can improve the activity of the catalysts. For example, Tan et al. [36] used the microporous MOFs confinement strategy to confine the sub-nano CoO_x clusters in the micropores of the ZIF-8-derived carbon-based nanomaterials. The micropores of the nanomaterial not only play a confining role on the CoO_x cluster, which makes the CoO_x cluster stable and prevents aggregation, but also interact with the CoO_x cluster to a certain extent, improve its electronic structure, and jointly promote the improvement of ORR/OER catalytic activity of the CoO_x cluster. Zhang et al. [37] proposed to use sulfurization to enhance the activity of iron clusters containing iron carbides (Fe_xC/Fe) for ORR catalysis. In contrast to its excellent activity in alkaline media, FeNC-S-Fe_xC/Fe exhibits better ORR activity and durability in acidic media. Its half-wave potential (0.821 V) is better than commercial Pt/C catalysts (20 wt%). Theoretical calculations confirm that the Fe_xC/Fe clusters, the Fe-S and C-S-C bonds construct the energy confined field and enhance the original FeN_x active center.

5.4 Metal Nanoparticles Encapsulated Carbon-Based Electrocatalysts for ORR

A variety of metal-based nanoparticle carbon materials, including metals, alloys, and compounds, can be obtained by simple pyrolysis process, which all show high ORR activity [35, 38]. However, these nanoparticles' dissociation, migration, and aggregation always result in decreased activity and stability. Anchoring metal nanoparticles on the surface of the carbon substrate or confining them in the cavities is an effective method to handle these problems [39].

An obvious advantage of MOF materials is that the composition of MOF can be changed to bind specific heteroatoms and metal species in situ by replacing the organic ligands or metal centers. In addition, additional functional metals can be introduced by constructing multi-metal center MOFs or confining metal nanoparticles to the cavities of MOFs [40].

Cui et al. [41] adopted a simple strategy to limit the growth of MOF in graphene aerogel (GA), and synthesized a new type of N-containing graphene aerogel cobalt in the catalyst (Co–N–GA) for ORR. As-prepared Co–N–GA exhibited a hierarchical porous structure and a high specific surface area ($466.6 \text{ m}^2 \text{ g}^{-1}$). Moreover, because of the synergistic effects of hierarchical pores, high specific surface area, N-doped carbon and internal metal Co, Co–N–GA catalyst showed excellent activity and stability for ORR. This strategy opened up a new platform to construct hierarchical porous GA-based catalysts as superior electrocatalysts for energy storage and conversion technologies.

Mu et al. [42] reported bifunctional oxygen electrocatalysts of based on ultra-fine CoFe alloy (4–5 nm) dispersed in defects enriched hollow porous Co–N-doped carbons made by annealing SiO_2 coated zeolitic imidazolate framework-67 (ZIF-67) encapsulated Fe ions. The open porous structure exposed more active sites inside ZIF-67 and provided efficient charge and mass transfer. The strong synergetic coupling among high-density CoFe alloys and Co–N_x sites in Co, N-doped carbon species ensures high ORR activity (Fig. 5.4a–d).

Wang et al. [43] developed a molten salt-assisted solid-state assembly strategy to prepare multifunctional Fe/Co Zn MOF composites. Further carbonization of MOF produced Fe/Co–N-doped mesoporous carbons (Fe/Co–NCs). The obtained NCs had many advantages, such as a sheet-like structure with high porosity and tubular macropores (15 nm) and an N-doped carbon skeleton with highly dispersed Fe/Co nanoparticles. The advantage of confined structure can promote the synergistic effect between active sites, and Fe/Co–NC showed high activity for ORR and HER. Among them, Fe–NC exhibited excellent ORR activity with a higher onset potential (0.963 V), half-wave potential (0.877 V vs. RHE in 0.1 M KOH), and excellent durability (95% current after 20,000 s maintain). The Co-NC exhibited high HER activity with a low overpotential of 242 mV at a current density of 10 mA cm^{-2} . The remarkable ORR and HER performance were mainly attributed to the simultaneous working of multiple active centers, such as N and metal species (Fe/Co) as active sites synergistically promoting ORR and HER processes.

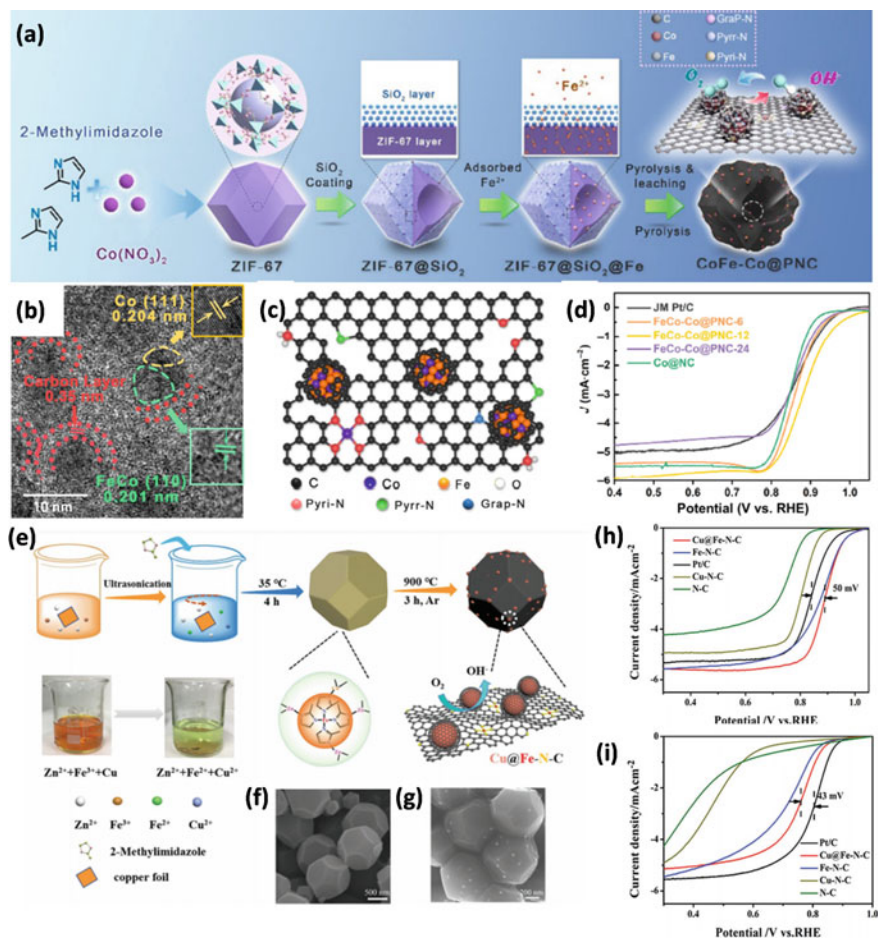


Fig. 5.4 Metal nanoparticles encapsulated carbon-based electrocatalysts for ORR. **a** Illustration of the preparation process of the CoFe-Co@PNC catalysts. **b** HR-TEM image of Fe, Co, N, and C of CoFe-Co@NPC-12. **c** Schematic diagram of the existence of each element in FeCo-Co@PNC-12. **d** ORR curves of various catalysts in O_2 -saturated 0.1 M KOH solution at 1600 rpm. Reproduced with permission [42]. Copyright 2020, Springer Nature. **e** Schematic of the synthesis procedure of Cu@Fe-N-C. SEM images of **f** FeCu-ZIF, and **g** Cu@Fe-N-C. **h** LSV curves of Cu@Fe-N-C, Fe-N-C, Pt/C, Cu-N-C, and N-C in O_2 -saturated 0.1 M KOH solutions with a rotation speed of 1600 rpm and a sweep rate of 10 $\text{mV}\cdot\text{s}^{-1}$. **i** LSV curves of Cu@Fe-N-C, Fe-N-C, Pt/C, Cu-N-C, and N-C in O_2 -saturated 0.5 M H_2SO_4 solutions with a rotation speed of 1600 rpm and a sweep rate of 10 $\text{mV}\cdot\text{s}^{-1}$. Reproduced with permission [44]. Copyright 2018, WILEY-VCH

Wang et al. [44] reduced Fe^{3+} to Fe^{2+} through copper sheets, and introduced Cu^{2+} , then mixed and stirred it with methanol solution containing 2-methylimidazole to obtain FeCu-ZIF precursor, and then subjected to simple pyrolysis to obtain Fe, Cu co-coordinated ZIF-derived carbon-based materials (Cu@Fe-NC) (Fig. 5.4e). The material had a regular truncated dodecahedron morphology, Fe is evenly distributed in the carbon framework, and Cu mainly exists in the form of carbon-coated copper particles (Fig. 5.4f, g). In terms of performance, Cu@Fe-N-C exhibited excellent ORR catalytic activity under both alkaline and acidic conditions (Fig. 5.4 h, i).

Chen et al. [45] synthesized a series of Co-ZnO (Co-ZnO@NC/CNT-T) coated in N-doped carbon/carbon nanotubes by annealing bimetallic MOF confining Co and Zn in N_2 atmosphere. In the hybrid, the metallic Co combines with ZnO that wrapped by NC, while coral-like carbon nanotubes are grown from Co-ZnO@NC nanoparticles. When applied to catalytic ORR, Co-ZnO@NC/CNT-700 has a half-wave potential of 0.86 V in 0.1 M KOH and a limiting current density of 5.98 mA cm^{-2} , even better than 20 wt% Pt/C. It was found that the presence of ZnO is closely related to high ORR catalytic activity from two aspects. On the one hand, ZnO catalyzes the formation of Co^0 , Co^{2+} , pyridinic and graphitic N as the main active species for ORR. On the other hand, ZnO promotes the growth of carbon nanotubes and micro/mesoporous structures, and improves the electrochemically active surface area and mass transfer in the ORR process.

5.5 Metal Nanoparticles Supported Carbon-Based Electrocatalysts for ORR

In addition to encapsulating metal nanoparticles in MOF-derived carbon-based materials, they can also be loaded onto other carbon-based materials. Transition metal nitride (M-N_x) is a kind of ORR catalyst like transition metal carbide [46]. Because it is easier to dissolve than other transition metals under high overpotential, transition metal nitride shows good stability, which is difficult to be etched and dissolved.

Varga et al. [47] formed nitrogen-doped graphene sheets ($\text{Co}_4\text{N/NG}$) modified by cobalt nitride (Co_4N) nanoparticles by mixing freeze-dried graphene oxide nanoparticles and cobalt acetate (II). The average particle size of Co_4N increased from 14 to 201 nm with the increase of cobalt content. Moreover, it showed ORR activity similar to that of Pt/C, and the highest reduction current density was as high as 4.1 mA cm^{-2} under alkaline conditions. In addition, the four-electron process was the main reaction pathway. In the case of Co-NC interaction, the cobalt atom carries more positive cations than the carbon atom is more conducive to the adsorption of oxygen molecules.

Tang et al. [48] discovered a general strategy mediated by metastable rock salt oxides for achieving high-density well-defined transition-metal nanocrystals encapsulated in N-doped carbon shells (M@NC) anchored on a substrate by a porous carbon network as highly active and durable bifunctional catalytic sites. Small-size

(15 ± 5 nm) well-dispersed $\text{Co}_2\text{Fe}_1@NC$ in a high density (metal loading up to 54.0 wt %) offered the zinc-air battery a record power density of 423.7 mW cm^{-2} . The dual protection from the complete graphitic carbon shells and the anchoring of the outer carbon network made $\text{Co}_2\text{Fe}_1@NC$ chemically and mechanically durable, giving the battery a long cycling life (Fig. 5.5a–d).

Hu et al. [45] developed a strategy to investigate the role of iron species in Fe–N–C nanohybrids for catalyzing ORR by delicately tuning the iron chemical state. By engineering peripheral substituents of iron porphyrin precursors, two Fe–N–C nanohybrids with metallic or oxidized iron species inside were achieved while holding a similar catalyst structure. Systematic experiments and theoretical analysis

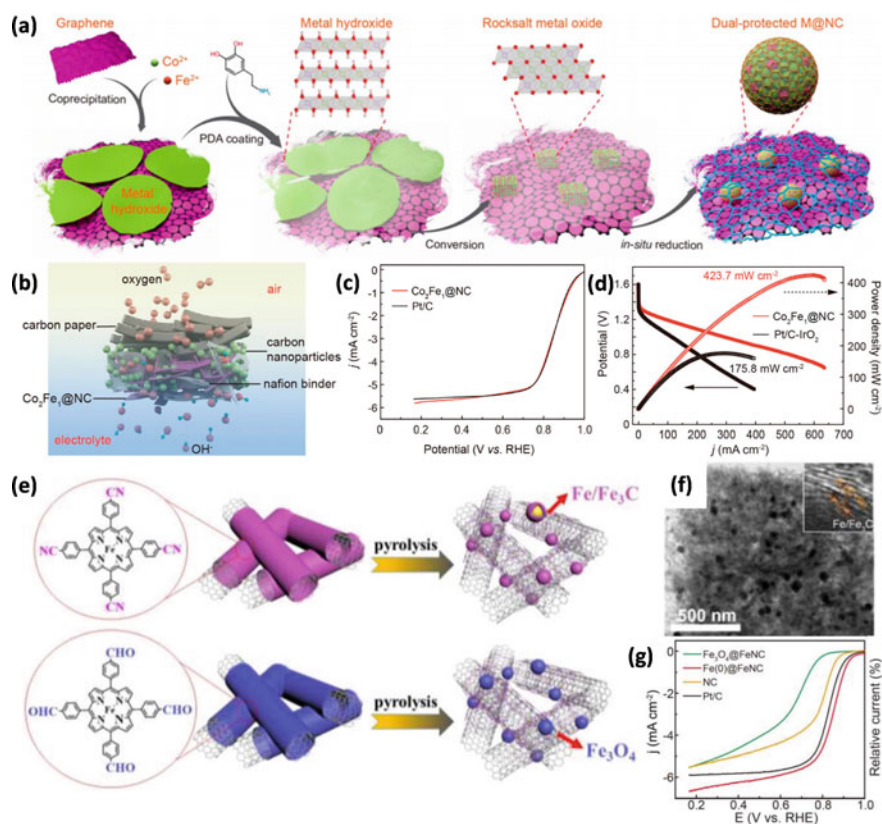


Fig. 5.5 Metal nanoparticles supported carbon-based electrocatalysts for ORR. **a** Synthesis and structural characterization of $\text{Co}_2\text{Fe}_1@NC$. **b** Scheme of a catalyst loaded gas diffusion air electrode in contact with liquid electrolyte and air. **c** Steady-state ORR polarization curves. **d** Discharge polarization curves and corresponding power density curves of CFB and PIB. Reproduced with permission [48]. Copyright 2020, American Chemical Society. **e** Schematic illustration of the preparation of $\text{Fe}(0)@FeNC$ and $\text{Fe}_3\text{O}_4@FeNC$ catalysts. **f** TEM images of $\text{Fe}(0)@FeNC$. **g** LSV curves of $\text{Fe}_3\text{O}_4@FeNC$, $\text{Fe}(0)@FeNC$, NC, and Pt/C for ORR. Reproduced with permission [45]. Copyright 2019, Elsevier

discovered that metallic iron species promoted the electrocatalytic activity of Fe–N_x sites for ORR. In contrast, oxidative ones inhibited O₂ adsorption on Fe–N_x sites, decreasing their ORR activity. (Fig. 5.5e–g).

For nonprecious transition metal oxides, although it exhibits good stability under acid, alkaline, and oxidation conditions and have certain ORR activity in alkaline solution, it is still a challenge to enhance their ORR activity. The low ORR activity is credited with the inherent large energy band of transition metal oxides, leading to its low electrical conductivity and poor surface oxygen adsorption capacity. Hence, this also suggests that they may not conducive to use as cathodic electrocatalysts in acid fuel cell [49]. Introducing defective structure into metal oxides is an effective means of improving the activity of electrocatalytic ORR by adjusting the atomic coordination environment and electronic structure to lead to surface strain effect, thereby optimizing the adsorption energy of ORR intermediates on the surface of the catalyst.

Therefore, Zhang et al. [50] prepared manganese defect Mn₃O₄ by calcining manganese glycolate. The Mn defect in Mn₃O₄ changed the electronic structure, thus improving the electrical conductivity and electron delocalization. In addition, the existence of manganese defects can pronouncedly reduce the desorption energy of OH*. The molecular orbital diagram showed that the bonding orbital energy of Mn²⁺–OH is different from that of Mn³⁺–OH, the former was lower than that of the latter, which indicated that the binding strength of the former was higher than that of OH*, which was consistent with the calculation of the reaction free energy of ORR. Therefore, the existence of manganese defects in Mn₃O₄ can be conducive to exhibit more Mn³⁺ as the main active site, thus promoting the activation of O₂ in ORR and the desorption of OH*, and effectively reducing the change of Gibbs free energy and theoretical overpotential in the rate-limiting step of ORR. As a result, the initial potential, half-wave potential, and the current density of Mn₃O₄ with Mn defects are superior to those of ordinary Mn₃O₄.

Because of its wide electronic structure and inherent physical properties, transition metal sulfides (TMSs) have a broad prospect in the field of electrocatalysis and have attracted widespread attention [51]. TMSs are new cluster crystals formed by the interaction between metal centers and sulfur elements, providing a good space for oxygen adsorption and electron transfer. The sulfidation of metals changes the surface chemical properties of transition metal sulfides and avoids oxidation in the metal center during the preparation of electrocatalysts, which are more stable than metal oxides in acidic electrolyte solutions [52].

Behret et al. [53] evaluated the electrocatalytic activity of a series of TMSs (Mn, Fe, Co, Ni, Cu, Zn) for ORR in acid electrolytes by measuring potentiodynamic and galvanostatic methods. The ORR activity of cobalt, iron and nickel sulfides was significantly higher in transition metal sulfides. To enhance the electrical conductivity of TMSs, carbon materials were used as carriers to disperse TMSs to obtain highly active ORR electrocatalysts. Exploring economical electrocatalysts for efficient and stable ORR is essential for future renewable energy applications.

In contrast, transition metal phosphides (TMPs) (TM = Fe, Co, Cu, Ni, W, and Mn) with electronic structures and properties are similar to carbides and nitrides, which

are significant substitute to take the place of Pt. Due to its series of advantages, such as high electrical conductivity, earth abundance reserves and good physical and chemical properties, it has aroused widespread attention [54]. As a result of its excellent catalytic activity and selectivity, it is widely used in ORR and other electrocatalytic reactions, especially cobalt phosphide and its derivatives [54].

Thus, Li et al. [55] used the supramolecular assembly-assisted one-pot method and used small organic molecules as the phosphorus source to prepare a unique cyclic hybrid nanostructure composed of interconnected CoP nanoparticles in a carbon matrix co-doped with phosphorus and nitrogen (CoP@PNC-DOS). Furthermore, CoP@PNC-DOS showed excellent ORR activity in alkaline medium (Eonset = 0.94 V, $E_{1/2}$ = 0.803 V and Tafel slope (85.6 mV dec⁻¹) close to Pt/C (92.5 mV dec⁻¹)), which was because of the synergistic effect of the hierarchical donut-like morphology, rich active centers and double-doped modulation carbon matrix.

5.6 Conclusion and Perspectives

The sluggish O₂ reduction due to its multi-electron transfer feature makes it the heart of fuel-cell chemistry. The desire to find non-precious metal alternatives to Pt-based ORR electrocatalysts is strong for a more affordable and applicable PEMFCs. The pyrolyzed porous carbon is usually structurally stable and possess unique electronic properties to offer high activity. Through reviewing the ongoing progress in carbon-based materials, some insights can be extracted with a view to realizing their practical application in the more demanding PEMFCs. However, there could be thousands and tens of thousands of combinations since the distribution and type of defective sites, heteroatom dopants and metal types in carbon nanomaterials are random and diverse. Fortunately, as the great progress and rapid development of computer technology, the use of high-throughput screening and machine learning technology in searching for the best active site for ORR may be the most efficient way. Besides, other significant challenges still exist, which are worthy of our further attention to developing the highly efficient carbon-based ORR electrocatalysts.

- (1) Modulating the electronic structure of the active sites accurately is the basis for studying different catalysts with different configuration. Therefore, more reasonable synthesis methods are needed to accurately modify the type, coordination structure and chemical environment of active center. For example, the doping of different elements, the preparation of multi-dimensional structures, and the construction of layered pores have been widely used in well-designed ORR electrocatalysts. Carbon electrocatalysts doped with multiple heteroatoms can further improve the electrocatalytic activity of ORR, which can be attributed to the synergistic effect between various heteroatoms. These heteroatoms can produce larger asymmetric spins, and the charge density is optimized for the carbon skeleton. In addition, due to the unique and adjustable structure of the precursor, the obtained electrocatalyst has an ultra-high specific

- surface area, layered pore structure, and high-density active centers with good dispersion, which will provide fast mass and protons transfer and enhance the catalytic activity of ORR.
- (2) Adjust the porous size and structure to expose more active specific surface area, introduce heteroatoms to provide more active site centers, and prevent the aggregation of $M-N_x$ sites from forming uniformly dispersed high-density active sites, which is useful for improving ORR catalytic activity of the electrocatalyst effectively. In addition, the size of catalysts is also closely related to the transport properties and electrocatalytic activity of ORR electrocatalysts. It has been proven that smaller electrocatalysts can provide more favorable quality and electron transfer processes. However, most of the synthesis routes of $M-N_x$ doped carbon-based catalysts involve high-temperature pyrolysis, which may produce two or more metal compound species at the same time, which is not conducive to determining the specificity of each species in catalytic effect. Therefore, this may be one of the critical issues for the future improvement of metal-doped carbon catalysts. In addition, there are severe obstacles to the development of carbon catalysts, that is, they are prone to agglomeration and are challenging to grow on the substrate during high-temperature processing, and may become another research hotspot to improve ORR transmission kinetics and improve electrocatalytic activity.
 - (3) The mechanism of how active sites interact with carbon substrates and co-promote the electrocatalytic ORR activity has not been understood. Normally, the theoretical simulations are employed to reveal the correlation with the electronic structure, adsorption properties, and electrocatalytic activity. However, there is a big difference between the practical application and theoretical modeling simulation. Combined with more powerful and effective experimental characterizations, even in situ or operando techniques are hence necessary to observe the real process of electrocatalysis, which will be very helpful to further understand the mechanism of the electrocatalytic reaction.
 - (4) The electrocatalytic ORR activity of metal-free carbon-based nanomaterials in alkaline conditions is usually higher than that in acidic conditions, for which include the quite different absorption intermediates and rate-determining steps in acidic and alkaline media. The current carbon-based ORR electrocatalysts are hence normally used in alkaline solutions, but not in acidic electrolytes. Since most of the practical fuel cells are more promising and competitive in acidic conditions (e.g., high efficiency and stability, non-effect of carbon dioxide), exploring and synthesizing more effective acidic carbon-based ORR electrocatalysts is of great significance.

All in all, carbon-based materials due to the multiple advantages of low cost, high efficiency, good stability, and long lifetime will undoubtedly have a promising application in the ORR field. Along with the present achievements and more advanced characterization methods combined with in situ techniques, the role of carbon-based materials in the electrocatalysis field will be able to further understand at a deeper level.

References

1. Y. Deng, J. Luo, B. Chi, H. Tang, J. Li, X. Qiao, Y. Shen, Y. Yang, C. Jia, P. Rao, S. Liao, X. Tian, Advanced atomically dispersed metal–nitrogen–carbon catalysts toward cathodic oxygen reduction in PEM fuel cells. *Adv. Energy Mater.* **11**, 2101222 (2021). <https://doi.org/10.1002/aenm.202101222>
2. H.S. Wroblowa, Y.C. Pan, G. Razumney, Electroreduction of oxygen: A new mechanistic criterion. *J. Electroanal. Chem. Interfacial Electrochem.* **69**, 195–201 (1976). [https://doi.org/10.1016/S0022-0728\(76\)80250-1](https://doi.org/10.1016/S0022-0728(76)80250-1)
3. C.H. Choi, H.-K. Lim, M.W. Chung, G. Chon, N. Ranjbar Sahraie, A. Altin, M.-T. Sougrati, L. Stievano, H.S. Oh, E.S. Park, F. Luo, P. Strasser, G. Dražić, K.J.J. Mayrhofer, H. Kim, F. Jaouen, The Achilles' heel of iron-based catalysts during oxygen reduction in an acidic medium. *Energy Environ. Sci.* **11**, 3176–3182 (2018). <https://doi.org/10.1039/c8ee01855c>
4. Z. Xing, D. Wang, T. Meng, X. Yang, Superb hydrogen evolution by a Pt nanoparticle-decorated Ni₃S₂ microrod array. *ACS Appl. Mater. Interfaces.* **12**, 39163–39169 (2020). <https://doi.org/10.1021/acscami.0c10476>
5. H. Li, X. Shu, P. Tong, J. Zhang, P. An, Z. Lv, H. Tian, J. Zhang, H. Xia, Fe-Ni alloy nanoclusters anchored on carbon aerogels as high-efficiency oxygen electrocatalysts in rechargeable Zn-Air batteries. *Small*, e2102002 (2021). <https://doi.org/10.1002/smll.202102002>
6. J. Zhang, J. Zhang, F. He, Y. Chen, J. Zhu, D. Wang, S. Mu, H.Y. Yang, Defect and doping Co-engineered non-metal nanocarbon ORR electrocatalyst. *Nano-Micro Lett.* **13**, 65 (2021). <https://doi.org/10.1007/s40820-020-00579-y>
7. Z. Zhu, H. Yin, Y. Wang, C.H. Chuang, L. Xing, M. Dong, Y.R. Lu, G. Casillas-Garcia, Y. Zheng, S. Chen, Y. Dou, P. Liu, Q. Cheng, H. Zhao, Coexisting single-atomic Fe and Ni sites on hierarchically ordered porous carbon as a highly efficient ORR electrocatalyst. *Adv. Mater.* **32**, e2004670 (2020). <https://doi.org/10.1002/adma.202004670>
8. L. Jiao, X. Wang, G. Diankov, H. Wang, H. Dai, Facile synthesis of high-quality graphene nanoribbons. *Nat. Nanotechnol.* **5**, 321–325 (2010). <https://doi.org/10.1038/nnano.2010.54>
9. L. Yang, J. Shui, L. Du, Y. Shao, J. Liu, L. Dai, Z. Hu, Carbon-based metal-free ORR electrocatalysts for fuel cells: Past, present, and future. *Adv. Mater.* **31**, e1804799 (2019). <https://doi.org/10.1002/adma.201804799>
10. Y. Zhao, L. Yang, S. Chen, X. Wang, Y. Ma, Q. Wu, Y. Jiang, W. Qian, Z. Hu, Can boron and nitrogen co-doping improve oxygen reduction reaction activity of carbon nanotubes? *J. Am. Chem. Soc.* **135**, 1201–1204 (2013). <https://doi.org/10.1021/ja310566z>
11. W.-J. Niu, Y.-P. Wang, J.-Z. He, W.-W. Liu, M.-C. Liu, D. Shan, L. Lee, Y.-L. Chueh, Highly stable nitrogen-doped carbon nanotubes derived from carbon dots and metal-organic frameworks toward excellent efficient electrocatalyst for oxygen reduction reaction. *Nano Energy* **63**, 103788 (2019). <https://doi.org/10.1016/j.nanoen.2019.05.074>
12. J.E. Park, M.-J. Kim, M.S. Lim, S.Y. Kang, J.K. Kim, S.-H. Oh, M. Her, Y.-H. Cho, Y.-E. Sung, Graphitic carbon nitride-carbon nanofiber as oxygen catalyst in anion-exchange membrane water electrolyzer and rechargeable metal-air cells. *Appl. Catal. B* **237**, 140–148 (2018). <https://doi.org/10.1016/j.apcatb.2018.05.073>
13. X. Xue, H. Yang, T. Yang, P. Yuan, Q. Li, S. Mu, X. Zheng, L. Chi, J. Zhu, Y. Li, J. Zhang, Q. Xu, N, P-coordinated fullerene-like carbon nanostructures with dual active centers toward highly-efficient multi-functional electrocatalysis for C₂O₂RR ORR and Zn-air battery. *J. Mater. Chem. A* **7**, 15271–15277 (2019). <https://doi.org/10.1039/c9ta03828k>
14. T. Gong, R. Qi, X. Liu, H. Li, Y. Zhang, N, F-codoped microporous carbon nanofibers as efficient metal-free electrocatalysts for ORR. *Nano-Micro Lett.* **11**, 9 (2019). <https://doi.org/10.1007/s40820-019-0240-x>
15. W. Li, D. Wang, Y. Zhang, L. Tao, T. Wang, Y. Zou, Y. Wang, R. Chen, S. Wang, Defect engineering for fuel-cell electrocatalysts. *Adv. Mater.* **32**, e1907879 (2020). <https://doi.org/10.1002/adma.201907879>
16. R. Paul, L. Zhu, H. Chen, J. Qu, L. Dai, Recent advances in carbon-based metal-free electrocatalysts. *Adv. Mater.* **31**, e1806403 (2019). <https://doi.org/10.1002/adma.201806403>

17. D. Yan, Y. Li, J. Huo, R. Chen, L. Dai, S. Wang, Defect chemistry of nonprecious-metal electrocatalysts for oxygen reactions. *Adv. Mater.* **29**, 1606459 (2017). <https://doi.org/10.1002/adma.201606459>
18. K. Chu, F. Wang, Y. Tian, Z. Wei, Phosphorus doped and defects engineered graphene for improved electrochemical sensing: Synergistic effect of dopants and defects. *Electrochem. Acta* **231**, 557–564 (2017). <https://doi.org/10.1016/j.electacta.2017.02.099>
19. X. Yan, Y. Jia, T. Odedairo, X. Zhao, Z. Jin, Z. Zhu, X. Yao, Activated carbon becomes active for oxygen reduction and hydrogen evolution reactions. *Chem. Commun.* **52**, 8156–8159 (2016). <https://doi.org/10.1039/c6cc03687b>
20. Y. Lin, P. Liu, E. Velasco, G. Yao, Z. Tian, L. Zhang, L. Chen, Fabricating single-atom catalysts from chelating metal in open frameworks. *Adv. Mater.* **31**, e1808193 (2019). <https://doi.org/10.1002/adma.201808193>
21. Y. Chang, J. Chen, J. Jia, X. Hu, H. Yang, M. Jia, Z. Wen, The fluorine-doped and defects engineered carbon nanosheets as advanced electrocatalysts for oxygen electroreduction. *Appl. Catal. B* **284**, 119721 (2021). <https://doi.org/10.1016/j.apcatb.2020.119721>
22. Y. Yamada, M. Yoneda, S. Fukuzumi, High and robust performance of H₂O₂ fuel cells in the presence of scandium ion. *Energy Environ. Sci.* **8**, 1698–1701 (2015). <https://doi.org/10.1039/c5ee00748h>
23. M. Wang, N. Zhang, Y. Feng, Z. Hu, Q. Shao, X. Huang, Partially pyrolyzed binary metal-organic framework nanosheets for electrochemical hydrogen peroxide synthesis. *Angew. Chem. Int. Ed.* **59**, 14373–14377 (2020). <https://doi.org/10.1002/anie.202006422>
24. K. Dong, J. Liang, Y. Wang, Z. Xu, Q. Liu, Y. Luo, T. Li, L. Li, X. Shi, A.M. Asiri, Q. Li, D. Ma, X. Sun, Honeycomb carbon nanofibers: A superhydrophilic O₂ -electrocatalyst enables ultrahigh mass activity for the two-electron oxygen reduction reaction. *Angew. Chem. Int. Ed.* **60**, 10583–10587 (2021). <https://doi.org/10.1002/anie.202101880>
25. Y. Deng, B. Chi, X. Tian, Z. Cui, E. Liu, Q. Jia, W. Fan, G. Wang, D. Dang, M. Li, K. Zang, J. Luo, Y. Hu, S. Liao, X. Sun, S. Mukerjee, g-C₃N₄ promoted MOF derived hollow carbon nanopolyhedra doped with high density/fraction of single Fe atoms as an ultra-high performance nonprecious catalyst towards acidic ORR and PEM fuel cells. *J. Mater. Chem. A* **7**, 5020–5030 (2019). <https://doi.org/10.1039/c8ta11785c>
26. L. Lin, W. Zhou, R. Gao, S. Yao, X. Zhang, W. Xu, S. Zheng, Z. Jiang, Q. Yu, Y.W. Li, C. Shi, X.D. Wen, D. Ma, Low-temperature hydrogen production from water and methanol using Pt/alpha-MoC catalysts. *Nature* **544**, 80–83 (2017). <https://doi.org/10.1038/nature21672>
27. U. Martinez, S. Komini Babu, E.F. Holby, H.T. Chung, X. Yin, P. Zelenay, Progress in the development of Fe-based PGM-free electrocatalysts for the oxygen reduction reaction. *Adv. Mater.* **31**, e1806545 (2019). <https://doi.org/10.1002/adma.201806545>
28. H. Zhang, H.T. Chung, D.A. Cullen, S. Wagner, U.I. Kramm, K.L. More, P. Zelenay, G. Wu, High-performance fuel cell cathodes exclusively containing atomically dispersed iron active sites. *Energy Environ. Sci.* **12**, 2548–2558 (2019). <https://doi.org/10.1039/c9ee00877b>
29. L. Jiao, J. Li, L.L. Richard, Q. Sun, T. Stracensky, E. Liu, M.T. Sougrati, Z. Zhao, F. Yang, S. Zhong, H. Xu, S. Mukerjee, Y. Huang, D.A. Cullen, J.H. Park, M. Ferrandon, D.J. Myers, F. Jaouen, Q. Jia, Chemical vapour deposition of Fe–N–C oxygen reduction catalysts with full utilization of dense Fe–N₄ sites. *Nat. Mater.* **20**, 1385–1391 (2021). <https://doi.org/10.1038/s41563-021-01030-2>
30. H. Jin, H. Zhou, D. He, Z. Wang, Q. Wu, Q. Liang, S. Liu, S. Mu, MOF-derived 3D Fe–N–S co-doped carbon matrix/nanotube nanocomposites with advanced oxygen reduction activity and stability in both acidic and alkaline media. *Appl. Catal. B* **250**, 143–149 (2019). <https://doi.org/10.1016/j.apcatb.2019.03.013>
31. W. Cheng, P. Yuan, Z. Lv, Y. Guo, Y. Qiao, X. Xue, X. Liu, W. Bai, K. Wang, Q. Xu, J. Zhang, Boosting defective carbon by anchoring well-defined atomically dispersed metal–N₄ sites for ORR, OER, and Zn–air batteries. *Appl. Catal. B Environ.* **260** (2020). <https://doi.org/10.1016/j.apcatb.2019.118198>
32. X. Xie, C. He, B. Li, Y. He, D.A. Cullen, E.C. Wegener, A.J. Kropf, U. Martinez, Y. Cheng, M.H. Engelhard, M.E. Bowden, M. Song, T. Lemmon, X.S. Li, Z. Nie, J. Liu, D.J. Myers, P.

- Zelenay, G. Wang, G. Wu, V. Ramani, Y. Shao, Performance enhancement and degradation mechanism identification of a single-atom Co–N–C catalyst for proton exchange membrane fuel cells. *Nat. Catal.* **3**, 1044–1054 (2020). <https://doi.org/10.1038/s41929-020-00546-1>
33. E.F. Holby, G. Wang, P. Zelenay, Acid stability and demetalation of PGM-free ORR electrocatalyst structures from density functional theory: A model for “single-atom catalyst” dissolution. *ACS Catal.* **10**, 14527–14539 (2020). <https://doi.org/10.1021/acscatal.0c02856>
 34. G. Yang, J. Zhu, P. Yuan, Y. Hu, G. Qu, B.A. Lu, X. Xue, H. Yin, W. Cheng, J. Cheng, W. Xu, J. Li, J. Hu, S. Mu, J.N. Zhang, Regulating Fe-spin state by atomically dispersed Mn–N in Fe–N–C catalysts with high oxygen reduction activity. *Nat. Commun.* **12**, 1734 (2021). <https://doi.org/10.1038/s41467-021-21919-5>
 35. Y. Wang, R. Gan, H. Liu, M. Dirican, C. Wei, C. Ma, J. Shi, X. Zhang, Fe₃O₄/Fe₂O₃/Fe nanoparticles anchored on N-doped hierarchically porous carbon nanospheres as a high-efficiency ORR electrocatalyst for rechargeable Zn-air batteries. *J. Mater. Chem. A* **9**, 2764–2774 (2021). <https://doi.org/10.1039/d0ta10205a>
 36. Y. Tan, W. Zhu, Z. Zhang, W. Wu, R. Chen, S. Mu, H. Lv, N. Cheng, Electronic tuning of confined sub-nanometer cobalt oxide clusters boosting oxygen catalysis and rechargeable Zn-air batteries. *Nano Energy* **83**, 10583 (2021). <https://doi.org/10.1016/j.nanoen.2021.105813>
 37. Y. Qiao, P. Yuan, Y. Hu, J. Zhang, S. Mu, J. Zhou, H. Li, H. Xia, J. He, Q. Xu, Sulfuration of an Fe–N–C catalyst containing Fe_xC/Fe species to enhance the catalysis of oxygen reduction in acidic media and for use in flexible Zn–Air batteries. *Adv. Mater.* **30**, e1804504 (2018). <https://doi.org/10.1002/adma.201804504>
 38. Q. Shi, Q. Liu, Y. Ma, Z. Fang, Z. Liang, G. Shao, B. Tang, W. Yang, L. Qin, X. Fang, High-performance trifunctional electrocatalysts based on FeCo/Co₂P hybrid nanoparticles for zinc-air battery and self-powered overall water splitting. *Adv. Energy Mater.* **10**, 1903854 (2020). <https://doi.org/10.1002/aenm.201903854>
 39. X. Liu, I.S. Amiinu, S. Liu, K. Cheng, S. Mu, Transition metal/nitrogen dual-doped mesoporous graphene-like carbon nanosheets for the oxygen reduction and evolution reactions. *Nanoscale* **8**, 13311–13320 (2016). <https://doi.org/10.1039/c6nr03247h>
 40. R.H. Morris, Six coordinate capped trigonal bipyramidal complexes, coordination. *Chem. Rev.* **350**, 105–116 (2017). <https://doi.org/10.1016/j.ccr.2017.06.019>
 41. Z. Zhu, Y. Yang, Y. Guan, J. Xue, L. Cui, Construction of a cobalt-embedded nitrogen-doped carbon material with the desired porosity derived from the confined growth of MOFs within graphene aerogels as a superior catalyst towards HER and ORR. *J. Mater. Chem. A* **4**, 15536–15545 (2016). <https://doi.org/10.1039/c6ta05196k>
 42. Z. Lei, Y. Tan, Z. Zhang, W. Wu, N. Cheng, R. Chen, S. Mu, X. Sun, Defects enriched hollow porous Co–N-doped carbons embedded with ultrafine CoFe/Co nanoparticles as bifunctional oxygen electrocatalyst for rechargeable flexible solid zinc-air batteries. *Nano Res.* **14**, 868–878 (2020). <https://doi.org/10.1007/s12274-020-3127-8>
 43. Y. Wang, Y. Pan, L. Zhu, H. Yu, B. Duan, R. Wang, Z. Zhang, S. Qiu, Solvent-free assembly of Co/Fe-containing MOFs derived N-doped mesoporous carbon nanosheets for ORR and HER. *Carbon* **146**, 671–679 (2019). <https://doi.org/10.1016/j.carbon.2019.02.002>
 44. Z. Wang, H. Jin, T. Meng, K. Liao, W. Meng, J. Yang, D. He, Y. Xiong, S. Mu, Fe, Cu-coordinated ZIF-derived carbon framework for efficient oxygen reduction reaction and zinc-air batteries. *Adv. Func. Mater.* **28**, 1802596 (2018). <https://doi.org/10.1002/adfm.201802596>
 45. Z. Li, L. Wei, W.-J. Jiang, Z. Hu, H. Luo, W. Zhao, T. Xu, W. Wu, M. Wu, J.-S. Hu, Chemical state of surrounding iron species affects the activity of Fe–Nx for electrocatalytic oxygen reduction. *Appl. Catal. B* **251**, 240–246 (2019). <https://doi.org/10.1016/j.apcatb.2019.03.046>
 46. J. Luo, X. Tian, J. Zeng, Y. Li, H. Song, S. Liao, Limitations and improvement strategies for early-transition-metal nitrides as competitive catalysts toward the oxygen reduction reaction. *ACS Catal.* **6**, 6165–6174 (2016). <https://doi.org/10.1021/acscatal.6b01618>
 47. T. Varga, G. Ballai, L. Vásárhelyi, H. Haspel, Á. Kukovecz, Z. Kónya, Co₄N/nitrogen-doped graphene: A non-noble metal oxygen reduction electrocatalyst for alkaline fuel cells. *Appl. Catal. B* **237**, 826–834 (2018). <https://doi.org/10.1016/j.apcatb.2018.06.054>

48. T. Tang, W.J. Jiang, X.Z. Liu, J. Deng, S. Niu, B. Wang, S.F. Jin, Q. Zhang, L. Gu, J.S. Hu, L.J. Wan, Metastable rock salt oxide-mediated synthesis of high-density dual-protected M@NC for long-life rechargeable zinc-air batteries with record power density. *J. Am. Chem. Soc.* **142**, 7116–7127 (2020). <https://doi.org/10.1021/jacs.0c01349>
49. D.M. Morales, M.A. Kazakova, S. Dieckhöfer, A.G. Selyutin, G.V. Golubtsov, W. Schuhmann, J. Masa, Trimetallic Mn–Fe–Ni oxide nanoparticles supported on multi-walled carbon nanotubes as high-performance bifunctional ORR/OER electrocatalyst in alkaline media. *Adv. Func. Mater.* **30**, 1905992 (2019). <https://doi.org/10.1002/adfm.201905992>
50. Y.-C. Zhang, S. Ullah, R. Zhang, L. Pan, X. Zhang, J.-J. Zou, Manipulating electronic delocalization of Mn₃O₄ by manganese defects for oxygen reduction reaction. *Appl. Catal. B* **277**, 119247 (2020). <https://doi.org/10.1016/j.apcatb.2020.119247>
51. S. Zhang, D. Zhai, T. Sun, A. Han, Y. Zhai, W.-C. Cheong, Y. Liu, C. Su, D. Wang, Y. Li, In situ embedding Co₉S₈ into nitrogen and sulfur codoped hollow porous carbon as a bifunctional electrocatalyst for oxygen reduction and hydrogen evolution reactions. *Appl. Catal. B* **254**, 186–193 (2019). <https://doi.org/10.1016/j.apcatb.2019.04.096>
52. A. Pendashteh, J.S. Sanchez, J. Palma, M. Anderson, R. Marcilla, Anchored NiCoMnS₄ nanoparticles on N-doped rGO: High-performance bifunctional electrocatalysts for rechargeable Zn-air batteries. *Energy Storage Mater.* **20**, 216–224 (2019). <https://doi.org/10.1016/j.ensm.2019.04.018>
53. H. Behret, H. Binder, G. Sandstede, Electrocatalytic oxygen reduction with thiospinels and other sulphides of transition metals. *Electrochim. Acta* **20**, 111–117 (1975). [https://doi.org/10.1016/0013-4686\(75\)90047-X](https://doi.org/10.1016/0013-4686(75)90047-X)
54. Z. Pu, T. Liu, I.S. Amiinu, R. Cheng, P. Wang, C. Zhang, P. Ji, W. Hu, J. Liu, S. Mu, Transition-metal phosphides: Activity origin, energy-related electrocatalysis applications, and synthetic strategies. *Adv. Func. Mater.* **30**, 2004009 (2020). <https://doi.org/10.1002/adfm.202004009>
55. Y. Li, Y. Liu, Q. Qian, G. Wang, G. Zhang, Supramolecular assisted one-pot synthesis of donut-shaped CoP@PNC hybrid nanostructures as multifunctional electrocatalysts for rechargeable Zn-air batteries and self-powered hydrogen production. *Energy Storage Mater.* **28**, 27–36 (2020). <https://doi.org/10.1016/j.ensm.2020.02.022>

Chapter 6

Carbon-Based Nanomaterials for Hydrogen Evolution Reaction



Bin Zhao and Siran Xu

Abstract Developing high-efficiency and strong stability hydrogen evolution reaction (HER) electrocatalysts is the critical and promising part of reducing the catalytic energy barrier and improving the efficiency of hydrogen production. For designing prominent HER electrocatalysts, challenges remain in creating large number of effective catalytic sites for HER while maintaining their robustness at high output volumes. Therefore, the development of effective anchoring of catalytic active sites on low-cost, highly conductive carbon carriers to effectively promote metal catalytic performance through strong metal-support interactions (SMSI) is a well-established strategy that has been widely investigated. Carbon-based nanomaterials have attracted extensive attention as a promising class of HER catalysts for green sustainable energy conversion and beyond, due to their low-cost, diverse forms and highly tunable electronic structures. Herein, a summary of the advanced research progress of various types of carbon-based catalysts has been discussed, mainly including the metal-free carbon-based nanomaterials, atomically dispersed metal carbon-based materials, metal nanoparticles supported carbon-based materials, and metal nanoparticles encapsulated carbon-based materials. Finally, some notable challenges and prospects that are instructive for the design and development of next-generation high-performance carbon-based electrocatalysts have been discussed.

6.1 Introduction

The limited fossil fuel has contributed to the rapid development of the economy while the harmful emissions from its combustion have also brought indelible damage to nature [1]. Therefore, it is necessary to explore sustainable green energy as a

B. Zhao · S. Xu (✉)
College of Materials Science and Engineering, Zhengzhou University, Zhengzhou 450001,
P. R. China
e-mail: siranxuhbnu@163.com

B. Zhao
e-mail: zhaobin270@163.com

means of reducing energy pressure even ensuring normal economic development and improving people's quality of life. Currently, converting cheap small molecules (e.g. water) into valuable fossil fuels (e.g. hydrogen energy) is one of the more promising solutions [2, 3]. At the same time, compared with local and intermittent energy sources such as solar, wind, geothermal, and hydroenergy, hydrogen's high energy density, and green and non-polluting combustion products make it the most promising alternative energy source [4]. Currently, coal gasification and steam reforming are the main methods for the large-scale production of hydrogen [5, 6]. However, these approaches not only increase the consumption of fossil fuels, but also irreparably damage nature with their combustion by-products such as carbon monoxide and carbon dioxide. Therefore, it is crucial to find a clean, efficient and sustainable strategy for hydrogen production.

National "The Fourteenth Five-Year Plan" proposed "hydrogen energy technology" as one of the national key R&D special projects to speed up the energy revolution and strengthen the country with science and technology, and actively respond to the national call for hydrogen energy green production strategy, electrolytic water hydrogen production technology is developing rapidly. At present, it is crucial to accelerate the significant industrialization of electrolytic water to hydrogen technology and promote the rapid development of new energy technology. Theoretically, a potential of 1.23 V is required to catalyze the electrolysis of water, but once the chemical reaction starts, additional activation energy needs to be overcome, and the presence of many constraints such as overpotential from electrode polarization, solution resistance, migration of ions and bubbles further slows down the rate of advancement of the reaction [7–9]. Therefore, the actual voltage of electrolytic water is greater than 1.23 V. The difference between the actual voltage and the theoretical potential called as overpotential. The overpotential has also become the most direct benchmark for evaluating the catalytic activity of electrocatalysts. Ruthenium-, iridium-, and platinum-based catalysts of noble metals have excellent catalytic activity and can effectively reduce the overpotential of electrolytic water reaction and accelerate the efficiency of electrolytic water hydrogen, but these catalysts are scarce and expensive on earth and difficult to be used in large-scale production, which greatly restricts the development of electrolytic water hydrogen technology and fundamentally limits the large-scale application of hydrogen energy [10–12]. Therefore, the exploration of inexpensive, efficient, stable, and abundant catalysts to replace precious metal catalysts for commercial production has become a key research direction in the development of new energy technologies.

However, before exploring clean and efficient hydrogen evolution reaction (HER) catalysts, it is necessary to understand the mechanism of HER catalysis. Under acidic conditions, the HER process consists of three steps with two different mechanisms (Fig. 6.1) [13, 14]. The first step is the discharge process, in which an electron is transferred to the catalyst surface to capture a proton, resulting in the formation of adsorbed hydrogen atoms (H_{ads}), also known as the Volmer reaction:



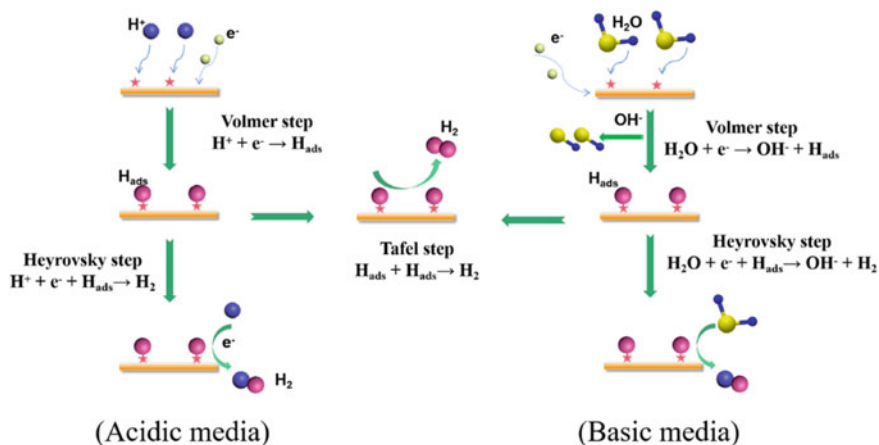
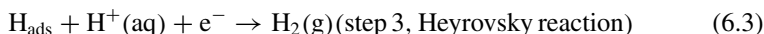
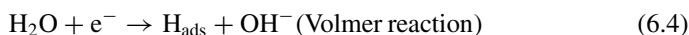


Fig. 6.1 Hydrogen evolution reaction mechanism under acidic and basic condition

There are two types of desorption according to different reaction kinetics: (1) Tafel reaction, where two H_{ads} atoms on the catalyst surface combine to form H_2 ; (2) Heyrovsky reaction, where H_{ads} atoms tend to combine with a second electron and another proton to form H_2 molecules when the H_{ads} coverage is low, which is also known as electrochemical desorption reaction:



In alkaline environment, the formation of adsorbed hydrogen atoms requires first breaking the H–O–H bond, and the HER process is more difficult in comparison [15, 16]. Three main reaction processes are also included, as follows:



Currently, theoretical evidence and numerous studies have shown that the conductivity, intrinsic catalytic activity, and the number of active sites of catalytic materials largely influence the HER catalytic activity, thus various strategies are proposed to enhance the HER performance, especially nanomaterials with high electrical conductivity as support [17–19]. Carbon, as one of the elements with a wide distribution in nature, was the first to attract research interest due to its low-cost and

high earth-abundant. Loading metal nanoparticles onto carbon nanomaterials with high electrical conductivity, large theoretical specific surface area, controllable structure, variable morphology, and corrosion resistance not only prevents aggregation and deactivation of metal nanoparticles, but also endows the catalyst more specific surface area, increases the number of accessible active sites, and accelerates the mass/electron transfer rate by using strong metal-support interactions (SMSI) [20–22]. Although the stability of conventional carbon-based loaded metal nanoparticles can be improved by strong metal-carrier interactions, they may still migrate and agglomerate under harsh conditions [23]. Fortunately, with the continuous innovation and development of carbon-based nanomaterials, in 2014, Bao et al. [24] successfully prepared three-dimensional transition metals Fe, Co into FeCo alloys and encapsulated them in nitrogen-doped carbon nanotubes (CNTs), which exhibited outstanding HER activity in acidic electrolytes. This metal-encapsulated carbon-based catalyst not only further prevents nanoparticle migration and aggregation due to its outstanding structural properties, but also further enhances the overall electrochemical stability of the catalyst due to the excellent corrosion resistance of its carbon shell.

In 2009, Dai et al. [25] successfully prepared nitrogen (N)-doped vertically aligned carbon nanotubes, which exhibited extremely high oxygen reduction reaction (ORR) catalytic activity, outstanding long-term stability. Subsequently, metal-free carbon-based materials have been widely explored as a new potential catalyst that exhibits excellent catalytic performance in electrochemical energy conversion and storage. Various heteroatoms (N, B, P, etc.), defects on carbon nanomaterials are also widely used as dopants for electrochemical hydrogen production to enhance the intrinsic catalytic activity [26]. In 2011, Zhang et al. [27] has prepared single-atom catalysts for the first time, and the concept of single-atom catalysts has provided a direction for the further development of electrocatalysis and further opened up the horizon of designing and building efficient electrochemical catalysts. Constructing single atom carbon-based materials can expose the active site to a greater extent, but the preparation method and characterization means are relatively complicated. Therefore, this section introduces the advanced development of HER electrochemical catalysts by systematically summarizing the four types of carbon-based electrocatalysts that have been widely reported so far: (1) metal-free carbon-based electrocatalysts; (2) atomically dispersed metal carbon-based electrocatalysts; (3) metal nanoparticles supported carbon-based electrocatalysts; and (4) metal nanoparticles encapsulated carbon-based electrocatalysts.

6.2 Metal-Free Carbon-Based Electrocatalysts for HER

Currently, Pt-based nanomaterials are still considered to be the most advanced and active HER catalysts due to their optimal binding ability with hydrogen. However, the high cost and scarcity of Pt-based catalysts severely hinder its large-scale application in the production of hydrogen [28, 29]. Therefore, it is crucial to develop

environmental-friendly, high-efficient, and low-cost catalysts as an alternative to the precious metal Pt. However, metal-free carbon-based nanocatalysts have rapidly flourished and have been explored extensively for energy conversion applications, and milestones have been achieved since low-cost carbon-based metal-free catalysts on N-doped carbon nanotube arrays as a highly promising alternative to Pt-based catalysts were successfully synthesized and showed promising catalytic properties in 2009 [25, 30].

As shown in Fig. 6.2a, various heteroatom-doped, edge-doped, defect-doped even including unmentioned charge transfer-doped are all evaluation factors that effectively influence the catalytic activity [30, 34–37]. In 2016, Yao et al. [31] was firstly reported and confirmed defect graphene as a trifunctional metal-free carbon-based electrocatalyst based on defect mechanism. As shown in Fig. 6.2b, carbon defect graphene (DG) was obtained via a facile nitrogen removal process from a N-doped carbon precursor. High-angle annular dark-field (HAADF) image of DG was measured in Fig. 6.2c, in addition to the normal hexagon structure of graphene, various combinations of structural defects were clearly observed near the lattice vacancies concentrated at the edges of the holes, including pentagonal, heptagonal, octagonal. Easy to speculate that the HER catalytic performance of DG catalysts was significantly enhanced compared to the NG catalyst, as shown in Fig. 6.2d, e, which exhibited significantly lower overpotential than that of NG catalyst. In addition to constructing defective engineering to improve catalytic activity, constructing edge active sites is also a feasible strategy. Qu et al. [32] Synthesized 2D mesoporous graphitic- C_3N_4 self-assembled on 2D graphene nanosheets (g-CN@G MMs) via in-suit selective growth without a template, shown in Fig. 6.2f. The pristine graphitic- C_3N_4 meshes with abundant mesoporous arranged regularly were shown in Fig. 6.2g. Meanwhile, two types of mesopore structures in line with the composition of g-CN@G MMs were observed in Fig. 6.2h. That mesh-on-mesh structure endowed the g-CN@G MMs with numerous exposed active sites, largely facilitating rapid charge transfer, as well as generating additional edges and defects as hydrogen bonding sites. Therefore, shown in Fig. 6.2i, j, the g-CN@G MMs catalyst exhibited lower overpotentials than the corresponding single component at the current density of 10 mA cm^{-2} .

Heteroatom dopant is also reported as a feasible strategy to alter the catalytic activity of metal-free carbon-based catalysts. Zhi et al. [38] firstly reported atomic sulfur-modified C_3N_4 material and successfully proved that sulfur doping can significantly enhance the activity of C_3N_4 for HER. That catalyst was synthesized via an in-suit polycondensation of sulfur-containing precursor with the existence of mesoporous carbon (MPC). Subsequently, they systematically investigated the effect of different dopants (S, P, B doping) on the catalytic performance of C_3N_4 -based materials combining comprehensive experimental and theoretical research, which were synthesized via an in-suit polycondensation of different precursors, respectively, shown in Fig. 6.2k [33]. In Fig. 6.2l, among three types of heteroatom-doped hybrids, S-doped C_3N_4 -based catalyst distinctly showed a lower onset potential of -55 mV than those of the pristine sample (-167 mV) and other dopant hybrids (P: -201 mV ; B: -254 mV). Then, to further understand the difference in HER activity caused

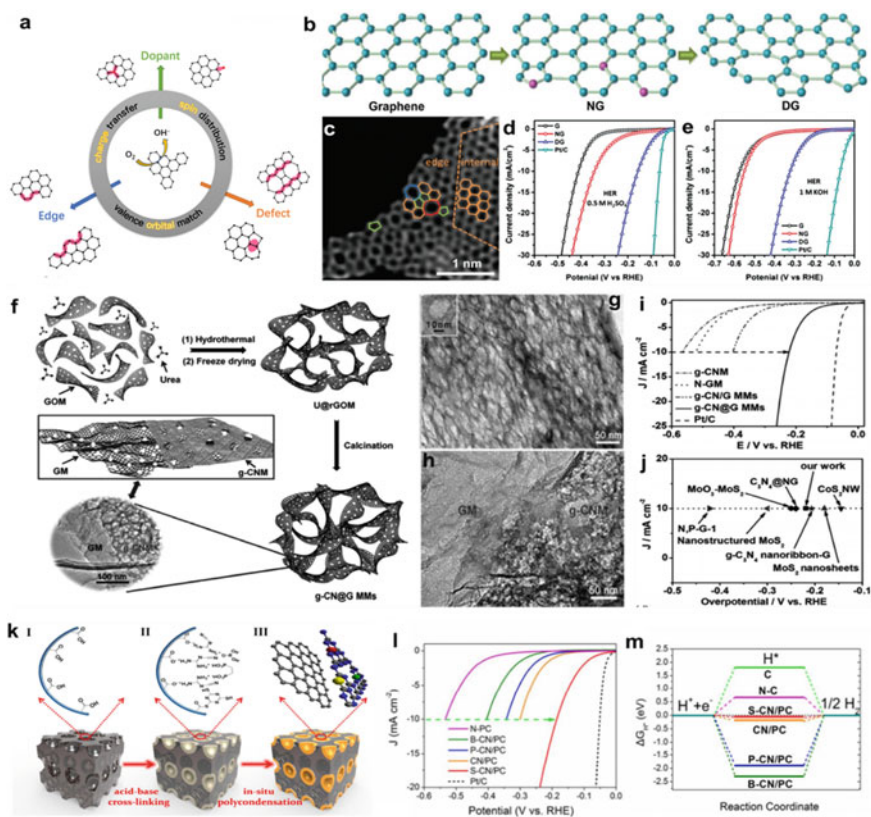


Fig. 6.2 Different metal-free carbon-based electrocatalysts for ORR. **a** Schematic illustration of various active sites and underlying mechanism of carbon nano-catalysts for ORR. **b** Abbreviated synthetic schematic of DG. **c** HAADF image of DG, in which the defects of pentagonal, heptagonal, and octagonal are marked in green, blue, and red respectively. LSV curves of the pristine graphene, NG, DG, and Pt/C in 0.5 H₂SO₄ **d** and 1 M KOH **e**. (**b–e**) Reproduced with permission [31]. Copyright 2016, WILEY–VCH. **f** Synthetic process illustration of g–CN@ G MMs. TEM images of g–C₃N₄ meshes **g** and g–CN@ G MMs **h**. **i** LSV curves of various prepared-catalysts (g–CNM, N–GM, g–CN/G MMs, g–CN@ G MMs). **j** The corresponding overpotentials of various catalysts at the current density of 10 mA cm^{–2}. **f–j** Reproduced with permission [32]. Copyright 2017, WILEY–VCH. **k** Preparation steps of the PC-based B/S/P-doped C₃N₄ catalysts. **l** The HER polarization curves of B/S/P-doped C₃N₄, pristine C₃N₄, and compared Pt/C. **m** The calculated ΔG_{H}^* value of various catalysts. **k–m**. Reproduced with permission [33]. Copyright 2017, American Chemical Society

by the dopant, the corresponding hydrogen adsorption Gibbs free energy (ΔG_{H}^*) was calculated. The calculated ΔG_{H}^* value of the doped catalysts was listed in Fig. 6.2m, compared to the pure C₃N₄ material, P-doped and B-doped samples all exhibited more negative ΔG_{H}^* values, implying the more difficult hydrogen adsorption. On the contrary, the S-doped compound exhibited more suitable ΔG_{H}^* values

of -0.03 eV even than the well-known Pt/C catalyst, which indicated better HER activity consistent with the numerical trend of the practical research values.

6.3 Atomically Dispersed Metal Carbon-Based Electrocatalysts for HER

Numerous experimental studies have shown that tuning the size of metal catalysts to the nanoscale can significantly contribute to the number of accessible active sites. However, these catalyst particles with small particle sizes tend to have high surface energy, which can lead to severe aggregation of nanoparticles, resulting in a significant decrease in electrocatalytic activity [39, 40]. Therefore, it is not only necessary to explore further innovations in small-size metal particles, but also to develop supporting materials with stable anchored metal active phases. In recent years, supported single-atom catalysts have been widely used in numerous reactions such as energy storage and green catalysis due to their maximum atom utilization efficiency [41, 42]. Among the variously reported supported-SACs, various carbon-based SACs consisting of C, N, and O existed in nature as elements abundant and prepared from easily available and inexpensive materials. As the most promising advanced hybrid nanocatalysts, carbon-based SACs are heavily used in advanced energy technologies and catalysis due to their unique physicochemical properties, such as tunable morphology, ordered porosity, and easy immobilization of the active phase [43]. This section mainly introduces the recently emerging carbon-based SACs with graphene, carbon–nitrogen, carbon nanotubes, and MOF-derived carbon shell as carbon carriers, and highlights their unique applications in hydrogen production for electrochemical water splitting.

Meanwhile, carbon-based SACs have made great progress in electrocatalysis due to the advantages of high electrical conductivity, large specific surface area, abundant carbon reserves, and a wide variety of carbon derivatives, especially graphene-based SACs [44–48]. However, pure graphene materials with relatively inert surfaces can only provide weak electronic metal-support interaction (EMSI) for metal nanoparticles, which is often insufficient to effectively control the electronic structure of the supported metal nanoparticles [49]. Therefore, several strategies have been explored to optimize the EMSI of graphene-based SACs. (1) The introduction of oxygen-containing groups on the surface of graphene can introduce additional electronic states near the Fermi energy level, thus changing its surface reactivity, such as GO, rGO [28, 50]. (2) The introduction of non-metallic (N, O and S) or metallic heteroatoms into graphene matrix can induce electronic redistribution or spin states in sp^2 -conjugated carbon substrates, thus adjusting the valence orbital energy of the active sites on the carbon surface [51–53]. The strong metal-support interaction not only causes strong orbital hybridization between the SACs and the carbon surface, which facilitates the electron transfer at its interface, but also further solidifies the

SACs on carbon substrate and facilitates the enhanced electrochemical stability of the carbon-based monoatomic catalyst [49].

In 2021, the Luo et al. [54] reported the synthesis of rich mesoporous graphene oxide (MGO) support via the low-intensity pulsed laser irradiation (LI) technique to obtain more surface dangling bonds. A series of experimental manipulations were then used to extract metal atoms from the corresponding metal foams using the surface dangling bonds of nanocarbon and evolve them directly into SACs. The specific synthesis mechanism of Fe/Co-SACs supported on N-doped MGO substrate was shown in the Fig. 6.3a. Figure 6.3b showed the LSV curves of Co-NMGO, which exhibited the outstanding HER activity with a lower overpotential of 146 mV at 10 mA cm^{-2} , and a smaller Tafel slope value (Fig. 6.3c), which was much smaller than those of Fe-NMGO (310 mV), NMGO (470 mV), and GO (600 mV) electrocatalyst. As shown in Fig. 6.3d, the current density value of the Co-NMGO electrocatalyst remained stable for at least 24 h with almost no energy loss, which signifies its good electrochemical stability. The proposed new synthetic method provides new ideas and insights to further enhance the metal-support interactions between carbon-based SACs. Su et al. [49] proposed a new strategy to modulate the electrocatalytic behavior of supported highly dispersed metal nanoparticles. The deposition of Ru nanoparticles on O-doped graphene modified with single metal atoms (e.g. Fe, Co, and Ni) for HER was systematically investigated by theoretical calculations and experimental explorations. As shown in Fig. 6.3e–g, DFT calculation was firstly proceeded to research this strategy theoretically. Firstly, the ideal structural model consisting of a highly stable Ru_{55} cluster with a diameter of about 1.2 nm supported on an O-doped graphitic nanosheet with highly atomically dispersed single atoms (called $\text{M}_1@OG$, with $M = \text{Fe, Co, and Ni}$) has been constructed. Meanwhile, binding energy and its corresponding adsorption free energy of H^* (Fig. 6.3f) of Ru_{55} on $\text{Fe}_1/\text{Co}_1/\text{Ni}_1@OG$ substrates were stronger than that of Ru_{55} on pure OG without metal-atom decoration. Fig. 6.3 g showed the electronic density of states (DOS), which revealed that the introduction of highly dispersed monometallic atoms induces significant states near the Fermi energy level, activating the inert carbon surface and significantly enhancing the interaction between its metal carriers. The underlying DFT calculations implied that single metal atoms and Ru clusters can synergistically modulate the HER activity through electronic coupling with O-doped graphene substrates. Subsequently, $\text{RuM}_1@OG$ was synthesized via a typical salt-template method to further verify the effect of SMSI between RuM_1 and OG substrate for HER. As an illustration in Fig. 6.3 h, i, $\text{RuCo}@OG$ exhibited superior HER activity with a lower overpotential of 13 mV than those of $\text{Ru}@OG$ (48 mV) at 10 mA cm^{-2} , even than the start-of-art Pt/C (31 mV). Meanwhile, the HER kinetics of as-prepared catalysts was exhibited through Tafel slopes shown in Fig. 6.3j, $\text{RuCo}@OG$ exposed the lowest Tafel slope value of 28.5 mV dec^{-1} , which coincided with the trend of LSV curve.

In addition, as a special structure of carbon-based SACs, metal- and N-doped carbon ($M\text{-N}_x\text{-C}$) materials can not only reinforce metal atoms through M–N coordination, thus further enhancing metal-carrier interactions, but also modulate the electronic structure of metal atoms through carbon–nitrogen tethering effects, which have been regarded as the most promising alternatives to the Pt-based noble-metal

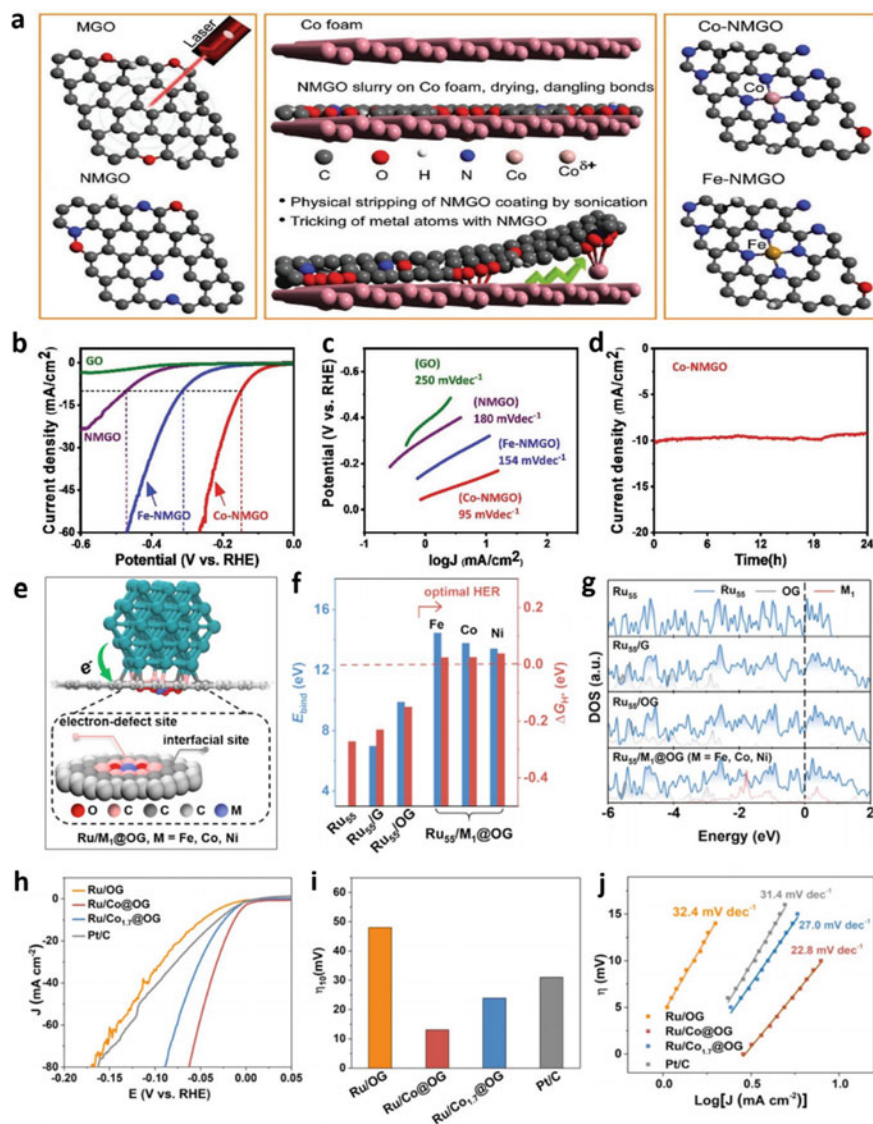


Fig. 6.3 Atomically dispersed metal carbon-based electrocatalysts with oxygen-containing groups. **a** Synthesis schematic of mesoporous GO prepared via LI method. **b** LSV curves, **c** Tafel slopes of Co-NMGO, Fe-NMGO, NMGO, and GO. **d** I-t measurements of Co-NMGO catalyst. **a-d** Reproduced with permission [54]. Copyright 2021, WILEY-VCH. **e** Ideal atomic structures models of Ru $_{55}$ supported on O-doped graphene with dispersed single metal atoms. **f** Binding energies (E_{bind}) of Ru $_{55}$ and Ru $_{55}$ /M $_1$ @OG, and its corresponding Gibbs adsorption free energy of H* (ΔG_{H^*}). **g** DOS of Ru $_{55}$ /M $_1$ @OG. **h** LSV curves, **i** the corresponding overpotentials, and **j** Tafel slopes of Ru/OG, RuCo/OG, RuCo $_{1.7}$ /OG, and commercial Pt/C. (**e-j**). Reproduced with permission [49]. Copyright 2021, WILEY-VCH

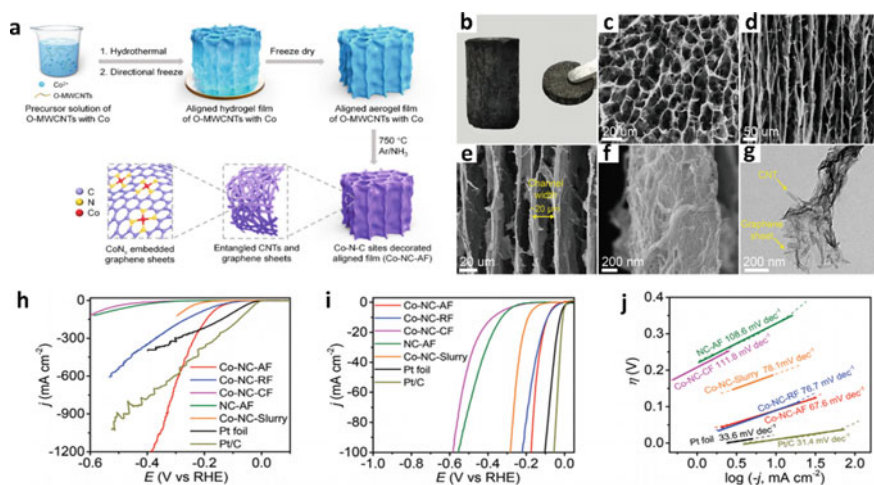


Fig. 6.4 Atomically dispersed metal carbon-based electrocatalysts with carbon–nitrogen tethering effects. **a** Detailed diagram of the synthesis process of Co–N–C sites embedded into the porous aligned film. **b** Macroscopic optical images of monolithic and thin-film Co–NC–AF material. **c–f** SEM images in different views, **g** TEM pattern of Co–NC–AF. **h, i** LSV curves, **j** Tafel slopes of Co–NC–AF, Co–NC–RF, Co–NC–CF, NC–AF, Co–NC–Slurry, Pt foil, and Pt/C (a–j). Reproduced with permission [55]. Copyright 2021, WILEY–VCH

electrocatalysts and thus have increasingly attracted attention [56–58]. Recently, Fei et al. [55] designed and fabricated single atom Co–N–C sites encapsulated into an aligned porous carbon film, which exhibited extremely excellent industrial HER activity and stability. As shown in Fig. 6.4a, Co–N–C sites decorated on aligned film (Co–NC–AF) were prepared via firstly constructing self-assembly into hydrogel film with strongly oxidized multiwall carbon nanotubes (O-MWCNTs) as a template, followed by freeze-drying and final annealing treatment. Figure 6.4b–g showed a schematic representation of the morphology and porous structure of the Co–NC–AF catalyst, in which it can be clearly observed that the intact MWCNTs serve as the overall derived backbone to enhance the stiffness and conductivity of the carbon network, while the graphene sheets serve as a substrate for the dispersed single-atom CoN_x sites. In addition, separate carbon film with vertically aligned large pores and nanochannels ($\sim 20 \mu\text{m}$) within the carbon wall network contributed to the smooth transport of ions and gases. Benefiting from its unique structural properties, Co–NC–AF exhibited excellent industrial electrochemical HER activity with an ultra-low overpotential of 343 mV at the large current density of 1 A cm^{-2} , and a small Tafel slope of 67.6 mV dec^{-1} , as shown in Fig. 6.4h–j. Meanwhile, at this high current density, the overpotential of Co–NC–AF catalyst can be stable for at least 32 h with almost no energy loss.

In addition, a variety of SAC catalysts with different structural properties are still designed and synthesized and exhibit excellent HER activity. The research development of various richly structured carbon-based SACs materials with strong metal

carrier interactions has provided rich insights and directions for further design of highly active and stable catalysts with commercial applications.

6.4 Metal Nanoparticles Supported Carbon-Based Electrocatalysts for HER

The development of highly active but low-cost catalysts remains one of the most critical impediments to achieving large-scale commercial production of hydrogen. Currently, there are numerous advanced catalysts fabricated via incorporating of zero-dimension (0D) electrochemically active metals nanoparticles onto catalytic supports, mainly including complex and variable carbon nanostructures, oxides electrodes, MoS₂ nanosheet, and so on [59, 60]. However, it is urgent to stably disperse metal nanoparticles on a suitable support to efficiently catalyze the HER process. Various carbon nanomaterials as high conductivity and low-cost support have generated widespread interest. Meanwhile, to improve the conductivity of supported-catalysts and avoid aggregation of metal nanoparticles, carbon material carriers such as reduced graphene oxide (rGO), [61–63] CNTs, and others are usually used as current integrators and further stabilize the dispersed metal active phase by building various defects, oxidation states, etc. [13, 19, 64].

CNTs as a special one-dimension (1D) carbon support were divided into single-walled carbon nanotube (SWCNTs) and MWCNTs. MWCNTs typically have the higher surface area to uniformly disperse metal nanoparticles, strong electrical conductivity to accelerate electron conduction rates, good chemical and mechanical stability to ensure electrochemical stability of the catalyst during long-term HER, strong coupling effect with active species to obtain SMSI, and are less expensive than highly conductive graphene [65–67]. Currently, Baek et al. [68] reported the synthesis of Ru nanoparticles uniformly deposited on MWCNTs as an excellent and stable HER catalyst. As shown in Fig. 6.5a, MWCNTs support with oxygenated functional groups (specifically, carboxylic acids, –COOH) was firstly fabricated via mildly oxidizing by nitric acid. Subsequently, benefiting from the numerous carboxylic acid bonds on the surface of MWCNT, Ru nanoparticles can be more stably anchored and dispersed on the carrier surface by forming ruthenium carboxylate complexes. Finally, the final catalytic product Ru-MWCNTs was obtained by further reduction of Ru nanoparticles and oxygen-containing groups by thermal reduction. Figure 6.5b, c showed the TEM images, in which well-dispersed and small-size (with the average size of 3.4 nm) Ru nanoparticles can be observed. Small particle size and uniform distribution are more conducive to exposing a large number of Ru active sites, which can be further illustrated in Fig. 6.5d, e. Compared with start-of-the-art Pt/C catalyst, Ru-MWCNTs exposed better electrochemical activity in 1.0 M KOH and 0.5 H₂SO₄ electrolytes (Fig. 6.5f–h), respectively. Especially, Ru-MWCNTs exhibited superior HER activity in alkaline with a lower overpotential of 17 mV at 10 mA cm⁻², which is less 16 mV than those of Pt/C (33 mV). However, it is still a daunting challenge

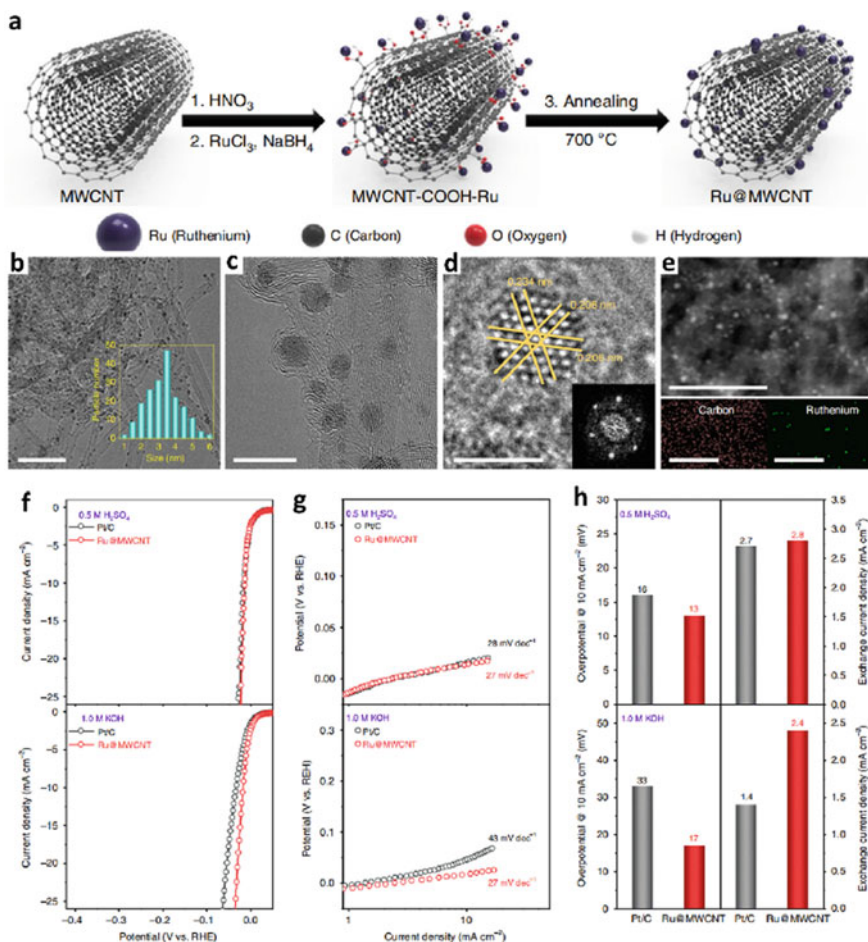


Fig. 6.5 Supported carbon-based electrocatalysts with CNT as support. **a** Diagram of the synthesis process. **b, c** TEM images, **d** HR-TEM image focused on Ru nanoparticles (The inset is the corresponding FFT pattern), **e** HAADF-STEM image (upper picture) and STEM-EDS element mapping (following pictures) of Ru@MWCNTs. **f–h** LSV curves, Tafel slopes and histogram of Pt/C and Ru@MWCNT at 1.0 M KOH and 0.5 M H₂SO₄, respectively. **a–h** Reproduced with permission [68]. Copyright 2020, Nature Publishing Group. **i** XRD pattern, **j, k** TEM images, **l** HRTEM image of Ru@Mo_xC–CNT. **m** LSV curves, **n** Tafel slopes of pure CNT, Mo_xC@CNT, Ru@CNT, Ru@Mo_xC–CNT, and Pt/C in 1.0 M KOH. **o** LSV curves of Ru@Mo_xC–CNT powder supported on Ni foam and Ni foam electrode. **p** Long-term stability curve of Ru–Mo₂C@CNT under the evolution of the potential required to maintain a high current density of 500 mA cm^{−2} stable for 1000 h (**i–p**). Reproduced with permission [69]. Copyright 2021, Nature Publishing Group

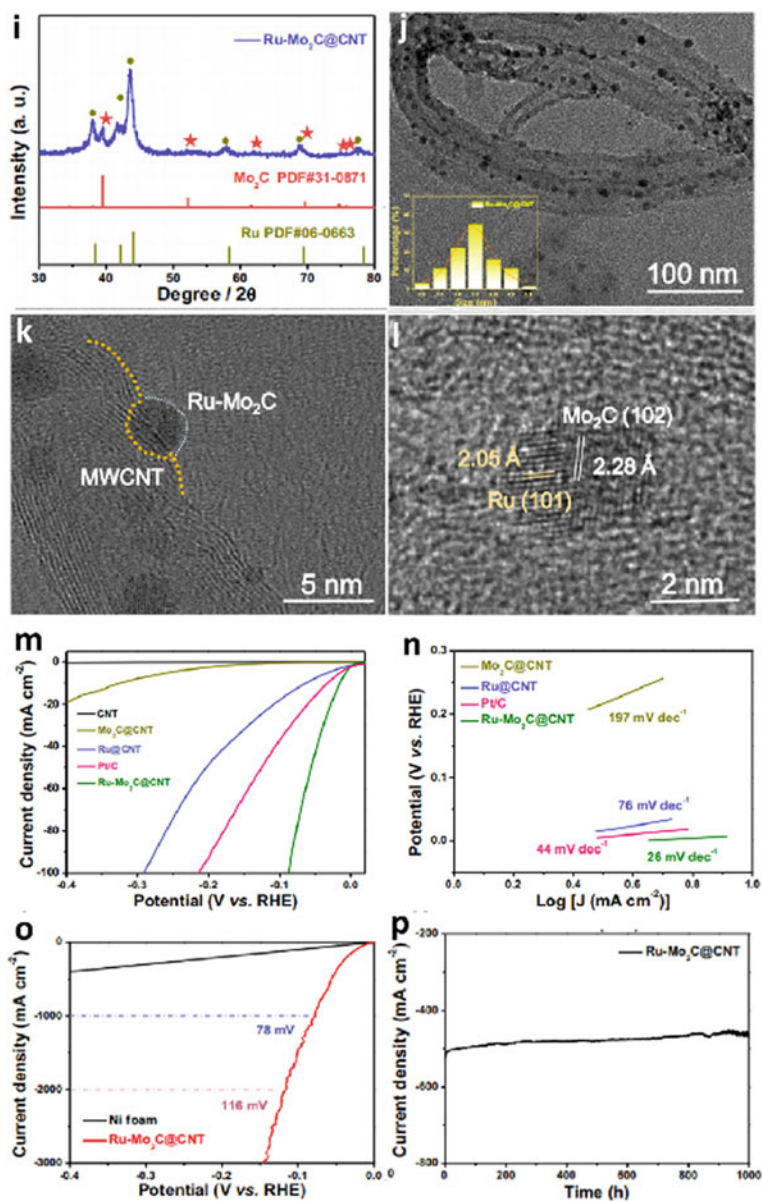


Fig. 6.5 (continued)

to achieve industrial production of carbon-based Ru nanoparticles for HER while reducing costs, increasing activity, and improving stability. Wu et al. [69] successfully fabricated ultra-small Ru-Mo_xC heterojunction nanoparticles (3.5 nm) supported on MWCNTs (Ru-MoC_x@MWCNTs) via a novel and straightforward solvent-free microwave pyrolysis method (Fig. 6.5i–l), which showed outstanding industrial HER performance with an ultra-low overpotential of 15 mV with 10 mA cm⁻² in 1.0 M KOH, and a low Tafel slope of 26 mV dec⁻¹. In addition, it is important to mention that Ru-MoC_x@MWCNTs with strong metal-support interaction exposed superior industrial HER activity as shown in Fig. 6.5m–p, which showed extremely low overpotential of 78 mV to afford the large current density of 1 mA cm⁻² in 1.0 KOH, and maintained it for at least 1000 h.

In addition, 2D graphene as a high-conductivity carrier, especially heterogeneous nitrogen (N)-doped graphene has become an intriguing material in the field of electrocatalysis. Numerous advanced reports show the doping of N, P, B, S, and other heteroatoms into carbon-based materials to optimize their electrocatalytic properties [70, 71]. The introduction of heteroatoms into the carbon lattice can effectively interfere with the electroneutrality of adjacent carbon atoms, thereby modulating the electronic properties and surface chemical states of carbon. Therefore, when N-doped graphene is used as a support, it can form surface strong coupling chemical bonds with metal nanoparticles to induce electron transfer and manipulate the electronic structure of the metal active phase, thus improving electrocatalytic activity. For example, the Hu et al. [72] synthesized the well-dispersed and ultra-small Ir nanoparticles (3.5 nm) supported on N-doped graphene nanosheets (Ir@NG). Ir@NG exhibited superior HER performance with an extremely low overpotential of 19 mV at 10 mA cm⁻², which is even less than those of commercial Pt/C catalyst. Meanwhile, Gibbs free energy of H adsorption of Ir@G without the introduction of N element, Ir@graphitic N (gN-G), and pyridinic N (pN-G) further proved that the doping of N elements can indeed optimize the HER activity of Ir nanoparticles. Furthermore, rGO flakes are a commonly studied type of graphene carrier material due to the active chemical bonding on the surface that effectively anchors the metal active phase, thus facilitating EMSI, dispersing and immobilizing the active site while further improving the long-term stability and corrosion resistance of the catalyst.

In recent years, many advanced literature reports show that surface graphene grown directly on porous carbon nanotube scaffolds can not only effectively eliminate the heavy stacking problem of conventional 2D graphene, but also provide a more stable anchor point for the loaded metal active phase than conventional graphene or carbon nanotubes alone [73, 74]. Furthermore, porous carbon benefits from abundant oxygen-containing surface functional groups and exhibits stronger reduction (low redox potential) than conventional carbon substrates such as carbon nanotubes or graphene oxide, which can make metal nanoparticles more easily chemically deposited and stably anchored on their surfaces, further enhancing their metal carrier interactions and thus effectively promoting HER performance [17, 55].

6.5 Metal Nanoparticles Encapsulated Carbon-Based Electrocatalysts for HER

The susceptibility of the metal active sites to corrosion during electrochemical measures severely affects the electrochemical stability of the electrocatalysts. In addition, the poor storage stability of catalysts with easier oxidation is also a major problem that the ideal catalyst needs to solve urgently [75]. Metal nanoparticles encapsulated in carbon materials are nanostructures with high chemical and thermal stability because the outer encapsulated carbon shell not only protects the metal nanoparticles from atmospheric oxygen-induced degradation and strong acidic and alkaline environments, but also effectively hinders the agglomeration of neighboring nanoparticles [76–79]. Currently, there are three types of metal nanoparticles encapsulated carbon-based materials are divided into metal nanoparticles encapsulated into CNTs, [80–82] MOFs, [83] and nanofibers [84].

Laasonen et al. [78] first investigated single-walled carbon nanotubes (SWNTs) surface decorated with single-shell carbon encapsulated iron nanoparticles as a novel highly active, durable, and low-cost electrocatalyst for HER, which was synthesized by a rapid and low-cost aerosol chemical vapor deposition method. The existence of a single carbon shell protected active metal centers from oxidation. Subsequently, Fang et al. [85] proposed a novel structure consisting of encapsulating ultra-fine Co nanoparticles in nitrogen-doped carbon nanotubes (N-CNTs) grafted onto rGO. As shown in Fig. 6.6a, Co@N-CNTs@rGo electrocatalyst was fabricated via GO-wrapped core-shell (Co, Zn)-bimetallic ZIF as precursors followed by annealing. The obvious rGo sheet structure can be found in the FE-TEM image, as shown in Fig. 6.6b. From the magnified FESEM image of Fig. 6.6c, numerous carbon nanotubes grown on rGo were uniformly extruded from all sides. Insert in Fig. 6.6d, ultra-fine Co nanoparticles with an average size of 8 nm encapsulated by the “bamboo joint-like” CNTs with only 3–4 carbon layers were also observed at the top of the CNTs. Inspired by the unique 3D hierarchical structure with rich active sites and expected composition, the as-obtained Co@N-CNTs@rGO composite exhibited excellent electrocatalytic performance with the ultra-low overpotential of 108 mV to afford the current density of 10 mA cm⁻² and a lower Tafel slope of 55 mV dec⁻¹ (Fig. 6.6e–g). Obviously, in 1.0 M KOH, Co@N-CNTs@rGo exposed strong long-term stability for 100 h with negligible decay during the continuous electrochemical process. Meanwhile, the DFT calculation showed the Gibbs free energy of H* (ΔG) of various catalysts. The H* adsorption of bare Co was too strong while the bare graphene was too weak, such all implied their lower activity toward HER. However, Co nanoparticles encapsulated into graphene, the ΔG was effectively tuned with nearly to zero.

Coating metal active centers with carbon layers are also an effective solution to improve catalyst durability. Meanwhile, the unique interfacial interaction between metal particles and carbon shells will also enable more catalytic active sites for HER, thus further enhancing electrocatalytic activity. The formation of carbon layers

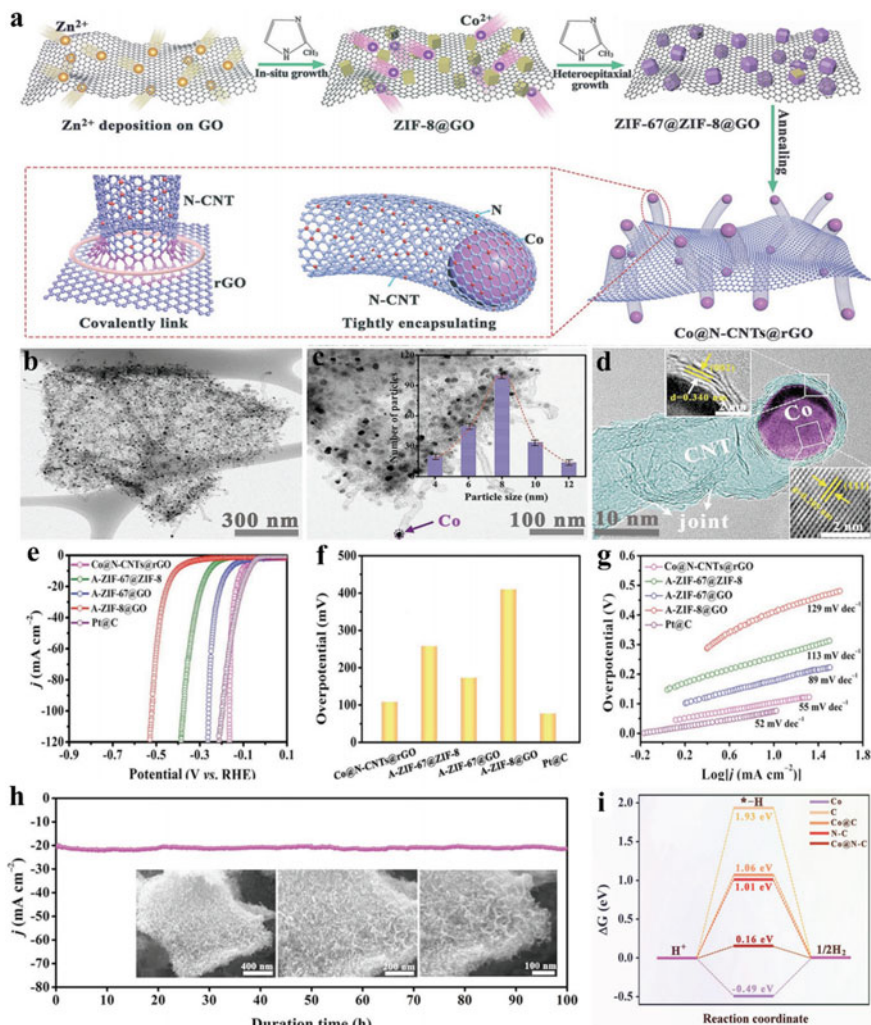


Fig. 6.6 Metal atom encapsulated carbon-based electrocatalysts. **a** The illustration of the synthetic process of Co@N-CNTs@rGO catalysts. **b, c** TEM images, **d** HRTEM image of Co@N-CNTs@rGO. **e** LSV curves, **f** overpotentials ($j = 10 \text{ mA cm}^{-2}$), **g** Tafel slopes of Co@N-CNTs@rGO, A-ZIF-67@ZIF-8, A-ZIF-67@GO, A-ZIF-8@GO and commercial Pt/C. **h** i-t curves of Co@N-CNTs@rGO at 20 mA cm^{-2} . **i** DFT calculation of H adsorption free energy. Reproduced with permission [85]. Copyright 2018, WILEY-VCH

mainly depended on MOF-derived, PANI-derived, and so on. Li et al. [86] fabricated the N-doped carbon encapsulated cobalt phosphide nanoparticles supported on N-doped graphene (CoP@NC-NG) with polyaniline (PANI) as carbon source (Fig. 6.7a). The C-shell layer covering the surface of CoP NPs derived from PANI not only acted as a protective layer to impede the dissolution of nanoparticles, but also

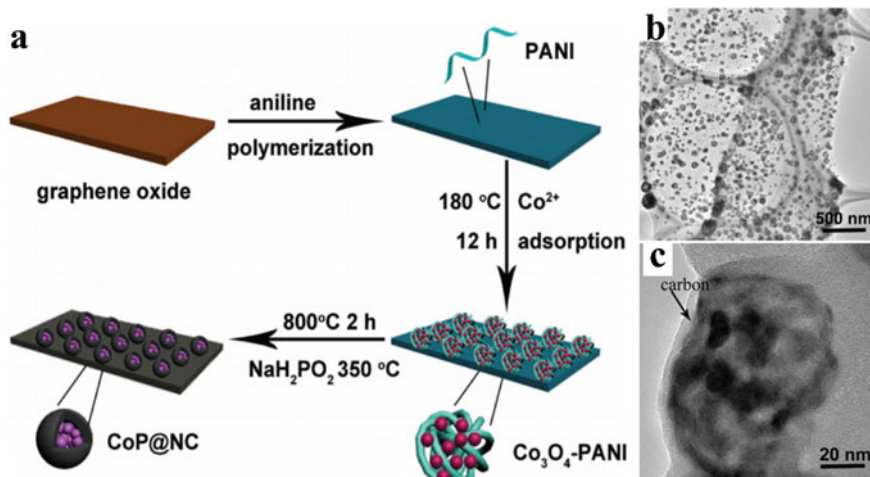


Fig. 6.7 Metal hybrids encapsulated carbon-based electrocatalysts. **a** Growth schematic of core-shell structure of CoP@NC. **b** TEM and **c** HRTEM images of CoP@NC. (a–c). Reproduced with permission [86]. Copyright 2018, WILEY-VCH

enhanced the electrical conductivity of nanoparticles. As an illustration in Fig. 6.7b, c, an obvious carbon shell can be found in TEM images, and CoP NPs coated in NC shell were well-dispersed with the benefit of N-doped graphene.

6.6 Conclusion and Prospects

Carbon nanomaterials have enormous potential as HER supports in terms of high electrical conductivity, strong electrochemical stability, highly adjustable electronic structure, and various structural features. In this chapter, the recently advanced perspectives of carbon-based nanomaterials as potential HER electrocatalysts have been summarized. Due to the efficient metal atom utilization, highly promising single-metal-atom carbon-based materials were first to be discussed. Secondly, carbon-based metal-free electrocatalysts were discussed in detail. Then, according to the different composite forms between metal nanoparticles and carbon materials, metal nanoparticles supported carbon-based materials and metal nanoparticles encapsulated carbon-based materials are depicted respectively. However, there are several unsolved problems about carbon-based nanomaterials, even if tremendous efforts are put into research systematically for the enhanced HER performance.

- (1) Improving the atomic utilization of metal active centers. Single metal-atom catalysts represent to a certain extent the maximization of metal atom utilization, which is conducive to the rational utilization of metal resources and the

economic potential of electrocatalytic systems. However, the linear relationship between the maximization of atomic utilization and the application area is still unclear, and it is not known whether the pursuit of maximization of atomic utilization can extend the field advantage. Currently, the synergy of single atomic sites with active sites in clusters and nanoparticles shows more favorable electrochemical activity than single metal sites. Therefore, the extent to which atomic utilization is appropriate remains to be explored.

- (2) **Catalytic mechanism.** To fully understand the origins of activity enhancement, further study of the underlying principles is needed. Only with a deeper understanding can we solve the bottleneck that the inherent linear scalar relationship limits the activity of carbon-based metal-free electrocatalysts, which may be a feasible strategy to surpass its active limit, and even expected to surpass carbon-based metal catalysts. Therefore, it is very necessary to explore what will happen to the surface of the carbon-based catalysts during HER. However, current theoretical studies are less concerned with the effect of surface reconstruction on the active epicenters of carbon-based catalysts. During the HER process, the existence of complicated surface reconstruction on the catalytic surface may cause changes in the chemical structure and environment of the active center, which further increases the difficulty of studying the potential catalytic mechanism. Therefore, on the one hand, the catalytic mechanism needs to be studied in greater depth, and on the other hand, various advanced in situ characterization techniques need to be developed to reveal the complex evolution of the active center during the HER process and provide better guidance for catalyst construct.
- (3) **Carbon corrosion.** Although loading the active center on carbon nanomaterials can effectively improve the corrosion resistance of the catalyst, a portion of the carbon atoms will be oxidized to CO₂ when exposed to strong acidic and alkaline environments or high overpotential for a long time, which will lead to the collapse of the catalyst structure and thus reduce the electrochemical performance. Therefore, it is essential to consider the design of carbon carriers with suitable defects to balance catalytic activity with long-term stability.
- (4) **Application.** In addition to the HER field, the application of carbon-based electrocatalysts in oxygen reduction reaction, oxygen evolution reaction, nitrogen reduction reaction, CO₂ reduction reaction, fuel cell, supercapacitor, and other fields is also expected to achieve favorable development.

References

1. P.W. Menezes, S. Yao, R. Beltrán-Suito, J.N. Hausmann, P.V. Menezes, M. Driess, Facile access to an active γ -NiOOH electrocatalyst for durable water oxidation derived from an intermetallic nickel germanide precursor. *Angew. Chem. Int. Ed.* **60**, 4640–4647 (2021). <https://doi.org/10.1002/anie.202014331>

2. W. Yang, S. Chen, Recent progress in electrode fabrication for electrocatalytic hydrogen evolution reaction: A mini review. *Chem. Eng. J.* **393**, 124726 (2020). <https://doi.org/10.1016/j.cej.2020.124726>
3. J. Theerthagiri, S.J. Lee, A.P. Murthy, J. Madhavan, M.Y. Choi, Fundamental aspects and recent advances in transition metal nitrides as electrocatalysts for hydrogen evolution reaction: A review. *Curr. Opin. Solid State Mater. Sci.* **24**, 100805 (2020). <https://doi.org/10.1016/j.cossms.2020.100805>
4. A. Ali, P.K. Shen, Nonprecious metal's graphene-supported electrocatalysts for hydrogen evolution reaction: Fundamentals to applications. *Carbon Energy* **2**, 99–121 (2020). <https://doi.org/10.1002/cey2.26>
5. Y. Pan, C. Zhang, Y. Lin, Z. Liu, M. Wang, C. Chen, Electrocatalyst engineering and structure-activity relationship in hydrogen evolution reaction: From nanostructures to single atoms. *Sci. China Mater.* **63**, 921–948 (2020). <https://doi.org/10.1007/s40843-019-1242-1>
6. W. Hua, H.-H. Sun, F. Xu, J.-G. Wang, A review and perspective on molybdenum-based electrocatalysts for hydrogen evolution reaction. *Rare Met.* **39**, 335–351 (2020). <https://doi.org/10.1007/s12598-020-01384-7>
7. Y. Wang, B. Kong, D. Zhao, H. Wang, C. Selomulya, Strategies for developing transition metal phosphides as heterogeneous electrocatalysts for water splitting. *Nano Today* **15**, 26–55 (2017). <https://doi.org/10.1016/j.nantod.2017.06.006>
8. S.-S. Lu, L.-M. Zhang, Y.-W. Dong, J.-Q. Zhang, X.-T. Yan, D.-F. Sun, X. Shang, J.-Q. Chi, Y.-M. Chai, B. Dong, Tungsten-doped Ni–Co phosphides with multiple catalytic sites as efficient electrocatalysts for overall water splitting. *J. Mater. Chem. A* **7**, 16859–16866 (2019). <https://doi.org/10.1039/C9TA03944A>
9. X. Xiao, L. Tao, M. Li, X. Lv, D. Huang, X. Jiang, H. Pan, M. Wang, Y. Shen, Electronic modulation of transition metal phosphide via doping as efficient and pH-universal electrocatalysts for hydrogen evolution reaction. *Chem. Sci.* **9**, 1970–1975 (2018). <https://doi.org/10.1039/C7SC04849A>
10. D. Chen, Z. Pu, R. Lu, P. Ji, P. Wang, J. Zhu, C. Lin, H.-W. Li, X. Zhou, Z. Hu, F. Xia, J. Wu, S. Mu, Ultralow Ru loading transition metal phosphides as high-efficient bifunctional electrocatalyst for a solar-to-hydrogen generation system. *Adv. Energy Mater.* **10**, 2000814 (2020). <https://doi.org/10.1002/aenm.202000814>
11. Z. Wu, Y. Zhao, H. Wu, Y. Gao, Z. Chen, W. Jin, J. Wang, T. Ma, L. Wang, Corrosion engineering on iron foam toward efficiently electrocatalytic overall water splitting powered by sustainable energy. *Adv. Func. Mater.* **31**, 2010437 (2021). <https://doi.org/10.1002/adfm.202010437>
12. L. Yan, H. Wang, J. Shen, J. Ning, Y. Zhong, Y. Hu, Formation of mesoporous Co/CoS/Metal–N–C@S, N-codoped hairy carbon polyhedrons as an efficient trifunctional electrocatalyst for Zn-air batteries and water splitting. *Chem. Eng. J.* **403**, 126385 (2021). <https://doi.org/10.1016/j.cej.2020.126385>
13. Y. Shi, B. Zhang, Recent advances in transition metal phosphide nanomaterials: Synthesis and applications in hydrogen evolution reaction. *Chem. Soc. Rev.* **45**, 1529–1541 (2016). <https://doi.org/10.1039/C5CS00434A>
14. D. Khalafallah, M. Zhi, Z. Hong, Recent trends in synthesis and investigation of nickel phosphide compound/hybrid-based electrocatalysts towards hydrogen generation from water electrocatalysis. *Top. Curr. Chem.* **377**, 29 (2019). <https://doi.org/10.1007/s41061-019-0254-3>
15. Z. Chen, X. Duan, W. Wei, S. Wang, B.-J. Ni, Recent advances in transition metal-based electrocatalysts for alkaline hydrogen evolution. *J. Mater. Chem. A* **7**, 14971–15005 (2019). <https://doi.org/10.1039/C9TA03220G>
16. Y. Pei, Y. Cheng, J. Chen, W. Smith, P. Dong, P.M. Ajayan, M. Ye, J. Shen, Recent developments of transition metal phosphides as catalysts in the energy conversion field. *J. Mater. Chem. A* **6**, 23220–23243 (2018). <https://doi.org/10.1039/C8TA09454C>
17. M. Kuang, Q. Wang, P. Han, G. Zheng, Cu, Co-embedded N-enriched mesoporous carbon for efficient oxygen reduction and hydrogen evolution reactions. *Adv. Energy Mater.* **7**, 1700193 (2017). <https://doi.org/10.1002/aenm.201700193>

18. Q. Lu, Y. Yu, Q. Ma, B. Chen, H. Zhang, 2D transition-metal-dichalcogenide-nanosheet-based composites for photocatalytic and electrocatalytic hydrogen evolution reactions. *Adv. Mater.* **28**, 1917–1933 (2016). <https://doi.org/10.1002/adma.201503270>
19. W. Zhou, J. Jia, J. Lu, L. Yang, D. Hou, G. Li, S. Chen, Recent developments of carbon-based electrocatalysts for hydrogen evolution reaction. *Nano Energy* **28**, 29–43 (2016). <https://doi.org/10.1016/j.nanoen.2016.08.027>
20. Y. Zheng, Y. Jiao, L.H. Li, T. Xing, Y. Chen, M. Jaroniec, S.Z. Qiao, Toward design of synergistically active carbon-based catalysts for electrocatalytic hydrogen evolution. *ACS Nano* **8**, 5290–5296 (2014). <https://doi.org/10.1021/nn501434a>
21. J. Wang, F. Xu, H. Jin, Y. Chen, Y. Wang, Non-noble metal-based carbon composites in hydrogen evolution reaction: Fundamentals to applications. *Adv. Mater.* **29**, 1605838 (2017). <https://doi.org/10.1002/adma.201605838>
22. Z. Shi, W. Yang, Y. Gu, T. Liao, Z. Sun, Metal-nitrogen-doped carbon materials as highly efficient catalysts: Progress and rational design. *Adv. Sci.* **7**, 2001069 (2020). <https://doi.org/10.1002/advs.202001069>
23. C. Gao, F. Lyu, Y. Yin, Encapsulated metal nanoparticles for catalysis. *Chem. Rev.* **121**, 834–881 (2021). <https://doi.org/10.1021/acs.chemrev.0c00237>
24. Y. Yang, Z. Lun, G. Xia, F. Zheng, M. He, Q. Chen, Non-precious alloy encapsulated in nitrogen-doped graphene layers derived from MOFs as an active and durable hydrogen evolution reaction catalyst. *Energy Environ. Sci.* **8**, 3563–3571 (2015). <https://doi.org/10.1039/C5EE02460A>
25. K. Gong, F. Du, Z. Xia, M. Durstock, L. Dai, Nitrogen-doped carbon nanotube arrays with high electrocatalytic activity for oxygen reduction. *Science* **323**, 760 (2009). <https://doi.org/10.1126/science.1168049>
26. L. Tao, Y. Wang, Y. Zou, N. Zhang, Y. Zhang, Y. Wu, Y. Wang, R. Chen, S. Wang, Charge transfer modulated activity of carbon-based electrocatalysts. *Adv. Energy Mater.* **10**, 1901227 (2020). <https://doi.org/10.1002/aenm.201901227>
27. B. Qiao, A. Wang, X. Yang, L.F. Allard, Z. Jiang, Y. Cui, J. Liu, J. Li, T. Zhang, Single-atom catalysis of CO oxidation using Pt₁/FeO_x. *Nat. Chem.* **3**, 634–641 (2011). <https://doi.org/10.1038/nchem.1095>
28. X. Wang, A. Vasileff, Y. Jiao, Y. Zheng, S.-Z. Qiao, Electronic and structural engineering of carbon-based metal-free electrocatalysts for water splitting. *Adv. Mater.* **31**, 1803625 (2019). <https://doi.org/10.1002/adma.201803625>
29. S. Zhao, D.-W. Wang, R. Amal, L. Dai, Carbon-based metal-free catalysts for key reactions involved in energy conversion and storage. *Adv. Mater.* **31**, 1801526 (2019). <https://doi.org/10.1002/adma.201801526>
30. R. Paul, L. Zhu, H. Chen, J. Qu, L. Dai, Recent advances in carbon-based metal-free electrocatalysts. *Adv. Mater.* **31**, 1806403 (2019). <https://doi.org/10.1002/adma.201806403>
31. Y. Jia, L. Zhang, A. Du, G. Gao, J. Chen, X. Yan, C.L. Brown, X. Yao, Defect graphene as a trifunctional catalyst for electrochemical reactions. *Adv. Mater.* **28**, 9532–9538 (2016). <https://doi.org/10.1002/adma.201602912>
32. Q. Han, Z. Cheng, J. Gao, Y. Zhao, Z. Zhang, L. Dai, L. Qu, Mesh-on-mesh graphitic-C₃N₄@graphene for highly efficient hydrogen evolution. *Adv. Func. Mater.* **27**, 1606352 (2017). <https://doi.org/10.1002/adfm.201606352>
33. Z. Pei, J. Gu, Y. Wang, Z. Tang, Z. Liu, Y. Huang, Y. Huang, J. Zhao, Z. Chen, C. Zhi, Component matters: Paving the roadmap toward enhanced electrocatalytic performance of graphitic C₃N₄-based catalysts via atomic tuning. *ACS Nano* **11**, 6004–6014 (2017). <https://doi.org/10.1021/acsnano.7b01908>
34. H. Huang, M. Yan, C. Yang, H. He, Q. Jiang, L. Yang, Z. Lu, Z. Sun, X. Xu, Y. Bando, Y. Yamauchi, Graphene nanoarchitectonics: Recent advances in graphene-based electrocatalysts for hydrogen evolution reaction. *Adv. Mater.* **31**, 1903415 (2019). <https://doi.org/10.1002/adma.201903415>
35. X. Gui, Z. Zeng, Y. Zhu, H. Li, Z. Lin, Q. Gan, R. Xiang, A. Cao, Z. Tang, Three-dimensional carbon nanotube sponge-array architectures with high energy dissipation. *Adv. Mater.* **26**, 1248–1253 (2014). <https://doi.org/10.1002/adma.201304493>

36. D. Yan, Y. Li, J. Huo, R. Chen, L. Dai, S. Wang, Defect chemistry of nonprecious-metal electrocatalysts for oxygen reactions. *Adv. Mater.* **29**, 1606459 (2017). <https://doi.org/10.1002/adma.201606459>
37. C. Tang, H.-F. Wang, Q. Zhang, Multiscale principles to boost reactivity in gas-involving energy electrocatalysis. *Acc. Chem. Res.* **51**, 881–889 (2018). <https://doi.org/10.1021/acs.accounts.7b00616>
38. Z. Pei, J. Zhao, Y. Huang, Y. Huang, M. Zhu, Z. Wang, Z. Chen, C. Zhi, Toward enhanced activity of a graphitic carbon nitride-based electrocatalyst in oxygen reduction and hydrogen evolution reactions via atomic sulfur doping. *J. Mater. Chem. A* **4**, 12205–12211 (2016). <https://doi.org/10.1039/C6TA03588D>
39. P. Zhai, M. Xia, Y. Wu, G. Zhang, J. Gao, B. Zhang, S. Cao, Y. Zhang, Z. Li, Z. Fan, C. Wang, X. Zhang, J.T. Miller, L. Sun, J. Hou, Engineering single-atomic ruthenium catalytic sites on defective nickel-iron layered double hydroxide for overall water splitting. *Nat. Commun.* **12**, 4587 (2021). <https://doi.org/10.1038/s41467-021-24828-9>
40. Y. Peng, B. Lu, S. Chen, Carbon-supported single atom catalysts for electrochemical energy conversion and storage. *Adv. Mater.* **30**, 1801995 (2018). <https://doi.org/10.1002/adma.201801995>
41. Y.-N. Chen, X. Zhang, Z. Zhou, Carbon-based substrates for highly dispersed nanoparticle and even single-atom electrocatalysts. *Small Methods* **3**, 1900050 (2019). <https://doi.org/10.1002/smt.201900050>
42. D. Liu, X. Li, S. Chen, H. Yan, C. Wang, C. Wu, Y.A. Haleem, S. Duan, J. Lu, B. Ge, P.M. Ajayan, Y. Luo, J. Jiang, L. Song, Atomically dispersed platinum supported on curved carbon supports for efficient electrocatalytic hydrogen evolution. *Nat. Energy* **4**, 512–518 (2019). <https://doi.org/10.1038/s41560-019-0402-6>
43. M.B. Gawande, P. Fornasiero, R. Zbořil, Carbon-based single-atom catalysts for advanced applications. *ACS Catal.* **10**, 2231–2259 (2020). <https://doi.org/10.1021/acscatal.9b04217>
44. Z. Pu, I.S. Amiinu, R. Cheng, P. Wang, C. Zhang, S. Mu, W. Zhao, F. Su, G. Zhang, S. Liao, S. Sun, Single-atom catalysts for electrochemical hydrogen evolution reaction: Recent advances and future perspectives. *Nano-Micro Letters* **12**, 21 (2020). <https://doi.org/10.1007/s40820-019-0349-y>
45. M. Fan, J. Cui, J. Wu, R. Vajtai, D. Sun, P.M. Ajayan, Improving the catalytic activity of carbon-supported single atom catalysts by polynary metal or heteroatom doping. *Small* **16**, 1906782 (2020). <https://doi.org/10.1002/sml.201906782>
46. K. Gao, B. Wang, L. Tao, B.V. Cunning, Z. Zhang, S. Wang, R.S. Ruoff, L. Qu, Efficient metal-free electrocatalysts from N-doped carbon nanomaterials: Mono-doping and Co-doping. *Adv. Mater.* **31**, 1805121 (2019). <https://doi.org/10.1002/adma.201805121>
47. F. Schedin, A.K. Geim, S.V. Morozov, E.W. Hill, P. Blake, M.I. Katsnelson, K.S. Novoselov, Detection of individual gas molecules adsorbed on graphene. *Nat. Mater.* **6**, 652–655 (2007). <https://doi.org/10.1038/nmat1967>
48. Y. Chen, S. Ji, Y. Wang, J. Dong, W. Chen, Z. Li, R. Shen, L. Zheng, Z. Zhuang, D. Wang, Y. Li, Isolated single iron atoms anchored on N-doped porous carbon as an efficient electrocatalyst for the oxygen reduction reaction. *Angew. Chem. Int. Ed.* **56**, 6937–6941 (2017). <https://doi.org/10.1002/anie.201702473>
49. P. Su, W. Pei, X. Wang, Y. Ma, Q. Jiang, J. Liang, S. Zhou, J. Zhao, J. Liu, G.Q. Lu, Exceptional electrochemical HER performance with enhanced electron transfer between Ru nanoparticles and single atoms dispersed on a carbon substrate. *Angew. Chem. Int. Ed.* **60**, 16044–16050 (2021). <https://doi.org/10.1002/anie.202103557>
50. Y. Zheng, Y. Jiao, Y. Zhu, L.H. Li, Y. Han, Y. Chen, A. Du, M. Jaroniec, S.Z. Qiao, Hydrogen evolution by a metal-free electrocatalyst. *Nat. Commun.* **5**, 3783 (2014). <https://doi.org/10.1038/ncomms4783>
51. Y. Liang, Y. Li, H. Wang, H. Dai, Strongly coupled inorganic/nanocarbon hybrid materials for advanced electrocatalysis. *J. Am. Chem. Soc.* **135**, 2013–2036 (2013). <https://doi.org/10.1021/ja3089923>

52. Y. Zhang, L. Guo, L. Tao, Y. Lu, S. Wang, Defect-based single-atom electrocatalysts. *Small Methods* **3**, 1800406 (2019). <https://doi.org/10.1002/smt.201800406>
53. H. Wang, Y. Liang, M. Gong, Y. Li, W. Chang, T. Mefford, J. Zhou, J. Wang, T. Regier, F. Wei, H. Dai, An ultrafast nickel–iron battery from strongly coupled inorganic nanoparticle/nanocarbon hybrid materials. *Nat. Commun.* **3**, 917 (2012). <https://doi.org/10.1038/ncomms1921>
54. K. Khan, T. Liu, M. Arif, X. Yan, M.D. Hossain, F. Rehman, S. Zhou, J. Yang, C. Sun, S.-H. Bae, J. Kim, K. Amine, X. Pan, Z. Luo, Laser-irradiated holey graphene-supported single-atom catalyst towards hydrogen evolution and oxygen reduction. *Adv. Energy Mater.* **11**, 2101619 (2021). <https://doi.org/10.1002/aenm.202101619>
55. R. Liu, Z. Gong, J. Liu, J. Dong, J. Liao, H. Liu, H. Huang, J. Liu, M. Yan, K. Huang, H. Gong, J. Zhu, C. Cui, G. Ye, H. Fei, Design of aligned porous carbon films with single-atom Co–N–C sites for high-current-density hydrogen generation. *Adv. Mater.* **33**, 2103533 (2021). <https://doi.org/10.1002/adma.202103533>
56. J. Yang, W. Liu, M. Xu, X. Liu, H. Qi, L. Zhang, X. Yang, S. Niu, D. Zhou, Y. Liu, Y. Su, J.-F. Li, Z.-Q. Tian, W. Zhou, A. Wang, T. Zhang, Dynamic behavior of single-atom catalysts in electrocatalysis: Identification of Cu–N₃ as an active site for the oxygen reduction reaction. *J. Am. Chem. Soc.* **143**, 14530–14539 (2021). <https://doi.org/10.1021/jacs.1c03788>
57. G. Yang, J. Zhu, P. Yuan, Y. Hu, G. Qu, B.-A. Lu, X. Xue, H. Yin, W. Cheng, J. Cheng, W. Xu, J. Li, J. Hu, S. Mu, J.-N. Zhang, Regulating Fe-spin state by atomically dispersed Mn–N in Fe–N–C catalysts with high oxygen reduction activity. *Nat. Commun.* **12**, 1734 (2021). <https://doi.org/10.1038/s41467-021-21919-5>
58. L. Cao, Q. Luo, W. Liu, Y. Lin, X. Liu, Y. Cao, W. Zhang, Y. Wu, J. Yang, T. Yao, S. Wei, Identification of single-atom active sites in carbon-based cobalt catalysts during electrocatalytic hydrogen evolution. *Nat. Catal.* **2**, 134–141 (2019). <https://doi.org/10.1038/s41929-018-0203-5>
59. D. Voiry, H.S. Shin, K.P. Loh, M. Chhowalla, Low-dimensional catalysts for hydrogen evolution and CO₂ reduction. *Nat. Rev. Chem.* **2**, 0105 (2018). <https://doi.org/10.1038/s41570-017-0105>
60. M. Ming, Y. Zhang, C. He, L. Zhao, S. Niu, G. Fan, J.-S. Hu, Room-temperature sustainable synthesis of selected platinum group metal (PGM = Ir, Rh, and Ru) nanocatalysts well-dispersed on porous carbon for efficient hydrogen evolution and oxidation. *Small* **15**, 1903057 (2019). <https://doi.org/10.1002/sml.201903057>
61. T. Liu, S. Wang, Q. Zhang, L. Chen, W. Hu, C.M. Li, Ultrasmall Ru₂P nanoparticles on graphene: A highly efficient hydrogen evolution reaction electrocatalyst in both acidic and alkaline media. *Chem. Commun.* **54**, 3343–3346 (2018). <https://doi.org/10.1039/C8CC01166D>
62. L. Wang, Y. Li, M. Xia, Z. Li, Z. Chen, Z. Ma, X. Qin, G. Shao, Ni nanoparticles supported on graphene layers: An excellent 3D electrode for hydrogen evolution reaction in alkaline solution. *J. Power Sour.* **347**, 220–228 (2017). <https://doi.org/10.1016/j.jpowsour.2017.02.017>
63. Y. Jiang, X. Li, S. Yu, L. Jia, X. Zhao, C. Wang, Reduced graphene oxide-modified carbon nanotube/polyimide film supported MoS₂ nanoparticles for electrocatalytic hydrogen evolution. *Adv. Func. Mater.* **25**, 2693–2700 (2015). <https://doi.org/10.1002/adfm.201500194>
64. L. He, F. Weniger, H. Neumann, M. Beller, Synthesis, characterization, and application of metal nanoparticles supported on nitrogen-doped carbon: Catalysis beyond electrochemistry. *Angew. Chem. Int. Ed.* **55**, 12582–12594 (2016). <https://doi.org/10.1002/anie.201603198>
65. T.-W. Lin, C.-J. Liu, J.-Y. Lin, Facile synthesis of MoS₃/carbon nanotube nanocomposite with high catalytic activity toward hydrogen evolution reaction. *Appl. Catal. B* **134–135**, 75–82 (2013). <https://doi.org/10.1016/j.apcatb.2013.01.004>
66. X. Sun, N. Habibul, H. Du, Co_{0.85}Se magnetic nanoparticles supported on carbon nanotubes as catalyst for hydrogen evolution reaction. *Chin. J. Catal.* **42**, 235–243 (2021). [https://doi.org/10.1016/S1872-2067\(20\)63632-4](https://doi.org/10.1016/S1872-2067(20)63632-4)
67. T.-W. Lin, C.-J. Liu, C.-S. Dai, Ni₃S₂/carbon nanotube nanocomposite as electrode material for hydrogen evolution reaction in alkaline electrolyte and enzyme-free glucose detection. *Appl. Catal. B* **154–155**, 213–220 (2014). <https://doi.org/10.1016/j.apcatb.2014.02.017>
68. D.H. Kweon, M.S. Okyay, S.-J. Kim, J.-P. Jeon, H.-J. Noh, N. Park, J. Mahmood, J.-B. Baek, Ruthenium anchored on carbon nanotube electrocatalyst for hydrogen production with enhanced Faradaic efficiency. *Nat. Commun.* **11**, 1278 (2020). <https://doi.org/10.1038/s41467-020-15069-3>

69. X. Wu, Z. Wang, D. Zhang, Y. Qin, M. Wang, Y. Han, T. Zhan, B. Yang, S. Li, J. Lai, L. Wang, Solvent-free microwave synthesis of ultra-small Ru-Mo₂C@CNT with strong metal-support interaction for industrial hydrogen evolution. *Nat. Commun.* **12**, 4018 (2021). <https://doi.org/10.1038/s41467-021-24322-2>
70. H. Tabassum, R. Zou, A. Mahmood, Z. Liang, S. Guo, A catalyst-free synthesis of B, N co-doped graphene nanostructures with tunable dimensions as highly efficient metal free dual electrocatalysts. *J. Mater. Chem. A* **4**, 16469–16475 (2016). <https://doi.org/10.1039/C6TA07214C>
71. T. Sun, Q. Wu, Y. Jiang, Z. Zhang, L. Du, L. Yang, X. Wang, Z. Hu, Sulfur and nitrogen codoped carbon tubes as bifunctional metal-free electrocatalysts for oxygen reduction and hydrogen evolution in acidic media. *Chem. Eur. J.* **22**, 10326–10329 (2016). <https://doi.org/10.1002/chem.201601535>
72. X. Wu, B. Feng, W. Li, Y. Niu, Y. Yu, S. Lu, C. Zhong, P. Liu, Z. Tian, L. Chen, W. Hu, C.M. Li, Metal-support interaction boosted electrocatalysis of ultrasmall iridium nanoparticles supported on nitrogen doped graphene for highly efficient water electrolysis in acidic and alkaline media. *Nano Energy* **62**, 117–126 (2019). <https://doi.org/10.1016/j.nanoen.2019.05.034>
73. K.-C. Pham, Y.-H. Chang, D.S. McPhail, C. Mattevi, A.T.S. Wee, D.H.C. Chua, Amorphous molybdenum sulfide on graphene-carbon nanotube hybrids as highly active hydrogen evolution reaction catalysts. *ACS Appl. Mater. Interfaces.* **8**, 5961–5971 (2016). <https://doi.org/10.1021/acsami.5b09690>
74. B. Cao, M. Hu, Y. Cheng, P. Jing, B. Liu, B. Zhou, X. Wang, R. Gao, X. Sun, Y. Du, J. Zhang, Tailoring the d-band center of N-doped carbon nanotube arrays with Co₄N nanoparticles and single-atom Co for a superior hydrogen evolution reaction. *NPG Asia Mater.* **13**, 1 (2021). <https://doi.org/10.1038/s41427-020-00264-x>
75. J. Liu, X. Wan, S. Liu, X. Liu, L. Zheng, R. Yu, J. Shui, Hydrogen passivation of M–N–C (M = Fe, Co) catalysts for storage stability and ORR activity improvements. *Adv. Mater.* **33**, 2103600 (2021). <https://doi.org/10.1002/adma.202103600>
76. Z. Wei, Y. Liu, Z. Peng, H. Song, Z. Liu, B. Liu, B. Li, B. Yang, S. Lu, Cobalt-ruthenium nanoalloys parceled in porous nitrogen-doped graphene as highly efficient difunctional catalysts for hydrogen evolution reaction and hydrolysis of ammonia borane. *ACS Sustain. Chem. Eng.* **7**, 7014–7023 (2019). <https://doi.org/10.1021/acssuschemeng.8b06745>
77. J.-Y. Wang, T. Ouyang, N. Li, T. Ma, Z.-Q. Liu, S. N co-doped carbon nanotube-encapsulated core-shelled CoS₂@Co nanoparticles: efficient and stable bifunctional catalysts for overall water splitting. *Sci. Bull.* **63**, 1130–1140 (2018). <https://doi.org/10.1016/j.scib.2018.07.008>
78. M. Tavakkoli, T. Kallio, O. Reynaud, A.G. Nasibulin, C. Johans, J. Sainio, H. Jiang, E.I. Kauppinen, K. Laasonen, Single-shell carbon-encapsulated iron nanoparticles: Synthesis and high electrocatalytic activity for hydrogen evolution reaction. *Angew. Chem. Int. Ed.* **54**, 4535–4538 (2015). <https://doi.org/10.1002/anie.201411450>
79. T. Ouyang, Y.-Q. Ye, C.-Y. Wu, K. Xiao, Z.-Q. Liu, Heterostructures composed of N-doped carbon nanotubes encapsulating cobalt and β-Mo₂C nanoparticles as bifunctional electrodes for water splitting. *Angew. Chem. Int. Ed.* **58**, 4923–4928 (2019). <https://doi.org/10.1002/anie.201814262>
80. X. Wang, Y. Zheng, J. Yuan, J. Shen, L. Niu, A.-J. Wang, Controllable synthesis of caterpillar-like molybdenum sulfide @carbon nanotube hybrids with core shell structure for hydrogen evolution. *Electrochim. Acta* **235**, 422–428 (2017). <https://doi.org/10.1016/j.electacta.2017.02.093>
81. J. Yu, G. Li, H. Liu, L. Zeng, L. Zhao, J. Jia, M. Zhang, W. Zhou, H. Liu, Y. Hu, Electrochemical flocculation integrated hydrogen evolution reaction of Fe@N-doped carbon nanotubes on iron foam for ultralow voltage electrolysis in neutral media. *Adv. Sci.* **6**, 1901458 (2019). <https://doi.org/10.1002/advs.201901458>
82. T. Li, G. Luo, K. Liu, X. Li, D. Sun, L. Xu, Y. Li, Y. Tang, Encapsulation of Ni₃Fe nanoparticles in N-doped carbon nanotube-grafted carbon nanofibers as high-efficiency hydrogen evolution electrocatalysts. *Adv. Func. Mater.* **28**, 1805828 (2018). <https://doi.org/10.1002/adfm.201805828>

83. J. Su, Y. Yang, G. Xia, J. Chen, P. Jiang, Q. Chen, Ruthenium-cobalt nanoalloys encapsulated in nitrogen-doped graphene as active electrocatalysts for producing hydrogen in alkaline media. *Nat. Commun.* **8**, 14969 (2017). <https://doi.org/10.1038/ncomms14969>
84. J. Wang, R. Zhu, J. Cheng, Y. Song, M. Mao, F. Chen, Y. Cheng, Co, Mo₂C encapsulated in N-doped carbon nanofiber as self-supported electrocatalyst for hydrogen evolution reaction. *Chem. Eng. J.* **397**, 125481 (2020). <https://doi.org/10.1016/j.cej.2020.125481>
85. Z. Chen, R. Wu, Y. Liu, Y. Ha, Y. Guo, D. Sun, M. Liu, F. Fang, Ultrafine Co nanoparticles encapsulated in carbon-nanotubes-grafted graphene sheets as advanced electrocatalysts for the hydrogen evolution reaction. *Adv. Mater.* **30**, 1802011 (2018). <https://doi.org/10.1002/adma.201802011>
86. J. Ma, M. Wang, G. Lei, G. Zhang, F. Zhang, W. Peng, X. Fan, Y. Li, Polyaniline derived N-doped carbon-coated cobalt phosphide nanoparticles deposited on N-doped graphene as an efficient electrocatalyst for hydrogen evolution reaction. *Small* **14**, 1702895 (2018). <https://doi.org/10.1002/sml.201702895>

Chapter 7

Carbon-Based Nanomaterials for Oxygen Evolution Reaction



Mengli Liu, Siran Xu, and Bang-An Lu

Abstract The oxygen evolution reaction (OER), one of the semi-reactions of water electrolysis, is expected to play an important role in the conversion and storage of energy in the future. The sluggish four-electron transfer reaction has become the primary bottleneck of electrochemical water splitting, which can be significantly alleviated with the development of low-cost and durable OER catalysts, fortunately. Carbon-based composite nanomaterials can function well in alkaline environments because of their excellent mechanical and electrical properties, low cost, high abundance, and large surface area. This chapter discusses recent breakthroughs in carbon-based OER electrocatalysts, mainly including metal-free catalysts, atomically dispersed metallic carbon, metal-encapsulated carbon nanoparticles, and carbon nanoparticles supported by metal nanoparticles. The knowledge offered in this chapter can be used to rationally design OER carbon-based composite nanomaterial catalysts, which may help shed light on the future of carbon-based OER development.

7.1 Introduction

In recent years, with the increase of the global population, the total energy demand has increased rapidly, leading to excessive consumption of traditional fossil energy and accompanied by increasingly serious environmental pollution problems [1, 2]. As a result, the urgent need for new energy forms and carriers, as well as the desire to reduce long-term excessive reliance on fossil energy, researchers in energy-related

M. Liu · S. Xu · B.-A. Lu (✉)

College of Materials Science and Engineering, Zhengzhou University, Zhengzhou 450001,
P. R. China

e-mail: balu@zzu.edu.cn

M. Liu

e-mail: 13592573680@163.com

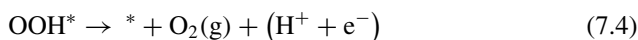
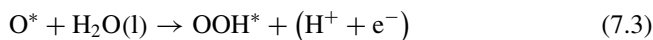
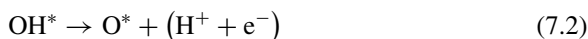
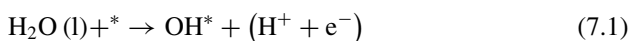
S. Xu

e-mail: siranxuhbnu@163.com

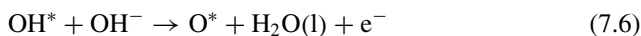
fields are exploring and developing environmentally friendly and sustainable new energy and production technologies. In order to achieve the goal of carbon neutrality and find alternatives to renewable energy and clean energy, such as wind energy, tidal energy, solar energy, and geothermal energy, a lot of efforts have been made [3, 4]. However, due to the lack of suitable energy storage technology, these intermittent energy sources cannot be widely used [5, 6]. Hydrogen energy has significant advantages as a zero-carbon energy source. Because of its high energy density, H₂ can be used to store large amounts of energy indefinitely. Low-pollution fuel cells can then be used to regenerate the electrical energy. Additional to this, the high-value-added chemicals can also be produced by using H₂ [7–9]. Fossil fuels, biomass, and water splitting are the three primary sources of hydrogen production currently available. However, hydrogen production from fossil fuels and biomass involves the use of limited fossil energy, resulting in environmental contamination. Electrochemical water splitting to produce hydrogen is therefore expected to become the primary method of producing hydrogen because of its durability and low pollution [10–12].

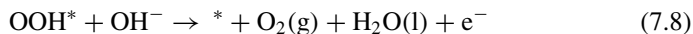
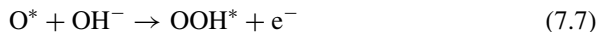
The electrocatalytic water splitting is the reverse process of the fuel cell reaction, including the hydrogen evolution reaction (HER) at the cathode and the oxygen evolution reaction (OER) at the anode [13–15]. Both of these reactions require efficient catalysts to accelerate the reaction kinetics. HER is a relatively simple two-electron transport process involving electrochemical H⁺ adsorption and H₂ desorption. In contrast, the OER process involves a complex four-electron-proton coupling process. Due to its slow kinetic reaction, it becomes a bottleneck for the production of hydrogen by electrochemical water splitting [16]. Meanwhile, OER is also an important semi-response of rechargeable metal-air batteries. However, due to the inherent slow kinetics of OER, the metal-air battery has low life, low energy conversion efficiency, and limited stability [17]. The reaction path of OER process in acidic and alkaline electrolytes is shown in the following formula:

Acid:



Alkaline:





In the formula, (l) and (g) are gas and liquid phases, respectively, * is the active site on the catalyst, and O^* , OH^* , OOH^* are adsorption intermediates.

The OER can be divided into four steps. Each step involves the transfer of an electron. The overpotential of OER can be determined by the free energy of the reaction of all four steps [18]. The energy barriers of different reaction intermediates are related to the catalyst's electronic structure and interface structure. This basic identification of OER mechanism and activity source is a prerequisite for designing advanced OER electrocatalysts [19, 20].

Generally speaking, there are two possible mechanism for the OER process, one is the traditional adsorbate evolution mechanism (AEM), and the other is the lattice oxygen mediated mechanism (LOM) [21–23]. AEM is considered to be a conventional OER mechanism. AEM involves four proton-coupled electron transfer processes centered on metal ions. The source of oxygen is mainly water molecules adsorbed in the electrolyte. Specifically, first, water molecules are adsorbed on the surface of the metal site through a single-electron oxidation process, forming an adsorbed *OH on the metal site (*). Then *OH forms *O species through proton coupling and electron removal. Another water molecule is adsorbed to form the *OOH intermediate in the next step. Finally, *OOH is oxidized, releasing O_2 , and the original clean metal active sites are restored. On the scale of reversible hydrogen electrodes, AEM usually produces activity independent of pH. However, LOM clearly pointed out the necessity of considering the surface of the dynamic catalyst, and the active sites on the surface of the dynamic catalyst are not limited to the metal center. The LOM concept involving the reaction of lattice oxygen was first proposed by Damjanovic and Jovanovic in 1976 [24]. In late 2015, Binninger et al. [25] proposed a more formal description and coined the term for the lattice oxygen evolution reaction in a typical LOM [25]. LOM involves the participation of lattice oxygen in the electrocatalyst, and oxygen is generated by lattice oxygen atoms. The first two steps are similar to those in AEM. However, in the third step, the adsorbed *O couples with the lattice oxygen on the electrocatalyst, releasing an oxygen molecule and leaving an oxygen vacancy. In order to produce adsorbed *H , the fourth step is supplemented with water and dissociated. The final deprotonation results in a clean metal site. Electrocatalyst electronic structure can be controlled by LOM's OER mechanism, which is based on LOM's metal–oxygen covalent bond [26].

The catalyst plays a critical role in accelerating the reaction rate and increasing the selectivity/efficiency of the OER. As a result, theoretical and experimental research on the design and development of effective and stable OER catalysts is still an important area of study. Despite being the most advanced OER electrocatalysts, IrO_2 and RuO_2 are not widely used because of their high cost and limited availability. In order to develop low-cost OER electrocatalysts with high activity and high stability, a great deal of work has been done thus far. For example, nitrides, phosphides,

sulfides, and selenides have been investigated as alternative OER electrocatalysts [27–32]. Carbon-based composites have shown surprising advantages in OER in recent years, including the acceptable cost of carbon matrix, the structural diversity provided by carbon-based composites, good electrical and thermal conductivity, and mechanical strength and lightness that traditional materials cannot match [33]. It also has a wide range of compositions and good conductivity, thanks to the addition of heteroatoms. The electrode becomes more stable when oxygen escapes thanks to this combination (bubble formation) [34]. Therefore, carbon-based nanocomposites have great potential in catalyzing OER.

OER carbon-based catalysts will be detailly introduced in this chapter including metal nanoparticle/alloy, atom dispersed metal–carbon, and metal hybrid carbon-based electrocatalysts. A summary of current research of carbon-based OER electrocatalysts in this field is also presented.

7.2 Metal-Free Carbon-Based Electrocatalysts for OER

Noble metals and their oxides, such as palladium, platinum, and RuO_2 , IrO_2 , are considered the most advanced OER catalysts. Besides, transition metal oxides, hydroxides, metal hybrids, chalcogenide compounds, and other reasonably inexpensive OER electrocatalysts of transition metals and related compounds have been identified based on extensive research. However, these transition metal-based catalysts will undergo oxidation, crystal structure changes, and uncontrolled dissolution when exposed to air or electrolytes. Therefore, in order to obtain high electrocatalytic activity and multifunctional carbon-based metal-free electrocatalyst, different carbon nanostructures are often doped with other heteroatoms and defect engineering, such as nitrogen (N), boron (B), sulfur (S), phosphorus (P), and fluorine (F) [35–39]. These may change the electronic structure of carbon materials and become active sites for catalytic reactions, although other factors affect electrocatalytic activity. The charge transfer efficiency of catalysts depends on various factors, such as specific surface area, number of active centers, conductivity, adsorption energy of intermediate products, and electrolyte stability.

In this context, carbon-based metal-free electrocatalysts for ORR have come a long way since their discovery in 2009 [40, 41]. Carbon-based metal-free electrocatalysts as a substitute for noble metal-based electrocatalysts have been widely researched to be effective OER catalysts [35, 42]. In 2013, it is reported for the first time that N-doped porous carbon prepared from melamine formaldehyde containing a heteroatom doped can be used as a carbon-based metal-free electrocatalyst (Fig. 7.1a, b), and showed better OER performance than IrO_2 (Fig. 7.1c). The observed OER performance is attributed to the favorable adsorption of positively charged C atoms by OH^- ions generated by charge transfer induced by adjacent N doping. Experimental and theoretical studies have also shown that the high oxygen evolution activity of

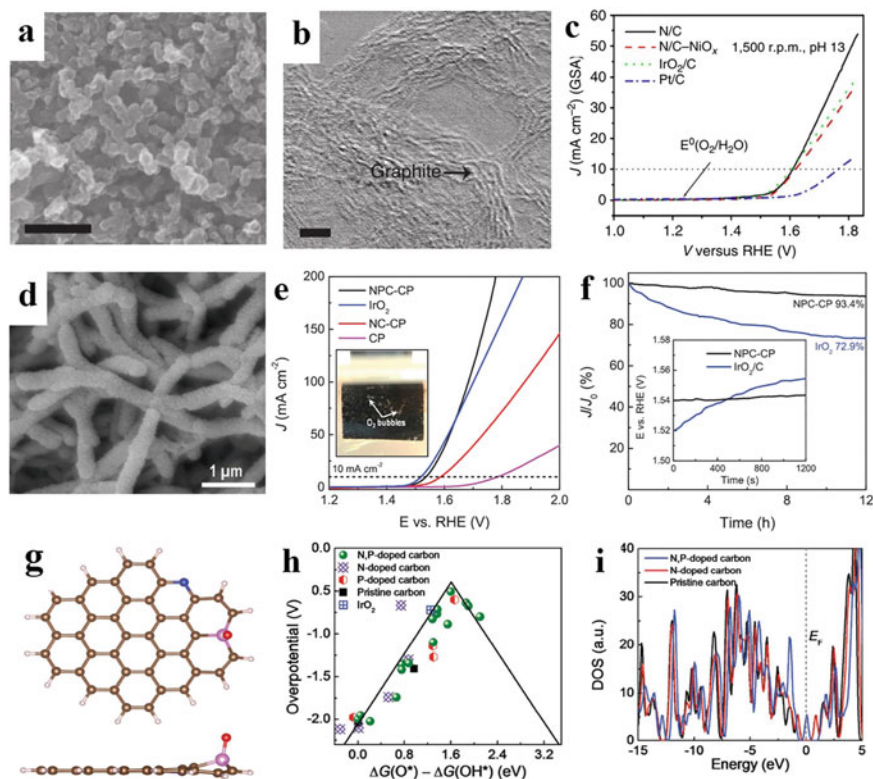


Fig. 7.1 Metal-free carbon-based electrocatalysts for OER. **a** and **b** The SEM and TEM images of the N/C. **c** Oxygen evolution activities of the N/C, N/C-NiO_x, IrO₂/C (20 wt%) and Pt/C (20 wt%) electrodes with KOH electrolyte (pH 13) analysed from RRDE system (loading catalyst: 0.2 mg cm⁻¹; rotation speed: 1500 r.p.m.; and scan rate: 5 mV s⁻¹) [35]. Copyright 2013, Nature Publishing Group. **d** SEM image of NPC-CP. **e** OER curves of NPC-CP, NC-CP, IrO₂, and pristine CP in O₂-saturated 1 M KOH (scan rate: 2 mV s⁻¹). **f** Chronoamperometric responses of NPC-CP and IrO₂ at a constant potential of 1.54 V. Inset in panel **f** shows the corresponding chronopotentiometry response curves with the constant current density held at 10 mA cm⁻². **g** Initial structure of N and P co-doped carbons and the corresponding structures. **h** Volcano plots of OER overpotential versus the difference between the adsorption energy of O* and OH*, that is, ΔG(O*) - ΔG(OH*), for the simulated carbon structures. **i** The DOS for the chemically doped carbon structures [43]. Copyright 2017, WILEY-VCH

nitrogen/carbon materials comes from pyridine nitrogen or/and quaternary-nitrogen-related active sites [35]. The N-P co-doped mesoporous carbon produced by pyrolysis of polyaniline aerogels generated in the presence of phytic acid in 2015 had a high surface area of around 1663 m² g⁻¹ and shown outstanding electrocatalytic activity in the OER and ORR. It is also attractive advantages after being used in zinc-air batteries. After mechanical charging, the two-electrode rechargeable battery is stable for up to 240 h and 180 cycles at 2 mA cm⁻². Its maximum power density is 55 mW cm⁻². In terms of alkaline electrolytes, it is comparable to commercial

metal air batteries. For chemical species' adsorption and catalytic activity, density functional theory (DFT) calculations show that a distance between the doping site and the edge of the carbon structure appears to be critical. For ORR and OER to function in both modes, a high-porosity foamed carbon network and N/P heteroatom co-doping are required [42]. Coincidentally, multi-stage porous N/P co-doped carbon nanofibers were immediately produced on conductive carbon paper by electrochemically induced polymerization in the presence of aniline monomer and phosphonic acid. (Fig. 7.1d). The synthesized material has stable stability (the activity decays little after 12 h of continuous operation) and high activity (Fig. 7.1e, f). Through DFT calculations, a model of double doping of N and P heteroatoms was constructed (Fig. 7.1g), and it was found that the P doping at the edge is more conducive to the precipitation of oxygen than the P dopant at the center. From a thermodynamic point of view, the ideal catalyst is the lower the overpotential, the better the catalytic performance. From the volcano plots of overpotential versus the difference between the adsorption energy of O* and OH* on the carbon nanostructures, it can be seen that N, P-doped carbon has the smallest overpotential (0.505 V) (Fig. 7.1h), even better than IrO₂. In addition, according to the density of states (DOS) (Fig. 7.1i), the N, P-doped carbon exhibits metallic properties with a relatively higher DOS crossing the Fermi level (E_F), which indicates that the electron transfer capability is improved and the charge distribution is optimized. Theoretically verified the effectiveness of the co-doping of N and P atoms in the collaborative creation of OER active sites and the improvement of the electronic conductivity of the carbon network [43]. Due to the effectiveness of heteroatom doping, carbon materials co-doped with three heteroatoms have been studied. By thermally activating a mixture of polyaniline-coated graphene oxide and ammonium hexafluorophosphate (AHF), a multifunctional electrocatalyst constituted of graphene doped with nitrogen, phosphorus, and fluorine is generated. The gas from the thermal decomposition of AHF promotes the formation of a template-free porous structure. The synthesized N, P, and F three-doped graphene exhibit good electrocatalytic activity for ORR, OER, and HER. It is further used as an OER-HER dual-function catalyst for oxygen and hydrogen production in an electrochemical water splitting device. The device is powered by an integrated Zn-air battery based on an air electrode made of the same ORR electrocatalyst. Therefore, low-cost metal-free trifunctional electrocatalysts have broad application prospects [39].

Carbon-based metal-free electrocatalysts can also benefit from construction defect engineering in addition to heteroatom doping. Nitrogen-doped ultra-thin carbon nanosheets (NCNs) can be made by pyrolyzing a citric acid and NH₄Cl mixture and then using a spontaneous gas foaming method. Ultra-thin sheet structure, ultra-high specific surface area (1793 m² g⁻¹), abundant edge defects, low overpotential, and stable ORR, OER and HER properties were achieved by synthesizing NCN-1000-5. Its high energy density, low charge/discharge voltage gap, high reversibility, and long cycle stability all come from the zinc-air rechargeable battery's use of NCN-1000-5 as the cathode catalyst. In ORR, OER, and HER, it is determined that the intrinsic active sites are the carbon atoms on the armchair's edge and adjacent graphite N dopants, thanks to DFT calculations [44].

7.3 Atomically Dispersed Metal Carbon-Based Electrocatalysts for OER

In recent years, the research on isolated metal atoms has increased dramatically, which has aroused widespread scientific interest in the new frontier field of atomic-level dispersion catalysis. The atomically dispersed active sites usually exhibit the most excellent catalytic activity [45]. In contrast to nanoparticle catalysts, atomically dispersed catalysts typically contain positively charged monodisperse metal atoms and coordination sites devoid of metal–metal bonds of the same metal. However, reducing the size of a metal particle to a single atom increases its surface free energy, making it easy to aggregate or Ostwald ripening. Therefore, it is necessary to anchor and strongly bond atomically dispersed metal atoms on a suitable carrier [46]. Carbon-based materials have proven to meet this need because they provide a large surface area. Metal ions can be stabilized on the carbonaceous carrier by forming ions or covalent bonds with heteroatoms (C, N, S, and P), thereby overcoming high aggregation tendency. Unique catalytic mechanisms, including electron transfer pathways or interactions with reactants, intermediaries, and products, are made possible by the singular electronic and geometric properties of the single atom (SAC). Scientific research and industrial applications have paid close attention to the unique properties and catalytic performance of atomic-level dispersion catalysts. As summarized in some excellent review articles [47, 48] the characterization of atomic-level dispersion catalysts is mainly based on some modern atomic resolution techniques, such as aberration-corrected high-angle circular dark-field scanning transmission electron microscopy (AC-HAADF-STEM). To identify scattered metal atoms on a carbon substrate, [49] X-ray absorption spectroscopy (XAS) is also useful, X-ray absorption near edge structure (XANES) provides information on the oxidation state of metal atoms, and extended X-ray absorption fine structure (EXAFS) technology provides detailed information about the coordination structure [50]. In addition, advanced theoretical modeling and simulation methods can build a reliable model for the active site to simulate the catalytic cycle [51]. The dispersed metal carbon-based electrocatalysts discussed in this chapter are typically formed of isolated atoms and carbon support materials that attach, restrict, or coordinate with isolated metal atoms.

The design and manufacture of isolated metal atoms as heterogeneous catalytically active substances can be traced back to 1995, which Thomas and colleagues reported that an oxygen-coordinated Ti SAC was used in the epoxidation reaction of cycloolefins [52]. The complex is grafted onto mesoporous silica and then calcined to synthesize. Until 2011, Zhang et al. [53] used the co-precipitation method to fix atomic Pt on the FeOx carrier and proposed the concept of single-atom catalysis for the first time. Since then, researchers' scientific interest in single atoms has increased dramatically, and atomic-level dispersed metal–carbon-based catalysts have entered a new stage of development.

In an earlier study, Jahan et al. [54] described the OER activity of Cu SAC in GO-MOF. Ding et al. [55] developed a sandwich structure in which a uniform polymer

ionic liquid (PIL) is coated on the surface of carbon nanotubes, and Co atoms are dispersed on the interface (Fig. 7.2a, b). In terms of electrochemical performance, the OER catalytic activity of CoSSPIL/CNT is significantly better than $\text{Co}_3\text{O}_4/\text{CNT}$

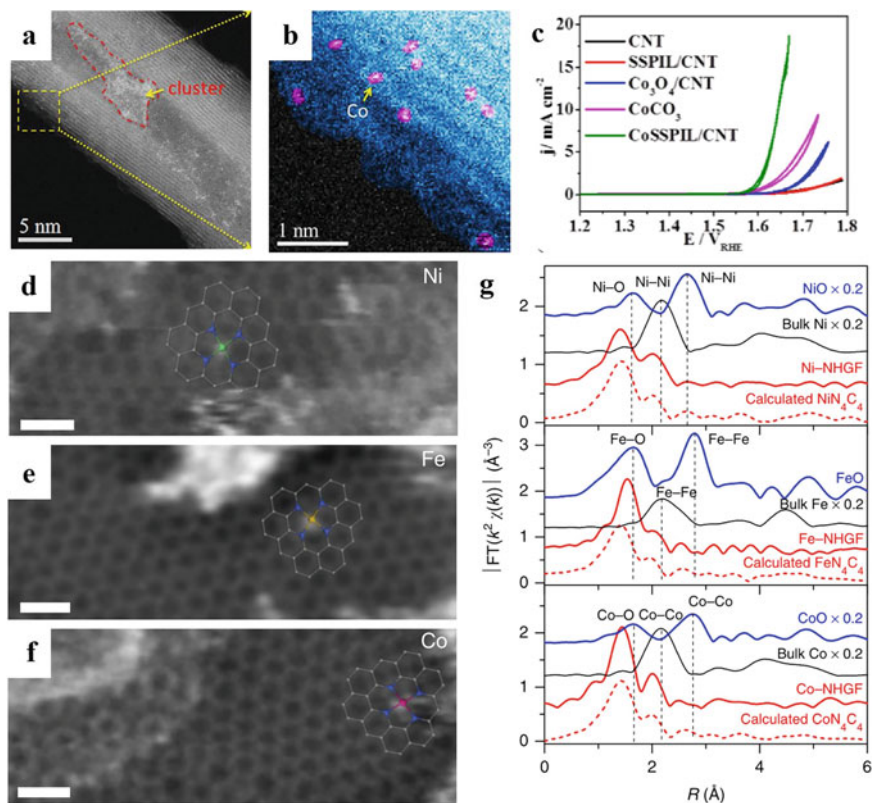


Fig. 7.2 Atomically dispersed metal carbon-based electrocatalysts for OER. **a** and **b** ADF-STEM images of the CoSSPIL/CNT. **c** CV of different samples normalized to the geometric area of the active electrode area [55]. Copyright 2017, WILEY-VCH. High-resolution TEM images enable the direct visualization of the atomic metals of **d** Ni, **e** Fe, and **f** Co embedded in the 2D graphene lattice. The overlaid schematics represent the structural models determined from XAFS analysis. Scale bars, 0.5 nm. The bright region at the top part of **d** is attributed to out-of-focus thick graphene layers or non-planar flakes. **g** Fourier transformed magnitudes of the experimental K-edge EXAFS signals of M-NHGFs along with reference samples (solid lines). The dashed lines represent calculated spectra based on a divacancy-based MN_4C_4 moiety enclosed in the graphene lattice. The Fourier transforms are not corrected for phase shift. **h** and **i** Proposed reaction scheme with the intermediates having optimized geometry of the single-site (**a**) and dual-site mechanisms (**b**) towards OER. **j** Free energy diagram at 1.23 V for OER over Fe-NHGF, Co-NHGF, and Ni-NHGF with a single-site mechanism, and Ni-NHGF with a dual-site mechanism. The highlights indicate the rate-determining step with the values of the limiting energy barrier labeled. **k** OER activity evaluated by LSV in 1 M KOH at a scan rate of 5 mV s^{-1} for NHGF, Fe-NHGF, Co-NHGF, and Ni-NHGF along with a RuO_2/C catalyst as a reference point. The data are presented with current-resistance (iR) correction [56]. Copyright 2018, Nature Publishing Group

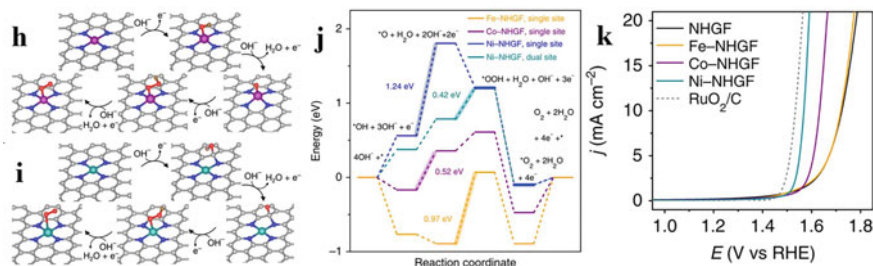


Fig. 7.2 (continued)

and CoCO_3 (Fig. 7.2c). In addition, the outstanding electronic conductivity of carbon nanotubes makes it a good carrier for OER. Subsequently, in order to identify the level of activity of different transition metals on OER, Fei et al. [56] reported a method of systematic X-ray absorption fine structure analysis and direct transmission electron microscopy imaging to identify a series of monodisperse atomic transition metals (such as Fe, Co, Ni) are embedded in nitrogen-doped porous graphene frameworks (NHGFs) (Fig. 7.2d–f). This work clearly determined their atomic structure and its correlation with the electrocatalytic activity of OER. Through in-depth analysis of EXAFS and XANES, it is proved that different M-NHGFs adopt the same MN_4C_4 group, have the same local atomic coordination configuration, and are embedded in graphene. In the crystal lattice (Fig. 7.2g). The clear structural configuration of MN_4C_4 allows the use of density functional theory (DFT) to investigate the catalytic performance of M-NHGFs on OER, indicating that the metal's catalytic activity and mechanism path are strongly dependent on the d orbital configuration. The activity trend is inversely proportional to the d orbital configuration, namely $\text{Ni-NHGF} > \text{Co-NHGF} > \text{Fe-NHGF}$ (Fig. 7.2h–j). Electrochemical tests have further confirmed this (Fig. 7.2k). Determining the atomic structure and its correlation with catalytic performance is a key step for the rational design and synthesis of noble metals or non-precious metal SACs with extremely high atom utilization and catalytic activity.

Since then, the transition metal Ni has been favored by researchers. Hou et al. [57] reported an electrocatalyst in which atom-dispersed nickel coordinated with nitrogen and sulfur in porous carbon nanosheets ($\text{SINiN}_x\text{-PC}$), which showed excellent activity and durability, even better than the commercial Ir/C . Theoretical and experimental results show that the well-dispersed SINiN_x species serves as the active site of OER. This unusual electrocatalytic activity is derived from the optimized density of states distribution of the SINiN_x center and the enhanced electron transfer capability spectrum measurement, which synergistically promotes the oxidation kinetics, according to experimental observations and theoretical calculations. Zhang et al. [58] reported a simple method to construct a hollow carbon matrix decorated with isolated nickel and N atoms (HCM@Ni-N). Combining experimental and theoretical methods revealed that effective electronic coupling through Ni–N

coordination is the key to regulating the OER mechanism. Precisely, the electronic coupling can significantly move the Fermi level downward, which may substantially impact the adsorption of the intermediate and the final OER kinetics. The new Ni-OG SACs developed by Li et al. [59] have a three-dimensional porous framework, a two-dimensional (2D) ultra-flaky structure, a single Ni atom uniformly distributed, a suitable Ni-O coordination, a significant activating effect on OER, and outstanding activity and durability.

Although some single-atom OER catalysts have been reported, [54–59] bimetallic catalysts with secondary metal introduction are generally more active than single-metal catalysts. Bai et al. [60] reported a cobalt-iron diatomic catalyst (Co-Fe-N-C), which was generated from atomically dispersed Co pre-catalyst (Co-N-C) by an in-situ electrochemical method in an iron-containing alkaline electrolyte. Compared with Co-N-C, Fe is necessary to enhance the activity of Co-Fe-N-C, and the former's activity increases with the increase of Fe content. Operando XAS data shows that Co-N-C undergoes significant structural changes after being immersed in an alkaline electrolyte, and Fe is incorporated in the electrochemical activation process to form a dimer Co-Fe structural element, which is the active site of OER. Han et al. [61] proposed a strategy for preparing heteroatom-doped bimetallic single-atom catalysts. Pyrolysis was used to create N-doped hollow carbon nanocubes (CoNi-SAs/NC) with atomically dispersed double Co-Ni sites using the dopamine-coated metal-organic framework (MOF) as a template. The atomically isolated bimetallic configuration in CoNi-SAs/NC was identified using a combination of microscopy and spectroscopy techniques. When used as an oxygen electrocatalyst in an alkaline medium, the resulting CoNi-SAs/NC hybrid material exhibits excellent catalytic performance in dual-function ORR/OER, which improves the efficiency of a realistic rechargeable zinc-air battery. According to theoretical calculations based on density functional theory, the synergistic effect of uniformly dispersed single atoms and adjacent Co-Ni bimetallic centers can optimize adsorption/desorption characteristics, reduce overall reaction barriers, and ultimately promote reversible oxygen electrocatalysis. This research provides ideas for the controlled synthesis of atomically isolated advanced materials. These research results will guide the further rational design and preparation of SACs with multiple active sites and a deep understanding of synergistic effects in energy-related catalysis applications.

7.4 Metal Nanoparticles Encapsulated Carbon-Based Electrocatalysts for OER

Transition metal (TM)-based electrocatalysts in OER face two major challenges: poor efficiency and unstable performance. It is possible to use nanoparticles made of TM encapsulated in carbon-based materials, which are stable against dissolution under operating conditions and prevent the agglomeration of small metal fragments [62]. In addition, the carbon shell's good electrical conductivity and high porosity

make it easier for electrons and electrolytes to move through the material. As a result, it is believed that the core structure of the transition metal particles influences the electronic structure of the thin carbon shell layer, thereby increasing its OER [18, 63]. The electronic effect of the metal-based core is dependent on the thickness of the graphite layer, which is worth noting. This effect will be reduced if the carbon layer is too thick. For carbon/transition metal composite catalysts, core-shell composite structure (i.e. carbon encapsulation) provides synergistic effect. Encapsulated metal nanoparticle carbon-based catalysts are discussed, as are the difficulties and opportunities currently facing this field.

Liang et al. [64] prepared a novel multilayer bent onion-like carbon nanosphere coated Co-N-C electrocatalyst (OLC/Co-N-C) by pyrolysis of surfactant P123-coated ZIF-67 precursor. With the addition of surfactant micelles, it was demonstrated that the mesoporous/microporous structure formed by the OLC/Co-N-C material during pyrolysis has a large electrochemical surface area and a high concentration of active sites. Due to the interaction of electronic and nanostructural effects, the OLC/Co-N-C catalysts exhibit superior ORR/OER performance ($E_{1/2} = 0.855$ V in 0.1 M KOH, $\eta_{10} = 344$ mV in 1.0 M KOH) and Zn-air battery performance (small charge/discharge voltage gap: 0.8 V at 2 mA cm⁻²), as well as long-term cycling stability (>100 h). Theoretical calculations explain the experimental results by demonstrating that the curvature of graphitic carbon is critical for the activity of meta-carbon atoms near graphite N and ortho/meta carbon atoms near pyridine N.

In addition to single atoms encapsulated in carbon materials, bimetallic nanoparticles embedded in carbon show similar activity enhancement. Wang et al. [65] successfully developed a simple strategy to control the synthesis of a rare hexagonally sealed (hcp) NiFe nanoparticle (NP) crystal structure encapsulated in a nitrogen-doped carbon (NC) shell (hcp-NiFe@NC). Under alkaline conditions, hcp-NiFe@NC exhibited superior OER activity than the conventional face-centered cubic (fcc) NiFe encapsulated in N-doped carbon shells (fcc-NiFe@NC). When the Fe/Ni ratio is ~5.4%, hcp-NiFe@NC exhibits excellent OER performance, and the NC coating on the NiFe surface also gives it high stability during the OER process. The results indicate that hcp-NiFe NP has good electronic properties, which accelerates the reaction on the NC surface and thus improves the catalytic activity of OER. Besides, Hao et al. [66] reported a novel method to prepare FeCo alloy nanoparticles (NPs) embedded with N, P co-doped carbon encapsulated N-doped carbon nanotubes (NPC/FeCo@NCNTs), where the NCNTs were derived from graphene oxide (GO) nanosheets and melamine. Specifically, the melamine-GO-PS-Fe-Co composites were obtained by strong complex interactions (e.g., electrostatic interactions, covalent and coordination bonds) between melamine, GO, PS (polystyrene spheres), FeCl₃, and Co(NO₃)₂. N-doped carbon nanotubes embedded with FeCo NPs (FeCo@NCNT) were generated by two-step calcination of the melamine-GO-PS-Fe-Co composites. The formation of NPC/FeCo@NCNT was achieved by calcination of FeCo@NCNT in polyphosphazenes (Fig. 7.3a, b). Interestingly, the electrocatalytic performance of NPC/FeCo@NCNT was greatly enhanced when it was used as a bifunctional catalyst for ORR and OER. In particular, the overpotential of NPC/FeCo@NCNT only needs 339.5 mV can provide a current density of

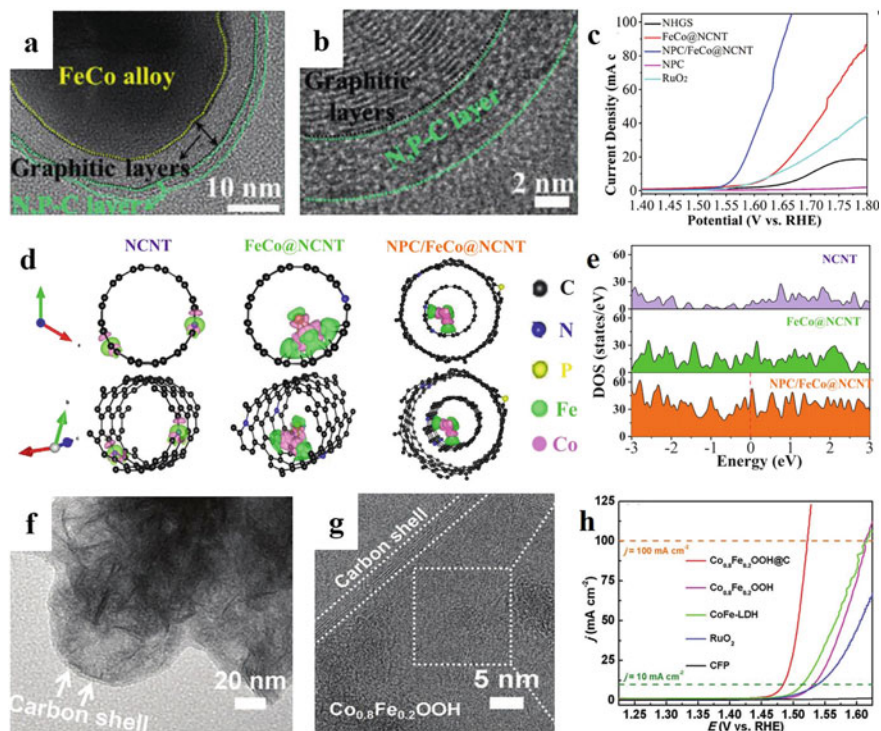


Fig. 7.3 Metal nanoparticles encapsulated carbon-based electrocatalysts for OER. **a** and **b** TEM images of NPC/FeCo@NCNT. **c** OER polarization curves of NHGS, FeCo@NCNT, NPC/FeCo@NCNT, NPC, and RuO₂ in 0.1 M KOH. **d** The optimized geometry models and **e** the calculated density of states of NCNT, FeCo@NCNT, and NPC/FeCo@NCNT [66]. Copyright 2021, WILEY-VCH. **f** TEM image and **g** HR-TEM image of the amorphorized Co_{0.8}Fe_{0.2}OOH@C nanosheets. **h** Polarization curves of Co_{0.8}Fe_{0.2}OOH@C nanosheets, Co_{0.8}Fe_{0.2}OOH, CoFe-LDH nanosheets, commercial RuO₂, and the CFP substrate at a scan rate of 5 mV s⁻¹ in 1.0 M KOH [67]. Copyright 2020, WILEY-VCH

10 mA cm⁻² for OER (Fig. 7.3c) and shows an onset potential of 0.92 V to drive ORR. More impressively, the bifunctional activity parameter (ΔE) of NPC/FeCo@NCNT is as low as 0.741 V, indicating that its bifunctional catalytic activity is better than most of the reported state-of-the-art bifunctional electrocatalysts. Three geometrical configurations, NCNT, FeCo@NCNT, and NPC/FeCo@NCNT, were constructed by density flooding theory (DFT) to simulate the occurring OER/ORR process (Fig. 7.3d). Figure 7.3e shows that all catalysts exhibit an ideal density of states, all above the Fermi energy level, indicating the high conductivity of these catalysts. The electronic states near the Fermi energy level of FeCo@NCNT are enhanced compared to those of NCNT, indicating the improved metallic character of the material. The metallic character of NPC/FeCo@NCNT can be enhanced due to the hybridization effect between the 2p state of the N atom and the adjacent C atom and the 3d state of the FeCo atom, resulting in a sharper peak near the Fermi energy level. The charge

distribution analysis shows that the coupling of FeCo clusters to NCNT can achieve direct electron transfer from FeCo to NCNT (Fig. 7.3d). The above analysis indicates that the interaction between FeCo NPs and NCNT and the presence of N and P co-doped carbon structures play an important role in the high catalytic performance of NPC/FeCo@NCNT. Han et al. [67] rationally designed and successfully synthesized efficient electrocatalysts made of amorphous $\text{Co}_{0.8}\text{Fe}_{0.2}\text{OOH}$ nanosheets encapsulated by carbon shells by using $\text{Co}_{0.8}\text{Fe}_{0.2}\text{P@C}$ nanosheets as efficient precatalysts (Fig. 7.3f, g). The conversion of cobalt-iron phosphide to the corresponding hydroxide was achieved by in situ electrochemical oxidation and deep structural reconstruction, during which phosphorus species were leached from the phosphide structure, and the residual cobalt-iron species were oxidized. Detailed structural analysis and characterization demonstrate the complete transformation from phosphorylated cobalt-iron to cobalt-iron hydroxide with a bulk phase amorphous structure. Thus, the amorphous $\text{Co}_{0.8}\text{Fe}_{0.2}\text{OOH@C}$ nanosheets have highly exposed active sites, abundant edge sites and pores, and an effective conducting framework, which synergistically achieves high oxygen precipitation activity. As a result, only low overpotentials of 254 and 292 mV are required to provide current densities of 10 and 100 mA cm^{-2} (Fig. 7.3h) with excellent stability (15 days of continuous stable operation at 100 mA cm^{-2}). However, in situ studies provide indirect evidence for structural and phase reconstruction during phosphorus leaching, and the origin of the OER active site in $\text{Co}_{0.8}\text{Fe}_{0.2}\text{OOH@C}$ nanosheets remains unclear. Therefore, theoretical and in situ/operational conditions analyses are needed as future directions to investigate the mechanism of structural reconstruction and the active catalytic sites on the $\text{Co}_{0.8}\text{Fe}_{0.2}\text{OOH}$ surface. Nevertheless, the present work opens a path for the rational design of amorphous nanomaterials to achieve efficient energy storage/conversion applications.

The activity performance of bimetallic transition metal hybrids encapsulated in carbon materials is also impressive. Cao et al. [68] reported a novel core-shell structure of a binary metal selenide hybrid electrocatalyst consisting of a selenide (cobalt, nickel) core and a nitrogen-doped carbon shell loaded on an electrochemically exfoliated graphite (EG) foil ($\text{EG}/(\text{Co}, \text{Ni})\text{Se}_2\text{-NC}$) on it. The hybrid catalysts were prepared by selenization of CoNi layered double hydroxide (CoNi-LDH)/zeolite imidazolate framework-67 (ZIF-67) nanosheet array. Due to the synergistic effect of the binary metals Co and Ni and N-doped carbon, the $\text{EG}/(\text{Co}, \text{Ni})\text{Se}_2\text{-NC}$ hybrid exhibited remarkable OER electrocatalytic performance at a current density of 10 mA cm^{-2} with a low overpotential of 258 mV and a small Tafel slope of 73.3 mV dec^{-1} , which was superior to commercial Ir/C and most reported binary cobalt selenide based materials. In situ electrochemical Raman spectroscopy combined with non-in situ X-ray photoelectron spectroscopy analysis showed that the ultra-high OER catalytic activity can be attributed to the highly active Co-OOH species and Ni elemental modification of the electron transfer process.

7.5 Metal Nanoparticles Supported Carbon-Based Electrocatalysts for OER

In addition to encapsulating metal nanoparticles in carbon-based materials, they can also be loaded onto carbon-based materials. Xu et al. [69] demonstrated that dual electrical behavior modulation on the electrocatalyst achieved enhanced electrochemical water oxidation. By hybridizing metallic Ni_3C nanoparticles with conductive carbon ($\text{Ni}_3\text{C}/\text{C}$), the intrinsic metallic properties will promote electron transport within the electrocatalyst phase and the conductive carbon carrier, thus promoting charge transport on the catalyst surface, significantly improving the OER catalytic performance compared to pure Ni_3C , NiO and NiO/C . In addition, the catalytic mechanism of $\text{Ni}_3\text{C}/\text{C}$ was investigated by XAFS characterization, HRTEM, and EELS spectroscopy; the $\text{NiOx}/\text{Ni}_3\text{C}/\text{C}$ heterostructure was shown to be an actual effective species for the OER process. Liang et al. [70] reported a hybrid material of Co_3O_4 nanocrystals grown on mild graphene oxide (Fig. 7.4a) as a high-performance bifunctional catalyst for oxygen reduction reaction (ORR) and oxygen precipitation reaction (OER). Although Co_3O_4 or graphene oxide alone has almost no catalytic activity, their hybrids exhibit unexpectedly high ORR activity, which is further enhanced by the nitrogen doping of graphene. The high activity for OER was also observed (Fig. 7.4c), making it a high-performance non-precious metal bi-functional catalyst for ORR and OER. To collect the interactions between Co_3O_4 and GO, X-ray absorption near edge structure (XANES) measurements were performed (Fig. 7.4b).

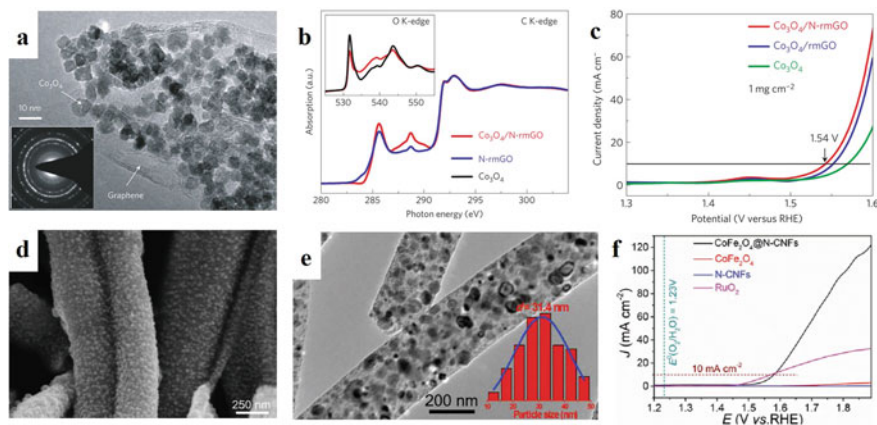


Fig. 7.4 Metal nanoparticles supported carbon-based electrocatalysts for OER. **a** TEM images of $\text{Co}_3\text{O}_4/\text{N-rmGO}$ hybrid. **b** C K-edge XANES of N-rmGO (blue curve) and $\text{Co}_3\text{O}_4/\text{N-rmGO}$ hybrid (red curve). Inset shows O K-edge XANES of Co_3O_4 (black curve) and $\text{Co}_3\text{O}_4/\text{N-rmGO}$ hybrid (red curve). **c** Oxygen evolution currents of $\text{Co}_3\text{O}_4/\text{N-rmGO}$ hybrid, $\text{Co}_3\text{O}_4/\text{rmGO}$ hybrid, and Co_3O_4 nanocrystal loaded onto Ni foam (to reach a high catalyst loading of $\sim 1 \text{ mg cm}^{-2}$) measured in 1 M KOH [70]. Copyright 2011, Nature Publishing Group. **d** and **e** The SEM and TEM images of the obtained $\text{CoFe}_2\text{O}_4/\text{N-CNFs}$. **f** LSV polarization curves of different catalysts [71]. Copyright 2017, WILEY-VCH

bond formation between CO_3O_4 and N-rmGO and changes in the chemical bonding environment of C, O, and Co atoms in the hybrid material may be responsible for the synergistic catalytic activity.

In addition to monometallic nanoparticles, polymetallic nanoparticles loaded on carbon materials are also performed strongly. Li et al. [71] demonstrated a feasible electrostatic spinning method for the simultaneous synthesis of CoFe_2O_4 nanoparticles (denoted as $\text{CoFe}_2\text{O}_4@\text{N-CNF}$) uniformly embedded in N-doped carbon nanofibers (Fig. 7.4d–e). By combining catalytically active CoFe_2O_4 nanoparticles with N-doped carbon nanofibers, the synthesized $\text{CoFe}_2\text{O}_4@\text{N-CNF}$ nanohybrids exhibited excellent OER performance compared to their single-component counterparts (pure CoFe_2O_4 and N-doped carbon nanofibers) and commercially available RuO_2 catalysts (Fig. 7.4f). The improved catalytic performance results from the unique one-dimensional structural features and the synergistic interaction between the constituents. Morales et al. [72] reported a highly active OER catalyst $\text{Fe}_{0.3}\text{Ni}_{0.7}\text{O}_x$ using oxygen-functionalized multi-walled carbon nanotubes as a carrier, which was essentially activated as a bifunctional ORR/OER catalyst by the additional addition of MnO_x . Carbon nanotube-loaded trimetallic (Mn–Ni–Fe) oxide catalysts demonstrated extremely low ORR and OER overpotentials. The combination of rare earth-rich transition metal oxides had a strong synergistic effect on catalytic activity. A four-electrode configuration cell assembly comprised an integrated two-layer bifunctional ORR/OER electrode system with each layer dedicated to ORR and OER to prevent the deactivation of ORR activity commonly observed at monolayer bifunctional ORR/OER electrodes after OER polarization was used to evaluate the suitability of the prepared catalysts for reversible ORR/OER electrocatalysis.

7.6 Conclusion and Perspective

Carbon-based OER catalysts have received intense attention in recent years because of their structural and compositional diversity, as well as their good electrocatalytic properties, which have outperformed traditional metal oxide or metal hydroxide electrodes and even noble metals, primarily under alkaline conditions. Although carbon itself does not contribute to these reactions, the high intrinsic OER activity, high possible surface area, and high electrical conductivity provided by the defective and heteroatom-doped structures result in excellent OER activity with low overpotential. The transition metals-doping can further boost carbon activity. Encasing metal or metal compound particles in thin graphite layers or nanotube structures is another strategy. The metal core's electronic effects can activate the carbon layer for OER. In general, these core–shell layer materials are more active than doped carbon (except for atomically dispersed materials).

Despite the exciting advances of carbon-based OER catalysts, there are still some challenging questions to be answered:

- (1) It is blurry for the real active sites and reaction mechanisms of various carbon-based materials. High-resolution in situ microscopy and spectroscopic techniques combined with advanced theoretical calculations (i.e., considering electrolytes and potentials) may help fully understand the role of doped elements and metal/metal compound cores.
- (2) Increasing the number of active sites is also an effective strategy to enhance OER performance. For example, the metal atom loading is very low for atomically dispersed catalysts. Increasing the metal loading while maintaining atomic dispersion is a challenging task. More advanced synthesis methods need to be developed.
- (3) To better evaluate the activity and stability of carbon-based electrocatalysts, the assessment of industrial electrolytic cell parameters is necessary. To date, almost all evaluation data are based on liquid cell test reports and may not represent the electrolytic cell's actual performance. The viability of carbon-based materials as anode and cathode catalysts should be evaluated in the industrial electrolytic cell. The results of such tests are essential to guide the future development of carbon-based electrocatalysts.
- (4) Development of in-situ characterization. Most transition metal-based catalysts undergo phase changes under OER conditions, including structure, valence state, and coordination environment. Most of the research works have used non-in situ techniques, which can only give the characterization results before and after OER measurements. However, the basic origin of the structural evolution information and self-reconstruction during OER is not fully understood. Therefore, the use of in situ techniques to detect intermediates and their adsorption/desorption behavior is essential to obtain direct experimental evidence for the proposed OER mechanism. The combination of in situ techniques, theoretical calculations, and electrochemical measurements can more effectively reveal the reaction mechanism and guide the rational design of optimized OER electrocatalysts.
- (5) Balancing the cost, stability, and universality of materials. Low cost, including synthetic feedstock and manufacturing process and robust stability, can be effectively operated in commercial facilities for several years. In addition to this, the ability to catalyze OER at a wide range of pH values, especially in acidic media and environmentally neutral electrolytes. However, so far, no OER electrocatalyst has been able to satisfy both of these advantages. Therefore, more efforts should be made in the future.

It provides some case studies for the design and development of new, efficient, low-cost, carbon based OER catalysts, and puts forward some challenges that still exist at present. This provides them with a great opportunity to surpass precious metal based OER catalysts in the clean energy and other technology markets. Continuing research and development in this exciting area will improve fuel economy and reduce the cost of producing important industrial chemicals.

References

1. M.G. Schultz, T. Diehl, G.P. Brasseur, W. Zittel, Air pollution and climate-forcing impacts of a global hydrogen economy. *Science* **302**, 624–627 (2003). <https://doi.org/10.1126/science.1089527>
2. Z. Wang, Z. Lin, P. Diao, Hybrids of iridium-cobalt phosphates as a highly efficient electrocatalyst for the oxygen evolution reaction in neutral solution. *Chem. Commun.* **55**, 3000–3003 (2019). <https://doi.org/10.1039/c8cc10278c>
3. Z. Yang, J. Zhang, M.C. Kintner-Meyer, X. Lu, D. Choi, J.P. Lemmon, J. Liu, Electrochemical energy storage for green grid. *Chem. Rev.* **111**, 3577–3613 (2011). <https://doi.org/10.1021/cr100290v>
4. N.L. Panwar, S.C. Kaushik, S. Kothari, Role of renewable energy sources in environmental protection: A review. *Renew. Sustain. Energy Rev.* **15**, 1513–1524 (2011). <https://doi.org/10.1016/j.rser.2010.11.037>
5. B. Li, M.I. Setyawati, H. Zou, J. Dong, H. Luo, N. Li, D.T. Leong, Emerging 0D transition-metal dichalcogenides for sensors, biomedicine, and clean energy. *Small* **13**, 1700527 (2017). <https://doi.org/10.1002/sml.201700527>
6. C. Le Quéré, M.R. Raupach, J.G. Canadell, G. Marland, L. Bopp, P. Ciais, T.J. Conway, S.C. Doney, R.A. Feely, P. Foster, P. Friedlingstein, K. Gurney, R.A. Houghton, J.I. House, C. Huntingford, P.E. Levy, M.R. Lomas, J. Majkut, N. Metzl, J.P. Ometto, G.P. Peters, I.C. Prentice, J.T. Randerson, S.W. Running, J.L. Sarmiento, U. Schuster, S. Sitch, T. Takahashi, N. Viovy, G.R. van der Werf, F.I. Woodward, Trends in the sources and sinks of carbon dioxide. *Nat. Geosci.* **2**, 831–836 (2009). <https://doi.org/10.1038/ngeo689>
7. W. Stedman, H. Kang, S. Lin, J.L. Kissil, M.S. Bartolomei, P.M. Lieberman, The art of splitting water. *Nature* **27**, 654–666 (2008). <https://doi.org/10.1038/451778a>
8. J. Song, Z.-F. Huang, L. Pan, K. Li, X. Zhang, L. Wang, J.-J. Zou, Review on selective hydrogenation of nitroarene by catalytic, photocatalytic and electrocatalytic reactions. *Appl. Catal. B* **227**, 386–408 (2018). <https://doi.org/10.1016/j.apcatb.2018.01.052>
9. L. Zhang, M. Zhou, A. Wang, T. Zhang, Selective hydrogenation over supported metal catalysts: from nanoparticles to single atoms. *Chem. Rev.* **120**, 683–733 (2020). <https://doi.org/10.1021/acs.chemrev.9b00230>
10. N. Ji, T. Zhang, M. Zheng, A. Wang, H. Wang, X. Wang, J.G. Chen, Direct catalytic conversion of cellulose into ethylene glycol using nickel-promoted tungsten carbide catalysts. *Angew. Chem. Int. Ed.* **47**, 8510–8513 (2008). <https://doi.org/10.1002/anie.200803233>
11. J.C. Serrano-Ruiz, R. Luque, A. Sepulveda-Escribano, Transformations of biomass-derived platform molecules: From high added-value chemicals to fuels *via* aqueous-phase processing. *Chem. Soc. Rev.* **40**, 5266–5281 (2011). <https://doi.org/10.1039/c1cs15131b>
12. S. Yang, Y. Gong, J. Zhang, L. Zhan, L. Ma, Z. Fang, R. Vajtai, X. Wang, P.M. Ajayan, Exfoliated graphitic carbon nitride nanosheets as efficient catalysts for hydrogen evolution under visible light. *Adv. Mater.* **25**, 2452–2456 (2013). <https://doi.org/10.1002/adma.201204453>
13. R. Subbaraman, D. Tripkovic, K.C. Chang, D. Strmcnik, A.P. Paulikas, P. Hirunsit, M. Chan, J. Greeley, V. Stamenkovic, N.M. Markovic, Trends in activity for the water electrolyser reactions on 3d M(Ni Co, Fe, Mn) hydr(oxy)oxide catalysts. *Nat. Mater.* **11**, 550–557 (2012). <https://doi.org/10.1038/nmat3313>
14. B.M. Hunter, H.B. Gray, A.M. Muller, Earth-abundant heterogeneous water oxidation catalysts. *Chem. Rev.* **116**, 14120–14136 (2016). <https://doi.org/10.1021/acs.chemrev.6b00398>
15. C. Spori, J.T.H. Kwan, A. Bonakdarpour, D.P. Wilkinson, P. Strasser, The stability challenges of oxygen evolving catalysts: Towards a common fundamental understanding and mitigation of catalyst degradation. *Angew. Chem. Int. Ed.* **56**, 5994–6021 (2017). <https://doi.org/10.1002/anie.201608601>
16. J. Song, C. Wei, Z. Huang, C. Liu, L. Zeng, X. Wang, Z. Xu, A review on fundamentals for designing oxygen evolution electrocatalysts. *Chem. Soc. Rev.* **49**, 2196–2214 (2020). <https://doi.org/10.1039/c9cs00607a>

17. H.-F. Wang, Q. Xu, Materials design for rechargeable metal-air batteries. *Matter* **1**, 565–595 (2019). <https://doi.org/10.1016/j.matt.2019.05.008>
18. L. Zhang, J. Xiao, H. Wang, M. Shao, Carbon-based electrocatalysts for hydrogen and oxygen evolution reactions. *ACS Catal.* **7**, 7855–7865 (2017). <https://doi.org/10.1021/acscatal.7b02718>
19. N.C.S. Selvam, L. Du, B. Xia, P.J. Yoo, B. You, Reconstructed water oxidation electrocatalysts: The impact of surface dynamics on intrinsic activities. *Adv. Func. Mater.* **31**, 2008190 (2020). <https://doi.org/10.1002/adfm.202008190>
20. N.T. Suen, S.F. Hung, Q. Quan, N. Zhang, Y.J. Xu, H.M. Chen, Electrocatalysis for the oxygen evolution reaction: recent development and future perspectives. *Chem. Soc. Rev.* **46**, 337–365 (2017). <https://doi.org/10.1039/c6cs00328a>
21. X. Rong, J. Parolin, A.M. Kolpak, A fundamental relationship between reaction mechanism and stability in metal oxide catalysts for oxygen evolution. *ACS Catal.* **6**, 1153–1158 (2016). <https://doi.org/10.1021/acscatal.5b02432>
22. D.A. Kuznetsov, M.A. Naem, P.V. Kumar, P.M. Abdala, A. Fedorov, C.R. Muller, Tailoring lattice oxygen binding in ruthenium pyrochloros to enhance oxygen evolution activity. *J. Am. Chem. Soc.* **142**, 7883–7888 (2020). <https://doi.org/10.1021/jacs.0c01135>
23. J.H. Montoya, L.C. Seitz, P. Chakthranont, A. Vojvodic, T.F. Jaramillo, J.K. Norskov, Materials for solar fuels and chemicals. *Nat. Mater.* **16**, 70–81 (2016). <https://doi.org/10.1038/nmat4778>
24. A. Damjanovic, B. Jovanovic, Anodic oxide films as barriers to charge transfer in O₂ evolution at Pt in acid solutions. *J. Electrochem. Soc.* **123**, 374–381 (1976). <https://doi.org/10.1149/1.2132828>
25. T. Binninger, R. Mohamed, K. Waltar, E. Fabbri, P. Levecque, R. Kotz, T.J. Schmidt, Thermodynamic explanation of the universal correlation between oxygen evolution activity and corrosion of oxide catalysts. *Sci. Rep.* **5**, 12167 (2015). <https://doi.org/10.1038/srep12167>
26. A. Grimaud, W. Hong, Y. Shao-Horn, J.M. Tarascon, Anionic redox processes for electrochemical devices. *Nat. Mater.* **15**, 121–126 (2016). <https://doi.org/10.1038/nmat4551>
27. B. Cao, G.M. Veith, J.C. Neuefeind, R.R. Adzic, P.G. Khalifah, Mixed close-packed cobalt molybdenum nitrides as non-noble metal electrocatalysts for the hydrogen evolution reaction. *J. Am. Chem. Soc.* **135**, 19186–19192 (2013). <https://doi.org/10.1021/ja4081056>
28. W. Zhou, J. Zhou, Y. Zhou, J. Lu, K. Zhou, L. Yang, Z. Tang, L. Li, S. Chen, N-doped carbon-wrapped cobalt nanoparticles on N-doped graphene nanosheets for high-efficiency hydrogen production. *Chem. Mater.* **27**, 2026–2032 (2015). <https://doi.org/10.1021/acs.chemmater.5b00331>
29. C. Lv, Q. Yang, Q. Huang, Z. Huang, H. Xia, C. Zhang, Phosphorus doped single wall carbon nanotubes loaded with nanoparticles of iron phosphide and iron carbide for efficient hydrogen evolution. *J. Mater. Chem. A* **4**, 13336–13343 (2016). <https://doi.org/10.1039/c6ta04329a>
30. S. Fu, C. Zhu, J. Song, M.H. Engelhard, X. Li, D. Du, Y. Lin, Highly ordered mesoporous bimetallic phosphides as efficient oxygen evolution electrocatalysts. *ACS Energy Lett.* **1**, 792–796 (2016). <https://doi.org/10.1021/acsenerylett.6b00408>
31. H. Wang, Z. Lu, S. Xu, D. Kong, J.J. Cha, G. Zheng, P.C. Hsu, K. Yan, D. Bradshaw, F.B. Prinz, Y. Cui, Electrochemical tuning of vertically aligned MoS₂ nanofilms and its application in improving hydrogen evolution reaction. *Proc. Natl. Acad. Sci.* **110**, 19701–19706 (2013). <https://doi.org/10.1073/pnas.1316792110>
32. S. Sun, Y. Sun, Y. Zhou, S. Xi, X. Ren, B. Huang, H. Liao, L.P. Wang, Y. Du, Z.J. Xu, Shifting oxygen charge towards octahedral metal: a way to promote water oxidation on cobalt spinel oxides. *Angew. Chem. Int. Ed.* **58**, 6042–6047 (2019). <https://doi.org/10.1002/anie.201902114>
33. J. Lai, A. Nsabimana, R. Luque, G. Xu, 3D porous carbonaceous electrodes for electrocatalytic applications. *Joule* **2**, 76–93 (2018). <https://doi.org/10.1016/j.joule.2017.10.005>
34. W. Xiao, J. Zhu, L. Han, S. Liu, J. Wang, Z. Wu, W. Lei, C. Xuan, H.L. Xin, D. Wang, Pt skin on Pd-Co-Zn/C ternary nanoparticles with enhanced Pt efficiency toward ORR. *Nanoscale* **8**, 14793–14802 (2016). <https://doi.org/10.1039/c6nr03944h>
35. Y. Zhao, R. Nakamura, K. Kamiya, S. Nakanishi, K. Hashimoto, Nitrogen-doped carbon nano-materials as non-metal electrocatalysts for water oxidation. *Nat. Commun.* **4**, 2390 (2013). <https://doi.org/10.1038/ncomms3390>

36. L. Yang, S. Jiang, Y. Zhao, L. Zhu, S. Chen, X. Wang, Q. Wu, J. Ma, Y. Ma, Z. Hu, Boron-doped carbon nanotubes as metal-free electrocatalysts for the oxygen reduction reaction. *Angew. Chem. Int. Ed.* **50**, 7132–7135 (2011). <https://doi.org/10.1002/anie.201101287>
37. B. Lu, J. Du, T. Sheng, N. Tian, J. Xiao, L. Liu, B. Xu, Z. Zhou, S. Sun, Hydrogen adsorption-mediated synthesis of concave Pt nanocubes and their enhanced electrocatalytic activity. *Nanoscale* **8**, 11559–11564 (2016). <https://doi.org/10.1039/c6nr02349e>
38. Z. Liu, F. Peng, H. Wang, H. Yu, W. Zheng, J. Yang, Phosphorus-doped graphite layers with high electrocatalytic activity for the O₂ reduction in an alkaline medium. *Angew. Chem. Int. Ed.* **50**, 3257–3261 (2011). <https://doi.org/10.1002/anie.201006768>
39. J. Zhang, L. Dai, Nitrogen, phosphorus, and fluorine tri-doped graphene as a multifunctional catalyst for self-powered electrochemical water splitting. *Angew. Chem. Int. Ed.* **55**, 13296–13300 (2016). <https://doi.org/10.1002/anie.201607405>
40. K. Gong, F. Du, Z. Xia, M. Durstock, L. Dai, Nitrogen-doped carbon nanotube arrays with high electrocatalytic activity for oxygen reduction. *Science* **323**, 760–764 (2009). <https://doi.org/10.1126/science.1168049>
41. J. Shui, M. Wang, F. Du, L. Dai, N-doped carbon nanomaterials are durable catalysts for oxygen reduction reaction in acidic fuel cells. *Sci. Adv.* **1**, e1400129 (2015). <https://doi.org/10.1126/sciadv.1400129>
42. J. Zhang, Z. Zhao, Z. Xia, L. Dai, A metal-free bifunctional electrocatalyst for oxygen reduction and oxygen evolution reactions. *Nat. Nanotechnol.* **10**, 444–452 (2015). <https://doi.org/10.1038/nnano.2015.48>
43. Y. Zhu, Y. Jing, A. Vasileff, T. Heine, S. Qiao, 3D synergistically active carbon nanofibers for improved oxygen evolution. *Adv. Energy Mater.* **7**, 1602928 (2017). <https://doi.org/10.1002/aenm.201602928>
44. H. Jiang, J. Gu, X. Zheng, M. Liu, X. Qiu, L. Wang, W. Li, Z. Chen, X. Ji, J. Li, Defect-rich and ultrathin N doped carbon nanosheets as advanced trifunctional metal-free electrocatalysts for the ORR, OER and HER. *Energy and Environmental Sciences* **12**, 322–333 (2019). <https://doi.org/10.1039/c8ee03276a>
45. C. Gao, J. Low, R. Long, T. Kong, J. Zhu, Y. Xiong, Heterogeneous single-atom photocatalysts: fundamentals and applications. *Chem. Rev.* **120**, 12175–12216 (2020). <https://doi.org/10.1021/acs.chemrev.9b00840>
46. J. Cordon, G. Jimenez-Oses, J.M. Lopez-de-Luzuriaga, M. Monge, The key role of Au-substrate interactions in catalytic gold subnanoclusters. *Nat. Commun.* **8**, 1657 (2017). <https://doi.org/10.1038/s41467-017-01675-1>
47. J. Guo, J. Huo, Y. Liu, W. Wu, Y. Wang, M. Wu, H. Liu, G. Wang, Nitrogen-doped porous carbon supported nonprecious metal single-atom electrocatalysts: From synthesis to application. *Small Methods* **3**, 1900159 (2019). <https://doi.org/10.1002/smt.201900159>
48. Y. Chen, S. Ji, C. Chen, Q. Peng, D. Wang, Y. Li, Single-atom catalysts: Synthetic strategies and electrochemical applications. *Joule* **2**, 1242–1264 (2018). <https://doi.org/10.1016/j.joule.2018.06.019>
49. J. Hong, C. Jin, J. Yuan, Z. Zhang, Atomic defects in two-dimensional materials: From single-atom spectroscopy to functionalities in opto-/electronics, nanomagnetism, and catalysis. *Adv. Mater.* **29**, 1606434 (2017). <https://doi.org/10.1002/adma.201606434>
50. B. Li, C. Zhao, S. Chen, J. Liu, X. Chen, L. Song, Q. Zhang, Framework-porphyrin-derived single-atom bifunctional oxygen electrocatalysts and their applications in Zn-air batteries. *Adv. Mater.* **31**, e1900592 (2019). <https://doi.org/10.1002/adma.201900592>
51. L. Cao, Q. Luo, W. Liu, Y. Lin, X. Liu, Y. Cao, W. Zhang, Y. Wu, J. Yang, T. Yao, S. Wei, Identification of single-atom active sites in carbon-based cobalt catalysts during electrocatalytic hydrogen evolution. *Nat. Catal.* **2**, 134–141 (2018). <https://doi.org/10.1038/s41929-018-0203-5>
52. T. Maschmeyer, F. Rey, G. Sankar, J.M. Thomas, Heterogeneous catalysts obtained by grafting metallocene complexes onto mesoporous silica. *Nature* **378**, 159–162 (1995). <https://doi.org/10.1038/378159a0>
53. B. Qiao, A. Wang, X. Yang, L.F. Allard, Z. Jiang, Y. Cui, J. Liu, J. Li, T. Zhang, Single-atom catalysis of CO oxidation using Pt₁/FeO_x. *Nat. Chem.* **3**, 634–641 (2011). <https://doi.org/10.1038/nchem.1095>

54. M. Jahan, Z. Liu, K.P. Loh, A graphene oxide and copper-centered metal organic framework composite as a tri-functional catalyst for HER OER, and ORR. *Adv. Funct. Mater.* **23**, 5363–5372 (2013). <https://doi.org/10.1002/adfm.201300510>
55. Y. Ding, A. Klyushin, X. Huang, T. Jones, D. Teschner, F. Girgsdies, T. Rodenas, R. Schlogl, S. Heumann, Cobalt-bridged ionic liquid polymer on a carbon nanotube for enhanced oxygen evolution reaction activity. *Angew. Chem. Int. Ed.* **57**, 3514–3518 (2018). <https://doi.org/10.1002/anie.201711688>
56. H. Fei, J. Dong, Y. Feng, C.S. Allen, C. Wan, B. Voloskiy, M. Li, Z. Zhao, Y. Wang, H. Sun, P. An, W. Chen, Z. Guo, C. Lee, D. Chen, I. Shakir, M. Liu, T. Hu, Y. Li, A.I. Kirkland, X. Duan, Y. Huang, General synthesis and definitive structural identification of MN_4C_4 single-atom catalysts with tunable electrocatalytic activities. *Nat. Catal.* **1**, 63–72 (2018). <https://doi.org/10.1038/s41929-017-0008-y>
57. Y. Hou, M. Qiu, M.G. Kim, P. Liu, G. Nam, T. Zhang, X. Zhuang, B. Yang, J. Cho, M. Chen, C. Yuan, L. Lei, X. Feng, Atomically dispersed nickel-nitrogen-sulfur species anchored on porous carbon nanosheets for efficient water oxidation. *Nat. Commun.* **10**, 1392 (2019). <https://doi.org/10.1038/s41467-019-09394-5>
58. H. Zhang, Y. Liu, T. Chen, J. Zhang, J. Zhang, X.W.D. Lou, Unveiling the activity origin of electrocatalytic oxygen evolution over isolated Ni atoms supported on a N-doped carbon matrix. *Adv. Mater.* **31**, e1904548 (2019). <https://doi.org/10.1002/adma.201904548>
59. Y. Li, Z. Wu, P. Lu, X. Wang, W. Liu, Z. Liu, J. Ma, W. Ren, Z. Jiang, X. Bao, High-valence nickel single-atom catalysts coordinated to oxygen sites for extraordinarily activating oxygen evolution reaction. *Adv. Sci.* **7**, 1903089 (2020). <https://doi.org/10.1002/advs.201903089>
60. L. Bai, C.S. Hsu, D.T.L. Alexander, H.M. Chen, X. Hu, A cobalt-iron double-atom catalyst for the oxygen evolution reaction. *J. Am. Chem. Soc.* **141**, 14190–14199 (2019). <https://doi.org/10.1021/jacs.9b05268>
61. X. Han, X. Ling, D. Yu, D. Xie, L. Li, S. Peng, C. Zhong, N. Zhao, Y. Deng, W. Hu, Atomically dispersed binary Co-Ni sites in nitrogen-doped hollow carbon nanocubes for reversible oxygen reduction and evolution. *Adv. Mater.* **31**, e1905622 (2019). <https://doi.org/10.1002/adma.201905622>
62. W. Zhou, T. Xiong, C. Shi, J. Zhou, K. Zhou, N. Zhu, L. Li, Z. Tang, S. Chen, Bioreduction of precious metals by microorganism: efficient gold@N-doped carbon electrocatalysts for the hydrogen evolution reaction. *Angew. Chem. Int. Ed.* **55**, 8416–8420 (2016). <https://doi.org/10.1002/anie.201602627>
63. Y. Xu, W. Tu, B. Zhang, S. Yin, Y. Huang, M. Kraft, R. Xu, Nickel nanoparticles encapsulated in few-layer nitrogen-doped graphene derived from metal-organic frameworks as efficient bifunctional electrocatalysts for overall water splitting. *Adv. Mater.* **29**. <https://doi.org/10.1002/adma.201605957>
64. Z. Liang, N. Kong, C. Yang, W. Zhang, H. Zheng, H. Lin, R. Cao, Highly curved nanostructure-coated Co, N-doped carbon materials for oxygen electrocatalysis. *Angew. Chem. Int. Ed.* **60**, 12759–12764 (2021). <https://doi.org/10.1002/anie.202101562>
65. T. Wang, J. Liang, Z. Zhao, S. Li, G. Lu, Z. Xia, C. Wang, J. Luo, J. Han, C. Ma, Y. Huang, Q. Li, Sub-6 nm fully ordered L_{10} -Pt-Ni-Co nanoparticles enhance oxygen reduction via Co doping induced ferromagnetism enhancement and optimized surface strain. *Adv. Energy Mater.* **9**, 1803771 (2019). <https://doi.org/10.1002/aenm.201803771>
66. X. Hao, Z. Jiang, B. Zhang, X. Tian, C. Song, L. Wang, T. Maiyalagan, X. Hao, Z.J. Jiang, N-doped carbon nanotubes derived from graphene oxide with embedment of FeCo nanoparticles as bifunctional air electrode for rechargeable liquid and flexible all-solid-state zinc-air batteries. *Adv. Sci.* **8**, 2004572 (2021). <https://doi.org/10.1002/advs.202004572>
67. X. Han, C. Yu, Y. Niu, Z. Wang, Y. Kang, Y. Ren, H. Wang, H.S. Park, J. Qiu, Full bulk-structure reconstruction into amorphized cobalt-iron oxyhydroxide nanosheet electrocatalysts for greatly improved electrocatalytic activity. *Small Methods* **4**, 2000546 (2020). <https://doi.org/10.1002/smt.202000546>
68. J. Cao, K. Wang, J. Chen, C. Lei, B. Yang, Z. Li, L. Lei, Y. Hou, K. Ostrikov, Nitrogen-doped carbon-encased bimetallic selenide for high-performance water electrolysis. *Nano-Micro Lett.* **11**, 67 (2019). <https://doi.org/10.1007/s40820-019-0299-4>

69. K. Xu, H. Ding, H. Lv, P. Chen, X. Lu, H. Cheng, T. Zhou, S. Liu, X. Wu, C. Wu, Y. Xie, Dual electrical-behavior regulation on electrocatalysts realizing enhanced electrochemical water oxidation. *Adv. Mater.* **28**, 3326–3332 (2016). <https://doi.org/10.1002/adma.201505732>
70. Y. Liang, Y. Li, H. Wang, J. Zhou, J. Wang, T. Regier, H. Dai, Co_3O_4 nanocrystals on graphene as a synergistic catalyst for oxygen reduction reaction. *Nat. Mater.* **10**, 780–786 (2011). <https://doi.org/10.1038/nmat3087>
71. T. Li, Y. Lv, J. Su, Y. Wang, Q. Yang, Y. Zhang, J. Zhou, L. Xu, D. Sun, Y. Tang, Anchoring CoFe_2O_4 nanoparticles on N-doped carbon nanofibers for high-performance oxygen evolution reaction. *Adv. Sci.* **4**, 1700226 (2017). <https://doi.org/10.1002/advs.201700226>
72. D.M. Morales, M.A. Kazakova, S. Dieckhöfer, A.G. Selyutin, G.V. Golubtsov, W. Schuhmann, J. Masa, Trimetallic Mn-Fe-Ni oxide nanoparticles supported on multi-walled carbon nanotubes as high-performance bifunctional ORR/OER electrocatalyst in alkaline media. *Adv. Func. Mater.* **30**, 1905992 (2019). <https://doi.org/10.1002/adfm.201905992>

Chapter 8

Carbon-Based Nanomaterials for Carbon Dioxide Reduction Reaction



Dongping Xue and Yifan Wei

Abstract Electrochemical reduction of CO₂ with renewable electricity has attracted much attention for producing fuels and value-added chemicals while reducing carbon emissions. Carbon-based nanomaterials are of particular interest due to their earth abundance and low cost. In this chapter, the latest progress and research status of four types of nanomaterials in electrocatalytic carbon dioxide reduction reaction (CO₂RR) have been discussed in detail, including metal-free carbon-based, atomically dispersed carbon-based, metal nanoparticles encapsulated carbon-based, and metal nanoparticles supported carbon-based nanomaterials. Finally, the challenges and opportunities faced by carbon-based nanomaterials in electrochemical CO₂RR have been proposed, as well as possible solutions in the future.

8.1 Introduction

Due to the continuous growth of human society's demand for energy, the consumption of non-renewable fossil fuels has increased dramatically, releasing a large amount of greenhouse gas carbon dioxide (CO₂). As of 2020, the concentration of CO₂ in the atmosphere has exceeded 414 ppm and continues to increase, causing environmental problems such as global warming and ocean acidification, which have attracted widespread attention [1]. In addition, there is an urgent need to explore technologies that can address both carbon emissions and the energy crisis, guided by the national strategy of "emission peak and carbon neutrality". In the past few decades, various technologies such as biochemical, electronic, photochemical, radiochemical, and thermochemical have been developed to reduce CO₂ [2–5]. Among them, electrocatalytic CO₂RR technology, with its simple experimental equipment, mild reaction conditions, and the use of renewable energy to provide electricity, is

D. Xue (✉) · Y. Wei
College of Materials Science and Engineering, Zhengzhou University, Zhengzhou 450001,
P. R. China
e-mail: xdongping1231@126.com

Y. Wei
e-mail: Ivan98cn@163.com

an effective way to achieve relatively “zero-emission” of CO₂ and store renewable energy [6–8]. In addition, electrocatalytic CO₂RR technology can utilize solar energy, wind energy, tidal energy, and other renewable energy sources to effectively reduce CO₂ into important fuels and chemical raw materials, such as formate/formic acid (HCOO⁻/HCOOH), carbon monoxide (CO), methane (CH₄), methanol (CH₃OH), ethylene (C₂H₄), and ethanol (C₂H₅OH). Such chemicals will be needed for a long time in the future, however, the current preparation methods are not only dominated by carbon-intensive fossil fuel methods, but also under harsh preparation conditions (Fig. 8.1) [9]. Therefore, utilizing electrocatalytic CO₂RR technology to make carbon chemicals may be a more sustainable alternative to this difficult-to-decarbonize approach.

Linear CO₂ molecules are relatively thermodynamically stable and chemically inert, reducing the kinetics of the reduction reaction, while the electrocatalytic reduction conversion efficiency is closely related to the slow kinetics of the rate-determining step [10]. Moreover, the selectivity of these catalysts remains low due to complicated reaction mechanisms [11]. In this regard, developing durable and highly efficient electrocatalysts is of vital importance to accelerate the reaction kinetics and thus improve the overall energy conversion efficiency. At present, the selection of electrocatalysts is mainly focused on precious metals such as Pt and Au [12]. However, the high cost, poor long-term stability, and low natural reserves of noble metal electrocatalysts hinder their commercialization. Carbon-based nanomaterials have become one of the main effective materials to replace noble metal catalysts due to the advantages of wide source of raw materials, controllable structure, good chemical stability, and electrical conductivity [13, 14]. Despite these advantages,

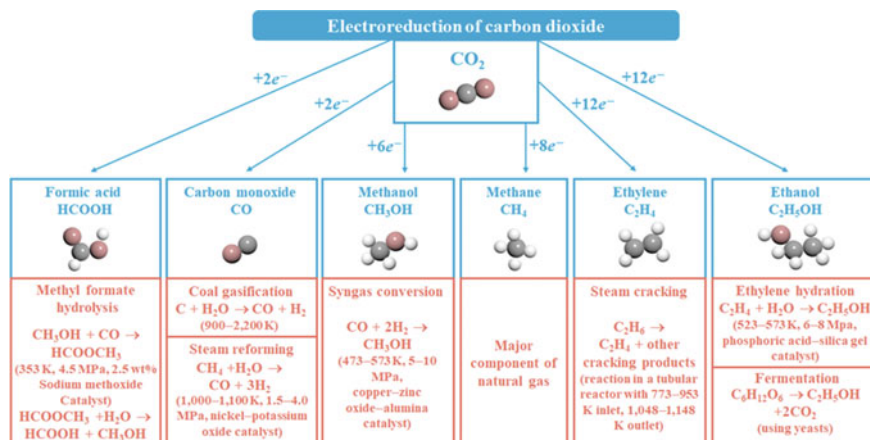


Fig. 8.1 Overview of select CO₂ electroreduction products, along with the current industrial methods to manufacture these products. The current large-scale methods to manufacture HCOOH, CO, CH₃OH, CH₄, C₂H₄, and C₂H₅OH are primarily fossil fuel based and, in most scenarios, require high pressure and/or high temperature to drive the process. The electroreduction of CO₂ could be an alternative sustainable pathway to such fossil fuel-based manufacturing methods

there is still a large gap between the electrocatalytic performance of pure carbon nanomaterials and precious metals.

After Dai's pioneering work on nitrogen-doped carbon nanotubes was published in 2009, high-performance CBN containing various defects have attracted the interest of many researchers [15]. The introduction of defects can affect the overall charge state of the carbon skeleton, thereby increasing the density and activity of potential active sites and improving the overall electrocatalytic performance of carbon nanomaterials [16, 17]. For example, edge and topological defects have been studied extensively in electrocatalytic reactions such as HER and oxygen reduction reaction (ORR) because of their different electrochemical and thermodynamic properties from the matrix material [18, 19]. Their potential for electrocatalytic CO₂ reduction has only recently been recognized. In addition, the doping of heteroatoms (N, B, P, etc.) [20] and the introduction of single metal atoms (Ni, Mn, and Cu, etc.) [21–23] can also effectively improve the performance of electrocatalytic CO₂ reduction. However, a major problem of nonprecious metal catalysts is their poor stability in practical catalytic processes, especially in harsh environments (e.g., strong acidity or alkalinity, high temperature, and high overpotential). Recently, to overcome the low stability of nonprecious metal catalysts under harsh reaction conditions, Bao et al. designed and fabricated unique chainmail catalysts by fully encapsulating transition metals through graphene shells, which can effectively improve the activity and stability of nonprecious-metal catalysts [24, 25]. Strong metal-support interaction (SMSI), commonly happening between metal and metal oxide support, has drawn significant attention in heterogeneous catalysis due to its capability of enhancing the activity and stability of catalysts. Herein, the strong interaction between metal oxide and carbon supports is discovered to significantly boost the performance for electrocatalytic CO₂ reduction reaction (CO₂RR) [26].

In this chapter, a systematic overview of the latest developments and structure-effect relationships in the electrocatalytic reduction of CO₂ from four classes of materials (metal-free carbon-based electrocatalysts, atomically dispersed metal carbon-based electrocatalysts, metal nanoparticles encapsulated/supported carbon-based electrocatalysts) have been presented. It is hoped that this chapter will provide a reference for researchers interested in CO₂ electrocatalytic reduction, to solve the technical bottlenecks from the aspect of catalytic materials and realize the industrialization of CO₂ electrocatalytic reduction in the near future.

Before conducting a detailed summary analysis of a certain class of materials, the commonly used evaluation parameters for electrocatalytic CO₂RR for the convenience of readers have been briefly summarized. The key performance parameters used to evaluate the activity, selectivity, and stability of electrocatalysts for CO₂RR are mainly overpotential, Faraday efficiency, Tafel slope, and energy efficiency.

- (1) Overpotential. Overpotential is the difference between working potential and theoretical potential, which reflects the driving force of ECR.
- (2) Energetic efficiency (EE). EE represents the overall energy utilization rate forming the target product.

- (3) Faradaic Efficiency (FE). FE represents the percentage of the charge consumed by the reaction to form the target product over the total charge transferred during the reaction. It can be calculated by Eq. (8.1):

$$FE = \frac{\alpha n F}{Q} \quad (8.1)$$

where α is the number of electrons transferred per molecule of the target product (e.g., $\alpha = 2$ for reduction of CO_2 to CO), n is the number of moles of the target product made by the reaction, F is the Faraday constant (96485 C mol^{-1}), and Q represents the charge passed during the entire reaction. The FE directly reflects the selectivity of the catalyst for ECR.

- (4) Tafel slope. The Tafel slope indicates the relationship between the overpotential and the logarithm of the current density, where the current density is obtained by dividing the total current by the geometric surface area of the working electrode. It is generally believed that the smaller the Tafel slope, the better the catalytic performance of the electrocatalyst.

8.2 Metal-Free Carbon-Based Electrocatalysts for CO_2RR

With the deepening of research, it has been found that the catalytic activity of undoped carbon nanomaterials can also be greatly improved by rationally regulating the intrinsic carbon defects within the carbon framework. Intrinsic carbon defects are formed by thermal vibrations of lattice atoms in the absence of any dopants, mainly including edges, vacancies, holes or topological defects [14, 27]. Among them, the intrinsic carbon defects used in ECR are mainly edge and topological defects. The main effects on the electrocatalytic CO_2RR catalysts are as follows: (1) Edge defects, which make the material edge full of a large number of unpaired π electrons, can effectively accelerate the transfer of electrons and reduce the formation energy of key intermediates. At the same time, the edge carbon atoms show higher charge density and can be used as active sites [27]. (2) Topological defects, the introduction of topological defects will interfere with the electronic symmetry of aromatic rings, causing local charge redistribution, and the adjacent carbon atoms can be optimized to become the active sites of the electrocatalyst [28–30]. Exploring the preparation of defective sites with suitable CO_2 activation/adsorption energies is an effective way to design high-performance CO_2RR catalysts. Thus, Wu et al. [31] prepared a defect-rich hierarchical porous carbon catalyst (DHPC) by pyrolysis of ZnO NP@ZIF-8 with the help of KNO_3 and ZnO nanoparticles (ZnO NPs), which acted as oxygen suppliers and carbon modifiers to facilitate carbon deficient site/Lewis base site generation (Fig. 8.2a, b). The mesoporous and carbon defect structure in DHPC improved its adsorption and activation efficiently for CO_2 . FE_{CO} can reach 99.5% at -0.5 V versus reversible hydrogen electrode (*vs.* RHE) in 0.5 M KHCO_3 medium. More importantly, such carbon material is useful even in a real

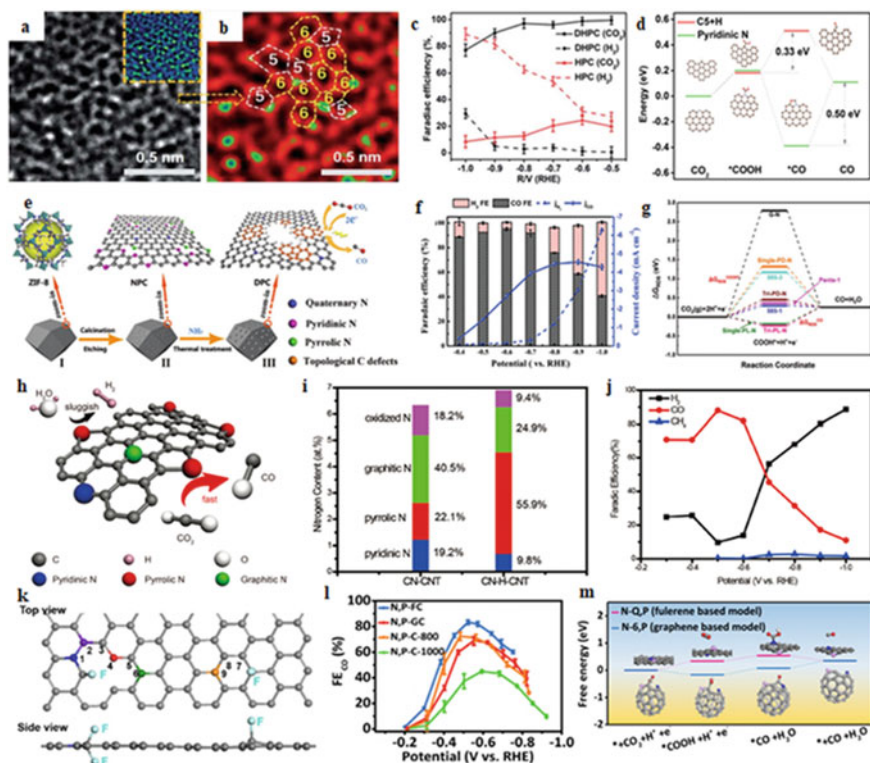


Fig. 8.2 Metal-free carbon-based electrocatalysts. Magnification of one segment of the HRTEM image **a** and **b** after fast Fourier transformation (FFT) filtering. **c** Faradaic efficiencies of DHPC and HPC in 0.5 M KHCO_3 at various potentials. **d** Free energy diagram for CO_2 reduction to CO over different defect sites. Reproduced with permission [31]. [32][43][45][46] Copyright 2020, Royal Society of Chemistry. **e** CO_2 electrochemical reduction capability of CN-H-CNTs and passivation for HER reaction. Summary of N atomic contents and total atomic concentrations in **f** CN-CNTs. Faradaic efficiency for CO , H_2 , and CH_4 versus potential on **g** CN-H-CNTs. Reproduced with permission. Copyright 2019, John Wiley and Sons. **h** Top view and side view of DFT model for FC. Gray atom: carbon, light blue atom: fluorine, other colorful atoms: carbon that calculated as active sites. **i** The FE_{CO} for various catalysts. **j** Free energy diagram of ECR reaction to CO on various catalysts. Reproduced with permission. Copyright 2017, John Wiley and Sons. **k** Top view and side view of DFT model for FC. Reproduced with permission. Copyright 2018, John Wiley and Sons. **l** FE for CO production at different applied potentials. **m** Free energy pathway of CO_2RR on N-Q,P and N-6,P. Reproduced with permission. Copyright 2019, Royal Society of Chemistry

sea-water medium with high CO faradaic efficiency as well (96.5% at -0.6 V) (Fig. 8.2c). According to the characterization test and theoretical calculation results, pentagon defects are proved to be electrocatalytic active centers, which can lead to local electron density redistribution, and have stronger adsorption on reactants and intermediates (Fig. 8.2d). Zhang et al. [32] reported a positive correlation between the electrocatalytic CO_2RR performance of carbon-based catalysts and the content

of intrinsic carbon defects within the catalysts. They synthesized a series of defective N-doped carbon spheres, it is demonstrated that the defective porous carbon catalyst without active heteroatom doping also exhibits good catalytic performance for electrocatalytic CO₂RR (Fig. 8.2e, f). The NEXAFS spectra show that the defects of sp^2 (octagonal and pentagonal) rather than the edges of sp^3 (armchair and zigzag) are positively related to the ECR activity of the defective porous carbon catalysts, and as the pyrolysis temperature increases, the more defects, the better the activity and selectivity of the catalyst. This conclusion is also verified by DFT calculation, for perfect sp^2 carbons, the free energies required for the formation of COOH* for armchair and zigzag edge defects increase significantly, while the free energy required for pentagonal defects decreases significantly (Fig. 8.2g). For the octagonal defect, due to the optimization of COOH* adsorption, part of the positive C atoms facilitates the conduction of electrons, which further promotes the reduction of COOH* to CO*. Although defect-based carbon materials exhibit a great potential in the diversity of electrocatalyst structural design. However, due to the difficulty of introducing a large number of specific types of defects, the structure-performance relationship between defective carbons and CO₂RR electrocatalysis has not been fully established.

Besides intrinsic defective carbon-based catalysts, heteroatom-doped carbon-based catalysts are another very important class of metal-free carbon-based electrocatalysts. Heteroatom doping with different electronegativity into the carbon network will introduce asymmetric charge, redistribute the spin density, break the electrical neutrality of carbon matrix, optimize the electronic properties of carbon materials to induce the generation of charged active sites [29, 33, 34]. In addition, the doping of heteroatoms can also stimulate the adjacent carbon atoms to improve the conductivity of carbon materials, thus enhancing the overall electrocatalytic activity of carbon materials [35]. The heteroatoms incorporated into carbon-based materials to enhance catalytic performance are generally B, [36] N, [37] O, [38] F, [39] P, [40] and S [41]. Among them, N atom is the most commonly used doped heteroatom because of its smaller atomic radius and larger electronegativity than carbon atom. N-doping in carbon nanomaterials generally forms four kinds of N-containing configurations including pyridinic, pyrrolic, graphitic, and oxidized N [42]. Most studies consider pyridinic-N as the primary active site for CO₂RR among the four N-containing configurations although different views are present. It is proposed that pyridinic-N can significantly enhance the binding of CO₂ or key intermediates as compared to graphitic-N or pyrrolic-N because of its accessible lone pair electrons. Zheng et al. [43] developed a unique vapor-etching method for tuning the configuration of nitrogen dopants in carbon frameworks. Selective etching takes advantage of the fact that H₂O molecules prefer to bond with carbon atoms around graphitic-N and pyridinic-N. After vapor etching, pyrrolic-N atoms with low water affinity are retained as the dominant N type in the obtained N-doped carbon network (designed as CN-H-CNT) (Fig. 8.2h) with a much increased content from 22.1 to 55.9 at % among the total N species (Fig. 8.2i). This steam-etched CN-H-CNT catalyst enables an excellent CO₂ reduction catalytic activity and HER suppression, with a high CO₂RR selectivity (~88%) toward the formation of CO under -0.5 V versus RHE. (Fig. 8.2j). The above work provides a new strategy for tuning the intrinsic

configuration of N-doped carbon and developing efficient and stable carbon cycle catalysts. On the other hand, doping F into the carbon lattice is different from N doping (replacement of carbon atoms in the lattice), which forms C-F bonds with covalent, ionic or semi-ionic properties [44]. Since F has the greatest electronegativity, the bonded carbon atoms will have more positive charges and become the active sites for electrocatalytic CO₂RR, which will be more favorable for the electrocatalytic CO₂RR [39]. Xie et al. [45] synthesized a F-doped carbon (FC) catalyst by simply pyrolyzing a mixture of commercial BP 2000 and polytetrafluoroethylene (PTFE) as a fluorine source (Fig. 8.2k). The FE of this catalyst electrocatalytic CO₂RR to CO reaches a maximum value (90%) at a lower overpotential (-0.51 V vs. RHE). Both experiments DFT calculations demonstrate that the key role of F doping in promoting the reduction of CO₂ to CO on metal-free carbon catalysts should have three functions: (1) Introduce a positive charge density between adjacent defect carbon atoms; (2) Introduce asymmetric spin density into adjacent defect carbon atoms; through these effects, carbon atoms become highly active and bind more strongly to COOH*, thereby increasing the reaction rate at lower overpotentials; (3) The Gibbs free energy of adsorbed H* is increased, resulting in the inhibition of the competitive hydrogen evolution reaction (HER) on the FC. In this regard, enhanced reduction of CO₂ to CO can be achieved over FC catalysts.

The diatomic co-doping may bring about the catalytic activity that the single heteroatom doped carbon material does not have because of the synergistic effect. Zhang et al. [46] prepared N,P-coordinated fullerene-like carbon (N,P-FC) and N,P-coordinated graphite-like carbon (N,P-FC) by soft-template pyrolysis method for electrocatalytic CO₂RR performance test. Different pyrolysis temperatures make the samples have different P/N atomic ratios, and the catalytic activity of the samples increases with the increase of the P/N atomic ratio. The N,P-FC obtained by pyrolysis at 900 °C has the best electrocatalytic CO₂RR activity (Fig. 8.2l). At the same time, it is found and confirmed by DFT that fullerene structure is more beneficial to electrocatalytic CO₂RR than graphene structure (Fig. 8.2m). Consequently, the above studies provide guidance and reference for designing and synthesizing high efficiency, high selectivity, and low cost heteroatom-doped carbon materials to replace metal catalysts for efficient electrocatalytic CO₂RR.

The co-doping of two different elements in carbon materials provides a new opportunity for the application of electrocatalysts. By properly adjusting the precursor, dopant type, doping ratio, and spatial distribution configuration, the electrocatalytic CO₂RR performance of the carbon-based catalyst is optimized.

8.3 Atomically Dispersed Metal Carbon-Based Electrocatalysts for CO₂RR

In recent years, atomically dispersed metal carbon-based nanomaterials have become popular and effective electrocatalysts for improving the performance of electrocatalytic CO₂RR due to their near 100% atomic utilization and excellent catalytic performance [47, 48]. Among them, the main reasons for the excellent electrocatalytic CO₂ reduction performance of metal-N-C catalysts are as follows. (1) Metal atoms directly combine with C-N atoms in carbon network to form metal activity centers with dispersed atoms [49]. (2) The size effect of single metal atoms gives carbon-based nanomaterials unique electronic structural characteristics and high specific surface area [50]. (3) The introduction of metal atoms changes the coordination environment of surface atoms, reduces the coordination number of surface atoms, decreases the overpotential of the catalyst, increases the current density of the catalyst, and reduces the Gibbs free energy of the formation of key intermediates and the desorption energy of the final product in ECR reaction [51]. M-N-C catalyst has been widely used in the study of ORR for decades, but were used to study electrocatalytic CO₂RR was for the first time proposed by Strasser et al. [52] in 2015 that Fe-N-C, Mn-N-C, and Fe, Mn-N-C have high electrocatalytic CO₂RR performance. The metals used to form M-N-C catalysts are mainly transition metals and individual precious metals such as Fe, Co, Ni, Cu, and Pd. Kattel et al. [53] prepared a N-doped carbon-supported Pd single-atom catalyst (Pd-NC) with Pd-N₄ sites. The well-dispersed Pd-N₄ active centers in the catalyst help stabilize the adsorbed CO₂ reduction intermediates, thereby enhancing the ECR ability at low overpotentials. However, due to the rarity and expensiveness of precious metals, low-cost transition single metal atom catalysts that can achieve the catalytic activity of precious metals are currently hot research topics. Wang et al. [54] successfully introduced a single P atom into an N-doped carbon-loaded single Fe atom catalyst (Fe-SAC/NPC), mainly in the form of a P-C bond for the electroreduction of CO₂ to CO in aqueous solution (Fig. 8.3a). Fe K-edge X-ray absorption spectroscopy (XAS) results indicate that the presence of P reduced the oxidation state of Fe in Fe-SAC/NPC. By fitting the FT-EXAFS spectra of Fe-SAC/NPC and Fe-SAC/NC in *R* space, the local structure of Fe was identified, in which each Fe atom was isolated by four N atoms and one O atom (Fig. 8.3b). This catalyst exhibited a CO Faradaic efficiency (FE_{CO}) of ~ 97% (Fig. 8.3c) and a stable CO partial current density (J_{CO} of ~ 5 mA cm⁻² for at least 24 h at a low overpotential of 320 mV with a Tafel slope of only 59 mV dec⁻¹, exceeding most reported single-atom catalysts and comparable to the most advanced gold catalysts to date. By combining experiments and DFT calculations, it was demonstrated that the presence of a single P atom increases the electron density at the Fe center and COOH* formation is greatly facilitated, resulting in excellent CO₂RR performance at low overpotentials. Among currently identified materials, Cu is the only recognized material catalyzing the production of a large number of hydrocarbons or alcohols in aqueous solutions [55, 56]. He et al. [57] design a facile procedure to synthesize through the hole carbon nanofibers (TCNFs) with abundant and homogeneously

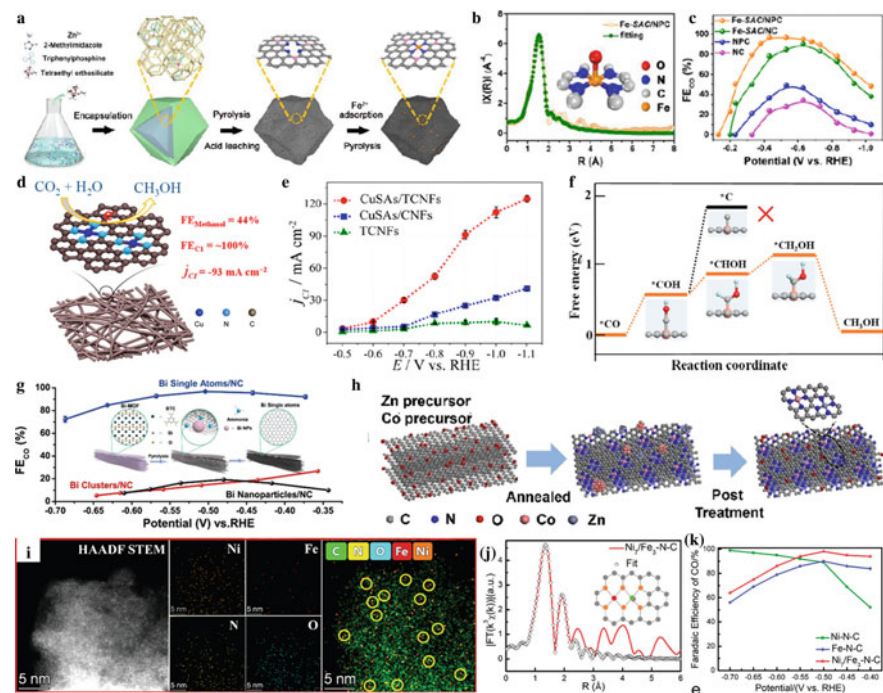


Fig. 8.3 Atomically dispersed metal carbon-based electrocatalysts. **a** Scheme of the synthesis of Fe-SAC/NPC. **b** R space fitting curve of Fe-SAC/NPC with the coordination model of Fe. **c** FE_{CO} of Fe-SAC/NPC. Reproduced with permission [54]. [57][58][60][61] Copyright 2021, John Wiley and Sons. **d** Synthesis procedure of CuSAs/THCF. **e** Partial current density of three samples. **f** Free energies for conversion of $*CO$ to CH_3OH on $Cu-N_4$ structure. Reproduced with permission. Copyright 2019, American Chemical Society. **g** Scheme of the transformation from Bi-MOF to single Bi atoms. Reproduced with permission. Copyright 2019, American Chemical Society. **h** Schematic illustration of ZnCoNC synthesis. Reproduced with permission. Copyright 2020, John Wiley and Sons. **i** HAADF STEM image and representative EDS chemical composition of the Ni_7/Fe_3-N-C sample. **j** Ni_7/Fe_3-N-C samples (Ni , Fe , O , N , and C atoms are represented in red, green, pink, orange and grey, respectively.) **k** FE of CO at various potentials. Reproduced with permission. Copyright 2021, Royal Society of Chemistry

distributed Cu single atoms (CuSAs) for efficient electrochemical CO_2RR (Fig. 8.3d). Due to the excellent mechanical properties, CuSAs/TCNFs can be directly used as the cathode for CO_2RR . Due to the synergistic effect of the through-hole carbon structure and abundant isolated Cu active sites, the CuSAs/TCNFs exhibited a FE of 44% and a methanol partial current density of -93 mA cm^{-2} as well as long-term stability (Fig. 8.3e). DFT calculations from CO^* to methanol were performed (Fig. 8.3f). According to DFT calculations, the reduction of COH^* to $CHOH^*$ on the $Cu-N_4$ structure has a moderate free energy barrier ($\sim 0.86 \text{ eV}$). In contrast, COH^* to C^* exhibits a higher reaction free energy barrier ($\sim 1.88 \text{ eV}$), which is also higher than that of other reaction steps in the CH_3OH generation process. Therefore, the Cu single-atom sites on the CuSAs/TCNFs catalysts tend to generate CH_3OH rather

than CH_4 . Besides transition metals, P-block metals are also widely used for electrocatalytic CO_2RR . For example, Li et al. [58] devised a simple and novel route to develop catalysts composed of single Bi atoms on N-doped carbon networks (Bi SAs/NCs) with hierarchical porosity for efficient CO reduction (Fig. 8.3g). Catalyst exhibits high intrinsic CO_2 reduction activity for CO conversion, with high FE_{CO} (97%) and large turnover frequency (5535 h^{-1}) at a low overpotential of 0.39 V versus RHE. Further experiments and DFT calculations reveal that the single-atom Bi- N_4 site is the main active center for CO_2 activation and rapid formation of the key intermediate COOH^* with a low free energy barrier.

Researchers further found that the interactions between tight single atoms can have a dramatic impact on catalytic performance compared to isolated atoms, as they can optimize intermediate adsorption and thus product distribution [59]. Gong et al. [60] synthesized Zn/Co-N-C catalysts by pyrolysis and post-acid treatment (Fig. 8.3 h). Performance test results show that Zn/Co-N-C has a high FE_{CO} of 93.2% was achieved at -0.5 V versus RHE and a CO current density of about 26 mAcm^{-2} at -0.5 V remained stable after a 30 h test. DFT calculations indicate that the electronic effect between Zn and Co lowers the energy barrier for the formation of COOH^* on the Zn site, promoting the reduction of CO_2 to CO. Arbiol et al. [61] prepared a quasi-double star Ni/Fe-N-C catalyst consisting of nearby Ni and Fe active sites by simple pyrolysis of Ni and Fe co-doped Zn-based MOFs in order to achieve high selectivity at low overpotentials during the CO_2 reaction (Fig. 8.3i). The atomic structure of the Ni/Fe-N-C catalyst was verified in detail by EXAFS spectra (Fig. 8.3 j), and based on the fitting results and the corresponding fitting parameters, it was demonstrated that a single Fe atom should be coordinated to four N atoms and one O atom. Performance testing found that the optimized Ni/Fe-NC catalyst exhibited unique selectivity (98% maximum $\text{FE}(\text{CO})$) at a low overpotential of 390 mV versus RHE, which was superior to its single metal counterpart (Ni-N-C and Fe-N-C catalysts) and other state-of-the-art M-N-C catalysts (Fig. 8.3k). DFT results further suggest that tuning catalytic CO_2RR performance through nearby Ni and Fe active sites may break the activity benchmark for single-metal counterparts, as adjacent Ni and Fe active sites not only act synergistically to reduce COOH^* formation and CO^* desorption reaction barriers, but also prevent the undesired hydrogen evolution reaction (HER) compared to their single metal counterparts.

By constructing suitable carbon precursor materials, individual metal atoms can be trapped and stabilized. Due to the large difference in electronegativity between metal and carbon atoms, sufficient charge transfer can be generated to make this structural unit (M-N-C/M-C) an active center for electrocatalysis, reducing the activation energy barrier and overpotential of the reaction. These strategies provide important guidance for the preparation of high-performance electrocatalytic CO_2RR catalysts and are also one of the current research hotspots.

8.4 Metal Nanoparticles Encapsulated/Supported Carbon-Based Electrocatalysts for CO₂RR

The best catalytic activity of atomically dispersed transition metal carbon-based catalysts is basically comparable to that of precious metals, but their poor stability seriously hinders their commercial application. Recently, to overcome the low stability of nonprecious metal catalysts, Bao et al. [24, 25] proposed a novel and promising strategy to design and fabricate unique chainmail catalysts by fully encapsulating transition metals through graphene shells. In this carbon layer encapsulated transition metal catalyst, the electron of transition metals can penetrate through the graphene shell to promote the catalytic reaction on the external graphene surface, while the graphene shell can completely prevent reaction molecules and medium from contacting the transition metals and therefore can protect the transition metals from damage in harsh conditions. It will improve both the activity and stability of nonprecious-metal catalysts [25]. For example, Ye et al. [62] prepared Fe@C hybrids by a two-step calcination method using MIL-101(Fe) as precursor (Fig. 8.4a). The activity and selectivity to CO for Fe@C, Fe/SiO₂, and Fe/CNT samples are summarized in Fig. 8.4b. Fe@C catalyst exhibits the highest catalytic activity toward the CO generation (55.75 $\mu\text{mol min}^{-1}$), the preferred selectivity toward CO over Fe@C catalyst (99.76%) become much obvious by evaluating in the fixed-bed reactor. DFT calculations were carried out to gain further insights into the nature of this catalytic process (Fig. 8.4c). Density of states (DOS) calculations show that the electronic structure of Fe nanoparticles near the Fermi energy level is modified to a metallic state by charge transfer and the Fermi energy level rises, thus ensuring the electron transfer of Fe nanoparticles to the reactants during catalysis and enhancing the catalytic performance.

Strong metal-support interaction (SMSI), commonly happening between metal and metal oxide support, has drawn significant attention in heterogeneous catalysis due to its capability of enhancing the activity and stability of catalysts. Herein, the strong interaction between metal and carbon supports is discovered to significantly boost the performance for electrocatalytic CO₂ reduction reaction (CO₂RR) [26]. He et al. [63] report the synthesis of copper clusters supported on defect-rich carbon (DRC) with an abundant microporous structure by a very simple synthetic route involving first impregnation at 800 °C and subsequent calcination at 600 °C. The dual confinement of carbon defects and microporosity effectively prevented metal aggregation during calcination, resulting in copper clusters with a diameter of ~1.0 nm and containing ~10 atoms (Fig. 8.4d). The resulting Cu clusters/DRC showed excellent performance in CO₂RR, with a high FE of 81.7% for CH₄ and a partial current density of 18.0 mA cm⁻² at 1.0 V versus RHE (Fig. 8.4e), which exceeded most Cu-based electrocatalysts. This can be attributed to the sub-nanoscale Cu clusters, whose *d*-band centers are shifted upwards compared to the nanoparticles, which can enhance the adsorption strength of H* and CO*, thus promoting the formation of CH₄ (Fig. 8.4f). In addition, the SMSI effect of Cu clusters and defective carbon also contributes significantly to the excellent performance by tuning the

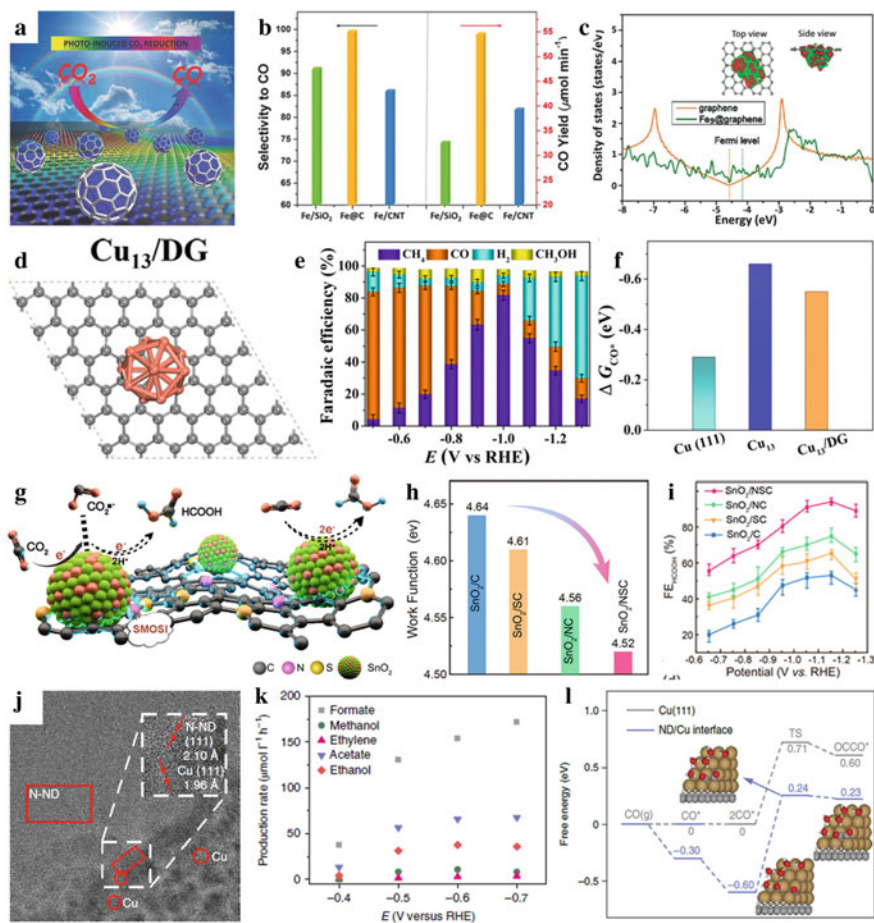


Fig. 8.4 Metal nanoparticles encapsulated and Metal nanoparticles supported carbon-based electrocatalysts. **a** Schematic illustration for the two-step preparation process for the core-shell structured Fe@C hybrid. **b** Photoinduced thermo-catalytic CO₂ conversion performance for Fe@C, Fe/SiO₂, and Fe/CNT catalysts in fixed bed reactor. **c** Projected density of states for the *p_z* orbitals of C atoms bonded with Fe atoms in the model of Fe₉@graphene in comparison with that of corresponding C atoms in pristine graphene model. The top and side views of the difference charge density of optimized Fe₉@graphene are shown as insertions. Reproduced with permission [62]. Copyright 2016, John Wiley and Sons. **d** Optimized structural model of Cu₁₃/DG. The pink and black represent Cu and C atoms, respectively. Faradaic efficiencies of **e** Cu/DRC at different potentials. **f** Adsorption energies of CO* intermediates on the above model. Reproduced with permission [63]. Copyright 2020, John Wiley and Sons. **g** Illustration of SMOSI enhancing the CO₂RR performance of SnO₂/NSC. **h** work function values. **i** FE_{HCOOH} and of SnO₂/C, SnO₂/SC, SnO₂/NC, and SnO₂/NSC. Reproduced with permission [26]. Copyright 2020, American Chemical Society. **j** HRTEM image of N-ND/Cu. The HRTEM image shows the presence of both Cu and nanodiamond as confirmed by lattice fringes of the selected regions in the micrograph. **k** Production rates for formate, methanol, ethylene, acetate and ethanol production by N-ND/Cu electrodes. **l** Free energy diagram for CO coupling on the Cu (111) surface (grey) and at the ND/Cu interface (blue). Reproduced with permission [64]. Copyright 2020, Springer Nature

electronic structure and improving the stability of the Cu clusters. Using molecular precursors, Hu et al. [26] have carefully designed a variety of doped and undoped carbon carriers with similar specific surface area, morphology and porous structure. It was found that these carriers were able to effectively load high density and small size SnO₂ NPs with a loading of approximately 60 wt.%. More importantly, systematic characterizations clearly revealed the existence of strong metal oxide-carrier interactions (SMOSI) between the SnO₂ nanoparticles and the doped carbon carriers (Fig. 8.4 g, h). The results show that the strongest SMOSI, SnO₂/NSC, has a CO₂RR selectivity of up to 94.4% for HCOOH and a partial current density of up to 56.0 mA cm⁻², which is superior to most Sn-based catalysts (Fig. 8.4i). Cui et al. [64] created a selective and reliable catalytic interface during the reduction of CO₂ to C₂ oxygenates by rationally tuning the assembly of N-doped nanodiamonds and copper nanoparticles (Fig. 8.4j). The catalyst exhibits a Faradaic efficiency of about 63% for C₂ oxygenates at an applied potential of only -0.5 V versus RHE (Fig. 8.4 k). In addition, the catalyst exhibits extremely high stability for up to 120 h. DFT calculations show that the binding of CO at the Cu/nanodiamond interface is significantly enhanced, reducing the apparent potential barrier of CO dimers and inhibiting the desorption of CO, thereby promoting the generation of C₂ (Fig. 8.4l). The design principles of this interface material-material platform will be applicable to various catalytic transformations, especially those requiring renewable energy input and aqueous conditions.

8.5 Conclusion and Perspectives

This chapter mainly introduces the research progress of carbon-based nanomaterials for CO₂ electrocatalytic reduction in recent years. Several efficient and typical carbon-based nanomaterials (non-metals, atomically dispersed metals, and metal nanoparticles) are selected for discussion. The differences of CO₂ electroreduction efficiency, product distribution and reduction process on various catalysts were analyzed. The special catalytic properties of these carbon-based nanomaterials and the mechanism behind them have improved the ideas for the development of efficient catalysts. Although the research on CO₂ electrocatalytic reduction has lasted for nearly half a century, the related work is almost limited to the scope of the laboratory, and it is still far from practical industrial application. In summary, it is believed that future research on electrocatalytic reduction of CO₂ needs to make breakthroughs in the following aspects.

- (1) Development of catalysts suitable for the reduction of CO₂ to alcohol products. Compared with other products of CO₂ electroreduction, alcohol liquid products have advantages in storage and transportation, and alcohols have higher energy density, so they are more suitable as target products to store CO₂ and electrical energy in the form of chemical energy. However, in many research reports, the conversion rate and the generation rate of alcohol are not ideal.

It is difficult to significantly increase the efficiency of alcohols by using only pure copper-based catalytic electrodes. Atomically dispersed metals are worth trying as catalytic materials, which are expected to catalyze the efficient and rapid reduction of CO₂ to alcohols.

- (2) Analysis of the mechanism of CO₂ reduction. Due to the lack of strong direct experimental observations to analyze the reaction mechanism (especially the aqueous reaction system), many mechanisms in the CO₂ reduction process are speculated by theoretical calculations. The theoretical calculations not only provide a reference for analyzing the reaction mechanism, but also provide a basis for the design of new catalysts. With the guidance of theoretical calculation results, researchers can purposefully synthesize new catalysts. However, for the same reduction process, there are also differences in the theoretical calculation results given by different researchers, and the proposed reaction processes are also different. However, for the same reduction process, there are also differences in the theoretical calculation results given by different researchers, and the proposed reaction processes are also different.

References

1. Y. Chen, Y. Zhang, G. Fan, L. Song, G. Jia, H. Huang, S. Ouyang, J. Ye, Z. Li, Z. Zou, Cooperative catalysis coupling photo-/photothermal effect to drive sabatier reaction with unprecedented conversion and selectivity. *Joule* **5**, 3235–3251 (2021). <https://doi.org/10.1016/j.joule.2021.11.009>
2. S. Ning, H. Xu, Y. Qi, L. Song, Q. Zhang, S. Ouyang, J. Ye, Microstructure induced thermodynamic and kinetic modulation to enhance CO₂ photothermal reduction: a case of atomic-scale dispersed Co-N species anchored Co@C hybrid. *ACS Catal.* **10**, 4726–4736 (2020). <https://doi.org/10.1021/acscatal.9b04963>
3. N. Li, J. Liu, J.J. Liu, L.Z. Dong, Z.F. Xin, Y.L. Teng, Y.Q. Lan, Adenine components in biomimetic metal-organic frameworks for efficient CO₂ photoconversion. *Angew. Chem. Int. Ed.* **58**, 5226–5231 (2019). <https://doi.org/10.1002/anie.201814729>
4. D.U. Nielsen, X.-M. Hu, K. Daasbjerg, T. Skrydstrup, Chemically and electrochemically catalysed conversion of CO₂ to CO with follow-up utilization to value-added chemicals. *Nat. Catal.* **2**, 95–95 (2018). <https://doi.org/10.1038/s41929-018-0152-z>
5. M.S. Frei, C. Mondelli, A. Cesarini, F. Krumeich, R. Hauert, J.A. Stewart, D. Curulla Ferré, J. Pérez-Ramírez, Role of zirconia in indium oxide-catalyzed CO₂ hydrogenation to methanol. *ACS Catal.* **10**, 1133–1145 (2019). <https://doi.org/10.1021/acscatal.9b03305>
6. D.D. Zhu, J.L. Liu, S.Z. Qiao, Recent advances in inorganic heterogeneous electrocatalysts for reduction of carbon dioxide. *Adv. Mater.* **28**, 3423–3452 (2016). <https://doi.org/10.1002/adma.201504766>
7. W. Zhang, Y. Hu, L. Ma, G. Zhu, Y. Wang, X. Xue, R. Chen, S. Yang, Z. Jin, Progress and perspective of electrocatalytic CO₂ reduction for renewable carbonaceous fuels and chemicals. *Advanced Science* **5**, 1700275 (2018). <https://doi.org/10.1002/advs.201700275>
8. T. Zheng, K. Jiang, H. Wang, Recent advances in electrochemical CO₂-to-CO conversion on heterogeneous catalysts. *Adv. Mater.* **30**, e1802066 (2018). <https://doi.org/10.1002/adma.201802066>
9. S. Verma, S. Lu, P.J.A. Kenis, Co-electrolysis of CO₂ and glycerol as a pathway to carbon chemicals with improved technoconomics due to low electricity consumption. *Nat. Energy* **4**, 466–474 (2019). <https://doi.org/10.1038/s41560-019-0374-6>

10. M. Liu, M. Liu, X. Wang, S.M. Kozlov, Z. Cao, P. De Luna, H. Li, X. Qiu, K. Liu, J. Hu, C. Jia, P. Wang, H. Zhou, J. He, M. Zhong, X. Lan, Y. Zhou, Z. Wang, J. Li, A. Seifitokaldani, C.T. Dinh, H. Liang, C. Zou, D. Zhang, Y. Yang, T.-S. Chan, Y. Han, L. Cavallo, T.-K. Sham, B.-J. Hwang, E.H. Sargent, Quantum-dot-derived catalysts for CO₂ reduction reaction. *Joule* **3**, 1703–1718 (2019). <https://doi.org/10.1016/j.joule.2019.05.010>
11. T.-T. Zhuang, Z.-Q. Liang, A. Seifitokaldani, Y. Li, P. De Luna, T. Burdyny, F. Che, F. Meng, Y. Min, R. Quintero-Bermudez, C.T. Dinh, Y. Pang, M. Zhong, B. Zhang, J. Li, P.-N. Chen, X.-L. Zheng, H. Liang, W.-N. Ge, B.-J. Ye, D. Sinton, S.-H. Yu, E.H. Sargent, Steering post-C–C coupling selectivity enables high efficiency electroreduction of carbon dioxide to multi-carbon alcohols. *Nat. Catal.* **1**, 421–428 (2018). <https://doi.org/10.1038/s41929-018-0084-7>
12. Y. Hori, Electrochemical CO₂ reduction on metal electrodes. *Mod. Aspects Electrochem.* **42**, 89–189 (2008). https://doi.org/10.1007/978-0-387-49489-0_3
13. X. Wan, X. Liu, Y. Li, R. Yu, L. Zheng, W. Yan, H. Wang, M. Xu, J. Shui, Fe-N-C electrocatalyst with dense active sites and efficient mass transport for high-performance proton exchange membrane fuel cells. *Nat. Catal.* **2**, 259–268 (2019). <https://doi.org/10.1038/s41929-019-0237-3>
14. S. Wang, H. Jiang, L. Song, Recent progress in defective carbon-based oxygen electrode materials for rechargeable zinc-air batteries. *Batteries Supercaps* **2**, 509–523 (2019). <https://doi.org/10.1002/batt.201900001>
15. K. Gong, F. Du, Z. Xia, M. Durstock, L. Dai, Nitrogen-doped carbon nanotube arrays with high electrocatalytic activity for oxygen reduction. *Science* **323**, 760–764 (2009). <https://doi.org/10.1126/science.1168049>
16. I.S. Amiinu, X. Liu, Z. Pu, W. Li, Q. Li, J. Zhang, H. Tang, H. Zhang, S. Mu, From 3D ZIF nanocrystals to Co-N_x/C nanorod array electrocatalysts for ORR, OER, and Zn-air batteries. *Adv. Func. Mater.* **28**, 1704638 (2018). <https://doi.org/10.1002/adfm.201704638>
17. Y. Jia, J. Chen, X. Yao, Defect electrocatalytic mechanism: concept, topological structure and perspective. *Mater. Chem. Front.* **2**, 1250–1268 (2018). <https://doi.org/10.1039/c8qm00070k>
18. C. Xie, D. Yan, W. Chen, Y. Zou, R. Chen, S. Zang, Y. Wang, X. Yao, S. Wang, Insight into the design of defect electrocatalysts: from electronic structure to adsorption energy. *Mater. Today* **31**, 47–68 (2019). <https://doi.org/10.1016/j.mattod.2019.05.021>
19. H. Zhao, C. Sun, Z. Jin, D.-W. Wang, X. Yan, Z. Chen, G. Zhu, X. Yao, Carbon for the oxygen reduction reaction: a defect mechanism. *J. Mater. Chem. A* **3**, 11736–11739 (2015). <https://doi.org/10.1039/c5ta02229k>
20. S. Liu, H. Yang, X. Su, J. Ding, Q. Mao, Y. Huang, T. Zhang, B. Liu, Rational design of carbon-based metal-free catalysts for electrochemical carbon dioxide reduction: a review. *J. Energy Chem.* **36**, 95–105 (2019). <https://doi.org/10.1016/j.jechem.2019.06.013>
21. H. Yang, Q. Lin, C. Zhang, X. Yu, Z. Cheng, G. Li, Q. Hu, X. Ren, Q. Zhang, J. Liu, C. He, Carbon dioxide electroreduction on single-atom nickel decorated carbon membranes with industry compatible current densities. *Nat. Commun.* **11**, 593 (2020). <https://doi.org/10.1038/s41467-020-14402-0>
22. T.K. Todorova, M.W. Schreiber, M. Fontecave, Mechanistic understanding of CO₂ reduction reaction (CO₂RR) toward multicarbon products by heterogeneous Copper-based catalysts. *ACS Catal.* **10**, 1754–1768 (2019). <https://doi.org/10.1021/acscatal.9b04746>
23. B. Zhang, J. Zhang, J. Shi, D. Tan, L. Liu, F. Zhang, C. Lu, Z. Su, X. Tan, X. Cheng, B. Han, L. Zheng, J. Zhang, Manganese acting as a high-performance heterogeneous electrocatalyst in carbon dioxide reduction. *Nat. Commun.* **10**, 2980 (2019). <https://doi.org/10.1038/s41467-019-10854-1>
24. D. Deng, K.S. Novoselov, Q. Fu, N. Zheng, Z. Tian, X. Bao, Catalysis with two-dimensional materials and their heterostructures. *Nat. Nanotechnol.* **11**, 218–230 (2016). <https://doi.org/10.1038/nnano.2015.340>
25. D. Deng, L. Yu, X. Chen, G. Wang, L. Jin, X. Pan, J. Deng, G. Sun, X. Bao, Iron encapsulated within pod-like carbon nanotubes for oxygen reduction reaction. *Angew. Chem. Int. Ed.* **52**, 371–375 (2013). <https://doi.org/10.1002/anie.201204958>

26. L.-P. Yuan, W.-J. Jiang, X.-L. Liu, Y.-H. He, C. He, T. Tang, J. Zhang, J.-S. Hu, Molecularly engineered strong metal oxide-support interaction enables highly efficient and stable CO₂ electroreduction. *ACS Catal.* **10**, 13227–13235 (2020). <https://doi.org/10.1021/acscatal.0c03831>
27. Y. Jiang, L. Yang, T. Sun, J. Zhao, Z. Lyu, O. Zhuo, X. Wang, Q. Wu, J. Ma, Z. Hu, Significant contribution of intrinsic carbon defects to oxygen reduction activity. *ACS Catal.* **5**, 6707–6712 (2015). <https://doi.org/10.1021/acscatal.5b01835>
28. J. Zhu, Y. Huang, W. Mei, C. Zhao, C. Zhang, J. Zhang, I.S. Amiinu, S. Mu, Effects of intrinsic pentagon defects on electrochemical reactivity of carbon nanomaterials. *Angew. Chem. Int. Ed.* **58**, 3859–3864 (2019). <https://doi.org/10.1002/anie.201813805>
29. J. Wu, T. Sharifi, Y. Gao, T. Zhang, P.M. Ajayan, Emerging carbon-based heterogeneous catalysts for electrochemical reduction of carbon dioxide into value-added chemicals. *Adv. Mater.* **31**, e1804257 (2019). <https://doi.org/10.1002/adma.201804257>
30. M. Chen, S. Wang, H. Zhang, P. Zhang, Z. Tian, M. Lu, X. Xie, L. Huang, W. Huang, Intrinsic defects in biomass-derived carbons facilitate electroreduction of CO₂. *Nano Res.* **13**, 729–735 (2020). <https://doi.org/10.1007/s12274-020-2683-2>
31. Q. Wu, J. Gao, J. Feng, Q. Liu, Y. Zhou, S. Zhang, M. Nie, Y. Liu, J. Zhao, F. Liu, J. Zhong, Z. Kang, A CO₂ adsorption dominated carbon defect-based electrocatalyst for efficient carbon dioxide reduction. *J. Mater. Chem. A* **8**, 1205–1211 (2020). <https://doi.org/10.1039/c9ta11473d>
32. W. Wang, L. Shang, G. Chang, C. Yan, R. Shi, Y. Zhao, G.I.N. Waterhouse, D. Yang, T. Zhang, Intrinsic carbon-defect-driven electrocatalytic reduction of carbon dioxide. *Adv. Mater.* **31**, e1808276 (2019). <https://doi.org/10.1002/adma.201808276>
33. S. Liu, H. Yang, X. Huang, L. Liu, W. Cai, J. Gao, X. Li, T. Zhang, Y. Huang, B. Liu, Identifying active sites of nitrogen-doped carbon materials for the CO₂ reduction reaction. *Adv. Func. Mater.* **28**, 1800499 (2018). <https://doi.org/10.1002/adfm.201800499>
34. L. Li, Y. Huang, Y. Li, Carbonaceous materials for electrochemical CO₂ reduction. *Energy-Chem* **2**, 100024 (2020). <https://doi.org/10.1016/j.enchem.2019.100024>
35. J. Zhao, H. Lai, Z. Lyu, Y. Jiang, K. Xie, X. Wang, Q. Wu, L. Yang, Z. Jin, Y. Ma, J. Liu, Z. Hu, Hydrophilic hierarchical nitrogen-doped carbon nanocages for ultrahigh supercapacitive performance. *Adv. Mater.* **27**, 3541–3545 (2015). <https://doi.org/10.1002/adma.201500945>
36. M. Tomisaki, S. Kasahara, K. Natsui, N. Ikemiya, Y. Einaga, Switchable product selectivity in the electrochemical reduction of carbon dioxide using boron-doped diamond electrodes. *J. Am. Chem. Soc.* **141**, 7414–7420 (2019). <https://doi.org/10.1021/jacs.9b01773>
37. X. Zou, M. Liu, J. Wu, P.M. Ajayan, J. Li, B. Liu, B.I. Yakobson, How nitrogen-doped graphene quantum dots catalyze electroreduction of CO₂ to hydrocarbons and oxygenates. *ACS Catal.* **7**, 6245–6250 (2017). <https://doi.org/10.1021/acscatal.7b01839>
38. Z. Ma, L. Tao, D. Liu, Z. Li, Y. Zhang, Z. Liu, H. Liu, R. Chen, J. Huo, S. Wang, Ultrafine nano-sulfur particles anchored on in situ exfoliated graphene for lithium–sulfur batteries. *J. Mater. Chem. A* **5**, 9412–9417 (2017). <https://doi.org/10.1039/c7ta01981e>
39. J. Kim, R. Zhou, K. Murakoshi, S. Yasuda, Advantage of semi-ionic bonding in fluorine-doped carbon materials for the oxygen evolution reaction in alkaline media. *RSC Adv.* **8**, 14152–14156 (2018). <https://doi.org/10.1039/c8ra01636d>
40. T. Liu, S. Ali, Z. Lian, C. Si, D.S. Su, B. Li, Phosphorus-doped onion-like carbon for CO₂ electrochemical reduction: the decisive role of the bonding configuration of phosphorus. *J. Mater. Chem. A* **6**, 19998–20004 (2018). <https://doi.org/10.1039/c8ta06649c>
41. W. Li, M. Seredych, E. Rodriguez-Castellon, T.J. Bandoz, Metal-free nanoporous carbon as a catalyst for electrochemical reduction of CO₂ to CO and CH₄. *Chemsuschem* **9**, 606–616 (2016). <https://doi.org/10.1002/cssc.201501575>
42. P. Wu, Y. Qian, P. Du, H. Zhang, C. Cai, Facile synthesis of nitrogen-doped graphene for measuring the releasing process of hydrogen peroxide from living cells. *J. Mater. Chem.* **22**, 6402–6412 (2012). <https://doi.org/10.1039/c2jm16929k>
43. X. Cui, Z. Pan, L. Zhang, H. Peng, G. Zheng, Selective etching of nitrogen-doped carbon by steam for enhanced electrochemical CO₂ reduction. *Adv. Energy Mater.* **7**, 1701456 (2017). <https://doi.org/10.1002/aenm.201701456>

44. W. Feng, P. Long, Y. Feng, Y. Li, Two-dimensional fluorinated graphene: synthesis, structures, properties and applications. *Adv. Sci.* **3**, 1500413 (2016). <https://doi.org/10.1002/advs.201500413>
45. J. Xie, X. Zhao, M. Wu, Q. Li, Y. Wang, J. Yao, Metal-free fluorine-doped carbon electrocatalyst for CO₂ reduction outcompeting hydrogen evolution. *Angew. Chem. Int. Ed.* **57**, 9640–9644 (2018). <https://doi.org/10.1002/anie.201802055>
46. X. Xue, H. Yang, T. Yang, P. Yuan, Q. Li, S. Mu, X. Zheng, L. Chi, J. Zhu, Y. Li, J. Zhang, Q. Xu, N. P-coordinated fullerene-like carbon nanostructures with dual active centers toward highly-efficient multi-functional electrocatalysis for CO₂RR ORR and Zn-air battery. *J. Mater. Chem. A* **7**, 15271–15277 (2019). <https://doi.org/10.1039/c9ta03828k>
47. Z. Wang, H. Jin, T. Meng, K. Liao, W. Meng, J. Yang, D. He, Y. Xiong, S. Mu, Fe, Cu-coordinated ZIF-derived carbon framework for efficient oxygen reduction reaction and zinc-air batteries. *Adv. Func. Mater.* **28**, 1802596 (2018). <https://doi.org/10.1002/adfm.201802596>
48. T. Ouyang, Y.Q. Ye, C.Y. Wu, K. Xiao, Z.Q. Liu, Heterostructures composed of N-doped carbon nanotubes encapsulating cobalt and beta-Mo₂C nanoparticles as bifunctional electrodes for water splitting. *Angew. Chem. Int. Ed.* **58**, 4923–4928 (2019). <https://doi.org/10.1002/anie.201814262>
49. C. Hu, R. Paul, Q. Dai, L. Dai, Carbon-based metal-free electrocatalysts: from oxygen reduction to multifunctional electrocatalysis. *Chem. Soc. Rev.* **50**, 11785–11843 (2021). <https://doi.org/10.1039/d1cs00219h>
50. J.N. Kuhn, W. Huang, C.K. Tsung, Y. Zhang, G.A. Somorjai, Structure sensitivity of carbon-nitrogen ring opening: Impact of platinum particle size from below 1 to 5 nm upon pyrrole hydrogenation product selectivity over monodisperse platinum nanoparticles loaded onto mesoporous silica. *J. Am. Chem. Soc.* **130**, 14026–14027 (2008). <https://doi.org/10.1021/ja805050c>
51. Y. Wang, P. Han, X. Lv, L. Zhang, G. Zheng, Defect and interface engineering for aqueous electrocatalytic CO₂ reduction. *Joule* **2**, 2551–2582 (2018). <https://doi.org/10.1016/j.joule.2018.09.021>
52. A.S. Varela, N. Ranjbar Sahraie, J. Steinberg, W. Ju, H.S. Oh, P. Strasser, Metal-doped nitrogenated carbon as an efficient catalyst for direct CO₂ electroreduction to CO and hydrocarbons. *Angew. Chem. Int. Ed.* **54**, 10758–10762 (2015). <https://doi.org/10.1002/anie.201502099>
53. Q. He, J.H. Lee, D. Liu, Y. Liu, Z. Lin, Z. Xie, S. Hwang, S. Kattel, L. Song, J.G. Chen, Accelerating CO₂ electroreduction to CO over Pd single-atom catalyst. *Adv. Func. Mater.* **30**, 2000407 (2020). <https://doi.org/10.1002/adfm.202000407>
54. X. Sun, Y. Tuo, C. Ye, C. Chen, Q. Lu, G. Li, P. Jiang, S. Chen, P. Zhu, M. Ma, J. Zhang, J.H. Bitter, D. Wang, Y. Li, Phosphorus induced electron localization of single iron sites for boosted CO₂ electroreduction reaction. *Angew. Chem. Int. Ed.* **60**, 23614–23618 (2021). <https://doi.org/10.1002/anie.202110433>
55. K.P. Kuhl, T. Hatsukade, E.R. Cave, D.N. Abram, J. Kibsgaard, T.F. Jaramillo, (2014) Electrocatalytic conversion of carbon dioxide to methane and methanol on transition metal surfaces. *Journal of the American Chemical Society*, 136: 14107–14113. <https://doi.org/10.1021/ja505791r>
56. A. Vasileff, C. Xu, Y. Jiao, Y. Zheng, S.-Z. Qiao, Surface and interface engineering in copper-based bimetallic materials for selective CO₂ electroreduction. *Chem* **4**, 1809–1831 (2018). <https://doi.org/10.1016/j.chempr.2018.05.001>
57. H. Yang, Y. Wu, G. Li, Q. Lin, Q. Hu, Q. Zhang, J. Liu, C. He, Scalable production of efficient single-atom copper decorated carbon membranes for CO₂ electroreduction to methanol. *J. Am. Chem. Soc.* **141**, 12717–12723. <https://doi.org/10.1021/jacs.9b04907>
58. E. Zhang, T. Wang, K. Yu, J. Liu, W. Chen, A. Li, H. Rong, R. Lin, S. Ji, X. Zheng, Y. Wang, L. Zheng, C. Chen, D. Wang, J. Zhang, Y. Li, Bismuth single atoms resulting from transformation of metal-organic frameworks and their use as electrocatalysts for CO₂ reduction. *J. Am. Chem. Soc.* **141**, 16569–16573 (2019). <https://doi.org/10.1021/jacs.9b08259>
59. P. Song, M. Luo, X. Liu, W. Xing, W. Xu, Z. Jiang, L. Gu, Zn single atom catalyst for highly efficient oxygen reduction reaction. *Adv. Func. Mater.* **27**, 1700802 (2017). <https://doi.org/10.1002/adfm.201700802>

60. W. Zhu, L. Zhang, S. Liu, A. Li, X. Yuan, C. Hu, G. Zhang, W. Deng, K. Zang, J. Luo, Y. Zhu, M. Gu, Z.J. Zhao, J. Gong, Enhanced CO₂ electroreduction on neighboring Zn/Co monomers by electronic effect. *Angew. Chem. Int. Ed.* **59**, 12664–12668 (2020). <https://doi.org/10.1002/anie.201916218>
61. T. Zhang, X. Han, H. Liu, M. Biset-Peiró, X. Zhang, P. Tan, P. Tang, B. Yang, L. Zheng, J.R. Morante, J. Arbiol, Quasi-double-star nickel and iron active sites for high-efficiency carbon dioxide electroreduction. *Energy Environ. Sci.* **14**, 4847–4857 (2021). <https://doi.org/10.1039/d1ee01592c>
62. H. Zhang, T. Wang, J. Wang, H. Liu, T.D. Dao, M. Li, G. Liu, X. Meng, K. Chang, L. Shi, T. Nagao, J. Ye, Surface-plasmon-enhanced photodriven CO₂ reduction catalyzed by metal-organic-framework-derived iron nanoparticles encapsulated by ultrathin carbon layers. *Adv. Mater.* **28**, 3703–3710 (2016). <https://doi.org/10.1002/adma.201505187>
63. Q. Hu, Z. Han, X. Wang, G. Li, Z. Wang, X. Huang, H. Yang, X. Ren, Q. Zhang, J. Liu, C. He, Facile synthesis of sub-nanometric copper clusters by double confinement enables selective reduction of carbon dioxide to methane. *Angew. Chem. Int. Ed.* **59**, 19054–19059 (2020). <https://doi.org/10.1002/anie.202009277>
64. H. Wang, Y.K. Tzeng, Y. Ji, Y. Li, J. Li, X. Zheng, A. Yang, Y. Liu, Y. Gong, L. Cai, Y. Li, X. Zhang, W. Chen, B. Liu, H. Lu, N.A. Melosh, Z.X. Shen, K. Chan, T. Tan, S. Chu, Y. Cui, Synergistic enhancement of electrocatalytic CO₂ reduction to C₂ oxygenates at nitrogen-doped nanodiamonds/Cu interface. *Nat. Nanotechnol.* **15**, 131–137 (2020). <https://doi.org/10.1038/s41565-019-0603-y>

Chapter 9

Carbon-Based Nanomaterials for Nitrogen Reduction Reaction



Yajin Wang, Dongping Xue, Siran Xu, and Bang-An Lu

Abstract Ammonia (NH_3) plays a vital role in food and industrial production and is a promising carbon-free energy storage carrier. At present, the main method of industrial synthesis of NH_3 is the Haber–Bosch method, which is carried out under high temperature and high pressure, consumes a large amount of energy and emits greenhouse gases, and this process is unsustainable. In recent years, the electrocatalytic nitrogen reduction reaction (NRR) has become a promising method for achieving green and sustainable NH_3 synthesis under ambient conditions, which has attracted the attention of researchers. However, due to the inertness of nitrogen molecules and the strong side reaction of hydrogen evolution, the catalytic activity and selectivity are low, which is still a huge challenge to the wide application of electrocatalytic NRR. Therefore, the design and development of an efficient NRR electrocatalyst is an important subject of theoretical and experimental research. Carbon-based nanomaterials have become a research hotspot in the field of electrocatalytic NRR due to their excellent electrical conductivity, chemical stability, adjustable electronic structure, and morphology characteristics. This chapter will start with the reaction mechanism of electrocatalytic NRR synthesis of NH_3 , and introduce the types of carbon-based nanomaterials. The focus is on the design of various carbon-based nanomaterials and the principle of improving NRR activity. The classification mainly includes metal-free carbon-based, atomically dispersed metal carbon-based, metal nanoparticles encapsulated carbon-based and metal nanoparticles supported carbon-based electrocatalysts. Finally, the problems faced by carbon-based nanomaterial catalysts

Y. Wang · D. Xue (✉) · S. Xu · B.-A. Lu
College of Materials Science and Engineering, Zhengzhou University, Zhengzhou 450001,
P. R. China
e-mail: xdongping1231@126.com

Y. Wang
e-mail: 13283861570@163.com

S. Xu
e-mail: siranxuhbnu@163.com

B.-A. Lu
e-mail: balu@zzu.edu.cn

for NRR and the design of carbon-based nanomaterial catalysts in the future are discussed and prospected.

9.1 Introduction

Ammonia (NH_3) and its derivatives are very important to modern society. Nitrogen (N_2) fixation is also a critical step in the earth's nitrogen cycle, the atmospheric N_2 can be used for a variety of nitrogen-containing molecules' biological synthesis, including ammonia, amino acids, nucleic acids, amines, nitrogen heterocycles, nitrates, and nitrites [1]. Nitrogen-containing chemicals are widely used in agriculture and chemical industries [2]. As a substitute for hydrogen (H_2), NH_3 containing 17.6 wt.% H is also considered an important hydrogen carrier. Compared with gaseous H_2 , it is easier to store and transport. Especially as carbon-free energy storage intermediate, NH_3 is completely burned to produce nitrogen (N_2) and water (H_2O), and will not emit harmful gases such as carbon monoxide (CO) and greenhouse gases such as carbon dioxide (CO_2) into the atmosphere [3, 4].

At present, the industrial production of NH_3 mainly adopts the Haber–Bosch process, which has been applied for more than 100 years. N_2 and H_2 are carried out under high temperature (300–600 °C) and high pressure (150–300 atm) conditions in the presence of iron-based catalysts. The energy consumption of this process accounts for 1–2% of the global total. Moreover, H_2 is obtained from steam methane reforming, which emits millions of tons of CO_2 every year, causing serious environmental problems [5]. Considering these energy and environmental costs, alternative processes need to be developed to achieve efficient N_2 reduction for the synthesis of NH_3 [6].

In the past few years, the emerging electrochemical ammonia synthesis process uses renewable electricity to directly synthesize NH_3 from N_2 and H_2O under ambient conditions and has received extensive attention from the scientific community [7]. The electrocatalytic process has many advantages, such as mild reaction conditions, simple infrastructure, less environmental pollution and so on. This process can provide an alternative way for the realization of green NH_3 synthesis (Fig. 9.1) [8].

Generally, electrocatalysis NRR involves three basic steps: 1) adsorption of nitrogen on catalytically active sites, 2) hydrogenation of adsorbed nitrogen and cracking of $\text{N}\equiv\text{N}$ bonds to generate ammonia, and 3) desorption of ammonia molecules from the catalyst surface [9]. It is quite difficult to adsorb and activate nitrogen molecules because the inertness of N_2 molecules with strong triple bonds [10]. The NRR process involves multiple proton-electron transfer reactions and different intermediate products. Therefore, a reasonable design of active sites on the catalyst is necessary. The ideal NRR catalyst should firstly have a strong adsorption capacity for N_2 molecules (that is, a lower activation energy), but the combination with intermediate species should be relatively weak (that is, a lower

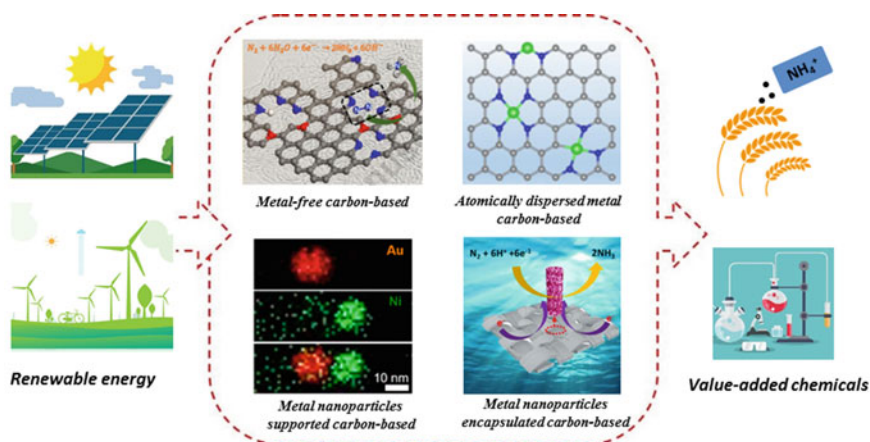
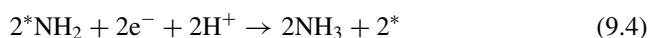


Fig. 9.1 Schematic illustration of carbon-based nanomaterials for NRR

adsorption energy) [11]. According to the way of nitrogen adsorption and hydrogenation the mechanisms can be divided into dissociative and associative. In the dissociation pathways, the $\text{N}\equiv\text{N}$ bond is destroyed before the hydrogenation reaction, and a single nitrogen atom is adsorbed on the surface of the catalyst, which is converted into NH_3 by the hydrogenation process. In the associative pathways, when the nitrogen molecule is hydrogenated, the two nitrogen atoms remain bonded to each other, [12] and there are two possible hydrogenation pathways: one is that the hydrogenation reaction occurs preferentially on the nitrogen atom farthest from the surface (assuming that the N_2 molecule is in the terminal coordination mode), and an NH_3 molecule is generated and dissociated, leaving an adsorbed nitrogen atom (or metal nitride $\text{M}\equiv\text{N}$ unit) on the surface of the catalyst, which is then hydrogenated to form a second NH_3 molecule. Another way of hydrogenation is that the two nitrogen centers of nitrogen atoms are alternately hydrogenated until one of the nitrates is converted to NH_3 and the $\text{N}\equiv\text{N}$ bond is broken (Fig. 9.2) [13, 14].

The detailed reaction steps are as follows:

Dissociative pathway:



Associative distal pathway:

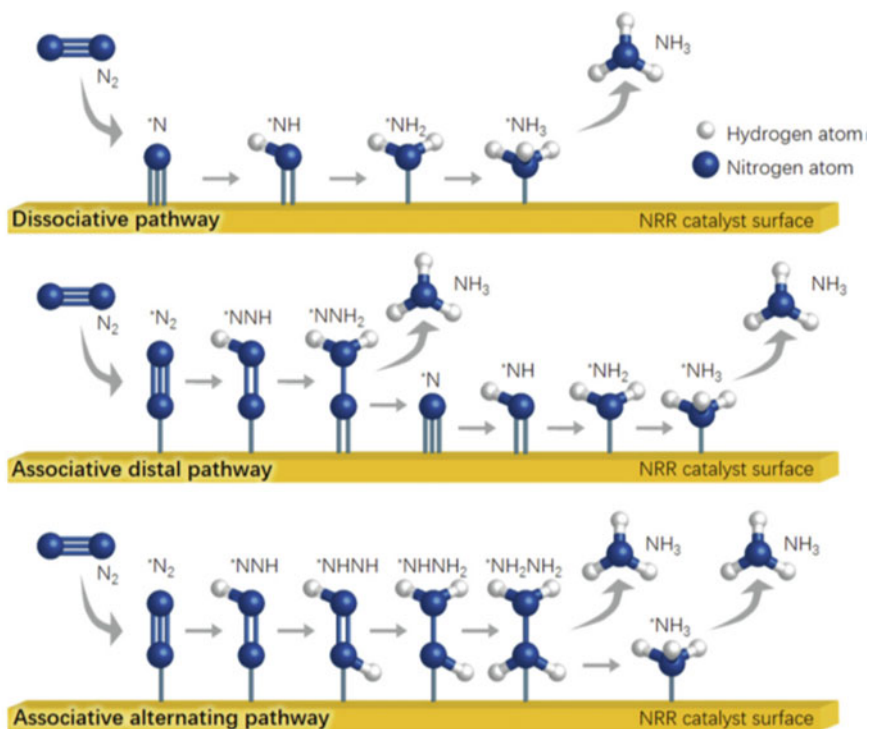
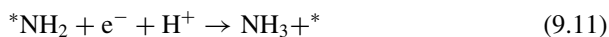
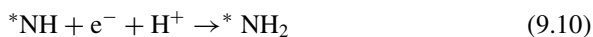
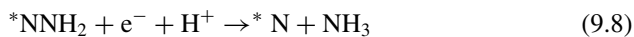
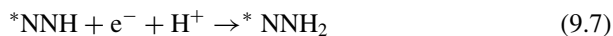
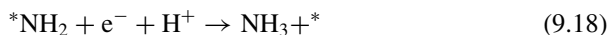
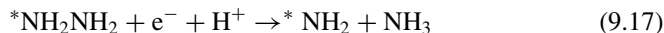
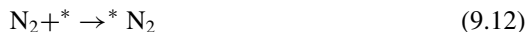


Fig. 9.2 Reaction Mechanisms for the NRR, including dissociative pathway, associative distal pathway, and associative alternating. Reproduced with permission [15]. Copyright 2019, Elsevier



Associative alternating pathway:



Despite rapid progress in this field of research, improving conversion efficiency is still a huge challenge, including low NH_3 yield and limited Faradaic efficiency (FE) [15].

In the electrochemical nitrogen reduction process, the design and development of suitable electrochemical NRR catalysts are still an important subject of theoretical and experimental research [16]. As one of the most abundant elements in the earth, carbon has been favored by many researchers for its controllable electronic structure, excellent electrical/thermal conductivity and abundant surface active sites [17, 18]. In the past few years, carbon-based electrocatalysts have shown great potential in energy conversion and storage. The introduction of cost-effective carbon-based materials into NRR may also be a promising catalyst. However, it is difficult for the original carbon materials to chemically adsorb N_2 , which directly inhibits NRR process of carbon-based materials [19]. The performance of NRR is intrinsically related to the electronic and surface structure of the catalyst. Therefore, modification of carbon-based materials is necessary by doping heteroatoms or constructing metal/carbon composite materials to increase the active sites and obtain high-efficiency NRR carbon-based catalysts [20, 21]. For example, Qiao et al. [20] systematically evaluated the potential of carbon sulfide doped materials (O, S, Se, Te) as NRR catalysts based on a combination of theoretical calculations and experimental observations. The charge accumulation induced by heteroatom doping promoted N_2 adsorption on carbon atoms, and spin polarization promoted the first potential determination step of protonation to form $*\text{NNH}$, which exhibited high intrinsic NRR activity. Establishing the correlation between the electronic structure of carbon-based materials and the performance of NRR.

In this chapter, several NRR carbon-based catalysts are summarized, including metal-free carbon-based, [22] atomically dispersed metal carbon-based, [23] metal nanoparticles/alloys carbon-based [24] and metal hybrids carbon-based electrocatalysts, [25] and we hope to guide for optimizing NRR carbon-based electrocatalysts.

9.2 Metal-Free Carbon-Based Electrocatalysts for NRR

In recent years, with the introduction of innovative concepts such as green chemistry and sustainable development, metal-free catalysts have gradually become a research hotspot and frontier in the field of catalysis [26]. Metal-free carbon-based catalyst has inherent advantages such as low cost and environmental friendliness, and it also has the advantages of large specific surface area, abundant pores, excellent activity, and long durability. More importantly, they can exhibit metal-like catalytic activity [27]. Metal-free carbon-based nanomaterials is also an ideal candidate material for designing high-performance NRR electrocatalysts [19]. Regarding the design and construction of metal-free carbon-based nanomaterials, heteroatom doping is considered to be effective method, [3] which can not only adjust the electronic structure and manipulate the surface characteristics, but also induce changes in the charge and spin density near the carbon atom. In this way, the adsorption/desorption behavior of reactants, intermediates and products on the surface of the catalyst can be adjusted, and electron transfer can be promoted [28].

The more commonly used non-metallic elements in heteroatom doping strategy are N, [29] B, [30] S, [31] and so on. Due to the large specific surface area and abundant pores of N-doped carbon nanomaterials, it can provide sufficient binding sites and fast mass transfer paths, so it is widely used in the capture of O_2 , CO_2 , and N_2 [32]. It is worth noting that N doping changes the electronic structure, induces the formation of defects and charge polarization, enhances the adsorption capacity, and leads to the improvement of catalytic performance [33]. Zhao et al. [34] reported that N-doped porous carbon (NPC) derived from ZIF-8 can be used to efficiently reduce the N_2 to ammonia at ambient environment. The content and species of N could be adjusted to enhance N_2 chemisorption and $N\equiv N$ breaking (Fig. 9.3a, b). The experimental results and theoretical calculation proved that high content of pyridine N and pyrrole N can promote the synthesis of ammonia. Wu et al. [35] reported a metal-organic framework-derived N-doped porous carbon as an electrocatalyst for NRR. The rate of ammonia production increases as the test temperature increases, indicating that adjusting the heating conditions could control the degree of N doping and graphitization, thereby optimizing the electronic structure and geometric structure of carbon, and improving NRR catalytic activity.

The B atom shows great potential in N_2 fixation. Since carbon (2.55) is more electronegative than boron (2.04), the B-C σ bond polarization is significant, which makes the B atoms positively charged; in addition, N_2 as a weak Lewis base is ideal for B doping to form a Lewis acid catalytic site to combine with N_2 . The sp^3 hybridized B atom also contains occupied orbitals and empty orbitals, which can effectively N_2 fixation (Fig. 9.3c) [27]. Yan et al. [22] proved that by promoting the adsorption of N_2 on the B-rich covalent organic framework through electrochemical excitation, high efficiency nitrogen reduction activity could be achieved (Fig. 9.3d). The simulation results showed that the B sites combine with N atoms under electrochemical conditions, and the resulting amorphous covalent organic framework had a stronger affinity for N_2 , which enhanced molecular collisions. At -0.2 V (vs. RHE)

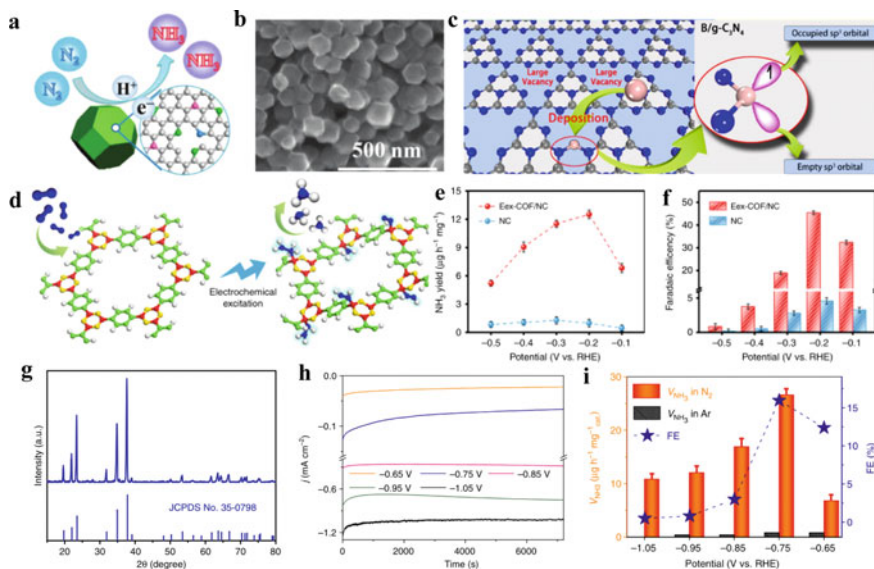


Fig. 9.3 Metal-free carbon-based electrocatalysts for NRR. **a** Schematic illustration and SEM image **b** of NPC for NRR. Reproduced with permission [19]. Copyright 2019, WILEY-VCH. **c** Design concept of a catalyst for N_2 fixation. Reproduced with permission [27]. Copyright 2018, American Chemical Society. **d** TEM images for B_4C nanosheets. **e, f** Chrono-amperometry curves **e**, NH_3 yields and Faradaic efficiencies (FEs) **f** at various potentials in N_2 -saturated 0.1 M HCl of B_4C/CPE . Reproduced with permission [22]. Copyright 2019, Nature Publishing Group. **g** XRD pattern for B_4C . **h** Chrono-amperometry curves at various potentials in N_2 -saturated 0.1 M HCl. **i** NH_3 yields and FE at each given potential in 0.1 M HCl. Reproduced with permission [36]. Copyright 2018, Nature Publishing Group

the ammonia production rate and FE were as high as $12.53 \mu\text{g h}^{-1} \text{mg}^{-1}$ and 45.43%, respectively (Fig. 9.3e-f). Sun et al. [36] reported that boron carbide nanosheets, as a high-performance electrochemical nitrogen fixation metal-free carbon-based nanomaterials (Fig. 9.3g), had good selectivity for the formation of NH_3 under ambient conditions. The chronoamperometric curves under different potentials showed good stability (Fig. 9.3h). Under -0.75 V (vs. RHE) potential, the catalyst had an ammonia yield of $26.57 \mu\text{g h}^{-1} \text{mg}^{-1}_{\text{cat}}$, and a FE of 15.95% (Fig. 9.3i). It is worth noting that it also exhibited high electrochemical stability and excellent selectivity.

In addition to the common N and B doping, the presence of S atoms can also enhance the physical and chemical adsorption capabilities of carbon-based nanomaterials for N_2 [37]. Li et al. [38] reported that S-doped 3D graphene could be used as an efficient and stable NRR catalyst. Because 3DG had high electron transport capacity and stable physical and chemical properties, it had good selectivity for the conversion of N_2 to NH_3 under an ambient environment. The results showed that in 0.05 M H_2SO_4 , the NH_3 yield of S-3DG is $38.81 \mu\text{g}_{NH_3} \text{mg}^{-1}_{\text{cat}} \text{h}^{-1}$, and the FE was 7.72% at -0.6 V (vs. RHE). It is worth noting that S-3DG exhibited excellent selectivity and durability.

In summary, the latest developments in metal-free carbon-based nanomaterials applied to NRR under an ambient condition was reviewed. Although significant progress has been made in different carbon nanomaterials, the catalytic mechanism of NRR catalysts still needs to be further understood to improve the performance of NRR catalysts and realize the practical application of electrocatalytic NRR as soon as possible.

9.3 Atomically Dispersed Metal Carbon-Based Electrocatalysts for NRR

Throughout the history of chemistry, it can be seen that the in-depth exploration of a single object can bring creative results and inspiring ways of thinking [39]. In recent years, the exploration of single-atom engineering has become more and more in-depth. Single-atom catalysts (SACs) have combined the advantages of homogeneous catalysts and heterogeneous catalysts in the development process, which show high catalytic efficiency, and have broad application prospects compared with bulk and nano-particle catalysts [40]. From the perspective of economy, environmental protection and sustainable development, it is particularly necessary to improve the utilization efficiency of metals of the same quality as much as possible [41]. SACs not only have higher catalytic activity and selectivity for various electrocatalytic reactions, but also can increase atom utilization and reduce costs in large-scale applications, so single-atom engineering is a kind of green and sustainable catalyst design strategy [42]. There are many advantages to shrinking metal nanoparticles into nanoclusters or even single atoms, but the high surface free energy of single atoms makes them easy to aggregate, so isolated atoms can be anchored on various substrates, and single metal atoms can be effectively dispersed through the carrier [43]. And use a single atom as the catalytic center, to maximize the use of metal elements to form a stable configuration [44]. In addition, the strong interaction between the individual atoms of SACs and the carrier leads to a tunable electronic structure that can improve electrocatalytic performance [45, 46]. Coincidentally, since the coordination number of metal ions is generally not very high, its single atom has good geometric uniformity as the catalytic center, and the unsaturated coordination environment has a positive effect on the reactants [47]. The adsorption and activation on the catalytic site play an important role and help reduce the energy barrier of the electrochemical reaction [48]. In addition, the identification of active sites on the atomic scale will lay the foundation for revealing the structure–activity/selectivity relationships and mechanisms of various electrocatalytic active sites [49]. So far, many advanced characterization techniques such as high-angle circular dark-field scanning transmission electron microscopy (HAADF-STEM) and X-ray absorption spectroscopy (XAS) have been used to reveal the structure of SACs [50, 51].

So far, through theoretical calculations, single transition metal atoms are anchored on different supporting substrates are able to effectively realize electrochemical

nitrogen-ammonia conversion. To obtain a highly active single-atom catalyst, careful selection of a suitable support substrate is essential for stabilizing the metal atoms dispersed on the support and establishing a strong metal-support interaction [52]. Among them, nitrogen-doped carbon material is considered to be a promising support substrate for anchoring metal atoms, forming a metal-nitrogen-carbon (M-N-C) material, which has good atomic stability and high catalytic activity [15]. For example, Xin et al. [21] reported that a single Mo atom anchored to nitrogen-doped porous carbon (SA-Mo/NPC) was used as a cost-effective NRR catalyst with high active site density and hierarchical porous carbon framework structure. Structural characterization showed that SA-Mo/NPC had a three-dimensional interconnected carbon framework with random open porous structure and Mo existed as a single atom (Fig. 9.4a, b). Compared with previously reported non-noble metal electrocatalysts, SA-Mo/NPC had a higher NH_3 yield ($34.0 \pm 3.6 \mu\text{g}_{\text{NH}_3} \text{h}^{-1} \text{mg}_{\text{cat}}^{-1}$) and Faradaic efficiency ($14.6 \pm 1.6\%$) (Fig. 9.4c) at room temperature 0.1 M KOH. This discovery provided a promising forerunner for the design of highly efficient and robust single-atom non-noble metal catalysts for electrocatalytic NRR.

Pennycook et al. [53] reported a class of Cu SACs based on a porous nitrogen-doped carbon network (NC-Cu SA), developed by a facile surfactant-assisted synthesis approach (Fig. 9.4d), which were investigated for their catalytic performance toward N_2 reduction in both alkaline and acidic solutions. The combination of experiments and first-principles calculations proved that the NC-Cu SA had an efficient NRR electrocatalysis (Fig. 9.4e). Due to the high density of exposed active sites and high porosity, Cu SAC exhibited high NH_3 yield and FE (Fig. 9.4f). As shown in Fig. 9.4g, it was proved that the NH_3 produced was indeed produced by the electrochemical reduction of the supplied N_2 through isotope labeling experiments [53]. Sun et al. [54] reported the study of the electrocatalytic reduction of ruthenium single atom to fix nitrogen at room temperature and pressure. Compared with Ru nanoparticles, a single Ru site on the N-doped porous carbon greatly promoted the selective electro-reduction of N_2 to NH_3 (Fig. 9.4h), and the addition of ZrO_2 could achieve higher FE. Experiments combined with density functional theory calculations showed that Ru sites containing oxygen vacancies were the main active centers, which can enhance N_2 adsorption, generate stable $^*\text{NNH}$ intermediates (Fig. 9.4i, j).

9.4 Metal Nanoparticles Encapsulated Carbon-Based Electrocatalysts for NRR

In order to achieve efficient nitrogen fixation, highly active electrocatalysts are required. In recent years, the research focus has shifted to the development of low-cost electrocatalysts composed of earth-rich elements, such as transition metals, whose unoccupied d orbitals can accept nitrogen electrons, thereby breaking the highly symmetrical $\text{N}\equiv\text{N}$ bond electron cloud. Therefore, nanostructures of various transition metal oxides, [55–57] sulfides, [58] nitrides, [59] and carbides [60] have been

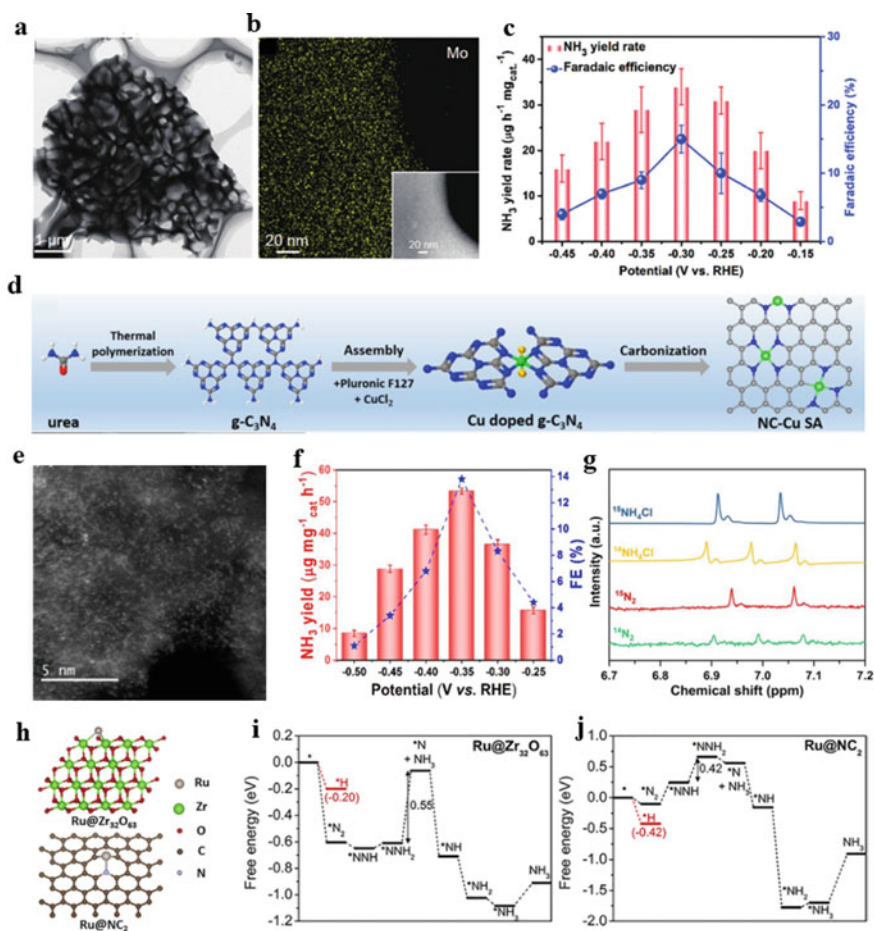


Fig. 9.4 Atomically dispersed metal carbon-based electrocatalysts for NRR. **a, b** TEM image of SA-Mo/NPC (**a**) and Mo EDS mapping (**b**). **c** NH_3 yield rate (red) and FE (blue) at each given potential of SA-Mo/NPC. Reproduced with permission [21]. Copyright 2019, WILEY-VCH. **d** Schematic illustration of the fabrication process, **e** HAADF-STEM images, **f** NH_3 yield rate and FE at different potentials in 0.1 M KOH, and **g** ^{15}N NMR spectra of the electrode after 12 h electrochemical reduction using $^{15}\text{N}_2$ as the feed gas of NC-Cu SA. Reproduced with permission [53]. Copyright 2019, American Chemical Society. **h** Calculation models for $\text{Ru@Zr}_{32}\text{O}_{63}$ and Ru/NC_2 . **i** Free-energy diagram for NRR on $\text{Ru@Zr}_{32}\text{O}_{63}$. **j** Free-energy diagram for NRR on Ru/NC_2 . Reproduced with permission [54]. Copyright 2018, Elsevier

explored as possible NRR electrocatalysts. However, because the nanostructured transition metal compound has a strong tendency to agglomerate and poor electrical conductivity, its activity and Faradaic efficiency are low. In addition, in many electrocatalytic energy storages, the catalytic material agglomerates and the volume increases during the cycle, [61] active site poisoning in the catalytic process, [62] etc. Therefore, some studies use carbon materials, including carbon nanosheets and

reduced graphene oxide (rGO) serves as a matrix to support these nanostructures, thereby avoiding their agglomeration and improving their electrical conductivity [63].

Numerous reports found that carbon coating of active materials is one of the ways to alleviate the deactivation of active materials. Active metal compound nanoparticles (such as elemental metals or metal oxides, sulfides, phosphides or carbides nanoparticles) [64, 65] are encapsulated in graphene, porous carbon or carbon nanotubes, or wrapped by a carbon shell, it not only can effectively protect it from harsh environments, and it can also resist aggregation and enhance durability. These materials have become a hot spot in the study of electrocatalytic energy conversion. In addition, carbon materials doped or even doped with heteroatoms (such as N, P, and S) [66–68] can greatly improve electrochemical activity due to their adjustment of structure and electronic changes. Therefore, coating transition metal nanoparticles with carbonaceous materials doped with multiple heteroatoms is an effective strategy for constructing high-activity and long-lasting electrocatalysts for energy conversion reactions, in which the synergy between the components may help produce the desired activity.

The introduction of carbon coating strategy into electrocatalytic NRR also achieved the purpose of improving electrocatalytic performance. Wen et al. [69] reported the preparation of independent 3D hybrid electrodes by *in-situ* growing N-doped carbon coated γ -Fe₂O₃ nanoparticles (γ -Fe₂O₃-NC/CF) (Fig. 9.5a). Figure 9.5b showed X-ray diffraction (XRD) pattern of γ -Fe₂O₃-NC/CF-700, and the main peak is very consistent with γ -Fe₂O₃ (JCPDS No. 39–1346). The transmission electron microscope (TEM) image of γ -Fe₂O₃-NC/CF-700 (Fig. 9.5c) showed that γ -Fe₂O₃ nanoparticles was composed of a large number of cross-linked nanoparticles embedded in a thin layer of carbon. The Faradaic efficiency and NH₃ yield on γ -Fe₂O₃-NC/CF-700 reached the highest values of 12.28% and 11.7×10^{-10} mol s⁻¹ cm⁻², and γ -Fe₂O₃-NC/CF-700 had stable NRR electrocatalytic ability (Fig. 9.5d). System characterization and comprehensive electrochemical studies showed that the γ -Fe₂O₃-NC/CF surface cation vacancies generated during the activation process were the main reason for improving the electrocatalytic activity of NRR [69]. Ding et al. [70] developed an interface engineering heterojunction consisting of CoS nanosheets anchored on TiO₂ nanofiber membranes. Figure 9.5e, f showed that the C@CoS@TiO₂ nanofiber membrane was composed of several micrometers nanofibers in length, which revealed the tight adhesion between the fibrous TiO₂ core and the layered CoS shell. The TiO₂ nanofiber membrane could uniformly limit the agglomeration of CoS nanosheets and greatly improve the NRR performance. The tight coupling between CoS and TiO₂ made charge transfer easier, resulting in rapid reaction kinetics at the heterogeneous interface. Carbon electroplating further improved the electrical conductivity and structural integrity of the heterojunction. The resulting C@CoS@TiO₂ electrocatalyst had a higher ammonia yield (8.09×10^{-10} mol s⁻¹ cm⁻²), FE (28.6%), and long-term durability (Fig. 9.5h).

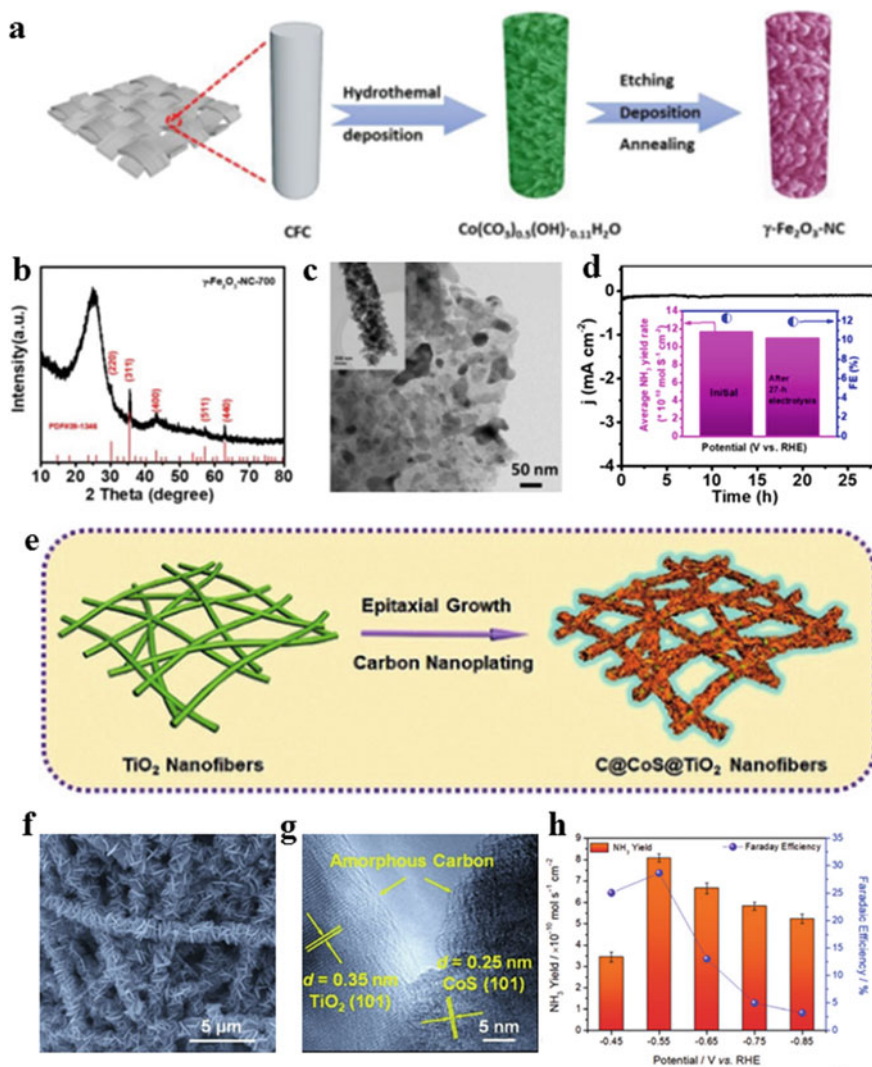


Fig. 9.5 Metal nanoparticles encapsulated carbon-based electrocatalysts for NRR. **a** Illustration of the synthesis process of $\gamma\text{-Fe}_2\text{O}_3\text{-NC/CF-700}$. **b**, **c** XRD pattern (**b**) and low- and high-magnification (inset) SEM images (**c**) and of $\gamma\text{-Fe}_2\text{O}_3\text{-NC/CF-700}$. **d** Long time-dependent current density curve for $\gamma\text{-Fe}_2\text{O}_3\text{-NC/CF-700}$ at -0.1 V (inset, NH_3 yield rates and FEs after charging at -0.1 V for 2 and 27 h). Reproduced with permission [69]. Copyright 2019, American Chemical Society. **e** Interfacial engineering of a TiO_2 nanofibrous membrane through coordination-driven epitaxial growth of CoS nanosheets followed by carbon nanoplating. **f** Low-magnification SEM images of a C@CoS@TiO_2 nanofibrous membrane. **g** HRTEM image of a C@CoS@TiO_2 nanofiber. **h** ammonia yields and Faradaic efficiencies of a C@CoS@TiO_2 nanofibrous membrane at different potentials. Reproduced with permission [70]. Copyright 2019, WILEY-VCH

9.5 Metal Nanoparticles Supported Carbon-Based Electrocatalysts for NRR

Supported metal nanoparticles catalyst is an important heterogeneous catalyst with the advantages of good recoverability and high atomic utilization [71]. It is widely used in various reactions and plays a vital role in the development of modern chemical industry. Metal nanoparticle catalysts have been widely used in heterogeneous catalysis because of their size dependence and high surface volume ratio [72]. Metal nanoparticles expose a large number of low coordination sites, which can be used as active sites to improve catalytic activity. However, the agglomeration of nanoparticles can lead to catalyst deactivation in many cases, which is then redistributed to restore performance [73, 74]. Therefore, it is very important to select the appropriate carrier. The selected material will not only play the role of carrier, but also interact strongly with metal components.

Metal catalysts supported on carbon materials are of great significance for the conversion of renewable energy. Carbon materials can not only fix metal nanoparticles and improve atomic utilization, but also affect the catalytic performance by engineering the electronic structure of active metal components [75]. The key parameters affecting the interaction between the load and the carbon substrate include metal properties, metal morphology, metal particle size, carbon structure, heteroatom doping, carbon coating and interface bonding [76]. The chemical environment and physical structure of carbon atoms will inevitably change the working function of the carrier, thus affecting the charge transfer between metal and carbon carrier [77]. Hybrid carbon atoms will redistribute electrons on the whole carbon carrier, resulting in the change of working function [78]. Although there are few reports on the charge transfer between precious metals and sp^3 hybrid diamond, it can be inferred that the charge will transfer from diamond to precious metals because the work function of diamond is less than that of all precious metals [79]. The contact interface between metal and carbon carrier controls the degree of metal carrier interaction and affects the coordination environment of metal [80]. In an ideal model system, metal nanoparticles are fixed on the surface of planar two-dimensional graphene. The corresponding structure is easy to simulate and study based on density functional theory (DFT) [81]. However, in practical catalysts, complex synthesis processes sometimes produce complex microstructure and form various types of metal/support interfaces [82]. Constructed heterojunctions and interfaces have been carefully established experimentally and theoretically [83].

As one of the most effective methods to adjust local electron arrangement, create rich active sites and improve charge transfer efficiency, they are jointly conducive to adjusting the chemical adsorption behavior of reaction intermediates, so as to enhance the intrinsic electrocatalytic activity [84]. In addition to electronic modulation through interface engineering to improve thermodynamics, fine nanostructure engineering also represents an effective way to maximize the exposure of catalytic active sites, shorten the mass transfer distance and promote the penetration of electrolyte [85]. Thus, the reaction kinetics is greatly accelerated. Structurally, the

branching hierarchy is particularly attractive for electrocatalysis due to the interconnection highway of electron transfer, open channels of mass diffusion and electrolyte penetration, and gas release. In addition, in order to improve the electrochemical stability of long-term operation, the direct integration of active components with conductive and solid matrix (such as carbonaceous materials and foamed nickel) is considered as an effective matrix for immobilized active components and enhancing electron transport capacity due to the chemical and electrical synergistic effects between active components [86].

Yan et al. [87] used a simple co-reduction method to achieve the amorphization of Au nanoparticles anchored on reduced graphite oxide (a-Au/CeO_x-RGO) in an ambient atmosphere (Fig. 9.6a). High-angle circular dark-field scanning transmission electron microscopy showed that Au nanoparticles were dispersed on the surface of CeO_x-RGO or RGO, with good dispersibility and similar particle size (~5 nm)

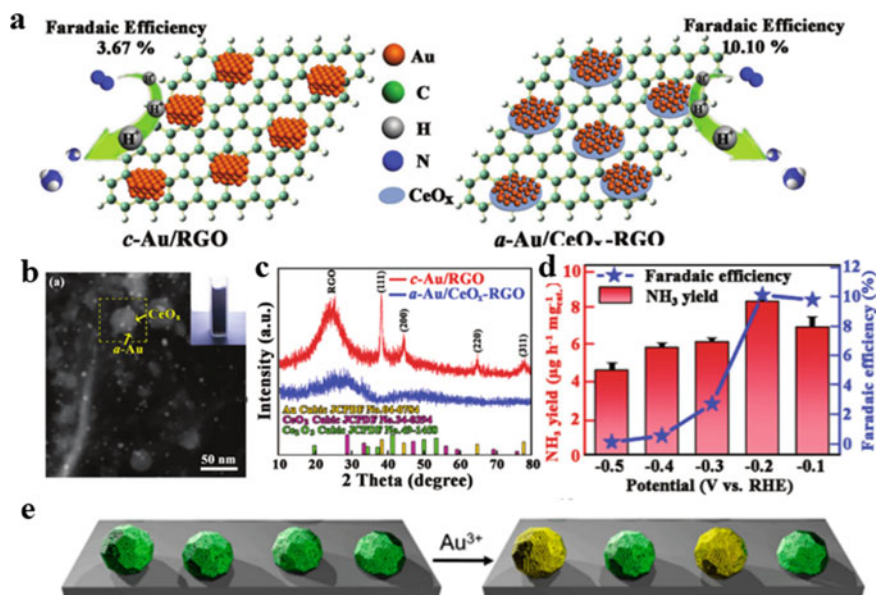


Fig. 9.6 Metal nanoparticles supported carbon-based electrocatalysts for NRR. **a** Schematic illustration for the electrochemical NRR by catalysts of a-Au/CeO_x-RGO and c-Au/RGO under ambient conditions. **b** Representative STEM image of the a-Au/CeO_x-RGO, and the inset is the photograph of a-Au/CeO_x-RGO suspended in water. **c** Representative XRD patterns of obtained a-Au/CeO_x-RGO (blue plot) and c-Au/RGO (red plot). **d** The yield of NH₃ (red) and FE (blue) at each given potential. Reproduced with permission [87]. Copyright 2017, WILEY-VCH. **e** Synthesis of donor-acceptor couples of Au and Ni nanoparticles. **f** EDX mapping results of Au₆/Ni. **g** NH₃ yield rate and FE at the corresponding potentials and **h** during the recycling test of Au₆/Ni. **i** The calculated electron density maps for N₂ adsorbed onto the surface of Au and electron-rich Au (Au + e⁻). **j** The calculated adsorption energies of N₂ and desorption energies of NH₃ adsorbed onto Au and Au + e⁻. **k** The N₂-TPD results of the Ni, Au₆/Ni, and Au₄₀/Ni catalysts normalized by the Au content. The insets show the corresponding structural models. Reproduced with permission [88]. Copyright 2019, American Chemical Society

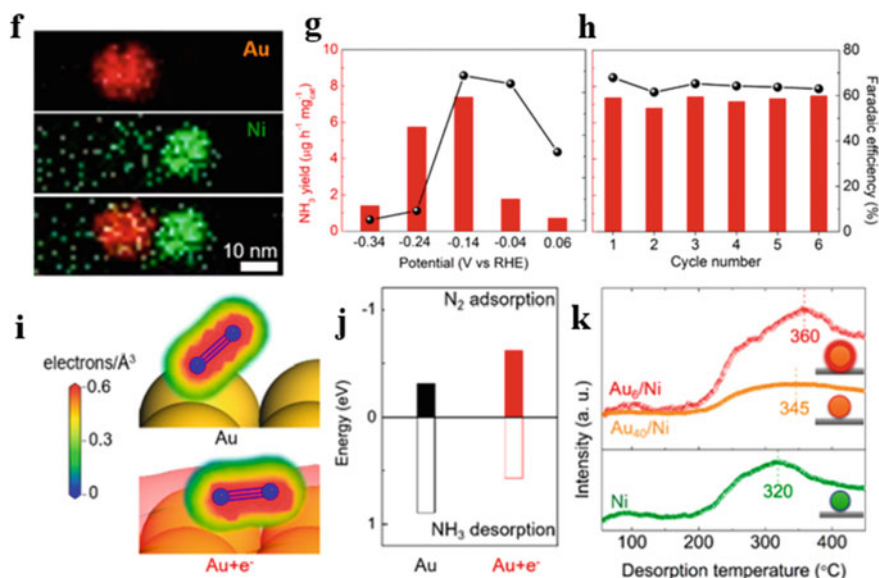


Fig. 9.6 (continued)

(Fig. 9.6b). XRD spectra confirmed that the CeO_x hybrid was amorphous/low crystalline, while the hybrid without CeO_x was polycrystalline (Fig. 9.6c). As a proof-of-concept experiment, the a-Au/CeO_x-RGO hybrid catalyst contained low precious metals (Au loading is 1.31 wt.%), and at -0.2 V versus RHE, it had a higher FE (10.10%) and ammonia yield (8.3 μg h⁻¹ mg⁻¹_{cat}) (Fig. 9.6d), which was significantly higher than the crystal counterpart (c-Au/RGO). It could even be comparable to the output and efficiency under severe temperature and/or pressure. Li et al. [88] proposed an effective method to increase the electron density of Au electrocatalysts by constructing an inorganic donor-acceptor coupling of Ni and Au nanoparticles (Fig. 9.6e), thereby significantly improved the NRR. The energy dispersive X-ray spectroscopy (EDX) elemental mapping images showed that Au nanoparticles were successfully deposited adjacent to Ni nanoparticles on a nitrogen-doped carbon carrier. At -0.14 V, the highest NH₃ yield was 7.4 μg h⁻¹ mg⁻¹_{cat}, and the FE was 67.8% (Fig. 9.6g). Most importantly, the Au₆/Ni-based electrode also provided a stable current density for NRR and provided repeatable NH₃ yield and FE at -0.14 V (vs. RHE) for 6 consecutive runs (Fig. 9.6h). Through theoretical simulation and experimental verification, the electron-rich Au surface induced the polarization of the adsorbed N₂ molecules, which was conducive to further adding hydrogen atoms to the electron-deficient N. After the catalytic surface changed from Au to the electron-rich Au model which happened obvious difference in the electron density of N₂ (Fig. 9.6i). This strong polarization effect also enhanced the pre-adsorption of N₂ molecules on the electron-rich Au surface, as predicted by the theoretically higher adsorption energy, and then passed through the N₂ temperature programmed

desorption (TPD) isotherm of the Au₆/Ni sample. The strong adsorption peak of N₂ was verified by experiments (Fig. 9.6k). It was also found that the desorption energy of NH₃ molecules on the electron-rich Au surface was reduced (Fig. 9.6j), indicating that the active sites were released quickly and new reactions could be carried out.

9.6 Conclusion and Perspectives

Understanding the relationship of structure and NRR activity is the key to exploring high-efficiency electrocatalysts. Effective electrocatalytic NRR depends to a large extent on electrocatalysts designed to solve interrelated competitive challenges: selectivity, efficiency and stability. This chapter summarizes the research progress of new carbon-based electrocatalytic NRR catalysts at home and abroad in recent years, including metal and its compound carbon materials, monoatomic carbon materials and non-metallic materials. It is a potential NRR catalyst that needs in-depth research in the future.

From experimental research and theoretical simulation, the activity of nanocarbon in electrocatalytic nitrogen reduction can be summarized into the following aspects: (1) The highly graphitized framework structure of nano-carbon provides a high-speed channel for electron migration; in addition, the porous structure facilitates the exposure of active sites, and the nano-confinement effect accelerates the reaction kinetics; (2) Surface defect sites of carbon nanomaterials, including structural vacancies, edges, surface functions and heteroatom doping are also critical to the catalytic activity of the active center. Fine-tuned electronic properties (such as electron density, charge transfer rate, and work function) and changes in surface physical properties enhance the affinity of nanocarbon materials for reactants; (3) The metal component, especially the transition metal species and the carbon nanomaterial composite, through the formation of the chemical bond between the two components on the interface and the synergistic effect of electron transfer, the catalytic performance of the surrounding carbon is further improved. The regulated spin structure improves the charge transfer ability, thereby promoting the redox cycle of metal ions as catalytic sites. At the same time, encapsulating the transition metal in the carbon frame or introducing a single-atom metal catalyst can provide abundant free electrons for the redox reaction, which significantly improves the reusability.

In some cases, the active center of the electrocatalyst may change, especially for variable structure and variable valence metal-based materials. Therefore, the structure/composition characteristics after electrolysis are recommended to determine the stable NRR active center of the electrocatalyst. In particular, *in-situ* photoelectron spectroscopy, synchrotron radiation and transmission electron microscopy are very useful for identifying the active structures/components of nitrogen-containing intermediates and their interaction with nitrogen-containing intermediates. In addition, it is recommended to design corresponding theoretical models for calculations based on stable structure information as much as possible. So as to provide a more reliable mechanism basis for the design of electrocatalysts. Most theoretical studies, such as

DFT calculations used to predict the research direction of high-efficiency electrocatalyst design, are based on appropriate simplifications of theoretical models. However, in the real-time operation of NRR, many factors need to be considered, such as structure/component evolution, adsorbent surface coverage, solvation effect, etc., in order to narrow the evaluation gap. In addition, it is very important to conduct theoretical research on electrocatalytic systems involving parameters such as salt concentration, pH and N₂ transport dynamics. Combining these two aspects can realize the design of an integrated, innovative and efficient non-nuclear reserve system.

In short, the conversion of N₂ to NH₃ in nature condition can show a broad potential for fertilizer production and significantly reduce global energy costs and carbon emissions. Despite the huge challenges, the combination of theoretical and experimental research, the combination of *in-situ*/operating parameter characterization techniques, and the combination of on-line rapid and accurate measurement of ammonia will further promote the development of high-efficiency catalytic activity and selective electrocatalysts for the production of NH₃. Moreover, the rational design of carbon catalysts with low cost, high activity, selectivity without sacrificing stability will be the focus of future research.

References

1. V. Rosca, M. Duca, M. Groot, M. Koper, Nitrogen cycle electrocatalysis. *Chem. Rev.* **109**, 2209–2244 (2009). <https://doi.org/10.1021/cr8003696>
2. B. Patil, Q. Wang, V. Hessel, J. Lang, Plasma N₂-fixation: 1900–2014. *Catal. Today* **256**, 49–66 (2015). <https://doi.org/10.1016/j.cattod.2015.05.005>
3. L. Shi, Y. Yin, S. Wang, H. Sun, Rational catalyst design for N₂ reduction under ambient conditions: strategies toward enhanced conversion efficiency. *ACS Catal.* **10**, 6870–6899 (2020). <https://doi.org/10.1021/acscatal.0c01081>
4. R. Song, J. Yang, M. Wang, Z. Shi, X. Zhu, X. Zhang, M. He, G. Liu, G. Qiao, Z. Xu, Theoretical study on P-coordinated metal atoms embedded in arsenene for the conversion of nitrogen to ammonia. *ACS Omega* **6**, 8662–8671 (2021). <https://doi.org/10.1021/acsomega.1c00581>
5. J. Erisman, M. Sutton, J. Galloway, Z. Klimont, W. Winiwarter, How a century of ammonia synthesis changed the world. *Nat. Geosci.* **1**, 636–639 (2008). <https://doi.org/10.1038/ngeo325>
6. J. Chen, R. Crooks, L. Seefeldt, K. Bren, R. Bullock, M. Darensbourg, P. Holland, B. Hoffman, M. Janik, A. Jones, M. Kanatzidis, P. King, K. Lancaster, S. Lymer, P. Pfromm, W. Schneider, R. Schrock, Beyond fossil fuel-driven nitrogen transformations. *Science* **360** (2018). <https://doi.org/10.1126/science.aar6611>
7. Y. Huang, N. Zhang, Z. Wu, X. Xie, Artificial nitrogen fixation over bismuth-based photocatalysts: fundamentals and future perspectives. *J. Mater. Chem. A* **8**, 4978–4995 (2020). <https://doi.org/10.1039/c9ta13589h>
8. A. Martín, T. Shinagawa, J. Pérez-Ramírez, Electrocatalytic reduction of nitrogen: from haber-bosch to ammonia artificial leaf. *Chem* **5**, 263–283 (2019). <https://doi.org/10.1016/j.chempr.2018.10.010>
9. W. Guo, K. Zhang, Z. Liang, R. Zou, Q. Xu, Electrochemical nitrogen fixation and utilization: theories, advanced catalyst materials and system design. *Chem. Soc. Rev.* **48**, 5658–5716 (2019). <https://doi.org/10.1039/c9cs00159j>
10. H. Jia, E. Quadrelli, Mechanistic aspects of dinitrogen cleavage and hydrogenation to produce ammonia in catalysis and organometallic chemistry: relevance of metal hydride bonds and dihydrogen. *Chem. Soc. Rev.* **43**, 547–564 (2014). <https://doi.org/10.1039/c3cs60206k>

11. P. Wang, F. Chang, W. Gao, J. Guo, G. Wu, T. He, P. Chen, Breaking scaling relations to achieve low-temperature ammonia synthesis through LiH-mediated nitrogen transfer and hydrogenation. *Nat. Chem.* **9**, 64–70 (2016). <https://doi.org/10.1038/nchem.2595>
12. X. Yan, D. Liu, H. Cao, F. Hou, J. Liang, S. Dou, Nitrogen reduction to ammonia on atomic-scale active sites under mild conditions. *Small Methods* **3** (2019). <https://doi.org/10.1002/smt.201800501>
13. X. Li, Q. Li, J. Cheng, L. Liu, Q. Yan, Y. Wu, X. Zhang, Z. Wang, Q. Qiu, Y. Luo, Conversion of dinitrogen to ammonia by FeN₃-embedded graphene. *J. Am. Chem. Soc.* **138**, 8706–8709 (2016). <https://doi.org/10.1021/jacs.6b04778>
14. R. Schrock, Catalytic reduction of dinitrogen to ammonia by molybdenum: theory versus experiment. *Angew. Chem. Int. Ed.* **47**, 5512–5522 (2008). <https://doi.org/10.1002/anie.200705246>
15. Y. Wan, J. Xu, R. Lv, Heterogeneous electrocatalysts design for nitrogen reduction reaction under ambient conditions. *Mater. Today* **27**, 69–90 (2019). <https://doi.org/10.1016/j.mattod.2019.03.002>
16. B. Yang, W. Ding, H. Zhang, S. Zhang, Recent progress in electrochemical synthesis of ammonia from nitrogen: strategies to improve the catalytic activity and selectivity. *Energy Environ. Sci.* **14**, 672–687 (2021). <https://doi.org/10.1039/d0ee02263b>
17. Y. Peng, B. Lu, S. Chen, Carbon-supported single atom catalysts for electrochemical energy conversion and storage. *Adv. Mater.* **30** (2018). <https://doi.org/10.1002/adma.201801995>
18. K. Zhao, X. Quan, Carbon-based materials for electrochemical reduction of CO₂ to C²⁺ oxygenates: recent progress and remaining challenges. *ACS Catal.* **11**, 2076–2097 (2021). <https://doi.org/10.1021/acscatal.0c04714>
19. S. Zhao, X. Lu, L. Wang, J. Gale, R. Amal, Carbon-based metal-free catalysts for electrocatalytic reduction of nitrogen for synthesis of ammonia at ambient conditions. *Adv. Mater.* **31** (2019). <https://doi.org/10.1002/adma.201805367>
20. Y. Yang, L. Zhang, Z. Hu, Y. Zheng, C. Tang, P. Chen, R. Wang, K. Qiu, J. Mao, T. Ling, S. Qiao, The crucial role of charge accumulation and spin polarization in activating carbon-based catalysts for electrocatalytic nitrogen reduction. *Angew. Chem. Int. Ed.* **59**, 4525–4531 (2020). <https://doi.org/10.1002/anie.201915001>
21. L. Han, X. Liu, J. Chen, R. Lin, H. Liu, F. Lü, S. Bak, Z. Liang, S. Zhao, E. Stavitski, J. Luo, R. Adzic, H. Xin, Atomically dispersed molybdenum catalysts for efficient ambient nitrogen fixation. *Angew. Chem. Int. Ed.* **58**, 2321–2325 (2019). <https://doi.org/10.1002/anie.201811728>
22. S. Liu, M. Wang, T. Qian, H. Ji, J. Liu, C. Yan, Facilitating nitrogen accessibility to boron-rich covalent organic frameworks via electrochemical excitation for efficient nitrogen fixation. *Nat. Commun.* **10** (2019). <https://doi.org/10.1038/s41467-019-11846-x>
23. X. Guo, S. Chen, H. Wang, Z. Zhang, H. Lin, L. Song, T. Lu, Single-atom molybdenum immobilized on photoactive carbon nitride as efficient photocatalysts for ambient nitrogen fixation in pure water. *J. Mater. Chem. A* **7**, 19831–19837 (2019). <https://doi.org/10.1039/c9ta06653e>
24. Y. Ma, T. Yang, H. Zou, W. Zang, Z. Kou, L. Mao, Y. Feng, L. Shen, S. Pennycook, L. Duan, X. Li, J. Wang, Synergizing Mo single atoms and Mo₂C nanoparticles on cnts synchronizes selectivity and activity of electrocatalytic N₂ reduction to ammonia. *Adv. Mater.* **32** (2020). <https://doi.org/10.1002/adma.202002177>
25. L. Li, J. Martinez, E. Carter, Prediction of highly selective electrocatalytic nitrogen reduction at low overpotential on a Mo-doped g-GaN monolayer. *ACS Catal.* **10**, 12841–12857 (2020). <https://doi.org/10.1021/acscatal.0c03140>
26. D. Liu, M. Chen, X. Du, H. Ai, K. Lo, S. Wang, S. Chen, G. Xing, X. Wang, H. Pan, Development of electrocatalysts for efficient nitrogen reduction reaction under ambient condition. *Adv. Funct. Mater.* **31** (2020). <https://doi.org/10.1002/adfm.202008983>
27. C. Ling, X. Niu, Q. Li, A. Du, J. Wang, Metal-free single atom catalyst for N₂ fixation driven by visible light. *J. Am. Chem. Soc.* **140**, 14161–14168 (2018). <https://doi.org/10.1021/jacs.8b07472>

28. X. Cui, C. Tang, Q. Zhang, A review of electrocatalytic reduction of dinitrogen to ammonia under ambient conditions. *Adv. Energy Mater.* **8** (2018). <https://doi.org/10.1002/aenm.201800369>
29. G. Chen, Y. Xu, L. Huang, A. Douka, B. Xia, Continuous nitrogen-doped carbon nanotube matrix for boosting oxygen electrocatalysis in rechargeable Zn-air batteries. *J. Energy Chem.* **55**, 183–189 (2021). <https://doi.org/10.1016/j.jechem.2020.07.012>
30. G. Chen, X. Cao, S. Wu, X. Zeng, L. Ding, M. Zhu, H. Wang, Ammonia electrosynthesis with high selectivity under ambient conditions via a Li⁺ incorporation strategy. *J. Am. Chem. Soc.* **139**, 9771–9774 (2017). <https://doi.org/10.1021/jacs.7b04393>
31. X. Liu, M. Antonietti, Moderating black powder chemistry for the synthesis of doped and highly porous graphene nanoplatelets and their use in electrocatalysis. *Adv. Mater.* **25**, 6284–6290 (2013). <https://doi.org/10.1002/adma.201302034>
32. L. Peng, L. Shang, T. Zhang, G. Waterhouse, Recent advances in the development of single-atom catalysts for oxygen electrocatalysis and zinc–air batteries. *Adv. Energy Mater.* **10** (2020). <https://doi.org/10.1002/aenm.202003018>
33. K. Tu, D. Tranca, F. Rodríguez-Hernández, K. Jiang, S. Huang, Q. Zheng, M. Chen, C. Lu, Y. Su, Z. Chen, H. Mao, C. Yang, J. Jiang, H. Liang, X. Zhuang, A novel heterostructure based on RuMo nanoalloys and N-doped carbon as an efficient electrocatalyst for the hydrogen evolution reaction. *Adv. Mater.* **32** (2020). <https://doi.org/10.1002/adma.202005433>
34. Y. Liu, Y. Su, X. Quan, X. Fan, S. Chen, H. Yu, H. Zhao, Y. Zhang, J. Zhao, Facile ammonia synthesis from electrocatalytic N₂ reduction under ambient conditions on N-doped porous carbon. *ACS Catal.* **8**, 1186–1191 (2018). <https://doi.org/10.1021/acscatal.7b02165>
35. S. Mukherjee, D. Cullen, S. Karakalos, K. Liu, H. Zhang, S. Zhao, H. Xu, K. More, G. Wang, G. Wu, Metal-organic framework-derived nitrogen-doped highly disordered carbon for electrochemical ammonia synthesis using N₂ and H₂O in alkaline electrolytes. *Nano Energy* **48**, 217–226 (2018). <https://doi.org/10.1016/j.nanoen.2018.03.059>
36. W. Qiu, X. Xie, J. Qiu, W. Fang, R. Liang, X. Ren, X. Ji, G. Cui, A. Asiri, G. Cui, B. Tang, X. Sun, High-performance artificial nitrogen fixation at ambient conditions using a metal-free electrocatalyst. *Nature Commun.* **9** (2018). <https://doi.org/10.1038/s41467-018-05758-5>
37. L. Xia, X. Wu, Y. Wang, Z. Niu, Q. Liu, T. Li, X. Shi, A. Asiri, X. Sun, S-doped carbon nanospheres: an efficient electrocatalyst toward artificial N₂ fixation to NH₃. *Small Methods* **3** (2018). <https://doi.org/10.1002/smt.201800251>
38. J. Wang, S. Wang, J. Li, S-doped three-dimensional graphene (S-3DG): a metal-free electrocatalyst for the electrochemical synthesis of ammonia under ambient conditions. *Dalton Trans.* **49**, 2258–2263 (2020). <https://doi.org/10.1039/c9dt04827h>
39. H. Li, C. Huang, Recent advances in the application of structural-phase engineering strategies in electrochemical nitrogen reduction reaction. *Adv. Mater. Interf.* **7** (2020). <https://doi.org/10.1002/admi.202001215>
40. Q. Zhang, J. Guan, Single-atom catalysts for electrocatalytic applications. *Adv. Funct. Mater.* **30** (2020). <https://doi.org/10.1002/adfm.202000768>
41. Y. Chen, S. Ji, C. Chen, Q. Peng, D. Wang, Y. Li, Single-atom catalysts: Synthetic strategies and electrochemical applications. *Joule* **2**, 1242–1264 (2018). <https://doi.org/10.1016/j.joule.2018.06.019>
42. J. Kim, H. Kim, H. Lee, Single-atom catalysts of precious metals for electrochemical reactions. *ChemSuschem* **11**, 104–113 (2018). <https://doi.org/10.1002/cssc.201701306>
43. M. Hu, J. Zhang, W. Zhu, Z. Chen, X. Gao, X. Du, J. Wan, K. Zhou, C. Chen, Y. Li, 50 ppm of Pd dispersed on Ni(OH)₂ nanosheets catalyzing semi-hydrogenation of acetylene with high activity and selectivity. *Nano Res.* **11**, 905–912 (2017). <https://doi.org/10.1007/s12274-017-1701-5>
44. Y. Lykhach, A. Bruix, S. Fabris, V. Potin, I. Matolínová, V. Matolín, J. Libuda, K. Neyman, Oxide-based nanomaterials for fuel cell catalysis: the interplay between supported single Pt atoms and particles. *Catal. Sci. Technol.* **7**, 4315–4345 (2017). <https://doi.org/10.1039/c7cy00710h>

45. X. Zhang, Z. Wu, X. Zhang, L. Li, Y. Li, H. Xu, X. Li, X. Yu, Z. Zhang, Y. Liang, H. Wang, Highly selective and active CO₂ reduction electrocatalysts based on cobalt phthalocyanine/carbon nanotube hybrid structures. *Nat. Commun.* **8** (2017). <https://doi.org/10.1038/ncomms14675>
46. H. Zhang, G. Liu, L. Shi, J. Ye, Single-atom catalysts: Emerging multifunctional materials in heterogeneous catalysis. *Adv. Energy Mater.* **8** (2018). <https://doi.org/10.1002/aenm.201701343>
47. A. Guan, Z. Chen, Y. Quan, C. Peng, Z. Wang, T. Sham, C. Yang, Y. Ji, L. Qian, X. Xu, G. Zheng, Boosting CO₂ electroreduction to CH₄ via tuning neighboring single-copper sites. *ACS Energy Lett.* **5**, 1044–1053 (2020). <https://doi.org/10.1021/acseenergylett.0c00018>
48. Y. Xiong, J. Dong, Z. Huang, P. Xin, W. Chen, Y. Wang, Z. Li, Z. Jin, W. Xing, Z. Zhuang, J. Ye, X. Wei, R. Cao, L. Gu, S. Sun, L. Zhuang, X. Chen, H. Yang, C. Chen, Q. Peng, C. Chang, D. Wang, Y. Li, Single-atom Rh/N-doped carbon electrocatalyst for formic acid oxidation. *Nat. Nanotechnol.* **15**, 390–397 (2020). <https://doi.org/10.1038/s41565-020-0665-x>
49. X. Li, X. Yang, J. Zhang, Y. Huang, B. Liu, In Situ/Operando techniques for characterization of single-atom catalysts. *ACS Catal.* **9**, 2521–2531 (2019). <https://doi.org/10.1021/acscatal.8b04937>
50. Y. Wang, W. Cheng, P. Yuan, G. Yang, S. Mu, J. Liang, H. Xia, K. Guo, M. Liu, S. Zhao, G. Qu, B. Lu, Y. Hu, J. Hu, J. Zhang, Boosting nitrogen reduction to ammonia on FeN₄ sites by atomic spin regulation. *Adv. Sci.* **8** (2021). <https://doi.org/10.1002/advs.202102915>
51. G. Yang, J. Zhu, P. Yuan, Y. Hu, G. Qu, B. Lu, X. Xue, H. Yin, W. Cheng, J. Cheng, W. Xu, J. Li, J. Hu, S. Mu, J. Zhang, Regulating Fe-spin state by atomically dispersed Mn-N in Fe-N-C catalysts with high oxygen reduction activity. *Nat. Commun.* **12** (2021). <https://doi.org/10.1038/s41467-021-21919-5>
52. J. Su, R. Ge, Y. Dong, F. Hao, L. Chen, Recent progress in single-atom electrocatalysts: concept, synthesis, and applications in clean energy conversion. *J. Mater. Chem. A* **6**, 14025–14042 (2018). <https://doi.org/10.1039/c8ta04064h>
53. W. Zang, T. Yang, H. Zou, S. Xi, H. Zhang, X. Liu, Z. Kou, Y. Du, Y. Feng, L. Shen, L. Duan, J. Wang, S. Pennycook, Copper single atoms anchored in porous nitrogen-doped carbon as efficient pH-universal catalysts for the nitrogen reduction reaction. *ACS Catal.* **9**, 10166–10173 (2019). <https://doi.org/10.1021/acscatal.9b02944>
54. H. Tao, C. Choi, L. Ding, Z. Jiang, Z. Han, M. Jia, Q. Fan, Y. Gao, H. Wang, A. Robertson, S. Hong, Y. Jung, S. Liu, Z. Sun, Nitrogen fixation by Ru single-atom electrocatalytic reduction. *Chem* **5**, 204–214 (2019). <https://doi.org/10.1016/j.chempr.2018.10.007>
55. C. Lv, C. Yan, G. Chen, Y. Ding, J. Sun, Y. Zhou, G. Yu, An amorphous noble-metal-free electrocatalyst that enables nitrogen fixation under ambient conditions. *Angew. Chem. Int. Ed.* **57**, 6073–6076 (2018). <https://doi.org/10.1002/anie.201801538>
56. Y. Zhang, W. Qiu, Y. Ma, Y. Luo, Z. Tian, G. Cui, F. Xie, L. Chen, T. Li, X. Sun, High-performance electrohydrogenation of N₂ to NH₃ catalyzed by multishelled Hollow Cr₂O₃ microspheres under ambient conditions. *ACS Catal.* **8**, 8540–8544 (2018). <https://doi.org/10.1021/acscatal.8b02311>
57. J. Han, X. Ji, X. Ren, G. Cui, L. Li, F. Xie, H. Wang, B. Li, X. Sun, MoO₃ nanosheets for efficient electrocatalytic N₂ fixation to NH₃. *J. Mater. Chem. A* **6**, 12974–12977 (2018). <https://doi.org/10.1039/c8ta03974g>
58. L. Zhang, X. Ji, X. Ren, Y. Ma, X. Shi, Z. Tian, A. Asiri, L. Chen, B. Tang, X. Sun, Electrochemical ammonia synthesis via nitrogen reduction reaction on a MoS₂ catalyst: theoretical and experimental studies. *Adv. Mater.* **30** (2018). <https://doi.org/10.1002/adma.201800191>
59. X. Yang, J. Nash, J. Anibal, M. Dunwell, S. Kattel, E. Stavitski, K. Attenkofer, J. Chen, Y. Yan, B. Xu, Mechanistic insights into electrochemical nitrogen reduction reaction on vanadium nitride nanoparticles. *J. Am. Chem. Soc.* **140**, 13387–13391 (2018). <https://doi.org/10.1021/jacs.8b08379>
60. Y. Luo, G. Chen, L. Ding, X. Chen, L. Ding, H. Wang, Efficient electrocatalytic N₂ fixation with mxene under ambient conditions. *Joule* **3**, 279–289 (2019). <https://doi.org/10.1016/j.joule.2018.09.011>

61. M. Jin, S. Lu, L. Ma, M. Gan, Y. Lei, X. Zhang, G. Fu, P. Yang, M. Yan, Different distribution of in-situ thin carbon layer in hollow cobalt sulfide nanocages and their application for supercapacitors. *J. Power Sources* **341**, 294–301 (2017). <https://doi.org/10.1016/j.jpowsour.2016.12.013>
62. F. Luo, Q. Zhang, K. Qu, L. Guo, H. Hu, Z. Yang, W. Cai, H. Cheng, Decorated PtRu electrocatalyst for concentrated direct methanol fuel cells. *ChemCatChem* **11**, 1238–1243 (2019). <https://doi.org/10.1002/cctc.201801801>
63. P. Chen, N. Zhang, S. Wang, T. Zhou, Y. Tong, C. Ao, W. Yan, L. Zhang, W. Chu, C. Wu, Y. Xie, Interfacial engineering of cobalt sulfide/graphene hybrids for highly efficient ammonia electrosynthesis. *Proc. Natl. Acad. Sci.* **116**, 6635–6640 (2019). <https://doi.org/10.1073/pnas.1817881116>
64. Y. Xu, W. Tu, B. Zhang, S. Yin, Y. Huang, M. Kraft, R. Xu, Nickel nanoparticles encapsulated in few-layer nitrogen-doped graphene derived from metal-organic frameworks as efficient bifunctional electrocatalysts for overall water splitting. *Adv. Mater.* **29** (2017). <https://doi.org/10.1002/adma.201605957>
65. D. Chung, S. Jun, G. Yoon, H. Kim, J. Yoo, K. Lee, T. Kim, H. Shin, A. Sinha, S. Kwon, K. Kang, T. Hyeon, Y. Sung, Large-scale synthesis of carbon-shell-coated FeP nanoparticles for robust hydrogen evolution reaction electrocatalyst. *J. Am. Chem. Soc.* **139**, 6669–6674 (2017). <https://doi.org/10.1021/jacs.7b01530>
66. P. Chen, T. Zhou, L. Xing, K. Xu, Y. Tong, H. Xie, L. Zhang, W. Yan, W. Chu, C. Wu, Y. Xie, Atomically dispersed iron-nitrogen species as electrocatalysts for bifunctional oxygen evolution and reduction reactions. *Angew. Chem. Int. Ed.* **56**, 610–614 (2017). <https://doi.org/10.1002/anie.201610119>
67. G. Chai, K. Qiu, M. Qiao, M. Titirici, C. Shang, Z. Guo, Active sites engineering leads to exceptional ORR and OER bifunctionality in P, N Co-doped graphene frameworks. *Energy Environ. Sci.* **10**, 1186–1195 (2017). <https://doi.org/10.1039/c6ee03446b>
68. Y. Hou, M. Qiu, T. Zhang, J. Ma, S. Liu, X. Zhuang, C. Yuan, X. Feng, Efficient electrochemical and photoelectrochemical water splitting by a 3d nanostructured carbon supported on flexible exfoliated graphene foil. *Adv. Mater.* **29** (2017). <https://doi.org/10.1002/adma.201604480>
69. Y. Li, Y. Kong, Y. Hou, B. Yang, Z. Li, L. Lei, Z. Wen, In situ growth of nitrogen-doped carbon-coated γ -Fe₂O₃ nanoparticles on carbon fabric for electrochemical N₂ fixation. *ACS Sustain. Chem. Eng.* **7**, 8853–8859 (2019). <https://doi.org/10.1021/acssuschemeng.9b00852>
70. Y. Liu, X. Chen, J. Yu, B. Ding, Carbon-nanoplated CoS@TiO₂ nanofibrous membrane: an interface-engineered heterojunction for high-efficiency electrocatalytic nitrogen reduction. *Angew. Chem. Int. Ed.* **58**, 18903–18907 (2019). <https://doi.org/10.1002/anie.201912733>
71. Q. Yan, P. Yin, H. Liang, Engineering the electronic interaction between metals and carbon supports for oxygen/hydrogen electrocatalysis. *ACS Mater. Lett.* **3**, 1197–1212 (2021). <https://doi.org/10.1021/acsmaterialslett.1c00266>
72. J. Wang, Z. Wei, S. Mao, H. Li, Y. Wang, Highly uniform Ru nanoparticles over N-doped carbon: pH and temperature-universal hydrogen release from water reduction. *Energy Environ. Sci.* **11**, 800–806 (2018). <https://doi.org/10.1039/c7ee03345a>
73. J. Lu, B. Fu, M. Kung, G. Xiao, J. Elam, H. Kung, P. Stair, Coking- and sintering-resistant palladium catalysts achieved through atomic layer deposition. *Science* **335**, 1205–1208 (2012). <https://doi.org/10.1126/science.1212906>
74. Q. Fu, W. Li, Y. Yao, H. Liu, H. Su, D. Ma, X. Gu, L. Chen, Z. Wang, H. Zhang, B. Wang, X. Bao, Interface-confined ferrous centers for catalytic oxidation. *Science* **328**, 1141–1144 (2010). <https://doi.org/10.1126/science.1188267>
75. O. Leenaerts, B. Partoens, F. Peeters, A. Volodin, C. Van Haesendonck, The work function of few-layer graphene. *J. Phys. Condensed Matter* **29**, 035003 (2017). <https://doi.org/10.1088/0953-8984/29/3/035003>
76. R. Garg, N. Dutta, N. Choudhury, Work function engineering of graphene. *Nanomaterials* **4**, 267–300 (2014). <https://doi.org/10.3390/nano4020267>
77. P. Liu, Q. Sun, F. Zhu, K. Liu, K. Jiang, L. Liu, Q. Li, S. Fan, Measuring the work function of carbon nanotubes with thermionic method. *Nano Lett.* **8**, 647–651 (2007). <https://doi.org/10.1021/nl0730817>

78. G. Gupta, D. Slanac, P. Kumar, J. Wiggins-Camacho, J. Kim, R. Ryoo, K. Stevenson, K. Johnston, Highly stable Pt/ordered graphitic mesoporous carbon electrocatalysts for oxygen reduction. *J. Phys. Chem. C* **114**, 10796–10805 (2009). <https://doi.org/10.1021/jp907015j>
79. S. Campisi, C. Chan-Thaw, A. Villa, Understanding heteroatom-mediated metal–support interactions in functionalized carbons: a perspective review. *Appl. Sci.* **8** (2018). <https://doi.org/10.3390/app8071159>
80. I. Gerber, P. Serp, A theory/experience description of support effects in carbon-supported catalysts. *Chem. Rev.* **120**, 1250–1349 (2020). <https://doi.org/10.1021/acs.chemrev.9b00209>
81. Y. Liu, H. Wang, T. Zhao, B. Zhang, H. Su, Z. Xue, X. Li, J. Chen, Schottky barrier induced coupled interface of electron-rich N-doped carbon and electron-deficient Cu: in-built lewis acid-base pairs for highly efficient CO₂ fixation. *J. Am. Chem. Soc.* **141**, 38–41 (2019). <https://doi.org/10.1021/jacs.8b08267>
82. Y. Lin, S. Zhang, Z. Xue, J. Zhang, H. Su, T. Zhao, G. Zhai, X. Li, M. Antonietti, J. Chen, Boosting selective nitrogen reduction to ammonia on electron-deficient copper nanoparticles. *Nat. Commun.* **10**, 4380 (2019). <https://doi.org/10.1038/s41467-019-12312-4>
83. Y. Cao, S. Mao, M. Li, Y. Chen, Y. Wang, Metal/Porous carbon composites for heterogeneous catalysis: old catalysts with improved performance promoted by N-doping. *ACS Catal.* **7**, 8090–8112 (2017). <https://doi.org/10.1021/acscatal.7b02335>
84. A. Wu, Y. Xie, H. Ma, C. Tian, Y. Gu, H. Yan, X. Zhang, G. Yang, H. Fu, Integrating the active OER and HER components as the heterostructures for the efficient overall water splitting. *Nano Energy* **44**, 353–363 (2018). <https://doi.org/10.1016/j.nanoen.2017.11.045>
85. T. Li, T. Lu, Y. Li, J. Yin, Y. Tang, M. Zhang, H. Pang, L. Xu, J. Yang, Y. Zhang, Interfacial engineering-induced electronic regulation drastically enhances the electrocatalytic oxygen evolution: immobilization of janus-structured NiS/NiO nanoparticles onto carbon nanotubes/nanofiber-integrated superstructures. *Chem. Eng. J.* **428** (2022). <https://doi.org/10.1016/j.cej.2021.131094>
86. S. Jeong, K. Hu, T. Ohto, Y. Nagata, H. Masuda, J. Fujita, Y. Ito, Effect of graphene encapsulation of NiMo alloys on oxygen evolution reaction. *ACS Catal.* **10**, 792–799 (2019). <https://doi.org/10.1021/acscatal.9b04134>
87. S. Li, D. Bao, M. Shi, B. Wulan, J. Yan, Q. Jiang, Amorphizing of Au nanoparticles by CeO_x-RGO hybrid support towards highly efficient electrocatalyst for N₂ reduction under ambient conditions. *Adv. Mater.* **29** (2017). <https://doi.org/10.1002/adma.201700001>
88. Z. Xue, S. Zhang, Y. Lin, H. Su, G. Zhai, J. Han, Q. Yu, X. Li, M. Antonietti, J. Chen, Electrochemical reduction of N₂ into NH₃ by donor–acceptor couples of Ni and Au nanoparticles with a 67.8% faradaic efficiency. *J. Am. Chem. Soc.* **141**, 14976–14980 (2019). <https://doi.org/10.1021/jacs.9b07963>

Chapter 10

Carbon-Based Nanomaterials for Metal-Ion Batteries



Yifan Wei, Huicong Xia, and Gan Qu

Abstract With the increasing dependence on fossil energy, environmental pollution has become a serious problem for human beings. Renewable energy has been developed to reduce the use of non-renewable sources. Clean energy, such as wind, solar and tidal power, suffers from time and space factors. Therefore, energy storage system is required to match the development of clean energy. Metal-ion batteries (MIBs) have attracted much attention due to their high-energy density and cycle life. Among MIBs, lithium-ion batteries (LIBs), sodium-ion batteries (SIBs), and potassium-ion batteries (PIBs) have attracted the most attention. However, metal ion batteries also face some problems. Due to the large radius of sodium/potassium ions, the active site cannot be fully utilized during the insertion/deinsertion process. In addition, charge transfer, ion transfer and volume change should be paid attention to in the exploit of electrode materials. In this regard, carbon-based nanomaterials show great potential. This chapter focuses on the application of carbon-based nanomaterials in MIBs, including metal-free carbon-based materials, atomically dispersed metal on carbon-based materials, metal nanoparticles encapsulated by carbon-based materials and metal nanoparticles supported on carbon-based materials. Finally, the application of carbon-based nanomaterials in metal batteries is briefly prospected, aiming to provide some enlightenment for the design and manufacture of MIBs.

Y. Wei · H. Xia · G. Qu (✉)

College of Materials Science and Engineering, Zhengzhou University, Zhengzhou 450001,
P. R. China

e-mail: gqu@zzu.edu.cn

Y. Wei

e-mail: Ivan98cn@163.com

H. Xia

e-mail: summer9209@126.com

10.1 Introduction

With the rapid development of society, the overuse of coal, oil, diesel, and other non-renewable energy resources results in the extreme shortage of traditional fossil energy in the world [1–5]. At the same time, over-consumption of fossil energy brings about serious environmental problems, such as the greenhouse effect, acid rain, haze, etc. Therefore, the development and utilization of renewable clean energy become the key to solving the energy crisis and environmental problems.

Metal-ion batteries (MIBs), such as lithium-ion batteries (LIBs), [6, 7] sodium-ion batteries (SIBs), [8–10] and potassium-ion batteries (PIBs) [11–13] have been widely studied in the fields of electrochemical energy storage. MIBs show well electrochemical stability with excellent specific density and energy density [14]. Because of the high specific density and abundant reserves, MIBs have achieved large-scale commercial applications. At present, LIBs are the most widely used MIBs in the market. LIBs play an indispensable role in the portable backup power supply, electronic devices, and electric vehicles, etc. Furthermore, LIBs act as a necessary part to promote the development of other clean energy sources. In addition, recent studies have shown that SIBs and PIBs also have the potential for commercialization in the future.

LIBs have firstly applied in the portable instrument (Fig. 10.1) but have not been effectively exploited in grid-scale supply systems. LIBs are the most promising

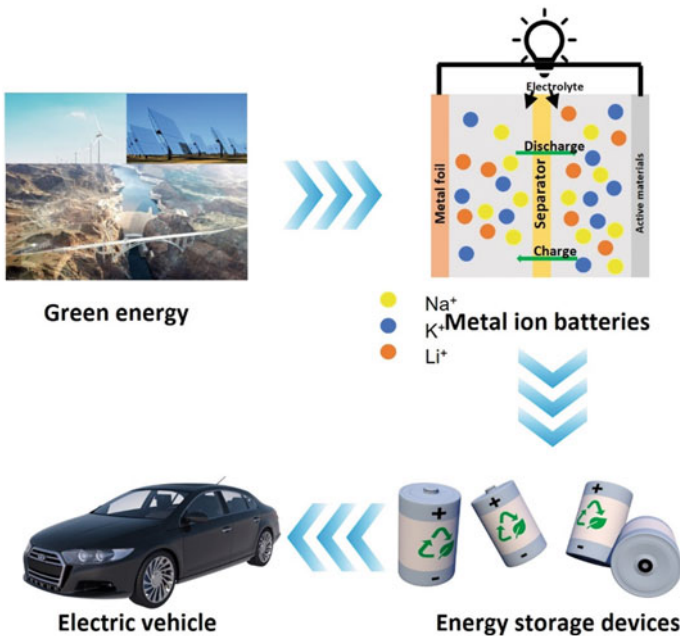


Fig. 10.1 Schematic diagram of metal-ion batteries in application

energy storage devices. Rachid et al. [15] firstly realized the assembly of LIBs in the early 1980s by intercalation/deintercalation of Li^+ in graphite. During the charging process, lithium ions move from the cathode, which goes across the separator and the electrolyte, and arrive on the anode side. Several common commercial cathodes have been developed, such as lithium cobalt oxide (LCO), lithium manganese oxide (LMO), lithium iron phosphate (LFP), lithium nickel cobalt aluminum oxide (NCA), and lithium nickel manganese cobalt oxide (NMC) [16]. The lithium oxides show the lower conductivity, which means the higher impedance. By mixing the lithium oxides with conductive carbon can improve the conductivity. The electrolyte is obtained by dissolving the lithium salts in organic solvents. Usually, lithium-hexafluorophosphate (LiPF_6) is widely used in laboratory research and commercial production [17].

SIBs have also attracted a great deal of attention in the energy storage field because of its high reserves in the earth. As mentioned above, lithium source is limited, and the price of LIBs is high. In order to mitigate this issue, the recent research focused on the next-generation energy storage systems. SIBs seem to be the best candidate. The SIBs and LIBs are more widely available and the SIBs exhibit similar electrochemistry as LIBs. Importantly, the sodium source is more abundant than that of Li. The cathode materials of SIBs are mainly categorized into polyanions, organic compounds and metal oxides, etc. Hard carbon materials, transition metals and their alloys are often used as anode materials. The electrolytes in SIBs should meet the following properties: (1) chemically stable, (2) thermally stable, and (3) electrochemically stable [18, 19]. NaClO_4 and NaPF_6 are often used as the electrolytes in SIBs [20].

PIBs show super-fast ionic conductivity in electrolytes and high working voltage, but the research on PIBs is still in the infancy [21–23]. The reserve of potassium in the earth is the most abundant, which leads to a low cost (the price of K_2CO_3 is similar to Na_2CO_3 , much cheaper than Li_2CO_3). Potassium shows a larger atomic radius (1.38 Å), while the Stokes radius of K^+ (3.6 Å) is the smallest among the Li, Na, and K. Therefore, K^+ -electrolyte shows the highest ion mobility and conductivity. However, there are still many challenges to solve in PIBs, such as poor K^+ reaction kinetics, large volume variations during the intercalation/deintercalation process, etc. [24].

For the kinds of MIBs, one of the biggest factors that restricting their energy density and specific density is the electrode materials. Thus, different electrode materials can lead to different energy densities and capacity densities. Taking the example of SIBs, Sb@porous carbon deriving from metal–organic framework shows the higher reversible capacity ($634.6 \text{ mA h g}^{-1}$) compared with that of $\text{Fe}_3\text{O}_4/\text{Fe}_{1-x}\text{S}$ @carbon-coated MoS_2 nanosheet (589 mA h g^{-1}) [25]. Therefore, the research on electrode materials is of great significance in improving the electrochemical performance in MIBs.

In the past years, carbon-based electrode materials have attracted wide attention. Up to now, a large number of carbon-based electrode materials with different compositions, crystal structures and morphologies have been reported. Carbon-based materials display great potential in MIBs due to their renewable essence, low price, porous

structure, and large specific surface area [26, 27]. In this section, carbon-based materials are classified as metal-free carbon-based materials, atomically dispersed metal on carbon-based materials, metal nanoparticles encapsulated carbon-based materials, and metal nanoparticles supported carbon-based materials. In this section, a series of carbon-based electrode materials are reviewed in MIBs. This chapter provides a clear direction for the future research and application of carbon-based materials in MIBs to achieve higher specific capacity and energy density.

10.2 Metal-Free Carbon-Based Materials for MIBs

As a widely used electrode material, carbon-based material shows the characteristics of low thermal expansion coefficient and low density. In addition, carbon-based material shows excellent conductivity. Therefore, the carbon-based material has received extensive attention. The traditional carbon materials, such as Ketjen Black (KB) and carbon black (SP, super P), are widely used in MIBs. It is reported that the heteroatom-doped carbon deriving from the nutshell provides additional holes or electrons delivers increased the conductivity. This strategy to improve the conductivity is widely studied in the electrode materials of MIBs. However, it is still a huge challenge to synthesize heteroatom-doped two-dimensional and three-dimensional (3D) carbon-based electrode materials with hierarchical pores.

The reported doping-atoms in electrode materials mainly include N, [28] P, [29] S, [30] etc. Huang et al. [31] synthesized the N-doped 3D mesoporous carbon nanosheets (N-CNS) by rational design. As shown in Fig. 2a, a carbon layer was uniformly deposited on the MgO nanosheet template after thermal annealing of the phenyl carbon (PC). The PC carbonizes on the surface of MgO during the annealing process. Then, the N-CNS can be obtained after acid pickling (HCl). It was worth mentioning that this method can be widely used to prepare the similar porous N-doped carbon-based materials after replacing the template with other nanostructures (e.g., SiO₂). As shown in Fig. 2b, the prepared electrode material showed numerous defects. The characterized graphite nitrogen, pyridine nitrogen and pyrrole nitrogen provided a large number of sites for adsorption of sodium and potassium ions. By adjusting the morphology, defect and nanostructures, the SIBs and PIBs have achieved excellent rate capability and cycle life. Zhang et al. [32] also utilized N as heteroatom to achieve the precise control of nitrogen-doped carbon-based materials through the pyrolysis of copolymers. Compared with graphitized N, edge nitrogen (pyrrole nitrogen and pyridine nitrogen) showed higher adsorption energy towards metal ion. The pyrolysis of polyaniline-co-polypyrrole (PACP) endowed more edge-nitrogen doped carbons (ENDCs) through releasing the free radicals from pyrrole and aniline. The pyrolysis conditions can be optimized to increase the doping level of N. The electron paramagnetic resonance (EPR, Fig. 2c) spectra of ENDCs and NDC900 (N-doped carbons formed under 900 °C) was used to interpret the structure of ENDCs. The *g* value of 2.0027 indicated the generation of unpaired electrons on *p*-conjugated carbon atoms.

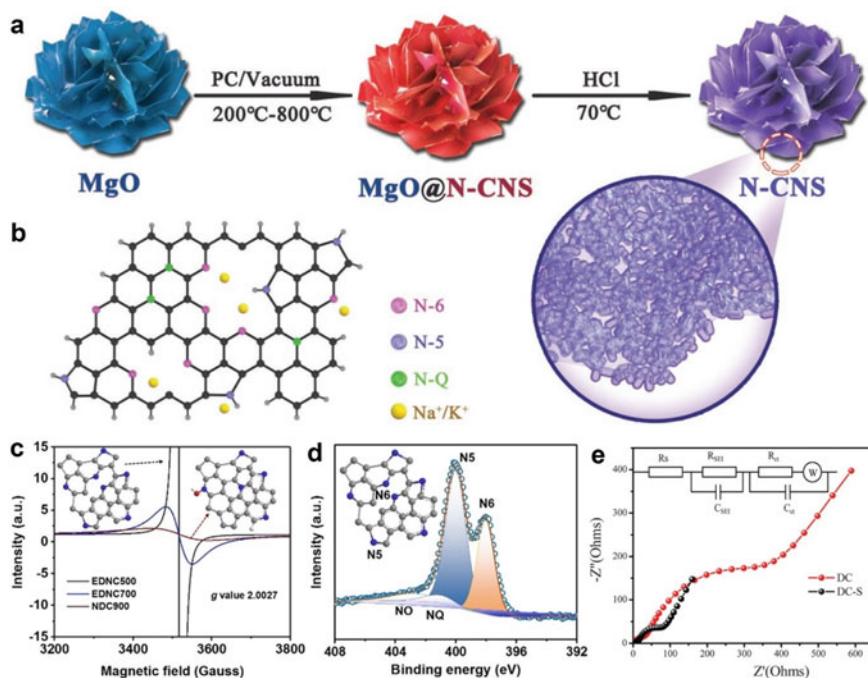


Fig. 10.2 Schematics of the synthesis process of hierarchical N-CNS and the N-CNS structure anode material in **a** SIBs and **b** PIBs. Reproduced with permission [31]. Copyright 2020, John Wiley. **c** EPR spectra of ENDNCs and NDC900. **d** High-resolution XPS spectra of N 1s from EDNC500; inset: the atomic structure of EDNC500. Reproduced with permission [32]. Copyright 2020, John Wiley. **e** Nyquist plots of DC-S and DC after the 1st cycle. Inserted image is the equivalent circuit. Reproduced with permission [30]. Copyright 2020, Royal Society of Chemistry

Similarly, high-resolution spectra of N 1s for EDNC500 (Fig. 2d) proved the existence of pyrrole nitrogen and pyridine nitrogen. The doped N mainly existed in the form of pyrrole- and pyridine-N rather than graphitized-N. [32] The S-doping also received extensive attention, especially in the application of SIBs. Because sodium has a larger radius than that of lithium. Therefore, the traditional host materials are not suitable for SIBs. Li et al. [30] reported the S-doped carbon-based material with increased layer spacing. The prepared S-doped disordered carbon (DC-S) achieved rapid insertion/deinsertion of sodium ion. As shown in Fig. 2e, compared with disordered carbon, the DC-S exhibits a lower SEI resistance (R_{SEI} , 14.3 Ω) and lower charge transfer resistance (R_{ct} , 52.4 Ω).

The incorporation of heteroatoms displays a positive effect on the ion storage properties of carbon-based materials. However, the correlation between structure and capacity has not been systematically investigated. Li et al. [33] combined experimental studies with first-principles calculations to study the mechanism of sodium ion storage. The charge profile of different atom-doped graphene-Na systems was simulated using Vienna Ab-initio Simulation Package (VASP, Fig. 3a-c) to show the

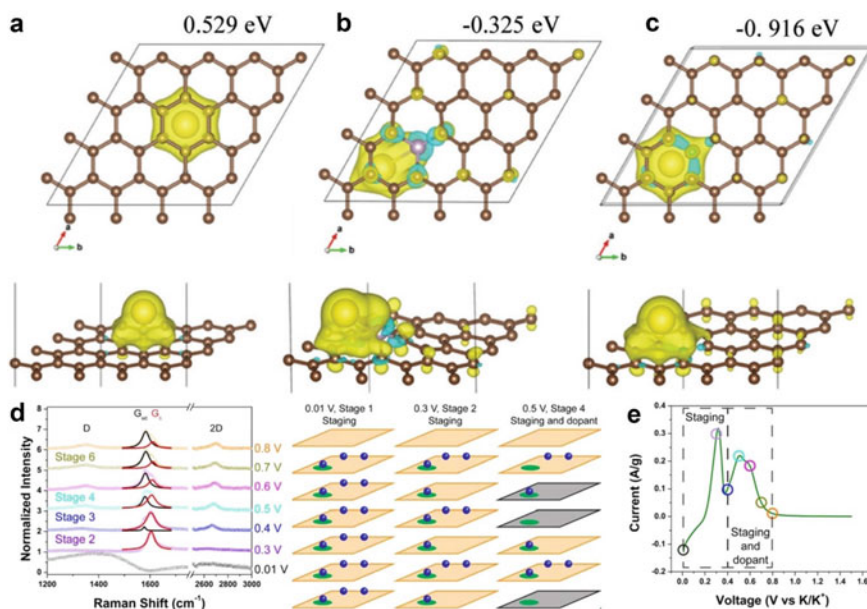


Fig. 10.3 Charge distribution plots of different graphene/Na systems simulated in VASP with the binding energies of sodium ions shown. **a** Pristine graphene. **b** P-doped graphene. and **c** B-doped graphene. Reproduced with permission [33]. Copyright 2017, John Wiley. **d** Raman spectra at selected voltages for N-FLG and the schematic of the staging and defect storage mechanism in N-FLG. **e** CVs at 0.05 mV/s for N-FLG. Reproduced with permission [34]. Copyright 2016, American Chemical Society

binding energy between sodium ions and the doped graphene samples. The repulsion between the heteroatoms and the positive charge made the Na ions closer to the negatively charged graphene sheet. In the region around the heteroatoms, the interaction between the sodium atoms and the graphene sheet was stronger. Share et al. [34] proved the change of doped N (N-FLG, N-doped few-layer graphene) and non-doped N (FLG, few-layer graphene) during charge process by *in-situ* Raman spectroscopy. Figure 3d showed the CV curve at sweep rate of 0.05 mV s^{-1} . Figure 3e showed the *in-situ* Raman spectra of N-FLG. With the increase of voltage, the intensity of G_{ce} peak decreased, when that of G_{uc} increased. These results illustrated that N-doping provides sites that can locally store K ions without damaging the formation of graphite intercalation compound (GIC) at stage 1.

10.3 Atomically Dispersed Metal on Carbon Materials for MIBs

In the field of energy storage, metal nanoparticles electrode materials often suffer from lower performances than the theoretical levels, which goes against the popular idea of green chemistry today. In recent years, atomically dispersed metal on carbon-based materials have attracted extensive attention due to their advantages of the high atom efficiency, unique electronic structure, adjustable surface characteristics, and low cost. In the electrochemical reaction, the single atom catalysts (SACs) exhibit high chemical activity and can quickly adsorb the reaction intermediates. The intermediate can eventually be completely reduced to the final product. At the same time, metal SAC receives electrons from the current and is further reduced to its original metal state [35].

However, atomically dispersed metal on carbon-based materials usually shows relatively low physical/chemical stability due to their high surface energy, which leads to a serious degradation in electrochemical process. In addition, metal atoms can easily agglomerate into metal nanoparticles during the preparation process. Many new synthetic strategies have been developed for SACs with better stability and improved performance.

Most of the atomically dispersed metal on carbon-based electrode materials are transition metals such as Fe, Co, Mn, Ni, Cu, etc. Zhang et al. [36] synthesized the metal-bis(iminobenzosemiquinoid) linked structure using Cu and Ni metal sources. Two-dimensional (2D) conjugated metal-organic framework materials (C-MOFs) showed the advantages of high intrinsic conductivity and large specific surface area. The results of experiments and theoretical calculations showed that phthalocyanine monomer and metal-bis(iminobenzosemiquinoid) linkages acted as active sites for Na^+ and SO_4^{2-} storage, respectively. The prepared electrode material showed a larger potential window, with an energy density of 51.6 Wh kg^{-1} and a peak power density of 32.1 kW kg^{-1} . As shown in Fig. 4a, the molecular electrostatic potential (MESP) showed that the phthalocyanine N connected to the Ni site represented by the purple ball as the electrophilic center was conducive to the adsorption of SO_4^{2-} , while M-N₄ connected to the Cu site represented by the yellow ball as the nucleophilic center was conducive to the adsorption of Na^+ . Through this strategy, Yuan et al. [37] synthesized the atomic-dispersed metal sites, including Ni, Fe, and Mn on N-rich nanosheets, which were used as electrodes with desired cycling and extremely high specific capacity in LIBs. According to the XRD patterns of Mn-N-C, Ni-N-C and Fe-N-C (Fig. 4b), there were no additional diffraction peaks except carbon, indicating that no impurity of metal-based particles. The N 1s spectra of XPS from Mn-N-C, Ni-N-C and Fe-N-C are shown in Fig. 4c. The formation of graphitic-N ($\sim 400.7 \text{ eV}$), pyrrolic-N ($\sim 399.8 \text{ eV}$) and pyridinic-N (398.2 eV) indicated the chemical states of the N 1s. In MIBs, the adsorption sites of ions are almost the same. Li et al. [38] synthesized cobalt atom-dispersed on graphene as an electrode material to solve the dendrite problem in LIBs. Generally, Li^+ can be absorbed on one top site (T) and three hollow sites (H1, H2, and H3) of Co-N-C, of which H1

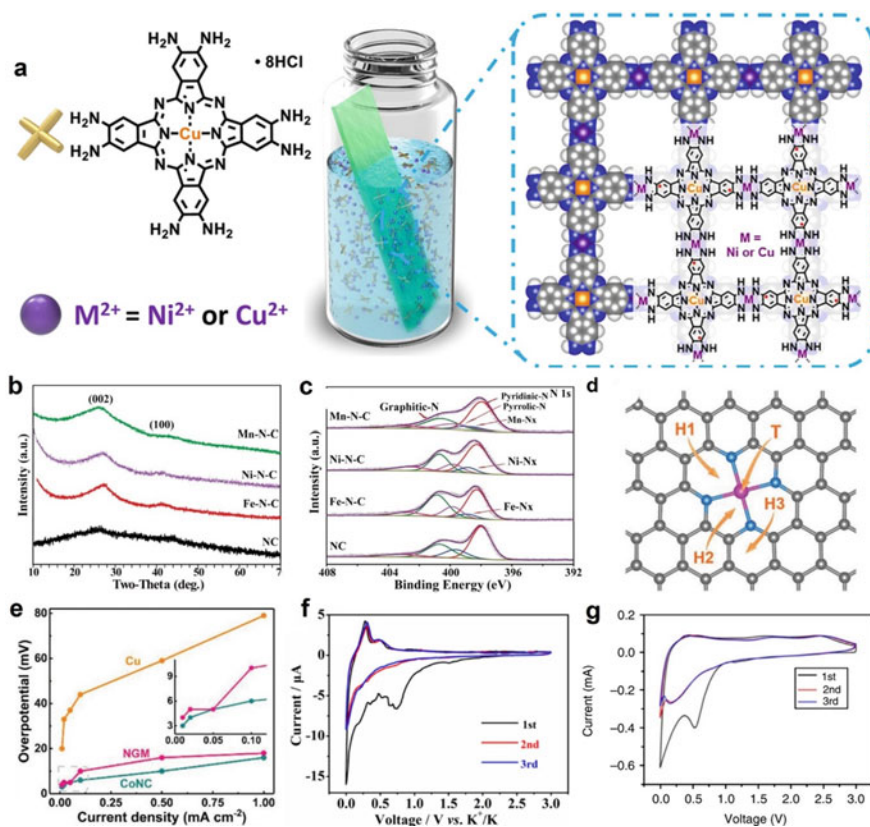


Fig. 10.4 Schematics of the synthesis process and structural characterization of SACs. **a** Schematic illustration of the in-situ growth of $\text{M}_2[\text{CuPc}(\text{NH}_2)_8]$ on carbon cloth. Reproduced with permission [36]. Copyright 2021, American Chemical Society. **b** XRD patterns. **c** N 1s spectra of XPS as-prepared Mn-N-C, Ni-N-C, Fe-N-C and NC. Reproduced with permission [37]. Copyright 2020, Royal Society of Chemistry. **d** Li adsorption sites on CoNC, the carbon, nitrogen, and cobalt are marked with gray, blue, and deep pink, respectively. Reproduced with permission [39]. Copyright 2018, John Wiley. **e** Cyclic voltammetry curve at 0.1 mV s^{-1} . Reproduced with permission [38]. Copyright 2014, Springer Nature. **f** Cyclic voltammetry curves at a scan rate of 0.01 mV s^{-1} in the voltage range of 0.01–3.0 V. Reproduced with permission [40]. Copyright 2017, John Wiley. **g** Li-nucleation overpotentials on Cu, CoNC, and NGM electrodes at different current densities. Reproduced with permission [38]. Copyright 2018, John Wiley

site affords the largest binding energy (-1.58 eV) toward a Li atom (Fig. 4d) which was also larger than the N sites in the N-doped graphene (NG) (-0.86 eV). These results confirmed that the Co- N_x -C structures can greatly enhance the ionophilicity of graphene. As a comparison, the nucleation overpotential of different substrates was measured to evaluate the lithophile and nucleation process on the surface of electrode materials (Fig. 4e) [39]. Compared with Cu and NGM, Co-N-C exhibited the lowest nucleation overpotential at a series of current densities. In addition, the atomically

dispersed metal on carbon-based materials is also widely used in PIBs. Xu et al. [40] synthesized N-doped carbon nanotubes with an edge-open layer-alignment structure by pyrolyzing the cobalt-containing metal–organic frameworks (ZIF-67). CV curves (Fig. 4f) showed that the strong peak at around 0 V corresponds to the intercalation of K^+ and the peak at 0.3 V corresponds to the extraction of K^+ . Similarly, Chen et al. [39] synthesized nitrogen-doped porous carbon prepared from a metal–organic framework as lithium anode. As shown in Fig. 4g, a distinct peak appears at 0.2 V during discharge from the second cycle onward, which could be ascribed to the generation of a new SEI film during the charge and discharge processes.

10.4 Metal Nanoparticles Encapsulated Carbon-Based Materials for MIBs

The theoretical specific capacity of transition metal oxides and alloy nanoparticles is much higher than that of conventional graphite anode. However, the poor conductivity and drastic volume changes in the charging/discharging processes often lead to irreversible capacity degradation. Through coating highly conductive carbon, the microstructure design and large specific surface area of the carbon shell can improve the electrochemical performance.

As mentioned above, alloy particles and transition metal compounds tend to agglomerate during synthesis. In order to solve this problem, a series of synthesis strategies were explored. As shown in Fig. 5a, Zhao et al. [41] developed a simple solvothermal method to produce NiS_2 nanocrystals with the $NiCl_2 \cdot 6H_2O$, $Na_2S_2O_3 \cdot 5H_2O$, and PVP (K-30) as precursors. NiS was successfully encapsulated by the amorphous N-doped box-like carbon (NiS@C) using polymerized dopamine (PDA) as carbon source. NiS particles are encapsulated by N-doped carbon cages via Ni-N bonds, exhibiting excellent sodium/potassium ions storage performance. The N-doped carbon makes the composites display high conductivity and fast ion diffusion channel, performing excellent rate performance. The top view (Fig. 5b) and side view (Fig. 5d) of the optimized geometry structures for NiS on N-doped carbon are corresponding to the XPS analysis. The DFT result shows that a spontaneous bridging between NiS and N-doped carbon via Ni-N bond is energetically favorable. The higher binding energy between NiS and N-doped carbon, which is much higher than the NiS without Ni-N bond (Fig. 5c), leads to a stronger adhesion between NiS and carbon shell, thus alleviating the volume change, pulverization, aggregation of NiS, and leading to a superior cycling stability [42]. The structural and chemical engineering of the solid electrolyte interface (SEI) in rechargeable batteries play a vital role in electrochemical performance. The underlying mechanism of the extraction sodium (Na) storage in metal-nitrogen was not yet revealed definitely due to the electrochemical inertness of metal-nitrogen (MN_x) to Na in the charge and discharge processes.

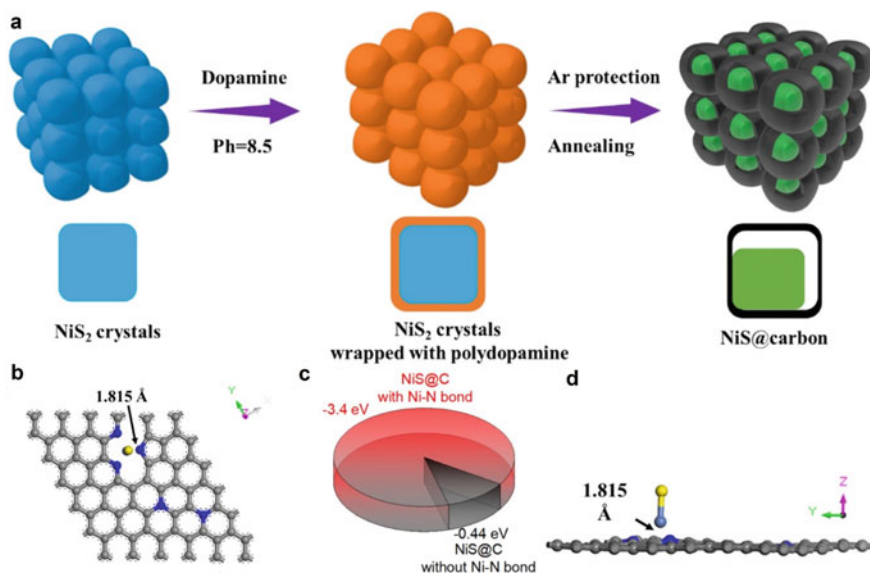


Fig. 10.5 Schematics of the synthesis process and structural characterization of Metal nanoparticles encapsulated carbon-based materials. **a** Schematic illustration of the preparation route of NiS@C. **b** Top view of optimized geometry structures of NiS adsorbed on N-doped carbon. **c** The binding energy of NiS on N-doped carbon (-3.40 eV) and undoped carbon (-0.44 eV). **d** Side view of optimized geometry structures of NiS adsorbed on N-doped carbon. Reproduced with permission [41]. Copyright 2020, Elsevier

Xia et al. [43] firstly proposed to uncover the mechanism using the *in-situ* acquired temperature-dependent Nyquist plots and *ex-situ* X-ray photoelectron spectroscopies. As shown in Fig. 6a–i, all of FeN_x/C samples contain Fe–N and Fe–Fe bonds, which means that the single atom site and cluster are on the carbon base. Wang et al. [44] encapsulated FeP and MnO (the related XPS spectrum shown in Fig. 7a and Fig. 7b) with the carbon shell respectively. Wang et al. [45] synthesized hollow FeP@carbon nanocomposite (H-FeP@C), which is prepared by phosphatizing the hollow Fe₃O₄ (H-Fe₃O₄) nanoparticles encapsulated with carbon. The hollow nanoparticles can solve the volume expansion problem and improve the utilization of electrode materials. The formation and disappearance of Li₂Se was monitored by XRD characterization (Fig. 7c) at different stages in the charging and discharging processes. In order to further alleviate the volume change, Zhang et al. [46] prepared the Fe₃O₄@Fe₃C core@shell nanoparticle which is well confined in the hollow carbon nanospindle. Among the charge and discharge processes, Fe₃O₄ will undergo volumetric expansion, dissolution, and fracture. Zhang innovatively coated the Fe₃O₄ with Fe₃C layer and carbon layer (Fig. d, e), facilitating excellent storage capacity. It can be found that the nanoparticle with a diameter of 15–20 nm from the high-magnification TEM image of Fe₃O₄@Fe₃C@C yolk-shell nanospindle owns a large void space of 75% in the nanospindle. The higher resolution TEM image

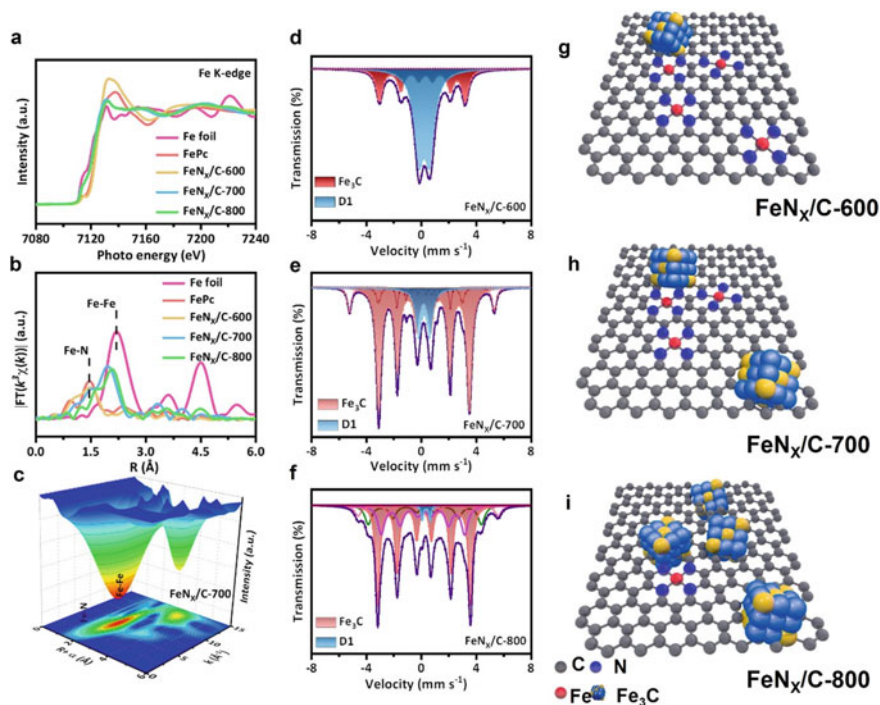


Fig. 10.6 Schematics of the synthesis process and structural characterization of Metal nanoparticles encapsulated carbon-based materials. **a** K-edge XANES spectra and **b** Fourier transforms of k^3 -weighted K-edge EXAFS spectra of $\text{FeN}_x/\text{C}-600$, $\text{FeN}_x/\text{C}-700$, $\text{FeN}_x/\text{C}-800$, Fe foil, and FePc, respectively. **c** Wavelet transform of the k^3 -weighted EXAFS data of $\text{FeN}_x/\text{C}-700$. **d-f** Room-temperature ^{57}Fe Mössbauer spectra of $\text{FeN}_x/\text{C}-600$, $\text{FeN}_x/\text{C}-700$, and $\text{FeN}_x/\text{C}-800$, respectively. **g-i** Schematic illustration of model systems of $\text{FeN}_x/\text{C}-600$, $\text{FeN}_x/\text{C}-700$ and $\text{FeN}_x/\text{C}-800$, respectively. Reproduced with permission [43]. Copyright 2022, Royal Society of Chemistry

indicates that the thickness of carbon layer with amount of micropores is 3–5 nm. Therefore, Zhang et al. proposed a Li ion storage mechanism that lithium ions enter through the outermost porous carbon material and then store Li at the interface between Fe_3O_4 and Fe_3C .

10.5 Metal Nanoparticles Supported Carbon-Based Materials for MIBs

In the charging and discharging processes, the drastic change of volume causes the decrease of cyclic performance and the increase of irreversible capacity limiting the performance of MIBs. In addition to the encapsulation strategy, the alloy particles

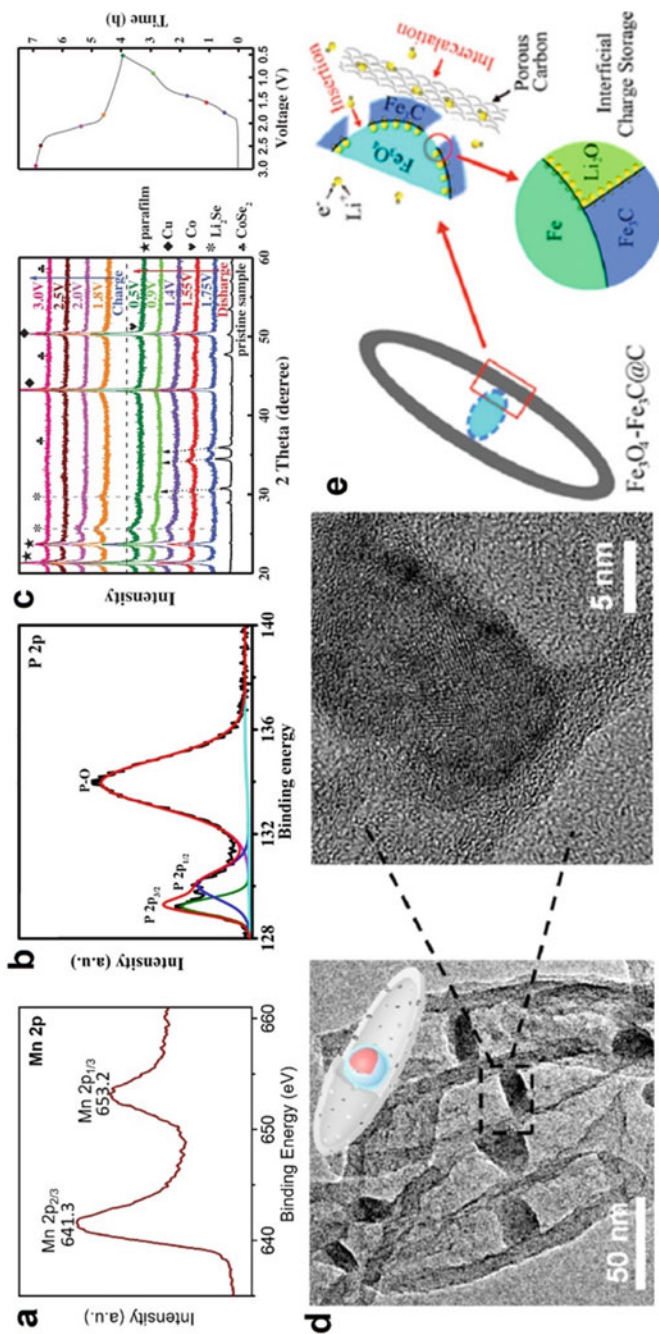


Fig. 10.7 Schematics of the structural characterization. **a** High-resolution Mn 2p XPS spectrum of MnO@NC nanocapsules. **b** P 2p XPS spectra of the H-FeP@C@GR nanocomposite. Reproduced with permission [44]. Copyright 2017, American Chemical Society. **c** XRD patterns of the CoSe₂@N-CF/CNTs electrodes obtained at various charge-discharge states for the 1st cycle. The corresponding charge-discharge curve. Reproduced with permission [45]. Copyright 2018, WILEY-VCH. **d** TEM images of Fe₃O₄@Fe₃C-C yolk-shell nanospindles (the inset shows the corresponding enlarged image of Fe₃O₄ (I) and Fe₃C (II)). Reproduced with permission [46]. Copyright 2015, American Chemical Society

and metal oxide, can be engineered through the *in-situ* growth and self-assemble technology to obtain the metal nanoparticles supported carbon-based anode materials. The metal particles and carbon layer connected by the van der Waals forces which resulting amounts of alkali metal ions (e.g., Na^+ , K^+ , and Li^+) spread in the interlayer. In addition, the effect of volume change can be alleviated to obtain robust rate performance and excellent cyclic stability.

As shown in Fig. 8a, Wang et al. [47] synthesized the porous MnSe/FeSe₂ (Mn-Fe-Se) inserted with interlaced carbon nanotubes by a simple chemical precipitation approach and a subsequent one-step carbonization and selenization of Mn-Fe Prussian blue analogs. Firstly, commercial carbon nanotubes were heated in a mixture of HNO_3 and H_2SO_4 . Then, the oxidized carbon nanotubes were obtained after the filter and drying processes. The oxidized carbon nanotubes were dispersed in the water with cetyltrimethylammonium bromide (CTAB). After adding the $\text{Mn}(\text{NO}_3)_2$

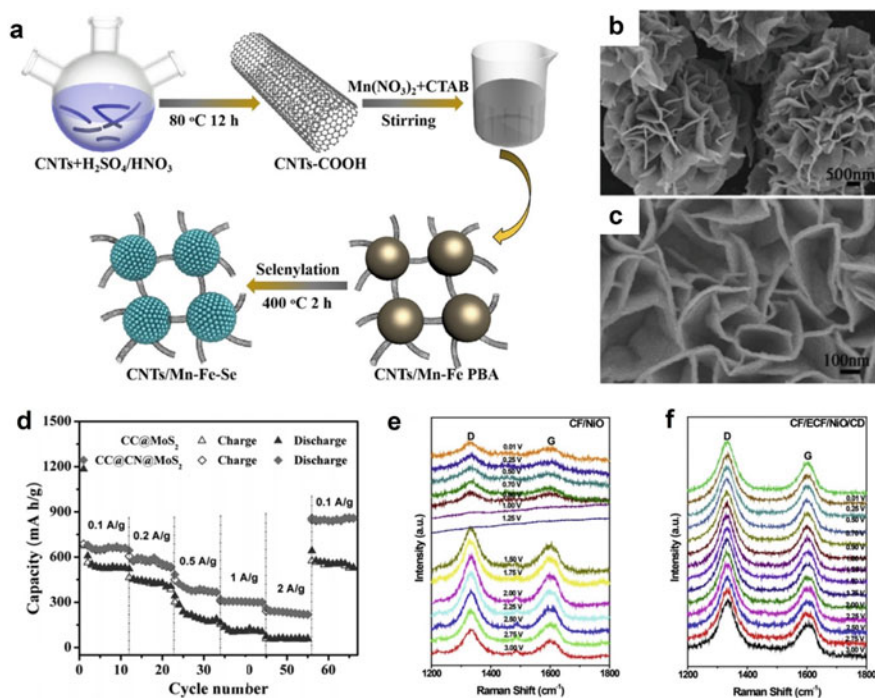


Fig. 10.8 Schematics of the morphology characterization and structural characterization. a Schematic representation of Mn-Fe-Se/CNTs composite. Reproduced with permission [47]. Copyright 2020, Elsevier. **b** Larger-magnification SEM images of SnS_2 with flower-like feature. **c** Larger-magnification SEM images of SnS_2 on CC showing the well-aligned nanosheet architecture. Reproduced with permission [48]. Copyright 2019, Elsevier. **d** Rate performance of the $\text{CC}@\text{CN}@\text{MoS}_2$ and $\text{CC}@\text{MoS}_2$ at various current densities, respectively. Reproduced with permission [49]. Copyright 2017, John Wiley. **e** *In-situ* Raman spectra of CF/NiO at different intercalated voltages. **f** *In-situ* Raman spectra of CF/ECF/NiO/CD at different intercalated voltages. Reproduced with permission [50]. Copyright 2020, Elsevier

and $K_3[Fe(CN)_6]$ precursors, Mn-Fe PBA/CNTs was obtained after agitation and centrifugation. Finally, Mn-Fe PBA/CNTs and selenium powder were physically mixed and heated in N_2 . Mn-Fe-Se /CNTs microspheres were obtained after the selenization process. Similarly, Mn-Se /CNTs can be prepared by the same method. Metal selenides show the special narrow-band gap and high theoretical specific capacity. In addition, Prussian blue analogues (PBAs), as a metal–organic framework composed of metal centers and organic links, are widely used as precursors of porous materials. Therefore, Mn-Fe-Se/CNTs can alleviate the volume effect and improve the specific capacity in energy storage fields. Mn-Fe-Se system shown improved cycling and rate performance in SIB and PIB. When used as anode in SIBs, the Mn-Fe-Se/CNT delivers superior cycling stability (552 mA h g^{-1} over 70 cycles) and favorable rate capability (411 mA h g^{-1} at 800 mA g^{-1}). Furthermore, Mn-Fe-Se/CNT shows high specific capacity (351 mA h g^{-1}) and unprecedented rate performance in PIBs. Wang et al. [48] prepared a vertically aligned SnS_2 nanosheets on carbon cloth by hydrothermal method. Firstly, carbon cloth (CC) was oxidized by H_2O_2 and washed by acetone and ethanol by ultrasonic treatment. Second, $SnCl_4 \cdot 5H_2O$ and thioacetamide (TAA) was dissolved in isopropanol. After hydrothermal treatment at 160 °C, the carbon cloth was washed with deionized water and anhydrous ethanol to obtain SnS_2/CC . SEM images of SnS_2 (Fig. 8b) show the densely agglomerated flower-like nanoplates on CC substrate, (Fig. 8c) showing the well-aligned nanosheet architecture. The thickness of each SnS_2 layer is measured to be 20 nm. The SnS_2 nanosheets array act as a network structure conducive to sodium ion migration in the electrolyte. In addition, CC has good flexibility, which is advantageous to alleviate the volume effect. Most importantly, the open 3D SnS_2/CC configuration provides good electrical conductivity and well contact towards electrolyte, reducing internal electron and ion transfer resistance and thereby improving power density. SnS_2/CC anode exhibits remarkably enhanced electrochemical properties with excellent reversible capacity and robust rate capability. Ren et al. [49] also used carbon cloth as the matrix and prepares ultra-thin MoS_2 nanosheets on the carbon cloth as the anode material. The $CC@CN@MoS_2$ was obtained by doping-N in the carbon cloth, thus improving the capacity and rate performance of MoS_2 . As shown in Fig. 8d, when circulating at different current densities of 0.1, 0.2, 0.5, 1.0, and 2.0 A g^{-1} , the $CC@CN@MoS_2$ electrode exhibits average discharge capacities of 660, 580, 394, 306, and 235 mA h g^{-1} , respectively. $CC@CN@MoS_2$ shows the higher capacity than that of $CC@MoS_2$, demonstrating its superior rate capability. Instead of sulfide and selenide, Tang et al. [50] successfully enhanced the lithium-ion storage chemistry of nickel oxide nanosheets by modulating the positions of p orbital energy levels through porous N-doped carbon fiber and carbon quantum dot (CDs) engineering. By comparing the $I_D:I_G$ of CF/NiO (Fig. 8e) and CF/ECF/NiO/CD (Fig. 8f), it is shown that CF contributes little to the lithium storage process of CF/NiO, but CF/ECF is greatly beneficial to the lithium storage process of CF/ECF/NiO/CD anode. It is proved that CF/ECF is one of the reasons for the high area capacity of CF/ECF/NiO/CD electrode.

10.6 Conclusion and Perspectives

Na-ion batteries are an attractive alternative to replace Li-ion batteries for smart grid and electric vehicle applications. Compared with other commonly used batteries, metal-ion batteries have higher energy density, especially sodium ion batteries, which are favored by capital because of their wide sources and great reserves. With the in-depth research on the charging and discharging process of metal ion batteries, the mechanism of metal-ion batteries becomes more and more clear. Carbon-based materials play an indispensable role in the design and commercial application of electrode materials for metal ion batteries. As a widely used electrode material, carbon-based nanomaterials stand out among all electrode materials because of their high specific capacity, excellent conductivity, low density, and storage capacity for metal ion batteries. However, for the application of metal ion battery, we put forward higher requirements, and the electrochemical performance of metal-ion batteries need to be further improved to meet the application requirements of new energy devices in the future. In the process of research, the shortcomings of the discharge process of metal ion batteries are as followed:

- (1) In terms of the negative electrode, the evolution of lithium and sodium on the surface of the negative electrode is the main reason that restricts the rapid charging, and not only the graphite negative electrode, but also the negative electrode with low lithium embedding potential will face this key problem.
- (2) The development of embedded cathode materials for multivalent metal ion batteries, such as magnesium ion battery, face two challenges: strong electrostatic effect and slow embedding/de-reaction kinetics. Polyvalent ions with high charge density have higher migration barrier in electrode materials, which will cause great structural change and lattice strain, and even lead to the collapse of electrode structure in the process of repeated embedding/stripping.
- (3) Take lithium-ion battery as an example, after the battery is charged and discharged for many times, the surface of lithium metal will continue to grow dendritic lithium crystal, a large number of sharp dendrites will produce stress on the diaphragm and Pierce it, resulting in short circuit explosion and other thermal control, bringing uncontrollable safety problems.

The electrode material prepared with carbon nanomaterials as the substrate has better electrical conductivity, which is also the basic condition for its good power density and energy density. Structural modification because of carbon-based nanomaterials, such as coated metal nanoparticles and loaded nanoparticles mentioned in the above paper, can solve the volume expansion problem in the charging and discharging process to a certain extent. At the same time, the outstanding three-dimensional grid structure can also be further experimental ion migration, to achieve the purpose of improving electrochemical performance. Of course, the challenges faced by metal ion batteries are far more than this. In the future, the infinite possibilities of carbon-based nanomaterials will bring more excellent carbon-based nanomaterial applied to metal ion batteries.

References

1. C. Zhang, Y.-L. Wei, P.-F. Cao, M.-C. Lin, Energy storage system: Current studies on batteries and power condition system. *Renew. Sustain. Energy Rev.* **82**, 3091–3106 (2018). <https://doi.org/10.1016/j.rser.2017.10.030>
2. H. Zhang, X. Yu, P.V. Braun, Three-dimensional bicontinuous ultrafast-charge and -discharge bulk battery electrodes. *Nat. Nanotechnol.* **6**, 277–281 (2011). <https://doi.org/10.1038/nnano.2011.38>
3. Y. Zhang, N. Hao, X. Lin, S. Nie, Emerging challenges in the thermal management of cellulose nanofibril-based supercapacitors, lithium-ion batteries and solar cells: a review. *Carbohydr. Polymers* **234** (2020). <https://doi.org/10.1016/j.carbpol.2020.115888>
4. Y. Zhang, L. Tao, C. Xie, D. Wang, Y. Zou, R. Chen, Y. Wang, C. Jia, S. Wang, (2020) Defect engineering on electrode materials for rechargeable batteries. *Adv. Mater.* **32**. <https://doi.org/10.1002/adma.201905923>
5. G. Zhou, L. Xu, G. Hu, L. Mai, Y. Cui, Nanowires for electrochemical energy storage. *Chem. Rev.* **119**, 11042–11109 (2019). <https://doi.org/10.1021/acs.chemrev.9b00326>
6. D. Deng, Li-ion batteries: basics, progress, and challenges. *Energy Sci. Eng.* **3**, 385–418 (2015). <https://doi.org/10.1002/ese3.95>
7. A. El Kharbachi, O. Zavorotynska, M. Latroche, F. Cuevas, V. Yartys, M. Fichtner, (2020) Exploits, advances and challenges benefiting beyond Li-ion battery technologies. *J. Alloys Compd.* **817**. <https://doi.org/10.1016/j.jallcom.2019.153261>
8. P. Bai, Y. He, X. Zou, X. Zhao, P. Xiong, Y. Xu, Elucidation of the sodium-storage mechanism in hard carbons. *Adv. Energy Mater.* **8**, 1703217 (2018). <https://doi.org/10.1002/aenm.201703217>
9. D. Bin, F. Wang, A.G. Tamirat, L. Suo, Y. Wang, C. Wang, Y. Xia, Progress in aqueous rechargeable sodium-ion batteries. *Adv. Energy Mater.* **8** (2018). <https://doi.org/10.1002/aenm.201703008>
10. Y. Cao, L. Xiao, M.L. Sushko, W. Wang, B. Schwenzer, J. Xiao, Z. Nie, L.V. Saraf, Z. Yang, J. Liu, Sodium ion insertion in hollow carbon nanowires for battery applications. *Nano Lett.* **12**, 3783–3787 (2012). <https://doi.org/10.1021/nl3016957>
11. J.-Y. Hwang, S.-T. Myung, Y.-K. Sun, Recent progress in rechargeable potassium batteries. *Adv. Funct. Mater.* **28** (2018). <https://doi.org/10.1002/adfm.201802938>
12. X. Lin, J. Huang, H. Tan, J. Huang, B. Zhang, $K_3V_2(PO_4)_2F_3$ as a robust cathode for potassium-ion batteries. *Energy Storage Mater.* **16**, 97–101 (2019). <https://doi.org/10.1016/j.ensm.2018.04.026>
13. J.C. Pramudita, D. Sehrawat, D. Goonetilleke, N. Sharma, An initial review of the status of electrode materials for potassium-ion batteries. *Adv. Energy Mater.* **7** (2017). <https://doi.org/10.1002/aenm.201602911>
14. A. Banerjee, V. Aravindan, S. Bhatnagar, D. Mhamane, S. Madhavi, S. Ogale, Superior lithium storage properties of α - Fe_2O_3 nano-assembled spindles. *Nano Energy* **2**, 890–896 (2013). <https://doi.org/10.1016/j.nanoen.2013.03.006>
15. R. Yazami, P. Touzain, A reversible graphite-lithium negative electrode for electrochemical generators. *J. Power Sour.* **9**, 365–371 (1983)
16. N. Nitta, F. Wu, J.T. Lee, G. Yushin, Li-ion battery materials: present and future. *Mater. Today* **18**, 252–264 (2015). <https://doi.org/10.1016/j.mattod.2014.10.040>
17. G. Zubi, R. Dufo-Lopez, M. Carvalho, G. Pasaoglu, (2018) The lithium-ion battery: State of the art and future perspectives. *Renew. Sustain. Energy Rev.* **89**, 292–308. <https://doi.org/10.1016/j.rser.2018.03.002>
18. B.L. Ellis, L.F. Nazar, Sodium and sodium-ion energy storage batteries. *Curr. Opin. Solid State Mater. Sci.* **16**, 168–177 (2012). <https://doi.org/10.1016/j.cossms.2012.04.002>
19. N. Yabuuchi, K. Kubota, M. Dahbi, S. Komaba, Research development on sodium-ion batteries. *Chem. Rev.* **114**, 11636–11682 (2014). <https://doi.org/10.1021/cr500192f>
20. J.-Y. Hwang, S.-T. Myung, Y.-K. Sun, Sodium-ion batteries: present and future. *Chem. Soc. Rev.* **46**, 3529–3614 (2017). <https://doi.org/10.1039/c6cs00776g>

21. L. Fan, R. Ma, Q. Zhang, X. Jia, B. Lu, Graphite anode for a potassium-ion battery with unprecedented performance. *Angewandte Chemie-Int. Edn.* **58**, 10500–10505 (2019). <https://doi.org/10.1002/anie.201904258>
22. R. Rajagopalan, Y. Tang, X. Ji, C. Jia, H. Wang, (2020) Advancements and challenges in potassium ion batteries: a comprehensive review. *Adv. Funct. Mater.* **30**. <https://doi.org/10.1002/adfm.201909486>
23. Y. Wu, H.-B. Huang, Y. Feng, Z.-S. Wu, Y. Yu, The promise and challenge of phosphorus-based composites as anode materials for potassium-ion batteries. *Adv. Mater.* **31** (2019). <https://doi.org/10.1002/adma.201901414>
24. W. Zhang, Y. Liu, Z. Guo, Approaching high-performance potassium-ion batteries via advanced design strategies and engineering. *Sci. Adv.* **5** (2019). <https://doi.org/10.1126/sciadv.aav7412>
25. Q. Li, W. Zhang, J. Peng, W. Zhang, Z. Liang, J. Wu, J. Feng, H. Li, S. Huang, Metal-organic framework derived ultrafine Sb@porous carbon octahedron via in situ substitution for high-performance sodium-ion batteries. *ACS Nano* (2021). <https://doi.org/10.1021/acsnano.1c05458>
26. Y. Pan, K. Xu, C. Wu, Recent progress in supercapacitors based on the advanced carbon electrodes. *Nanotechnol. Rev.* **8**, 299–314 (2019). <https://doi.org/10.1515/ntrev-2019-0029>
27. X. Wang, L. Liu, Z. Niu, Carbon-based materials for lithium-ion capacitors. *Mater. Chem. Front.* **3**, 1265–1279 (2019). <https://doi.org/10.1039/C9QM00062C>
28. H.G. Wang, Z. Wu, F.L. Meng, D.L. Ma, X.L. Huang, L.M. Wang, X.B. Zhang, Nitrogen-doped porous carbon nanosheets as low-cost, high-performance anode material for sodium-ion batteries. *Chemoschem* **6**, 56–60 (2013). <https://doi.org/10.1002/cssc.201200680>
29. C. Zhang, N. Mahmood, H. Yin, F. Liu, Y. Hou, Synthesis of phosphorus-doped graphene and its multifunctional applications for oxygen reduction reaction and lithium ion batteries. *Adv. Mater.* **25**, 4932–4937 (2013). <https://doi.org/10.1002/adma.201301870>
30. W. Li, M. Zhou, H.M. Li, K.L. Wang, S.J. Cheng, K. Jiang, A high performance sulfur-doped disordered carbon anode for sodium ion batteries. *Energy Environ. Sci.* **8**, 2916–2921 (2015). <https://doi.org/10.1039/c5ee01985k>
31. H. Huang, R. Xu, Y. Feng, S. Zeng, Y. Jiang, H. Wang, W. Luo, Y. Yu, Sodium/potassium-ion batteries: boosting the rate capability and cycle life by combining morphology, defect and structure engineering. *Adv. Mater.* **32**, e1904320 (2020). <https://doi.org/10.1002/adma.201904320>
32. W. Zhang, Z. Cao, W. Wang, E. Alhajji, A.H. Emwas, P. Costa, L. Cavallo, H.N. Alshareef, A site-selective doping strategy of carbon anodes with remarkable K-ion storage capacity. *Angew. Chem. Int. Ed.* **59**, 4448–4455 (2020). <https://doi.org/10.1002/anie.201913368>
33. Z. Li, C. Bommier, Z.S. Chong, Z. Jian, T.W. Surta, X. Wang, Z. Xing, J.C. Neuefeind, W.F. Stickle, M. Dolgos, P.A. Greaney, X. Ji, Mechanism of Na-ion storage in hard carbon anodes revealed by heteroatom doping. *Adv. Energy Mater.* **7** (2017). <https://doi.org/10.1002/aenm.201602894>
34. K. Share, A.P. Cohn, R. Carter, B. Rogers, C.L. Pint, Role of nitrogen-doped graphene for improved high-capacity potassium ion battery anodes. *ACS Nano* **10**, 9738–9744 (2016). <https://doi.org/10.1021/acsnano.6b05998>
35. L. Ma, G. Zhu, D. Wang, H. Chen, Y. Lv, Y. Zhang, X. He, H. Pang, (2020) Emerging metal single atoms in electrocatalysts and batteries. *Adv. Funct. Mater.* **30**. <https://doi.org/10.1002/adfm.202003870>
36. P. Zhang, M. Wang, Y. Liu, S. Yang, F. Wang, Y. Li, G. Chen, Z. Li, G. Wang, M. Zhu, R. Dong, M. Yu, O.G. Schmidt, X. Feng, Dual-redox-sites enable two-dimensional conjugated metal-organic frameworks with large pseudocapacitance and wide potential window. *J. Am. Chem. Soc.* **143**, 10168–10176 (2021). <https://doi.org/10.1021/jacs.1c03039>
37. M.W. Yuan, Z.M. Sun, L. Lin, H. Yang, D. Wang, K.B. Yin, C.Y. Nan, G.B. Sun, H.F. Li, S.L. Ma, Atomically dispersed metal sites anchored in N-doped carbon nanosheets with enhanced Li storage performance. *Mater. Chem. Front.* **4**, 2157–2167 (2020). <https://doi.org/10.1039/d0qm00191k>

38. H. Liu, X. Chen, X.B. Cheng, B.Q. Li, R. Zhang, B. Wang, X. Chen, Q. Zhang, Uniform lithium nucleation guided by atomically dispersed lithiophilic CoN_x sites for safe lithium metal batteries. *Small Methods* **3**, 9 (2018). <https://doi.org/10.1002/smt.201800354>
39. F. Zheng, Y. Yang, Q. Chen, High lithium anodic performance of highly nitrogen-doped porous carbon prepared from a metal-organic framework. *Nat. Commun.* **5**, 5261 (2014). <https://doi.org/10.1038/ncomms6261>
40. P. Xiong, X. Zhao, Y. Xu, Nitrogen-doped carbon nanotubes derived from metal-organic frameworks for potassium-ion battery anodes. *Chemsuschem* **11**, 202–208 (2018). <https://doi.org/10.1002/cssc.201701759>
41. X. Zhao, F.Y. Gong, Y.D. Zhao, B. Huang, D. Qian, H.E. Wang, W.H. Zhang, Z.J. Yang, Encapsulating NiS nanocrystal into nitrogen-doped carbon framework for high performance sodium/potassium-ion storage. *Chem. Eng. J.* **392**, 123675 (2020). <https://doi.org/10.1016/j.cej.2019.123675>
42. G.Y. Zhu, L. Wang, H.N. Lin, L.B. Ma, P.Y. Zhao, Y. Hu, T. Chen, R.P. Chen, Y.R. Wang, Z.X. Tie, J. Liu, Z. Jin, Walnut-like multicore-shell MnO encapsulated nitrogen-rich carbon nanocapsules as anode material for long-cycling and soft-packed lithium-ion batteries. *Adv. Func. Mater.* **28**, 1800003 (2018). <https://doi.org/10.1002/adfm.201800003>
43. H. Xia, L. Zan, G. Qu, Y. Tu, H. Dong, Y. Wei, K. Zhu, Y. Yu, Y. Hu, D. Deng, J. Zhang, Evolution of a solid electrolyte interphase enabled by FeN_x/C catalysts for sodium-ion storage. *Energy Environ. Sci.* **15**, 771–779 (2022). <https://doi.org/10.1039/d1ee02810c>
44. X. Wang, K. Chen, G. Wang, X. Liu, H. Wang, Rational design of three-dimensional graphene encapsulated with hollow FeP @carbon nanocomposite as outstanding anode material for lithium ion and sodium ion batteries. *ACS Nano* **11**, 11602–11616 (2017). <https://doi.org/10.1021/acsnano.7b06625>
45. J. Yang, H. Gao, S. Men, Z. Shi, Z. Lin, X. Kang, S. Chen, CoSe_2 nanoparticles encapsulated by N-doped carbon framework intertwined with carbon nanotubes: High-performance dual-role anode materials for both Li- and Na-ion batteries. *Adv. Sci.* **5**, 1800763 (2018). <https://doi.org/10.1002/advs.201800763>
46. J. Zhang, K. Wang, Q. Xu, Y. Zhou, F. Cheng, S. Guo, Beyond yolk-shell nanoparticles: Fe_3O_4 @ Fe_3C core@shell nanoparticles as yolks and carbon nanospindles as shells for efficient lithium ion storage. *ACS Nano* **9**, 3369–3376 (2015). <https://doi.org/10.1021/acsnano.5b00760>
47. J.M. Wang, B.B. Wang, X.J. Liu, J.T. Bai, H. Wang, G. Wang, Prussian blue analogs (PBA) derived porous bimetal (Mn, Fe) selenide with carbon nanotubes as anode materials for sodium and potassium ion batteries. *Chem. Eng. J.* **382**, 123050 (2020). <https://doi.org/10.1016/j.cej.2019.123050>
48. L.Q. Wang, J.R. Yuan, Q.Q. Zhao, Z.T. Wang, Y.Q. Zhu, X.L. Ma, C.B. Cao, Supported SnS_2 nanosheet array as binder-free anode for sodium ion batteries. *Electrochim. Acta* **308**, 174–184 (2019). <https://doi.org/10.1016/j.electacta.2019.04.019>
49. W. Ren, H. Zhang, C. Guan, C. Cheng, Ultrathin MoS_2 nanosheets@metal organic framework-derived N-doped carbon nanowall arrays as sodium ion battery anode with superior cycling life and rate capability. *Adv. Funct. Mater.* **27** (2017). <https://doi.org/10.1002/adfm.201702116>
50. Y. Huang, H. Yang, T. Xiong, D. Adekoya, W. Qiu, Z. Wang, S. Zhang, M.S. Balogun, Adsorption energy engineering of nickel oxide hybrid nanosheets for high areal capacity flexible lithium-ion batteries. *Energy Storage Mater.* **25**, 41–51 (2020). <https://doi.org/10.1016/j.ensm.2019.11.001>

Chapter 11

Carbon-Based Nanomaterials for Metal-Sulfur/Selenium Batteries



Wei jie Chen, Kai Guo, Huicong Xia, and Gan Qu

Abstract With the rapid development of mobile electronic devices and electric vehicles, traditional lithium-ion batteries (LIBs) can no longer satisfy human's requirement due to the limited energy density. Nowadays, the metal-sulfur/selenium (M-S/Se) batteries have attracted widespread attention due to the high theoretical energy density. Among the M-S/Se batteries, lithium-sulfur (Li-S) batteries receive more attention. Li-S batteries show a high theoretical specific capacity (1675 mA h g^{-1}) and high energy density (2600 W h kg^{-1}). However, Li-S batteries still face some problems: (i) Due to the soluble polysulfide (LiPSs), the "shuttle effect" can cause the loss of sulfur components and corrosion of Li anode. (ii) The electrical conductivity of S_8 and $\text{Li}_2\text{S}_2/\text{Li}_2\text{S}$ is poor, lots of conductive additives need to be introduced into the sulfur cathode, making the theoretical energy density difficult to be achieved. (iii) The volume change during the charge/discharge processes is about 80%, which leads to the structural collapse. For the M-S/Se batteries, there exist the similar problems to be solved. Over the past years, efforts have been devoted to constructing conductive scaffolds to enhance the specific capacity, cycling stability and rate delivery of M-S/Se batteries. Carbon-based materials present the porous nanostructures and high conductivity, which have been employed as host materials and interlayer materials to promote the electrochemical performance. In this chapter, the investigations of carbon-based materials in M-S/Se batteries are summarized. Finally, carbon-based materials applied in M-S/Se batteries were briefly prospected, aiming at providing some thoughts for the design of electrode materials in M-S/Se batteries.

W. Chen · K. Guo · H. Xia · G. Qu (✉)
College of Materials Science and Engineering, Zhengzhou University, Zhengzhou 450001,
P. R. China
e-mail: gqu@zzu.edu.cn

W. Chen
e-mail: chenweijie990822@163.com

K. Guo
e-mail: gk15937961601@163.com

H. Xia
e-mail: summer9209@126.com

11.1 Introduction

With the rapid development of electronic device and electric vehicle, traditional lithium-ion batteries cannot meet the market demand due to their low theoretical energy density [1]. Metal-sulfur/selenium batteries (M-S/Se batteries) have gradually grasped people's attention for their higher energy density (both mass and volume energy density) Fig. 11.1.

Among metal-sulfur/selenium batteries, Li-S batteries attract the most attention. Since the Li-S batteries were found in the 1960s, this new rechargeable system has drawn much public attention because of high specific capacity (1672 mA h g^{-1} and $3467 \text{ mA h cm}^{-3}$) and energy density (2600 W h kg^{-1}). [2] However, the LIBs based on LiCoO_2 , [3] LiFePO_4 [4] have been the most popular energy storage devices, which show the long cycle stability. [5] Although the traditional LIBs have a higher voltage platform, the specific capacity of those systems are much lower than that of sulfur. [6–8] Li-S batteries have a superhigh density capacity, calculated on the basis of the Li anode and S cathode. [9, 10] Furthermore, the sulfur is the byproducts of petroleum industry, which means the abundant resources of nature [11]. Meanwhile, sulfur is non-toxic compared to the traditional metal-based cathode, providing promising future for application [12] Table 11.1.

Different from rocking chair batteries (intercalation/deintercalation chemistry [13]), Li-S batteries suffer from a multi-phase conversion ($\text{S}_{8(\text{solid})}$ - $\text{Li}_2\text{S}_{n(\text{liquid})}$ - $\text{Li}_2\text{S}_{1/2(\text{solid})}$ [14]) during redox processes. In the discharge process, there are two obvious platform at 2.3–2.4 V and 2.1–2.0 V, [15] corresponding to phase-change reaction process. For the first platform at about 2.3 V, solid S_8 transfers to soluble lithium polysulfides (LiPSs) mostly Li_2S_8 , Li_2S_6 , and Li_2S_4 , when the second one

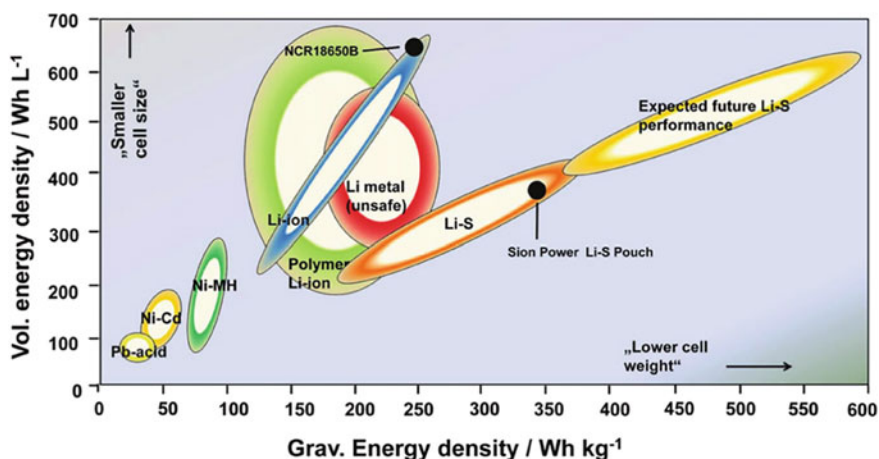


Fig. 11.1 Performance comparison of Li-S batteries with other batteries. The abscissa represents the mass energy density and the ordinate represents the volume energy density. Reproduced with permission [2]. Copyright 2018, John Wiley

Table 11.1 Comparison of physical properties of cathode materials for Li-ion batteries and M-S/Se batteries. Bold represents the best performance, Italic represents average performance, and Bold italic represents the worst performance

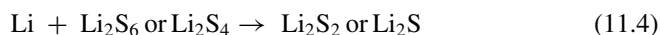
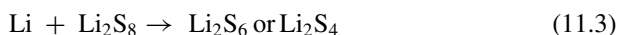
Cathode	Parameter			
	Conductivity (S m ⁻¹)	Volume specific capacity (mA h cm ⁻³)	Density (g cm ⁻³)	Mass specific capacity (mA h g ⁻¹)
LiFePO ₄	<i>10⁻⁷ ~ 10⁻⁶</i>	1080	<i>0.7 (loose loading)</i>	170
S	<i>5 × 10⁻²⁸</i>	3467	<i>2.07</i>	1675
Se	10⁻³ ~ 10⁻¹	3270	4.82	<i>672</i>

at about 2.1 V corresponds to the conversion of soluble LiPSs to insoluble lithium sulfides (Li₂S₂ and Li₂S) [16, 17]. At the end of discharge process, the polar voltage suddenly increase because of the accumulation of insulated products (mostly Li-S) at cathode surface.

The overall reaction of Li-S batteries is:



Usually, the step-by-step reactions are:



Li-S batteries encounter the following problems:

- (i) The intermediate products Li₂S_n (8 ≥ n ≥ 4) can be easily dissolved into ether-based electrolyte.[18] The dissolution of Li₂S_n facilitate the faster ion transfer and reaction kinetics.[19] However, the sluggish kinetic of conversion from Li₂S_{4/6/8} to Li₂S_{1/2} leads to the accumulation of Li₂S_n at the cathode side, which causes the serious “shuttle effect”. [20] Under the drive of concentration gradient, Li₂S_n can pass through the separator and react with Li foil leading to the loss of active matter, low coulomb efficiency and fast capacity decay. It is more serious under high loading conditions.
- (ii) Meanwhile, the insulator nature of S₈ (5 × 10⁻³⁰ S m⁻¹) and Li₂S_{1/2} (10⁻¹² S m⁻¹) introduces large polarization phenomenon, poor rate capacity, and sluggish reaction kinetics [21]. Therefore, lots of conductive additives are needed at the cathode side to ensure the fast electron transmission. Even so, part of S powder and conductive additive are still in poor contact (often named

dead sulfur). As a result, theoretical energy density (2600 W h kg^{-1}) is difficult to be achieved.

- (iii) The density of S and Li_2S are 2.07 and 1.66 g cm^{-3} , respectively. Calculated based on active matter, the volume change is about 80% during lithiation/delithiation progress, which leads to structural degradation and poor cycle stability.

Nearly all of the elements in group VIA are high-energy density cathode materials that can be coupled with alkali metal anode (such as Li, Na, K) [22]. Selenium, *d*-electron containing member of group 16 (VIA) with high electrical conductivity ($\sim 10^{-3} \text{ S m}^{-1}$), was firstly regarded as positive electrode in Li, Na ion batteries by Abouimrane [23]. So far, two different mechanisms have been revealed in Li-Se batteries. In ether-based electrolyte, the mechanism of Li-Se batteries is similar to that of Li-S batteries [24]: (i) there are two platform at 2.1 and 2.0 V , respectively; (ii) there will present soluble polyselenides during discharge process. While in ester-based electrolyte, just one platform is shown [25]. Abouimrane et al. [26] verified the different mechanisms in the two types of electrolytes. When Li_2Se , Se, and $\text{Li}_2\text{Se} + \text{Se}$ were introduced into EC (ethylene carbonate)/EMC (ethyl methyl carbonate), there was no dissolution phenomenon. Namely, the conversion mechanism of Li-Se batteries was similar to that of the traditional Li-ion batteries (intercalation/deintercalation chemistry) in ester-based electrolyte, while the reaction mechanism in Li-Se batteries was the same as that of Li-S batteries in ether-based electrolyte. Although Se showed much higher electrical conductivity, the volume expansion of cathode was 153% leading to serious structural damage and poor cycling stability (Fig. 11.2).

The anode based on sodium and potassium also has been studied for decades, including Na-S, K-S, Na-Se, and K-Se batteries. Due to the higher reserves of Na ($2.30 \text{ wt.}\%$) and K ($2.10 \text{ wt.}\%$) on earth (20 ppm for Li), these energy storage

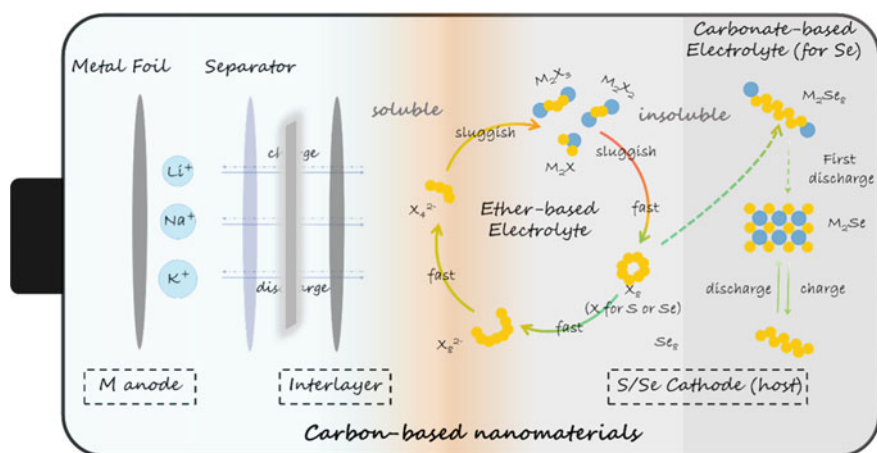


Fig. 11.2 Schematic diagram of reaction mechanisms between cathode and anode in M-S/Se cell

Table 11.2 The cathode density, discharge product density and volume change for Li-S, Na-S, K-S, Li-Se, Na-Se, and K-Se batteries

Cathode	Parameter		
	Cathode matter density (g cm ⁻³)	Discharge product density (g cm ⁻³)	Volume charge (% based on cathode)
Li-S	2.07	1.66 (Li ₂ S)	78
Na-S		1.86 (Na ₂ S)	170
K-S		1.805 (K ₂ S)	294
Li-Se	4.81	2.0 (Li ₂ Se)	153
Na-Se		2.58 (Na ₂ Se)	196
K-Se		2.29 (K ₂ Se)	320

systems have also attracted extensive attention. These systems show the same reaction mechanism as Li-S and Li-Se batteries Table 11.2.

Although M-S/Se batteries have attracted considerable attention, the above problems still limited the industrialization of M-S/Se batteries. On the cathode side, a lot of efforts have devoted to designing host, interlayer materials, [27] and modifide separator to slove the problems [28]. Carbon-based nanomaterials have shown great potential in this regard.

Carbon is one of the most important elements in nature, which has sp , sp^2 and sp^3 hybrid electronic hybridizaition orbitals. The superhigh electrical conductivity can accelerate electron transfer during the redox reactions. In the conventional energy storage systems, carbon is often used as anode (such as Graphene and Hard Carbon) and conductive additives in electrodes (such as Super P, Carbon Black, and Ketjen Black) [29]. By controlling the synthesis condition, various types of carbon materials can be prepared, such as carbon spheres, nanotubes, fibers, etc. At the infancy state of the study, many works focused on constructing porous carbon with special morphology. The large specific surface area and pore volume can buffer the large volume change of sulfur cathode and facilitate the uniform deposition of sulfur during charge/discharge progress.

In 2009, Nazar et al. [30] used CMK-3 as host materials to store sulfur by molten method, opening the door to the study of host materials for sulfur cathode. Heteroatom-doped carbon materials can introduce polar sites at atomic level, which show strong interaction between carbon matrix and polysulfides. Due to the introduce of heteroatoms, the polar carbon material in turn can enhance the adsorption ability and improve the sluggish reaction kinetics [31]. In addition, heteroatom-doped can improve the electric conductivity of carbon materials [32]. Through the doping of various heteroatoms, the polarity of the carbon material surface can be adjusted to achieve better catalytic effect.

In order to further increase the adsorption ability between the host and LiPSs, metal-based compounds are focused on. The metal with unfilled d -orbit not only showed higher catalytic effect towards the multi-phase coversion in M-S/Se batteries

but also displayed a higher adsorption energy for LiPSs, thus facilitating the improved cycling stability and high performance in M-S/Se batteries.

In the field of oxygen reduction reaction, single atom catalysts (SACs) draw extensive attention during the past decades [33–36]. Since 2018, SACs have been introduced into M-S/Se batteries, showing large potential in the applications of M-S/Se batteries [37–39]. Researchers have constructed M-H-C (M: metal, H: heteroatom, and C: carbon) electrocatalysts by introducing metal atoms and heteroatoms into carbon materials simultaneously. Through such a combination, metal atom coupled with different nonmetallic atom (B, N, O, P, and S) can be built [40, 41]. Although the exact reaction mechanism is still unclear, the M-H-C structure can act as an ideal model to improve the electrochemical performance.

Various metal-based compounds (metal borides, nitrides, oxides, phosphides, sulfides, and selenides) embedded in carbon materials are investigated in M-S/Se batteries [42, 43]. These metal compounds showed larger binding energy towards polysulfides, especially the metal oxides. In addition, the structure can be conveniently adjusted, showing a promising potential for application. The research on building (multi-components) metal compounds heterostructure became one of the most hot area in the past 3 years.

Herein, we summarize different types of carbon-based nanomaterials in M-S/Se batteries, including metal-free carbon-based materials, atomically dispersed metal on carbon-based materials, metal nanoparticles encapsulated by carbon-based materials, and supported carbon-based materials in M-S/Se batteries. This chapter aims at describing the recent progresses of carbon-based nanomaterials in M-S/Se batteries and putting forward an outlook in the future of carbon-based nanomaterials.

11.2 Metal-Free Carbon-Based Materials for MSBs

Metal-sulfur/selenium batteries (MSBs) have received extensive attention from the scientific community in recent years due to the higher theoretical energy density than that of the traditional lithium-ion batteries. However, the inherent shuttle effect of metal-sulfur/selenium batteries and the large-volume effect of sulfur/selenium still plague researchers. In the past ten years, scientists have made many efforts to improve the performance in MSBs. Metal-free carbon-based materials have become a promising candidate due to their larger specific surface area, higher conductivity, and better adjustability.

Carbon materials showed great potential in the early stage of Li-S batteries cathode research. In 2009, Nazar et al. [30] creatively used CMK-3 as the sulfur cathode, which made a significant breakthrough in Li-S batteries. CMK-3 was one of the most famous members among the mesoporous carbon families. CMK-3 showed the uniform pore size, large pore volume, network of cross-linked pores and high electrical conductivity. CMK-3 was synthesized using the nano-casting method, and then the CMK-3/sulfur composite cathode was prepared by the melt diffusion method. The molten sulfur entered the micropores of CMK-3 under capillary action. Figure 11.3a

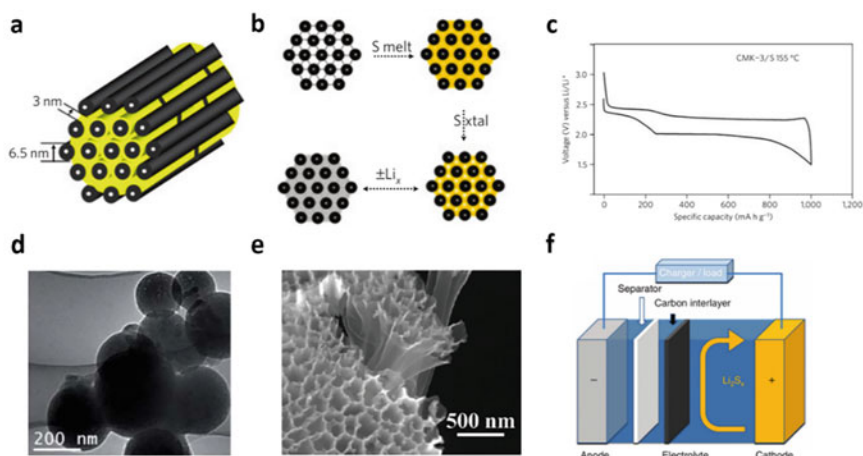


Fig. 11.3 Preliminary study on Li-S battery. **a** Schematic diagram of the sulfur (yellow) confined in the interconnected pore structure of CMK-3. **b** Schematic diagram of composite synthesis by impregnation of molten sulfur, followed by its densification on crystallization. The lower diagram represents subsequent discharging–charging with Li. **c** Galvanostatic charge–discharge curves for the first cycle of CMK-3/S material at a current rate of 168 mA g^{-1} . Reproduced with permission [30]. Copyright 2009, Springer Nature. **d** TEM images of carbon spheres. Reproduced with permission [44]. Copyright 2010, RSC Publishing. **e** Hollow carbon nanofiber encapsulated sulfur. Reproduced with permission [45]. Copyright 2011, American Chemical Society. **f** Schematic configuration of a Li–S battery with a bifunctional microporous carbon interlayer inserted between the sulfur cathode and the separator. Reproduced with permission [46]. Copyright 2012, Springer Nature

is a schematic diagram of CMK-3/sulfur composite, which was composed of interconnected mesoporous carbon and sulfur distributed between the pores. Figure 11.3b is a schematic diagram of CMK-3 and the subsequent discharge process. The CMK-3/sulfur composite showed great performance in the electrochemical performance test. The discharge curve presented two voltage platforms (Fig. 11.3c). Through this method, the CMK-3/sulfur composite provided nearly 80% of the theoretical capacity (1320 mA h g^{-1}), bringing new hope in the application of Li-S batteries. In 2010, Gao et al. [44] prepared a sulfur/carbon sphere composite by mixing the sublimated sulfur and microporous carbon spheres. The reaction of the sulfur cathode was well confined inside the carbon spheres, promoting the reversibility and discharge capacity and the reversible capacity remains at 650 mA h g^{-1} after 500 cycles at 400 mA g^{-1} (Fig. 11.3d). In 2011, Cui et al. [45] used anodized aluminum oxide (AAO) as a template to prepare hollow carbon nanofiber arrays through the thermal carbonization of polystyrene. The thin carbon wall ensured the rapid transmission of electrons. The high specific surface area of the carbon fiber array was favorable to the deposition of Li_2S (Fig. 11.3e). In addition, researchers also tried to suppress the shuttle effect through the intermediate layer. In 2012, Manthiram et al. [46] reported a new strategy to suppress the shuttle effect. Dual-function microporous carbon paper

acted as interlayer between the cathode and the separator, which improved the utilization of active materials and achieves high capacity, long cycle life and fast charging rate (Fig. 11.3f).

Although carbon materials show the advantages of high conductivity and specific surface area, the binding energy towards polysulfides is weak. Thus, Heteroatom-doped carbon materials with polar groups were studied. In 2016, Zhang et al. [47] used density functional theory calculations to simulate a series of heteroatom-doped graphene nanoribbons and evaluated their ability to anchor sulfur and polysulfides (Fig. 11.4a, b). In addition, multi-heteroatom co-doping was further put forward and investigated in Li-S batteries. In 2020, Huang et al. [31] used heteroatom-doped porous graphene framework (HGF) to accelerate the sulfur reduction reaction (SRR) kinetics. Figure 11.4c shows the EIS curves of different heteroatom-doped materials. Through Fig. 11.4d, we can use the Arrhenius formula to calculate the activation energy (E_a) of SRR (Fig. 11.4e).

In addition to Li-S batteries, batteries with sodium/potassium anode materials and sulfur/selenium cathode materials were also researched. In 2012, Amine et al. [23]

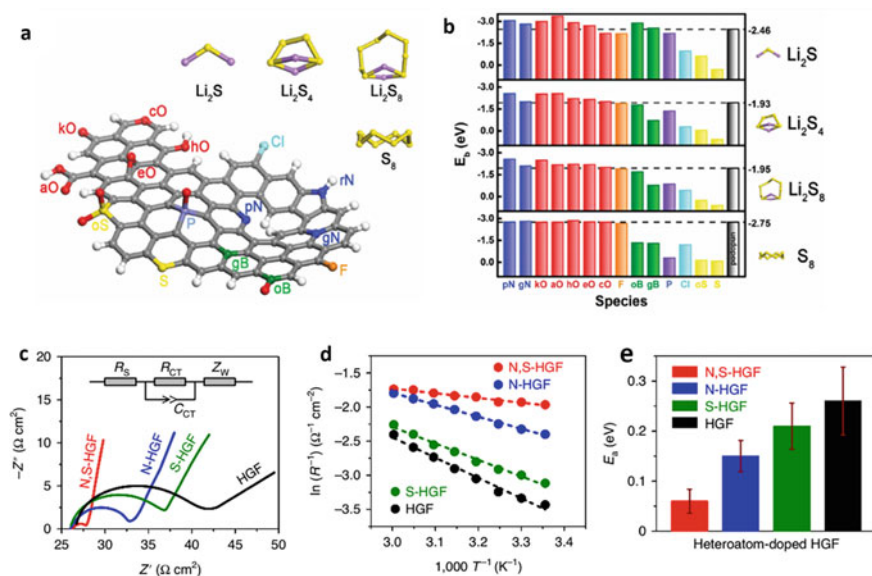


Fig. 11.4 Heteroatom-doped carbon materials for Li-S battery. **a** The schematic diagram of X-doped nanocarbon materials ($X = N, O, F, B, P, S, Cl$). **b** The binding energy E_b (eV) between different polysulfides intermediates and doped graphene, and the binding energies of Li_2S , Li_2S_4 , Li_2S_8 , and S_8 interacting with pristine materials are shown as grey bars and dashed lines for reference. Reproduced with permission [47]. Copyright 2016, John Wiley. **c** Electrochemical impedance spectroscopy (EIS) of heteroatom-doped HGFs in SRR. **d** The linear relationship between logarithmic values of the reciprocal of charge transfer resistance and the reciprocal of absolute temperatures. **e** Activation energies for the SRR process among various heteroatom-doped HGFs at the onset potential. Reproduced with permission [31]. Copyright 2020, Springer Nature

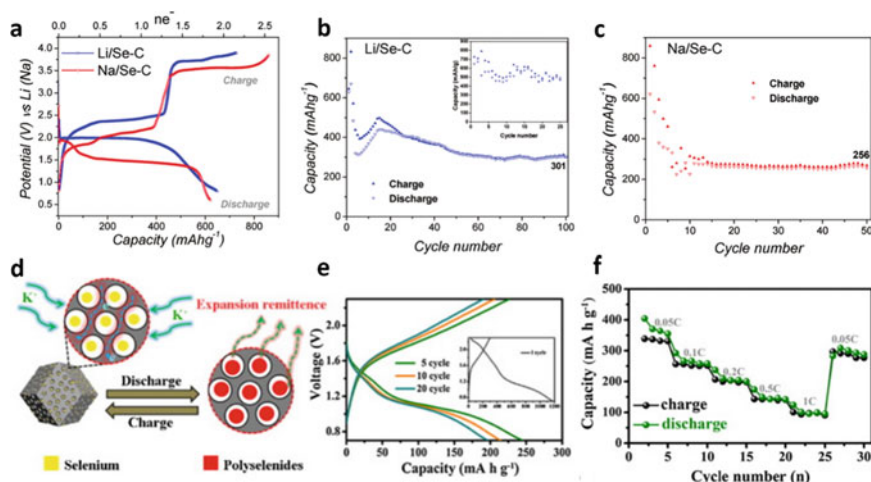


Fig. 11.5 Metal-free carbon-based materials for other M-S/Se batteries (except Li-S battery). **a** Voltage profiles for Li/Se-C and Na/Se-C during the first discharge/charge. **b, c** The capacity retention of Li/Se-C **b** and Na/Se-C **c** cycled at 50 and 10 mA g⁻¹ (inset) current density. Reproduced with permission [23]. Copyright 2012, American Chemical Society. **d** Mechanism schematic diagram during discharge–charge process in rechargeable K-Se batteries. **e** The galvanostatic discharge–charge curves. **f** Rate capability at different current densities. Reproduced with permission [48]. Copyright 2019, Elsevier

reported an S/Se composite coupled with Li and Na anodes. Figure 11.5a shows the 1st charge/discharge curves of Li/Se-C and Na/Se-C. The reversible capacity of the Li/Se-C can be maintained at 500 mA h g⁻¹ after 25 cycles at low current density. The Se_xS_y-C cathode was also produced with the S and Se as precursors, which showed a higher theoretical specific capacity than the pure Se and better conductivity than the pure S. In 2018, Xu et al. [48] used Se/N doped porous carbon composite cathode for secondary K-Se batteries (Fig. 11.5d-f). The specific discharge capacities at 0.05, 0.1, 0.2, 0.5, and 1 C are 405, 267, 211, 150, and 101 mA h g⁻¹, respectively. Therefore, in addition to Li–S batteries, carbon materials also presented promising application in Na/K-S/Se batteries.

11.3 Atomically Dispersed Metal on Carbon-Based Materials for MSBs

Although pure carbon materials and doped carbon materials have shown improved performance in M-S/Se batteries. However, the weak electrostatic force towards LiPSs still cannot meet the industrial demand in M-S/Se batteries. Therefore, atomically dispersed metal on carbon-based materials were investigated to further advance the performance in M-S/Se batteries.

As a kind of atomically dispersed metal on carbon-based materials, SACs have gained extensive attention for the nearly 100% atom utilization and the high-efficient active sites. Meanwhile, the optimized SACs were ideal model in researching the whole reaction kinetics during redox processes. In 2018, Hou et al. [49] successfully produced porous Fe, N co-doped graphene through a one-step scalable calcination process. According to X-ray absorption spectroscopy and DFT calculations, iron atoms not only coordinated with the four nitrogen atoms in graphene layer and formed Fe-N₄ sites, but also coordinated with the two nitrogen atoms on the edge of graphene and form Fe-N₂ sites (Fig. 11.6a). The Fe, N co-doped graphene achieved an efficient suppression of the shuttle effect. In 2021, Xiong et al. [50] used the self-template and self-reduction method to prepare nitrogen-doped graphene SACs with a unique W-O₂N₂-C coordination structure (W/NG) and high W loading (8.6 wt.%). The theoretical calculations and experiments proved that the MSBs with W/NG modified separator showed a great improvement in performance. Figure 11.6b shows the HAADF-STEM image of W/NG. A large number of isolated W atoms were observed on the surface of W/NG. Through the X-ray near-edge absorption fine structure spectrum (XANES) in Fig. 11.6c, the white line intensity of W/NG was higher than that of W foil and WO₂, indicating that W element in W/NG shows an oxidized electronic structure. Figure 11.6d shows the k₃-weighted Fourier transform extended X-ray absorption fine structure (FT-EXAFS) curve of W/NG, W-foil and WO₂. The main peak at 1.42 Å belongs to the W-O coordination. The main peak of W/NG at 1.32 Å moved to the lower *R* position, indicating the changed coordination. What's more, the W-W coordination peak of W-foil located at 2.6 Å, which was negligible in the W/NG spectrum, indicating that most W atoms were dispersed and coordinate with N and O. From Fig. 11.6e, the *i*₀ of the W/NG@PP batteries is higher than that of the other two samples, which proved that W/NG is more efficient in promoting the redox reaction kinetics. Through this work, W from W-N₂O₂-C was a multifunctional active center, which can not only effectively adsorb polysulfides, but also promoted the kinetic transformation of LiPSs. Pan et al. [51] developed a simple strategy to assemble uniformly dispersed Co-N₄ active sites. The cross-linked carbon left with a three-dimensional porous layered carbon structure. The porous carbon layer not only improved ion conductivity, but also buffered the volume expansion (Fig. 11.6f). In 2020, Li et al. [52] was inspired by the biocatalytic molybdenase with stable Mo-S bonds and developed porous Mo-N-C nanosheets with atom-dispersed Mo-N₂/C sites as the host. Theoretical calculations showed that Mo-N-C can not only reduce the activation energy of Li₂S₄ to Li₂S conversion, but also reduce the decomposition barrier of Li₂S (Fig. 11.6g). In 2017, Dong et al. [53] designed a quasi-two-dimensional Co@N-C composite with a honeycomb structure as a multifunctional sulfur host through template method. The honeycomb structure provided high specific surface area to load sulfur and promoted the transmission of electrons (Fig. 11.6h-j).

In summary, by virtue of the high atom utilization, the single-atom catalysts favored the adsorption and catalytic conversion of polysulfides/selenides, achieving the improved electrochemical performance in M-S/Se batteries.

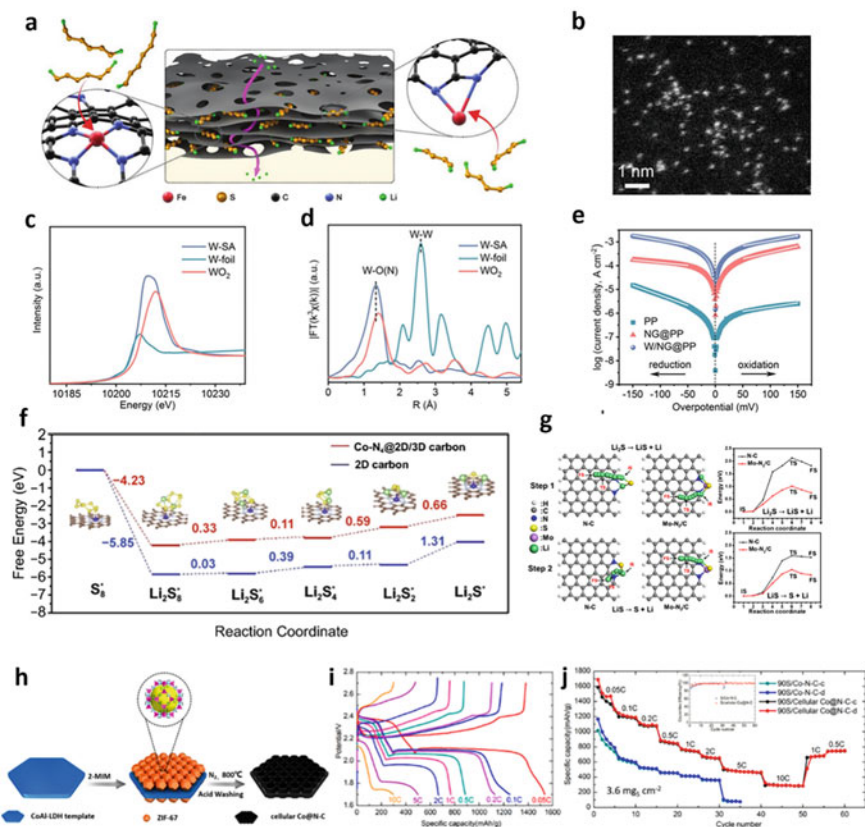


Fig. 11.6 SACs for M-S/Se batteries. **a** Schematic illustration of the confinement of sulfur and polysulfides in the layer structure and the additional ionic diffusion pathways (purple arrow line) through the holey structure (the black sheets). Reproduced with permission [49]. Copyright 2018, John Wiley. **b** Magnified HAADF-STEM image of W/NG. **c** XANES of W-SA, W-foil and WO_2 . **d** k^3 -weighted FT-EXAFS spectra at W L3-edge of W/NG and the references. **e** Tafel plots of the Li_2S oxidation process. Reproduced with permission [50]. Copyright 2021, John Wiley. **f** Energy profiles for the reduction of LiPSs on $\text{Co-N}_4@2\text{D}/3\text{D}$ carbon and 2D carbon substrates, the inset showing the optimized adsorption conformations of intermediate species on $\text{Co-N}_4@2\text{D}/3\text{D}$ carbon and 2D carbon substrates. Reproduced with permission [51]. Copyright 2021, Springer Nature. **g** Decomposition pathways of Li_2S to LiS and LiS to S on $\text{Mo-N}_2/\text{C}$ and N-C . Reproduced with permission [52]. Copyright 2020, American Chemical Society. **h** The schematic illustration of the step-by-step synthesis strategy for the cellular $\text{Co}@N\text{-C}$ composite. **i** The discharge and charge voltage profiles at increasing current rates from 0.05 to 10 C. **j** The rate performances of the 90S/cellular $\text{Co}@N\text{-C}$ and 90S/ Co-N-C electrodes at different current rates (inset: coulombic efficiency versus cycle number). Reproduced with permission. [53] Copyright 2017, American Chemical Society

11.4 Metal Nanoparticles Encapsulated by Carbon-Based Materials for MSBs

In recent years, metal oxides, [54] metal sulfides, [55] metal phosphides [56] and bimetal compounds [57–59] have been studied to not only effectively adsorb polysulfides/selenides, but also further promote the polysulfides/selenides conversion. Metal compounds encapsulated by carbon shell showed higher conductivity and lighter weight than pure metal compounds. Therefore, metal nanoparticles encapsulated by carbon-based materials have attracted lots of attention.

In 2017, Manthiram et al. [60] rationally designed carbon@Fe₃O₄ (YSC@Fe₃O₄) yolk-shell nanobox as the sulfur host (Fig. 11.7a–d). Benefiting from the unique structure, YSC@Fe₃O₄ showed many advantages. As a polar center, Fe₃O₄ can effectively adsorb polysulfides and promote the conversion of polysulfides. Meanwhile, the porous structure of the yolk-shell structure can retain sulfur and buffer the large volume expansion of sulfur during the lithiation process. Finally, the carbon shell acted as a nanocontainer, restricting the diffusion of polysulfides. Through this yolk-shell structure, they succeeded in improving the performance of Li-S batteries. In addition to metal oxides, metallic compounds formed with non-metallic elements of the main oxygen group are also introduced into Li-S batteries.[61, 62] As a similar work, Tan et al. [63] obtained the S/FeSe₂@C composite material based on the S/Fe₃O₄@C through the selenization reaction. Compared with S/Fe₃O₄@C cathode, S/FeSe₂@C cathode showed better sulfur utilization, higher rate performance and longer cycle life. FeSe₂ was utilized because the metal selenide is theoretically more conductive than that of metal oxides and metal sulfides. In short, they further developed the potential of metal nanoparticles encapsulated by carbon-based materials, which once again improved the performance of Li-S batteries (Fig. 11.7e–g). Instead of using single metal compounds in the middle layer, carbon materials encapsulating alloy nanoparticles were also a competitive choice. In 2021, Zhang et al. [64] successfully developed Nitrogen-doped carbon-coated CoFe alloy (CoFeCN@C) nanoparticles for the functionalization of commercial polypropylene separators in Li-S batteries. The N-doped carbon provided abundant transport channels for ions and electrons, when CoFe nanoparticles provided active sites to adsorb and catalyze polysulfides conversion (Fig. 11.7h–j).

11.5 Metal Nanoparticles Supported Carbon-Based Materials for MSBs

Carbon can not only be used as a shell for coating alloy nanoparticles, but also can be used as a substrate to load various metal nanoparticles and form the metal nanoparticles supported carbon-based materials.

Choosing a metal-based compound is the most important problem. In 2016, Cui et al. [65] used kapok tree as a template and carbon source to synthesize a series of

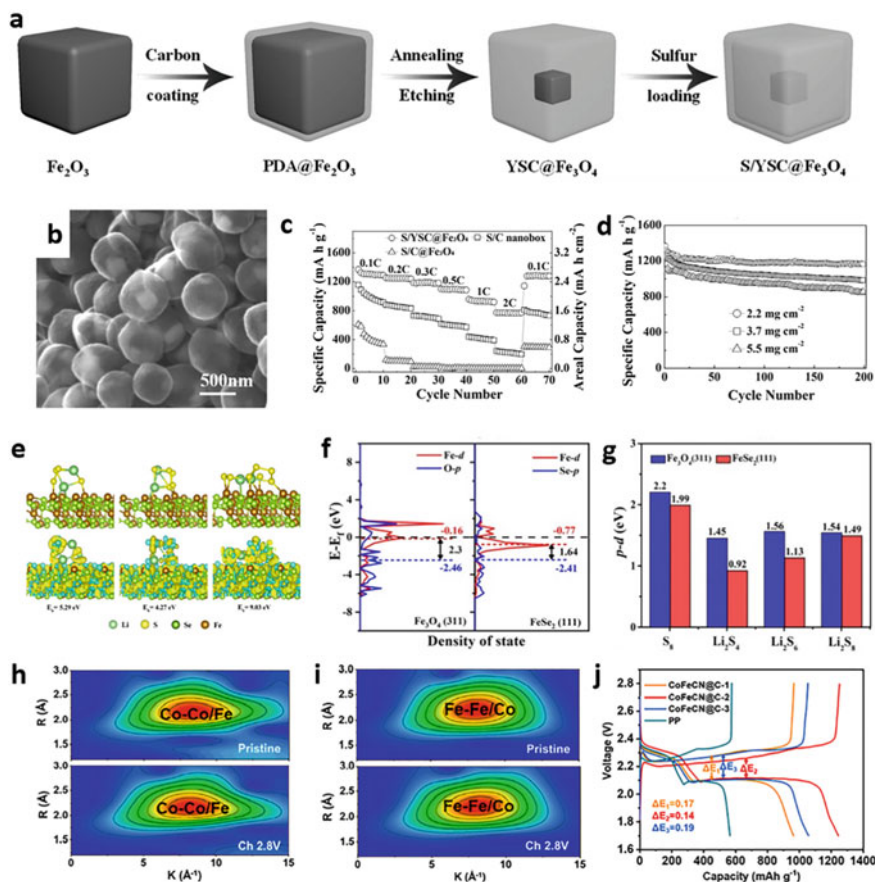


Fig. 11.7 Metal nanoparticles encapsulated by carbon-based materials for MSBs. **a** Schematic of the synthetic procedure of the S/YSC@Fe₃O₄ composite. **b** TEM images of YSC@Fe₃O₄. **c** Rate performances at various cycling rates of the S/C@Fe₃O₄, S/YSC@Fe₃O₄, and S/C nanobox electrodes. **d** Cycling performance of the S/YSC@Fe₃O₄ electrodes with different sulfur loadings. Reproduced with permission [60]. Copyright 2017, John Wiley. **e** The optimized configurations and electronic differential density of FeSe₂(111) binding with Li₂S₈. **f** Density of states analysis of *p* bands of anions and *d* bands of Fe in the pristine Fe₃O₄ (311) and FeSe₂ (111). **g** Calculated energy gap of Fe₃O₄ (311) and FeSe₂ (111) absorbed with S₈, Li₂S₄, Li₂S₆, and Li₂S₈, respectively. Reproduced with permission [63]. Copyright 2021, Elsevier. WT-EXAFS spectra of **h** Co and **i** Fe K-edge at different states of charge in the first cycle. **j** Galvanostatic charge/discharge profiles at 0.1C. Reproduced with permission [64]. Copyright 2021, Elsevier

non-conductive metal oxide nanoparticles supported on porous carbon nanoplates through the biological template method. They used a series of carbon nanoparticles composite matrix as the host to improve the performance. Among them, MgO, CeO₂ and La₂O₃ composite carbon matrix showed higher capacity and better cycle stability (Fig. 11.8a). In 2018, Ding et al. [66] developed a multifunctional

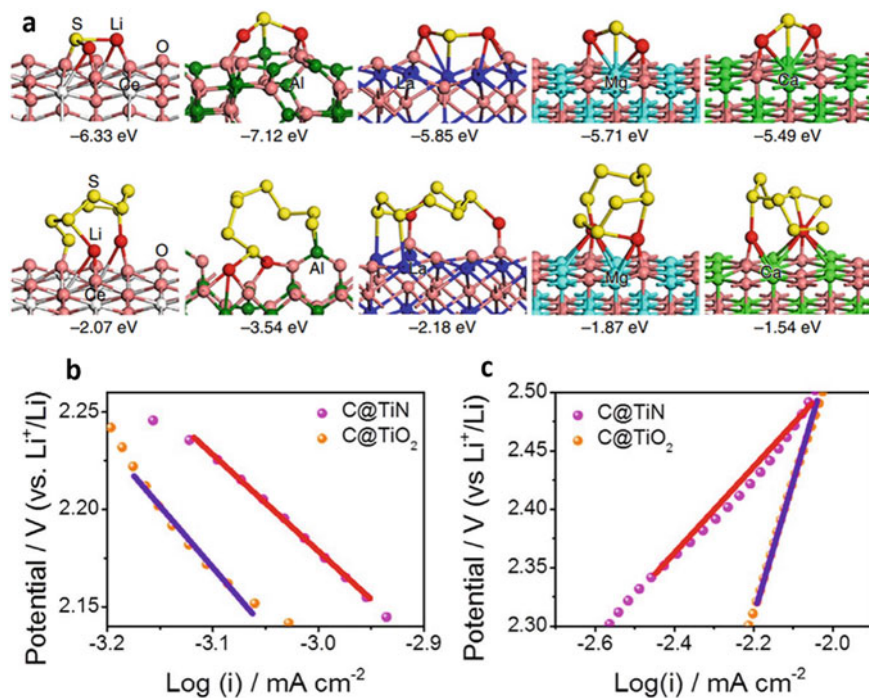


Fig. 11.8 Metal compound composite carbon material. **a** Optimized geometries of most stable Li_2S and Li_2S_8 on the metal oxide surface. Reproduced with permission [65]. Copyright 2016, Springer Nature. **b** and **c** Tafel plots for C@TiN and C@TiO₂ electrodes during reduction and oxidation processes. Reproduced with permission [66]. Copyright 2019, Elsevier

polysulfides medium based on hollow carbon nanospheres supported on titanium nitride (C@TiN) double-shell nanospheres, which successfully achieved the physical confinement, chemical adsorption and catalysis effect towards the sulfur species conversion. C@TiN-S composite material (with a sulfur content of about 70%) as cathode material exhibited faster reaction kinetics and stronger adsorption ability towards polysulfides than C@TiO₂-S composite material (Figs. 11.8b, c).

In addition to metal oxides and metal nitrides, researchers have also studied the metal phosphides and metal borides combining with carbon matrix. In 2021, Sun et al. [67] prepared rGO-CNT-CoP (amorphous) as sulfur host to gain insight into the advantages of amorphous CoP in Li-S batteries. Through the experiments and calculations, the strategy of amorphous cobalt phosphide grown on reduced graphene oxide-multi-walled carbon nanotubes (rGO-CNT-CoP (amorphous)) improved the electrochemical performance in Li-S batteries (Fig. 11.9a–c). Wang et al. [68] reported the molten salt-assisted dissolution and growth on ZIF-8 and ZIF-67 to prepare a new type of 2D heterostructure nanosheets composed of binary sulfiphilic CoB and nitrogen, boron-codoped porous carbon (NBC). Figure 11.9d shows the rate performance for CoB/NBC-S, CoB-S and NBC-S. CoB/NBC-S performed higher

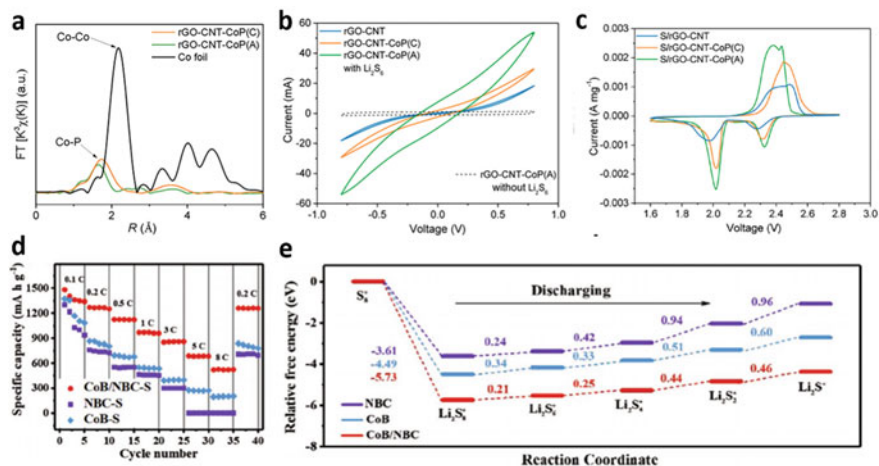


Fig. 11.9 Metal phosphides and metal borides combining with carbon matrix. **a** EXAFS spectra for Co K-edge of rGO-CNT-CoP (crystalline) and rGO-CNT-CoP (amorphous). **b** CV curves results of Li₂S₆-symmetric cells employing rGO-CNT, rGO-CNT-CoP (crystalline), and rGO-CNT-CoP (amorphous) as electrodes at 200 mV s⁻¹. **c** CV curves of S/rGO-CNT, S/rGO-CNT-CoP (crystalline), and S/rGO-CNT-CoP (amorphous) electrodes at 0.1 mV s⁻¹. Reproduced with permission [67]. Copyright 2021, American Chemical Society. **d** Rate performance for CoB/NBC-S, CoB-S, and NBC-S. **e** The energy profiles for the reduction of sulfur and polysulfides. Reproduced with permission [68]. Copyright 2021, John Wiley

specific capacity than that of the other two samples. As shown in Fig. 11.9e, the Gibbs free energy of the reduction reaction on the surface of CoB/NbC was significantly lower than that of CoB and NBC, which indicated that CoB/NBC was more thermodynamically favorable for the reduction of sulfur than CoB and NBC. Based on these experiments and electrochemical analysis, the interface electron interaction between NBC and CoB caused charge redistribution in the interface region, accelerating ion/electron transfer and facilitating the uniform deposition of solid sulfur species. The advanced catalytic effect and binary sulfophilicity for CoB/NBC greatly promoted the oxidation–reduction kinetics and chemical adsorption towards polysulfides, even at high sulfur content, high sulfur loading and high rates.

Researchers have gradually realized that single metal compound cannot meet the development for high energy batteries. Thus, a new efficient catalyst with high conductivity was urgently needed. In recent works, heterostructure materials have attracted widespread attention due to their strong adsorption ability and high catalytic activity. In 2017, Yang et al. [69] reported a TiO₂-TiN heterostructure that combined the advantages of strong adsorption towards polysulfides (from TiO₂), high electrical conductivity, and catalytic effect (Fig. 11.10a–c). This strategy provided a new way to prepare a multifunctional interlayer in Li-S batteries. In 2018, Qiao et al. [70] prepared a 2D heterostructure of MoN-VN as a new type of sulfur host. Figure 11.10d shows the in-situ synchrotron radiation X-ray contour map of S/MoN-VN and the corresponding discharge curve. The whole reduction process can be clearly revealed.

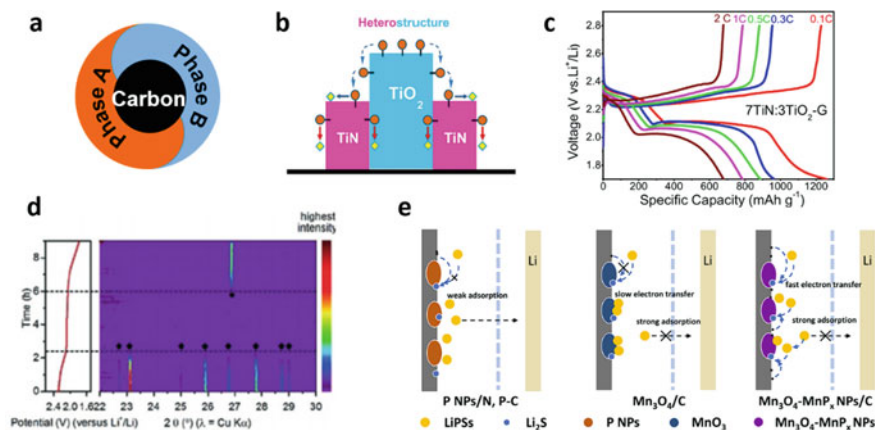


Fig. 11.10 Heterostructure materials for Li-S battery. **a** Schematic diagram of a heterostructure combined with a carbon-based material. **b** Schematic of LiPSs conversion processes on TiO_2 -TiN heterostructure surface. **c** Charge/discharge profiles of the cell with the 7TiN:3TiO₂-G coating layer at different C-rates within a potential window of 1.7–2.8 V versus Li^+/Li . Reproduced with permission [69]. Copyright 2017, RSC Publishing. **d** In situ synchrotron XRD contour plot of the S/MoN-VN with the corresponding discharge curve. Reproduced with permission [70]. Copyright 2018, John Wiley. **e** Schematic of the principle of the Mn_3O_4 - MnP_x heterostructure. Reproduced with permission [71]. Copyright 2021, Elsevier

In 2021, Zhang et al. [71] prepared a Mn_3O_4 - MnP_x heterostructure by in-situ crystallization of Mn_3O_4 - MnP_x on amorphous phosphorus nanoparticle-decorated carbon nanosheets. Experiment and DFT calculations show that Mn_3O_4 has a strong adsorption capacity for polysulfides. Meanwhile, MnP_x can also significantly catalyze the conversion reaction between sulfur and polysulfides. The synergistic effect of Mn_3O_4 and MnP_x facilitates simple redox kinetics and efficient absorption of polysulfides.

11.6 Conclusion and Perspectives

In the past ten years, M-S/Se batteries have made considerable progresses with the understanding on the basic principles of M-S/Se batteries. Carbon-based materials as host materials and interlayer materials play a vital role in the commercialization in Li-S batteries. The catalysts represented by carbon-based nanomaterials stand out by virtue of high electrical conductivity, light weight, excellent mass transfer rate, strong adsorption, and highly catalytic ability. The superhigh electrical conductivity can accelerate electron transfer during redox processes. Even heteroatom-doped carbon matrix shows weak adsorption towards polysulfides. By coupling with SACs or metal compounds, the strong binding energy and highly catalytic activity can be achieved. In addition, single-component compound show limited catalytic effect towards multi-conversion reactions. Therefore, heterostructure (with two phases or more) supported

on carbon matrix are developed for the adjustable composites and structure in past three years, showing great potential for industrial application. Although there are many studies on the cathode side, the problems of Li-S batteries are still serious, including the unstable performance for catalysts, poor rate capability, and limited performance under high sulfur/selenium loading. These difficulties and challenges bring a huge block on the development and promotion of M-S/Se batteries. In addition, the catalytic mechanism should be further studied in future. Finally, we believe that the carbon-based nanomaterials will play important role in boosting the electrochemical performance and promoting the industrialization in M-S/Se batteries. Meanwhile, the Li-S batteries are complex energy storage system, including electrolyte, host materials, separator, and Li anode. Each part needs to be reasonably investigated and optimized. It is believed that M-S/Se batteries will be industrialized in the energy market in combination with carbon-based nanomaterials in the future.

References

1. Q. Pang, X. Liang, C.Y. Kwok, L.F. Nazar, Advances in lithium–sulfur batteries based on multifunctional cathodes and electrolytes. *Nat. Energy* **1**, 16132 (2016). <https://doi.org/10.1038/nenergy.2016.132>
2. Z.W. Seh, Y. Sun, Q. Zhang, Y. Cui, Designing high-energy lithium-sulfur batteries. *Chem. Soc. Rev.* **45**, 5605–5634 (2016). <https://doi.org/10.1039/c5cs00410a>
3. K. Kang, Y.S. Meng, J. Breger, C.P. Grey, G. Ceder, Electrodes with high power and high capacity for rechargeable lithium batteries. *Science* **311**, 977–980 (2006). <https://doi.org/10.1126/science.1122152>
4. A.K. Padhi, K.S. Nanjundaswamy, J.B. Goodenough, Phospho-olivines as positive-electrode materials for rechargeable lithium batteries. *J. Electrochem. Soc.* **144**, 1188–1194 (2019). <https://doi.org/10.1149/1.1837571>
5. J. Cabana, L. Monconduit, D. Larcher, M.R. Palacin, Beyond intercalation-based Li-ion batteries: the state of the art and challenges of electrode materials reacting through conversion reactions. *Adv. Mater.* **22**, E170–192 (2010). <https://doi.org/10.1002/adma.201000717>
6. J.P. Paraknowitsch, A. Thomas, Doping carbons beyond nitrogen: an overview of advanced heteroatom doped carbons with boron, sulphur and phosphorus for energy applications. *Energy Environ. Sci.* **6**, 9821–9826 (2013). <https://doi.org/10.1039/c3ee41444b>
7. X. Li, X. Pu, S. Han, M. Liu, C. Du, C. Jiang, X. Huang, T. Liu, W. Hu, Enhanced performances of Li/polysulfide batteries with 3D reduced graphene oxide/carbon nanotube hybrid aerogel as the polysulfide host. *Nano Energy* **30**, 193–199 (2016). <https://doi.org/10.1016/j.nanoen.2016.10.015>
8. H. Sun, G. Zhu, Y. Zhu, M.C. Lin, H. Chen, Y.Y. Li, W.H. Hung, B. Zhou, X. Wang, Y. Bai, M. Gu, C.L. Huang, H.C. Tai, X. Xu, M. Angell, J.J. Shyue, H. Dai, High-safety and high-energy-density lithium metal batteries in a novel ionic-liquid electrolyte. *Adv. Mater.* **32**, e2001741 (2020). <https://doi.org/10.1002/adma.202001741>
9. P.G. Bruce, S.A. Freunberger, L.J. Hardwick, J.M. Tarascon, Li-O₂ and Li-S batteries with high energy storage. *Nat. Mater.* **11**, 19–29 (2011). <https://doi.org/10.1038/nmat3191>
10. Y.X. Yin, S. Xin, Y.G. Guo, L.J. Wan, Lithium-sulfur batteries: electrochemistry, materials, and prospects. *Angew. Chem. Int. Ed.* **52**, 13186–13200 (2013). <https://doi.org/10.1002/anie.201304762>
11. S. Evers, L.F. Nazar, New approaches for high energy density lithium-sulfur battery cathodes. *Acc. Chem. Res.* **46**, 1135–1143 (2013). <https://doi.org/10.1021/ar3001348>

12. A. Manthiram, Y. Fu, S.H. Chung, C. Zu, Y.S. Su, Rechargeable lithium-sulfur batteries. *Chem. Rev.* **114**, 11751–11787 (2014). <https://doi.org/10.1021/cr500062v>
13. C. Delmas, M. Maccario, L. Croguennec, F. Le Cras, F. Weill, Lithium deintercalation in LiFePO_4 nanoparticles *via* a domino-cascade model. *Nat. Mater.* **7**, 665–671 (2008). <https://doi.org/10.1038/nmat2230>
14. B. Dunn, H. Kamath, J.M. Tarascon, Electrical energy storage for the grid: a battery of choices. *Science* **334**, 928–935 (2011). <https://doi.org/10.1126/science.1212741>
15. H. Wang, Y. Yang, Y. Liang, J.T. Robinson, Y. Li, A. Jackson, Y. Cui, H. Dai, Graphene-wrapped sulfur particles as a rechargeable lithium-sulfur battery cathode material with high capacity and cycling stability. *Nano Lett.* **11**, 2644–2647 (2011). <https://doi.org/10.1021/nl200658a>
16. X. Ji, L.F. Nazar, Advances in Li–S batteries. *J. Mater. Chem.* **20**, 9821–9826 (2010). <https://doi.org/10.1039/b925751a>
17. A. Manthiram, Y. Fu, Y.S. Su, Challenges and prospects of lithium-sulfur batteries. *Acc. Chem. Res.* **46**, 1125–1134 (2013). <https://doi.org/10.1021/ar300179v>
18. Z. Wei Seh, W. Li, J.J. Cha, G. Zheng, Y. Yang, M.T. McDowell, P.C. Hsu, Y. Cui, Sulphur-TiO₂ yolk-shell nanoarchitecture with internal void space for long-cycle lithium-sulphur batteries. *Nat. Commun.* **4**, 1331 (2013). <https://doi.org/10.1038/ncomms2327>
19. Y.V. Mikhaylik, J.R. Akridge, Polysulfide shuttle study in the Li/S battery system. *J. Electrochem. Soc.* **151** (2004). <https://doi.org/10.1149/1.1806394>
20. X. Liang, C. Hart, Q. Pang, A. Garsuch, T. Weiss, L.F. Nazar, A highly efficient polysulfide mediator for lithium-sulfur batteries. *Nat. Commun.* **6**, 5682 (2015). <https://doi.org/10.1038/ncomms6682>
21. L. Ji, M. Rao, H. Zheng, L. Zhang, Y. Li, W. Duan, J. Guo, E.J. Cairns, Y. Zhang, Graphene oxide as a sulfur immobilizer in high performance lithium/sulfur cells. *J. Am. Chem. Soc.* **133**, 18522–18525 (2011). <https://doi.org/10.1021/ja206955k>
22. X. Gu, T. Tang, X. Liu, Y. Hou, Rechargeable metal batteries based on selenium cathodes: progress, challenges and perspectives. *J. Mater. Chem. A* **7**, 11566–11583 (2019). <https://doi.org/10.1039/c8ta12537f>
23. A. Abouimrane, D. Dambournet, K.W. Chapman, P.J. Chupas, W. Weng, K. Amine, A new class of lithium and sodium rechargeable batteries based on selenium and selenium-sulfur as a positive electrode. *J. Am. Chem. Soc.* **134**, 4505–4508 (2012). <https://doi.org/10.1021/ja211766q>
24. K. Han, Z. Liu, J. Shen, Y. Lin, F. Dai, H. Ye, A free-standing and ultralong-life lithium-selenium battery cathode enabled by 3D mesoporous carbon/graphene hierarchical architecture. *Adv. Func. Mater.* **25**, 455–463 (2015). <https://doi.org/10.1002/adfm.201402815>
25. Q. Cai, Y. Li, L. Wang, Q. Li, J. Xu, B. Gao, X. Zhang, K. Huo, P.K. Chu, Freestanding hollow double-shell Se@CN_x nanobelts as large-capacity and high-rate cathodes for Li-Se batteries. *Nano Energy* **32**, 1–9 (2017). <https://doi.org/10.1016/j.nanoen.2016.12.010>
26. Y. Cui, A. Abouimrane, C.J. Sun, Y. Ren, K. Amine, Li-Se battery: absence of lithium polyselenides in carbonate based electrolyte. *Chem. Commun.* **50**, 5576–5579 (2014). <https://doi.org/10.1039/c4cc00934g>
27. S. Tu, X. Chen, X. Zhao, M. Cheng, P. Xiong, Y. He, Q. Zhang, Y. Xu, A polysulfide-immobilizing polymer retards the shuttling of polysulfide intermediates in lithium-sulfur batteries. *Adv. Mater.* **30**, e1804581 (2018). <https://doi.org/10.1002/adma.201804581>
28. J. He, Y. Chen, A. Manthiram, Vertical Co_9S_8 hollow nanowall arrays grown on a celgard separator as a multifunctional polysulfide barrier for high-performance Li–S batteries. *Energy Environ. Sci.* **11**, 2560–2568 (2018). <https://doi.org/10.1039/c8ee00893k>
29. Z.L. Yu, B. Qin, Z.Y. Ma, J. Huang, S.C. Li, H.Y. Zhao, H. Li, Y.B. Zhu, H.A. Wu, S.H. Yu, Superelastic hard carbon nanofiber aerogels. *Adv. Mater.* **31**, e1900651 (2019). <https://doi.org/10.1002/adma.201900651>
30. X. Ji, K.T. Lee, L.F. Nazar, A highly ordered nanostructured carbon-sulphur cathode for lithium-sulphur batteries. *Nat. Mater.* **8**, 500–506 (2009). <https://doi.org/10.1038/nmat2460>

31. L. Peng, Z. Wei, C. Wan, J. Li, Z. Chen, D. Zhu, D. Baumann, H. Liu, C.S. Allen, X. Xu, A.I. Kirkland, I. Shakir, Z. Almutairi, S. Tolbert, B. Dunn, Y. Huang, P. Sautet, X. Duan, A fundamental look at electrocatalytic sulfur reduction reaction. *Nat. Catal.* **3**, 762–770 (2020). <https://doi.org/10.1038/s41929-020-0498-x>
32. L. Qie, W. Chen, H. Xu, X. Xiong, Y. Jiang, F. Zou, X. Hu, Y. Xin, Z. Zhang, Y. Huang, Synthesis of functionalized 3D hierarchical porous carbon for high-performance supercapacitors. *Energy Environ. Sci.* **6**, 2497–2504 (2013). <https://doi.org/10.1039/c3ee41638k>
33. B. Singh, M.B. Gawande, A.D. Kute, R.S. Varma, P. Fornasiero, P. McNeice, R.V. Jagadeesh, M. Beller, R. Zboril, Single-atom (iron-based) catalysts: synthesis and applications. *Chem. Rev.* **121**, 13620–13697 (2021). <https://doi.org/10.1021/acs.chemrev.1c00158>
34. C. Wan, X. Duan, Y. Huang, Molecular design of single-atom catalysts for oxygen reduction reaction. *Adv. Energy Mater.* **10**, 1903815 (2020). <https://doi.org/10.1002/aenm.201903815>
35. J. Zhang, H. Yang, B. Liu, Coordination engineering of single-atom catalysts for the oxygen reduction reaction: a review. *Adv. Energy Mater.* **11**, 2002473 (2020). <https://doi.org/10.1002/aenm.202002473>
36. C.X. Zhao, B.Q. Li, J.N. Liu, Q. Zhang, Intrinsic electrocatalytic activity regulation of M-N-C single-atom catalysts for the oxygen reduction reaction. *Angew. Chem. Int. Ed.* **60**, 4448–4463 (2021). <https://doi.org/10.1002/anie.202003917>
37. J. Wang, L. Jia, H. Lin, Y. Zhang, Single-atomic catalysts embedded on nanocarbon supports for high energy density lithium-sulfur batteries. *Chemsuschem* **13**, 3404–3411 (2020). <https://doi.org/10.1002/cssc.202000702>
38. K. Zhang, Z. Chen, R. Ning, S. Xi, W. Tang, Y. Du, C. Liu, Z. Ren, X. Chi, M. Bai, C. Shen, X. Li, X. Wang, X. Zhao, K. Leng, S.J. Pennycook, H. Li, H. Xu, K.P. Loh, K. Xie, Single-atom coated separator for robust lithium-sulfur batteries. *ACS Appl. Mater. Interf.* **11**, 25147–25154 (2019). <https://doi.org/10.1021/acsami.9b05628>
39. Z. Zhuang, Q. Kang, D. Wang, Y. Li, Single-atom catalysis enables long-life, high-energy lithium-sulfur batteries. *Nano Res.* **13**, 1856–1866 (2020). <https://doi.org/10.1007/s12274-020-2827-4>
40. C. Wang, H. Song, C. Yu, Z. Ullah, Z. Guan, R. Chu, Y. Zhang, L. Zhao, Q. Li, L. Liu, Iron single-atom catalyst anchored on nitrogen-rich MOF-derived carbon nanocage to accelerate polysulfide redox conversion for lithium sulfur batteries. *J. Mater. Chem. A* **8**, 3421–3430 (2020). <https://doi.org/10.1039/c9ta11680j>
41. G. Zhou, S. Zhao, T. Wang, S.Z. Yang, B. Johannessen, H. Chen, C. Liu, Y. Ye, Y. Wu, Y. Peng, C. Liu, S.P. Jiang, Q. Zhang, Y. Cui, Theoretical calculation guided design of single-atom catalysts toward fast kinetic and long-life Li-S batteries. *Nano Lett.* **20**, 1252–1261 (2020). <https://doi.org/10.1021/acs.nanolett.9b04719>
42. J. He, G. Hartmann, M. Lee, G.S. Hwang, Y. Chen, A. Manthiram, Freestanding 1T MoS₂/graphene heterostructures as a highly efficient electrocatalyst for lithium polysulfides in Li-S batteries. *Energy Environ. Sci.* **12**, 344–350 (2019). <https://doi.org/10.1039/c8ee03252a>
43. L. Ji, X. Wang, Y. Jia, Q. Hu, L. Duan, Z. Geng, Z. Niu, W. Li, J. Liu, Y. Zhang, S. Feng, (2020) Flexible electrocatalytic nanofiber membrane reactor for lithium/sulfur conversion chemistry. *Adv. Funct. Mater.* **30**. <https://doi.org/10.1002/adfm.201910533>
44. B. Zhang, X. Qin, G.R. Li, X.P. Gao, Enhancement of long stability of sulfur cathode by encapsulating sulfur into micropores of carbon spheres. *Energy Environ. Sci.* **3**, 1531–1537 (2010). <https://doi.org/10.1039/c002639e>
45. G. Zheng, Y. Yang, J.J. Cha, S.S. Hong, Y. Cui, Hollow carbon nanofiber-encapsulated sulfur cathodes for high specific capacity rechargeable lithium batteries. *Nano Lett.* **11**, 4462–4467 (2011). <https://doi.org/10.1021/nl2027684>
46. Y.S. Su, A. Manthiram, Lithium-sulphur batteries with a microporous carbon paper as a bifunctional interlayer. *Nat. Commun.* **3**, 1166 (2012). <https://doi.org/10.1038/ncomms2163>
47. T.-Z. Hou, X. Chen, H.-J. Peng, J.-Q. Huang, B.-Q. Li, Q. Zhang, B. Li, Design principles for heteroatom-doped nanocarbon to achieve strong anchoring of polysulfides for lithium-sulfur batteries. *Small* **12**, 3283–3291 (2016). <https://doi.org/10.1002/smll.201600809>

48. X. Huang, Q. Xu, W. Gao, T. Yang, R. Zhan, J. Deng, B. Guo, M. Tao, H. Liu, M. Xu, Rechargeable K-Se batteries based on metal-organic-frameworks-derived porous carbon matrix confined selenium as cathode materials. *J. Colloid Interf. Sci.* **539**, 326–331 (2019). <https://doi.org/10.1016/j.jcis.2018.12.083>
49. Y. Wang, D. Adekoya, J. Sun, T. Tang, H. Qiu, L. Xu, S. Zhang, Y. Hou, Manipulation of edge-site Fe–N₂ moiety on holey Fe, N codoped graphene to promote the cycle stability and rate capacity of Li–S batteries. *Adv. Func. Mater.* **29**, 1807485 (2018). <https://doi.org/10.1002/adfm.201807485>
50. P. Wang, B. Xi, Z. Zhang, M. Huang, J. Feng, S. Xiong, Atomic tungsten on graphene with unique coordination enabling kinetically boosted lithium-sulfur batteries. *Angew. Chem. Int. Ed.* **60**, 15563–15571 (2021). <https://doi.org/10.1002/anie.202104053>
51. R. Wang, R. Wu, C. Ding, Z. Chen, H. Xu, Y. Liu, J. Zhang, Y. Ha, B. Fei, H. Pan, Porous carbon architecture assembled by cross-linked carbon leaves with implanted atomic cobalt for high-performance Li-S batteries. *Nano-Micro Lett.* **13**, 151 (2021). <https://doi.org/10.1007/s40820-021-00676-6>
52. F. Ma, Y. Wan, X. Wang, X. Wang, J. Liang, Z. Miao, T. Wang, C. Ma, G. Lu, J. Han, Y. Huang, Q. Li, Bifunctional atomically dispersed Mo-N₂/C nanosheets boost lithium sulfide deposition/decomposition for stable lithium-sulfur batteries. *ACS Nano* **14**, 10115–10126 (2020). <https://doi.org/10.1021/acsnano.0c03325>
53. Y. Li, J. Fan, J. Zhang, J. Yang, R. Yuan, J. Chang, M. Zheng, Q. Dong, A honeycomb-like Co@N-C composite for ultrahigh sulfur loading Li-S batteries. *ACS Nano* **11**, 11417–11424 (2017). <https://doi.org/10.1021/acsnano.7b06061>
54. L.-L. Gu, J. Gao, C. Wang, S.-Y. Qiu, K.-X. Wang, X.-T. Gao, K.-N. Sun, P.-J. Zuo, X.-D. Zhu, Thin-carbon-layer-enveloped cobalt-iron oxide nanocages as a high-efficiency sulfur container for Li-S batteries. *J. Mater. Chem. A* **8**, 20604–20611 (2020). <https://doi.org/10.1039/d0ta07579e>
55. R. Hu, Y. Ouyang, T. Liang, X. Tang, B. Yuan, J. Liu, L. Zhang, L. Yang, M. Zhu, Inhibiting grain coarsening and inducing oxygen vacancies: the roles of Mn in achieving a highly reversible conversion reaction and a long life SnO₂–Mn–graphite ternary anode. *Energy Environ. Sci.* **10**, 2017–2029 (2017). <https://doi.org/10.1039/c7ee01635b>
56. Z. Shen, M. Cao, Z. Zhang, J. Pu, C. Zhong, J. Li, H. Ma, F. Li, J. Zhu, F. Pan, H. Zhang, Efficient ni₂co₄p₃ nanowires catalysts enhance ultrahigh-loading lithium-sulfur conversion in a microreactor-like battery. *Adv. Func. Mater.* **30**, 1906661 (2019). <https://doi.org/10.1002/adfm.201906661>
57. H. Li, L. Fei, R. Zhang, S. Yu, Y. Zhang, L. Shu, Y. Li, Y. Wang, FeCo alloy catalysts promoting polysulfide conversion for advanced lithium-sulfur batteries. *J. Energy Chem.* **49**, 339–347 (2020). <https://doi.org/10.1016/j.jechem.2020.02.050>
58. Z. Qiao, F. Zhou, Q. Zhang, F. Pei, H. Zheng, W. Xu, P. Liu, Y. Ma, Q. Xie, L. Wang, X. Fang, D.-L. Peng, Chemisorption and electrocatalytic effect from Co_xSn_y alloy for high performance lithium sulfur batteries. *Energy Storage Mater.* **23**, 62–71 (2019). <https://doi.org/10.1016/j.ensm.2019.05.032>
59. Z. Shi, Z. Sun, J. Cai, Z. Fan, J. Jin, M. Wang, J. Sun, Boosting dual-directional polysulfide electrocatalysis via bimetallic alloying for printable Li–S batteries. *Adv. Func. Mater.* **31**, 2006798 (2020). <https://doi.org/10.1002/adfm.202006798>
60. J. He, L. Luo, Y. Chen, A. Manthiram, Yolk-shelled C@Fe₃O₄ nanoboxes as efficient sulfur hosts for high-performance lithium-sulfur batteries. *Adv. Mater.* **29**, 1702707 (2017). <https://doi.org/10.1002/adma.201702707>
61. X.Y. Yu, H. Hu, Y. Wang, H. Chen, X.W. Lou, Ultrathin MoS₂ nanosheets supported on N-doped carbon nanoboxes with enhanced lithium storage and electrocatalytic properties. *Angew. Chem. Int. Ed.* **54**, 7395–7398 (2015). <https://doi.org/10.1002/anie.201502117>
62. X.Y. Yu, H.B. Wu, L. Yu, F.X. Ma, X.W. Lou, Rutile TiO₂ submicroboxes with superior lithium storage properties. *Angew. Chem. Int. Ed.* **54**, 4001–4004 (2015). <https://doi.org/10.1002/anie.201411353>

63. W. Sun, Y. Li, S. Liu, C. Liu, X. Tan, K. Xie, Mechanism investigation of iron selenide as polysulfide mediator for long-life lithium-sulfur batteries. *Chem. Eng. J.* **416**, 129166 (2021). <https://doi.org/10.1016/j.cej.2021.129166>
64. Y. Hu, C. Cheng, T. Yan, G. Liu, C. Yuan, Y. Yan, Z. Gu, P. Zeng, L. Zheng, J. Zhang, L. Zhang, Catalyzing polysulfide redox conversion for promoting the electrochemical performance of lithium-sulfur batteries by CoFe alloy. *Chem. Eng. J.* **421**, 129997 (2021). <https://doi.org/10.1016/j.cej.2021.129997>
65. X. Tao, J. Wang, C. Liu, H. Wang, H. Yao, G. Zheng, Z.W. Seh, Q. Cai, W. Li, G. Zhou, C. Zu, Y. Cui, Balancing surface adsorption and diffusion of lithium-polysulfides on nonconductive oxides for lithium-sulfur battery design. *Nat. Commun.* **7**, 11203 (2016). <https://doi.org/10.1038/ncomms11203>
66. Y. Wang, R. Zhang, Y.-C. Pang, X. Chen, J. Lang, J. Xu, C. Xiao, H. Li, K. Xi, S. Ding, Carbon@titanium nitride dual shell nanospheres as multi-functional hosts for lithium sulfur batteries. *Energy Storage Mater.* **16**, 228–235 (2019). <https://doi.org/10.1016/j.ensm.2018.05.019>
67. R. Sun, Y. Bai, M. Luo, M. Qu, Z. Wang, W. Sun, K. Sun, Enhancing polysulfide confinement and electrochemical kinetics by amorphous cobalt phosphide for highly efficient lithium-sulfur batteries. *ACS Nano* **15**, 739–750 (2021). <https://doi.org/10.1021/acsnano.0c07038>
68. Z. Li, P. Li, X. Meng, Z. Lin, R. Wang, The interfacial electronic engineering in binary sulfiphilic cobalt boride heterostructure nanosheets for upgrading energy density and longevity of lithium-sulfur batteries. *Adv. Mater.* **33**, e2102338 (2021). <https://doi.org/10.1002/adma.202102338>
69. T. Zhou, W. Lv, J. Li, G. Zhou, Y. Zhao, S. Fan, B. Liu, B. Li, F. Kang, Q.-H. Yang, Twinborn TiO₂-TiN heterostructures enabling smooth trapping-diffusion-conversion of polysulfides towards ultralong life lithium-sulfur batteries. *Energy Environ. Sci.* **10**, 1694–1703 (2017). <https://doi.org/10.1039/c7ee01430a>
70. C. Ye, Y. Jiao, H. Jin, A.D. Slattery, K. Davey, H. Wang, S.Z. Qiao, 2D MoN-VN heterostructure to regulate polysulfides for highly efficient lithium-sulfur batteries. *Angew. Chem. Int. Ed.* **57**, 16703–16707 (2018). <https://doi.org/10.1002/anie.201810579>
71. K. Guo, G. Qu, J. Li, H. Xia, W. Yan, J. Fu, P. Yuan, J. Zhang, Polysulfides shuttling remedies by interface-catalytic effect of Mn₃O₄-MnP_x heterostructure. *Energy Storage Mater.* **36**, 496–503 (2021). <https://doi.org/10.1016/j.ensm.2021.01.021>

Chapter 12

Carbon-Based Nanomaterials for Metal-Air Batteries



Yue Yu and Huicong Xia

Abstract Metal-air batteries (MABs) recently have received much attention due to their possible higher energy efficiency and lower cost. However, the full utilization of the high specific capacity remains challenging and requires the exploration of appropriate electrode materials. Carbon nanomaterials simultaneously display high electrical conductivities, high specific surface areas and good stabilities with little volume expansion during the charge–discharge process. The high electrical conductivity facilitates charge transfer and high specific surface area provide channels for electrolyte and oxygen diffusion. Porous structures with high surface areas enable rapid electrolyte diffusions and charge transfers, which is beneficial for fast charge and discharge. The chemical properties of carbon nanomaterials can be varied via introducing chemical dopants. The incorporation of heteroatoms can significantly change the nanostructure and electrochemical performance of carbon nanomaterials. In this chapter, we summarize research progress on carbon-based nanomaterials with enhanced performance for rechargeable metal-air batteries. In each section, we describe the synthesis, physical and chemical characterizations, and innovation of carbon-based nanomaterials for each application. Finally, we conclude the perspectives and critical challenges that need to be addressed for designing carbon nanomaterials to improve the electrochemical performance of MABs with higher energy density and power density.

12.1 Introduction

With the ever-increasing demand for the transition from fossil fuels to clean and renewable energy, great efforts have been devoted to the development of sustainable energy harvesting, conversion, and storage [1–3]. Batteries of various types

Y. Yu · H. Xia (✉)

College of Materials Science and Engineering, Zhengzhou University, Zhengzhou 450001,
P. R. China

e-mail: summer9209@126.com

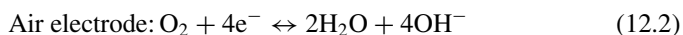
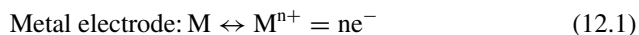
Y. Yu

e-mail: yy013682@gs.zzu.edu.cn

have been an essential medium bridging energy harvesting and utilization. Li-ion batteries (LIBs), due to the high energy storage capability, have successfully dominated the consumer market since their initial commercialization in the 1990s [4]. However, LIBs face a number of challenges, especially the safety issues and the uprising cost of battery materials [5–7]. To avoid these problems, the development of alternative electrochemical energy storage and conversion technologies (e.g., Na-ion batteries, Li-metal batteries, metal-sulfur batteries, fuel cells, and metal-air batteries) has led to intensive research activity [8, 9]. MABs are assembled from a metal anode (e.g., Li, Na, K, Mg, Al, Zn) and an air-breathing cathode that are immersed in a proper electrolyte, generating electricity through the redox reaction between the metal anode and oxygen [10–12]. The half-open structure of a metal-air battery allows the direct oxygen supply from ambient air as the cathode reactant, therefore enabling high capacities and energy densities. Generally, based on the electrolyte, these MABs can be divided into aqueous and nonaqueous systems, corresponding to two typical batteries of Zn–air and Li–air, respectively. Li-air batteries (LABs) and Zn-air batteries (ZABs) are two types of metal-air batteries that have attracted most attention [13, 14]. Li-air batteries (with Li_2O_2 as the discharge product) can deliver a superior theoretical performance of a large energy density of $11,429 \text{ W h kg}^{-1}$ (based on the mass of Li metal), a high specific capacity of 3860 mA h g^{-1} (based on the mass of Li metal), and a cell voltage as high as 2.96 V. For Zn-air batteries the theoretical energy density is 1350 W h kg^{-1} (based on the mass of Zn metal), still about fivefold higher than Li-ion batteries. Moreover, Zn-air batteries also have the advantage of low cost ($\sim \$10 \text{ kW}^{-1} \text{ h}^{-1}$) compared with Li-ion batteries ($\$400\text{--}800 \text{ kW}^{-1} \text{ h}^{-1}$). Besides Li-air and Zn-air batteries, other types of MABs also have their own superiorities. For example, Al-air batteries exhibit the highest volumetric capacity (8040 A h L^{-1}), and Na-air batteries show smaller charge overpotentials than Li-air batteries.[15, 16] Therefore, the metal-air battery family has great potential to serve as next-generation electrochemical energy-storage devices.

MABs usually contain four major parts: an air electrode, metal electrode, electrolyte, and separator, as illustrated in Fig. 12.1. For most MABs, the air electrode reactant O_2 is obtained from the ambient air rather than encapsulated in the cell. Therefore, the air electrode usually consists of only an electrocatalyst layer to reduce the electrode overpotential and a gas-diffusion layer (GDL) to enhance the oxygen diffusion between the ambient air and the catalyst surface [17].

The electrode reactions of rechargeable MABs vary with the metal electrodes and the type of electrolytes. Generally, for metal-air batteries with aqueous electrolyt99es the electrode reactions are in the following form:



where M stands for the metal (Zn, Al, Mg, Fe, etc.) and n represents the metal ion charge number. The metal ions generated on the metal electrode during the discharge

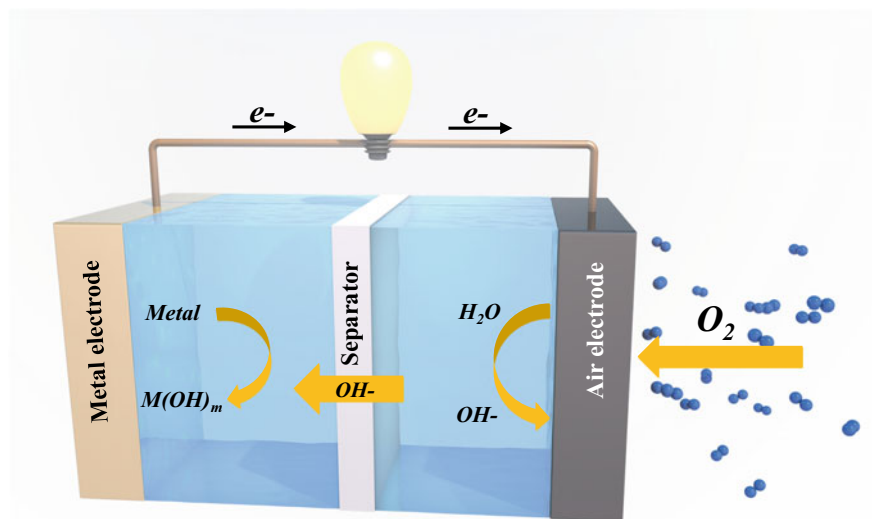
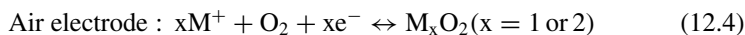
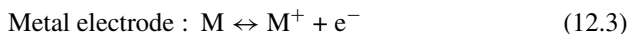


Fig. 12.1 Schematic diagram of MABs

process may further react with OH^- in the alkaline electrolyte. On the air electrode, the conversions between oxygen and water take place during the discharge and charge processes, which have been widely investigated as oxygen reduction reaction (ORR, discharge) and oxygen evolution reaction (OER, charge) for the applications in fuel cells, water splitting, and so forth [18].

For Li-, Na-, and K-air batteries with aprotic electrolytes, oxygen reacts with metal ions on the air electrode, and the discharge product on the air electrode can be metal superoxides or peroxides. The electrode reactions are as follows:



The oxygen molecules are first reduced to superoxide ion and then bound with metal ions. However, according to the hard-soft acid–base theory (HSAB), Li^+ with a small ionic radius is a hard Lewis acid, which is unstable with O_2^- . Therefore, the Li superoxides will disproportionate to form Li_2O_2 , the main discharge product for Li-air batteries, while for Na^+ and K^+ with increasing ionic radius, the combination with O_2^- becomes more stable and the proportion of superoxides in the discharge product increases. The peroxides and superoxides generated during the discharge process deposit on the air electrode, and decompose to metal ion and oxygen when charging. The air electrode ORR and OER processes significantly distinguish from

those in aqueous electrolytes. Moreover, as the Li, Na, and K metals are sensitive to the H₂O and CO₂ in air, metal-air batteries with these anodes are usually operated in pure O₂ and are denoted as Li-O₂, Na-O₂, and K-O₂ batteries [19–21].

Inspired by alkali metal-O₂ batteries, alkali metal-CO₂ batteries using greenhouse gas as the active material, not only serve as energy storage devices, but also decrease CO₂ accumulation in the atmosphere. The battery structure and electrochemical principles of alkali metal-CO₂ batteries are similar to those of alkali metal-O₂ batteries, except for the electrolyte and the active material. The CO₂ reduction reaction (CO₂RR) and CO₂ evolution reaction (CO₂ER) happen at the surface of catalyst of the cathode as:



The CO₂ insulator/three-phase reaction interface and side reactions/high decomposition barrier of M₂CO₃ are respectively the major challenges hindering CO₂RR and CO₂ER kinetics. Because the M₂CO₃ solid is more stable than the M₂O₂ solid, the reversible conversion of CO₂RR and CO₂ER in alkali metal-CO₂ batteries is more difficult.

The major obstacles that limit the practical applications of MABs are the overall energy efficiency and long-term cyclability, which are currently less than a quarter of the commercially available lithium-ion batteries. The air electrode is the key factor that determines the battery performance, where the conversion between oxygen and metal hydroxide takes place. Practical MABs leans on the development of a stable air-electrode with superior ORR and OER catalytic activities [22]. The air-electrode should also fulfill the following criteria:

- (i) High chemical/electrochemical stability for reversible electrochemical reaction under acceptable charge/discharge voltage with minimum irreversible parasitic reaction [23].
- (ii) Suitable porosity for controllable dictate product size and improved rechargeability. Less packed electrodes with large void volume (e.g., CNT vs. carbon black) can ease electrolyte penetration and assure arrival of both active species, i.e., O₂ and metal ion, to the catalytic reaction sites. Adequate porosity can not only facilitate mass transport and efficient product accumulation, but also dictate product size and efficient rechargeability [24].
- (iii) High electrical conductivity for better electron transfer from the insulator and insoluble discharge product to cathode surface at low overpotentials [25].

The intrinsic sluggish reaction kinetics on the air electrode, including ORR during the discharge process and OER during the charging process, contribute most to the high polarization and the inferior electrode reversibility of MABs [26]. Therefore, the rational design of efficient bifunctional oxygen catalysts has attracted intensive research interest with the purpose of accelerating the reaction kinetics and lowering the discharge/charge overpotentials to achieve better battery performances [27]. So far, various materials have been explored as bifunctional oxygen electrocatalysts,

including metal oxides, metal hydroxides, metal sulfides, carbon materials, and their composites [28–31].

Amongst, carbon materials are the most popular candidates to construct efficient bifunctional oxygen catalysts for MABs, due to their high electrical conductivity, high chemical stability, versatile porous nanostructure, tunable physical and chemical properties, and low cost [32]. Remarkably, the electronic structure of carbon materials can be facilely modified via multiple regulation strategies (e.g., heteroatom doping, defect engineering, surface engineering, etc.) to achieve variable electrocatalytic properties [33]. Because of its attractive properties, such as high electronic conductivity, lightweights, and cost-effectiveness, porous carbon structures had been mostly employed in MABs [34].

The standard air-breathing cathode is composed of a high surface area carbonaceous material, a polymer binder, and possibly a catalyst mixed together and applied on a metal (commonly nickel or stainless steel) current collector [35]. The carbon serves as a conductive substrate supporting ORR and OER, providing channels for oxygen diffusion and, in some cases, accommodating catalysts for improved electrochemical activity, and is thus regarded as one of the most important components affecting MABs performance [36].

Herein, we introduce the advanced development of materials for MABs electrode by systematically summarizing the four types of carbon-based materials that have been widely reported so far: (1) metal-free carbon-based materials; (2) atomically dispersed metal carbon-based materials; (3) metal nanoparticles supported carbon-based materials; (4) metal nanoparticles encapsulated carbon-based materials. This chapter aims to describe the recent progress and prospects of carbon-based nanomaterials for metal-air batteries and put forward an outlook on the future of carbon-based nanomaterials.

12.2 Metal-Free Carbon-Based Materials for MABs

The premier application of cathode in MABs is thin carbon composite electrode. Given the advantages of porosity, lightweight, and high electrical conductivity, porous carbon materials, for example, Ketjen Black, and carbon-related materials, for example, graphene, are the most potential candidates for MABs. [37, 38]. A series of results about discharge product and specific capacity were published based on these carbon electrodes, in addition, the technology of MABs has also progressed greatly [34, 39].

Carbon nanotubes (CNTs) have relatively high surface areas and also a high aspect ratio, which is favorable to the formation of the continuous path from the current collector to the electrochemical active sites as the material for composite electrode [40]. Hirokazu et al. [41] present the fabrication of solid-state lithium–air cells using an air electrode with an inorganic solid electrolyte and a CNT catalyst. That air electrodes using inorganic solid electrolytes and carbon materials for solid-state lithium–air batteries show good potential for development. Although the carbon

nanotubes used as catalyst and as conductive additive aggregated, a cell capacity of about 400 mA h g^{-1} was obtained.

Mirzaeian et al. [45] found that the battery performance depended on the morphology of the carbon as well. Therefore it is important to develop new carbon-based electrodes to improve the kinetics of the air cathode and to enhance the battery performance. Generally speaking, the introduction of defects into host materials can generate more active sites for electrochemical reactions. Recently, nitrogen-doped carbon powder as cathode material in lithium–air batteries showed improvement to the discharge capacity because of the high surface area, porosity and electrocatalytic activity. The doped heteroatoms are available to tailor the chemical and electronic nature of carbon-based materials. Li et al. [42] employed Nitrogen-doped carbon nanotubes (N-CNTs) as cathode for Li–air batteries (Fig. 12.2a). The N-CNTs were synthesized by a floating catalyst chemical vapor deposition (FCCVD) method. It was demonstrated that nitrogen doping into carbon nanotubes not only increased the discharge capacity but also enhanced the reversibility in the charge/discharge process. This finding is opening a rational and promising direction in developing carbon electrode for Li–air batteries. N-CNTs were investigated as cathode material for Li–air batteries and exhibited a specific discharge capacity of 866 mA h g^{-1} , which was about 1.5 times as that of CNTs (Fig. 12.2f). The results indicated that the N-CNTs electrode showed high electrocatalytic activities for the cathode reaction thus improving the Li–air battery performance.

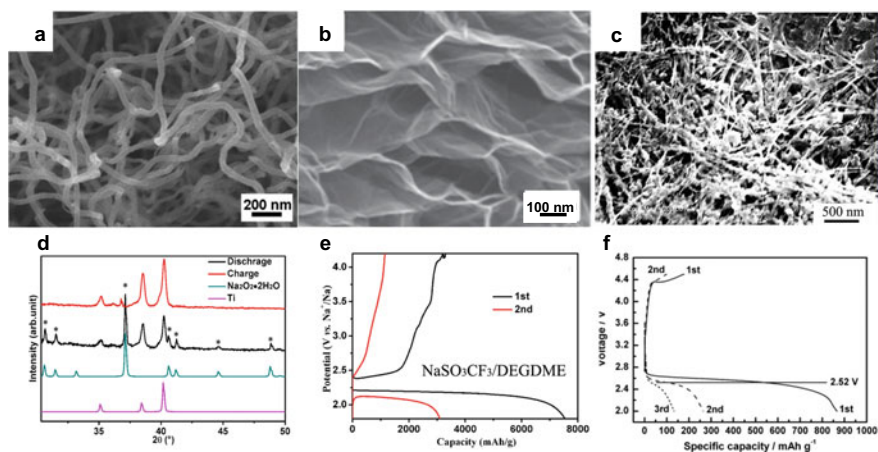


Fig. 12.2 Morphology of 1D, 2D, and 3D carbon nanomaterials and performance in metal-air batteries. SEM image of **a** CNTs. Reproduced with permission [42]. Copyright 2011, Elsevier B.V. **b** Graphene nanosheets. Reproduced with permission [43]. Copyright 2011, The Royal Society of Chemistry. **c** 3D CNT papers. **d** XRD patterns of the CNT paper cathode after deep discharging and charging. **e** First two discharge/charge cycles with cut-off potentials from 1.8 to 4.2 V. Reproduced with permission [44]. Copyright 2013, Elsevier B.V. **f** The voltage profiles of N-CNTs electrodes cycled in a voltage range of 2.0–4.5 V at a current density of 75 mA g^{-1} in the first three cycles. Reproduced with permission [42]. Copyright 2011, Elsevier B.V.

The carbon nanotubes presented good performance in MABs, but the limited surface area of the one-dimensional (1D) morphology restricted the active sites. two-dimensional (2D) carbon materials possess abundant active sites, thus exhibiting much enhanced electrochemical and catalytic properties compared to 1D carbon materials. Li et al. [43] reported graphene nanosheets (GNSs) introduced as cathode active materials in non-aqueous LABs and delivered a high capacity of 8705.9 mA h^{-1} at a current density of 75 mA g^{-1} . The unique structures of GNSs form an ideal 3D 3-phase electrochemical area and the diffusion channels for the electrolyte and O_2 , which increase the efficiency of the catalyst reaction (Fig. 12.2b). In addition, the active sites at the edge significantly contribute to the superior electrocatalytic activity towards ORR. Although the detailed mechanism for the oxygen reduction reaction on GNSs in a nonaqueous electrolyte is unclear, it has revealed that GNSs can deliver an extremely high discharge capacity, showing promising applications in MABs.

Although the performance is improved in the 1D and 2D carbon electrodes to some extent, the reversible capacity is relatively limited, due to the structural anisotropy of the 1D or 2D electrodes. As a result, both the electron transport and mass transport of reactants in 1D or 2D electrodes are restricted by the structural characteristics of the 1D and 2D electrodes. To resolve this issue, the nanostructure design of three-dimensional (3D) carbon electrodes has been developed. It has been confirmed that 3D architectures are effective for facilitating the mass transport of reactants through the electrode, improving both the power density and the energy density of metal-air batteries simultaneously. Jian et al. [44] demonstrate that a 3D interpenetrating CNT paper without binders and additives could serve as an ideal catalyst for Na-O_2 batteries. The CNT paper exhibits the discharge and charge capacities of 7530 and 3300 mA h g^{-1} , respectively, at a current density of 500 mA g^{-1} (Fig. 12.2e). The overpotential gap is as small as 200 mV . The XRD pattern confirms that the crystalline discharge product particles in the positive electrode of the battery after full discharge are $\text{Na}_2\text{O}_2 \cdot 2\text{H}_2\text{O}$ (Fig. 12.2d). Many $\text{Na}_2\text{O}_2 \cdot 2\text{H}_2\text{O}$ particles distributed along the carbon nanotubes can be observed in the SEM image of the CNT paper cathode after deep discharge, which leads to the high capacity of the carbon nanotube paper (Fig. 12.2c).

It can be said that non-metallic carbon-based materials have considerable research value as electrode materials for non-aqueous electrolyte metal-air batteries. In addition, non-metallic carbon-based materials can also play an important role as carriers in composite electrode materials.

In addition, researchers have also conducted extensive research on metal-free carbon-based electrode materials for metal-air batteries with aqueous electrolytes. Rechargeable zinc-air batteries have attracted the most attention among aqueous electrolyte metal-air batteries due to their abundant zinc reserves, high theoretical energy density (1086 W h kg^{-1}), and intrinsic safety. However, due to the inherently slow kinetic processes of ORR and OER during cathode discharge and charging, insufficient power density and energy efficiency greatly hinder the wide application of rechargeable Zn-air batteries. However, the best-performing industrial-level OER/ORR catalysts still rely heavily on noble metal catalysts. The high cost and poor

stability make the development of efficient and stable non-precious metal OER/ORR bifunctional catalysts an urgent problem. Because of great potential in high performance and high stability as well as abundant carbon resources, carbon materials have become a promising substitute for precious metal catalysts.

In 2022, Wu et al. [46] developed a high-throughput plasma-enhanced chemical vapor deposition method to fabricate N and O co-doped vertical graphene films with favorable morphologies and preferred doping configurations. The vertically aligned graphene arrays are excellent substrates for anchoring active catalytic species due to their unique morphology and excellent charge transfer ability, and the co-doping of N and O is mainly at pyridinic sites next to C vacancies in the graphene structure and is extremely active in promoting the ORR-OER redox process in Zn-air batteries.

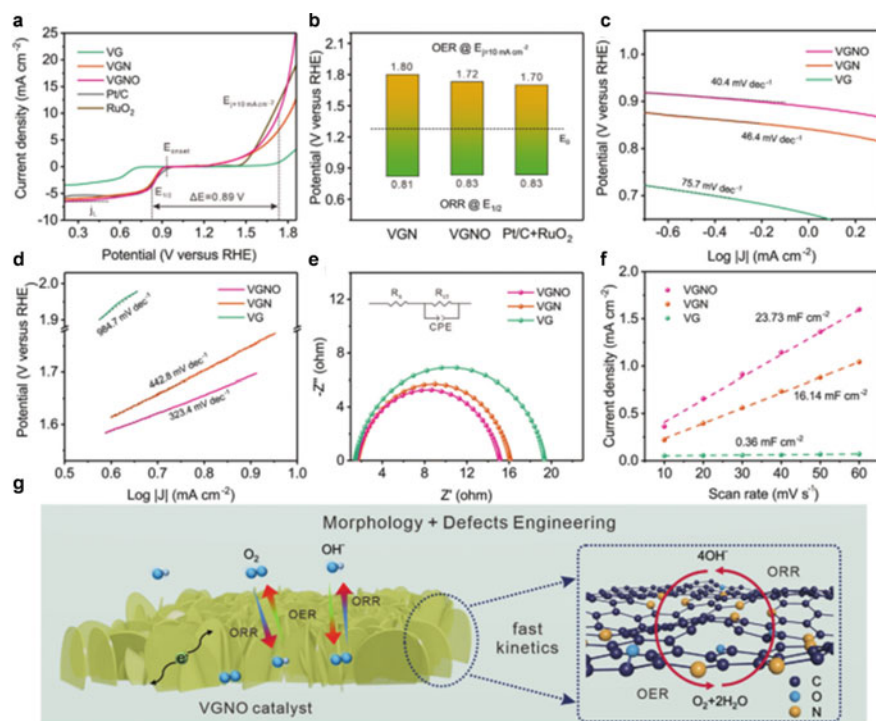


Fig. 12.3 Schematic diagram of electrochemical performance test and reaction mechanism of VGNO. **a** LSV polarization curves of different catalysts for ORR and OER in 0.1 m KOH solutions with iR-correction; **b** Comparison of potential gap between EOER and EORR for VGN, VGNO, and Pt/C + RuO₂. Tafel plots and corresponding slopes of various catalysts for **c** ORR and **d** OER. **e** Nyquist plots of various catalysts (the inset is the equivalent circuit). **f** Current density differences at 1.07 V plotted against scan rates and corresponding electrical double-layer capacitance of various catalysts. **g** Schematic representation of synergistic morphology and defects benefits for ORR and OER of VGNO catalysts. Reproduced with permission [46]. Copyright 2022, The Authors. Advanced Science published by Wiley-VCH GmbH

In Fig. 12.3a, the N and O co-doped vertical graphene (VGNO) catalyst exhibits remarkable ORR activity with an onset potential (E_{onset}) of 0.92 V, half-wave potential ($E_{1/2}$) of 0.83 V and a diffusion limiting current density (j_L) of 6.3 mA cm⁻² (at 0.3 V), which is comparable to that of commercial Pt/C (E_{onset} of 0.98 V and $E_{1/2}$ of 0.83 V). Meanwhile, the OER performance of VGNO surpasses that of VG and vertical graphene (VGN) with a low overpotential below 500 mV acquired at 10 mA cm⁻², which is very close to that for the benchmark RuO₂ catalyst. The bifunctional ORR-OER activity of catalysts was assessed by the potential gap between the OER potential acquired at 10 mA cm⁻² and half-wave potential of ORR (Fig. 12.3b). Generally, a smaller potential gap indicates superior oxygen catalytic activity, as shown in Fig. 12.3b, VGNO yields a low potential gap value of 0.89 V, outperforming single doped VGN and being comparable to the mixed catalyst Pt/C + RuO₂. VGNO also gives a smaller Tafel slope with respect to VGN and non-doped samples, indicating accelerated electrochemical reaction kinetics of ORR and OER (Fig. 12.3c, d). The superior kinetics was also verified by the electrochemical impedance spectroscopy (EIS), with the smallest electron transfer resistance (R_{ct}) during the ORR process (Fig. 12.3e). electrochemical surface areas (ECSA) of vertically aligned graphene arrays (VG), VGN, and VGNO were estimated by the double layer capacitance (CDL) calculated via CV measurement at different scan rates. The CDL of VGNO is as large as 23.73 mF cm⁻², compared with the low value of 16.14 mF cm⁻² for VGN and 0.36 mF cm⁻² for VG, as shown in Fig. 12.3f. This indicates that the ECSA of VGNO is higher than VG and VGN. The higher ECSA could also indicate porous and well-exposed graphene surficial structure, which is indicative of the population of electrochemically active sites. Overall, such data are demonstrative of the advantageous morphologies and preferable doping configurations of the co-doped VGNO, which help enable fast redox kinetics behind the outstanding ORR and OER performances without using precious and expensive Pt and Ru resources (Fig. 12.3g).

It can be seen that carbon-based materials also have considerable potential in aqueous electrolyte metal-air batteries.

12.3 Atomically Dispersed Metal Carbon-Based Materials for MABs

Heterogeneous single-atom catalysts (SACs) referring to atomically dispersed active metal centers on a support have attracted considerable interest in recent years [47]. The attention is because of the special electronic structure and maximized atomic utilization of such materials, which differ greatly from those of conventional nano- or subnano-counterparts [48]. Moreover, the single-atom nature of the active centers in SACs and the resulting low-coordination environment and the enhanced metal-support interactions all provide robust catalytic performance in a number of heterogeneous reactions, such as the carbon dioxide reduction, hydrogen evolution

reaction and photocatalytic reactions [49]. In principle, it is vital to explore the electrochemistry and catalytic mechanism when SACs are applied in MABs.

Zhao et al. [50] synthesized a single-atom Pt catalyst supported on holey ultrathin g-C₃N₄ nanosheets (Pt-CNHS) via a facile liquid-phase reaction of g-C₃N₄ and H₂PtCl₆ (Fig. 12.4a). The single-atom Pt can achieve high dispersibility and stability, which can promote the utilization efficiency as well as enhance the electrochemical activity. When employed as LABs cathode catalyst, Pt-CNHS exhibits excellent electrocatalytic activity. LABs utilizing Pt-CNHS show much higher discharge specific capacities than those with pure CNHS. LABs with Pt-CNHS cathode can be cycled stably for 100 times under the discharge capacity of 600 mA h g⁻¹. Based on experimental results and density functional theory calculations, the superior electrocatalytic activity of Pt-CNHS can be ascribed to the large surface area, the enhanced electrical conductivity and the efficient interfacial mass transfer through Pt atoms and porous structure of CNHS.

Hu et al. [51] employ metal–organic frameworks (MOF)-assisted spatial confinement and ionic substitution strategies to synthesize Ru single atoms riveted with nitrogen-doped porous carbon (Ru SAs-NC) as the electrocatalytic material (Fig. 12.4b). By using the optimized Ru_{0.3} SAs-NC as electrocatalyst in the oxygen-breathing electrodes, the developed LAB can deliver the lowest overpotential of only

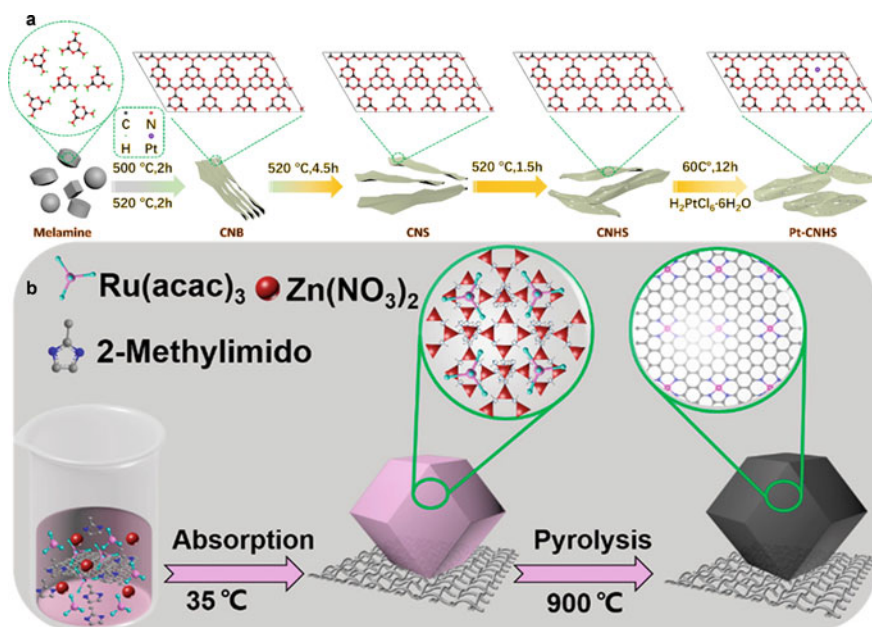


Fig. 12.4 Schematic synthetic procedure of Atomically dispersed metal carbon-based materials. **a** Schematic synthetic of Pt-CNHS. Reproduced with permission [50]. Copyright 2019, Elsevier B. V. **b** Ru SAs-NC on the flexible CC. Reproduced with permission [51]. Copyright 2020, American Chemical Society

0.55 V at 0.02 mA cm⁻². Moreover, *in-situ* DEMS results quantify that the e⁻/O₂ ratio of LOBs in a full cycle is only 2.14, indicating a superior electrocatalytic performance in LAB applications. Theoretical calculations reveal that the Ru–N₄ serves as the driving force center, and the amount of this configuration can significantly affect the internal affinity of intermediate species. The rate-limiting step of the ORR on the catalyst surface is the occurrence of 2e⁻ reactions to generate Li₂O₂, while that of the OER pathway is the oxidation of Li₂O₂. This work broadens the field of vision for the design of single-site high-efficiency catalysts with maximum atomic utilization efficiency for LABs.

Due to the high-cost constraints of noble metal-based catalysts, the development of non-noble metal catalysts is a difficult and necessary topic. Wu et al. [52] prepared an efficient ORR electrocatalyst by co-anchoring atomic dispersed Fe and Ni dual metal sites on N-S co-doped defect-rich porous carbon frameworks by pyrolysis of metal precursors. When used to assemble the air cathode of the liquid or flexible solid-state primary Mg-air battery and Zn-air battery, the obtained Fe, Ni-SAs/DNSC delivers high voltage and power density, superior than that of the benchmark cathode based on Pt catalyst (Fig. 12.5a–c).

Recently, Liu et al. [53] used density functional theory (DFT) calculations to screen SACs on N-doped graphene (SAm@NG, Me = Cr, Mn, Fe, Co, Ni, Cu) for CO₂ reduction and evolution reaction. Among them, SACr@NG shows the promising potential as an effective electrocatalyst for the reversible Li-CO₂ batteries. To verify the validity of the DFT calculations, a two-step method has been developed to fabricate SAm@NG on a porous carbon foam (SAm@NG/PCF) with similar loading of ~8 wt.% (Fig. 12.5d). Consistent with the theoretical calculations, batteries with the SACr@NG/PCF cathodes exhibit a superior rate performance and cycling ability, with a long cycle life and a narrow voltage gap of 1.39 V over 350 cycles at a rate of 100 μA cm⁻². This work not only demonstrates a principle for catalysts selection for the reversible Li-CO₂ batteries but also a controllable synthesis method for single atom catalysts.

In summary, metal atom-dispersed carbon-based materials can be used as catalysts for key reactions in metal-air batteries with excellent performance and great research prospects.

12.4 Metal Nanoparticles Encapsulated Carbon-Based Materials for MABs

Nano-confinement of metal nanoparticles in various carbon-based materials enables novel functionalities with unique physical and chemical properties for metal-air batteries with enhanced performance. The nanocarbon-based encapsulated metal particle materials can combine the high catalytic activity of metal particles with the large specific surface area and high electrical conductivity of carbon-based materials, and produce a synergistic effect to maintain electrode stability [54]. Furthermore,

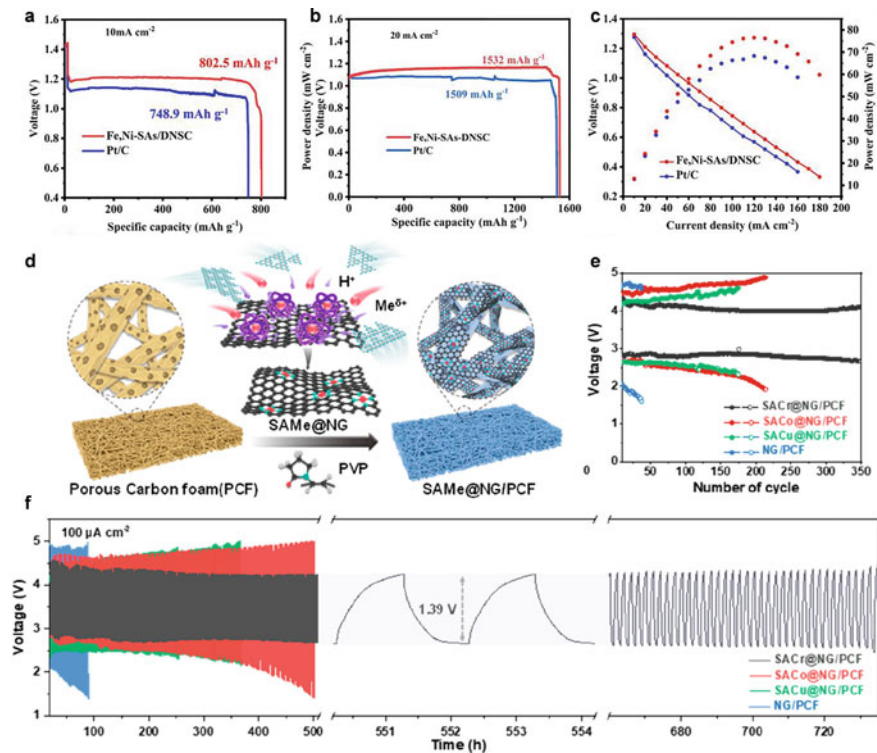


Fig. 12.5 Characterization and charge–discharge performance evaluation. **a** Specific capacities for primary Zn-air battery. **b** Specific capacities for liquid Mg-air batteries with Fe, Ni-SAs/DNSC and Pt/C cathode. **c** The discharge polarization curves of liquid Mg-air battery. Reproduced with permission [52]. Copyright 2021, Elsevier B.V. **d** Schematics of the synthesis of SAME@NG/PCF. **e** Discharge and charge voltage and **f** time–voltage curves of the four cathodes at a current density of $100 \mu\text{A cm}^{-2}$ with a limited capacity of $100 \mu\text{A h cm}^{-2}$. Reproduced with permission [53]. Copyright 2021, American Chemical Society

encapsulation of catalysts into nanocarbons has been shown to effectively suppress aggregation [55]. Meanwhile, the regional enrichment of electron density caused by the direct exposure of catalyst nanoparticles is one of the main reasons for the local distribution of discharge products, and the encapsulation of nanoparticles can eliminate the local electron density enrichment caused by direct exposure of catalyst nanoparticles, so metal Encapsulation of nanoparticles is an extremely critical approach to the development of cathode materials for MABs.

Huang et al. [56] prepared a series of carbon nanotubes-encapsulated noble metal nanoparticles (Pd, Pt, Ru and Au) by wet impregnation followed by thermal annealing, and systematically investigated their performances in LABs. The as-prepared hybrid materials exhibited superior OER activity than the conventional cathodes materials with noble metal nanoparticles direct supported on CNTs, thus demonstrating the feasibility of the strategy.

Wu et al. [57] reported the synthesis of the ultrasmall Pt-coated hollow graphene nanocages as cathode in LABs. They first developed a novel architecture of porous carbon material, the 3D hollow graphene nanocages (HGNs). Subsequently, Pt-HGN was obtained by depositing Pt catalysts on HGNs by physical vapor deposition (PVD) (Fig. 12.6a). The charge voltage plateau can reduce to 3.2 V at the current density of 100 mA g^{-1} , even maintain below 3.5 V when the current density increased to 500 mA g^{-1} (Fig. 12.6b, c). The unique hollow graphene nanocages matrix can not only provide numerous nanoscale tri-phase regions as active sites for efficient oxygen

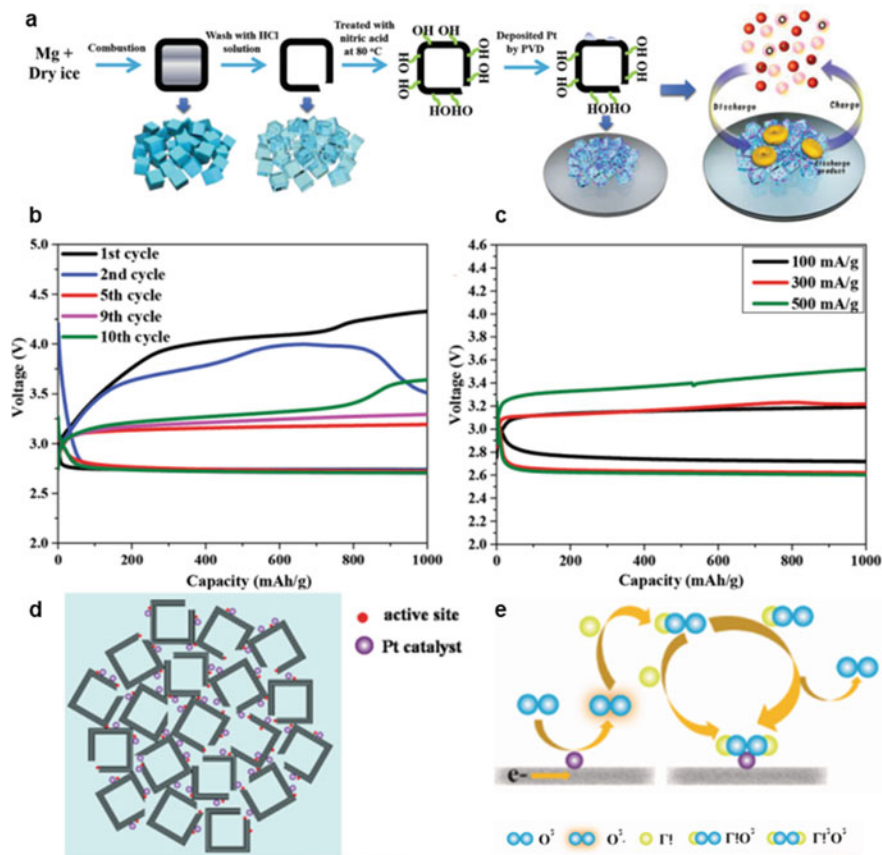


Fig. 12.6 Synthesis strategy, performance and mechanism of Pt-HGN. **a** Schematic illustration for synthesis of Pt-coated hollow graphene nanocages. **b** Galvanostatic discharge/charge profiles of LABs with Pt-HGNs as cathode catalysts at 100 mA g^{-1} in the voltage range of 2.2–4.5 V versus Li^+/Li with the fixed capacity of 1000 mAh g^{-1} . **c** Discharge/charge profiles of $\text{Li}-\text{O}_2$ batteries with Pt-HGNs cathode catalysts at different current densities in the voltage range of 2.2–4.5 V versus Li^+/Li with the fixed capacity of 1000 mAh g^{-1} . **d** The schematic illustrations of the active sites in the substrate of Pt-HGNs. **e** The mechanism for the nucleation of Li_2O_2 on Pt catalyst. Reproduced with permission [57]. Copyright 2016, WILEY-VCH Verlag GmbH & Co. KGaA, Weinheim

reduction, but also offer sufficient amount of mesoscale pores for rapid oxygen diffusion (Fig. 12.6d). Furthermore, with strong atomic-level oxygen absorption into its subsurface, ultrasmall Pt catalytically serves as the nucleation site for Li_2O_2 growth (Fig. 12.6e). The Li_2O_2 is subsequently induced into a favorable form with small size and amorphous state, decomposed more easily during recharge. Meanwhile, the conductive hollow graphene substrate can enhance the catalytic activity of noble metal Pt catalysts due to the graphene-metal interfacial interaction. Benefiting from the above synergistic effects between the hollow graphene nanocages and the nano-sized Pt catalysts, the ultrasmall Pt-decorated graphene nanocage cathode exhibits enhanced electrochemical performances.

Although noble metal materials have outstanding performance as cathode materials for MABs, the excessively expensive cost has drawn attention to the development of non-precious metal materials as substitutes for noble metal materials. Although noble metal materials have outstanding performance as cathode materials for MABs, the excessively expensive cost has drawn attention to the development of non-precious metal materials as substitutes for noble metal materials.

Li et al. [58] developed FeNi nanoparticles encapsulated in nitrogen-doped carbon frame (FeNi-NP/NC) as the cathode catalyst for Al-air batteries via confined pyrolysis of the polydopamine-coated MOF. The battery equipped with FeNi-NP/NC cathode, at a discharge current density of 1 mA cm^{-2} , can achieve a discharge voltage above 1.55 V and maintained for over 24 h.

In addition, Xia et al. [59] further improved the catalytic performance by alloying noble metals with non-noble metals while reducing the loading of noble metals. They designed and prepared a composite catalyst for high-performance LABs, which comprises of CoPt NPs loaded on functionalized porous carbon with hydroxyl (OH^-) and amino (NH_2^-) groups as the link bridge. Density functional theory (DFT) calculations suggest the enhanced metal-support interaction and reduced theoretical ORR/OER overpotential via introducing functional groups on the surface of the carbon substrate. Moreover, these two functional groups are ubiquitous in biochar, and the preparation process is common and simple. For this, they use crab shell waste as a sustainable carbon source through carbonization, activation, and sol-gel method to synthesize activated functional carbon (AFC) and fabricate CoPt/AFC catalyst. The as-prepared catalyst is expected to have a large specific surface area, rich pore structures, and good electrical conductivity. Attributed to these favorable features, the LOBs with the CoPt/AFC cathode could present a large discharge capacity, low charge and discharge overpotential, and good cycle stability. *In-situ* Raman was also used to confirm that CoPt/AFC cathode could effectively suppress the formation of Li_2CO_3 in the reaction. This work could introduce a new avenue to design and fabricate high-performance and sustainable cathode catalyst for LABs.

In conclusion, the encapsulation of metal nanoparticles in carbon-based materials provides great development prospects for advancing the application of MABs.

12.5 Metal Nanoparticles Supported Carbon-Based Materials

Despite the unique advantages of metal nanoparticles encapsulated in carbon-based materials, the design of encapsulation structures is still a major challenge [60]. Therefore, loading metal nanoparticles on carbon-based materials has more structural possibilities and is more feasible.

Kang et al. [61] reported the use of Ru-modified CNTs (CNT/Ru) as cathode catalysts of Na-air batteries, which exhibited excellent catalytic performance and stable cycling performance. The dual catalytic role of CNT/Ru is confirmed to be responsible for promoting oxygen reduction at low potentials.

Luo et al. [62] synthesized a series of AuPt nanoparticles supported on multi-walled carbon nanotubes ($\text{Au}_x\text{Pt}/\text{MWNTs}$) catalysts with ultrafine distribution for Al-air battery cathode to enhance the oxygen reduction reaction. Among them, $\text{Au}_{0.67}\text{Pt}/\text{MWNTs}$ catalyst with metal loading of 10.2 wt.% (Au: 4.1 wt.%, Pt: 6.1 wt.%) exhibited a superior ORR catalytic activity and competitive durability to 20 wt% Pt/C catalyst. When applied as Al-air battery, appropriate increasing Au loading encourage better battery performance. $\text{Au}_{1.68}\text{Pt}/\text{MWNTs}$ with 8.95 wt.% of Au and as little as 5.3 wt.% Pt content exhibit larger specific capacity (921 mA h g^{-1}) and power density (146.8 mW cm^{-2}) as well as better durability than 20 wt.% Pt/C catalyst when it is assembled as cathode in Al-air battery.

Dai et al. [63] synthesized a well-dispersed catalyst of ruthenium nanoparticles anchored on the nitrogen-doped reduced graphene oxide (Ru/N-rGO), acting as an efficient bifunctional catalyst for Li-O₂ batteries. The introduction of N dopants provides an enhanced metal-support interaction and homogeneous anchoring sites for ruthenium nanoparticles on the graphene substrate with a high specific surface area. Upon the initial discharge process, the homogeneous ruthenium nanoparticles serve as the nucleation sites for the growth of film-like Li₂O₂, which preferentially decomposes at a reduced charge overpotential; the subsequent deep discharge is associated with a modified Li₂O₂ morphology via LiO₂ disproportionation in solution, endowing substantial improvement of the specific capacity in Li-O₂ batteries. Meanwhile, in comparison with the pristine nitrogen-doped rGO (N-rGO) electrode, the surface coordination of ruthenium promotes charge transfer and mass transport through the discharge product layer, leading to faster reaction kinetics toward Li₂O₂ formation and decomposition. Moreover, the strong ruthenium-support interaction is helpful to reduce carbon defects and thus suppresses Li₂CO₃ formation. As a result, the electrodes exhibit a high specific capacity of $17,074 \text{ mA h g}^{-1}$ (Fig. 12.7a), a low charge polarization of 0.51 V (Fig. 12.7b), a superior power density of 25.6 mW mg^{-1} at a current density of 11.1 mA mg^{-1} and a voltage of 2.3 V (Fig. 12.7c), as well as a long-term cycling stability (Fig. 12.7d). The strong superoxide adsorption ability of Ru/N-rGO was the major decipher for the structural modulation of the discharge products. As shown in Fig. 12.7e, Ru/N-rGO exhibited a much higher superoxide adsorption efficiency of 84.7% compared to those of 55.5% for Ru/rGO, 48.8% for N-rGO, and 29.4% for rGO. Remarkably, both N doping and Ru loading promoted

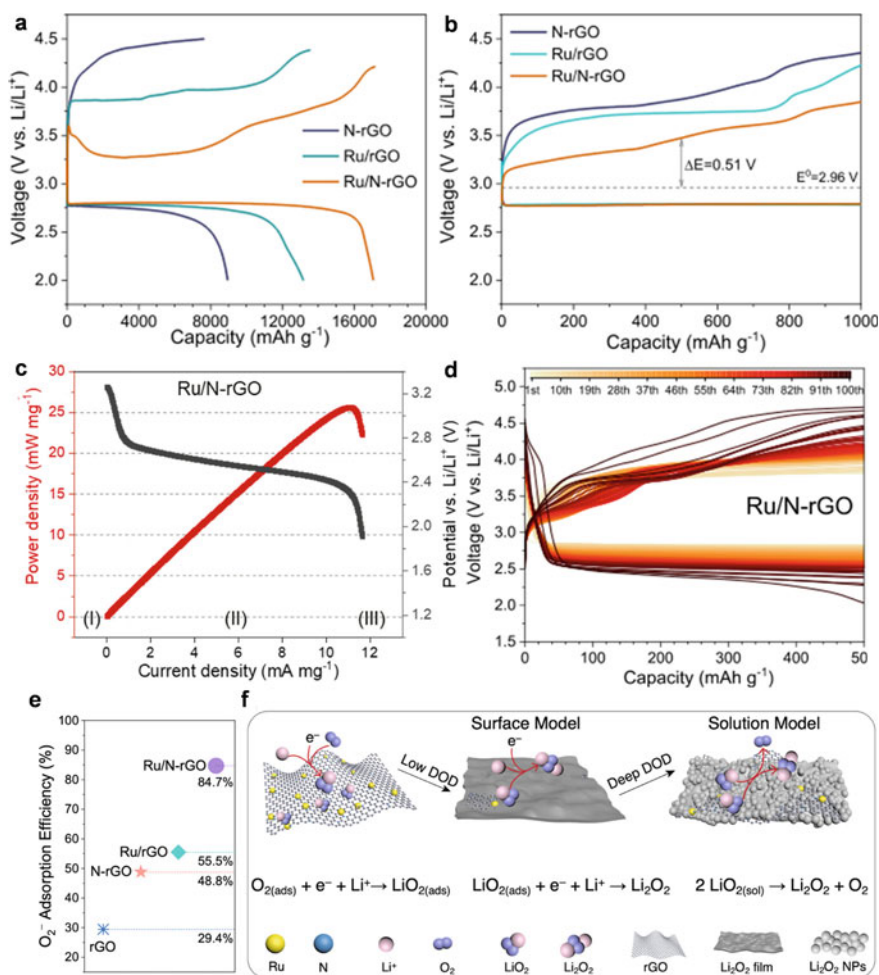


Fig. 12.7 Cell performance and discharge mechanism of Ru/N-rGO catalysts. **a** The initial deep galvanostatic discharge-charge curves of Ru/N-rGO (orange), Ru/rGO (blue), and N-rGO (dark) electrodes at a current density of 500 mA g^{-1} . **b** Discharge-charge profiles for the first cycle with the cathode catalyst of Ru/N-rGO (orange), Ru/rGO (blue), and N-rGO (dark) at a limited capacity of 1000 mA h g^{-1} at a current density of 100 mA g^{-1} ; **c** Polarization/power density curves (0.01 mA s^{-1}) of Ru/N-rGO; **d** Galvanostatic cycling profiles of Ru/N-rGO electrodes at a current density of 100 mA g^{-1} to the fixed capacity of 500 mA h g^{-1} ; **e** Superoxide adsorption efficiency for rGO, N-rGO, Ru/rGO, and Ru/N-rGO calculated from the corresponding UV-vis spectra. **f** Schematic of the discharge mechanism for Ru/N-rGO

the adsorption of superoxide species due to the large adsorption strength of Ru and N dopants toward superoxide. Furthermore, the authors speculate that the growth of discharge products on Ru/N-rGO at low DOD is mainly a surface growth model. When the further discharging proceeded, the reaction interface was transferred from the discharge product/cathode interface to the discharge product/electrolyte interface. At this stage, the solution model dominated the growth of the discharge product. based on such morphology evolution, a two-stage discharge mechanism on Ru/N-rGO catalysts is proposed, including a surface model and a solution model for Li_2O_2 growth (Fig. 12.7f). Reproduced with permission. [63] Copyright 2021, American Chemical Society.

Nevertheless, there exist shortcomings with mono metal catalysts from materials preparation to electrochemical processes. First, for example, the preparation for monodispersed Ru nanoparticles was often achieved under mild experimental conditions without the generation of stable crystal surfaces, further affecting catalytic activity in Li- CO_2 batteries. Second, the incompatibility between the discharge products and mono metal nanomaterials might lead to severe agglomeration and dropping during long cycles. Zhang et al. [64] designed a composite of ruthenium-copper nanoparticles highly co-dispersed on graphene (Ru-Cu-G) as efficient air cathodes for Li- CO_2 batteries. The Li- CO_2 batteries with Ru-Cu-G cathodes exhibit ultra-low overpotential and can be operated for 100 cycles with a fixed capacity of 1000 mA h g^{-1} at 200 and 400 mA g^{-1} . The synergistic effect between Ru and Cu not only regulates the growth of discharge products, but also promotes CO_2 reduction and evolution reactions by changing the electron cloud density of the surface between Ru and Cu. This work may provide new directions and strategies for developing highly efficient air cathodes for Li- CO_2 batteries, or even practical Li-air batteries.

Furthermore, when metal nanoparticles coexist with atomically dispersed sites, the electronic synergy between the two can further enhance the performance of the catalyst. Recently, Lin et al. [65] fabricate a new catalyst containing well defined ruthenium atomic cluster (Ru_{AC}) and single atom Ru- N_4 (Ru_{SA}) composite sites on carbon nanobox substrate ($\text{Ru}_{\text{AC}+\text{SA}}@\text{NCB}$), by utilizing the different complexation effects between Ru cation and amine group ($-\text{NH}_2$) on carbon quantum dots (CQDs) or nitrogen moieties on NCB (Fig. 12.8a-d). Systematic experimental and theoretical investigations demonstrate the vital role of electronic synergy between Ru_{AC} and Ru- N_4 in improving the electrocatalytic activity toward CO_2ER and CO_2RR . The electronic properties of Ru- N_4 sites are essentially modulated by the adjacent Ru_{AC} species, which optimize the interactions with key reaction intermediates thereby reduce the energy barriers in the rate-determining steps of CO_2RR and CO_2ER . Remarkably, the $\text{Ru}_{\text{AC}+\text{SA}}@\text{NCB}$ based cell displays unprecedented overpotentials as low as 1.65 and 1.86 V at ultrahigh rates of 1 and 2 A g^{-1} , and two-fold cycling lifespan than the baselines. The findings provide a novel strategy to construct catalysts with composite active sites comprising multiple atom assemblies for high-perform metal- CO_2 batteries.

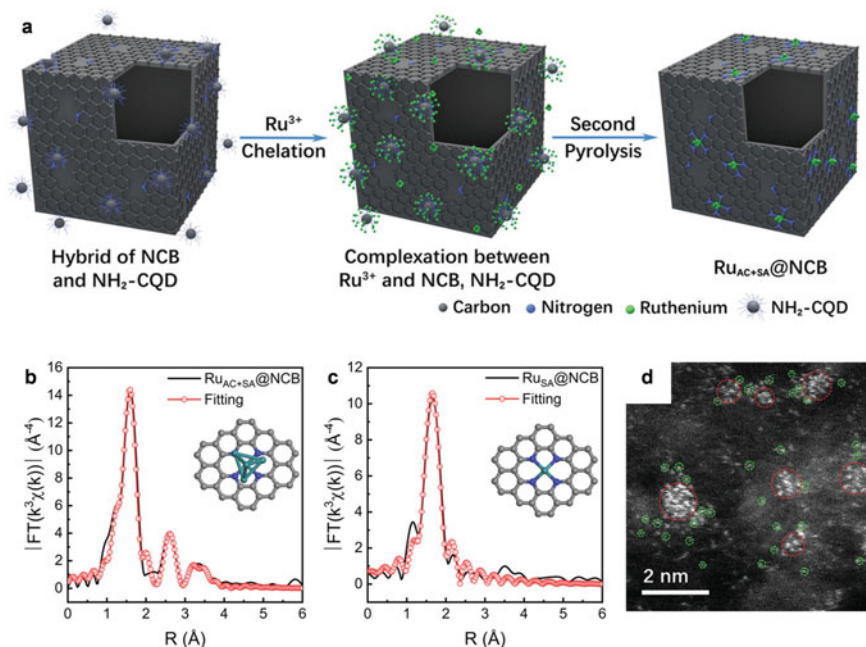


Fig. 12.8 Synthesis strategy and characterization. **a** Schematic illustrating the synthesis procedure for Ru_{AC+SA}@NCB. **b** and **c** EXAFS fitting curves at R space for Ru_{AC+SA}@NCB and Ru_{SA}@NCB sample, respectively. **d** HAADF-STEM images of Ru_{AC+SA}@NCB. Reproduced with permission [65]. Copyright 2022, Wiley–VCH GmbH

12.6 Conclusion and Perspectives

Enormous progress has been made in carbon-based nanomaterials as cathode bifunctional catalysts for metal-air batteries. However many metal-air batteries in published work still operate in pure oxygen environments. In-depth research is also required to suppress side reactions that occur when working in ambient air. In addition, the reactive oxygen intermediate species in the cathodic redox process can cause strong carbon corrosion of the carbon substrate, which can lead to insufficient catalyst stability. It is extremely important to study how to inhibit carbon corrosion to improve the cycling stability of carbon-based catalysts. The porous structure of carbon materials is extremely important for catalytic performance. Considering the enrichment of discharge products at the micrometer scale, the diffusion of gases, and the exposure of active sites, careful exploration of the optimal combination of pore size and distribution is required. Single-atom catalysts have been extensively studied. However, isolated atoms may not be able to accommodate multiple reaction steps and reaction intermediates, and the introduction of dual-active sites provides a promising solution to this problem. In addition, metal clusters inevitably appear during the synthesis of

single-atom catalysts, and understanding the synergy between metal clusters and single-atom sites is also an attractive topic.

During the exploration of cathode materials for MABs, carbon-based materials have received extensive attention due to their high electrical conductivity, large specific surface area, and low cost. With the improvement of people's understanding of the battery mechanism of MABs and the understanding of material design engineering, starting from the use of pure carbon materials as the air electrode of metal-air batteries, and then trying the doping of heteroatoms, various composite methods with metal materials, the development of MABs have made considerable progress. However, there is still a long way to go before the large-scale application of metal-air batteries. The slow kinetics of key reactions on the electrode during charge and discharge, the deposition of by-products, and the low stability of catalysts are all problems that need to be overcome. Carbon-based nanomaterials have shown great research prospects in MABs, and we believe that with continued in-depth research, carbon-based nanomaterials will continue to lead the advancement of MABs.

References

1. S. Chu, A. Majumdar, Opportunities and challenges for a sustainable energy future. *Nature* **488**, 294–303 (2012). <https://doi.org/10.1038/nature11475>
2. C. Liu, F. Li, L.-P. Ma, H.-M. Cheng, (2010) Advanced materials for energy storage. *Adv. Mater.* **22**, E28–E62. <https://doi.org/10.1002/adma.200903328>
3. S. Chu, Y. Cui, N. Liu, The path towards sustainable energy. *Nat. Mater.* **16**, 16–22 (2017). <https://doi.org/10.1038/nmat4834>
4. J.B. Goodenough, K.-S. Park, The Li-ion rechargeable battery: a perspective. *J. Am. Chem. Soc.* **135**, 1167–1176 (2013). <https://doi.org/10.1021/ja3091438>
5. J.M. Tarascon, M. Armand, Issues and challenges facing rechargeable lithium batteries. *Nature* **414**, 359–367 (2001). <https://doi.org/10.1038/35104644>
6. J.B. Goodenough, Y. Kim, Challenges for rechargeable Li batteries. *Chem. Mater.* **22**, 587–603 (2010). <https://doi.org/10.1021/cm901452z>
7. N. Nitta, F. Wu, J.T. Lee, G. Yushin, Li-ion battery materials: present and future. *Mater. Today* **18**, 252–264 (2015). <https://doi.org/10.1016/j.mattod.2014.10.040>
8. D. Larcher, J.M. Tarascon, Towards greener and more sustainable batteries for electrical energy storage. *Nat. Chem.* **7**, 19–29 (2015). <https://doi.org/10.1038/nchem.2085>
9. M.D. Slater, D. Kim, E. Lee, C.S. Johnson, Sodium-ion batteries. *Adv. Funct. Mater.* **23**, 947–958 (2013). <https://doi.org/10.1002/adfm.201200691>
10. D. Geng, N. Ding, T.S.A. Hor, S.W. Chien, Z. Liu, D. Wu, X. Sun, Y. Zong, From lithium-oxygen to lithium-air batteries: challenges and opportunities. *Adv. Energy Mater.* **6** (2016). <https://doi.org/10.1002/aenm.201502164>
11. G. Girishkumar, B. McCloskey, A.C. Luntz, S. Swanson, W. Wilcke, Lithium-air battery: promise and challenges. *J. Phys. Chem. Lett.* **1**, 2193–2203 (2010). <https://doi.org/10.1021/jz1005384>
12. J.-S. Lee, S. Tai Kim, R. Cao, N.-S. Choi, M. Liu, K.T. Lee, J. Cho, Metal-air batteries with high energy density: Li-air versus Zn-air. *Adv. Energy Mater.* **1**, 34–50 (2011). <https://doi.org/10.1002/aenm.201000010>
13. Y. Li, H. Dai, Recent advances in zinc-air batteries. *Chem. Soc. Rev.* **43**, 5257–5275 (2014). <https://doi.org/10.1039/C4CS00015C>

14. P.G. Bruce, S.A. Freunberger, L.J. Hardwick, J.-M. Tarascon, Li–O₂ and Li–S batteries with high energy storage. *Nat. Mater.* **11**, 19–29 (2012). <https://doi.org/10.1038/nmat3191>
15. T.A. Ha, C. Pozo-Gonzalo, K. Nairn, D.R. MacFarlane, M. Forsyth, P.C. Howlett, An investigation of commercial carbon air cathode structure in ionic liquid based sodium oxygen batteries. *Sci Rep* **10**, 7123 (2020). <https://doi.org/10.1038/s41598-020-63473-y>
16. J. Ryu, M. Park, J. Cho, Advanced technologies for high-energy aluminum–air batteries. *Adv. Mater.* **31**, 1804784 (2019). <https://doi.org/10.1002/adma.201804784>
17. H.-F. Wang, Q. Xu, Materials design for rechargeable metal-air batteries. *Matter* **1**, 565–595 (2019). <https://doi.org/10.1016/j.matt.2019.05.008>
18. M.K. Debe, Electrocatalyst approaches and challenges for automotive fuel cells. *Nature* **486**, 43–51 (2012). <https://doi.org/10.1038/nature11115>
19. C. Xu, K. Zhang, D. Zhang, S. Chang, F. Liang, P. Yan, Y. Yao, T. Qu, J. Zhan, W. Ma, B. Yang, Y. Dai, X. Sun, Reversible hybrid sodium–CO₂ batteries with low charging voltage and long-life. *Nano Energy* **68** (2020). <https://doi.org/10.1016/j.nanoen.2019.104318>
20. M. Balaish, J.W. Jung, I.D. Kim, Y. Ein-Eli, A critical review on functionalization of air-cathodes for nonaqueous Li–O₂ batteries. *Adv. Funct. Mater.* **30** (2019). <https://doi.org/10.1002/adfm.201808303>
21. J. Park, J.-Y. Hwang, W.-J. Kwak, Potassium–oxygen batteries: Significance, challenges, and prospects. *J. Phys. Chem. Lett.* **11**, 7849–7856 (2020). <https://doi.org/10.1021/acs.jpcclett.0c01596>
22. J. Suntivich, H.A. Gasteiger, N. Yabuuchi, H. Nakanishi, J.B. Goodenough, Y. Shao-Horn, Design principles for oxygen-reduction activity on perovskite oxide catalysts for fuel cells and metal–air batteries. *Nat. Chem.* **3**, 546–550 (2011). <https://doi.org/10.1038/nchem.1069>
23. K. Chen, D.-Y. Yang, G. Huang, X.-B. Zhang, Lithium–air batteries: air-electrochemistry and anode stabilization. *Acc. Chem. Res.* **54**, 632–641 (2021). <https://doi.org/10.1021/acs.accounts.0c00772>
24. L.C. Greenburg, C.O. Plaza-Rivera, J.-W. Kim, J.W. Connell, Y. Lin, Architecture transformations of ultrahigh areal capacity air cathodes for lithium-oxygen batteries. *Batteries Supercaps* **4**, 120–130 (2021). <https://doi.org/10.1002/batt.202000201>
25. F. Cheng, J. Chen, Metal–air batteries: from oxygen reduction electrochemistry to cathode catalysts. *Chem. Soc. Rev.* **41**, 2172–2192 (2012). <https://doi.org/10.1039/C1CS15228A>
26. Y. Bae, H. Park, Y. Ko, H. Kim, S.K. Park, K. Kang, Bifunctional oxygen electrocatalysts for lithium-oxygen batteries. *Batteries Supercaps* **2**, 311–325 (2019). <https://doi.org/10.1002/batt.201800127>
27. M. Kuang, G. Zheng, Nanostructured bifunctional redox electrocatalysts. *Small* **12**, 5656–5675 (2016). <https://doi.org/10.1002/smll.201600977>
28. X. Wen, Q. Zhang, J. Guan, Applications of metal–organic framework-derived materials in fuel cells and metal-air batteries. *Coord. Chem. Rev.* **409**, 213214 (2020). <https://doi.org/10.1016/j.ccr.2020.213214>
29. L. Liu, Z. Niu, J. Chen, Unconventional supercapacitors from nanocarbon-based electrode materials to device configurations. *Chem. Soc. Rev.* **45**, 4340–4363 (2016). <https://doi.org/10.1039/C6CS00041J>
30. G. Li, M.A. Mezaal, R. Zhang, K. Zhang, L. Lei, Electrochemical performance of MnO₂-based air cathodes for zinc-air batteries. *Fuel Cells* **16**, 395–400 (2016). <https://doi.org/10.1002/fuce.201500077>
31. Y. Xu, A. Sumboja, Y. Zong, J.A. Darr, Bifunctionally active nanosized spinel cobalt nickel sulfides for sustainable secondary zinc–air batteries: examining the effects of compositional tuning on OER and ORR activity. *Catal. Sci. Technol.* **10**, 2173–2182 (2020). <https://doi.org/10.1039/C9CY02185J>
32. Q. Zhang, C. Wang, Z. Xie, Z. Zhou, Defective/doped graphene-based materials as cathodes for metal–air batteries. *Energy Environ. Mater.* n/a (2021). <https://doi.org/10.1002/eem2.12293>
33. M.-M. Titirici, R.J. White, N. Brun, V.L. Budarin, D.S. Su, F. del Monte, J.H. Clark, M.J. MacLachlan, Sustainable carbon materials. *Chem. Soc. Rev.* **44**, 250–290 (2015). <https://doi.org/10.1039/C4CS00232F>

34. L. Dai, Y. Xue, L. Qu, H.-J. Choi, J.-B. Baek, Metal-free catalysts for oxygen reduction reaction. *Chem. Rev.* **115**, 4823–4892 (2015). <https://doi.org/10.1021/cr5003563>
35. H. Woo, J. Kang, J. Kim, C. Kim, S. Nam, B. Park, Development of carbon-based cathodes for Li-air batteries: present and future. *Electron. Mater. Lett.* **12**, 551–567 (2016). <https://doi.org/10.1007/s13391-016-6183-1>
36. D. Aurbach, B.D. McCloskey, L.F. Nazar, P.G. Bruce, Advances in understanding mechanisms underpinning lithium–air batteries. *Nat. Energy* **1**, 16128 (2016). <https://doi.org/10.1038/nenergy.2016.128>
37. W. Zhang, S. Zhu, R. Luque, S. Han, L. Hu, G. Xu, Recent development of carbon electrode materials and their bioanalytical and environmental applications. *Chem. Soc. Rev.* **45**, 715–752 (2016). <https://doi.org/10.1039/C5CS00297D>
38. R.L. McCreery, Advanced carbon electrode materials for molecular electrochemistry. *Chem. Rev.* **108**, 2646–2687 (2008). <https://doi.org/10.1021/cr068076m>
39. L. Qu, Y. Liu, J.-B. Baek, L. Dai, Nitrogen-doped graphene as efficient metal-free electrocatalyst for oxygen reduction in fuel cells. *ACS Nano* **4**, 1321–1326 (2010). <https://doi.org/10.1021/nn901850u>
40. K. Gong, F. Du, Z. Xia, M. Durstock, L. Dai, Nitrogen-doped carbon nanotube arrays with high electrocatalytic activity for oxygen reduction. *Science* **323**, 760–764 (2009). <https://doi.org/10.1126/science.1168049>
41. H. Kitaura, H. Zhou, Electrochemical performance of solid-state lithium-air batteries using carbon nanotube catalyst in the air electrode. *Adv. Energy Mater.* **2**, 889–894 (2012). <https://doi.org/10.1002/aenm.201100789>
42. Y. Li, J. Wang, X. Li, J. Liu, D. Geng, J. Yang, R. Li, X. Sun, Nitrogen-doped carbon nanotubes as cathode for lithium–air batteries. *Electrochem. Commun.* **13**, 668–672 (2011). <https://doi.org/10.1016/j.elecom.2011.04.004>
43. Y. Li, J. Wang, X. Li, D. Geng, R. Li, X. Sun, Superior energy capacity of graphene nanosheets for a nonaqueous lithium–oxygen battery. *Chem Commun (Camb)* **47**, 9438–9440 (2011). <https://doi.org/10.1039/c1cc13464g>
44. Z. Jian, Y. Chen, F. Li, T. Zhang, C. Liu, H. Zhou, High capacity Na–O₂ batteries with carbon nanotube paper as binder-free air cathode. *J. Power Sources* **251**, 466–469 (2014). <https://doi.org/10.1016/j.jpowsour.2013.11.091>
45. P.J. Hall, M. Mirzaei, S.I. Fletcher, F.B. Sillars, A.J.R. Rennie, G.O. Shitta-Bey, G. Wilson, A. Cruden, R. Carter, Energy storage in electrochemical capacitors: Designing functional materials to improve performance. *Energy Environ. Sci.* **3** (2010). <https://doi.org/10.1039/c0ee00004c>
46. Z. Wu, Y. Yu, G. Zhang, Y. Zhang, R. Guo, L. Li, Y. Zhao, Z. Wang, Y. Shen, G. Shao, In situ monitored (N, O)-doping of flexible vertical graphene films with high-flux plasma enhanced chemical vapor deposition for remarkable metal-free redox catalysis essential to alkaline zinc-air batteries. *Adv. Sci. (Weinh)*, e2200614 (2022). <https://doi.org/10.1002/advs.202200614>
47. Y. Wang, H. Su, Y. He, L. Li, S. Zhu, H. Shen, P. Xie, X. Fu, G. Zhou, C. Feng, D. Zhao, F. Xiao, X. Zhu, Y. Zeng, M. Shao, S. Chen, G. Wu, J. Zeng, C. Wang, Advanced electrocatalysts with single-metal-atom active sites. *Chem. Rev.* **120**, 12217–12314 (2020). <https://doi.org/10.1021/acs.chemrev.0c00594>
48. H. Fei, J. Dong, D. Chen, T. Hu, X. Duan, I. Shakir, Y. Huang, X. Duan, Single atom electrocatalysts supported on graphene or graphene-like carbons. *Chem. Soc. Rev.* **48**, 5207–5241 (2019). <https://doi.org/10.1039/C9CS00422J>
49. S. Ding, M.J. Hülsley, J. Pérez-Ramírez, N. Yan, Transforming energy with single-atom catalysts. *Joule* **3**, 2897–2929 (2019). <https://doi.org/10.1016/j.joule.2019.09.015>
50. W. Zhao, J. Wang, R. Yin, B. Li, X. Huang, L. Zhao, L. Qian, Single-atom Pt supported on holey ultrathin g-C₃N₄ nanosheets as efficient catalyst for Li–O₂ batteries. *J. Colloid Interf. Sci.* **564**, 28–36 (2020). <https://doi.org/10.1016/j.jcis.2019.12.102>
51. X. Hu, G. Luo, Q. Zhao, D. Wu, T. Yang, J. Wen, R. Wang, C. Xu, N. Hu, Ru single atoms on N-doped carbon by spatial confinement and ionic substitution strategies for high-performance Li–O₂ batteries. *J. Am. Chem. Soc.* **142**, 16776–16786 (2020). <https://doi.org/10.1021/jacs.0c07317>

52. X. Zhang, Y. Li, M. Jiang, J. Wei, X. Ding, C. Zhu, H. He, H. Lai, J. Shi, Engineering the coordination environment in atomic Fe/Ni dual-sites for efficient oxygen electrocatalysis in Zn-air and Mg-air batteries. *Chem. Eng. J.* **426** (2021). <https://doi.org/10.1016/j.cej.2021.130758>
53. Y. Liu, S. Zhao, D. Wang, B. Chen, Z. Zhang, J. Sheng, X. Zhong, X. Zou, S.P. Jiang, G. Zhou, H.M. Cheng, Toward an understanding of the reversible Li-CO₂ batteries over metal-N₄-functionalized graphene electrocatalysts. *ACS Nano* (2021). <https://doi.org/10.1021/acs.nano.1c10007>
54. M. Karuppanan, Y. Kim, S. Gok, E. Lee, J.Y. Hwang, J.-H. Jang, Y.-H. Cho, T. Lim, Y.-E. Sung, O.J. Kwon, A highly durable carbon-nanofiber-supported Pt-C core-shell cathode catalyst for ultra-low Pt loading proton exchange membrane fuel cells: facile carbon encapsulation. *Energy Environ. Sci.* **12**, 2820–2829 (2019). <https://doi.org/10.1039/C9EE01000A>
55. Q. Dong, H. Wang, S. Ji, X. Wang, Q. Liu, D.J.L. Brett, V. Linkov, R. Wang, (2019) Mn nanoparticles encapsulated within mesoporous helical N-doped carbon nanotubes as highly active air cathode for zinc-air batteries. *Adv. Sustain. Syst.* **3**, 1900085. <https://doi.org/10.1002/adsu.201900085>
56. X. Huang, H. Yu, H. Tan, J. Zhu, W. Zhang, C. Wang, J. Zhang, Y. Wang, Y. Lv, Z. Zeng, D. Liu, J. Ding, Q. Zhang, M. Srinivasan, P.M. Ajayan, H.H. Hng, Q. Yan, Carbon nanotube-encapsulated noble metal nanoparticle hybrid as a cathode material for Li-oxygen batteries. *Adv. Funct. Mater.* **24**, 6516–6523 (2014). <https://doi.org/10.1002/adfm.201400921>
57. F. Wu, Y. Xing, X. Zeng, Y. Yuan, X. Zhang, R. Shahbazian-Yassar, J. Wen, D.J. Miller, L. Li, R. Chen, J. Lu, K. Amine, Platinum-coated hollow graphene nanocages as cathode ssed in lithium-oxygen batteries. *Adv. Funct. Mater.* **26**, 7626–7633 (2016). <https://doi.org/10.1002/adfm.201602246>
58. G. Li, D. Yu, J. Song, F. Hu, L. Li, S. Peng, FeNi nanoparticles encapsulated in nitrogen-doped carbon frame for efficient and stable Al-air batteries. *Mater. Lett.* **296** (2021). <https://doi.org/10.1016/j.matlet.2021.129890>
59. H. Xia, Q. Xie, Y. Tian, Q. Chen, M. Wen, J. Zhang, Y. Wang, Y. Tang, S. Zhang, (2021) High-efficient CoPt/activated functional carbon catalyst for Li-O₂ batteries. *Nano Energy* **84**. <https://doi.org/10.1016/j.nanoen.2021.105877>
60. C. Gao, F. Lyu, Y. Yin, Encapsulated metal nanoparticles for catalysis. *Chem. Rev.* **121**, 834–881 (2021). <https://doi.org/10.1021/acs.chemrev.0c00237>
61. J.-H. Kang, W.-J. Kwak, D. Aurbach, Y.-K. Sun, Sodium oxygen batteries: one step further with catalysis by ruthenium nanoparticles. *J. Mater. Chem. A* **5**, 20678–20686 (2017). <https://doi.org/10.1039/c7ta06584a>
62. Z. Luo, L. Yin, L. Xiang, T.X. Liu, Z. Song, Y. Li, L. Zhou, K. Luo, K. Wu, J. Jiang, AuPt nanoparticles/ multi-walled carbon nanotubes catalyst as high active and stable oxygen reduction catalyst for Al-air batteries. *Appl. Surf. Sci.* **564** (2021). <https://doi.org/10.1016/j.apsusc.2021.150474>
63. W. Dai, Y. Liu, M. Wang, M. Lin, X. Lian, Y. Luo, J. Yang, W. Chen, Monodispersed ruthenium nanoparticles on nitrogen-doped reduced graphene oxide for an efficient lithium-oxygen battery. *ACS Appl. Mater. Interf.* **13**, 19915–19926 (2021). <https://doi.org/10.1021/acsami.0c23125>
64. Z. Zhang, C. Yang, S. Wu, A. Wang, L. Zhao, D. Zhai, B. Ren, K. Cao, Z. Zhou, Exploiting synergistic effect by integrating ruthenium-copper nanoparticles highly Co-dispersed on graphene as efficient air cathodes for Li-CO₂ batteries. *Adv. Energy Mater.* **9** (2019). <https://doi.org/10.1002/aenm.201802805>
65. J. Lin, J. Ding, H. Wang, X. Yang, X. Zheng, Z. Huang, W. Song, J. Ding, X. Han, W. Hu, Boosting energy efficiency and stability of Li-CO₂ battery via synergy between Ru atom cluster and single atom Ru-N₄ site in electrocatalyst cathode. *Adv. Mater.* e2200559 (2022). <https://doi.org/10.1002/adma.202200559>

Chapter 13

Summary and Perspectives



Huicong Xia, Dongping Xue, and Jia-Nan Zhang

Abstract With the popularization of portable electronic products and the progress of technology, portable, flexible, portable and wearable electronic devices have attracted many scientists and developers because of their potential applications, such as artificial electronic skin, multi-dimensional energy storage devices and biocompatible electronic devices. The booming of carbon-based electrode materials affords broader options towards practical applications of energy storage and conversion under different conditions. Facing the opportunities and challenges, many researchers have devoted a lot of time and energy. However, there are still many challenges in practical industrial applications. In this chapter, the challenges as well as perspective for the advancement of the carbon-based electrode materials are discussed.

Research on the exploration of carbon-based materials as platforms for electrochemical catalysis for energy conversion and storage is certainly one of the most active topics among the chemistry and materials community. Thanks to the efforts of researchers, significant progress have been made in recent years in the development of carbon-based, and electrochemical catalysis for energy conversion and storage.

The increasing demand for energy sources and the shortage of fossil fuels have become the major concerns these days. To make full use of renewable energy sources, researches on energy storage and conversion have attracted extensive attention. To meet the ever-increasing demand for energy sources, a large number of researchers focus on developing high-performance energy conversion and storage devices. Extensive studies on catalysts have been carried out and applied in various types of electrochemical reactions. The design and optimization of catalysts are considered as

H. Xia · D. Xue · J.-N. Zhang (✉)
College of Materials Science and Engineering, Zhengzhou University, Zhengzhou 450001,
P. R. China
e-mail: zjn@zzu.edu.cn

H. Xia
e-mail: summer9209@126.com

D. Xue
e-mail: xdongping1231@126.com

one of the main routes to achieve high performance of the electrochemical energy conversion and storage device. In this regard, carbon-based nanomaterials have drawn considerable attention due to the high surface areas, which provides a large number of active sites for electrochemical reaction and facilitate ion/electron diffusion kinetics. In addition, the various electrochemical reaction can be effectively catalyzed by carbon-based materials, such as metal-free carbon-based nanomaterials, atomically dispersed metal carbon-based nanomaterials, metal nanoparticles supported/encapsulated carbon-based materials. With the flourishing development of various carbon-based nanomaterials, there have been some insights into the design and mechanisms for electrocatalysts. However, there is still a lack of books with related works and research frontier in this area, which is conducive to the scientific researchers and novices.

This book aims at covering all these aspects and discussing the recent achievements and various electrochemical reactions. The book is comprised of four sections. The first section discusses the fundamental synthesis, characterization techniques, and catalytic effects on the energy conversion and storage mechanism. The second section elaborately reviews various types of electrocatalytic reactions on carbon-based materials and their performance. The third section focuses on batteries about carbon-based materials with different storage mechanisms. At the last one, the following enlightenment in terms of theoretical development and experimental research will be provided to the general readers: (1) Precise design and construction of local atomic and electronic structures at the interface of catalysts; (2) Selective activation and directed the conversion of carbon-based energy-carrying molecules at the interface; 3) Interaction mechanism and regulation of catalyst solid surface interface properties under environment and external field.

There is no doubt that carbon-based nanomaterials in electrochemical catalysis are useful platforms for energy conversion and storage applications. It is anticipated that the content will further supply unambiguous understanding for all these components and the importance of the field and discuss current trends of different carbon-based materials for current ongoing works. We hope that this book can help readers design and develop new electrochemical energy materials based on carbon-based nanomaterials, and apply them to the world economy shortly.

Index

A

Aberration Correction-Scanning
Transmission Electron Microscopy
(AC-STEM), 55

Activated carbon, 16

Activation energy, 236

Active centers, 178

Active chemical bonding, 136

Active metal centers, 137

Active metals nanoparticle, 133

Active site, 261, 265, 272

Adsorption and bonding, 65

Agglomerate, 222

Aggregation state of heavy atoms, 59

Air breathing electrode, 258

Al-air batteries, 262

Alloy nanoparticles, 217, 238

Alloy-supported carbon-based
nanomaterial, 40

Analysis of the mechanism of CO₂
reduction, 182

Annular Bright-Field (ABF), 58

Anodized aluminum oxide, 233

Asymmetric charge, 174

Atomically dispersed metal, 217

Atomically dispersed metal carbon-based
electrocatalysts, 154

Atomically dispersed metal carbon-based
electrocatalysts for CO₂RR, 176

Atomically dispersed metal carbon-based
materials, 108, 235, 258

Atomic coordination state, 56

Atomic radius, 211

Atomic structure changes in real time, 54

B

Bader charge, 75

Ball milling, 16

Band gap, 16

Behavior of extranuclear electrons, The, 74

Bifunctional oxygen electrocatalysts, 252

Binding energy, 242

Binding energy of electrons, 66

Bond length, 69

Boron doping, 25

Brunner-Emmet-Teller (BET)
measurements, 66

C

Carbon-based electrocatalysts, 126, 128

Carbon-based nanomaterials, 16, 176

Carbon corrosion, 140

Carbon derivatives, 129

Carbon layers, 137, 157

Carbon nanomaterials, 3

Carbon nanostructures, 133

Carbon nanotube, 16, 263

Carbon nitride, 16

Carbon precursor, 178

Carbon reserves, 129

Carbon skeleton, 171

Carbon sphere, 233

Carbon wall network, 132

Catalytic activity, 2

Catalytic effects, 5

Catalytic mechanism, 140

Catalytic selectivity, 6

Central metal atom, 17

Chainmail catalysts, 179
Challenges, 169
Change of the dipole moment, The, 72
Characterization approaches, 55
Charge accumulation, 191
Charge transfer, 18
Charge transfer-doped, 127
Charge transport, 4
Chemical coordination, 87
Chemical groups, The, 72
Clusters, 140, 159
CO₂ activation/adsorption energies, 172
CO₂ evolution reaction, 252
CO₂ reduction reaction, 6, 252
Coercivity, 73
Confinement, 179
Confinement effect, 5, 86, 87
COOH* adsorption, 174
Coordination environment, 176
Coordination number, 69, 176
Coordination of each element, 62
CO partial current density, 176
Copper clusters, 179
Co-precipitation, 20
Core@shell nanoparticle, 218
Crystallization state, 63
Cyclic performance, 219

D

D-band centers, 179
Dead sulfur, 230
Decomposition barrier, 236, 252
Defect engineering, 16
Defect Graphene (DG), 127
Defect mechanism, 127
Defects, 173, 175
Defects and heteroatoms, 53
D electron, 17
Density functional theory, 38, 262
Density functional theory calculations, 234
Density Of States (DOS), 75, 180
Design and construction, 272
Development of catalysts suitable for the reduction of CO₂ to alcohol products, 181
DFT calculations, 181
Diameter, 130
Diatomic co-doping, 175
Diffusion limiting current density, 257
Direct carbonization, 23
Direct methanol fuel cell, 41
Direct visualization, 53

Discharge product, 260
Doping evaporation, 23
D-orbit, 231
Double layer capacitance, 257

E

Edge active site, 127
Edge defects, 174
Edge engineering, 20
Edge site, 16
Electrical conductivity, 133
Electric field effect, 93
Electrocatalysts, 2
Electrocatalytic behavior, 130
Electrocatalytic carbon dioxide reduction reaction, 169
Electrochemical ammonia synthesis, 188
Electrochemical energy storage, 6
Electrochemical impedance spectroscopy, 257
Electrochemical reaction, 215
Electrochemical reduction-reoxidation, 20
Electrochemical surface areas, 257
Electrode materials, 218, 223
Electrolytic water hydrogen production technology, 124
Electron cloud density, 265
Electron conduction, 56
Electron-deficient, 85
Electronegativity, 178
Electron Energy Loss Spectrum (EELS), 56
Electronic environment of metal species, 74
Electronic factor, 90
Electronic Metal-Support Interaction (EMSI), 90
Electronic orbitals, 54
Electronic state of target atoms, 69
Electronic structure, 16, 84, 272
Electronic synergy, 265
Electron Paramagnetic Resonance (EPR), 71
Electron-rich, 85
Electron transfer, 85
Electron transfer resistance, 257
Electrophilic center, 215
Element distribution, 55
Emission peak and carbon neutrality, 169
Encapsulated carbon shell, 137
Encapsulating, 179
Energetic efficiency, 171
Energy band, 75
Energy barrier, 178

Energy conversion efficiency, 170
Energy crisis, 169
Energy density, 211, 255
Energy Dispersive Spectrometer (EDS), 56
Environmental problems, 210
Ester-based electrolyte, 230
Ether-based electrolyte, 230
Evaluation parameters, 171
Existing forms of metals, The, 58
Experimental explorations, 130
Ex-situ, in-situ, and operando techniques, 53
Extended X-ray Absorption Fine Structure Spectroscopy (EXAFS), 69

F

Faradaic efficiency, 195
Faraday efficiency, 171
Fermi energy level, 179
First-principles, 53
First-principles calculations, 213
Floating catalyst chemical vapor deposition, 254
Four-electron, 104
Fourier Transform Infrared Spectrum (FT-IR), 72
Fuel cells, 251
Fuels and chemical raw materials, 170

G

Gas-diffusion layer, 250
Geometry structures, 217, 218
Gibbs free energy, 176
Gibbs free energy of reaction, 75
Global warming, 169
Graphene, 16, 261, 263
Graphene-based electrocatalyst, 27
Graphene-based SACs, 129
Graphite intercalation compound, 214
Greenhouse gas, 252
Group VIA, 230

H

Haber-Bosch process, 188
H* adsorption, 137
Half-wave overpotential, 106
Half-wave potential, 257
Hard-soft acid-base theory, 251
HER kinetics, 130
Heteroatom dopant, 127
Heteroatom-doped carbon, 17

Heteroatom-doped carbon materials, 234
Heteroatom doping, 16, 174
Heterogeneous catalysis, 179
Heterostructure, 242
Heyrovsky reaction, 125
High-Angle Annular Dark-Field (HAADF), 58
High current density, 134
High selectivity, 175
Host materials, 231, 242, 243
Hydrogen adsorption, 128
Hydrogen energy, 124
Hydrogen evolution reaction, 6, 16, 124, 125
Hydrogen oxidation reaction, 104
Hydrothermal synthesis, 27
Hysteresis loops, 74

I

Identify defect types, 59
Identify the active sites, 53
Identify the element types, 62
Indirect validation, 53
Industrial HER activity, 136
Infrared absorption spectrum, The (IR), 72
Inherent pore, 16
Insertion/deinsertion, 213
In-situ and operando XAS, 71
In-situ STEM, 59
In-suit selective growth, 127
Interaction force between host and guest, 54
Intercalation/deintercalation chemistry, 230
Intercalation/deintercalation process, 211
Interface engineering, 90
Interlayer materials, 242
Intermediates, 180
Intrinsic carbon defects, 174
Intrinsic conductivity, 215
Ion diffusion channel, 217
Ion/electron diffusion kinetics, 272
Ionic or semi-ionic properties, 175
Iron carbide, 37
Irreversible capacity, 219

K

Ketjen Black, 253

L

Large scattering angle, 58
Laser Irradiation (LI), 130

Lattice oxygen mediated mechanism, The, 149
Lattice vacancies, 127
Lewis acid, 251
Li-air batteries, 251
Li-ion batteries, 250
Liquid-phase electrodeposition, 25
Lithium-Ion Batteries (LIBs), 6, 210, 228
Lithium-sulfur batteries, 250
Loading metal nanoparticles, 126
Local atomic, 272
Local charge redistribution, 172
Lone pair electrons, 174
Long-term stability, 177
Low temperature thermal solution method, 23

M

Magnetic moment, 74
Magnetic properties of materials, The, 73
Magnetization, 73, 74
Magnetization curves, 73
Mass and volume energy density, 228
Mass transfer, 56
Mass transport, 263
Maximization of atomic utilization, 140
Mechanism of HER catalysis, 124
Melt diffusion method, 232
Mesh-on-mesh structure, 127
Metal aggregation, 179
Metal-air batteries, 257
Metal-based compounds, 238
Metal encapsulated, 5, 6, 126
Metal-free, 4
Metal-free carbon-based electrocatalysts, 151
Metal-free carbon-based electrocatalysts for CO₂RR, 172
Metal-free carbon-based materials, 126, 212, 235, 253
Metal nanoparticles encapsulated, 219
Metal nanoparticles encapsulated/supported carbon-based electrocatalysts for CO₂RR, 179
Metal nanoparticles encapsulated by carbon-based materials, 113, 238, 239, 259
Metal nanoparticles encapsulated carbon-based electrocatalysts, 158
Metal nanoparticles supported, 221
Metal nanoparticles supported carbon-based electrocatalysts, 160

Metal nanoparticles supported carbon-based materials, 123, 263
Metal-O₂ batteries, 252
Metal-organic framework, 217, 222, 258
Metal oxide support, 179
Metal precursors, 259
Metal-sulfur/selenium batteries, 6, 232
Metal supported, 4
Metal-support interaction, 5, 17, 262
M-H-C structure, 232
M-N coordination, 130
M-N_x-C, 130
Modifide separator, 231
Molecular dynamics simulation calculations, 53
Molecular electrostatic potential, 215
Molten salt-assisted acid exfoliation, 20
Monitor catalyst surface evolution, 54
Mössbauer spectroscopy, 74
M-S/Se batteries, 236, 237
Multiple proton-electron transfer, 188

N

Na-air batteries, 263
Nanotechnology, 1
N-doped carbon spheres, 174
Next-generation energy storage systems, 211
NH₃ yield, 195, 196
Nitrogen-doped, 217
Nitrogen fixation, 193
Nitrogen reduction reaction, 6
Non-metallic heteroatom doping, 105
Nonprecious metal catalysts, 179
Normal hexagon structure, 127

O

Ocean acidification, 169
One-dimensional, 3
Onset potential, 257
Optimal binding ability, 126
Orbital hybridization, 129
Overpotential, 171, 176, 258
Oxidized carbon nanotubes, 221
Oxygenated functional groups, 133
Oxygen evolution reaction, 6, 140, 147, 251
Oxygen reduction reaction, 16, 104, 255, 263
Oxygen vacancy defect, 20

P

Paramagnetic substances, 71, 72
Pentagon defects, 173
Peroxides, 251
Peroxymonosulfate, 32
Photocatalytic reactions, 258
Physical/chemical stability, 215
Physical vapor deposition, 261
Polar voltage, 229
Polymer electrolyte membrane electrolysis cell, 41
Polymerized dopamine, 217
Polysulfide, 236
Pore size distribution of mesopores, The, 66
Pore size or pore volume, 66
Porosity, 254
Porous carbon structures, 253
Porous structure, 212
Positions of metals, The, 58
Potassium-ion batteries, 210
Power density, 259
Practical industrial application, 181
Proton exchange membrane fuel cell, 104
Prussian Blue Analogues (PBAs), 222
Pyridine nitrogen, 212, 213
Pyridinic, 256
Pyridinic-N, 174
Pyrrole nitrogen, 213

Q

Quantum size effects, 54

R

Raman spectrometer (Raman), 63
Rate capability, 222
Rate Determination Step (RDS), 75, 265
Rate-limiting step, 259
Rate performance, 222
Reaction intermediates, 62, 215, 266
Reaction kinetics, 4, 211, 223
Reaction mechanism, 182, 187
Reaction path of OER process, The, 148
Reduced graphene oxide, 20
Regional structure information, 69
Relative content, 62
Renewable clean energy, 210
Renewable energy, 169, 170
Reversible capacity, 211
Rocking chair batteries, 228

S

Scanning Electron Microscopy (SEM), 54, 55
Scanning Tunneling Microscope (STM), 56
Sea-water medium, 173
Selected Area Electron Diffraction (SAED), 56
Selective activation, 272
Self-assemble technology, 221
Self-supporting material, 38
Shuttle effect, 236
Simulation calculations, 53
Single-atom catalyst, 27, 29, 129, 215, 232, 266, 267
Single-atom resolution, 56
Single carbon shell, 137
Sodium-ion batteries, 210
Soft-template pyrolysis method, 175
Solid surface interface, 272
Sp²-conjugated carbon substrates, 129
Spatial confinement, 89
Spatial distribution, 62
Specific surface area, 66, 259
Spin density, 175
Spin polarization, 191
Spontaneous gas foaming, 20
Stable anchor point, 136
Strong Metal-Support Interactions (SMSI), 126, 130, 179
Structure-activity relationships, 53
Structure-effect relationships, 171
Sub-Ångstrom resolution, 59
Sulfur reduction reaction kinetics, 234
Superoxides, 251
Supported carbon-based materials, 238
Supported-catalysts, 133
Surface and interface effects, 54
Surface characteristics, 215
Surface chemical states, 136
Surface chemistry, 87
Surface coupling reaction, 23
Surface element species, The, 66
Surface energy, 215
Surface-Enhanced Infrared Absorption Spectroscopy (SEIRAS), 54
Surface morphology, 56
Surface reactivity, 129
Synergistic effect, 177
Synthesis of intramolecular defect formers, 23

T

Tafel reaction, 125

Tafel slope, [176](#), [257](#)
Target products, [181](#)
Theoretical calculations, [182](#), [191](#), [215](#)
Theoretical capacity, [233](#)
Thermally induced defects, [20](#)
Three-dimensional, [3](#)
Three-phase reaction interface, [252](#)
Topological defect, [23](#), [172](#)
Traditional adsorbate evolution mechanism,
The, [149](#)
Transition metal compounds, [217](#)
Transmission Electron Microscopy (TEM),
[54](#), [55](#)
Turnover frequency, [178](#)
2D graphene, [136](#)
Two-dimensional, [3](#)
Two-electron, [104](#)

U

Ultrasonic-assisted liquid phase exfoliation,
[20](#)
Unpaired electrons, The, [71](#)

V

Vacancy, [19](#)
Valence and spin state, [74](#)

Vapor etching, [174](#)
Vibrating Sample Magnetometer (VSM),
[73](#)
Vibration frequency of the probe molecule,
The, [73](#)
Vienna Ab-initio Simulation Package, [213](#)
Volmer reaction, [124](#)
Voltage platform, [233](#)
Volume effect, [232](#)
Volumetric capacity, [250](#)

X

X-ray absorption fine structure, [236](#)
X-ray absorption near-edge structure
spectrum (XANES), [69](#)
X-ray Absorption Spectrometer (XAS), [63](#)
X-ray absorption spectroscopy, [176](#)
X-Ray Diffractometer (XRD), [62](#)
X-ray near-edge absorption fine structure
spectrum, [236](#)
X-ray Photoelectron Spectroscopy (XPS),
[62](#), [218](#)

Z

Zero-dimensional, [3](#)
Zn-air batteries, [255](#), [256](#)